



Ecole doctorale n°158 : Cerveau, Cognition, Comportement (ED3C)

*Laboratoire : équipe inDEV, unité Inserm NeuroDiderot UMR1141,
CEA, NeuroSpin, UNIACT*

Mapping Newborn Brain Development:

Analyses of large multi-modal imaging dataset

Par Andrea Gondová

Thèse de doctorat de Neurosciences

Dirigée par Dr. Jessica Dubois

Date de soutenance prévue : le 11 décembre 2023

Devant un jury composé de :

François ROUSSEAU	• Professeur HDR, IMT Atlantique	<i>Rapporteur</i>
Lilla ZOLLEI	• Associate Professor, Harvard Medical School	<i>Rapporteuse</i>
Elda FISCHI-GOMEZ	• Senior Research Scientist, École Polytechnique Fédérale de Lausanne	<i>Examinatrice</i>
Daniel MARGULIES	• Directeur de Recherche, Université Paris Cité, CNRS	<i>Examineur</i>
Jessica DUBOIS	• Directrice de Recherche, Université Paris Cité, Inserm	<i>Directrice de thèse</i>
Tomoki ARICHI	• Senior Clinical Lecturer, King's College London	<i>Membre invité</i>
Jean-François MANGIN	• Directeur de Recherche, Université Paris-Saclay, CEA	<i>Membre invité</i>

Title: Mapping Newborn Brain Development: Analyses of large multi-modal imaging dataset

Abstract:

The perinatal period plays a critical role in brain development, and its perturbations due to prematurity may lead to long-term neurodevelopmental impairments. This PhD research aimed to investigate these prematurity-related alterations in developmental trajectories using a multimodal *in vivo* dataset including magnetic resonance imaging (MRI) from the *developing Human Connectome Project*. We examined preterm infants and full-term neonates at various scales, including grey matter microstructure, white matter structural connectivity, and functional connectivity. Our analyses employed multivariate and machine learning approaches to integrate information from diverse MRI markers, revealing the benefits of such approaches in understanding atypical brain development and identifying markers of adverse outcomes.

Firstly, we characterized the distances between preterms and full-terms within the primary sensorimotor network based on microstructural properties of white matter tracts using complementary diffusion tensor imaging (DTI) and neurite orientation dispersion and density imaging (NODDI) measures with Mahalanobis approach. Our findings revealed tract-specific vulnerability to prematurity, particularly in infants born at earlier gestational ages, and suggested potential associations with altered neurodevelopmental outcomes.

However, predicting individual outcomes using these microstructural descriptors proved challenging, emphasizing the difficulty of shifting from group-based comparisons to the identification of *at-risk* individuals, particularly in small datasets. A parallel study aimed to employ predictive modelling based on microstructural inputs from cortical regions previously reported highly predictive of outcomes by another group. Our inability to replicate these findings with larger training dataset and extended validation aligned with known replicability issues within the machine learning domain and underscored the need for more robust practices in implementing reliable and generalisable predictive tools. Furthermore, we employed a machine learning approach to explore global cortical microstructure differences between preterm infants at term-equivalent age and full-term neonates, revealing prominent alterations with prematurity in lateral and medial inferior frontal lobes.

Finally, we explored the interplay between microstructural similarities across cortical and subcortical regions and the maturation of functional connectivity, longitudinally in preterms and compared to full-terms. Our work presented an alternative approach for studying complex relationships between different aspects of early brain development and demonstrated

how these complex microstructural-functional relationships evolve during development and are altered with prematurity.

In summary, our PhD research highlighted the important role of MRI in studying typical and atypical infant brain development. Integrating complementary MRI-derived markers and employing advanced statistical and machine learning methods, as illustrated in our work, has the potential to enhance our understanding and prediction of neurodevelopmental outcomes and to drive the improvements of care leading to enhanced quality of life of vulnerable populations in the future.

Keywords: early brain development, prematurity, neurodevelopmental outcome, magnetic resonance imaging (MRI), multimodal MRI, diffusion MRI, resting-state functional MRI, multivariate analyses, machine learning, prediction

Titre : Cartographie du développement du cerveau du nouveau-né : Analyses de grandes bases de données d'imagerie multimodales

Résumé :

La période périnatale joue un rôle essentiel dans le développement du cerveau, et ses perturbations dues à la prématurité peuvent avoir des conséquences neurodéveloppementales à long terme. Cette recherche doctorale visait à étudier ces altérations liées à la prématurité au niveau des trajectoires développementales en utilisant la base de données du *developing Human Connectome Project* incluant de l'imagerie par résonance magnétique (IRM) multimodale *in vivo*. Nous avons examiné des nourrissons prématurés et des nouveau-nés à terme à différentes échelles, y compris la microstructure de la substance grise, la connectivité structurelle de la substance blanche et la connectivité fonctionnelle. Nos analyses ont utilisé des approches multivariées et d'apprentissage automatique pour intégrer les informations provenant de divers marqueurs IRM, révélant les avantages de telles approches pour comprendre le développement atypique du cerveau et identifier les marqueurs du devenir neurodéveloppemental.

Tout d'abord, nous avons caractérisé les distances entre prématurés et nouveau-nés à terme au sein du réseau sensorimoteur primaire en nous basant sur les propriétés microstructurelles des tracts de substance blanche évaluées par des mesures complémentaires d'imagerie du tenseur de diffusion (DTI) et d'imagerie de dispersion des orientations et de densité des neurites (NODDI), et sur l'approche de Mahalanobis. Nos résultats ont révélé une vulnérabilité spécifique à la prématurité, en particulier chez les enfants nés à des âges gestationnels plus précoces, et ont suggéré des associations potentielles avec le devenir neurodéveloppemental.

Cependant, il s'est avéré difficile de prédire le devenir individuel à l'aide de ces descripteurs microstructurels, ce qui souligne la difficulté de passer de comparaisons basées sur des groupes à l'identification d'individus à risque, en particulier dans les petits ensembles de données. Une étude parallèle visait à utiliser une modélisation prédictive basée sur des entrées microstructurelles provenant de régions corticales précédemment signalées comme hautement prédictives du devenir par un autre groupe. Notre incapacité à reproduire ces résultats avec des données d'entraînement plus larges et une validation étendue est cohérente avec les problèmes de reproductibilité connus dans le domaine de l'apprentissage automatique et souligne la nécessité de pratiques plus robustes dans la mise en œuvre d'outils prédictifs fiables et généralisables. De plus, nous avons utilisé une approche d'apprentissage automatique pour explorer les différences globales de microstructure corticale entre les nourrissons

prématurés à l'âge équivalent au terme et les nouveau-nés à terme, révélant des altérations importantes avec la prématurité au niveau des lobes frontaux inférieurs latéraux et médians.

En outre, nous avons exploré les interactions entre les similitudes microstructurelles des régions corticales et sous-corticales et la maturation de la connectivité fonctionnelle, de manière longitudinale chez les prématurés et en comparaison avec les nouveau-nés de référence. Notre travail a présenté une approche alternative pour étudier les relations complexes entre les différents aspects du développement précoce du cerveau et a démontré comment ces relations microstructurelles-fonctionnelles complexes évoluent au cours du développement et sont modifiées avec la prématurité.

En résumé, notre recherche doctorale a mis en évidence le rôle important de l'IRM dans l'étude du développement cérébral typique et atypique du nourrisson. L'intégration de marqueurs complémentaires dérivés de l'IRM et l'utilisation de méthodes statistiques et d'apprentissage automatique avancées, comme illustré dans notre travail, ont le potentiel d'améliorer notre compréhension et la prédiction du devenir neurodéveloppemental, pouvant conduire à l'amélioration des soins et ainsi de la qualité de vie des populations vulnérables à l'avenir.

Mots clefs : développement cérébral précoce, prématurité, devenir neurodéveloppemental, imagerie par résonance magnétique (IRM), IRM multimodale, IRM de diffusion, IRM fonctionnelle au repos, analyses multivariées, apprentissage automatique, prédiction

Acknowledgments

‘No man is an island entire of itself’¹

I am grateful to many friends and colleagues for their help and guidance during this PhD.

First of all, I would like to express my sincere *thank you* to my supervisor Jessica Dubois for introducing me to the endlessly fascinating world of early brain development, for creating a safe and nurturing environment that encourages learning and questioning, for thoughtful guidance and corrections, and for being an inspiring example of the power that lies in kindness and patient determination.

I also want to thank Sara Neumane for her instrumental help throughout the thesis, for grounding all the ‘methodological exercises’ in clinical insights and always bringing it back to the baby, for her kind advice and reassurance, and for demonstrating that in life, there is never one correct way of doing things.

Additionally, I would like to express my gratitude to my colleagues and collaborators that actively contributed to the work presented in this manuscript: Tomoki Arichi, Jean-François Mangin, and Lucie Hertz-Pannier for their precious help, advice, and careful review of the articles. Yann Leprince, for his insightful comments and reliable support with all technical and methodological questions. It would have not been possible to accomplish this work without all your support.

I also thank all the babies and families that have volunteered their time for the research and to the whole dHCP team for collecting, curating, and making the data available to the scientific community.

I am also grateful to the jury members for accepting to review my work and for their comments.

The whole *baby team*! Parvaneh Adibpour, for many informative and interesting discussions and inputs, for willingness to share her experience and provide advice, for her sensitivity and compassion without judgment, and for bringing sunshine wherever she goes. To Dollyane Muret, whose rigour, determination, and honesty can be an example to us all, for her insightful comments on my work and for her support and advice with all the questions - work and life. And of course, all other team members past and present, Laurie Devisscher, Alexia Gerard, Alexandra Brandstätter, Marion Pavaux, for their scientific insights and for making going to the office a wonderful experience.

I would also like to thank the wider *inDev* team and *Neurospin* colleagues, Justine Fraize and Clément Poiret, with whom was on a parallel PhD track (I accomplished a lot simply mirroring your example), Eliot Kerdreux for his top organisation of social life of the team, David Germanaud for interesting conversations, Catherine Chiron, Aurélie Lebrun, Pierre-Yves Postic, Lucas Arcamone, Julia Micaux, and all the others who were there to help me with any types of questions and problems and offer support when necessary.

I am also grateful to the whole OSSIG team for allowing me to expand my scientific horizons, for giving me opportunity to participate in amazing community, for making me feel helpful, and for recharging by batteries with their passion and care.

¹ John Donne

Finally, I would like to thank my friends who supported me throughout this journey. Vicky Hohendorf and Daniel Hunter, with whom I started my academic path many years ago, for their friendship and moral support, and for the evidence that the best things are random – like choosing a seat next to the right people in a lecture theatre. To Daniel Fernández-Llaneza for debating anything and everything just for the fun of it and for endlessly expanding my reading list.

My deepest gratitude goes to Kristína Križanová – listing all the reasons why would fill a chapter – she calms nerves when needed, brings joy when needed, and scolds when necessary. Everyone deserves a friend like her although not many are as lucky as me to find them.

And of course, my family that has always been there to help and love me. My *maminka*, for instilling in me the passion for learning and exploring, because there is always another metaphorical mountain to climb. My *ocinko*, for teaching me all about moral strength and resilience to carry on, uncomplaining, not by lectures but by everyday example. My brother Dalibor, who despite being the youngest is often the voice of reason in our family and whose kind support, perceptive assessment, and pragmatic advice has helped me on many crossroads during my journey.

*...za život člověk vidí kdesi čosi,
kde všade bol a čo si v sebe nosí...²*



This project has received funding from the European Union's Horizon 2020 research and innovation programme under grant agreement No 800945 — NUMERICS — H2020-MSCA-COFUND-2017

² Honza Nedvěd

Table of contents

Acknowledgments.....	5
Table of contents	7
List of figures.....	9
List of tables.....	11
List of abbreviations	12
PART I: Early brain development and prematurity	14
<i>Chapter 1: Early brain development and impact of prematurity.....</i>	<i>15</i>
1.1. Early stages of brain development.....	16
1.1.1. Laminar structure of the foetal neocortex	16
1.1.2. Development of transient neural circuits	17
1.2. Developmental processes during the preterm and early post-term periods	18
1.2.1. Increasing cortical complexity	18
1.2.2. Shift from transient to permanent circuitry during the preterm period.....	20
1.2.3. Myelination: increasing the efficiency of structural connections	22
1.2.4. Functional development.....	24
1.2.5. Complex relationships between structural and functional organization during development.....	25
1.3. Prematurity and neurodevelopment	27
1.3.1. Preterm infants: a specific population.....	27
1.3.2. Brain differences between preterm and term-born infants as TEA	28
1.3.3. Prematurity and neurodevelopmental outcomes.....	32
1.3.4. Prediction of neurodevelopmental outcomes in premature children	33
Statement of interest	41
<i>Chapter 2: Methods for multimodal assessment of infant brain development.....</i>	<i>44</i>
2.1. Data for the study of early brain development.....	44
2.1.1. Multimodal MRI data: dataset acquisition and dHCP pre-processing.....	46
2.1.2. Neurodevelopmental outcomes at 18 months	49
2.2. Processing and analyses	50
2.2.1. Assessment of GM and WM microstructure with dMRI	50
2.2.2. Investigating structural and functional connectivity.....	54
2.2.3. Brain parcellation.....	60
2.2.4. Multivariate analyses of early MRI-derived markers of development	65
PART II: Experimental work	72
<i>Chapter 3: Effect of prematurity on the sensorimotor network.....</i>	<i>73</i>
Preface.....	73
<i>Published paper: Early structural connectivity within the sensorimotor network:</i>	
<i>Deviations related to prematurity and association to neurodevelopmental outcome...75</i>	
Afterword.....	111
<i>Poster: Early structural connectivity within SM network</i>	<i>112</i>

Chapter 4: Individual prediction of specific features and developmental outcomes....	113
Preface.....	113
4.1. Potential of the SM network characterization for predicting outcomes	114
Poster: Predicting neurodevelopmental outcomes.....	120
4.2. Cortical microstructure as a biomarker for early prediction of outcomes	121
Published paper: Predicting neurodevelopmental outcomes from neonatal cortical microstructure: A conceptual replication study.	122
4.3. Cortical microstructure as a biomarker of prematurity at birth	157
Poster: Cortical microstructure for prematurity prediction	160
Afterword.....	161
Chapter 5: Relationship between grey-matter microstructural similarity and functional connectivity	162
Preface.....	162
Paper: Bridging the gap between microstructural grey-matter similarity and functional connectome: A multi-modal MRI study in preterm and full-term infants	163
PART III: Discussion and general conclusion	202
Chapter 6: Discussion.....	203
6.1. Non-invasive examination of early brain development	204
6.1.1. Magnetic resonance imaging of typical and atypical populations	204
6.1.2. Prematurity: modulator of brain development or clinical phenotype?	206
6.1.3. What can we gain from ‘almost healthy’ cohorts?.....	207
6.1.4. Would a single snapshot be ever enough?	208
6.2. What can we ‘see’ with MRI?: link to underlying neurobiology.....	209
6.2.1. Assessing brain’s microstructure: dMRI as a tool for ‘virtual histology and dissection’	209
6.2.2. Resting state functional connectivity in infants	214
6.2.3. Relating functional and structural development	215
6.3. Linking the early brain features to later neurodevelopment	217
6.3.1. Machine learning for personalized predictions.....	217
6.3.2. Difficulties with predicting later outcomes from early MRI	219
Chapter 7: General conclusion	221
Global references.....	223
ANNEXE.....	263
Annexe 1: Résumé des travaux de thèse	264
Annexe 2: Whole-brain tractography in PT/FT infants.....	271
Annexe 3: Supplementary materials	278
Annexe 4: CV and Publications	310

Note to readers, references used throughout the manuscript are listed in the section **Global references** at the end of the manuscript with exception of the references employed within the three presented articles - these are located at the end of their respective article sections.

List of figures

Figure 1.1 Overview of principal events in typical human brain development.....	15
Figure 1.2. Schematic model of developing laminar structure in the human neocortex.	16
Figure 1.3. Sulci and gyri development during gestation.	19
Figure 1.4. Cortical development during the preterm period.....	20
Figure 1.5. Transient compartments from preterm period to full-term birth.	21
Figure 1.6. Myelogenesis in the human brain.....	23
Figure 1.7. Resting-state networks in adults and preterms.	25
Figure 1.8. Global burden of prematurity.	28
Figure 1.9. Examples of common types of white matter injury in preterm infants.	30
Figure 1.10. Graphical overview of studies performed within the presented PhD work.....	43
Figure 2.1. Available subjects within the dHCP cohort.	45
Figure 2.2. Summary of the main stage of the anatomical MRI's processing pipeline.	47
Figure 2.3. Neurodevelopmental categories included in the BSID-III assessment	49
Figure 2.4. Maps of DTI and NODDI-derived metrics for an example full-term neonate.....	52
Figure 2.5. Sensitivity of tractography results to methodological choices.	56
Figure 2.6. Example tractography pipeline.....	57
Figure 2.7. Functional connectivity (FC) estimation across a set of predefined ROIs.....	59
Figure 2.8. Employed anatomical parcellations.....	63
Figure 2.9. Example of random parcellation in the dHCP template space	65
Figure 2.10. Simplified example of Mahalanobis distance.....	66
Figure 3.1. Regions of interest, sensorimotor tracts, and diffusivity metrics for a representative full-term infant.....	83
Figure 3.2. Outcome assessment at around 18 months of corrected age	90
Figure 3.3. Diffusion metrics across tracts and cohort subgroups.....	91
Figure 3.4. Results of the Mahalanobis analyses.	92
Figure 3.5. Significant correlations between Mahalanobis distances and neurodevelopmental scores at 18mCA	95
Figure 4.1. Overview of the predictive pipeline.	117
Figure 4.2. Example parcellation	131
Figure 4.3. Nested validation pipeline.	134
Figure 4.4. Distribution of cortical FA.....	136
Figure 4.5. Visual description of the Cohorts A,B, and C.....	137

Figure 4.6. Predictive results	140
Figure 4.7. Overlap of global FA	143
Figure 4.8. Results of the prematurity status prediction.	158
Figure 4.9. Localisation of 5 clusters for prematurity prediction	159
Figure 5.1. Grey matter connectome in infant groups.	169
Figure 5.2. Mutual information (MI) results of groups comparisons.	170
Figure 5.3. Functional connectome in infant groups.	172
Figure 5.4. Relationship between GC and FC connectivity per ROI pair	173
Figure 5.5. Mutual information (MI) between GC and FC.....	174
Figure 5.6. Longitudinal evolution of GC and FC.....	175
Figure 5.7. Directionality of GC-FC relationships.	177
Figure 5.8. Network-based comparisons of longitudinal GC-FC relationships.....	179

List of tables

Table 1.1. Overview of recent neurodevelopmental outcome prediction studies.	34
Table 3.1. Detailed clinical and sociodemographic information for the 59 pairs of infants. ...	89
Table 4.1. Description of Cohort A, B, C (Cohort D is a random subset of C).	127
Table 4.2. Composition of Cohorts A,B, and C in terms of categorised BSID-III composite scores.....	138
Table 4.3. Results of the nested validation	142

List of abbreviations

AD – axial diffusivity	FCA – fuzzy clustering analysis
ADHD – attention deficit hyperactivity disorder	FDR – false discovery rate
ASD – autism spectrum disorder	fNN – fully connected neural network
AUC – area under receiver operating characteristic curve	fODF – fibre orientation density function
BEDPOSTX – Bayesian estimation of diffusion parameters obtained using sampling techniques	FT – full-term infant
BG – basal ganglia	GA – gestational age
BOLD – blood oxygen level-dependent signal	GC – grey matter connectivity
BSID-III – Bayley scales of infant development third edition	GM – grey matter
Bstem – brainstem	GMM – Gaussian mixture models
Caud – caudate nucleus	GPU – graphics processing unit
CHARMED – composite hindered and restricted water diffusion	HARDI – high angular resolution diffusion imaging
CLD – chronic lung disease	ICA – independent component analysis
CNN – convolutional neural network	IMD – index of multiple deprivation
CP – cortical plate	IUGR – intrauterine growth restriction
CSD – constrained spherical deconvolution	IZ – intermediate zone
CSF – cerebrospinal fluid	Lenti – lenticular nucleus
CST – corticospinal tract	LOOCV – leave one out cross-validation
cuDIMOT – CUDA diffusion modelling toolbox	M – Mahalanobis distance
cUS – cranial ultrasonography	M1 – lateral portion of the primary motor cortex (precentral region)
CV – cross-validation	MAE – mean absolute error
dHCP - developing Human Connectome Project	MB – multi-band
DIAMOND – distribution of anisotropic microstructural environments in diffusion-compartment imaging	mCA – months of corrected age
DKI – diffusion kurtosis imaging	M-CRIB-S – Melbourne children's regional infant brain surface parcellation
DKT – Desikan-Killiany-Tourville atlas	MD – mean diffusivity
dMRI – diffusion-weighted magnetic resonance imaging	MEG – magnetoencephalography
Draw-EM – developing brain region annotation with expectation maximization	ML – machine learning
DTI – diffusion tensor imaging	MRI – magnetic resonance imaging
DWMA – diffuse white matter abnormalities	MSEL – Mullen scales of early learning
EEG – electroencephalography	MZ – marginal zone
EPI – echo-planar imaging	NDI – neurite density index
F/M – female/male	NEC – necrotizing enterocolitis
FA – fractional anisotropy	NICU – neonatal intensive care unit
FC – functional connectivity	NIRS – near infrared spectroscopy
	NODDI – neurite orientation dispersion and density imaging
	NPV – negative predictive value
	NSMDA – neuro-sensory motor development assessment,
	ODI – orientation dispersion index
	ParaC – medial portions of the primary sensori-motor cortices (paracentral region)
	PC – principal component
	PCA – principal component analysis
	PMA – postmenstrual age
	PPV – positive predictive value

PROBTRACKX – probabilistic tracking with crossing fibers
PT – preterm infant
Q-CHAT – quantitative checklist for autism in toddlers
R – Pearson’s correlation coefficient
R² – coefficient of determination
RD – radial diffusivity
RF – random forest
ROI – region of interest
ROP – retinopathy of prematurity
rs-fMRI – resting-state functional magnetic resonance imaging
RSN – resting-state networks
S1 – lateral portion of the primary somatosensory cortex (postcentral region);
SENS – sensitivity
SES – socio-economic status
SHARD – spherical harmonics and radial decomposition

sMSM – multimodal surface matching with higher-order smoothness constraints
SNR – signal-to-noise ratio
SP – subplate
SPEC – specificity
SPM – statistical parametric mapping
SVM – support vector machine
SVR – support vector regression
SVZ – subventricular zone
T1w/T2w – T1-weighted/T2-weighted
TDI – toddler temporal-spatial deviation index
TE – echo time
TEA – term-equivalent age
Thal – thalamus
TR – repetition time
VZ – ventricular zone
wGA – weeks of gestational age
WM – white matter

PART I: Early brain development and prematurity |

Chapter 1: Early brain development and impact of prematurity

Brain development is a complex, multi-stage process that begins in early gestation and extends through adolescence. The most profound morphological and cellular transformations occur in the prenatal and early postnatal periods, during which the simple embryonic neural tube transforms into the highly complex central nervous system (*Figure 1.1*) (Lagercrantz, 2016). This chapter aims to provide an overview of the developmental processes underlying cortical and subcortical maturation and establishment of early structural and functional connectivity. We mostly focus on the preterm period (between 26 - 37 weeks of gestational age - wGA), drawing from a diverse set of methodological approaches, including detailed anatomical descriptions through *post mortem* histology methods and non-invasive *in vivo* neuroimaging, particularly magnetic resonance imaging (MRI) (methodological MRI descriptions are the focus of *Chapter 2*). We then briefly describe effects of prematurity on typical brain development and neurodevelopmental impairments observed in this clinically important population.

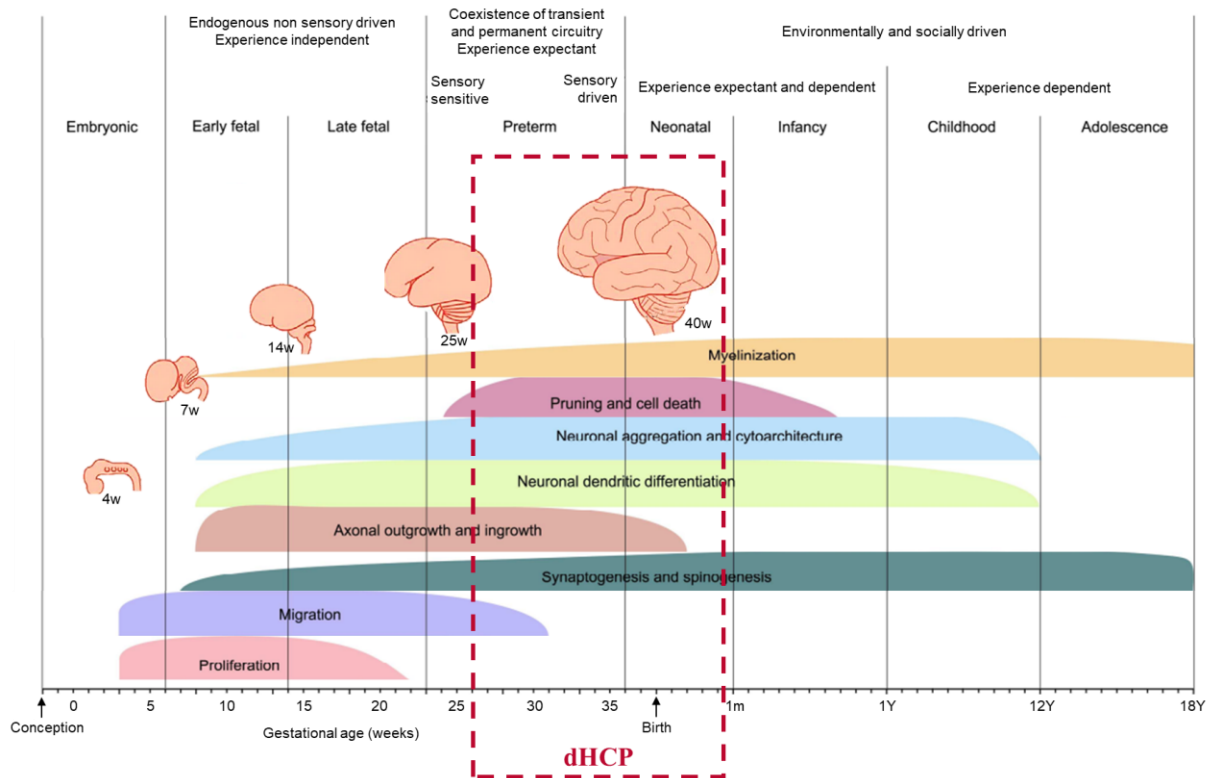


Figure 1.1 Overview of principal events in typical human brain development, emphasizing their sequential and overlapping nature and shift from activity-independent to activity-dependent development with age. The highlighted red box denotes the specific developmental period studied in the current work using the data from the *developing Human Connectome Project* (dHCP). Adapted from (Lagercrantz, 2016; Kostović et al., 2019).

1.1. Early stages of brain development

The following sections focus on the early stages of brain development before 26wGA.

1.1.1. Laminar structure of the foetal neocortex

Two critical processes lay a foundation for subsequent cerebral development during embryonic and early foetal periods: neuronal (and glial) proliferation and neural migration. By 14wGA (start of the 2nd trimester), cerebral tissues are organized in five **transient zones**, some of which lack a direct counterpart in adults (Bystron et al., 2008; Vasung et al., 2016) (*Figure 1.2*), ordered from lateral ventricles to brain periphery.

Firstly, **proliferative zones** (ventricular and subventricular zones, VZ/SVZ) serve as a proliferation hubs that contain progenitor cells of excitatory and inhibitory neurons, and glial cells (Kriegstein & Alvarez-Buylla, 2009). Relative volume of VZ/SVZ decreases exponentially from 15-22wGA, coinciding with the completion of neurogenesis (Vasung et al., 2019). Neurogenesis continues to a limited extent even in later prenatal and postnatal stages in SVZ and subgranular zone of hippocampus (Shankle et al., 1999).

Next, the **intermediate zone** (IZ) consists largely of axonal fibres, increased extracellular matrix and lower neuronal density compared to the proliferative zones. IZ is known as 'foetal white matter' reflecting its function in the mature brain. The IZ is enveloped by the **subplate zone** (SP) which serves as an axonal 'waiting compartment' during formation of cortical circuits (Kostovic & Rakic, 1990).



Figure 1.2. Schematic model of developing laminar structure in the human neocortex. **Legend:** VZ - ventricular zone; SVZ - subventricular zone; IZ - intermediate zone; PP - preplate zone; SP - subplate zone; CP - cortical plate; MZ - marginal zone. Adapted from (Bystron et al., 2008).

The **cortical plate** (CP) is a target of post-migratory neurons organized in coherent radial columns before the 3rd trimester and a precursor of the mature grey matter (Khan et al., 2019; Bataille et al., 2018). Glutamatergic excitatory projection neurons follow a pattern of radial migration guided by glial cell scaffolds, resulting in an 'inside-out' cortical layer organization (i.e. the last neurons to arrive form the outermost layers of the CP). GABA(γ -aminobutyric acid)-expressing neurons on the other hand migrate tangentially from multiple regions, including lateral and medial ganglionic eminences and the adjacent preoptic/anterior entopeduncular area, and exhibit more protracted neurogenic and migratory periods than glutamatergic excitatory neurons (Stiles & Jernigan, 2010; Tau & Peterson, 2010; Kolasinski et al., 2013). Neuronal migration to CP coincides with substantial increase in its surface and thickness. The neuronal positioning and differentiation are driven by molecular and genetic factors (Kang et al., 2011; Bakken et al., 2016) that shape the organization of CP into regions with specific microstructural characteristics (Kostović & Judaš, 2015). Lastly, the **marginal zone** (MZ) represents the outermost layer above the CP and later becomes layer 1 of the mature cortex (Bystron et al., 2008).

1.1.2. Development of transient neural circuits

As neurons reach their target locations in CP, they start extending axons and dendrites to establish connections, i.e. synapses, with other neurons. Early synaptogenesis relies heavily on interactions with underlying scaffolds formed by radial glial cells and tangentially migrating neurons (Allen, 2013), and the regulation of transcription factor expression through guidance molecule gradients (Sur & Rubenstein, 2005; Rakic et al., 2009). Thus, the earliest stages of circuit formation (including transient thalamo-cortical, cortico-cortical, and cortico-thalamic connections) occur independently of neural activity and inputs (Rakic et al., 2009; Lewis et al., 2013). But throughout gestation, axonal and dendritic growth and branching become increasingly influenced by spontaneous (and later evoked) synaptic activity (Mire et al., 2012) (Mizuno et al., 2010) (Pletikos et al., 2014) (Molnár et al., 2020)

Major projection fibres, including thalamic fibres passing through the internal capsule, cortico-ponto-cerebellar, basal ganglia, and basal forebrain fibres are already present in the early foetal period (by 17wGA) (Kostovic & Rakic, 1980; Kostović & Jovanov-Milošević, 2006; Huang et al., 2009; Wilkinson et al., 2017), along with limbic bundles like the fornix, stria terminalis, and cingulum (Vasung et al., 2019). In the midfoetal period (17w-25wGA), efferent fibres from SP and CP penetrate their targets in the striatum, pons, and spinal cord (Judas et al., 2005). The cortico-cortical fibres of the corpus callosum exhibit increased growth

(Vasung et al., 2010). Some forming cortico-cortical association fibres, including the inferior longitudinal fasciculus, fronto-occipital fasciculus, middle longitudinal fasciculus, and vertical occipital fasciculus, also become recognizable at this period (Song et al., 2017; Vasung et al., 2017). At this stage, afferent pathways do not yet penetrate the CP but establish transient synaptic connections with neurons in the SP of sensory and association areas. The relocation of the connections from SP to CP marks the shift from transient to permanent cortical circuitry observed during the preterm period (Kostović & Judoš, 2010; Kostović et al., 2019).

The development of structural pathways is accompanied by changes in the predominant fibre orientation within the IZ (future white matter), which initially exhibits mostly radial coherence similar to CP due to a mixture of radial glia, penetrating blood vessels, and radial axons (Xu et al., 2014) and then shifts to a predominantly tangentially oriented patterns from around 22wGA (Mitter et al., 2015)

1.2. Developmental processes during the preterm and early post-term periods

Preterm period is interesting both biologically and clinically because, in addition to *post mortem* studies, the brain development can be monitored *in vivo* in prematurely-born infants using a combination of imaging methods, for example structural MRI (e.g., MRI with T1 and T2 weighting, diffusion MRI), and functional techniques such as electroencephalogram (EEG), near infrared spectroscopy (NIRS), or resting-state functional MRI (rs-fMRI). Additionally, the early post-term period can be explored in healthy full-term newborns. In the following sections, we provide a concise overview of the developmental processes from the preterm period (26w-37wGA) up to the early post-term period (44wGA) as these age ranges correspond to the ages at scan within dHCP dataset used in our work.

1.2.1. Increasing cortical complexity

Cortical plate (CP) continues to expand in surface area throughout the preterm period. Concurrently, this phase is also characterized by significant changes in cortical surface morphology, particularly the emergence of complex gyral and sulcal patterns. Development of primary sulci begins during the foetal stage around 20wGA, and continues in the preterm period with emergence of secondary sulci from 32wGA, and tertiary sulci after 38wGA (Dubois et al., 2019; de Vareilles et al., 2023) (*Figure 1.3*).

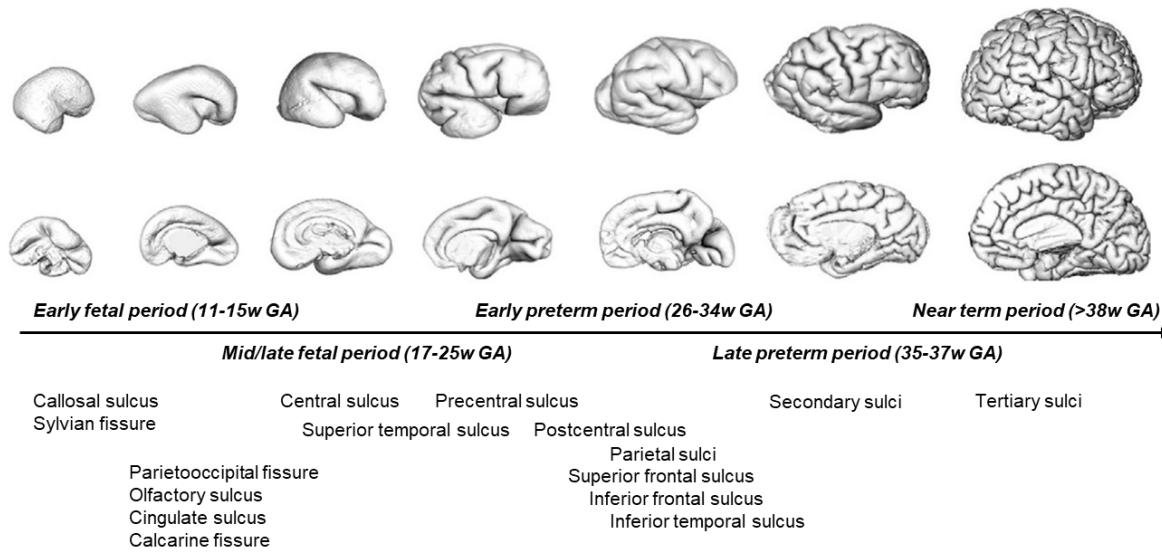


Figure 1.3. Sulci and gyri development during gestation. Adapted from (Kostovic & Vasung, 2009).

From the cytoarchitectural perspective, the radial coherence of the CP due to radial glia and radial orientation of neuronal apical dendrites observed in the foetal stages progressively diminishes through the preterm period by a gradual elaboration of neuronal dendrites, ingrowth of axonal fibres, and the development of horizontal laminations of the cortex (Mrzljak et al., 1988; Mrzljak et al., 1992; Garel et al., 2001; Kostovic et al., 2002; Vasung et al., 2016; Khan et al., 2019) (*Figure 1.4a*). These changes underlie the increases in CP thickness and the reported decreases in cortical diffusion anisotropy during this period (McKinstry et al., 2002; Yu et al., 2016; Khan et al., 2019; for review: Ouyang et al., 2019) (*Figure 1.4b*).

Significant variability in cytoarchitecture, subplate thickness, and genetic and transcriptomic profiles exist across cortical areas giving rise to distinct areal identities (Brodmann, 1908; Kostovic et al., 2002) (H. Huang et al., 2013) (Yun et al., 2020). Human-specific ‘protomap’ of cytoarchitectonic areas describing conserved patterns of regional specialization with diverse developmental trajectories is thought to be initiated already in the foetal period under genetic control, gradients of morphogens and distinct transcriptional programs (Piao et al., 2004; O’Leary et al., 2007; Stahl et al., 2013) and then further refined by region-specific maturation signals, extrinsic signalling from ingrowing axons, and activity-dependent processes (Cadwell et al., 2019).

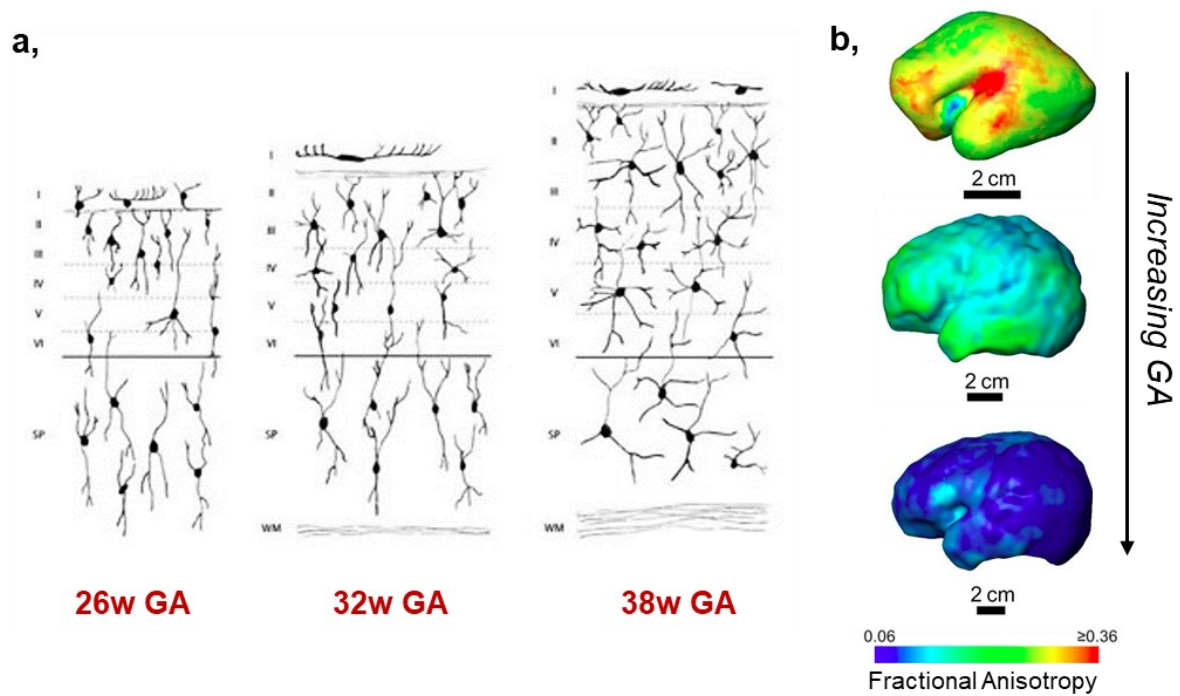


Figure 1.4. Cortical development during the preterm period. **a**, Schematic depiction of cortical layers with increasing maturation of cortical and subplate neurons and increasing elaboration of their dendritic spines alongside the tangential organization of white matter. **b**, Heterogenous decrease of cortical diffusion anisotropy during the preterm period coinciding with the complexifying cortical cytoarchitecture. Adapted from (Mrzljak et al., 1988; Yu et al., 2016; Batalle et al., 2018).

1.2.2. Shift from transient to permanent circuitry during the preterm period

Preterm period is marked by a significant reorganization of cortical circuits corresponding to the formation of permanent brain circuitry and a gradual resolution of the SP (Kostović & Judaš, 2010). From 26wGA, thalamo-cortical afferents relocate from SP to establish connections with CP layer IV (Kostović & Jovanov-Milošević, 2006; Krsnik et al., 2017). Transient circuitry nevertheless persists in other areas of the SP, which reaches its peak volume and thickness between 26-32wGA depending on cerebral regions. Notably, the SP persists longer in associative cortical regions, where the relocation of long associative cortico-cortical fibres spans from 23-38wGA (Kostović & Judaš, 2010; Vasung et al., 2016) (*Figure 1.5*). The presence of the SP is one of the main signs of cortical immaturity in brain development (Kostovic & Vasung, 2009) and SP disappears only postnatally in some regions resulting from axon relocation, extracellular matrix loss, and white matter reorganization (Kostovic & Rakic, 1990) (Kostović, 2020).

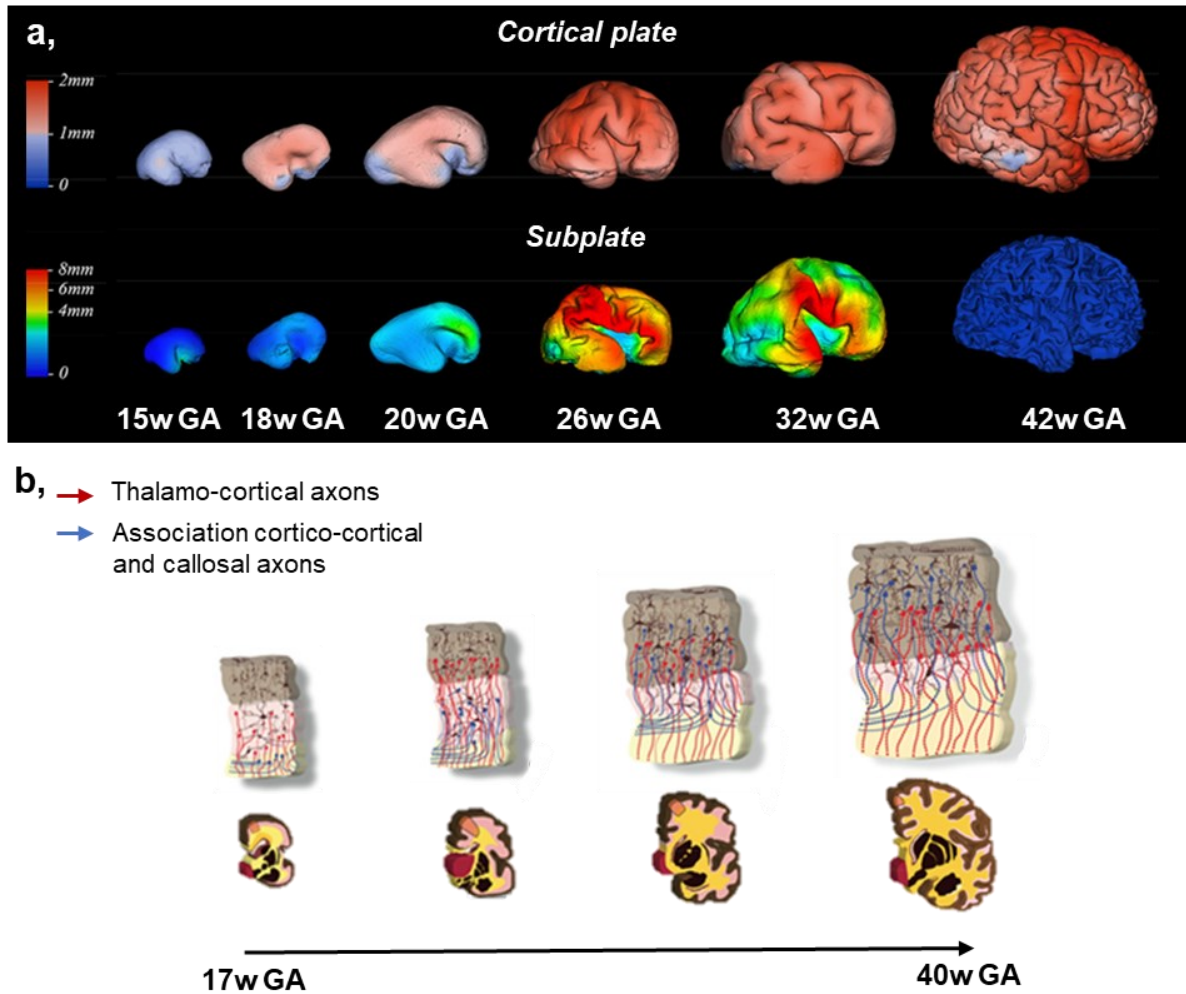


Figure 1.5. Transient compartments from preterm period to full-term birth. **a,** Changes in cortical plate and subplate thickness. Subplate lingers for an extended period in associative cortical regions. **b,** Development of cortical connectivity in the transient foetal zones together with the associated changes in dendritic arborisation of cortical and subplate neurons, and changes in cortical morphology during the same period. Neurons in **brown**, thalamo-cortical axons in **red**, cortico-cortical axons in **blue**. Adapted from (Takahashi et al., 2012; Vasung et al., 2016; Vasung et al., 2019).

By 30wGA, long-distance connections are well-developed in the cingulate, entorhinal, and hippocampal cortices (Kostović et al., 1993). Between 31-36wGA, rapid increase in white matter (IZ) volume is driven by growth of long intra-hemispheric (associative) and inter-hemispheric (callosal) pathways (Huang et al., 2009; Takahashi et al., 2012; Vasung et al., 2017). Initially, this involves excess callosal axons which undergo pruning postnatally (Kostovic et al., 2014). In fact, the majority of pathways formed prenatally exhibit an excess of axons, which are subsequently pruned in the most intense manner during the first year after birth, and later at a slower pace, through interaction with environmental inputs (Kostovic et al., 2014). Development of fibre pathways continues postnatally with the formation of U-fibres, accompanied by dendritic arborization and spine formation, synapse overproduction and

elimination, as well as axonal pruning, to refine the cortical circuitry and structural connectivity through interactions with the environmental inputs (Kostovic et al., 2014; for review: Dubois et al., 2015).

Developing structural connectivity, i.e. anatomical connections linking a set of neural elements or brain regions, in the preterm period can be also described using graph-based metrics. Such investigations have revealed a general trend towards increased local and global efficiency of the structural networks (Batalle et al., 2017; Song et al., 2017; Ní Bhroin et al., 2020) and a reduction in their characteristic path length (Brown et al., 2014; van den Heuvel et al., 2015). The observed trends suggest enhanced network integration during the early development that facilitates the exchange of information between distant regions, as well as heightened network segregation that supports specialized information processing between interconnected brain regions (Rubinov & Sporns, 2010). Network evaluations also suggest widespread progressive strengthening of connections within and between cortical lobes and hemispheres (Brown et al., 2014; Batalle et al., 2017b; Wu et al., 2023).

Hemispheric asymmetries within structural connectivity were reported from direct evaluations based on local diffusion indices and spatial localizations of tracts (Dubois et al., 2009; Dubois et al., 2016) as well as graph connectivity metrics (Y. Wu et al., 2023). However, it's worth noting that studies examining the evolution of connectivity strength sometimes yield conflicting results (even when employing same diffusion metrics to characterize the structural networks), highlighting the methodological challenges associated with reliable delineation of structural connectivity in infant MRI data.

1.2.3. Myelination: increasing the efficiency of structural connections

Myelination is another important process that occurs concurrently and subsequently to axonal pruning to enhance the efficiency of cortical circuits and structural connectivity. During myelination, oligodendrocytes orchestrate myelin production and wrapping of axonal fibres with myelin sheaths from neural bodies to periphery, resulting in accelerated conduction of neural transmission (Fletcher et al., 2021). While initiated in the latter half of gestation in some deep brain regions, its most intense phase occurs around term, peaks during the first postnatal year, and continues into childhood and adolescence (Lagercrantz, 2016).

Myelination occurs with asynchronous spatiotemporal progression throughout the white matter (Van der Knaap & Valk, 1993; Baumann & Pham-Dinh, 2001) which has been extensively studied by histological approaches, and confirmed by myelin-sensitive MRI evaluations (Carmody et al., 2004; Dubois et al., 2006; Deoni et al., 2012; Smyser et al.,

2016;Melbourne et al., 2016 for review: Dubois et al., 2014) (*Figure 1.6*). Myelination progresses in a stereotyped sequence which begins in early active nerves like the long pyramidal motor tracts, and olfactory and visual pathways (Lagercrantz, 2016). It follows a caudo-rostral gradient, progressing from central to peripheral regions, occurring sooner and more rapidly in sensory pathways (somatosensory, visual, auditory) than in motor pathways, and in projection fibres than in associative ones (Yakovlev & Lecours, 1967). Asymmetries in connectivity between hemispheres are paralleled by left-right asynchronies in myelination (Dubois et al., 2009; Dubois et al., 2016).

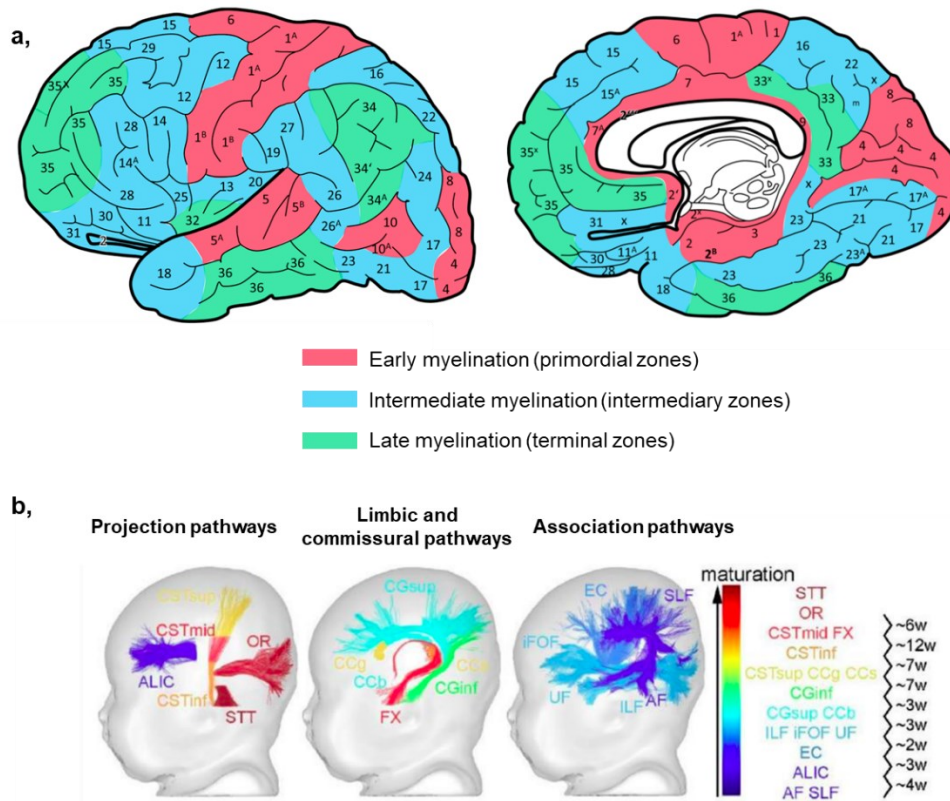


Figure 1.6. Myelogenesis in the human brain. **a,** Subcortical regions of the earliest myelinating primordial zone show myelination by the end of gestation and correspond mainly to primary sensorimotor areas. Myelination then continues postnatally in intermediary, then terminal zones corresponding to unimodal and multimodal associative areas, respectively. Arabic numerals indicate cortical areas according to the beginning of myelination (1 earliest, 36 latest). Adapted from (Zilles, 2018, originally from Flechsig, 1901). **b,** White matter maturation asynchrony in healthy infants evaluated by mutliparametric MRI. Pathways are ordered and coloured according to their maturation with maturational delays (in weeks) between pairs of pathways. Adapted from (Dubois et al., 2015, originally from Kulikova et al., 2015). **Legend:** AF arcuate fasciculus; ALIC anterior limb of the internal capsule; CC corpus callosum (g/b/s genu/body/splenium); CG cingulum (inf/sup inferior/superior parts); CST cortico-spinal tract (inf/mid/sup inferior/middle/superior portions); EC external capsule; FX fornix; iFOF inferior fronto-occipital fasciculus; ILF inferior longitudinal fasciculus; OR optic radiations; SLF superior longitudinal fasciculus; STT spino-thalamic tract; UF uncinat fasciculus.

1.2.4. Functional development

In this section, we transition from examining structural brain development to exploring the coinciding changes in brain functioning. Formation and maturation of cortical circuits are accompanied by substantial changes in brain activity. From 24wGA onwards, EEG recordings reveal a shift in neural activity patterns from sudden bursts to more continuous activity (Vanhatalo & Kaila, 2006; Wallois, 2010).

By 26wGA, functional networks observed with resting-state fMRI begin to encompass diverse cortical regions and the cerebellum, with progressive development throughout the preterm period (Doria et al., 2010; Smyser et al., 2010; van den Heuvel et al., 2015). Notably, the strengthening of thalamo-cortical functional connections is significant between the 29-31wGA period. The cortico-cortical connectivity also intensifies, as indicated by the increased synchrony of the spontaneous neural activity across cortical regions, i.e. functional connectivity, and proceeds at varying developmental patterns across networks. This progression appears to follow a sequence of occipital to temporal, then frontal, and parietal expansion (Fransson et al., 2009; Doria et al., 2010; Smyser et al., 2010; Jakab et al., 2014; van den Heuvel et al., 2015).

While homologous regions in both hemispheres initially exhibit similar mirrored connectivity profiles, this similarity decreases during development, leading to more diverse regional relationships and inter-hemispheric asymmetries (Taymourtash et al., 2023; Williams et al., 2023).

At term age (~40wGA), the architecture of functional networks, including visual, auditory, somatosensory, motor, frontoparietal, and executive control networks, appears similar to adults' (Fransson et al., 2009; van den Heuvel et al., 2015; Toulmin et al., 2015; Turk et al., 2019; Eyre et al., 2021; Dall'Orso et al., 2022)(*Figure 1.7*). However, graph-based evaluations of the functional networks have suggested that, in contrast to adults, cortical hubs critical for functional integration across networks are still primarily located in primary sensory and sensory-motor regions (Fransson et al., 2009; van den Heuvel et al., 2015). Functional network centrality then primarily increases within visual regions and decreases within the motor and auditory regions in term-born infants (Fenn-Moltu et al., 2023)

Postnatally, maturation, fine-tuning, and specialization of functional networks progresses asynchronously, following a primary-to-higher function order from primary sensorimotor/auditory networks to the visual, and then default-mode networks (Hoff et al., 2013; Gao et al., 2015; Cao et al., 2017; Larivière et al., 2020; Eyre et al., 2021).

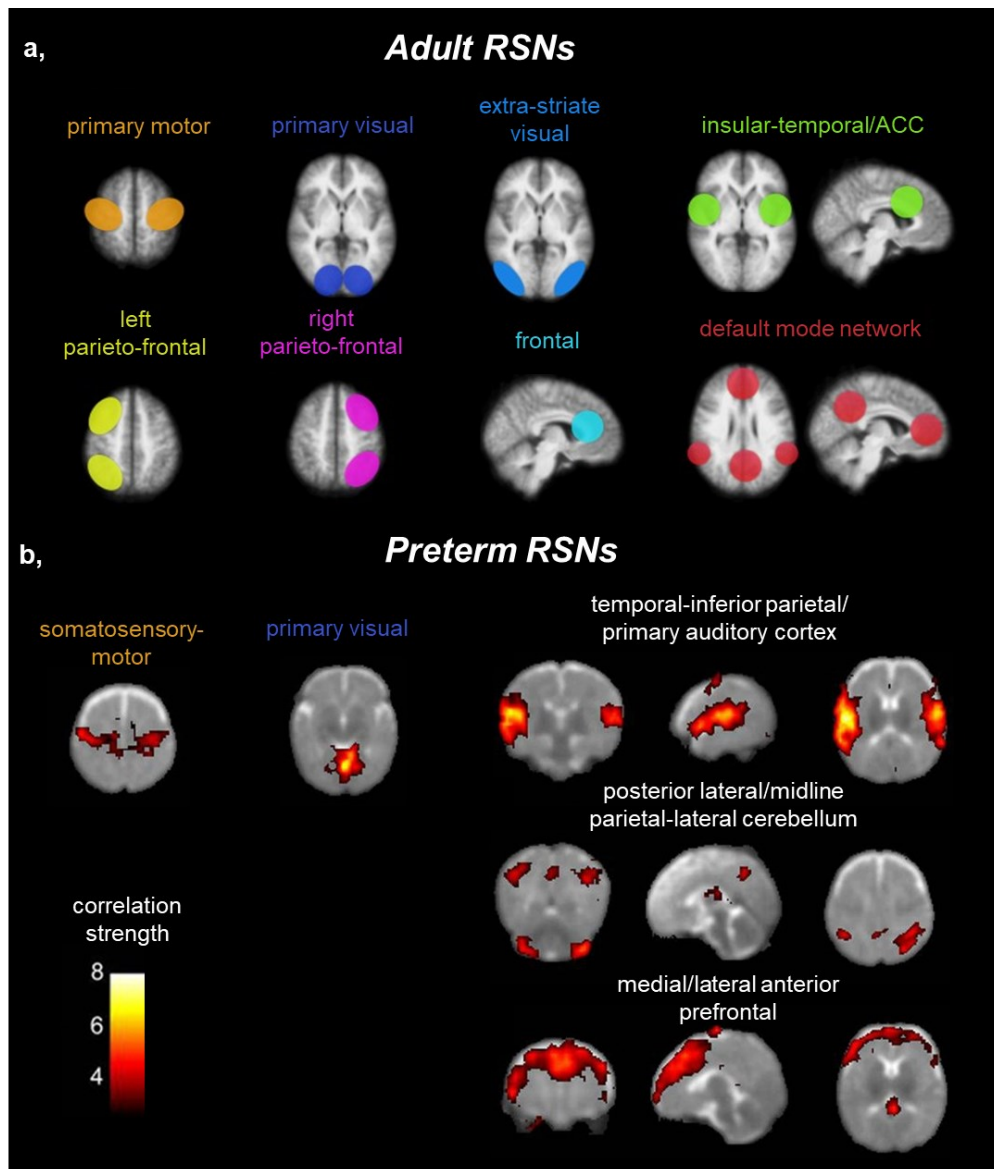


Figure 1.7. Resting-state networks in adults and preterms. **a**, Eight commonly reported resting-state networks (RSNs) that regroup areas with strong functional synchrony in adults. **b**, As comparison, five RSNs consistently identified in preterm infants. Adapted from (Fransson et al., 2007; van den Heuvel & Hulshoff Pol, 2010; Hoff et al., 2013)

1.2.5. Complex relationships between structural and functional organization during development

In previous sections, we explored the intricate and asynchronous nature of early brain maturation across brain regions and networks, hinting at a complex interplay between structural and functional development.

Fundamentally, axonal pathways and their synaptic connections form the essential foundation for functional connectivity. The relationship with the structural framework becomes

prominent with the intense growth of inter- and intra-hemispheric connections in the late foetal and early preterm period, coinciding with significant functional changes in neural activity patterns (Kostović & Judoš, 2010). As early as 24wGA, sensory inputs like sound trigger evoked cortical responses, aligning with the migration of thalamic afferents from sensory and associative thalamic nuclei to the SP and then the CP (Milh et al., 2007; Kostović & Judoš, 2010). The transition to sensory-expectant functioning is critical for wiring and refining the developing functional circuitry (Penn & Shatz, 1999; Milh et al., 2007). Furthermore, evoked responses in pain perception pathways indicate functionality between 29-30 wGA, additionally illustrating the early development of sensory functions in parallel to the establishment of the anatomical substrate (Anand & Hickey, 1987; Lee et al., 2005; Kostović & Jovanov-Milošević, 2006; Lagercrantz & Changeux, 2009).

Additionally, myelination, a structural change, impacts functional aspects by increasing conduction velocities reflected in reduced peak latencies of cortical responses observed with EEG (Demerens et al., 1996; Barrera et al., 2013). Of note, although these changes in peak latencies were reported to be associated with fibre myelination in afferent visual pathways and acoustic radiations in auditory network, other factors such as microstructural organization of the CP and SP, and cortical folding also likely contribute to this effect (Dubois et al., 2006; Roberts et al., 2009; Adibpour et al., 2015; Dubois, et al., 2016). At later ages, myelination may allow to maintain peak latencies while the brain size and white matter connection lengths increase (Dubois et al., 2016).

Additionally, cytoarchitectonically defined cortical areas provide anatomical basis for characterisation of functionally relevant units, with regional and laminar microstructure, as well as molecular and transcriptomic profiles able to differentiate sensory, motor, and associative brain regions (Zilles & Amunts, 2015) suggesting at least a limited role of underlying microstructure and cortico-cortical connectivity in functional specialization.

However, this relationship is bidirectional. The shift from activity-independent to activity-dependent development of cortical circuits occurs early in the foetal period (Rakic et al., 2009; Lewis et al., 2013), marked by the emergence of spontaneous synchronized bursts of neuronal activity (Sun et al., 2010). While the precise mechanisms underlying these bursts are debated, their instructive role in the establishment and maturation of early neuronal circuits and structural connectivity, neuronal differentiation, synaptogenesis, synaptic elimination, and axonal pruning is increasingly recognised in both animal models and preterm infants (Vecchierini et al., 2007; Hanganu-Opatz, 2010; Benders et al., 2015; Luhmann et al., 2016; Whitehead et al., 2017; Arichi et al., 2017; Mukherjee & Kanold, 2023)..

In the cortex, activity-dependent mechanisms are believed to drive progressive refinement and formation of distinct boundaries between functional areas through a combination of neuronal differentiation, synaptogenesis, and axonal formation and signalling leading to functional specialization (Cadwell et al., 2019). Furthermore, neuronal activity, both spontaneous and sensory evoked, directly regulates axon myelination by influencing activity-dependent differentiation of oligodendrocytes and inducing myelin formation through neurotransmitter release (Demerens et al., 1996; Barrera et al., 2013; White & Krämer-Albers, 2014; Wake et al., 2015; for review: Dubois et al., 2014).

Hence, activity-dependent plasticity tightly intertwines early structural and functional development. Insights gained from structural descriptions contribute significantly to understanding neuronal activity development and functional connectivity, and vice versa. Interestingly, in rodent models, peripheral-driven neuronal activity also appears to influence maturation of brain vasculature (Lacoste et al., 2014; Whiteus et al., 2014; Guilbert et al., 2022), suggesting intricate relationships not only between multiple aspects of the brain development, but also its broader environment. This interplay, especially crucial in early stages, potentially diminishes as the structure stabilizes, establishing a more permanent foundation for the adaptations of the functional connectome to new demands as neonates rapidly acquire skills and respond to their environment (Ciarrusta et al., 2022). This is supported by differences in structure–function coupling in older children (Baum et al., 2020) and the increasing differences between structural and functional networks in adults (Yeo et al., 2011).

1.3. Prematurity and neurodevelopment

1.3.1. Preterm infants: a specific population

Our understanding of development during the preterm period largely relies on *in vivo* assessments of preterm-born neonates. However, comparing preterm babies at term equivalent age (TEA) to their full-term born peers consistently reveals the significant impact of premature birth on brain features. These observations highlight the extreme vulnerability of the complex maturational processes during the preterm period and their role in long-term development and prompt questions about the generalizability of findings obtained from preterm neonates to typically developing populations. Advances in *in utero* foetal imaging, particularly in data processing and motion artifact correction, hold promise for assessing the typical developmental trajectories of healthy fetuses *in vivo* (Jakab et al., 2015; Pollatou et al., 2022). However, challenges remain, including generally lower spatial resolutions which impact the ability to

detect subtle abnormalities or small anatomical structures accurately (Bekiesinska-Figatowska et al., 2016).

Moreover, preterm infants remain a critical population in brain development research due to their high worldwide prevalence and the substantial individual and societal burden of long-term neurodevelopmental impairments frequently associated with prematurity (Blencowe et al., 2012) (*Figure 1.8.*).

Prematurity, defined as birth before 37wGA, is categorized into four groups: extremely preterm (<28 wGA), very preterm (28–32 wGA), moderate (32–34 wGA), and late preterm (34–36 wGA). These distinctions are clinically relevant, as the impact of prematurity is closely tied to prematurity levels (Harrison & Goldenberg, 2016). In the subsequent sections, we offer a non-exhaustive description of the prematurity-related alterations of brain features at TEA. We then focus on the established associations between prematurity and long-term neurodevelopmental outcomes and summarize recent efforts focused on predicting the individual outcomes from early MRI-derived markers. (The group association studies of brain alterations at TEA with later neurodevelopmental outcomes are not the primary focus of this chapter.)

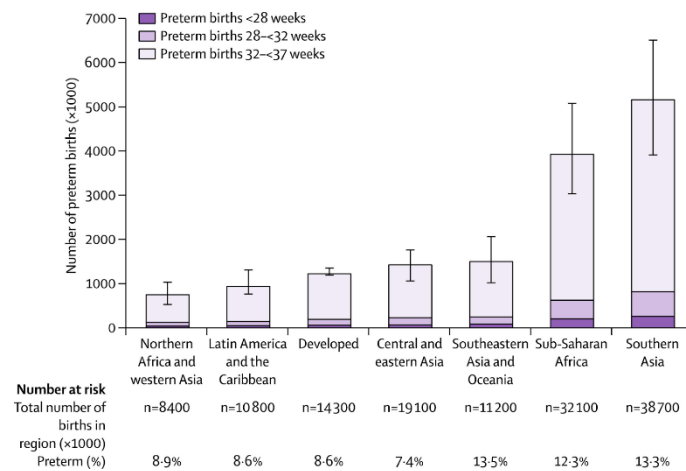


Figure 1.8. Global burden of prematurity. Estimated preterm birth by level of prematurity and region for the year 2010. Moderate and late preterm infants make up majority of the preterm births around the globe (Blencowe et al., 2012).

1.3.2. Brain differences between preterm and term-born infants as TEA

Preterm birth disrupts typical developmental events of the 3rd trimester, shifting them to an abnormal *ex utero* environment, with significant pathophysiological consequences affecting the immature respiratory and gastrointestinal systems (Rubarth & Quinn, 2015; Erickson et al., 2021; Bazaciu & Neu, 2019), as well as thermoregulatory mechanisms (Pereira

et al., 2016). Additionally, it can impact the emergence of spontaneous sensorimotor behaviours, which are influenced by altered sensory stimulations and motor experiences in the external environment compared to the typical *in utero* setting (Fagard et al., 2018). These changes result in marked differences in PT infants compared to FT peers at TEA, with the effects inversely correlated with the length of gestation (Volpe, 2019).

On the morphological level, PT infants at TEA exhibit smaller global and regional brain volumes, including key cortical and subcortical regions (Peterson et al., 2000; Srinivasan et al., 2007; Kesler et al., 2008; Tam et al., 2009; Ball et al., 2012; Chiarelli et al., 2021). Interestingly, cortices of PT infants seem thicker in the somatosensory, frontal and insular regions (Dimitrova et al., 2021), with negative association between cortical thickness and GA at birth persisting into infancy (Jha et al., 2019). Extreme PT infants at TEA also display reduced brain growth (characterized by biparietal diameter and interhemispheric distance) (Kidokoro et al., 2014) and cortical surface area (Ajayi-Obe et al., 2000). Ventriculomegaly due to increased volume of cerebrospinal fluid (CSF) (Kuban et al., 1999) was also observed. Cortical gyrification, a marker of grey matter maturation, is decreased in PT at TEA (Dubois et al., 2019a) especially in the frontal lobe (Pittet et al., 2019).

PT brain also presents significant alterations in the white matter, including decreased global volumes (Cismaru et al., 2016). White matter injuries, such as periventricular leukomalacia, periventricular haemorrhagic venous infarction, and punctate lesions, are frequent in extreme/very premature born infants (Inder et al., 2021), profoundly affecting the underlying white matter pathways and the overall structural connectivity (Bassi et al., 2011; Thompson et al., 2012; Thompson et al., 2014; Arichi et al., 2014; Brouwer et al., 2016; Tusor et al., 2017; Lean et al., 2019; Smyser et al., 2019) (*Figure 1.9a*). Even in the absence of overt brain lesions, diffuse excessive high signal intensity (DEHSI), also referred to as diffuse white matter abnormalities (DWMA) (Counsell et al., 2003; Kline, Illapani, et al., 2021), lead to alterations in volume and microstructure of a wide range of pathways, including major thalamo-cortical pathways and corpus callosum (Ball et al., 2013; Malavolti et al., 2017), and influence network properties of structural networks (Kline, Illapani, et al., 2021) (*Figure 1.9b*), and myelination (Dudink et al., 2007; Dubois et al., 2008; Counsell et al., 2008; Walsh et al., 2014). The predominance of white matter abnormalities in PT infants underscores the vulnerability of rapid axonal pathway development which depends on its maturational stage (Kostovic et al., 2014; Li et al., 2015). For example, thalamo-cortical pathways alterations seem characteristic of early preterms, while those of long association fibres are more prominent features in later preterms (Kostovic et al., 2014)

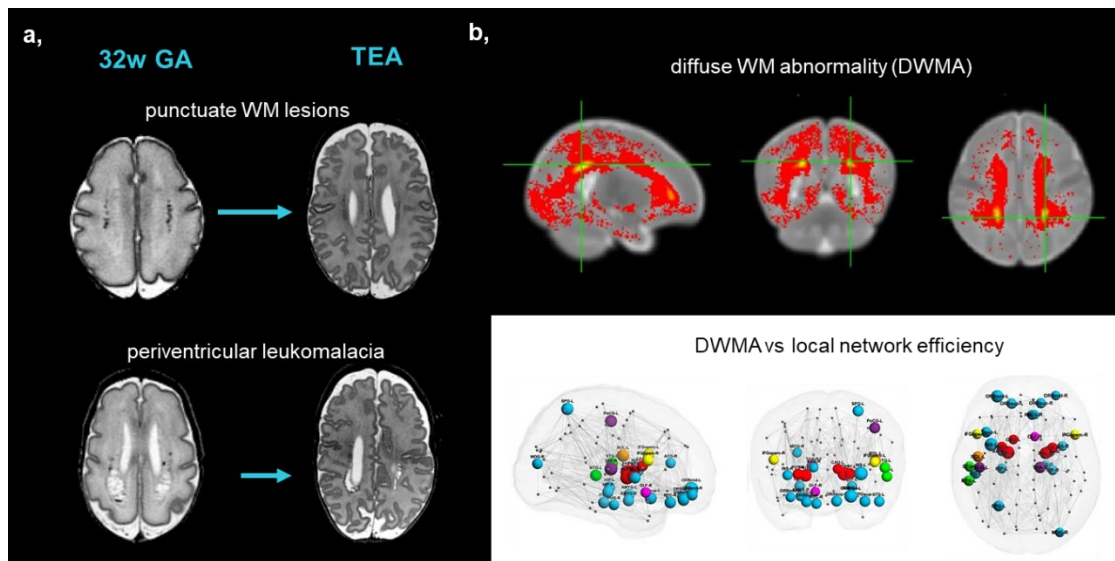


Figure 1.9. Examples of common types of white matter injury in preterm infants. **a**, Progression of punctuate WM lesions and periventricular leukomalacia from birth to TEA. **b**, Diffuse white matter abnormalities (DWMA), i.e. increases in WM signal intensity on T2w MRI, shown as a heatmap of DWMA over 343 very preterm infants (GA at birth ≤ 32 w) at TEA (top row). Nodes in which DWMA volume was negatively correlated with local efficiency are shown in the bottom row. Adapted from (Plaisier et al., 2014; Kline, Illapani, et al., 2021).

Assessments of the microstructure of the cortical and subcortical regions also highlight global and region-specific differences in PT grey matter at TEA, again underlining the heterogeneity of prematurity effects on different brain areas (McKinstry et al., 2002; Ball, Srinivasan, et al., 2013; Eaton-Rosen et al., 2015; Smyser et al., 2016; Yu et al., 2016; Eaton-Rosen et al., 2017; Bataille et al., 2019; Ouyang, Jeon, et al., 2019; Dimitrova et al., 2021). Some of the abnormalities in the grey matter regions can be related to injuries of underlying axonal pathways suggesting the tightly linked nature of the white and grey matter development during the preterm period (Kostovic et al., 2014; Smyser et al., 2016). Delayed cerebral grey-white matter differentiation and altered disappearance of transient compartments (e.g., the subplate) was also described in PT infants (Hüppi et al., 1996; Maalouf et al., 1999; Hagmann et al., 2009; Pittet et al., 2019).

Cumulative maturity scores based on combined measures (for example myelination, degree of cortical folding, visibility of neural migration, descriptions of transient compartments) consistently distinguish FT and PT subjects at TEA and increase with gestational duration (Woodward et al., 2006; Walsh et al., 2014; Kidokoro et al., 2014; Pittet et al., 2019). Yet, PT infants at TEA exhibit both delayed and accelerated maturation patterns compared to FT newborns (Pittet et al., 2019).

On the network level, higher segregation and lower capacity, i.e. amount of information transfer, of structural networks impacting both cortico-subcortical and short-distance cortico-cortical connections have been described in PT (Ball et al., 2014; Kline, Yuan, et al., 2021; Sa de Almeida et al., 2021). Higher modularity and lower global efficiency of PT vs FT infants suggests a delayed transition from a local architecture, focused on short-range connections, to a more distributed architecture with efficient long-range connections in those infants with likely adverse developmental consequences (Ball et al., 2014; Kline, Yuan, et al., 2021). The disruption of structural connectivity patterns including the prolonged segregation might affect information exchange across brain regions and seems to persist over time (Pandit et al., 2014; Fischi-Gómez et al., 2015; Fischi-Gomez et al., 2016; Irzan et al., 2021).

In terms of functional connectivity, both severe white matter lesions and diffuse white matter abnormalities observed in PT infants impact connectivity across multiple regions (He & Parikh, 2015), and in proportion to the injury severity (Smyser et al., 2013). In the absence of injuries, PT infants display spatially diffuse alterations of the functional connectivity, including thalamo-cortical and cortico-subcortical pathways (Smyser et al., 2010; Ball et al., 2016; Keunen et al., 2017; Brenner et al., 2021), within cortical regions (Chiarelli et al., 2021; Eyre et al., 2021), and fewer long-range connections (Smyser et al., 2010). Functional connectivity in PT infants is also characterized by dense local connectivity with reduced strength compared to FT neonates (Scheinost et al., 2016), with higher centrality in visual regions and lower centrality in motor regions (Fenn-Moltu et al., 2023). Again, alterations of the functional connectivity seem to persist over time (Damaraju, 2010; Wehrle et al., 2018). Interestingly, development of topological organization of the functional connectivity within the sensorimotor network in PT infants was more dependent on age at scan rather than age at birth in the absence of brain injury, suggesting at least partial ongoing functional organization despite atypical environmental exposure (Dall’Orso et al., 2022). This might be in line with previously suggested higher genetic influences on network topographies, while environmental influences might primarily shape the connectivity strengths (Burger et al., 2022).

Thus, prematurity disrupts critical brain growth and organization, increasing the risk of future neurodevelopmental impairments. The impact varies based on the region and level of prematurity. Understanding how these alterations relate to adverse neurodevelopmental outcomes holds significant clinical and scientific relevance due to the high prevalence of such impairments among preterm-born populations. In the following section, we will provide a brief overview of neurodevelopmental risks associated with premature birth.

1.3.3. Prematurity and neurodevelopmental outcomes

Prematurity poses significant risks to neurodevelopment, evident in enduring adverse outcomes observed in prematurely born individuals across various follow-up ages (Goldenberg et al., 2008; Lundequist et al., 2015; Luu et al., 2017; Moore et al., 2013). These encompass neurodevelopmental impairments such as cerebral palsy, severe cognitive deficits, and sensory impairments (Longo et al., 2021; Marret et al., 2013; McGowan & Vohr, 2019; Serenius et al., 2016). The prevalence rates are highest in the most extreme preterms, inversely related to level of prematurity (Saigal & Doyle, 2008). Although the incidence of severe effects has been decreasing in developed countries reflecting improvements in neonatal care (Arnaud et al., 2021), preterm infants remain at risk of delayed developmental milestones and neurodevelopmental abnormalities, not diagnosed as impairments, that may impact their education, health, social outcomes, and overall quality of life over the long term. These delays often span multiple domains, suggesting a general impairment rather than deficits in specific domain, highlighting the complex interrelated nature of behavioural acquisitions during the development (Saigal & Doyle, 2008).

For instance, premature infants are vulnerable to motor problems, particularly affecting fine motor skills and generalized coordination abilities (McGowan & Vohr, 2019; A. J. Spittle & Orton, 2014). Delays and impairments in the motor domain can affect subsequent skills acquisitions and adversely affect learning (Mulder et al., 2010). Language development can also be compromised, impacting individual's communication, cognitive processes, and social interactions (Foster-Cohen et al., 2010; McGowan & Vohr, 2019). Moreover, cognitive and behavioural difficulties across multiple domains are also prevalent in PT population, including executive functioning, working memory, and attention (Bhutta et al., 2002; Woodward et al., 2006; Nosarti et al., 2007; Breeman et al., 2016; Allotey et al., 2018). The risk of attention deficit hyperactivity disorder (ADHD) also increases with higher prematurity levels (Lindström et al., 2011).

These impairments persist into childhood and adulthood, affecting socio-emotional development (Montagna & Nosarti, 2016; Johnson et al., 2010; Joseph et al., 2017) and increasing the likelihood of psychiatric diagnosis (Lund et al., 2011; Nosarti et al., 2012). Consequently, prematurity can profoundly impact the quality of life, including academic achievement, employment prospects, and overall well-being (Stahlmann et al., 2009; Mulder et al., 2010; Lobo et al., 2013; Baumann et al., 2016; ; Kroll et al., 2017; Jaekel et al., 2019).

The impact extends to families and holds significant societal and economic implications (Saigal & Doyle, 2008; A. Spittle & Treyvaud, 2016; Stahlmann et al., 2016; Khurana et al., 2020).

Even late preterm infants without perinatal brain injuries exhibit neurodevelopmental problems, emphasizing the need for routine assessments and targeted care for all preterm children (Williams & Pugh, 2018; Pierrat et al., 2021).

Early developmental interventions, particularly those initiated in the neonatal intensive care unit (NICU), could improve long-term neurodevelopment in this population through non-pharmacological interventions (Palisano et al., 2000; Spittle & Treyvaud, 2016). However, identifying at-risk infants in need of targeted interventions, even in severe conditions like cerebral palsy, remains challenging before 18 to 24 months of age (Palisano et al., 2000). Inadequate patient stratification might be one of the reasons why, despite significant efforts, clinical trials of neuroprotective interventions have shown varying effect sizes in mitigating adverse effects of preterm birth (Benzies et al., 2013; Spittle & Treyvaud, 2016; Hughes et al., 2016; Haslbeck et al., 2020; Khurana et al., 2020). Early and reliable identification of at-risk individuals could significantly enhance these results and at the same time optimize the allocation of limited healthcare resources (Parikh, 2016).

Advanced MRI at TEA serves as a crucial tool for identifying altered brain development including lesions or abnormalities that could suggest risk of vulnerabilities in preterm infants (Banihani et al., 2021). Detection of these alterations can aid in developing MRI prognostic biomarkers for predicting later neurodevelopmental outcomes and tailoring interventions to improve perceptions, acquisitions, and learnings in preterm babies, particularly when combined with advanced image analysis and individual-specific predictive modelling with machine learning.

1.3.4. Prediction of neurodevelopmental outcomes in premature children

Given the critical need for early identification of infants at risk of neurodevelopmental impairments, many studies have investigated alterations of brain features in preterm infants at TEA and their association with later outcomes (van't Hooft et al., 2015; Vo Van et al., 2022). While group studies provide valuable insights, they are not adapted for individual outcome prediction. To address this gap, recent research has turned to predictive modelling, including machine learning, to establish links between early MRI-derived markers and later outcomes.

Predictive models have been developed for various outcomes in premature infants, including mortality (Mangold et al., 2021), sepsis (Persad et al., 2021), and retinopathy of prematurity (Zhang et al., 2021). However, fewer studies have explored links to later

neurodevelopment, primarily focusing on motor, cognitive, and language outcomes (van Boven et al., 2022; Baker & Kandasamy, 2023). *Table 1.1* summarizes studies that employ MRI-derived markers (anatomical, diffusion or functional MRI) around birth or at TEA, involving cohorts that include PT subjects (except one of the two studies focusing on cortical microstructure, which focused on FT subjects), to predict later neurodevelopmental outcomes.

Table 1.1. Overview of recent neurodevelopmental outcome prediction studies. Table summarized recent studies aiming to predict neurodevelopmental outcomes in PT and FT subjects using MRI-derived markers around birth or TEA. Entries are categorized based on MRI-modality of the input features and include information on cohort composition, outcome measures, and reported results of the best predictive model within the study. Additionally, we note any unique or non-standard approaches in the predictive pipeline used by the authors. Legend: AUC - area under receiver operating characteristic curve, BSID-III - Bayley Scales of Infant Development Third Edition, CNN - convolutional neural network, CV - cross-validation, DTI - diffusion tensor imaging, DWMA - diffuse white matter abnormality, FA - fractional anisotropy, fNN - fully connected neural network, GA - gestational age, LOOCV - leave one out cross-validation, MAE - mean absolute error, mCA - months of corrected age, MD - mean diffusivity, MSEL - Mullen Scales of Early Learning, N - sample size, NPV - negative predictive value, NSMDA - Neuro-Sensory Motor Development Assessment, PMA - postmenstrual age, PPV - positive predictive value, Q-CHAT - Quantitative Checklist for Autism in Toddlers, R - Pearson's correlation coefficient, TDI - Toddler Temporal-spatial Deviation Index, TEA - term-equivalent age.

Anatomical MRI		
(Moeskops et al., 2017)	Sample: <28 wGA (N=153 max) Age at prediction: 30/40wPMA Outcome: motor and cognitive BSID-III scores at 26-35mCA Task: classification score <85	AUC: 0.85 (motor) 0.81 (cognitive)
	Inputs: tissue volumes, inner cortical surface area, gyrification index, global mean curvature, and median cortical thickness Model: support vector machine (SVM) with linear kernel Validation: Leave 5% Out CV (500 rounds)	
(Shin et al., 2021)	Sample: ≤32 wGA (N=46) Age at prediction: near-term/TEA Outcome: motor BSID-II (Korean) score at 12mCA Task: classification score <85	AUC: 0.925
	Inputs: T1w and T2w-derived radiomics features Model: tree ensemble Validation: 8-fold CV Note: feature selection on the whole dataset	
(Wagner et al., 2022)	Sample: <32 wGA (N=166) Age at prediction: near birth Outcome: motor BSID-III score at 18mCA (and others) Task: classification score <85	AUC: 0.81
	Inputs: T1w and T2w-derived radiomics features Model: ElasticNet Validation: LOOCV	

Diffusion MRI (dMRI)*descriptors of white matter microstructure:*

(Schadl et al., 2018)	Sample: ≤ 32 wGA and birth weight ≤ 1500 g (N=60) Age at prediction: ~ 36 wPMA Outcome: motor and cognitive BSID-III scores at 18-22mCA Task: classification score < 85	AUC: 0.912 (motor) 1 (cognitive)
	Inputs: averaged regional DTI-derived metrics Model: logistic regression Validation: LOOCV	
(Cahill-Rowley & Rose, 2016)	Sample: ≤ 32 wGA and birth weight ≤ 1500 g (N=52) Age at prediction: ~ 36 wPMA Outcome: motor TDI at 20mCA Task: classification < -1 standard deviation	AUC: 0.83-1 (different subtests)
	Inputs: averaged regional DTI-derived metrics Model: Logistic regression Validation: LOOCV	
(Vassar et al., 2020)	Sample: ≤ 32 wGA and birth weight ≤ 1500 g (N=59) Age at prediction: TEA Outcome: language BSID-III scores at 18-22mCA Task: classification score < 85	AUC: 0.50 (language), 0.62 (expressive lang), 0.32 (receptive lang.)
	Inputs: averaged regional DTI-derived metrics Model: logistic regression Validation: LOOCV	
(Valavani et al., 2022)	Sample: ≤ 33 wGA (N=89) Age at prediction: TEA Outcome: language BSID-III score at 24mCA Task: classification score < 85	Balanced Accuracy: 91%
	Inputs: histogram-based peak widths of DTI-derived metrics (WM skeletons) Model: random forest Validation: LOOCV Note: top features evaluated from the whole dataset	

descriptors of cortical microstructure:

(Ouyang et al., 2020)	Sample: PT+FT (N=46) Age at prediction: 31-42w Outcome: motor, cognitive, language BSID-III scores at 24mCA Task: regression	R: 0.54 (cognitive) 0.47 (language)
	Inputs: regional cortical fractional anisotropy Model: support vector machine with linear kernel Validation: LOOCV	

whole-brain microstructure image:

(Saha et al., 2020)	Sample: < 31 wGA (N=77) Age at prediction: near birth Outcome: motor NSMDA at 24m CA Task: classification score > 0	AUC: 0.72 (patch-based AUC 0.60)
---------------------	--	--

Inputs: whole brain FA map cut into patches
Model: CNN
Validation: 10-fold CV within 90% training set
Note: not clear how patches were split into folds (potential within-subject data leakage), image classified abnormal if at least 27% patches abnormal, abnormal class augmented to reduce imbalance by rigid transformations, abnormality score cutoff score >0 (very mild delays)

structural connectivity:

(Kawahara et al., 2017)	Sample: <32 wGA (N=115) Age at prediction: after birth and/or 40 wPMA Outcome: motor and cognitive BSID-III scores at 18mCA Task: regression	MAE / R: 10.64 / 0.263 (motor) 10.49 / 0.162 (cognitive)
	Inputs: whole-brain tractography derived connectome Model: CNN Validation: 3-fold CV Note: multiple scans for the same subject likely randomly split across folds	
(Brown et al., 2019)	Sample: 24–32 wGA (N=115) Age at prediction: ~36 wPMA Outcome: motor and cognitive BSID-III scores at 18mCA Task: classification score ≤85 and regression	Accuracy: 72.5% (motor), 59.5% (cognitive) R: 0.44 (motor) 0.44 (cognitive)
	Inputs: whole-brain tractography derived connectome Model: support vector machine / linear regression Validation: Leave 2 Out CV (1000 rounds)	
(Girault et al., 2019)	Sample: <37 wGA (N=37) Age at prediction: TEA Outcome: cognitive MSEL at 25mCA Task: classification score <110 (median for full-term cohort) and regression	Accuracy: 89.5% (FT), 83.8% (PT) R: 0.98 (FT) 0.96 (PT)
	Input: whole-brain tractography derived connectome Model: sequential model including CNN and linear regression Validation: stratified 10-fold CV (with integrated grid-search)	
(Chen et al., 2020)	Sample: <32 wGA (N=80) Age at prediction: TEA Outcome: cognitive BSID-III score at 24mCA Task: classification score <90 and regression	AUC: 0.75 MAE / R: 16.2 / 0.47
	Input: tractography derived connectome Model: CNN (pre-trained in ImageNet) Validation: 5-fold CV (1 fold retained as hold-out) Note: oversampling to balance classes with SMOTE	

Functional MRI (fMRI)

(He et al., 2018)	Sample: <32 wGA (N=28) Age at prediction: TEA Outcome: cognitive BSID-III score at 24mCA Task: classification score <85	AUC: 0.76
	Inputs: functional connectivity Model: support vector machine Validation: 10-fold CV	

Note: feature selection with autoencoder

(He et al., 2020)	Sample: <32 wGA (N=33) Age at prediction: TEA Outcome: motor, cognitive, language BSID-III scores at 24mCA Task: classification score <85	AUC: 0.84 (motor), 0.86 (cognitive), 0.66 (language)
	Inputs: functional connectivity Model: fully-connected NN (fNN) Validation: 5-fold CV (50 rounds) Note: multi-task and multi-stage (pre-trained on children & adults), fine-tuned in infants	
Multimodal MRI		
(Janjic et al., 2020)	Sample: <32 wGA (N=103/115 Motor/Cognitive) Age at prediction: TEA Outcome: motor and cognitive BSID-III scores at 12mCA Task: classification score <85	PPV / NPV (%): 90.9 / 96.7 (cognitive) 100 / 99.1 (cognitive)
	Inputs: metabolite ratios (from MR spectroscopy) and two DTI (FA+MD) characteristics in six manually defined ROIs Model: fully connected neural network ensemble with vote aggregation Validation: 4-fold CV Note: two-step strategy, first locate if preterm in ‘developmental delay common relaxed zones’ based on similarity to other delayed neonates, if yes, continue with prediction	
(He et al., 2021)	Sample: ≤ 32 wGA (N=257/108 pre-train/tune) Age at prediction: TEA Outcome: motor, cognitive, language BSID-III scores at 24mCA Task: classification score ≤90 and regression	AUC: 0.85 (motor) 0.87 (cognitive) 0.85 (language)
	Inputs: structural connectome; functional connectome, DWMA from T2w Model: CNN-fNN fusion Validation: nested 5-fold CV Note: separate model per modality (functional/structural connectome - CNN, DWMA quantification/ clinical features - fNN)	MAE / R: 11.6 / 0.63 (motor) 11.7 / 0.62 (cognitive) 10.5 / 0.63 (language)
(Fenchel et al., 2022)	Sample: FT (N=187) Age at prediction: TEA Outcome: social-emotional Q-CHAT at 17-25mCA Task: regression	RMSE / R: 9.60 / 0.188
	Inputs: Morphometric similarity network Model: Connectome-based Predictive Modelling (CPM) with linear regression Validation: LOOCV followed by 10-fold CV (100 rounds)	

The reported outcome prediction studies primarily targeted very preterm infants and evaluated neurodevelopmental outcomes between 12-36 months of corrected age (mCA). The most common assessment tool was the Bayley Scales of Infant Development Third Edition (BSID-III) (Bayley, 2006), although Neuro-Sensory Motor Development Assessment (NSMDA) (Burns et al., 1989), Mullen Scales of Early Learning (MSEL) (Mullen, 1995),

Toddler Temporal-spatial Deviation Index (TDI) (Cahill-Rowley & Rose, 2016), and Quantitative Checklist for Autism in Toddlers (Q-CHAT) (Allison et al., 2008). Machine learning models, including logistic and linear regression, random forests, support vector machines, fully connected neural networks, and convolutional networks, were employed for both continuous regression and binary classification. In the classification settings, researchers first categorized outcomes as normal or abnormal using predefined thresholds, with some inconsistencies in the classification thresholds between studies (Saha et al., 2020; Chen et al., 2020; He et al., 2021).

Because of the quantitative metrics of brain maturation it provides, diffusion MRI was the most used modality for neurodevelopmental outcome prediction, either by evaluating region-based microstructure or structural connectivity but led to variable results. For example, using random forest algorithms with white matter dysmaturation biomarkers as inputs achieved a balanced accuracy of 91% in predicting BSID-III-derived language outcomes at 24mCA, but using averaged regional white matter diffusion tensor imaging (DTI) metrics did not reach meaningful prediction levels for BSID-III-derived language outcomes at 18-22mCA using logistic regression (Vassar et al., 2020). In contrast, regional white matter microstructure effectively predicted motor and cognitive BSID-III scores at 18-22 mCA leading to AUC (i.e. area under receiver operating characteristic curve) of 0.91 for motor and 1 for cognitive outcomes (Schadl et al., 2018), but it is important to note that the validation in this study was performed on a very limited number of subjects.

Structural connectivity derived from whole-brain tractography has also been a popular MRI-derived marker for predicting BSID-III scores (Kawahara et al., 2017; Brown et al., 2019; Chen et al., 2020) and cognitive MSEL scores at 25 mCA (Girault et al., 2019) in both classification and regression contexts. For example, support vector machine based on structural connectivity estimates achieved accuracy of 73% in motor outcome prediction (Brown et al., 2019). The highest cognitive outcome results based on structural connectivity were obtained with convolutional neural networks pretrained on the large image database (ImageNet) and then fine-tuned to infants leading to AUC of 0.75 (Chen et al., 2020).

Gray matter microstructural features have also been used to successfully predict continuous cognitive and language BSID-III scores at 24mCA with support vector machine (Ouyang et al., 2020). Whole-brain fractional anisotropy maps were also used directly to predict abnormal motor NSMDA outcomes at 24mCA with patch-based convolutional neural networks reaching AUC of 0.72 (Saha et al., 2020).

Anatomical MRI markers such as tissue volumes combined with morphological surface features (Moeskops et al., 2017) or T1w/T2w-derived radiomics features (Shin et al., 2021; Wagner et al., 2022) have also been employed for motor BSID-III score prediction in very preterm infants, all leading to reported AUC above 0.8.

Functional connectivity was used to predict neurodevelopmental outcomes in only two studies. In the first, a support vector machine predicted cognitive BSID-III scores at 24mCA with an AUC of 0.76 based on functional connectivity inputs reduced using a stacked sparse autoencoder (He et al., 2018). In the second study (He et al., 2020), neural networks were employed to predict motor, cognitive, as well as language outcomes. A multi-stage setup involved pre-training networks on adult and older-children's data, then fine-tuning to the infant domain. This was the only study that attempted to jointly predict all three BSID-III scores in a multi-task manner, leading to enhanced prediction accuracy.

Overall, models using anatomical, diffusion, and functional inputs yielded variable results. Combined with diversity in cohorts and modelling approaches, it is challenging to definitively determine the most effective modality and descriptors for predicting neurodevelopmental outcomes. In absence of clear evidence of superior predictive performance for inputs requiring complex pre-processing, such as white matter tractography, a practical approach may involve utilizing more straightforward measures, such as aMRI-based morphometrics or regional microstructural descriptors.

Recently, efforts to combine complementary information from different MRI modalities have also been attempted with promising results. In one study, metabolic ratios derived from magnetic resonance spectroscopy combined with microstructural descriptors predicted motor and cognitive BSID-III outcomes at 12mCA with positive predictive value (PPV) and negative predictive value (NPV) over 90% (Janjic et al., 2020). In another study, combining functional and structural connectivity markers, T2w-derived estimates of diffuse white matter abnormalities, and additional clinical information improved predictions of motor, cognitive, and language BSID-III scores at 24mCA compared to using each modality alone (He et al., 2021). Additionally, several studies benefited from incorporating clinical, demographic, and environmental variables, resulting in improved predictions of neurodevelopmental outcomes (Kawahara et al., 2017; Moeskops et al., 2017; Schadt et al., 2018; He et al., 2018, 2020; Valavani et al., 2022).

However, as mentioned earlier, comparing results across reported studies and across MRI modalities is challenging due to significant variations in cohort composition, outcome measures, prediction and assessment ages, and validation strategies. Despite these variations,

the studies share several limitations, notably small sample sizes. Most studies had fewer than 115 subjects, except for Wagner et al., (2022) with 166 subjects. This limitation is particularly critical for complex deep learning architectures, which might require larger datasets for effective training. To address this, He et al., (2020) and He et al., (2021) used a **transfer-learning approach** by pre-training models on a larger dataset of older children and adults, then fine-tuning them on PT subjects. This multi-stage approach showcased improved predictive results, suggesting potential for future studies in the absence of large datasets. One study used pretraining on a large image database (ImageNet) (Chen et al., 2020) to improve training. This is an interesting choice for learning of structural connectomes due to differences in spatial dependencies of pixels between natural images and structural connectivity matrices. The potential positive impact of such transfer learning will require further evaluation and will likely depend on source-target domain similarity (Zhuang et al., 2021).

Most studies also faced data **imbalance issues**, with a small number of high-risk infants compared to low-risk ones, which can significantly affect the learning ability of predictive models (Haixiang et al., 2017). Various techniques were explored to tackle this, including oversampling during data augmentation or synthetic minority over-sampling technique (SMOTE) (Kawahara et al., 2017; Chen et al., 2020; Valavani et al., 2022). Additionally, some studies potentially suffered from **data leakage**, either by incorporating feature selection step on the level of the entire dataset (including the testing set) (Shin et al., 2021) or potentially risked leakage of subject-specific information between training and testing (Kawahara et al., 2017; Saha et al., 2020).

Validation approaches also varied, with most using k-fold or leave-one-out cross-validation which are often reported to lead to inflated estimates of predictive performance (Varoquaux, 2018). Combined with the previously mentioned limitations, further research, including external independent validation of the reported results, will be needed before these methods can be turned into reliable predictive tools for enhanced preterm infant care. Nevertheless, these examples clearly demonstrate the potential of utilizing early MRI makers for predicting individual neurodevelopmental outcomes and should serve as an inspiration for future investigations.

Statement of interest

To conclude the preceding chapter, early brain development is a dynamic process accompanied by a complex series of structural and functional changes. Studying the perinatal period offers insights into the foundational mechanisms that shape crucial aspects of human life, such as cognition and behaviour. The importance of this early period is underscored by the **early vulnerability** of typical brain developmental trajectories to adverse life experiences, such as premature birth, making neonatal conditions a significant contributor to the global burden of disease (Vos et al., 2020). A recent global report has revealed a concerning statistic: 1 in 10 children is born prematurely (before 37wGA) (World Health Organization et al., 2023), with preterm survivors reported to face lifelong health consequences including an increased likelihood of disability and developmental delays (Pierrat et al., 2017, 2021a)

Improved understanding of both **typical and atypical neurodevelopmental trajectories** around birth could allow us to identify early neurobiological markers of the neurodevelopmental outcomes and their alterations in prematurity. This would significantly contribute to **prognostication efforts for at-risk individuals**, with hope to provide insights necessary for the development of targeted interventions to support optimal development within the vulnerable populations. These insights, in turn, have the potential to inform and enrich research across a spectrum of disciplines, including neuroscience, developmental psychology, and education.

With these practical implications in mind, in this PhD work, we aimed to investigate the alterations of early brain development in the context of prematurity and contrast them to typically developing full-term infants, as well as to explore early brain development more broadly in terms of developing structure-function during the early period. In our work, we employed a large database - the *developing Human Connectome Project* (dHCP) - which links together multimodal magnetic resonance imaging (MRI) that has in recent years emerged as a powerful tool for *in vivo* investigations of the period around birth, with clinical and behavioural information to provide complementary views of typical and atypical development.

We evaluated development of preterm and full-term infants at multiple scales with three main aims: *i*, to demonstrate deviations related to prematurity in the structural connectivity of a specific functional network (*Chapter 3*), *ii*, to evaluate modelling approaches of the individual prediction of specific features and developmental outcomes (*Chapter 4*), and *iii*, to investigate the relationships between grey-matter microstructural similarity and functional connectivity (*Chapter 5*). We used different types of connectivities including white matter **structural**

connectivity estimated from **diffusion MRI** using seed-based and whole-brain tractography methods, as well as **functional connectivity** derived from **resting-state functional MRI** data. Additionally, we investigated an alternative measure of ‘**grey matter connectivity**’ through microstructural similarity across cortical and subcortical regions and its relationship to functional connectivity (*Chapter 5*). The estimation of these connectivities was based on cortical and subcortical regions derived by **parcellation** strategies based on **anatomical MRI**. Throughout the thesis, we provide examples of adapted multivariate approaches that take into account complementary information from different MRI markers, including **Mahalanobis distance** to quantify **tract-specific prematurity effects** on sensorimotor networks (*Chapter 3*), and **machine learning** for identification of patterns across the cortical microstructural features that **discriminate preterm and term-born subjects** as well as potential **individual prediction of neurodevelopmental outcomes** at 18 months (*Chapter 4*). *Figure 1.10.* provides a graphical overview of the studies performed in the presented PhD work. In the next chapter (2), we aim to provide a global overview of the processing and analysis strategies employed in our work and expand on concepts underlying these methods.

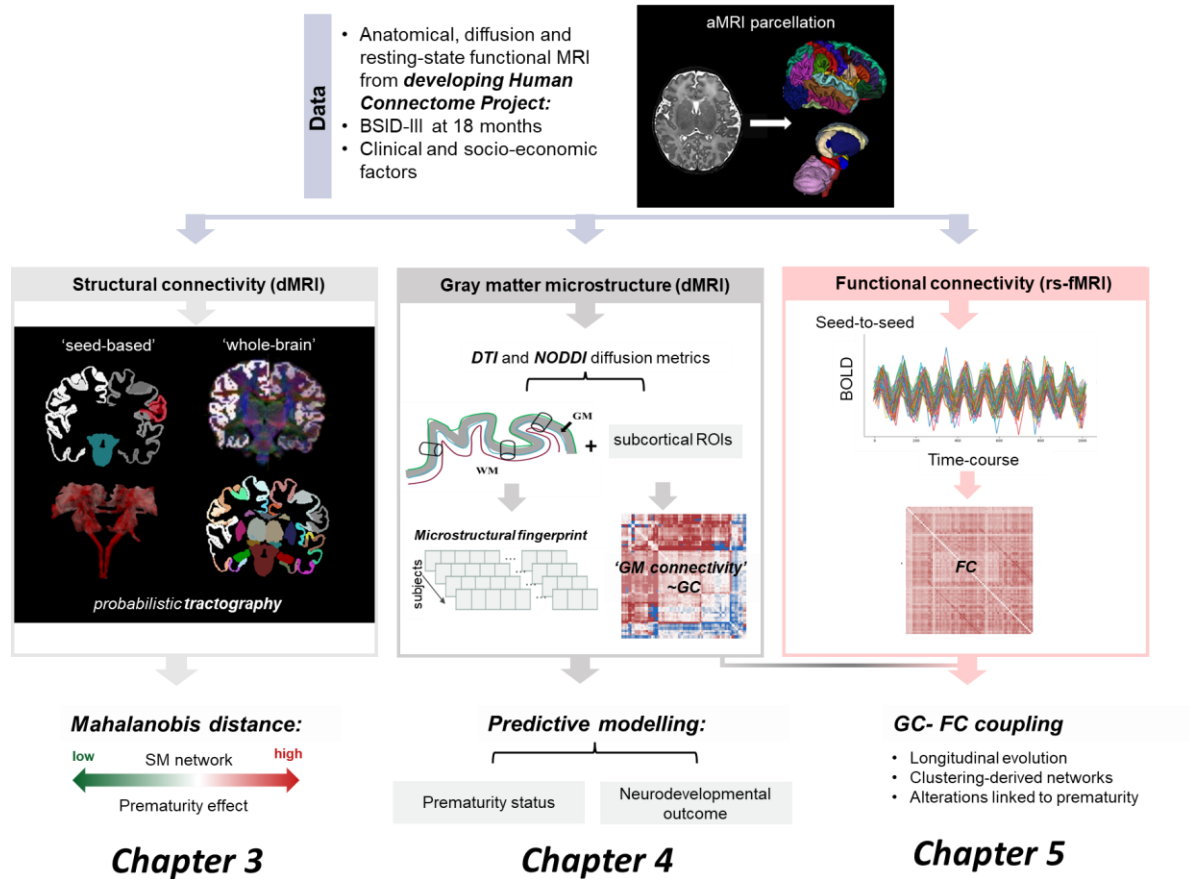


Figure 1.10. Graphical overview of studies performed within the presented PhD work. We leveraged a large multimodal MRI database of the developing Human Connectome Project (dHCP) to study atypical and typical developmental trajectories in terms of gray matter microstructure as well as structural and functional connectivity. **Legend:** aMRI: anatomical MRI; dMRI: diffusion MRI; rs-fMRI: resting-state functional MRI; DTI: diffusion tensor imaging; NODDI: neurite orientation dispersion and density imaging; SM: sensorimotor; GC: grey matter connectivity; FC: functional connectivity; BSID-III: Bayley Scales of Infant and Toddler Development, Third Edition; BOLD: blood oxygen level-dependent signal.

Chapter 2: Overview of methods for multimodal assessment of infant brain development

The goal of this chapter is twofold. Firstly, it serves as a methods section in which we aim to provide an overview of general characteristics of the employed dataset and give a global overview of the methods used for the data processing and analyses employed in this thesis. These foundational elements were adapted to address specific research questions and their detailed descriptions can be found in dedicated method sections within *Chapters 3, 4, and 5*. This chapter is also the opportunity to provide a description of the used techniques with a wider presentation of underlying concepts to clarify their choice and potential limitations.

2.1. Data for the study of early brain development

Our understanding of early brain development has been greatly enhanced due to the emergence of non-invasive neuroimaging techniques, particularly magnetic resonance imaging (MRI), which allows the study of structural and functional development *in vivo*. Recently, there has been a substantial growth in the size and complexity of MRI datasets. In our work, we utilized one of these datasets, the *developing Human Connectome Project* (dHCP), created through collaboration between King's College London (KCL, Center for the Developing Brain), Imperial College London, and Oxford University (Hughes et al., 2017) and made open to the scientific community (<https://www.developingconnectome.org/>). This PhD thesis also benefited from a close collaboration with Dr Tomoki Arichi (Clinical Senior Lecturer in the former center, KCL).

In the 3rd dHCP release, the database currently includes information on 783 subjects (median gestational age - GA at birth - 39.3 weeks [23w - 43.6w], 54% male) (*Figure 2.1a*). The cohort consists of subjects born at full term (FT) (578 subjects with median GA at birth of 40.1w [37w - 43.6w] and PMA at scan of 41.4w [37.4w - 44.9w]) as well as preterm subjects (PT) scanned at term-equivalent age (TEA) (140 subjects with median GA at birth of 32.1w [23w, 36.9w] and PMA at scan of 41w [37.1w, 45.1w]). Additionally, 156 PT subjects were also scanned close to birth (median GA at birth 31.7w [23.6w, 36.4w], median PMA at scan 34.4w [26.7w, 36.9w]), some of which also have the scan at TEA allowing for the longitudinal assessments.

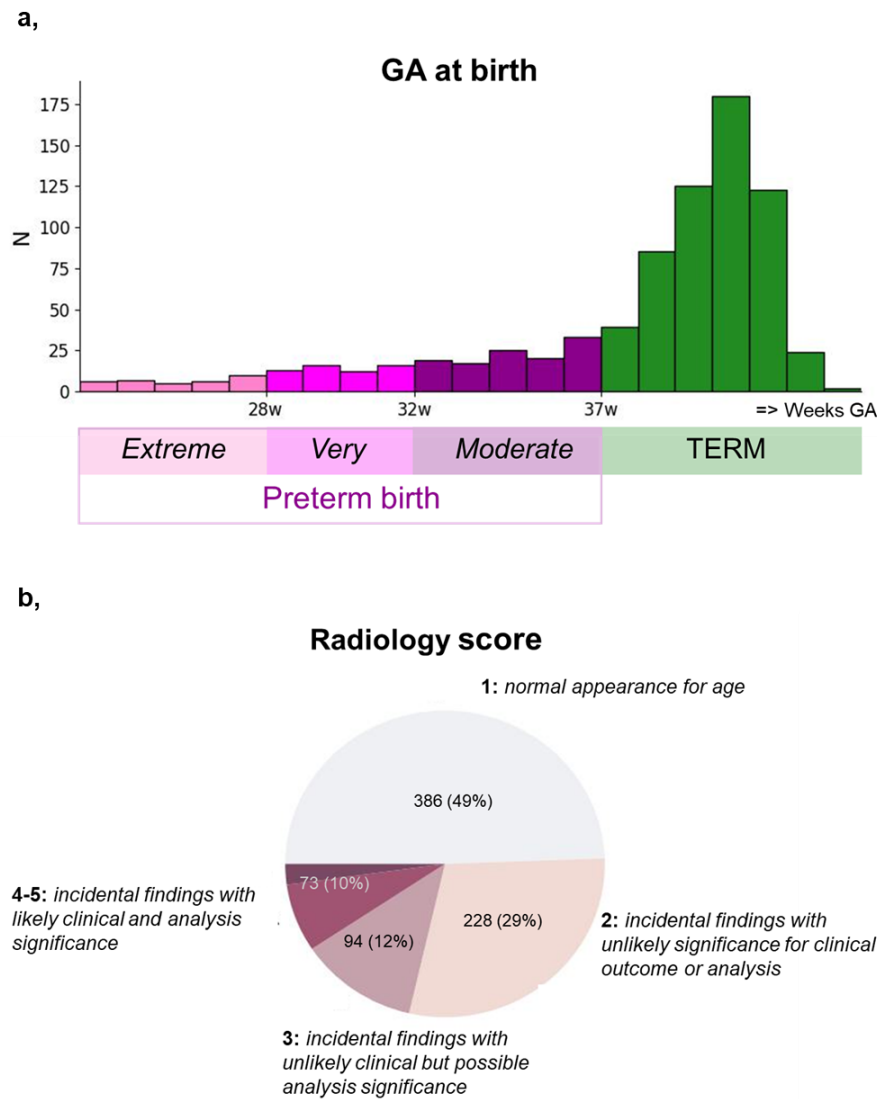


Figure 2.1. Available subjects within the dHCP cohort. **a,** Distribution of GA at birth of infants within the dHCP 3rd release. **b,** Distribution of radiology scores across dHCP infants.

The subject data consists of multimodal *anatomical, diffusion, and resting-state functional MRI* (aMRI, dMRI, rs-fMRI, respectively), combined with a broad spectrum of supplementary information including parental demographics, maternal medical history, and subjects' birth-related medical details, thus providing a unique opportunity for the study of both the early brain maturation in healthy FT infants and to assess the impact of prematurity on the typical brain developmental processes.

Moreover, infants were recruited with specified inclusion and exclusion criteria (detailed description at: developingconnectome.org/study-inclusion-and-exclusion-criteria). In this thesis, we additionally excluded subjects whose radiological score, assessed by an

experienced radiologist and reported within the data description provided by the dHCP team, was above 3, i.e. described incidental findings with likely clinical and analysis significance (*Figure 2.1b*). We considered that the inclusion of predominantly low-risk infants without overt brain abnormalities might provide a representative cohort that reflects the majority of preterm and full-term births (Blencowe et al., 2012).

Utilization of additional exclusion criteria, description of the dataset’s quality control and of environmental and clinical variables are described throughout the PhD manuscript chapters, when applied or relevant.

2.1.1. Multimodal MRI data: dataset acquisition and dHCP pre-processing

The dHCP study design largely aligns with the Human Connectome Project protocol (Van Essen et al., 2013). However, due to the unique age range of the cohort, additional optimization of imaging and processing parameters was integrated during data acquisition, reconstruction, and pre-processing. MRI data was acquired with a Philips 3-Tesla Achieva scanner (Philips Medical Systems, Best, Netherlands). Subjects were scanned during natural sleep, using a neonatal head coil and motion-tolerant imaging system optimized for the dHCP study (Hughes et al., 2017; Cordero-Grande et al., 2018; Hutter et al., 2018). The acquisition protocol optimized for the properties of the neonatal brain is summarized in (Edwards et al., 2022). The released dataset contains high-resolution anatomical, diffusion, and resting state functional MRI data provided both in their raw formats and post-application of the processing pipelines. More details on these modalities are provided in the *Section 2.2*. In addition to data in individual acquisition space, the pre-computed registration warps allowing to connect different modalities and each individual to age-matched templates are also available within the dHCP database.

- ***Anatomical MRI (aMRI)***

Given the considerable differences between properties of neonatal and adult brains affecting MRI contrasts, including higher water content and incomplete white matter myelination in infants, the primary data for the subsequent steps, like ROI delineation essential for dMRI and rs-fMRI analysis, is based on T2-weighted (T2w) rather than T1-weighted anatomical images. These T2w images resulted from acquisition and reconstruction using optimized protocols (Cordero-Grande et al., 2018b; Edwards et al., 2022), yielding super-resolved images with an isotropic voxel size of 0.5mm. Preprocessing follows a specialized fully-automated pipeline tailored to

neonatal brains (Makropoulos et al., 2018b) and includes bias-correction, cortical surface extraction, and segmentation using the Draw-EM (Developing brain Region Annotation with Expectation Maximization) algorithm (Makropoulos et al., 2014) (Figure 2.2.).

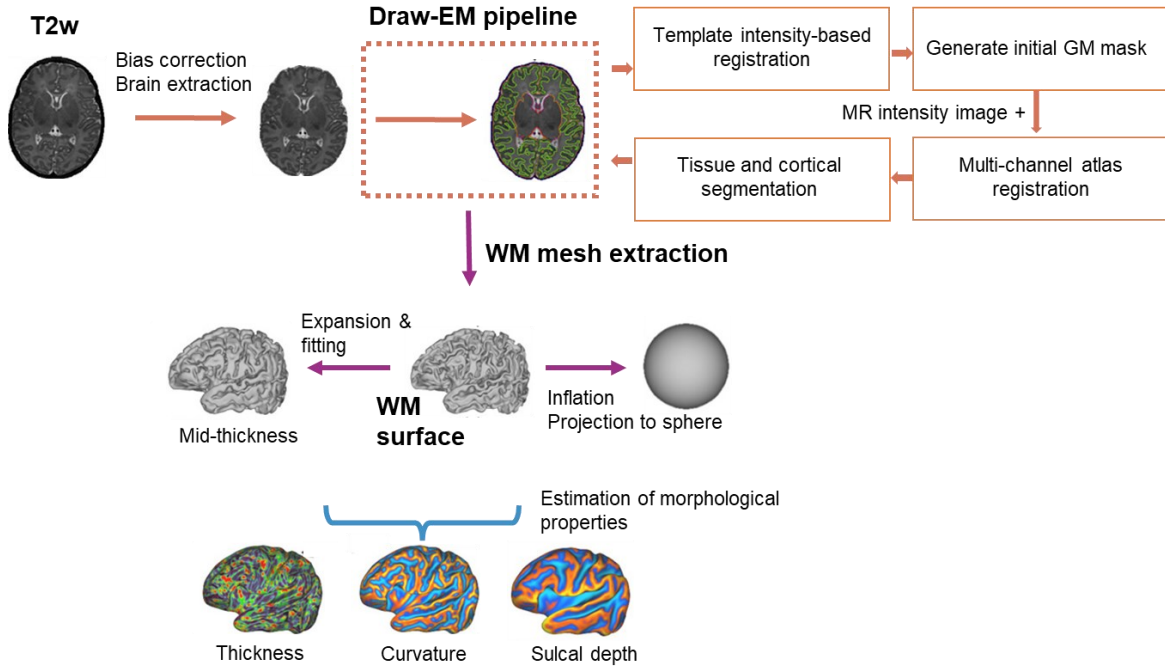


Figure 2.2. Summary of the main stage of the anatomical MRI's processing pipeline. The provided data was used for delineating cortical and subcortical ROIs and for driving the extraction of the regional metrics in experimental works. Adapted from (Makropoulos et al., 2018b).

- **Diffusion MRI (dMRI)**

Diffusion data was acquired and reconstructed using a multi-shell high angular resolution diffusion imaging (HARDI) protocol with 4 b-shells ($b = 0$ s/mm²: 20 repeats; and $b = 400, 1,000, 2,600$ s/mm²: 64, 88, and 128 directions, respectively) as outlined by (Hutter et al., 2018). Pre-processing, detailed on the dHCP 3rd release website (<https://biomedica.github.io/dHCP-release-notes/dwi-shard.html#ref1>), included denoising (Cordero-Grande et al., 2019), Gibbs ringing correction (Kellner et al., 2016), fat shift suppression (Christiaens et al., 2020), susceptibility-induced distortion correction (Andersson et al., 2003), as well as motion artifact correction and slice-to-volume reconstruction using the spherical harmonics and radial decomposition (SHARD) approach leading to an isotropic voxel size of 1.5 mm (Cordero-Grande et

al., 2019; Christiaens et al., 2021). The data was also corrected for inter-slice inhomogeneities (Pietsch et al., 2021) and rigidly aligned to individual anatomical spaces (Jenkinson et al., 2002). The pre-processed diffusion data was used to estimate diffusion metrics for evaluating the tissue microstructure of the developing brain (see *Section 2.2.1.*) and to drive the structural connectivity analyses (see *Section 2.2.2.*).

Before making the choice to use the SHARD-preprocessed data for the diffusion analyses, we compared some diffusion tensor imaging (DTI) quantification measures (see *2.2.1.* for a detailed description of the DTI model) following SHARD pipeline and FSL EDDY (pre-processed data also available from the dHCP database) (Bastiani et al., 2019). We assessed fractional anisotropy (FA) and mean diffusivity (MD) maps in white matter, and specifically in internal capsule, as well as structural connectivities in primary sensorimotor networks. SHARD data showed globally lower FA estimates and streamline numbers than EDDY data, and the motion correction seemed to be more efficient across subjects (less residual motion artifacts). In addition, both methods showed expected age-related changes in diffusion metrics and comparable sensorimotor connectivities (results not presented). While we expected that the choice of SHARD vs EDDY method would not influence the results of subsequent analyses (comparison of groups, evaluation of the impact of various factors, etc.), we must admit that our final choice relied on non-scientific criteria (we preferred to use the SHARD pre-processed data, as the tools were developed by the KCL team, in agreement with Dr Arichi).

- ***Resting-state functional MRI (rs-fMRI)***

Rs-fMRI protocol involved a 15-minute acquisition using a high temporal resolution multiband EPI protocol (TE=38 ms; TR=392 ms; MB factor=9x; 2.15 mm isotropic) (Price, 2015). Preprocessing employed the dHCP neonatal fMRI pipeline (Fitzgibbon et al., 2020b), including field map estimation and motion distortion correction (Andersson et al., 2003; Andersson & Sotiropoulos, 2016), along with ICA denoising (Salimi-Khorshidi et al., 2014). Individual functional-to-anatomical registration was performed using boundary-based registration (Jenkinson & Smith, 2001) and the warps are provided within the dHCP database. The available rs-fMRI data was used for the whole-brain functional connectivity estimation (see *Section 2.2.2.*).

2.1.2. Neurodevelopmental outcomes at 18 months

Age-appropriate neurodevelopmental and behavioural evaluations were also performed in the dHCP study design to assess the subject outcomes at 18 months of corrected age (mCA). Specifically, we relied on reported Bayley Scales of Infant and Toddler Development, Third Edition - BSID-III results (Bayley, 2006), which demonstrated the highest completion rate among conducted neurodevelopmental assessments (77%) during follow-up (Edwards et al., 2022). BSID-III is a popular tool for diagnosing developmental delays in early childhood (Del Rosario et al., 2021), used as a prevalent outcome metric across studies aiming to link early brain development to later behavioural performance (Baker & Kandasamy, 2023). The scores encompass 5 distinct developmental categories: cognition, receptive and expressive language, and fine and gross motor functions, yielding age-standardized scaled scores (mean 10, standard deviation 3) with higher values denoting better infant development and scores below 7 indicating developmental delay in a respective domain. The scaled scores aggregate into 3 composite scores representing global cognitive, language, and motor abilities of the subject (Figure 2.3).

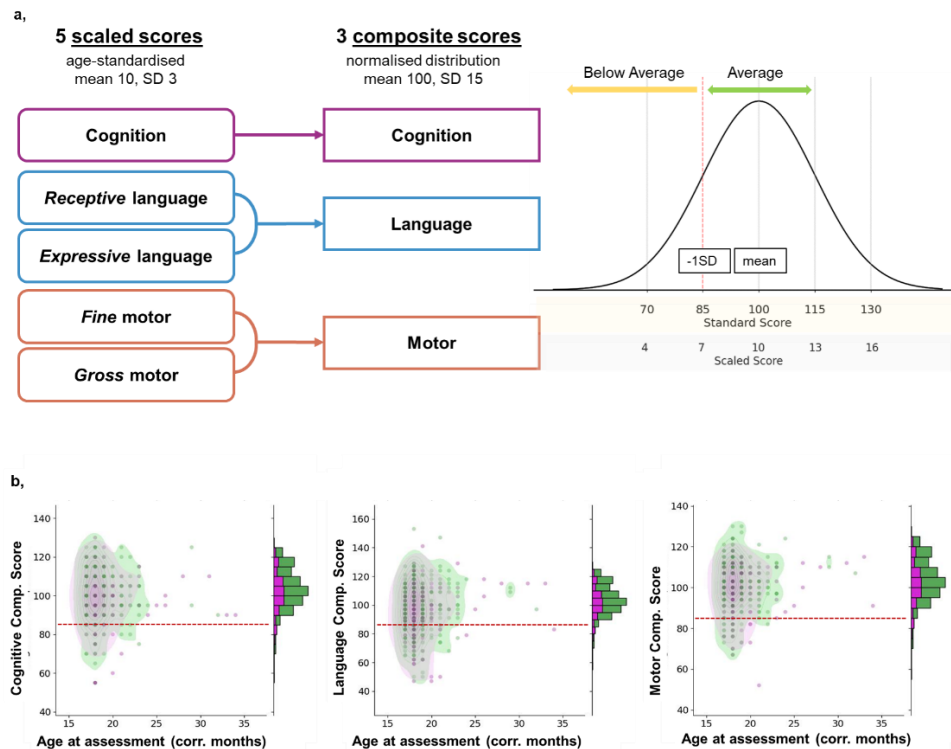


Figure 2.3. Neurodevelopmental categories included in the BSID-III assessment (a) as well as the distributions of all available Cognitive, Language, and Motor composite scores across 604 subjects with available BSID-III scores: preterm (magenta) and full-term (green) subjects (b). The distribution suggests most infants within the dHCP database are at low risk of neurodevelopmental delays. SD: standard deviation.

The use of corrected age for the assessment is crucial, particularly for PT infants, as it adjusts chronological age based on the time from birth to estimated term-equivalent age (TEA). This ensures the use of appropriate behavioural tests despite changes in chronological age. In the dHCP database, BSID-III assessment was available for 604 infants with median corrected age at assessment of 18 [17-34] mCA (months of corrected age). In our work, we considered only the subjects assessed at around 18 mCA (between 17 and 21 m).

2.2. Processing and analyses

2.2.1. Assessment of GM and WM microstructure with dMRI

2.2.1.1. Diffusion models and derived metrics

dMRI provides various quantitative parameters that can be used to assess the microstructural profiles of developing white and grey matter in infants. This is done by investigation of diffusion of water molecules, or rather its restriction (e.g. within the intracellular space) and hindrance (e.g. tortuosity of the extracellular space), in the presence of aligned structures such as axonal fibres and interactions with tissue components in heterogeneous brain regions. To describe diffusion in 3-dimensional space, the diffusion signal is characterized using diverse mathematical models.

In this work, we first relied on the most used model: **Diffusion Tensor Imaging** (DTI) (Basser et al., 1994). At each voxel, DTI calculates a 3x3 symmetric diffusion tensor which can be represented by an ellipsoid. The magnitude of diffusion along the ellipsoid's 3 principal axes of diffusion is described by its eigenvalues ($\lambda_1, \lambda_2, \lambda_3$) which are used to derive useful interpretable metrics: **axial diffusivity** (AD), or λ_1 , which aligns with the direction of the highest diffusivity; **radial diffusivity** (RD), the mean diffusivity along the remaining two axes of the ellipsoid perpendicular to the principal axis; and **mean diffusivity** (MD), the mean diffusivity in all three directions (Figure 2.4). Additionally, **fractional anisotropy** (FA) is quantified to describe the normalized diffusion along the principal axis relative to perpendicular axes:

$$AD = \lambda_1 \quad (2.1)$$

$$RD = (\lambda_2 + \lambda_3)/2 \quad (2.2.)$$

$$MD = (\lambda_1 + \lambda_2 + \lambda_3)/3 \quad (2.3.)$$

$$FA = \frac{\sqrt{3} \sqrt{\sum_{i=1}^3 (\lambda_i - MD)^2}}{\sqrt{2} \sqrt{\sum_{i=1}^3 \lambda_i^2}} \quad (2.4.)$$

Nevertheless, since DTI reveals only the dominant fibre orientation within each voxel, it can lead to erroneous estimates of the microstructural properties of the underlying tissues, especially in areas with more complex fibre configurations, such as crossing or kissing fibres. Moreover, DTI-derived metrics can lack specificity in separating factors like neurite density or volume fractions, making it less suitable for complex tissue compositions, for example GM, or voxels that contain several tissue compartments with different diffusion properties. Additionally, the DTI model assumes the Gaussian distribution of diffusion in each voxel, which is not entirely adequate, especially in heterogeneous tissues (Jensen & Helpert, 2010) or for high b-values (Grinberg et al., 2011).

In this work, DTI estimation was performed with FSL's DTIFIT, and the choice was made to use only a single b-value of 1000 s/mm² to estimate the DTI model, as the utility of including more diffusion directions may be outweighed by the non-Gaussian contribution of high b-value acquisitions (Pines et al., 2020).

To counter the DTI limitations with hope to capture more nuanced microstructural insights, different more complex and potential more biologically relevant alternatives of diffusion models were proposed, including diffusion kurtosis imaging (DKI) (Jensen et al., 2005) or ball and sticks (Behrens et al., 2003). In our work, we aimed to complement DTI-derived metrics with metrics derived from another such model - the *Neurite Orientation Dispersion and Density Imaging* (NODDI) (Zhang et al., 2012). NODDI characterizes underlying tissue microstructure as three compartments: intra-neurite compartment, modelled as stick; extra-neurite space, described by anisotropic Gaussian diffusion; and the free water compartment with isotropic Gaussian diffusion. NODDI provides two key metrics: *neurite density index* (NDI) and neurite *orientation dispersion index* (ODI) (Figure 2.4) which might be particularly valuable for the analysis of areas with mixed fibre orientations and tissue compositions. However, similarly to other multi-compartment models, NODDI requires multi-shell high angular resolution diffusion images (HARDI) to model the diffusion signal and estimate its parameters, strongly limiting its use to studies which have such data available. Furthermore, in contrast to more easily interpretable DTI-derived diffusivities, NODDI-derived metrics are not always straightforward to interpret. The synergy of the NODDI-derived metrics with established ones, like those obtained from DTI, may serve both to enhance and to validate the observed findings.

In this work, we estimated NODDI using the CUDA 9.1 Diffusion Modelling Toolbox (cuDIMOT) NODDI Watson model implementation for GPUs (Hernandez-Fernandez et al., 2019). For more details on the NODDI model computations and the method developed for the

post-processing of the calculated NDI and ODI maps, I refer the readers to the detailed descriptions in specific chapters describing the experimental work (*Chapters 3, 4, and 5*).

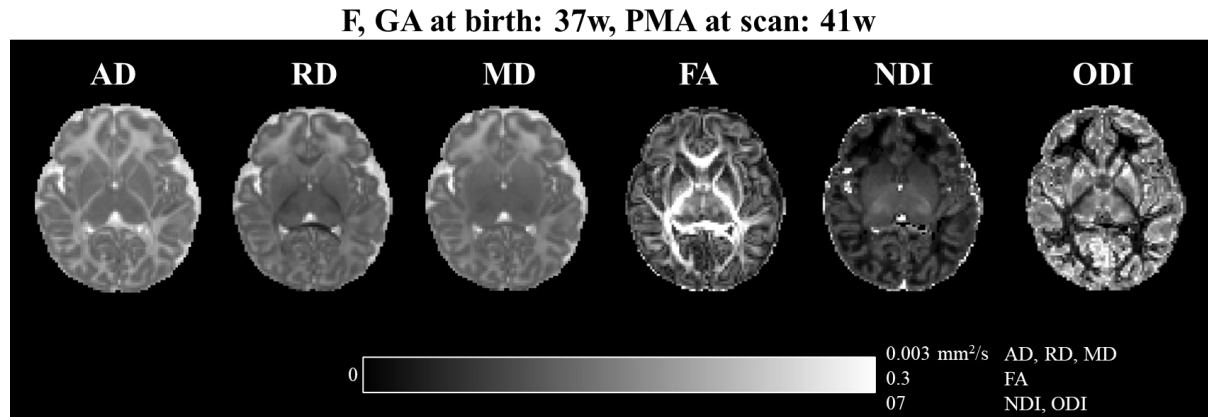


Figure 2.4. Maps of DTI and NODDI-derived metrics for an example full-term neonate from the dHCP database.

2.2.1.2. Diffusion metrics and the underlying neurodevelopmental processes

DTI and NODDI reveal complex brain maturation patterns (Qiu et al., 2015; Ouyang, Dubois, et al., 2019). In **white matter (WM)**, diffusion studies reveal a global pattern of age-related increase in FA and decrease in diffusivities (AD, RD, MD) from foetal period to early postnatal years (Hermoye et al., 2006; Dubois et al., 2008; Geng et al., 2012; Mishra et al., 2013; Yu et al., 2014; Wilson et al., 2021). NDI in preterm newborns and early postnatal years follows a similar age-dependent increase, while changes in ODI display varied region-dependent patterns (Jelescu et al., 2015; Batalle et al., 2017a; Kimpton et al., 2021; Zhao et al., 2021). These changes reflect underlying developmental processes. Initially, progressive axonal organization into coherent fascicles leads to a preferential diffusion along the fibres, increasing AD and FA, and decreasing RD. Coinciding increases in NDI suggest FA changes during the pre-myelination period characterized by proliferation and differentiation of oligodendrocytes which subsequently settle along the axons (Baumann & Pham-Dinh, 2001), are driven by rising neurite density and regional complexity (Batalle et al., 2019b) rather than solely fiber coherence (Drobyshevsky et al., 2005; Wimberger et al., 1995) or axonal membrane properties (Prayer et al., 2001) suggested previously. Additionally, brain water content decreases with age. Combined with oligodendrocyte proliferation that precedes the myelination, the increased cellular density leads to decreases of all three diffusivities. FA increases even further as “true” myelination (ensheathment of myelin around axons by oligodendrocytes) progresses in parallel

to axonal fibres (Zanin et al., 2011; Snaidero et al., 2014; Simons & Nave, 2016). The resulting decreased axonal membrane permeability due to myelin sheath leads to further RD decrease. However, complex axonal configurations, such as crossing, fanning, bending, or branching, are common in the white matter (Jeurissen et al., 2013) and pose challenges for DTI-based estimations due to its limitations in differentiating multiple fibre orientations. ODI differences across white matter regions could help elucidate this complexity (Kunz et al., 2014), highlighting the benefits of complementing DTI with NODDI evaluations to inform on a complex regionally dependent variability that includes changes in geometrical organization and neurite density which DTI metrics alone might not capture effectively (Kunz et al., 2014).

DTI and NODDI metrics can also provide insights into the development of *grey matter (GM)*, in particular the cerebral cortex (Ball, Srinivasan, et al., 2013; H. Huang et al., 2009, 2013). The immature cortex exhibits high FA and AD due to its organized radial architecture, but maturation involves reduction in both FA and AD accompanied by increases in ODI (Ball, Srinivasan, et al., 2013; Smyser et al., 2016; Eaton-Rosen et al., 2017). These changes reflect microstructural modifications, including synaptogenesis and synapse pruning, dendritic arborization, myelination of intracortical white matter, and axonal growth, progressively disrupting the early radial organization (Bystron et al., 2008). Dramatic decrease in water content and increase in tissue density lead to decrease in MD values (and overall diffusivities). Period before 38wGA is also accompanied by decreases in NDI which might reflect cortical expansion in some cortical areas (Batalle et al., 2019b). FA remains relatively stable after 38wGA (Ball, Srinivasan, et al., 2013), although, recent research has suggested a biphasic age-dependent change in both FA and NDI: initially decreasing until ~38wGA, then increasing in older neonates while ODI remains constant (Batalle et al., 2019b). This shift would align with histological studies which emphasize the dominance of increasing geometric complexity in the prenatal period (increase in ODI). Beyond 38wGA, the cortex's radial organization is no longer evident, thus minimally impacting ODI, while important increases in neurite density contribute to decreased MD and AD (Rakic et al., 2009; Lu et al., 2013).

Similarly, global changes in diffusion metrics with development were also reported in subcortical structures, including grey nuclei and thalamus, characterized by increases in FA and decreases in AD, MD, and RD (Nossin-Manor et al., 2013a; Qiu et al., 2013; Zheng, Zhao, et al., 2023). These likely reflect rapid changes in connections to and from deep grey matter structures and the increasing myelin content resulting in increased fibre integrity (Batalle et al., 2017a; Zheng, Wang, et al., 2023). Globally, previous work indicates that subcortical structures become more like WM and more dissimilar to cortical GM with age (Galdi et al., 2020).

Despite discernible global trends, important spatiotemporal asynchronies in maturation have been observed for both white matter (Lebel et al., 2012; Geng et al., 2012; Nossin-Manor et al., 2013b; Dubois et al., 2014; Batalle et al., 2017a; Kimpton et al., 2021; for review: Ouyang, Dubois, et al., 2019) and cortical grey matter regions (Ball, Srinivasan, et al., 2013; Huang et al., 2013; Yu et al., 2016; Neil & Smyser, 2018) which result in significant regional variations in age-related changes of DTI and NODDI metrics. Interestingly, the changes in cortical microstructural properties seem related to associated white-matter tracts confirming that brain maturation might be better viewed as maturation of networks and systems rather than separate regions of grey and white matter (Smyser et al., 2016; Friedrichs-Maeder et al., 2017).

Thus, DTI and NODDI provide tools for a comprehensive assessment of both GM and WM microstructure during early development and can allow comparisons of microstructural variation across regions and between different infant populations, particularly for the assessment of alterations resulting from effects of prematurity and their implications for later neurodevelopmental outcomes.

2.2.2. Investigating structural and functional connectivity

The human brain can be represented as a network of interconnected regions at both structural and functional levels. In the following sections, we briefly present the conceptual background underlying assessment of structural and functional connectivity using dMRI and rs-fMRI, respectively. We then introduce methods employed to estimate structural and functional connectivity in the infant brain within this PhD work.

2.2.2.1. Structural connectivity: anatomical organization of the WM

Structural connectivity in the brain, defined by spatial and topological arrangement of white matter connections (fibres) between distinct anatomical elements, can be studied using dMRI-based tractography methods. Various non-invasive tractography approaches have been developed to map these structural connections by reconstructing three-dimensional white matter pathways based on various diffusion MRI models.

These methods globally involve two main steps: first, estimating fibre orientations at the voxel level, and second, step-wise propagation of streamlines based on these local fibre orientations. Streamlines are then assigned to pairs of regions of interest (ROIs) to reconstruct the structural pathways. Assignment can be seed-based, where streamlines are initiated from specific seed ROIs during construction, or achieved through a ‘brute force’ (whole-brain)

method, where streamlines are initiated randomly from larger areas, for example the entire white matter, and are subsequently assigned to ROI pairs based on connectivity likelihood estimated from tractography results and a set of inclusion and exclusion criteria to filter out non-relevant streamlines (Jeurissen et al., 2019; Rheault et al., 2022). The quality of structural reconstructions heavily depends on the diffusion model used to estimate fibre orientations, on the tractography method, and specific parameter settings (Schilling et al., 2021) (*Figure 2.5a*).

Regarding the *diffusion model*, DTI has been widely used to estimate fibre orientations in infant and foetal studies (for example: Berman et al., 2005; Dubois et al., 2006; Tymofiyeva et al., 2012; Ouyang et al., 2016; Yepes-Calderon et al., 2017; Friedrichs-Maeder et al., 2017). However, DTI's limitation of estimating a single fibre orientation per voxel often resulting in underestimation of tract complexity (Farquharson et al., 2013) (*Figure 2.5b*). This is particularly significant as up to 90% of brain voxels may contain multiple fibre orientations (Jeurissen et al., 2013).

To address these limitations, advanced models estimating multiple fibre orientations within each voxel have been employed in infant structural connectivity studies (Bassi et al., 2008; Roze et al., 2012; Takahashi et al., 2012; Jaimes et al., 2018). Some variations of these models extend DTI into multi-compartment approach which represent diffusion signal as a sum of diffusion signals caused by individual compartments, including parametric ball-and-sticks model (Behrens et al., 2007), composite hindered and restricted water diffusion (CHARMED) (Assaf & Basser, 2005), or distribution of anisotropic microstructural environments in diffusion-compartment imaging (DIAMOND) (Scherrer et al., 2016). Another class of methods estimates a fibre orientation distribution function (fODF), which indicates the probability distribution that a fibre points in a specific direction on a sphere. These methods include Q-ball Imaging (Tuch, 2004), Diffusion Spectrum Imaging (DSI) (Wedeen et al., 2005), or spherical deconvolution-based methods such as Constrained Spherical Deconvolution (CSD) (Tournier et al., 2004). However, these methods might often require more advanced diffusion imaging techniques (such as HARDI employed in the acquisition of the current cohort) or impractical scan times for infant studies (Seunarine & Alexander, 2014). In recent years, several data-driven and machine learning methods have shown promise in estimating fODF from dMRI, providing model-free estimations that might avoid sub-optimal assumptions inherent in diffusion models (Lin et al., 2019; Nath et al., 2019; Karimi et al., 2021)

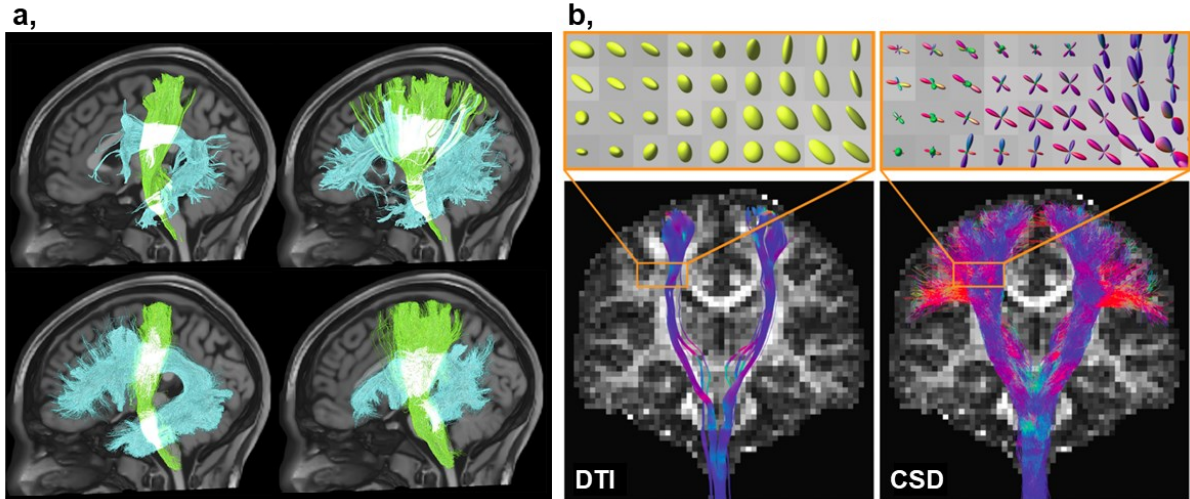


Figure 2.5. Sensitivity of tractography results to methodological choices. **a**, Variability in delineation of the corticospinal tract (green) and arcuate fasciculus (cyan) using four different tractography settings. The same pathway exhibits notable variations in size, shape, and streamline density, emphasizing the impact of different settings on tractography reconstructions. Adapted from (Schilling et al., 2021). **b**, Example of fiber tracking within sensorimotor WM regions using DTI (right) and CSD (left) fiber estimates, superimposed on coronal FA maps of a healthy (adult) subject. The CSD fiber orientation estimates within individual voxels highlight the presence of multiple fiber orientations, particularly the expected fan-shaped configuration of streamlines of the cortico-spinal tract, which is inadequately represented by DTI, resulting in significant differences between the tractograms. Adapted from (Farquharson et al., 2013).

After estimating fibre orientations within diffusion data, streamlines are seeded and constructed incrementally. *Tractography methods* can be categorized into deterministic and probabilistic approaches, depending on how the direction of streamline propagation is sampled from fibre estimates. Deterministic methods use a fixed fibre direction at each tracing step. For example, DTI-based deterministic tractography connects the first eigenvectors to reconstruct pathways of white matter fibres with streamline propagation methods (Jones et al., 1999; Mori et al., 1999). Probabilistic methods randomly sample the direction of the next step from the distribution of fibre orientations, aiming to account for uncertainties in fibre orientation estimates and data noise (Behrens et al., 2003; Jones, 2008; Farquharson et al., 2013), although sometimes leading to spurious streamlines (Sarwar et al., 2019).

In one of our PhD studies focusing on sensorimotor connections (Chapter 3, Figure 2.6a), we estimated fibre orientations using Bayesian Estimation of Diffusion Parameters Obtained using Sampling Techniques (BEDPOSTX with GPU acceleration) (Jbabdi et al., 2012). This involves a parametric model similar to the ball-and-stick model, which divides the diffusion signal into several anisotropic components representing fibre orientation (stick) and an isotropic component (ball) (Behrens et al., 2007). In contrast to the ball-and-stick, we

employed a deconvolution against a zeppelin response (Behrens et al., 2007; Jbabdi et al., 2012; Sotiropoulos et al., 2016) as it was suggested to improve estimations, especially in areas with low anisotropy inherent in neonatal dMRI data (Bastiani et al., 2019; Sotiropoulos et al., 2016). Model parameter distributions at each voxel were constructed using Markov Chain Monte Carlo sampling. We then performed seed-based tractography using GPU-accelerated Probabilistic Tracking with Crossing Fibers (PROBTRACKX) (Behrens et al., 2007; Hernandez-Fernandez et al., 2019) to sample streamlines between predefined seed regions within the primary sensorimotor system. The resulting output described the connectivity density distribution between ROI pairs. The use of exclusion and termination criteria, along with tractography settings, and analysis of the reconstructed sensorimotor network, are detailed in the dedicated methods section in *Chapter 3*.

In another study, we also employed a whole-brain tractography approach for the estimation of structural connectivity based on a multi-shell two-tissue (MS2T) constrained spherical deconvolution (CSD) (Dhollander et al., 2019) of the diffusion data followed by probabilistic tracking with second-order Integration over Fiber Orientation Distributions (iFOD2) algorithm (Tournier et al., 2010). The details are provided in a dedicated chapter within the *Annexe 2* (see *Figure 2.6b* for example identification of sensorimotor network connections).

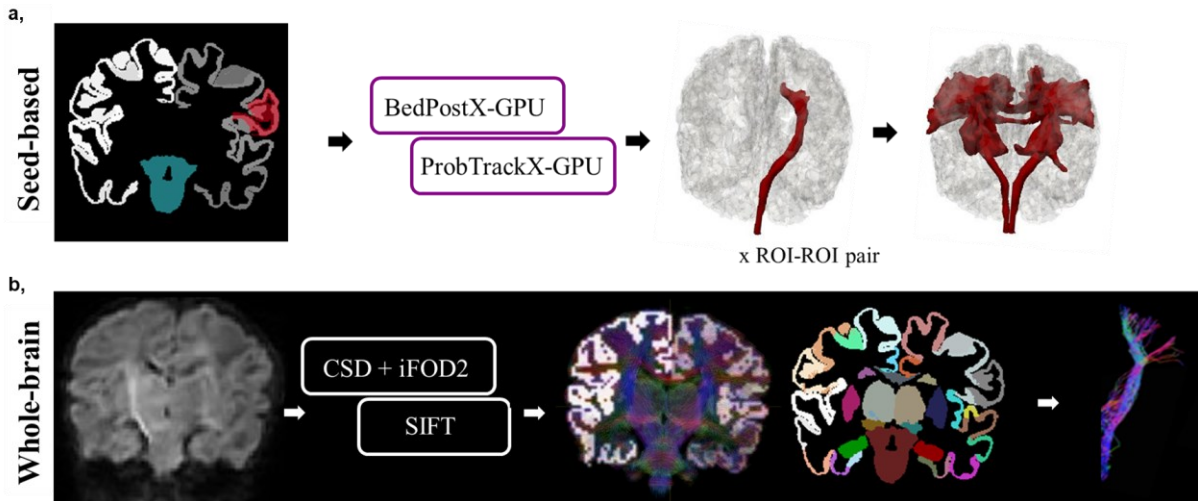


Figure 2.6. Example tractography pipeline for seed-based (a) and whole-brain (b) estimation of structural sensorimotor connectivity.

2.2.2.2. *Functional connectivity: synchronous activity patterns across brain regions*

In contrast to the structural connectome which maps direct white matter connections, functional connectivity refers to the coordinated brain activity across different brain regions. Resting-state functional MRI (rs-fMRI) measures blood oxygen level-dependent (BOLD) signals, reflecting changes in regional metabolic demand (e.g., oxygen consumption, and related blood flow changes) and providing indirect indication of regional neuronal activity (Ogawa et al., 1990; S. M. Smith et al., 2009). Functional connectivity is evaluated by analysing synchronicity in BOLD signal patterns across brain regions, using temporal correlation or other statistical relationships (Friston, 1994). The fundamental assumption is that regions exhibiting similar BOLD fluctuations over time, even during task-free spontaneous activity ('resting-state'), are functionally connected (Cole et al., 2010).

The analysis of rs-fMRI in terms of functional connectivity has gained popularity for studying the emergence of functional architecture from infancy through early childhood (Hoff et al., 2013; Cao et al., 2017; Eyre et al., 2021; Yu et al., 2021; Williams et al., 2023) as reviewed in (Cao et al., 2017; Keunen et al., 2017; Zhang et al., 2019). Additionally, resting-state functional connectivity can be assessed using encephalographic recordings, such as EEG and MEG; however, a detailed examination of these approaches is beyond the scope of this section.

Two primary approaches exist for estimating functional connectivity and can be regrouped under seed-based and data-driven categories (Smith & Beckmann, 2017). ***Seed-based methods*** utilize predefined ROIs to calculate relationships of the ROI to the rest of the brain or between a set of ROIs (Farahani & Karwowski, 2019) using measures like temporal correlation (covariance), cross-correlation (Cao & Worsley, 1999), coherence analysis (Sun et al., 2004) phase-spectrum delays (Sun et al., 2005), statistical parametric mapping (SPM) (Dale et al., 2000; Greicius et al., 2003; Penny et al., 2007), or global network models such as Bayes nets (Ide et al., 2013) (*Figure 2.7*). Partial correlation can be used for multiple ROIs analysis, approximating direct links within structural networks (Liégeois et al., 2020). However, ROI selection based on prior knowledge can introduce significant bias into the connectivity estimates (Smith & Beckmann, 2017). Notably, using inaccurate ROIs for network estimation can greatly undermine the results, emphasizing the need for caution when using potentially inappropriate ROI definitions derived from structural atlases (Smith et al., 2011).

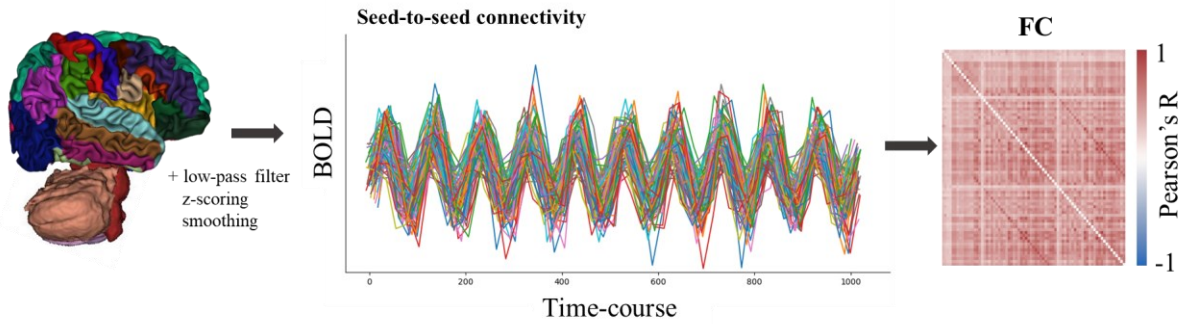


Figure 2.7. Functional connectivity (FC) estimation across a set of predefined ROIs. Firstly, time-series data is extracted from these ROIs to reduce noise. This can be achieved by averaging the BOLD signal value at each time point across the seed's voxels or employing more sophisticated approaches such as Principal Component Analysis (PCA) (Margulies et al., 2010). Subsequently, the extracted time series are then interrelated between regions to create connectivity matrices depicting ROI-ROI connections.

Data-driven methods aim to explore the multivariate structure of data without prior knowledge of seed regions. Decomposition methods, including Independent Component Analysis (ICA) and its more complex alternatives like probabilistic ICA or dual-regression ICA, identify independent components representing data structure that can be described by spatial and temporal maps (Cole et al., 2010). Despite their popularity, these methods face challenges in determining the optimal number of components and dealing with signal variations such as the ones related to physiological noise (Baumgartner et al., 2000; Cole et al., 2010; Margulies et al., 2010; Bijsterbosch et al., 2017).

Clustering methods, such as fuzzy clustering analysis (FCA) or hierarchical clustering analysis (HCA), partitions rs-fMRI data into clusters based on a chosen similarity measure (Li et al., 2009). The goal is to group voxels that are functionally connected or exhibit similar patterns of functional connectivity with the rest of the brain (Cohen et al., 2008). Various variations of clustering methods have been developed and applied to rs-fMRI connectivity delineations (for review: Khosla et al., 2019).

While approaches mentioned above describe undirected connectivity, the study of 'effective' connectivity, which assesses directional influence between regions, has also been proposed (in infants based on EEG recordings: Bosch-Bayard et al., 2022). This is often achieved using Granger causality or dynamic causal modelling (Friston, 2011). In rs-fMRI such approaches are heavily debated due to slow haemodynamics and time delays resulting in low temporal resolutions (Stokes & Purdon, 2017; Bielczyk et al., 2019).

Once the functional connectivities are delineated, their intrinsic properties are often analysed using graph theory-based methods to explain functional relationships across brain

regions (for review of basic concepts: Wang et al., 2010; guidelines on building graphs: Yu et al., 2018, examples related to brain development: Power et al., 2010).

In our PhD work (*Chapter 5*), we used the pre-processed rs-fMRI data provided within the dHCP database to compute whole-brain functional connectivity within a set of delineated ROIs, represented as Pearson’s correlation between the median time courses of the respective region pairs.

2.2.3. Brain parcellation

The assessment of GM microstructural properties and the estimation of structural and functional connectivity require a precise delineation of ROIs. In the following section, we provide a concise overview of different strategies used to define ROIs and describe specific parcellation choices in our PhD work.

2.2.3.1. Atlas-based parcellation

Brain parcellation, a common MRI analysis step, divides the brain into distinct (mostly) contiguous regions, aiming to regroup locations with similar properties like cytoarchitecture, patterns of structural connectivity, or functional activity among others, that should reflect meaningful structural and/or functional areas (Moghimi et al., 2021).

Anatomical parcellations divide the brain using anatomical landmarks to create an atlas with distinct labels for each region (Geyer et al., 2011). For example, cortical sulci around each gyrus can delineate boundaries of anatomically-defined cortical regions (Moghimi et al., 2021). However, inter-individual variability of brain morphology challenges this approach. For example, variations in sulci position and shape can hinder precise identification, impacting resulting parcellations (Destrieux et al., 2010). High-resolution MRI and new automated sulci identification methods may enhance consistency (Borne et al., 2020).

Structural parcellations may also be constructed based on patterns of structural connectivity estimated from white matter tractography (Roca et al., 2009, 2010; Mars et al., 2011; Baldassano et al., 2015; Thompson et al., 2020) to define functionally relevant regions based on an assumption that structural connections can be a determinant of a region’s functional role (Passingham et al., 2002). For parcellation of subcortical regions, the diffusion properties of voxels can substitute the connectivity estimation with tractography due to deeper white matter penetration (Wiegell et al., 2003; Solano-Castiella et al., 2010). However, using cortical diffusion properties might not be as effective due to their strong overall homogeneity (Behrens et al., 2003).

Functional parcellations are constructed from rs-fMRI or task-based fMRI by grouping voxels with similar functional properties from functional connectivity or using voxel connectivity profiles or ‘functional connectivity fingerprints’ (Barnes et al., 2010; Goulas et al., 2012; Jung et al., 2014; Gordon et al., 2016). Additionally, combining multiple complementary properties into multimodal parcellations (for example myeloarchitecture and cortical thickness with task-based functional data) was also proposed to enhance boundary accuracy of resulting parcellations (Glasser et al., 2016; in infants: Li et al., 2023). Structural, functional, and multimodal parcellations use data-driven algorithms to group voxels (or cortical surface vertices) based on their properties. The choice of similarity measure and algorithm greatly impacts parcellation outcomes as they rely on specific assumptions about data structure (for detailed review: Moghimi et al., 2021).

For all types of parcellation, **reference atlases**, constructed from single or multiple subjects, are then applied to new data using automated volumetric or surface-based spatial normalization (Fischl, 2004; Ardekani et al., 2005; Oliveira & Tavares, 2014). The choice of reference atlases can significantly affect resulting parcellation accuracy within individuals, especially in fine-grained regions, if the morphological difference of the individual to the reference atlas is too large (Heckemann et al., 2006; Aljabar et al., 2009). This is especially important when atlases, defined mostly in adults, are applied to the neonate or infant brain due to inherent differences in their anatomy (for example brain size and level of sulcation), as well as imaging quality including lower data resolutions. Selecting appropriate, preferably morphologically similar and/or age-matched reference atlas can enhance parcellation accuracy (Aljabar et al., 2009).

For this reason, in our PhD work, we relied on a neonatal-specific cortical atlas adapted for infants at TEA compatible with the DKT atlas (Klein & Tourville, 2012) available with the surface-based parcellation tool - Melbourne Children's Regional Infant Brain (M-CRIB-S) (Adamson et al., 2020), allowing to subdivide each cortical hemisphere into 31 ROIs (*Figure 2.8a*). Surface-based cortical parcellation was chosen over volumetric methods due to its suggested improvement of alignment of cortical landmarks, including cortical folds, leading to potentially more accurate areal boundaries (Coalson et al., 2018). The surface-based approaches might be especially useful at the boundaries of brain regions with complex anatomical features or close spatial proximity, where volumetric approaches might fail more often. We used the M-CRIB-S tool, heavily based on Freesurfer's automated parcellation pipeline (Fischl, 2012), to register the M-CRIB-S(DKT) cortical template to dHCP surface data through curvature-based spherical mapping. This spherical registration included linear and

non-linear displacement of surface vertices in spherical space, while optimizing the agreement of local curvatures of subject surfaces with the template to improve the final alignment of sulci and gyri and thus the resulting parcellations (Bozek et al., 2018). This anatomical parcellation provided a common consistent framework facilitating analyses in all studies of this PhD work, including assessments of cortical microstructure, as well as structural and functional connectivity.

As expected, we observed good parcellation performance in subjects with similar age to the age of the atlas template cohort (infants at TEA), but the quality decreased as subjects' ages moved further from this cohort (*Figure 2.8a*). This decline in parcellation quality could have potential down-stream effects on the analysis and comparisons of results, especially in younger subjects.

To address parcellation errors in early PT sessions, during a supervised project of a master student (Marion Pavaux), we attempted to leverage conserved within-subject morphological patterns in subjects with longitudinal follow-up by projecting the high-quality M-CRIB-S-derived parcellations at TEA to the subject's earlier sessions (rather than parcellating the early session). The projection was performed using the Multimodal Surface Matching with higher-order smoothness constraints (sMSM) method, which aligns cortical surfaces based on areal features like curvatures or myelin maps while using a novel strain-based surface distortion penalization (Robinson et al., 2018). However, our efforts did not outperform projecting TEA parcellations 'through the template', i.e. when using the surface-registration warps to-and-from 40w surface templates provided within the dHCP database which were previously constructed using the multimodal surface matching approach (Bozek et al., 2018). Our results suggested the need for additional optimization or inclusion of complementary information for alignment. Alternatively, significant morphological and folding changes, characteristic of the period between preterm birth and TEA, may limit alignment improvement even with the additional optimisations compared to the 'through the template' approach, where projection warps were created by alignment to a local age-group template first and only subsequently registered to a 40-week template (Bozek et al., 2018).

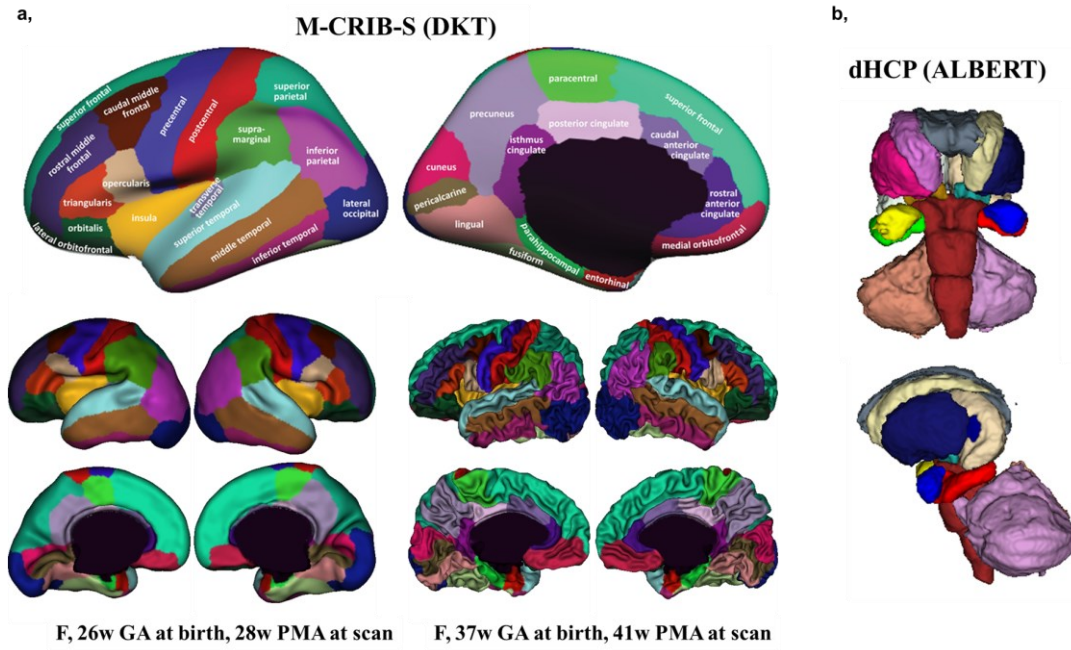


Figure 2.8. Employed anatomical parcellations. **a**, DKT parcellation scheme used to define cortical ROIs (Klein & Tourville, 2012) and example parcellation results for the youngest scan in the dHCP cohort (28w PMA at scan) as well as exemplar FT infant. **b**, Example of subcortical ROI provided in the dHCP parcellations (Gousias et al., 2012) for the same FT subject. Volumetric parcels were converted to surface to aid the visualization.

Additionally, we also explored the MarsAtlas cortical parcellation strategy (Auzias et al., 2016), offering finer regional delineation than the DKT scheme. This method is based on the HIP-HOP cortical parametrization method, which subdivides the cortex using an orthogonal coordinate system defined by primary and secondary sulci (Auzias et al., 2013). Manual delineation of necessary sulci in 8 infants performed by Dr. Sara Neumane (post-doc in the team) allowed us to define MarsAtlas regions with reasonable parcellation quality. However, for large-scale analyses, manual segmentations were impractical. We experimented with an automated sulci recognition strategy using convolutional neural networks implemented in the BrainVISA package (Borne et al., 2020). However, since the model was trained on the adults, it was not fully adapted to handle infant data, resulting in sulci recognition errors with downstream effects on MarsAtlas delineations. Ongoing efforts to adapt the automated sulci recognition model to various populations, including infants, show promise for effective subgyral parcellations of the infant cortex.

Finally, relying solely on surface-based cortical parcellations may overlook subcortical structure and deep brain regions which are crucial to the brain functional development. To include selected subcortical regions in our analyses, we utilized the individual volumetric

parcellation provided within the dHCP database (*Figure 2.8b*). To mitigate potential border errors, we eroded the provided masks, and, in tractography studies, further refined the masks by excluding voxels with a high probability of including CSF voxels (*Chapter 3*). For analyses combining cortical and subcortical regions, we projected the surface-based cortical parcellations to their respective individual volumetric spaces.

2.2.3.2. Random parcellation

Considering challenges with atlases derived based on adult anatomy in delineating infant brain regions, a strategy of dividing brain into random, equally sized ROIs, shows promise for studying brain development across diverse populations and age groups (Fenchel et al., 2020). Such random parcellation might provide more unbiased and computationally efficient ROI delineations, although the difficulties with projecting such parcellations to individual subjects (to ensure inter-subject regional agreement for the subsequent analyses) remains similar and depends on the quality of registration strategy.

Assuming appropriate granularity of the chosen random parcellation, this approach theoretically still reduces input dimensionality compared to voxel (or vertex)-wise analyses, enhancing computational efficiency, while retaining critical detail irrespective of adult, anatomical, or other priors. This might be particularly interesting in predictive studies, where the main objective of parcellating the brain might be a dimensionality reduction independent of regional priors rather than characterisation of brain organization.

In our PhD work (*Chapter 4*), we partitioned cortical surfaces into 128, 256, 512, and 1024 randomly defined bilateral regions of similar size (*Figure 2.9*) using the k-means clustering algorithm, with distances between cortical vertices determined via the Dijkstra-path with edges between vertices weighted by a Euclidean distance. An optimization procedure balanced vertex distribution across regions. To ensure the region correspondence between subjects, the random parcellation was performed for each clustering number in the 40w dHCP surface template space (Bozek et al., 2018) after excluding the cingulate region by a manual segmentation (this was performed to focus on the evaluation of the same cortical locations as in the M-CRIB-S which also excludes the cingulate area). The resulting random parcellations were then projected to the subjects' anatomical space using transformations available from the dHCP database.

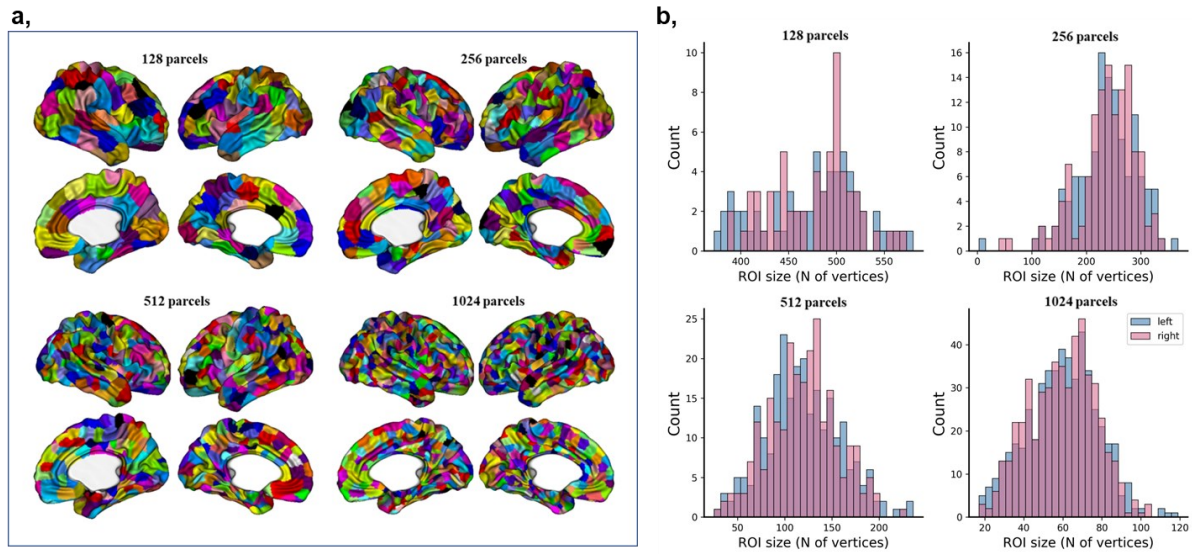


Figure 2.9. Example of random parcellation in the dHCP template space (a). Distribution of number of vertices (N) per parcel for left and right hemispheres (b).

2.2.4. Multivariate analyses of early MRI-derived markers of development

Employing multivariate analysis of MRI data opens new perspectives for exploring both typical and atypical early brain development. Integrating complementary MRI markers into a unified modelling strategy can offer a more precise characterisation compared to univariate approaches, as suggested in prior studies on maturation of white matter bundles or cortical microstructure (Dubois et al., 2014; Kulikova et al., 2015; Nossin-Manor et al., 2015; Lebenberg et al., 2019). In recent years, researchers have increasingly sought to analyse both white and grey matter development, often focusing on healthy newborns, either by computing multiparametric maturational distances or by employing supervised and unsupervised machine learning methods which are described in the following sections. Note that by "multivariate analysis", we refer to approaches where multiple descriptors are integrated within a single model, rather than employing them in parallel and then interpreting to highlight commonalities or differences across these descriptors.

2.2.4.1. Multivariate maturational distance: deviations from typical developmental trajectory

Previously, multiparametric descriptions have been used to study white matter maturation (Dubois et al., 2008; Prastawa et al., 2010; Vardhan et al., 2012; Sadeghi et al., 2013). However, these evaluations have been predominantly univariate which limits the ability to differentiate WM bundles at different maturational stages by overlooking crucial

interrelationships between MRI markers and challenges the interpretations due to the need for numerous comparisons, potentially leading to conflicting findings.

To address these limitations, several studies (Kulikova et al., 2015; Devisscher et al., 2021; Li et al., 2022; Liang et al., 2022) have employed a *multiparametric Mahalanobis distance* (M) approach to characterize maturation. This method enables the comparison of multiple parameters to their typical values in a reference group, most often adults. The Mahalanobis distance is a statistical measure that quantifies the distance between a multivariate data point (\vec{x}) and a reference multivariate distribution characterized by a mean vector ($\vec{\mu}$) and a covariance matrix (S):

$$M(\vec{x}) = \sqrt{(\vec{x} - \vec{\mu})^T S^{-1} (\vec{x} - \vec{\mu})} \quad (2.5)$$

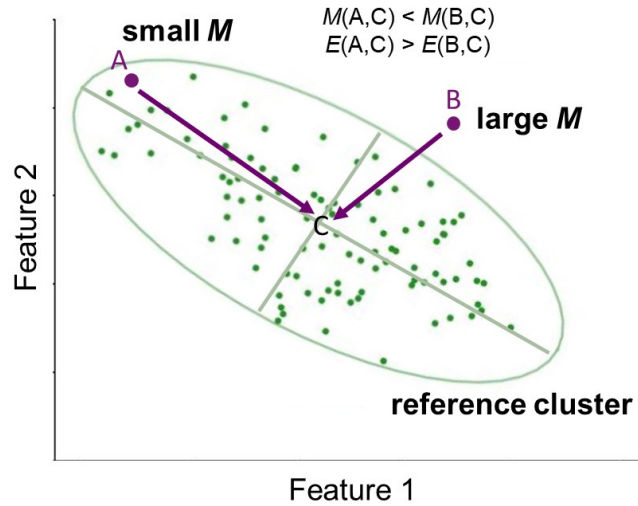


Figure 2.10. Simplified example of Mahalanobis distance which considers feature variability and multicollinearity within the reference group (**green cloud**) when determining the distance of new data point (**magenta**) to the reference group. Distributions of two features are shown as a green oval with mean C. Although the Euclidean distance (E) of B to C is smaller than that of A to C, it results in higher Mahalanobis distance (M) because the point B is outside normal variability of the features in the reference population.

Thus, Mahalanobis distance offers advantages by considering interdependencies among multiple features, providing a comprehensive assessment of a multivariate space defined by complementary metrics. Additionally, it adjusts for typical variation in each feature, resulting in a more accurate dissimilarity measure compared to more simple approaches like Euclidean distance. Moreover, Mahalanobis distance normalizes features by their respective standard deviations, preventing dominance by metrics with larger scales. These characteristics make

Mahalanobis distance an effective measure to identify genuine differences not evident when considering features individually (*Figure 2.10*) and have contributed to its popularity in recent studies focused on analysing maturational asynchronies across white and grey matter regional microstructure and white matter bundle-specific characteristics.

For example, Kulikova et al., (2015) assessed maturation across 18 white matter bundles in healthy infants during the first postnatal year using four MRI markers (quantitative T1 and T2 relaxation times, DTI AD and RD), confirming expected maturational asynchronies and the temporal ordering of bundle maturation. Notably, the multivariate approach outperformed univariate approaches in discriminating between different maturational stages. Similarly, Liang et al., (2022) studied maturation in healthy neonates compared to adults, but rather than assessing multiple bundles, focused on three subdivisions of the superior longitudinal fasciculus (SLF), a complex associative tract in the frontoparietal cortex. Mahalanobis distance computed from DTI and NODDI-derived measure (AD, RD, MD, FA, NDI, ODI) measures described a heterogeneous maturation among SLF branches on the ventral-dorsal axis.

Apart from analysing bundle-specific characteristics, regional white matter microstructural descriptors were also evaluated to determine maturational distances relative to adult references (Li et al., 2022). This involved employing the Mahalanobis distance computed using diffusion metrics derived from both DTI and DKI. The results again underscored asynchronous maturation across white matter tracts, aligning with the established myelination sequence (Kinney et al., 1988).

Additionally, maturation of the GM was also evaluated in comparison to the adult reference with Mahalanobis approach by Devisscher et al., (2021) to investigate the microstructural maturation of somatotopic territories within precentral and postcentral gyri in healthy newborns based on Mahalanobis distance to adult population (computed from AD, NDI, and ODI measures). Results suggested advanced maturation in the leg compared to mouth regions of the somatomotor cortex, highlighting central-to-peripheral maturation in the grey matter, which is in line with previously suggested commonalities between white and grey matter maturation (Smyser et al., 2016).

All the aforementioned studies focused on typical developmental trajectories in healthy newborns in comparison to adult reference. However, employing the Mahalanobis approach for studying atypical development remains unexplored. In one study of this PhD work (*Chapter 3*), we aimed to apply the Mahalanobis approach to assess how prematurity affects microstructural traits in sensorimotor tracts. This quantitative assessment involved comparing

features of a given sensorimotor tract in PT infants to its typical values in a reference group of healthy full-term (FT) infants at TEA. In this setting, small distances indicated a close resemblance of the preterm infant to the FT reference, while large distances suggested specific effects of prematurity on the tract microstructural characteristics. The variations in Mahalanobis distances across tracts were interpreted as differential effects of prematurity on the tracts within the sensorimotor network (further details presented in *Chapter 3*).

2.2.4.2. Data-driven exploration of patterns within neonatal MRI data with clustering

Another popular approach to explore multiparametric information is using **clustering**. In the context of early brain development studies, this unsupervised method can identify regions or subjects sharing common features or exhibiting similar patterns of activity, microstructure, or connectivity in a data-driven manner. During clustering, data points are assigned to clusters based on a measure of their (di)similarity and the assignment is iteratively optimized to maximize the quality of assignment using a pre-selected metric.

An example is the popular k-mean clustering, which partitions data points into pre-selected numbers of clusters and iteratively optimizes their assignment to minimize cluster variance, i.e. internal coherence of clusters. However, this criterion biases resulting clusters toward convex and isotropic shapes (Jain, 2008), emphasizing the importance of the chosen quality measure which is driven by the assumption about the underlying distribution of data within the multivariate space, and its implications on the resulting cluster shape. Thus, despite being labelled as data-driven, the results derived by clustering algorithms heavily depend on the selected similarity metrics and optimisation strategies.

Recently, these methods have been applied to study early brain development. For instance, in rs-fMRI data analysis, k-means clustering was utilized to derive resting state functional networks in FT newborns, revealing hierarchical and replicable networks such as sensorimotor, visual, default mode, ventral attention, and high-level vision (Molloy & Saygin, 2022) with results consistent with previously defined resting state networks in neonates using ICA (Eyre et al., 2021). This approach also highlighted high inter-individual variability across subjects, especially in the ventral attention networks. Clustering has also been employed to study cortical development. For example, Huang et al., (2022) employed k-mean clustering to examine the regionalisation of cortical surface development from 31wGA to 2 years, and parcellate cortex into clusters based on the region-based developmental trajectory of the cortical surface, leading to three distinct developmental clusters. Incorporating microstructural information with morphological assessments, Fenchel et al., (2020) used an affinity

propagation clustering approach, including DTI and NODDI metrics, to derive similarity networks in individual FT infants at birth. The derived network corresponded to known functional distinctions, such as sensorimotor, limbic, and association regions, and were spatially mapped onto known cytoarchitectonic tissue classes.

Furthermore, microstructural properties of the neonate cortex were also investigated based on diffusion properties alone, using AD, NDI, ODI, and a clustering approach with Gaussian Mixture Models (GMM) algorithm (Ginzburg et al., 2021). Authors were able to derive distinct clusters which were thought to reflect different stages of cortical maturation, for example, regrouping insula and cingulate regions and primary sensorimotor cortices into a common cluster with more advanced maturation. Microstructural properties of the cerebral cortex were further investigated with the GMM algorithm in 1-5m old infants based on quantitative T1 and T2 relaxation times and DTI-derived AD (Lebenberg et al., 2019), and resulting cortical clusters were in notable agreement with *postmortem* studies of white matter myelination (Flechsig, 1920; Kinney et al., 1988). Together, these studies have provided valuable insights into the heterogeneous maturation patterns across distinct cortical clusters and hinted at the common patterns of the grey and white matter maturation. Finally, an interesting novel multimodal approach was introduced by (Ball et al., 2017), which employed clustering on a combination of imaging and clinical data to define new features linked to both antenatal and postnatal adverse outcomes.

In one of our PhD works (*Chapter 5*), we also employed clustering analysis to explore both atypical and typical profiles of regional similarity in terms of GM microstructure and functional connectivity. We employed hierarchical clustering (Ward's method) to analyse inter-regional relationships, identify patterns and compare them between modalities to study relationships between functional and structural development longitudinally in preterm (PT) infants from birth to term-equivalent age (TEA). Additionally, we compared alterations associated with prematurity by comparing PT at TEA to those of full-term (FT) infants. More details on this approach are presented in the dedicated *Chapter 5*.

2.2.4.3. Supervised machine learning: differentiating altered development between PT and FT and predicting neurodevelopmental outcomes

Another data-driven approach employed to investigate early brain development is supervised machine learning, a broad term describing computationally intensive algorithms that seek to capture intricate relationships within data by associating inputs with provided output labels. For example, ***logistic regression***, a simple form of supervised learning and a

generalized linear model for predicting categorical outcomes, computes label prediction as a linear combination of input features adjusted by weights transformed into probabilities via the logistic function. The resulting odds ratio indicates the probability of a data point (e.g., subject) belonging to a given label. During training, weights are iteratively adjusted at each pass through the training set using methods like Gradient Descent (or other similar optimiser) to minimize an objective function, such as the sum of squared errors between known and predicted target labels (Pedregosa et al., 2011). Diverse supervised machine learning algorithms including support vector machines, random forests, and neural networks, vary in architectural complexity and assumptions about input-output relationships, but the underlying principle remains the same: iteratively learning parameters to enhance predictive accuracy of categorical or continuous output labels over time by minimizing an objective function (Sarker, 2021).

The ability of machine learning to uncover latent associations within datasets facilitates the development of descriptive, predictive and recommendation tools, with significant efforts directed toward building models that could aid in the early detection of abnormal brain development, including neurodevelopmental outcomes. We have described the efforts to relate early MRI markers to later neurodevelopmental outcomes in PT infants in *Chapter 1*. Additionally, *descriptive tools based on machine learning* can be used to study typical and atypical brain development at the time of MRI assessment.

For example, Ball et al., (2016) utilized functional connectivity inputs to differentiate PT and FT infants at TEA with 80% balanced accuracy (0.92 AUC). Employing random forest-based feature selection followed by support vector machine with non-linear basis function kernel classification, the authors demonstrated global differences in functional connectivity between PT and FT infants at TEA and suggested that the most predominant connectivity alterations were located between subcortical structures (especially nuclei of the basal ganglia) and higher-level cortex. This was in line with previous studies that suggested a particular vulnerability of subcortical grey matter to injury or altered development after preterm birth (Smyser et al., 2010; Ball et al., 2012), and the global effects of prematurity on subcortical–cortical systems as a whole (Ball, Boardman, et al., 2013; Fische-Gómez et al., 2015; Toulmin et al., 2015).

Similarly, Taoudi-Benchekroun et al., (2022) achieved accurate prediction of GA at birth as a continuous outcome using random forests and fully connected neural networks (mean absolute error of 2.21 weeks, Pearson’s correlation of 0.82, $p < 0.001$), this time based on structural connectivity inputs in PT and FT infants at TEA. The features important for

predictions predominantly involved temporal regional and thalami, in addition to the basal ganglia and temporal regions, and again highlighted alterations in frontal and basal ganglia regions. Additionally, authors developed a model to predict postmenstrual age at scan trained only on FT infants which was then used to compute a brain maturational index (predicted age minus actual age) of the PT infants which was significantly correlated with motor outcomes at 18mCA.

These examples highlight that alterations of the neural substrate of brain maturation with implications for future neurodevelopment is detectable at term equivalent age from MRI-markers of functional and structural connectivity, and that machine learning could provide a fairly unbiased strategy for detection of these alterations. In different studies of our PhD work (subsections of *Chapter 4*), we investigated the applicability of early MRI markers for both classifying infants into PT and FT groups based on their early cortical microstructural properties and predicting later outcomes using inputs from white matter connectivity and cortical microstructure. Detailed approaches for these investigations are presented in their respective subsections of Chapter 4.

PART II: Experimental work

Chapter 3: Effect of prematurity on the sensorimotor network

Preface

The late second and third trimesters of gestation, as well as the neonatal period, represent a critical window for the dynamic refinement and maturation of brain networks, including the sensorimotor network. Disturbances during this period linked to premature birth can impact the integrity of emerging networks, potentially leading to long-lasting neurodevelopmental consequences, even in low-risk cohorts (Williams & Pugh, 2018; Pierrat et al., 2021b). In this chapter, we focus on the investigation of the impact of prematurity on the microstructural characteristics of the sensorimotor (SM) system in infants at term-equivalent age (TEA) and its potential association with later neurodevelopmental outcomes.

The choice to focus on the **SM cerebral network** was motivated by its foundational place in early brain development and in the infant's behavioural acquisitions, facilitating interaction with and learning from the environment through the processing of sensory information, motor activities, and related sensory feedback (perception-action loop). The SM network, already established during the preterm period in terms of structural connections (Dubois et al., 2014; Ouyang, Dubois, et al., 2019), plays a crucial role in shaping the structural and functional connectome of the whole brain during the neonatal period (van den Heuvel et al., 2015; Zhao et al., 2019). It serves as a backbone for achieving developmental milestones, from sensorimotor to cognitive functions, including language acquisitions (Thibault et al., 2021), executive functions (van der Fels et al., 2019), and intellectual abilities (Heineman et al., 2018).

Our study cantered on the connections between a primary subset of cortical and subcortical regions that form the complex, highly distributed and interconnected somatosensory and motor systems in the mature brain, namely, *for the cortex*, the *precentral* and *postcentral gyri*, the *paracentral lobule*, and for subcortical structures, the *thalamus*, *caudate* and *lenticular nuclei*, and *brainstem*. We intentionally excluded non-primary cortical areas, which typically mature later in development. A seed-based probabilistic tractography was employed to establish the structural connectivity within the *a priori* selected components of the SM network, providing sensitivity to specific localized effects of prematurity on particular tracts.

To quantitatively evaluate the alterations of a given SM tract in the preterm population, we compared its microstructural features to the typical values in a reference group of healthy term-born infants. We employed the Mahalanobis distance as a suitable and robust metric for

such assessment, given its ability to consider both inter-subject variability and correlations among parameters within the reference group. This approach allowed us to capture the differential effect of prematurity on SM tracts, even when microstructural features were not drastically different to typical values. To gain further insights into prematurity-linked alterations of the SM network, we further evaluated relationships between the described tract-based Mahalanobis distances and later neurodevelopmental outcomes.

The presented investigations were performed in collaboration with S. Neumane (PhD, MD, post-doc in inDEV team). In addition to the publication of this work as a full-length article in the special issue of the journal *Frontiers in Neuroscience*, research topic: *Imaging the Developing Connectome of Perinatal Brain* (see the article included in the following section (Neumane*, Gondová* et al., 2022), *co-first authors), the work was presented as a poster at the annual meeting of the Organisation of Human Brain Mapping (OHBM) 2023 (Gondová et al., (2023b) included at the end of the chapter).

Paper: Early structural connectivity within the sensorimotor network: Deviations related to prematurity and association to neurodevelopmental outcome

Sara Neumane^{1,2,3*} Andrea Gondova^{1,2*} Yann Leprince² Lucie Hertz-Pannier^{1,2} Tomoki Arichi^{3,4} Jessica Dubois^{1,2}

1. Inserm, NeuroDiderot, Université Paris Cité, Paris, France

2. CEA, NeuroSpin UNIACT, Université Paris-Saclay, Paris, France

3. School of Biomedical Engineering and Imaging Sciences, Centre for the Developing Brain, King's College London, London, United Kingdom

4. Paediatric Neurosciences, Evelina London Children's Hospital, Guy's and St Thomas' NHS Foundation Trust, London, United Kingdom

Reference: Neumane, S., Gondova, A., Leprince, Y., Hertz-Pannier, L., Arichi, T., & Dubois, J. (2022). Early structural connectivity within the sensorimotor network: Deviations related to prematurity and association to neurodevelopmental outcome. *Frontiers in Neuroscience*, 16.

#1 Abstract

Consisting of distributed and interconnected structures that interact through cortico-cortical connections and cortico-subcortical loops, the sensorimotor (SM) network undergoes rapid maturation during the perinatal period and is thus particularly vulnerable to preterm birth. However, the impact of prematurity on the development and integrity of the emerging SM connections and their relationship to later motor and global impairments are still poorly understood. In this study we aimed to explore to which extent the early microstructural maturation of SM white matter (WM) connections at term-equivalent age (TEA) is modulated by prematurity and related with neurodevelopmental outcome at 18 months corrected age. We analysed 118 diffusion MRI datasets from the developing Human Connectome Project (dHCP) database: 59 preterm (PT) low-risk infants scanned near TEA and a control group of full-term (FT) neonates paired for age at MRI and sex. We delineated WM connections between the primary SM cortices (S1, M1 and paracentral region) and subcortical structures using probabilistic tractography and evaluated their microstructure with diffusion tensor imaging (DTI) and neurite orientation dispersion and density imaging (NODDI) models. To go beyond tract-specific univariate analyses, we computed a maturational distance related to prematurity based on the multi-parametric Mahalanobis distance of each PT infant relative to the FT group. Our results confirmed the presence of microstructural differences in SM tracts between PT and FT infants, with effects increasing with lower gestational age at birth. Maturational distance analyses highlighted that prematurity has a differential effect on SM tracts with higher distances and thus impact on (i) cortico-cortical than cortico-subcortical connections; (ii)

* first co-authors

projections involving S1 than M1 and paracentral region; and (iii) the most rostral cortico-subcortical tracts, involving the lenticular nucleus. These different alterations at TEA suggested that vulnerability follows a specific pattern coherent with the established WM caudo-rostral progression of maturation. Finally, we highlighted some relationships between NODDI-derived maturational distances of specific tracts and fine motor and cognitive outcomes at 18 months. Our results expand understanding of the significant impact of premature birth and early alterations on the emerging SM network even in low-risk infants, with possible relationship with neurodevelopmental outcomes. This encourages further exploration of these potential neuroimaging markers for prediction of neurodevelopmental disorders, with special interest for subtle neuromotor impairments frequently observed in preterm-born children.

#2 Introduction

The cerebral somatosensory and motor systems consist of distributed networks of specialized interconnected cortical and subcortical grey matter (GM) regions, interacting through white matter (WM) tracts, that support a wide variety of sensory and motor functions that are essential for nearly every human behaviour across the lifespan. In somatosensation, inputs from peripheral receptors are first conveyed by peripheral nerves, then through the spinal cord to the brainstem dorsal column nuclei. These nuclei further connect to the thalamus which sends projections to cortical somatosensory areas, particularly the primary somatosensory cortex (S1) located on the postcentral gyrus. On the other hand, the primary motor cortex (M1) in the precentral gyrus, is critical for motor behaviour, exerting its influence over the body's muscles through its output to a variety of descending pathways, the main being the direct cortical innervation of motoneurons via the corticospinal tract (CST). S1 and M1 are reciprocally connected, directly via short-range intra-hemispheric and homotopic interhemispheric pathways, and indirectly via some cortico-subcortical pathways predominately involving the thalamus and the basal ganglia (BG). The BG notably include the caudate nucleus, putamen and globus pallidus: the first two functionally constitute the striatum (receiving most of the BG inputs), while the last two are grouped anatomically in the lenticular nucleus, with the globus pallidus representing one of the key output structures of the BG (Leisman et al., 2014).

Interactions between somatosensory and motor systems, observable in mature brains (Hatsopoulos and Suminski, 2011; Tomasino and Gremese, 2016), are particularly important during the early stages of neurodevelopment. The late second and third trimesters of gestation, as well as the neonatal period, are a critical time for the dynamic refinement and maturation of

brain networks through several complex processes (Dubois et al., 2014; Kostović et al., 2019), laying the foundations of structural connectivity that underlie later neurodevelopment (Gilmore et al., 2018). As projection and interhemispheric tracts show rapid growth before 28 weeks of gestational age (wGA) (Keunen et al., 2017; Kostović et al., 2019), the general architecture of the sensorimotor (SM) network is already established during the preterm period, making it one of the earliest brain systems to mature (Dubois et al., 2014; Ouyang et al., 2019; Machado-Rivas et al., 2021). It may therefore play a pivotal role for the optimal development of secondary and associative networks in their earliest stages and for organizing the structural and functional connectome throughout the neonatal period (Ball et al., 2014; van den Heuvel et al., 2015; Zhao et al., 2019).

This crucial maturation phase is also highlighted by the adverse effects of preterm birth (before 37wGA) on neurodevelopment. The sudden need to adapt to extra-uterine life does not provide the optimal conditions for physiological neurodevelopmental mechanisms, resulting in variable structural and/or functional abnormalities (Suzuki, 2007). The related diffuse cerebral dysmaturation (Back, 2015; Volpe, 2021) alters the integrity of the emerging neural networks (Suzuki, 2007; Back, 2015), with early maturing regions suffering the largest adverse effects with a greater degree of prematurity (lower GA at birth) (Knight et al., 2018).

Magnetic resonance imaging (MRI) including diffusion MRI (dMRI) has been extensively used to evaluate the consequences of preterm birth on brain development. Even in the absence of focal cerebral lesions, prematurity is associated with disturbances in brain growth, in particular in GM structures including the BG and thalamus (Keunen et al., 2012; Padilla et al., 2015; Loh et al., 2020), and pervasive widespread abnormalities in GM and WM microstructure, maturation and connectivity (Ball et al., 2013b; Batalle et al., 2018). In particular, the WM of preterm infants at term-equivalent age (TEA) has a more “immature” microstructural profile compared with term-born neonates, consistent with delayed and/or disrupted WM development and maturation (Thompson et al., 2011; Kelly et al., 2016a,2020). The extent of early WM abnormalities (even in the absence of overt brain lesion) has been related to poorer neurodevelopmental outcome (Duerden et al., 2015; Barnett et al., 2018; Kelly et al., 2020; Pannek et al., 2020). Preterm infants are also at higher risk of impaired neuromotor function (Williams et al., 2010; Odd et al., 2013; Spittle and Orton, 2014), that can manifest as poorer fine and gross motor skills compared with term-born controls (Evensen et al., 2020). Although long-lasting WM alterations in SM tracts have been observed during childhood and adolescence in these populations (Groeschel et al., 2014; Dewey et al., 2019; Thompson et al., 2020), the relationship between neonatal SM network structural alterations and neuromotor

impairment in low-risk preterm infants (including moderate to late preterm and/or preterm babies without perinatal brain injury) has been less systematically explored. Also, assessing early WM maturational delays across the different SM tracts and analysing the correlation with outcome would enable a better understanding of the pathophysiology of the disorders resulting from deviations in typical developmental processes.

In this study, we thus aimed to assess how preterm birth impacts SM network maturation at TEA in the absence of overt cerebral lesions, and the potential effect on later neurodevelopmental outcome. We hypothesized that SM network would show significantly altered microstructure in preterm infants compared to full-term neonates, with distinct patterns of maturation delay across the SM tracts, and that these alterations are associated with motor and global neurodevelopmental outcomes. For this purpose, we studied a large cohort of low-risk preterm infants at TEA and full-term neonates from the developing Human Connectome Project (dHCP) (Edwards et al., 2022), and investigated the effects of prematurity on WM microstructure and maturation of SM tracts using complementary approaches based on diffusion MRI data and tractography (Dubois et al., 2014, 2016; Ouyang et al., 2019). We dissected an unprecedented set of SM cortico-cortical and cortico-subcortical tracts and computed quantitative metrics from two complementary models: the widely used Diffusion Tensor Imaging (DTI) model (Dubois et al., 2014; Pecheva et al., 2018; Ouyang et al., 2019) and the more specific 3 tissue compartments model of neurite orientation dispersion and density imaging (NODDI) (Zhang et al., 2012; Kunz et al., 2014; Batalle et al., 2017; Kimpton et al., 2021). To overcome the limitations inherent to univariate dMRI approaches which cannot reflect the inter-related complexity of processes involved in early brain maturation, we used the multivariate Mahalanobis distance approach to compare the preterm and full-term groups (Kulikova et al., 2015; Dean et al., 2017; Li et al., 2022). This allowed us to consider multiple metrics and to quantify the tract-specific maturational gap at TEA between a preterm infant and the reference group of full-term neonates, with the added advantage of taking into account inter-subject variability in the reference group, as well as correlations between input metrics. Moreover, using the Mahalanobis distance measure with different sets of DTI and NODDI complementary metrics allowed the effect of maturation and complex underlying WM microstructural processes to be accounted for. Finally, we evaluated the relationships between the aforementioned distances for the different SM connections and neurodevelopmental outcome at 18 months of corrected age (mCA).

#3 Methods

#3.1. Subjects

This study included a sample of preterm and full-term neonates taken from the dHCP cohort, collected at St Thomas' Hospital London, UK from 2015 to 2020.¹⁴ This project received UK NHS research ethics committee approval (14/LO/1169, IRAS 138070), and written informed consent was obtained from the parents of all participant infants. From the overall cohort, we identified 59 preterm (PT) infants (33 males, gestational age at birth – GA at birth: median 31.7 weeks, range [23.7w–36.0w]) scanned near TEA (median post-menstrual age –PMA: 41.3w, range [38.4w–44.9w]), and a control group of 59 full-term born (FT) infants (GA at birth: median 40.1w, range [37.4w–42.3w]) matched to the preterm population on age at MRI and sex. Preterm infants were subdivided into infants born extremely to very preterm (GA at birth < 32w, N = 33; PTEV group) or moderate to late preterm (GA at birth ≥ 32w, N = 26; PTML group). The corresponding controls are subsequently noted FTEVCt and FTMLCt, respectively. All included infants were deemed healthy at TEA, i.e., were without major brain focal lesions or any overt abnormality of clinical significance on structural MRI as evaluated by an expert pediatric neuroradiologist (dHCP radiological score in the range 1-3).²⁵

#3.1.1. Neonatal characteristics at birth

Obstetric factors (i.e., multiple pregnancy status, intrauterine growth restriction –IUGR, maternal antenatal steroids and magnesium therapy, delivery method) as well as infant characteristics at birth (i.e., Apgar scores at 1 and 5 min, birth weight, length, and head circumference) were extracted from the dHCP records.

Specific postnatal risk factors previously recognized to be related with neonatal brain abnormalities, including diffuse and regional WM microstructural alterations (Pogribna et al., 2013; Brouwer et al., 2017; Barnett et al., 2018; Parikh et al., 2021), were also considered. These included NICU variables (i.e., total duration of ventilatory support and oxygen therapy, and parenteral nutrition) which were binarized using thresholds established in previous studies (need of mechanical ventilation beyond 7 days, and of parenteral nutrition longer than 21 days) (Brouwer et al., 2017). Sepsis was considered as any situation where an infant received antibiotics, as there was not enough information to retain only confirmed episodes of postnatal sepsis. Additionally, we derived a neonatal morbidities binary factor to summarize the presence

⁴ <http://www.developingconnectome.org/>

⁵ <https://biomed.github.io/dHCP-release-notes/download.html>

of at least one of the following 4 morbidities associated with prematurity (or the absence of all 4): chronic lung disease, necrotizing enterocolitis (NEC), retinopathy of prematurity (ROP) and abnormal cranial ultrasonography (cUS). Of note, detailed neonatal medical records were available only for infants admitted to the neonatal intensive care unit (NICU) after birth: 51 PT (86%) and 2 FT (3%, admitted for sepsis treatment, without further complications).

Comparisons between PT and FT groups in terms of the described variables and factors were performed with suitable tests (Wilcoxon rank sum test for ordinal and continuous variables; Fisher's exact test for binary factors; Pearson's Chi-squared test for non-binary nominal factors) in R (version 4.0.5, 2021.03.31).

#3.1.2. Outcome assessment and infant characteristics at 18 months

Family socio-economic status (SES) was measured using the index of multiple deprivation (IMD) which is a UK geographically defined composite social risk score comprising data on income, employment, health, education, living environment, and crime calculated from the mother's home address at the time of birth.

Neurodevelopmental outcome was assessed at St Thomas' Hospital, London by two experienced assessors using the Bayley Scales of Infant and Toddler Development, Third Edition –BSID-III (Bayley, 2006). We only considered assessments performed at around 18 mCA (between 17 and 21 m), which was available for 44 (75%) PT infants and 53 (90%) FT infants (median age: 18.3 m). Five distinct developmental categories (cognition, receptive and expressive language, and fine and gross motor function) were assessed yielding age-standardized respective scaled scores (mean 10, SD 3), with higher values indicating better infant development and scores lower than 7 indicating developmental delay in that domain.

Comparisons between PT and the FT groups were performed with t-tests corrected for multiple comparisons using Benjamini–Hochberg false discovery rate (FDR) correction across scores. The effect of sub-groups (PTEV, PTML, FTEVCt, and FTMLCt) on neurodevelopmental outcomes was assessed using one-way ANOVA.

Of note, the 5 BSID-III scaled scores can be summarized into the widely used 3 composite cognitive, language, and motor scores (mean 100, SD 15). The results of the entire analyses performed using them can be found in the *Annexe 3.1. Supplementary materials: BSID-III composite score results section*.

#3.2. Magnetic resonance imaging data acquired at term-equivalent age

Magnetic resonance imaging (MRI) data was acquired using a Philips 3-Tesla Achieva scanner (Philips Medical Systems, Best, Netherlands). All infants were scanned during natural sleep using a neonatal head coil and imaging system optimized for the dHCP study as previously described (Hughes et al., 2017).

We used anatomical and diffusion MRI data available in its pre-processed state from the dHCP database (third release) (Edwards et al., 2022). The structural data was a result of acquisition and reconstruction using optimized protocols (Cordero-Grande et al., 2018) leading to super-resolved T2w images with an isotropic spatial voxel size of 0.5 mm. Processing followed a dedicated pipeline for segmentation and cortical surface extraction for T2w images of neonatal brains (Makropoulos et al., 2018), with bias-correction, brain extraction, and segmentation using Draw-EM (Developing brain Region Annotation with Expectation Maximisation) algorithm (Makropoulos et al., 2014). White matter surface (inner cortical surface) meshes provided within the dHCP database were used for the segmentation of cortical regions of interest (ROIs), while volumetric segmentations were directly used to extract subcortical ROIs (cf. section Selection and delineation of regions of interest). Additionally, derived hemispheric, WM and cortical masks (also referred to as cortical ribbons) were also used for the tractography analysis (cf. section SM connectivity reconstruction).

Acquisition and reconstruction of the diffusion data followed a multi-shell high angular resolution diffusion imaging (HARDI) protocol with 4 b-shells ($b = 0 \text{ s/mm}^2$: 20 repeats; and $b = 400, 1,000, 2,600 \text{ s/mm}^2$: 64, 88, and 128 directions, respectively) (Hutter et al., 2018) and was pre-processed with correction for motion artifacts and slice-to-volume reconstruction using the SHARD approach, leading to an isotropic voxel size of 1.5 mm (Christiaens et al., 2021). Pre-processed data was used for the fitting of diffusion models (cf. *section #3.3.1. Estimation of diffusion models*) and for the tractography analysis (cf. *section #3.3.3. SM connectivity reconstruction*).

#3.3. Assessment of sensorimotor network microstructure

To estimate WM microstructural characteristics within the SM network, we first quantified complementary diffusion metrics from the available diffusion data. Structural connections between pairs of anatomically defined SM regions, including cortical primary SM cortices and key sub-cortical structures, were delineated using probabilistic tractography. The diffusion metrics were then extracted for the selected connections of interest and used to study developmental differences between the cohort subgroups.

#3.3.1. Estimation of diffusion models

The DTI model was fitted to the diffusion data using a single shell ($b = 1,000 \text{ s/mm}^2$) and calculated with FSL's DTIFIT. The choice of using only a single b-value was made because the utility of including more diffusion directions may be outweighed by the non-Gaussian contribution of high b-value acquisitions (Pines et al., 2020). DTI maps were computed for four metrics: fractional anisotropy (FA) and Mean Diffusivity (MD) which are a composite of axial diffusivity (AD) and radial diffusivity (RD).

Additionally, multi-shell diffusion data were used to derive the NDI and ODI maps from the NODDI model (Zhang et al., 2012) using the CUDA 9.1 Diffusion Modelling Toolbox (cuDIMOT) NODDI Watson model implementation for GPUs (Hernandez-Fernandez et al., 2019). We used the MCMC optimization algorithm and default settings to fit the NODDI model to our infant data. The NODDI-derived maps were then post-processed to reduce the observed noise. Briefly, we used ODI maps to detect possible errors using an alpha-trimming strategy. The voxels presenting values outside the threshold range (fixed upper value of 0.95 and the lower limit being the first groove of the histogram of values) were either (i) normalized by the immediate surrounding values (i.e., the mean of the voxel's immediate environment after the removal of extreme values), or (ii) set to 0, if no voxels in the "normal" range were found in their environment. The same erroneous voxels were also corrected in NDI maps in the same fashion.

#3.3.2. Selection and delineation of regions of interest

Pre-processed structural data was used to parcellate 13 ROIs (6 in each hemisphere and 1 bilateral, *Figure 3.1A*) relevant for the developing SM network, focusing on the primary core of cortical and deep GM structures. Regarding cortical regions, we considered primary sensory and motor cortices which are essential for processing peripheral somatosensory inputs and for initiating and controlling motor behaviours, through cortico-subcortical loops including thalamus, BG and brainstem. We then disregarded non-primary cortical areas, which mature later during typical development. Three cortical ROIs were thus defined on the cortical surface of each hemisphere using the M-CRIB-S surface-based parcellation tool optimized for the term-born neonates (Adamson et al., 2020) whose labelling scheme replicates the Desikan-Killiany-Tourville (DKT) atlas (Klein and Tourville, 2012): the postcentral gyrus as the anatomical proxy of the lateral portion of the primary somatosensory cortex (hereafter referred to as S1 for the sake of simplification), the precentral gyrus as the lateral portion of the primary motor cortex (referred to as M1), and the paracentral lobule (referred to as ParaC)

corresponding to the medial surface of the hemisphere in the continuation of the precentral and postcentral gyri, including the medial portions of the primary SM cortices. The central sulcus was required as a landmark to delineate these pre- and post-central regions, explaining the choice of a surfacic parcellation tool. Individual surface ROIs were then projected to the cortical ribbon defined in the anatomical volumes, and further dilated by one voxel into the WM to ease the tractography process.

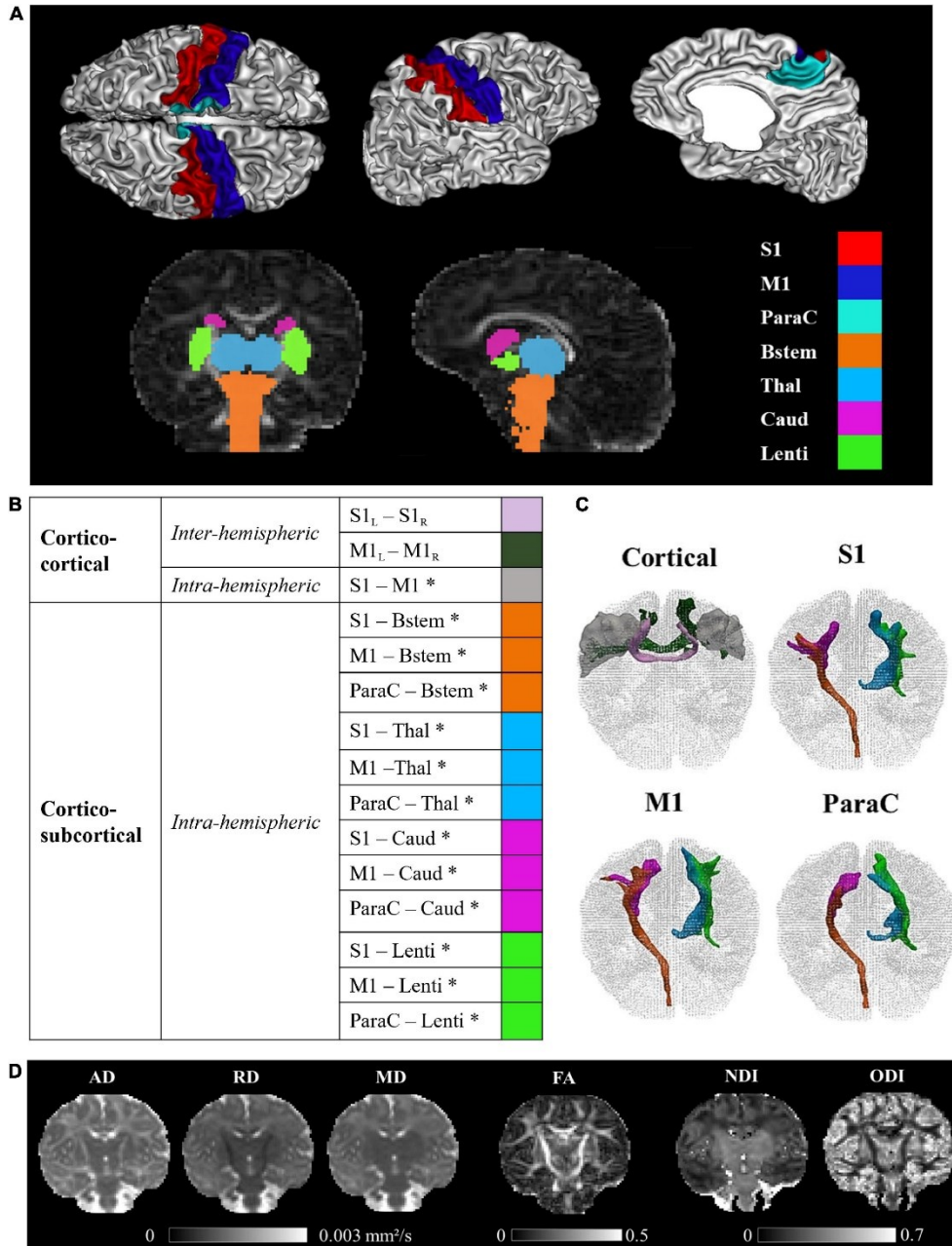


Figure 3.1. Regions of interest, sensorimotor tracts, and diffusivity metrics for a representative full-term infant (GA at birth 40.4w, PMA at MRI 44.1w). **(A)** Visualization of the cortical and subcortical ROIs used as tractography seeds. **(B)** List of the SM tracts of interest. **(C)** 3D reconstructions of SM tracts. **(D)** Metric maps resulting from DTI (AD, RD, MD, FA) and NODDI (NDI, ODI) models. GA,

gestational age (in weeks); PMA, post-menstrual age (in weeks); ROIs, regions of interest; SM, sensorimotor; S1, lateral portion of the primary somatosensory cortex (postcentral gyrus); M1, lateral portion of the primary motor cortex (precentral gyrus); ParaC, medial portions of the primary sensorimotor cortices (paracentral area); Bstem, brainstem; Thal, thalamus; Caud, caudate nucleus; Lenti, lenticular nucleus; L, left; R, right. *Intra-hemispheric tracts, evaluated in left and right hemispheres separately. DTI, diffusion tensor imaging; metrics: AD, axial diffusivity; RD, radial diffusivity; MD, mean diffusivity; FA, fractional anisotropy; NODDI, neurite orientation dispersion and density imaging metrics; NDI, neurite density index; ODI, orientation dispersion index.

Regarding sub-cortical structures, the most relevant to be studied at early developmental stages are the main input/output and relay structures, implicating in particular the brainstem, the thalamus, the dorsal striatum (composed of the putamen and caudate nucleus) that can be considered as the main BG input structure for SM projections, and the internal segment of the globus pallidus (GPi), one of the major output structures of the BG (Leisman et al., 2014). Identifying these specific GM structures on MR images is quite challenging in infants due to the inter-subject variability and rapid changes in morphological characteristics and sizes during the perinatal period. In addition, the precise segmentation of structures of interest also depends on the possibilities offered by the tool validated for neonatal population. The subcortical ROIs were thus defined using a volumetric GM parcellation based on Draw-EM algorithm segmentation (Makropoulos et al., 2014) provided within the dHCP data release, namely medial brainstem (Bstem) and for each hemisphere: thalamus (Thal, fusing high and low intensity regions), caudate nucleus (Caud, part of the striatum) and lenticular nucleus (Lenti, containing the putamen as well as the GPi).

These cortical ROIs (bilateral M1, S1, and ParaC region) and subcortical ROIs (brainstem and bilateral thalamus, caudate and lenticular nuclei), used as seeds for the tractography, were aligned to the diffusion space with FSL 6.0's FLIRT.

#3.3.3. Sensorimotor connectivity reconstruction

Individual dissections of SM connections, which to our knowledge have never been achieved in neonates and infants until now, were performed using an automated tractography-based approach benefitting from multi-shell MRI data. For each subject, probabilistic tractography estimating multiple diffusion orientations within a voxel (Behrens et al., 2007) was used to reconstruct connections between the selected ROI pairs (designated as tracts thereafter). Briefly, for each subject, we first modelled crossing fibres within each voxel of the multi-shell diffusion data using a GPU accelerated version of FSL's Bayesian Estimation of Diffusion Parameters Obtained using Sampling Techniques modelling Crossing Fibres (BEDPOSTX), with default settings apart from the deconvolution model with zeppelins

(Hernández et al., 2013). Then, the pre-selected ROIs were used as seed masks to derive region-to-region structural connections using the GPU implementation of the Probabilistic Tractography with crossing fibers (ProbTrackX) available with FSL 6.0 (Hernandez-Fernandez et al., 2019), and the default (one-way) setting with a loop check. The resulting output describe the density of WM connections between the ROI pair.

To improve the tractography results, and to reduce the incidence of erroneous streamlines, we employed exclusion masks. These exclusion masks were based on a mask of CSF created by thresholding the MD maps (voxels with $MD > 2.10\text{--}3\text{mm}^2/\text{s}$ were considered as CSF) and corrected by removing voxels with $FA > 0.25$ (which might correspond to WM voxels in the corpus callosum but close to the ventricles with CSF partial volume effects). The exclusion masks were further adapted to exclude all other brain structures apart from the considered ROIs pair. Additionally, where the pair of ROIs were ipsilateral, i.e., in a single hemisphere, the entire contralateral hemisphere was also excluded. No supplementary constraints were included in the tractography runs.

Reconstructed tracts were then thresholded at 5% of the maximum fibre density of the evaluated tract. This was not performed for cortico-cortical inter-hemispheric tracts, whose reconstructions were used in their original state due to low streamline numbers.

The final list of SM tracts of interest (corresponding to homotopic inter-hemispheric tracts, short-range S1–M1 intra-hemispheric tracts, and long-range intra-hemispheric cortico-subcortical tracts) is described in *Figure 3.1B*. We visually validated the accuracy of the tracts reconstructions for several subjects and observed expected topographies (e.g., the S1 and M1 projections toward the ventral anterior and lateral portions of the thalami). Note that the (inter- and intra-hemispheric) cortico-cortical tracts involving paracentral regions could not be evaluated due to frequent and variable tractography errors identified upon visual examination. Also, connections between subcortical structures were not studied because of their proximity which could alter the tractography performance.

#3.3.4. Extraction of tract-specific metrics

DTI and NODDI-derived metrics (FA, MD, AD, RD, NDI, ODI) were extracted from each individual tract by calculating the weighted average value (metric \bar{X}) using the following equation:

$$\bar{X} = \frac{\sum(d_i \times x_i)}{\sum d_i}$$

where i denotes the tract voxels, d_i is the fiber density at voxel i of a tract, and x_i is value of the metric at voxel i (Hua et al., 2008). This weighted approach gave more weight to the central portion (with higher fiber density) compared to the tract periphery, rendered the measures independent on the number of streamlines assessed by the tractography algorithm, and limited the effect of potential artifacts related to tractography reconstruction.

#3.4. Univariate tract-specific analyses

To investigate tract-specific relationships between the diffusion metrics and subject characteristics (prematurity, clinical factors, etc.), we performed three sets of univariate analyses on the tract diffusion metrics (see *Annexe 3.1. Supplementary materials: Descriptive univariate analysis* section for the methods and results). This allowed us to identify parameters for the later multivariate analysis. In the univariate analyses, we did not observe interaction between hemisphere and the infant group for any of the six evaluated metrics justifying the averaging of the diffusion metrics over the left and right tracts. Additionally, evaluated clinical variables were not associated, or were only weakly associated, with the diffusion metrics in the PT group, which led us not to consider them as confounders. In contrast, we observed a strong association between the tract-specific diffusion metrics and (i) infant group (PTEV, PTML, FT) or GA at birth; (ii) PMA at scan; and (iii) WM residuals (estimated as the residuals of the linear model considering the metric averaged over the whole WM mask as a function of GA at birth and PMA at scan). The tract-specific diffusion metrics were therefore adjusted for PMA at scan and WM residuals in all the subsequent analyses that aimed to study the effect of prematurity level or GA at birth. As a proxy of the maturational gap between PT and FT, we calculated the relative percentage difference in the metric values between each PT infant and its matched FT control, and averaged this over the PTEV and PTML groups independently.

#3.5. Multivariate tract-specific analyses on effects of prematurity

In order to characterize the potential difference at TEA between the microstructural profiles of PT infants compared to FT neonates for each tract, we used a previously proposed multiparametric approach based on the Mahalanobis distance (Kulikova et al., 2015). The goal was to evaluate the distance between each individual PT infant and the FT group as a reference, by taking into account the inter-subject variability within the FT group and the collinearity between a set of diffusion metrics.

Firstly, we scaled each diffusion metric between [0;1], considering all tracts and the mean WM in all the PT and FT infants. The tract scaled metrics were then corrected for GA at

birth, PMA at scan and WM residuals, considering each of the three groups independently (PTEV, PTML, and entire FT group) and keeping the respective group value means. Next, we divided the PT and FT individual tract metric values by their respective metric means from the FT group.

For the calculation of the Mahalanobis distance, it is beneficial to choose independent metrics that provide complementary information. With this in mind, we decided to subset the six metrics into three parallel analysis streams based on the nature of the metrics and models used to derive them. AD and RD, which are direct measures of the diffusivity within the tracts, were retained as set 1. More complex but commonly used DTI metrics: MD and FA, formed set 2. Finally, NODDI metrics (NDI and ODI) formed an independent set 3 to dissociate them from the more widely established DTI metrics and test their relevance for microstructure in the context of SM network and prematurity.

For a given tract, the Mahalanobis distance (D_{tract}) for a given PT individual was then computed using the following equation:

$$D_{tract}(\vec{x}) = \sqrt{(\vec{x} - \vec{\mu})^T S^{-1} (\vec{x} - \vec{\mu})}$$

where \vec{x} is a multivariate vector describing the PT individual tract-specific metrics, $\vec{\mu} = [1, \dots, 1]$ is the mean vector for the corresponding FT group, and S is a covariation matrix for diffusion metrics in FT infants.

In the interpretation, the smaller the distance, the closer the individual preterm infant is to the distribution within the control FT cohort. Differences in distances across tracts can thus be interpreted as a differential, tract-specific effect of prematurity on maturation.

Regarding statistical analyses, we first evaluated whether the distances for each of the two PT subgroups were significantly different from 0 (meaning that the PT subgroups are different from the FT reference group) using one-sample Wilcoxon signed rank tests corrected for multiple comparisons (FDR) across all tracts and metric sets. We further evaluated the effect of tracts and PT subgroups on the Mahalanobis distances using global ANOVA modelling with these two factors. We additionally compared distances between the two PT subgroups based on unpaired t-tests with FDR correction for multiple comparisons. Both ANOVA and t-tests were performed after checking for normality of the Mahalanobis tract values using Shapiro–Wilk test corrected for multiple comparisons across sets.

To establish whether SM tracts were differentially affected by the prematurity level, we compared all possible pairs of tracts within each PT group, using paired t-tests corrected for multiple comparisons (FDR) across all studied metric sets and tracts.

We finally evaluated the relationship between this maturational distance related to prematurity and neurodevelopmental outcome. For each tract, we evaluated Pearson's correlations between the Mahalanobis distances in each metrics set and the 5 BSID-III scaled scores, considering infants with outcome data in each group separately (PTEV N = 24; PTML N = 20) given the between-subgroup differences observed in distances but not BSID-III scores (see #4 *Results* section). The reported results were corrected for multiple comparisons (FDR) across all tract and metric sets.

Statistical analyses were performed in R (version 4.0.5, 2021.03.31). Statistical tests throughout the analyses were considered with a 0.95 significance level.

#4 Results

#4.1. Cohort characteristics

A summary of the demographic and clinical characteristics for each group and detailed results of the group comparisons are presented in *Table 3.1*. Obstetric factors, multiple pregnancies, IUGR, and delivery by caesarean section were significantly more frequent in the PT group compared to FT (30.5 vs 1.5, 31 vs 2, and 68 vs 49%, respectively). As expected, PT infants differed significantly from FT group in weight, length, and head circumference at birth, as well as Apgar scores. Among the neonates admitted to NICU, only PT needed surfactant, ventilatory support and parenteral nutrition, with 7 (13%) infants needing mechanical ventilation >7 days and 4 (7.5%) parenteral nutrition >21 days.

Morbidities linked to prematurity were seen in 25 PT infants (56.8% of the 44 with available data), including chronic lung disease for 18 infants (15 needing oxygen at discharge), 16 infants had an abnormality identified on cUS during NICU period, 6 had NEC and 2 had ROP. Of note, weight, length, and head circumference at TEA were not available in the dHCP dataset for all infants.

As would be expected, some differences were observed in Radiology scores at TEA between PT and FT babies, with more PT infants having a neuroradiology score equal to 3.

Selected clinical descriptors for the 4 infant subgroups included in the next descriptive analyses are presented in *Annexe 3.1 Supplementary Table 1*.

	Preterm group (N = 59)			Full-term controls (N = 59)			p
	NA	N (%)	Median (IQR) [Range]	NA	N (%)	Median (IQR) [Range]	
Obstetric factors							
Multiple pregnancy, <i>twins</i>		18 (30.5)			1 (1.7)		****
IUGR, <i>yes</i>	4	17 (30.9)□		2	1 (1.8)□		****
Maternal antenatal steroids, <i>given</i>		48 (81.4)			/		
Maternal antenatal magnesium sulphate, <i>yes</i>	3	25 (44.6)□			/		
Mode of delivery, <i>cesarean section</i>		40 (67.8)			29 (49.2)		*
Newborn characteristics at birth							
Gestational age (weeks)			31.7 (28.8; 34.1) [23.7; 36.0]			40.1 (39.4; 41.1) [37.4; 42.3]	****
GA grouping (by wGA)							
Extremely PT (<28 w)		10 (16.9)			0		
Very PT (≥28 to <32 w)		23 (39.0)			0		
Moderate to late PT (≥32 to < 37 w)		26 (44.1)			0		
Full-term birth (≥37 w)		0			59 (100)		
Sex, <i>male</i>		33 (55.9)			33 (55.9)		#
Birth weight (kg)			1.48 (1.10; 1.99) [0.54; 3.06]			3.47 (3.24; 3.74) [2.44; 4.14]	****
Birth length (cm)	38		44 (40; 47) [29; 53]	11		52 (50; 54) [46; 57]	****
Birth head circumference (cm)	2		29 (26; 31) [21.5; 35]	1		35 (34; 35.5) [31.5; 37]	****
Neonatal period factors							
Admitted in NICU, <i>yes</i>		51 (86.4)			2 (3.4)		****
Apgar score at first minute			7 (5; 9) [1; 10]			9 (8.5; 9) [1; 10]	****
Apgar score at fifth minute			9 (8; 9.5) [1; 10]			10 (10; 10) [6; 10]	***
Surfactant, <i>given</i>	13	22 (47.8)□			/		
Mechanical ventilation > 7 days	5	7 (12.9)□			0		***
Ventilatory support, <i>total days</i>	5		3.0 (1.0; 19.5) [0.0; 90.0]		/		
Oxygen needed, <i>total days</i>	5		1.0 (0.0; 23.8) [0.0; 99.0]		/		
Parenteral nutrition > 21 days	5	4 (7.4)□			0		**
Parenteral nutrition, <i>total days</i>	5		5.0 (0.0; 12.0) [0.0; 29.0]		/		
Postnatal sepsis		14 (23.7)			4 (6.8)		*
Neonatal morbidities, <i>yes</i>	15	25 (56.8)□			0		
CLD/O2 dependency at discharge	5	18 (33.3)/15 (27.7)□			/		
Necrotizing enterocolitis	5	6 (11.2)□			/		
Retinopathy of prematurity	5	2 (3.7)			/		
Any abnormal cUS	16	14 (32.5)□			/		
MRI scan around TEA							
PMA (weeks) at MRI			41.3 (40.1; 42.1) [38.4; 44.9]			41.3 (40.2; 42.1) [38.3; 44.7]	#
Radiology score			2 (1; 3) [1; 3]			1 (1; 2) [1; 3]	*
1. Normal appearance for age		22 (37.3)			35 (59.3)		
2. Incidental findings with unlikely significance for clinical outcome or analysis		18 (30.5)			17 (28.8)		
3. Incidental findings with unlikely clinical significance but possible analysis significance		19 (32.2)			7 (11.9)		
Median IQR: interquartile range (25%; 75%); range: [minimum; maximum]. NA: data not available (number of subjects). □Percentage over the available data (see NA for missing data). Comparisons were performed with suitable tests (Wilcoxon rank sum test for ordinal and continuous variables; Fisher's exact test for binary factors; Pearson's Chi-squared test for non-binary nominal factors). #No comparisons performed since these variables were used for pairing the full-term infants to preterm ones. cUS, cranial ultrasonography; CLD, chronic lung disease; FT, full-term birth; IUGR, intrauterine growth restriction; NICU, neonatal intensive care unit; PMA, post-menstrual age; PT, preterm birth; TEA, term equivalent age; wGA, weeks of gestational age p-value ≤ 0.0001 [****], ≤0.001 [***], ≤0.01 [**], < 0.05 [*], <0.1 [.] , ≥0.1 [ns].							

Table 3.1. Detailed clinical and sociodemographic information for the 59 pairs of infants.**#4.2. Neurodevelopmental outcome and characteristics at 18 months**

Significant differences were observed in IMD scores reported at 18mCA (n = 96) (Supplementary Table 2), with PT families tending to live in more deprived areas than the FT ones (quintiles ≤ 3 for 64.3 vs 29.6%, respectively, data not shown).

Among the 97 infants with available BSID-III data, no significant differences between PT and FT controls were observed for the corrected age at assessment. Paired t-tests on scaled scores showed no significant differences between PT and FT groups after correcting the results for multiple comparisons (*Figure 3.2*). BSID-III scaled scores across PTEV, PTML FTEVCt

and FTMLCt subgroups (presented in *Annexe 3.1. Supplementary Figure 1*) also showed no significant group effect.

Over the whole cohort, only a small number of infants showed scaled scores indicating a developmental delay (scores below 7 and corresponding to $< -1SD$), with no significant difference between PT and FT. These consisted of developmental delay in 30.9% of infants for expressive communication (N = 30, 19 PT), 14.4% for receptive communication (N = 14, 7 PT), 11.3% for gross motor (N = 11, 5 PT), 6.2% for fine motor (N = 6, 4 PT) and cognition (N = 6, 4 PT).

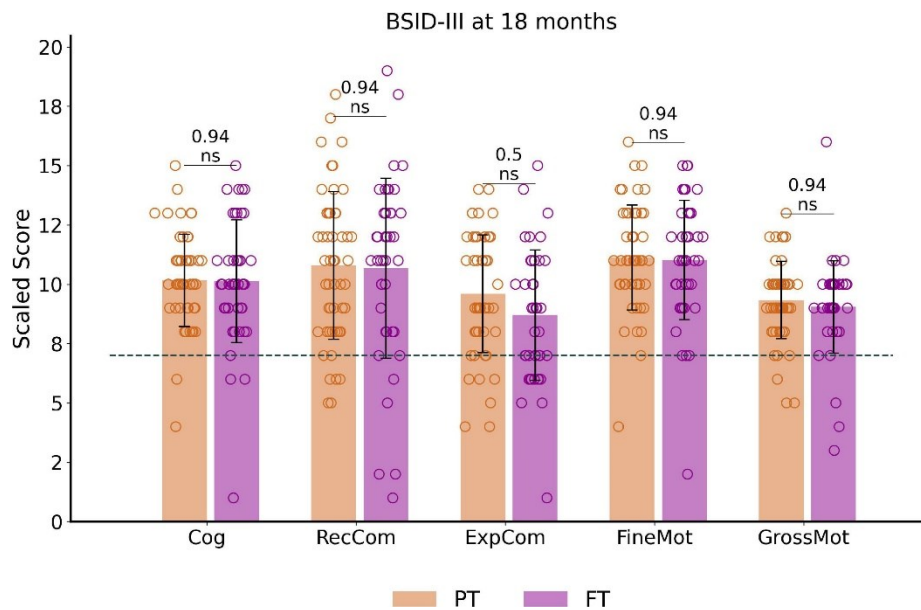


Figure 3.2. Outcome assessment at around 18 months of corrected age: BSID-III scaled scores distribution and comparisons between preterm and full-term infant groups. The dotted line corresponds to the pathological threshold, with scores < 7 ($< -1SD$) indicating a developmental delay. Of note, only one extreme PT (male, born at 27.6wGA) presented severe developmental delay (scores $< -3SD$) for cognitive and both communication scores (with fine motor score at $-2SD$ and gross motor score on the norm values). Reported p -values come from t -tests corrected for multiple comparisons. See Supplementary Figure 3.1 or infant subgroup analysis using one-way ANOVA. BSID-III, Bayley Scales of Infant and Toddler Development, Third edition. PT, preterm; FT, full-term. Cog, cognitive; RecCom, receptive communication; ExpCom, expressive communication; FineMot, fine motor; GrossMot, gross motor scaled scores; ns, non-significant.

#4.3. Sensorimotor tract reconstructions

Visual inspection of the automated reconstructions for all tracts was performed on some randomly selected infants which allowed us to evaluate the quality of reconstructions for all the 15 tracts of interest, in a similar way across PT and FT infants. Examples of individual tract

reconstructions and diffusion metric maps are shown in *Figures 3.1C,D* for a representative FT infant.

#4.4. Univariate tract-specific metrics

Tract-specific distributions of diffusion metrics across the 4 infant groups are presented in *Figure 3.3*. Visual assessment suggested important microstructural differences between groups. Results of the univariate analyses are presented in *Annexe 3.1. Supplementary materials: Descriptive univariate analysis* section. Interestingly, we observed that AD, RD, MD (controlled for the effects of PMA at scan and WM microstructure) decreased with GA at birth in all tracts, while corrected FA, NDI and ODI increased.

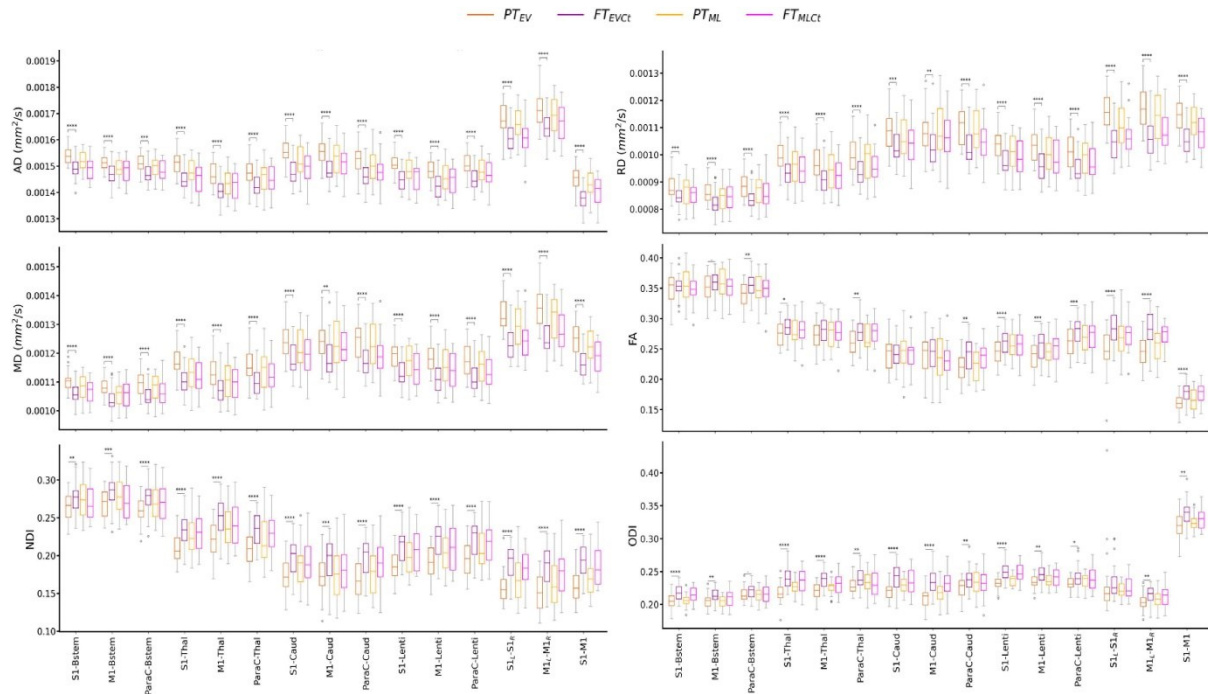


Figure 3.3. Diffusion metrics across tracts and cohort subgroups: extreme to very preterm group (PTEV, dark orange) compared to paired full-term controls (FTEVct, dark purple), and moderate to late preterm group (PTML, light orange) compared to paired controls (FTMLct, light purple). Significances are results of the tract-specific paired t-tests between paired groups, corrected for multiple comparisons. Only the comparisons between PTEV – FTEVct reached significance. Refer to Figure 3.1 legend for abbreviations and to Table 3.1 for p-value legend.

The analysis of the relative percent difference in diffusion metrics between the PT and paired FT neonates allowed us to estimate a proxy of the maturational gap related to prematurity for each PTEV and PTML group (*Annexe 3.1. Supplementary Figure 3.2*). Visual inspection suggested a larger gap in the PTEV subgroup than in PTML, highlighting the effect of prematurity degree on tract microstructural characteristics. However, the observed

variability between the metrics rendered the interpretation of different maturational patterns across tracts difficult, justifying the need for a multivariate approach.

#4.5. Mahalanobis distance of preterm subjects from the typical full-term profile

To explore the impact of prematurity on tract-specific microstructure, we computed multi-metric Mahalanobis distances of PT subgroups (PTEV and PTML independently) to all FT infants as reference, using the 3 metric sets: set 1 (AD and RD), set 2 (MD and FA), and set 3 (NDI and ODI) (Figure 3.4). For a given tract, computed Mahalanobis distance can be understood as a maturational distance for a given PT infant compared to the FT group.

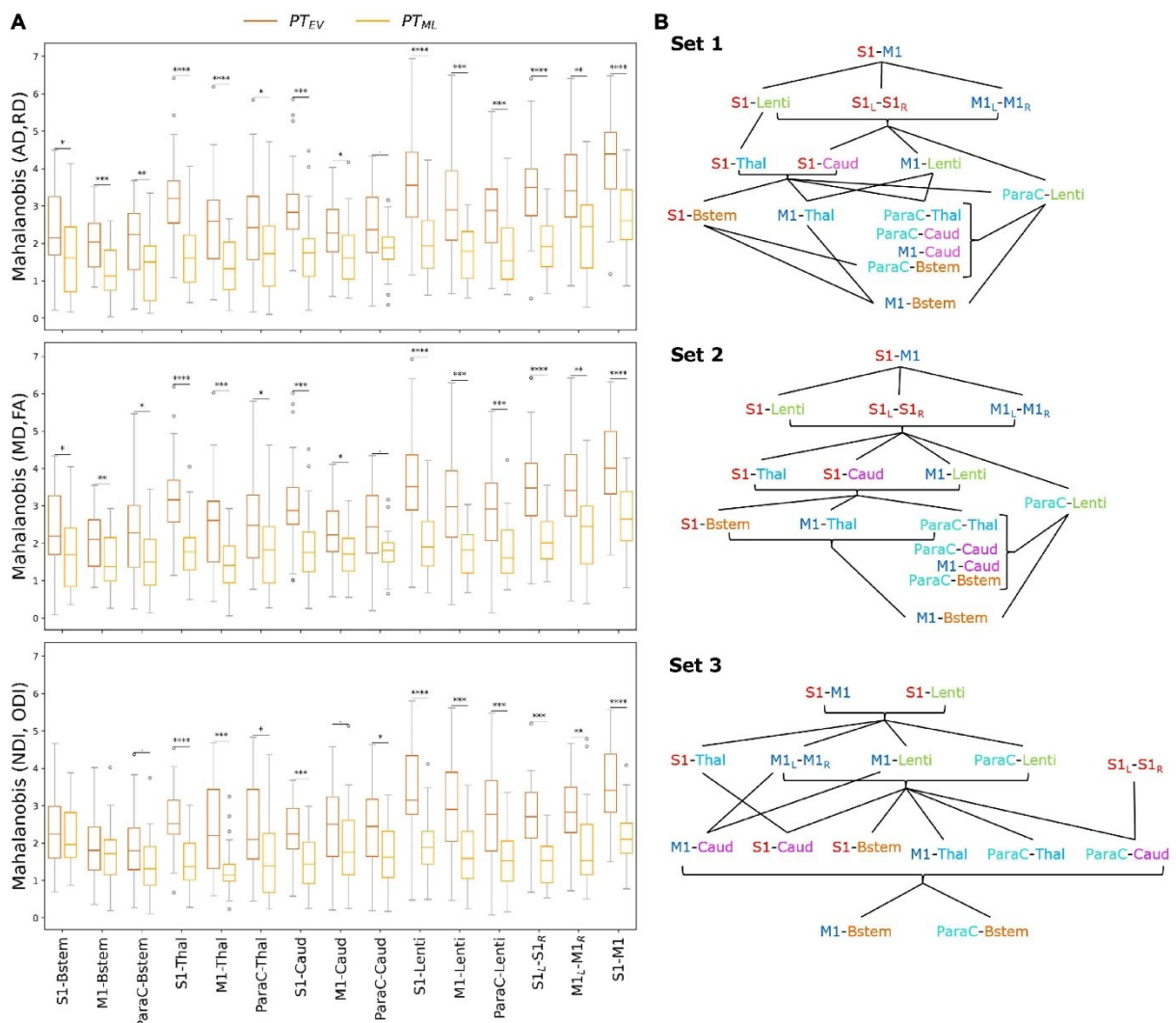


Figure 3.4. Results of the Mahalanobis analyses. **(A)** Multi-metric Mahalanobis distance across tracts and PT subgroups (PTEV and PTML with FT controls as reference) at TEA. The smaller the distance, the less the microstructural profile of the PT infant differs from the FT reference group. Note that the effect of prematurity is globally smaller for PTML than for PTEV infants across the studied SM tracts. Significances are results of the comparison of Mahalanobis distances (PTEV vs PTML) with unpaired t-tests (p-values corrected for multiple corrections) for each set and each tract. For visualization purposes, outliers (mean \pm 3SD) were removed (6 points for PTEV, 3 for PTML infants). **(B)** Order of the SM tracts in the PTEV subgroup based on the Mahalanobis distance per metrics set (higher values

on the top), highlighting the differential effect of prematurity on SM tracts microstructure. The lines represent the significant differences between tracts according to paired t-tests (corrected for multiple comparisons) over the PTEV group (for visualization purposes, the statistical threshold was relaxed to $p < 0.1$). Metrics sets: 1 (AD, RD); 2 (MD, FA); 3 (NDI, ODI). Refer to Figure 3.1 legend for ROIs color code and abbreviations.

For both PT subgroups (PTEV and PTML), all sets and all tracts, distances were highly significantly different from 0 as assessed by Wilcoxon tests corrected for multiple comparisons (all $p < 0.001$), suggesting that SM network microstructure is affected by prematurity, even moderate/late. Considering all PT infants, ANOVA modeling on distances for each set confirmed the expected effects of group, tract, and the interaction between group and tract for all three sets (*Annexe 3.1. Supplementary Table 3*). As expected, the distance increased with the prematurity levels, with unpaired t-tests per tract comparing the two PT subgroups revealing higher distances in PTEV than in PTML (*Figure 3.4A*). In addition, the tracts were not affected in the same manner: distances were different between PTEV and PTML for all tracts except for ParaC-Caud in both DTI sets (1 and 2), and for set 3: S1-Bstem, M1-Bstem, ParaC-Bstem and M1-Caud.

#4.5.1. Tract-specific effects of prematurity

To further evaluate the differential effect of prematurity on specific tracts, we subsequently compared distances for each pair of tracts through paired t-tests in each PT subgroup independently (*Annexe 3.1. Supplementary Figure 3.3*). Many more significant tract-by-tract differences were observed in the PTEV than in the PTML group (69 vs 26/105 for set 1; 70 vs 22/105 for set 2; 61 vs 23/105 for set 3), but the trends were rather consistent between the two PT subgroups.

Focusing on the PTEV subgroup, the significant differences between tracts assessed by the paired t-tests allowed us to propose an ordering of the tracts based on the relative effects of prematurity on microstructural characteristics (*Figure 3.4B*). For sets 1 and 2 (DTI sets), the orderings were highly similar, with, somewhat schematically, the following tracts showing the lowest to highest distances: (1) M1-Bstem; (2) ParaC-Bstem, S1-Bstem, M1-Thal, ParaC-Thal, M1-Caud, ParaC-Caud; (3) M1-Lenti, ParaC-Lenti, S1-Thal, S1-Caud; (4) S1-Lenti, S1L-S1R, M1L-M1R; (5) S1-M1. For set 3 (NODDI set), the ordering showed schematically, from the lowest to highest distances of tracts: (1) M1-Bstem, ParaC-Bstem; (2) S1-Bstem, M1-Thal, ParaC-Thal, M1-Caud, ParaC-Caud, S1-Caud; (3) S1-Thal, M1-Lenti, ParaC-Lenti, S1L-S1R, M1L-M1R; (4) S1-Lenti, S1-M1 (*Figure 3.4B*).

Despite a few differences in the ordering of a couple of tracts, the results were quite consistent across the three sets and revealed a differential impact of prematurity on the SM tracts microstructure. Overall, the tract ordering based on maturational distances highlighted a coherent caudo-rostral and central-to-periphery pattern, with: the cortico-Brainstem tracts presenting the lowest distances and thus the least impact of prematurity; the cortico-Thalamic and cortico-Caudate tracts showing “intermediate” distances; the cortico-Lenticular tracts appearing with the highest distances among the cortico-subcortical tracts; and the cortico-cortical tracts revealing the highest prematurity impact. Inter-hemispheric tracts (S1L-S1R and M1L-M1R) showed lower distances than the intra-hemispheric tracts (S1–M1). S1 tracts generally had higher distances than the M1 and ParaC tracts, both presenting similar profiles.

This approach of tract ordering based on the maturational distance related to prematurity was not considered for the PTML subgroup as tract pairwise comparisons were less systematically significant than in the PTEV group and the ordering was more difficult to synthesize. For this subgroup, the distances of all tracts were more homogeneous (*Annexe 3.1. Supplementary Figure 3*), which may be associated with a lesser effect of prematurity on the microstructural profiles of the SM tracts.

#4.5.2. Tract-specific maturational distance associated with neurodevelopmental outcome

Finally, we assessed whether maturational distances related to prematurity at TEA might be related to outcome (BSID-III scaled scores) at 18mCA, considering each PT subgroup independently. Pearson correlations showed significant results only in PTEV group (N = 24), for Set 3 (NODDI) (*Annexe 3.1. Supplementary Table 4*) and for specific tracts: M1-Bstem and ParaC-Bstem distances were both negatively correlated with Cognitive scaled score and Fine motor score, while M1-Lenti, ParaC-Lenti and S1–M1 tracts were also negatively correlated with Fine motor score (the lower the maturational distance, the higher the score and thus the better the outcome) (*Figure 3.5*). Interestingly, these five tracts showed different levels of distances over the PTEV group, with M1- and ParaC-Bstem having a distance closest to 0, whereas S1–M1 was the tract with the highest distance; and M1- and ParaC-Lenti presented a similar and intermediate distance.

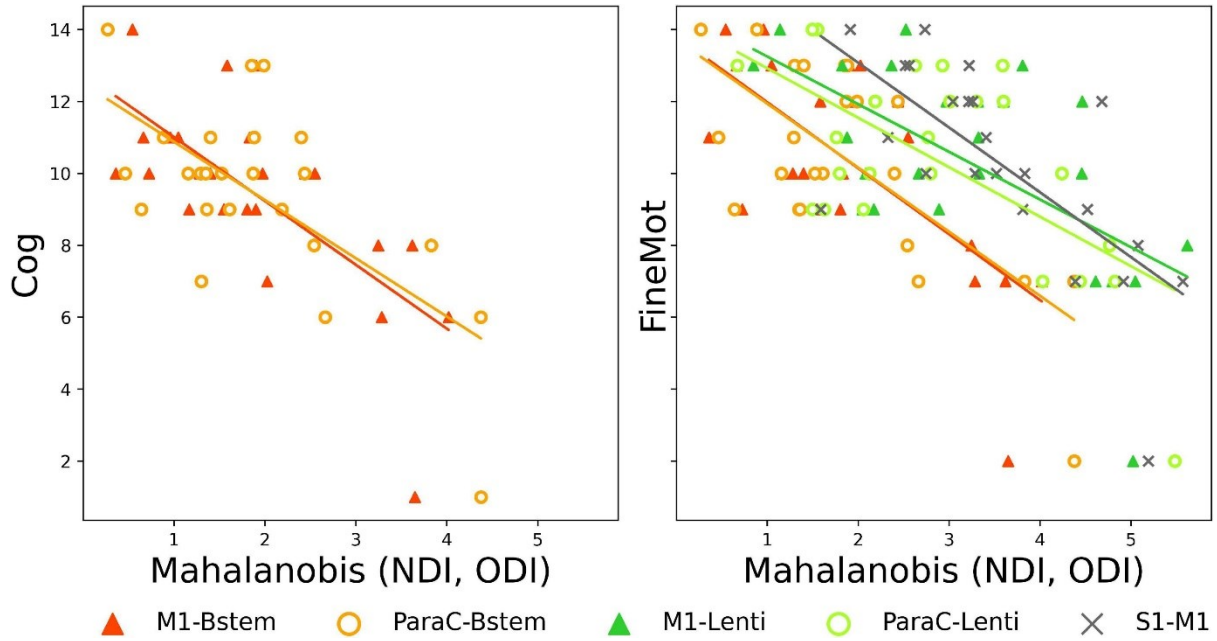


Figure 3.5. Significant correlations between Mahalanobis distances and neurodevelopmental scores at 18mCA, for NODDI set. Scatter plots of the significant Pearson correlations between tract-specific maturational distance related to prematurity at TEA in PTEV group and BSID-III scores. Cog, cognitive; FineMot, fine motor scaled scores. Refer to Figure 3.1 legend for abbreviations.

#5 Discussion

In this study, we considered an unprecedented set of primary SM cortico-cortical and cortico-subcortical tracts that are thought to underpin a wide range of early SM experiences. We observed significant differences in diffusion MRI derived metrics of WM microstructure between low-risk PT and FT infants at TEA. Multi-parametric assessment showed that the maturational gap differs with the prematurity level and across SM tracts, with alterations particularly affecting S1-related tracts and more rostral tracts. Importantly, these findings are of functional significance as correlations were also observed between specific measures of microstructural maturation within particular tracts and neurodevelopmental outcomes evaluated at 18mCA.

#5.1. Exploring the developing sensorimotor network microstructure with diffusion magnetic resonance imaging

#5.1.1. A robust automated approach to delineate primary sensorimotor tracts in neonates

After meeting the challenge of extracting reliable individual SM tracts by optimizing the settings of an automated tractography-based approach benefitting from the dHCP multi-shell dMRI data, we explored the WM maturational differences of low-risk preterm infants at

TEA compared to full-term neonates. We then quantified the microstructure of each tract by extracting DTI and NODDI-derived diffusion metrics using a weighting approach which privileges the core of the tract and avoids potential bias linked to some inter-individual differences in tract volumes.

#5.1.2. Relevance of diffusion MRI models to characterize white matter maturation

DTI and NODDI models present different trade-offs between complexity, biological plausibility, robustness, and run-time duration (Jelescu and Budde, 2017). Despite its widespread use in most studies of WM development (Dubois et al., 2014; Ouyang et al., 2019), DTI-derived metrics can be affected by several microstructural features and lack specificity to disentangle the complex properties of voxels containing crossing, kissing and fanning fibers (Zhang et al., 2012; Jeurissen et al., 2013). In contrast, NODDI allows a more sophisticated and biologically plausible multi-compartment model, relevant for developmental studies (Chang et al., 2015; Genc et al., 2017; Mah et al., 2017; Kimpton et al., 2021), but requires multi-shell data and increased processing time. Although potentially sub-optimal, we opted for default settings of diffusivities in the NODDI model, which were optimized for the adult WM but not for infants (Guerrero et al., 2019). In the absence of gold standards for infant-specific NODDI fitting to evaluate the metric maps, this was performed to maintain some consistency with previous studies (Guerrero et al., 2019; Fenchel et al., 2020).

Overall, the resulting metrics maps were consistent among PT and FT subjects, and metric differences across tracts were largely coherent between DTI and NODDI results in all infants. Once controlled for the effects of PMA at scan and global WM microstructure, we observed that AD, RD, MD decreased with GA at birth in all tracts, while FA, NDI and ODI increased. Globally, MD differences across tracts presented an opposite pattern to NDI (Kimpton et al., 2021), and differences in RD were highly similar to MD in all tracts, and opposite to FA in cortico-subcortical tracts, confirming that variations in MD and FA are likely largely driven by RD. Such diverse profiles across tracts might result from differences in both intrinsic microstructure (similar to adults) and in maturation (according to different myelination stages across tracts) (Dubois et al., 2014). During WM development, MD tends to decrease and NDI to increase with the growth of fibres and membranes, acting as barriers to the random water motion, while FA tends to increase, reflecting several factors including the presence of compact fibre tracts and increasing myelination (Beaulieu and Allen, 1994; Batalle et al., 2017; Kimpton et al., 2021). ODI describes the orientational dispersion of fibres within a tract, which is highly variable across tracts and likely changes during the growth and maturation of crossing

fibres (Raghavan et al., 2021). Interestingly, in a few tracts, we did not observe significant relationship between FA or ODI (corrected for PMA at scan and WM residuals) and GA at birth, suggesting that both metrics might be less sensitive to detect subtle variations of microstructure in the settings of this study. Further analyses (beyond the scope of this study) could be performed to evaluate the potential correlations between all these metrics, as performed in previous studies (Kunz et al., 2014).

Moreover, the results of the maturational distance analyses underlined a high coherence between DTI sets which seemed fairly intuitive and in line with previous studies (Li et al., 2022). The differences observed between the DTI and NODDI sets (with NODDI set presenting more compact and roughly lower Mahalanobis distances values across tracts, with subtle variations in the main order of distances) suggested that NODDI metrics provide complementary information, probably due to their differing sensitivity to neurites growth and maturation. Thus, in line with previous studies (Batalle et al., 2017; Kimpton et al., 2021), our results highlighted the complementarity of these models and confirmed the relevance of NODDI-derived metrics for the study of WM microstructure maturation in the context of prematurity.

#5.2. Studying the effects of prematurity on sensorimotor network maturation at term-equivalent age

#5.2.1. Hypotheses about the differential effect of prematurity across primary sensorimotor tracts

In contrast to the majority of previous studies, we focused on low-risk PT infants without overt brain abnormality at TEA, which is representative of the majority of children now born preterm in developed countries. Despite the presence of specific clinical risk factors in some of the PT infants (e.g., morbidities related to prematurity), the absence of a significant difference in the BSID-III outcome at 18 months of age between PT and FT infants corroborated that the included PT infants were at low-risk for neurodevelopment impairment.

In this study, we hypothesized that WM microstructure within SM tracts would show a significant maturational delay at TEA in PT infants compared to FT neonates, with distinct patterns as a function of GA at birth and across cortico-subcortical and cortico-cortical tracts. This was based on the assumption that early peripheral stimuli are essential for the emerging SM network maturation, and that preterm birth is associated with modified SM stimuli and experiences, notably related to numerous and various procedures in NICU (Mörelus et al., 2006; Gibbins et al., 2008), which might have a differential effect on somatosensory and motor

systems (Duerden et al., 2018; Schneider et al., 2018; Jones et al., 2022). Of direct relevance, previous studies have reported either higher tactile sensitivity in PT infants at TEA (André et al., 2020), tactile hyporeactivity, lower brain responses (Maitre et al., 2017) and/or undifferentiated integration of nociceptive versus non-nociceptive stimuli (Fabrizi et al., 2011), in association with WM abnormalities (Brummelte et al., 2012; Zwicker et al., 2013).

#5.2.2. Approaching the effects of prematurity on WM microstructure with univariate analyses

Univariate dMRI approaches, based on individual derived metrics, are commonly applied to reveal WM developmental changes in the neonatal brain (Kunz et al., 2014; Ouyang et al., 2019). These analyses were thus used to evaluate the effects of several factors on the diffusion metrics measured in SM tracts.

Firstly, these were not related to the infants' sex in our cohort. Combined with previous studies which showed inconsistent results (Pannek et al., 2014; Barnett et al., 2018; Kimpton et al., 2021), this observation suggests that sex effects may vary according to the studied brain regions. Surprisingly, we also observed no effect of main perinatal clinical risk factors (including preterm morbidities), despite numerous studies describing associations of WM abnormalities with obstetric, neonatal and postnatal factors (Pogribna et al., 2013; Brouwer et al., 2017; Barnett et al., 2018; Parikh et al., 2021), and with exposure to cumulative risk factors (Barnett et al., 2018). These negative results might be partly due to the specific study of low-risk PT infants.

In line with previous literature, we observed that diffusion metrics –even measured at TEA– were dependent on PMA at MRI (de Bruïne et al., 2011; van Pul et al., 2012; Kimpton et al., 2021) and were influenced by prematurity (Kunz et al., 2014; Kelly et al., 2016a; Batalle et al., 2017; Thompson et al., 2019; Dibble et al., 2021; Kimpton et al., 2021), with PTEV infants showing more “immature” microstructural profiles (higher AD, RD, MD, lower FA, NDI, ODI) than PTML and FT infants. Interestingly, when group analyses were performed at the tract level, PTML showed no difference with the FT paired group, suggesting that the specific SM tracts studied here might not contribute significantly to the well-described whole-brain WM diffusion abnormalities in moderate-late PT (Kelly et al., 2016a; Thompson et al., 2019).

#5.2.3. Evaluating the maturational distances related to prematurity with a multivariate approach

We then aimed to evaluate the maturational gap between PT infants and their full-term peers, based on SM tracts microstructural characteristics at TEA. Although univariate dMRI approaches allow some inference about the effects of prematurity on SM tract microstructure, they cannot reflect the inter-related complexity of processes involved in early brain maturation (Kostović et al., 2019), and are limited by the difficulties interpreting findings related to single metrics which are sensitive to different underlying microstructural properties and maturational processes. Also, quantifying the maturational degree across regions requires comparison of an infant's data with a mature reference to account for “intrinsic” microstructural differences (Dubois et al., 2014). To overcome these limitations, we implemented an original multivariate approach already validated in neonatal and paediatric data (Kulikova et al., 2015; Dean et al., 2017; Li et al., 2022), that took advantage of the complementary information described by different DTI and NODDI metrics, to enable better characterization of SM tract maturation and the effects of prematurity as compared to typical development. Multivariate Mahalanobis distance was calculated in respect to a reference group (FT neonates) which provided typical values for the given tract. Importantly, this approach also allowed to take into consideration both the inherent variability of the diffusion metrics across tracts in the FT group and the correlations between these metrics. For each tract, the resulting maturational distance related to prematurity could be interpreted as a developmental gap between a PT infant at TEA and the FT control group.

#5.2.4. Highlighting the tract-specific effects of prematurity on SM network

Focusing on the PTEV group, the comparison of distances across tracts highlighted the differential impact of prematurity on the SM tracts at TEA. For all sets of diffusion metrics, the impact increased in a caudo-rostral and central-to-peripheral manner following the typical progression of WM growth and myelination during infancy (Yakovlev and Lecours, 1967; Dubois et al., 2014) and within the CST tract (Kimpton et al., 2021), suggesting that early maturing tracts are less impacted. Furthermore, while this spatial pattern is globally consistent with previous studies of preterm infants (Wu et al., 2017; Knight et al., 2018), our results raise several interesting points regarding the functional role of the different SM tracts and related GM structures during development.

Firstly, we observed a differential impact of prematurity among tracts related to different cortical seeds. S1-subcortical tracts were systematically more impacted than M1- and

ParaC-subcortical tracts. This suggests that S1 tracts may have a specific vulnerability to the deleterious effects of prematurity, possibly due to the altered SM perceptions and experiences as a result of early exposure to the ex-utero environment. Alternatively, the observed differences may reflect compensatory faster and/or more efficient maturational “catch-up” mechanisms in the M1/ParaC-subcortical tracts during the first post-natal weeks after preterm birth.

The similar profiles seen in the ParaC-subcortical tracts and related M1-subcortical tracts are less straightforward to interpret as the paracentral lobule includes both motor and somatosensory regions. Given the somatotopic organization of S1 and M1, this could suggest that connections related to the lower limb representations are less impacted by prematurity, which may be linked to the possible advanced maturation of these representations at early ages (Devisscher et al., 2021). A further possible explanation is that a greater number of motor fibres than sensory fibres were included in ParaC- tracts.

Secondly, the prematurity impact was also variable across sub-cortical related tracts. Of these, the cortico-Brainstem tracts appeared the least impacted. As these mainly correspond of CST fibres that myelinate early, notably at the level of the PLIC (Dubois et al., 2014; Kulikova et al., 2015; Kimpton et al., 2021), this is consistent with connections that have more advanced maturation at the time of birth being less vulnerable to prematurity (Wu et al., 2017). In agreement with the acknowledged vulnerability of thalamocortical connections following preterm birth (Ball et al., 2013a), the cortico-Thalamic tracts showed higher impact than cortico-Brainstem tracts, giving an “intermediate” profile compared to other studied tracts. The specific functional role of the thalamus, with essential input and output projections to the different SM regions, might help to modulate this vulnerability compared to other sub-cortical structures (Duerden et al., 2018; Schneider et al., 2018). Similarly, the cortico-Caudate tracts showed “intermediate” profile. This might result from an interplay between the high vulnerability of the caudate nuclei to prematurity (Nosarti et al., 2014; Back, 2015; Loh et al., 2017) and the adverse effects on the major efferent projections (McClendon et al., 2014) compared with more “preserved” afferent connections (from SM cortices). The cortico-Lenticular tracts systematically presented the maturational distance profile with the greatest impact of prematurity, suggesting their specific vulnerability. In addition to the known structural consequences of preterm birth on BG growth (Loh et al., 2017, 2020), different hypotheses can be proposed to explain this specific profile, especially knowing the anatomo-functional particularities of these tracts. As the dissected tracts include both (afferent) cortico-putaminal and (efferent) pallido-cortical fibres, the observed alteration may involve both the

input (putamen) and output (GPi) structures of the BG, which have different functions in cortico-BG loops. We hypothesize that maturation of the efferent pallido-cortical fibres is specifically altered by prematurity, with functional effects on information reaching SM cortices, which might secondarily induce alterations of the descending cortico-striatal and cortico-pallidal fibres.

Finally, we observed the highest impact of prematurity in the cortico-cortical tracts, suggesting a particular vulnerability of these rostral structures, in line with the well-described caudo-rostral maturational pattern. Inter-hemispheric tracts presented lower impact than intra-hemispheric S1–M1 tracts, in line with the late and protracted maturation of such short-range connections (Kostović et al., 2019).

While interesting, the results should be interpreted cautiously given the limitations of diffusion MRI and tractography with relation to the image spatial resolution and the size of neonatal structures, and the presence of crossing fibres notably at the level of the corona radiata. However, the rare high-quality of dHCP neonatal data, the use of HARDI acquisition, the consistency of the tract's delineation and the multivariate approach allowed us to overcome, at least partially, these limitations. In the future, it would be interesting to further investigate whether the vulnerability of SM tracts to prematurity is stable over development or whether “catch-up” development is present for some tracts, either before or after TEA. This would require the longitudinal evaluation of maturational distances defined with similar settings.

#5.3. Relating the early microstructure of sensorimotor tracts with neurodevelopmental outcome

The final aim of this study was to investigate the relationship between SM microstructural characteristics at TEA and neurodevelopmental outcome at 18mCA. In the specific low-risk preterm cohort studied, no substantial developmental delay or specific disability was expected, as confirmed by the results in terms of BSID-III scores.

Nevertheless we hypothesized that correlations would exist between diffusion metrics profiles and BSID-III scores based on previous studies showing that, even in the absence of overt brain lesions, neonatal microstructural WM measures are associated with neurodevelopmental outcome in toddlers and children (van Kooij et al., 2012; Duerden et al., 2015; Barnett et al., 2018; Girault et al., 2019; Kelly et al., 2020; Pannek et al., 2020; Parikh et al., 2021). In particular, reduced neonatal FA (especially in the PLIC) has been associated with delayed psychomotor development and motor disability at different ages (Rose et al., 2007; Skranes et al., 2007; De Bruïne et al., 2013; Groeschel et al., 2014; Kelly et al., 2016b), and

neonatal NODDI metrics have been found to relate to later neurodevelopmental outcomes (Kelly et al., 2016b; Young et al., 2019).

Our results showed negative correlations in PTEV infants between maturational distances and Cognitive and Fine motor scaled scores for a number of tracts in the NODDI set only. This suggested that the early microstructural information as modelled by NODDI is more sensitive than DTI based metrics such as FA for detecting subtle WM tract alterations related to later neurodevelopmental impairments in preterm infants (Batalle et al., 2017; Kimpton et al., 2021). Moreover, early SM tract microstructure was further correlated with cognitive outcomes, confirming essential developmental interactions between the SM system and higher-order functions, and the common clinical overlap of motor and cognitive impairments in the PT population.

Regarding the tracts concerned, we first observed that fine motor score was related to five tracts with different maturational distance profiles: M1-Brainstem and ParaC-Brainstem which were the least impacted by prematurity; M1-Lenti and ParaC-Lenti with intermediate profile; and S1–M1 with the greatest impact. This suggested that the degree of maturational gap at TEA by itself is not the only factor explaining motor outcomes.

In the light of our results showing the high vulnerability of lenticular tracts to prematurity, it is not surprising that microstructural alterations in the motor tracts connected to this key BG structure may underpin early SM impairments with further consequences on fine motor skill acquisition (Leisman et al., 2014). Likewise, as intra-hemispheric SM connections contribute to improve SM integration and functions, the correlation observed for S1–M1 tract suggests that early impact of prematurity on these tracts may alter later neuromotor development.

Maturational distances for M1-Brainstem and ParaC-Brainstem tracts were also correlated with cognitive scores, suggesting that early microstructural alterations in these tracts might have global functional consequences, beyond motor skills. Nevertheless, further studies are needed to better understand the involvement in these developmental domains of the brainstem, a complex structure that plays an essential role as a relay for a large number of connections from the whole nervous system, in addition to the functions associated with its many GM sub-structures.

The observed relationships in PTEV infants between SM tract microstructure at TEA and outcome at 18mCA are of particular interest in the context of prematurity, as even low-risk populations are at increased risk of –sometimes subtle– neuromotor impairments (e.g., developmental coordination disorder) (Edwards et al., 2011; Spittle and Orton, 2014; Zwicker,

2014; Groeschel et al., 2019). These disorders are generally not visible enough to be diagnosed until much later (often at school age) (Williams et al., 2010; de Jong et al., 2012; Van Hus et al., 2014), which underlines the need for early diagnostic biomarkers. Thus, the specific impact of prematurity on the five primary SM tracts previously mentioned should be further explored, in order to investigate their potential value as early markers of motor and/or other neurodevelopmental disorders such as developmental coordination disorder.

Nevertheless, whilst relating early brain markers and long-term outcome has important clinical relevance, previous studies have described that environmental factors (e.g., socio-familial) could explain the greatest part of interindividual variability in neurodevelopment later in childhood, with the influence of perinatal risk factors diminishing over time (Thompson et al., 1998; Miceli et al., 2000; Anderson and Doyle, 2008; Linsell et al., 2015). Thus, future studies should incorporate more accurate predictive models to intend to approach the complex relationship between early brain characteristics, environmental factors and outcome.

#6 Conclusion

Using an unprecedented combination of diffusion MRI data and innovative analysis methods, our results confirmed that prematurity impacts early microstructural development of the primary SM network, even in low-risk preterm infants. We further found that these effects differ according to the level of prematurity and across the SM tracts, with the most rostral tracts as well as those involving S1 showing the greatest vulnerability to prematurity at TEA. Our study also showed the complementarity between DTI and NODDI models as well as the interest of using multiparametric approaches for assessing maturational processes and microstructural developmental differences. Longitudinal studies incorporating earlier MRI evaluation as well as behavioral follow-up through to later childhood would provide a better understanding of the impact of early-life disturbances in SM tracts microstructure on neurodevelopmental outcomes.

#7 References

- Adamson, C. L., Alexander, B., Ball, G., Beare, R., Cheong, J. L. Y., Spittle, A. J., et al. (2020). Parcellation of the neonatal cortex using Surface-based Melbourne Children's Regional Infant Brain atlases (M-CRIB-S). *Sci. Rep.* 10:4359. doi: 10.1038/s41598-020-61326-2
- Anderson, P. J., and Doyle, L. W. (2008). Cognitive and educational deficits in children born extremely preterm. *Semin. Perinatol.* 32, 51–58. doi: 10.1053/j.semperi.2007.12.009
- André, V., Durier, V., Beuchée, A., Roué, J.-M., Lemasson, A., Hausberger, M., et al. (2020). Higher tactile sensitivity in preterm infants at term-equivalent age: A pilot study. *PLoS One* 15:e0229270. doi: 10.1371/journal.pone.0229270
- Back, S. A. (2015). Brain Injury in the Preterm Infant: New Horizons for Pathogenesis and Prevention. *Pediatr. Neurol.* 53, 185–192. doi: 10.1016/j.pediatrneurol.2015.04.006

- Ball, G., Aljabar, P., Zebari, S., Tusor, N., Arichi, T., Merchant, N., et al. (2014). Rich-club organization of the newborn human brain. *Proc. Natl. Acad. Sci. U. S. A.* 111, 7456–7461. doi: 10.1073/pnas.1324118111
- Ball, G., Srinivasan, L., Aljabar, P., Counsell, S. J., Durighel, G., Hajnal, J. V., et al. (2013b). Development of cortical microstructure in the preterm human brain. *Proc. Natl. Acad. Sci. U. S. A.* 110, 9541–9546. doi: 10.1073/pnas.1301652110
- Ball, G., Boardman, J. P., Aljabar, P., Pandit, A., Arichi, T., Merchant, N., et al. (2013a). The influence of preterm birth on the developing thalamocortical connectome. *Cortex* 49, 1711–1721. doi: 10.1016/j.cortex.2012.07.006
- Barnett, M. L., Tusor, N., Ball, G., Chew, A., Falconer, S., Aljabar, P., et al. (2018). Exploring the multiple-hit hypothesis of preterm white matter damage using diffusion MRI. *NeuroImage Clin.* 17, 596–606. doi: 10.1016/j.nicl.2017.11.017
- Batalle, D., Edwards, A. D., and O’Muircheartaigh, J. (2018). Annual Research Review: Not just a small adult brain: Understanding later neurodevelopment through imaging the neonatal brain. *J. Child Psychol. Psychiatry* 59, 350–371. doi: 10.1111/jcpp.12838
- Batalle, D., Hughes, E. J., Zhang, H., Tournier, J.-D., Tusor, N., Aljabar, P., et al. (2017). Early development of structural networks and the impact of prematurity on brain connectivity. *NeuroImage* 149, 379–392. doi: 10.1016/j.neuroimage.2017.01.065
- Bayley, N. (2006). *Bayley Scales of Infant and Toddler Development*, 3rd Edn. San Antonio, TX: Harcourt Assessment.
- Beaulieu, C., and Allen, P. S. (1994). Determinants of anisotropic water diffusion in nerves. *Magn. Reson. Med.* 31, 394–400. doi: 10.1002/mrm.1910310408
- Behrens, T. E. J., Berg, H. J., Jbabdi, S., Rushworth, M. F. S., and Woolrich, M. W. (2007). Probabilistic diffusion tractography with multiple fibre orientations: What can we gain? *NeuroImage* 34, 144–155. doi: 10.1016/j.neuroimage.2006.09.018
- Brouwer, M. J., Kersbergen, K. J., van Kooij, B. J. M., Benders, M. J. N. L., van Haastert, I. C., Koopman-Esseboom, C., et al. (2017). Preterm brain injury on term-equivalent age MRI in relation to perinatal factors and neurodevelopmental outcome at two years. *PLoS One* 12:e0177128. doi: 10.1371/journal.pone.0177128
- Brummelte, S., Grunau, R. E., Chau, V., Poskitt, K. J., Brant, R., Vinall, J., et al. (2012). Procedural pain and brain development in premature newborns. *Ann. Neurol.* 71, 385–396. doi: 10.1002/ana.22267
- Chang, Y. S., Owen, J. P., Pojman, N. J., Thieu, T., Bukshpun, P., Wakahiro, M. L. J., et al. (2015). White Matter Changes of Neurite Density and Fiber Orientation Dispersion during Human Brain Maturation. *PLoS One* 10:e0123656. doi: 10.1371/journal.pone.0123656
- Christiaens, D., Cordero-Grande, L., Pietsch, M., Hutter, J., Price, A. N., Hughes, E. J., et al. (2021). Scattered slice SHARD reconstruction for motion correction in multi-shell diffusion MRI. *NeuroImage* 225:117437. doi: 10.1016/j.neuroimage.2020.117437
- Cordero-Grande, L., Hughes, E. J., Hutter, J., Price, A. N., and Hajnal, J. V. (2018). Three-dimensional motion corrected sensitivity encoding reconstruction for multi-shot multi-slice MRI: Application to neonatal brain imaging. *Magn. Reson. Med.* 79, 1365–1376. doi: 10.1002/mrm.26796
- De Bruïne, F. T., Van Wezel-Meijler, G., Leijser, L. M., Steggerda, S. J., Van Den Berg-Huysmans, A. A., Rijken, M., et al. (2013). Tractography of white-matter tracts in very preterm infants: A 2-year follow-up study. *Dev. Med. Child Neurol.* 55, 427–433. doi: 10.1111/dmcn.12099
- de Bruïne, F. T., van Wezel-Meijler, G., Leijser, L. M., van den Berg-Huysmans, A. A., van Steenis, A., van Buchem, M. A., et al. (2011). Tractography of developing white matter of the internal

- capsule and corpus callosum in very preterm infants. *Eur. Radiol.* 21, 538–547. doi: 10.1007/s00330-010-1945-x
- de Jong, M., Verhoeven, M., and van Baar, A. L. (2012). School outcome, cognitive functioning, and behaviour problems in moderate and late preterm children and adults: A review. *Semin. Fetal. Neonatal Med.* 17, 163–169. doi: 10.1016/j.siny.2012.02.003
- Dean, D. C., Lange, N., Travers, B. G., Prigge, M. B., Matsunami, N., Kellett, K. A., et al. (2017). Multivariate characterization of white matter heterogeneity in autism spectrum disorder. *NeuroImage Clin.* 14, 54–66. doi: 10.1016/j.nicl.2017.01.002
- Devisscher, L., Chauvel, M., Rolland, C., Labra, N., Aubrain, K., Leroy, F., et al. (2021). “Disentangling the differential maturation of sensorimotor cortices in newborns compared to adults,” in *Proceedings of the OHBM 2021 – Organization for human brain mapping, virtual meeting, France.*
- Dewey, D., Thompson, D. K., Kelly, C. E., Spittle, A. J., Cheong, J. L. Y., Doyle, L. W., et al. (2019). Very preterm children at risk for developmental coordination disorder have brain alterations in motor areas. *Acta Paediatr.* 1992, 1649–1660. doi: 10.1111/apa.14786
- Dibble, M., Ang, J. Z., Mariga, L., Molloy, E. J., and Bokde, A. L. W. (2021). Diffusion Tensor Imaging in Very Preterm, Moderate-Late Preterm and Term-Born Neonates: A Systematic Review. *J. Pediatr.* 232, 48–58.e3. doi: 10.1016/j.jpeds.2021.01.008
- Dubois, J., Adibpour, P., Poupon, C., Hertz-Pannier, L., and Dehaene-Lambertz, G. (2016). MRI and M/EEG studies of the White Matter Development in Human Fetuses and Infants: Review and Opinion. *Brain Plast.* 2, 49–69. doi: 10.3233/BPL-160031
- Dubois, J., Dehaene-Lambertz, G., Kulikova, S., Poupon, C., Hüppi, P. S., and Hertz-Pannier, L. (2014). The early development of brain white matter: A review of imaging studies in fetuses, newborns and infants. *Neuroscience* 276, 48–71. doi: 10.1016/j.neuroscience.2013.12.044
- Duerden, E. G., Foong, J., Chau, V., Branson, H., Poskitt, K. J., Grunau, R. E., et al. (2015). Tract-Based Spatial Statistics in Preterm-Born Neonates Predicts Cognitive and Motor Outcomes at 18 Months. *AJNR Am. J. Neuroradiol.* 36, 1565–1571. doi: 10.3174/ajnr.A4312
- Duerden, E. G., Grunau, R. E., Guo, T., Foong, J., Pearson, A., Au-Young, S., et al. (2018). Early Procedural Pain Is Associated with Regionally-Specific Alterations in Thalamic Development in Preterm Neonates. *J. Neurosci.* 38, 878–886. doi: 10.1523/JNEUROSCI.0867-17.2017
- Edwards, A. D., Rueckert, D., Smith, S. M., Abo Seada, S., Alansary, A., Almalbis, J., et al. (2022). The Developing Human Connectome Project Neonatal Data Release. *Front. Neurosci.* 16:886772. doi: 10.3389/fnins.2022.886772
- Edwards, J., Berube, M., Erlandson, K., Haug, S., Johnstone, H., Meagher, M., et al. (2011). Developmental coordination disorder in school-aged children born very preterm and/or at very low birth weight: A systematic review. *J. Dev. Behav. Pediatr.* 32, 678–687. doi: 10.1097/DBP.0b013e31822a396a
- Evensen, K. A. I., Ustad, T., Tikanmäki, M., Haaramo, P., and Kajantie, E. (2020). Long-term motor outcomes of very preterm and/or very low birth weight individuals without cerebral palsy: A review of the current evidence. *Semin. Fetal. Neonatal Med.* 25:101116. doi: 10.1016/j.siny.2020.101116
- Fabrizi, L., Slater, R., Worley, A., Meek, J., Boyd, S., Olhede, S., et al. (2011). A Shift in Sensory Processing that Enables the Developing Human Brain to Discriminate Touch from Pain. *Curr. Biol.* 21, 1552–1558. doi: 10.1016/j.cub.2011.08.010
- Fenchel, D., Dimitrova, R., Seidlitz, J., Robinson, E. C., Batalle, D., Hutter, J., et al. (2020). Development of Microstructural and Morphological Cortical Profiles in the Neonatal Brain. *Cereb. Cortex* 30, 5767–5779. doi: 10.1093/cercor/bhaa150

- Genc, S., Malpas, C. B., Holland, S. K., Beare, R., and Silk, T. J. (2017). Neurite density index is sensitive to age related differences in the developing brain. *NeuroImage* 148, 373–380. doi: 10.1016/j.neuroimage.2017.01.023
- Gibbins, S., Stevens, B., Beyene, J., Chan, P. C., Bagg, M., and Asztalos, E. (2008). Pain behaviours in Extremely Low Gestational Age infants. *Early Hum. Dev.* 84, 451–458. doi: 10.1016/j.earlhumdev.2007.12.007
- Gilmore, J. H., Knickmeyer, R. C., and Gao, W. (2018). Imaging structural and functional brain development in early childhood. *Nat. Rev. Neurosci.* 19, 123–137. doi: 10.1038/nrn.2018.1
- Girault, J. B., Munsell, B. C., Puechmaille, D., Goldman, B. D., Prieto, J. C., Styner, M., et al. (2019). White matter connectomes at birth accurately predict cognitive abilities at age 2. *NeuroImage* 192, 145–155. doi: 10.1016/j.neuroimage.2019.02.060
- Groeschel, S., Holmström, L., Northam, G., Tournier, J.-D., Baldeweg, T., Latal, B., et al. (2019). Motor Abilities in Adolescents Born Preterm Are Associated With Microstructure of the Corpus Callosum. *Front. Neurol.* 10:367. doi: 10.3389/fneur.2019.00367
- Groeschel, S., Tournier, J.-D., Northam, G. B., Baldeweg, T., Wyatt, J., Vollmer, B., et al. (2014). Identification and interpretation of microstructural abnormalities in motor pathways in adolescents born preterm. *NeuroImage* 87, 209–219. doi: 10.1016/j.neuroimage.2013.10.034
- Guerrero, J. M., Adluru, N., Bendlin, B. B., Goldsmith, H. H., Schaefer, S. M., Davidson, R. J., et al. (2019). Optimizing the intrinsic parallel diffusivity in NODDI: An extensive empirical evaluation. *PLoS One* 14:e0217118. doi: 10.1371/journal.pone.0217118
- Hatsopoulos, N. G., and Suminski, A. J. (2011). Sensing with the Motor Cortex. *Neuron* 72, 477–487. doi: 10.1016/j.neuron.2011.10.020
- Hernández, M., Guerrero, G. D., Cecilia, J. M., García, J. M., Inuggi, A., Jbabdi, S., et al. (2013). Accelerating fibre orientation estimation from diffusion weighted magnetic resonance imaging using GPUs. *PLoS One* 8:e61892. doi: 10.1371/journal.pone.0061892
- Hernandez-Fernandez, M., Reguly, I., Jbabdi, S., Giles, M., Smith, S., and Sotiropoulos, S. N. (2019). Using GPUs to accelerate computational diffusion MRI: From microstructure estimation to tractography and connectomes. *NeuroImage* 188, 598–615. doi: 10.1016/j.neuroimage.2018.12.015
- Hua, K., Zhang, J., Wakana, S., Jiang, H., Li, X., Reich, D. S., et al. (2008). Tract Probability Maps in Stereotaxic Spaces: Analyses of White Matter Anatomy and Tract-Specific Quantification. *NeuroImage* 39, 336–347. doi: 10.1016/j.neuroimage.2007.07.053
- Hughes, E. J., Winchman, T., Padormo, F., Teixeira, R., Wurie, J., Sharma, M., et al. (2017). A dedicated neonatal brain imaging system. *Magn. Reson. Med.* 78, 794–804. doi: 10.1002/mrm.26462
- Hutter, J., Tournier, J. D., Price, A. N., Cordero-Grande, L., Hughes, E. J., Malik, S., et al. (2018). Time-efficient and flexible design of optimized multishell HARDI diffusion. *Magn. Reson. Med.* 79, 1276–1292. doi: 10.1002/mrm.26765
- Jelescu, I. O., and Budde, M. D. (2017). Design and validation of diffusion MRI models of white matter. *Front. Phys.* 28:61. doi: 10.3389/fphy.2017.00061
- Jeurissen, B., Leemans, A., Tournier, J., Jones, D. K., and Sijbers, J. (2013). Investigating the prevalence of complex fiber configurations in white matter tissue with diffusion magnetic resonance imaging. *Hum. Brain Mapp.* 34, 2747–2766. doi: 10.1002/hbm.22099
- Jones, L., Verriotes, M., Cooper, R. J., Laudiano-Dray, M. P., Rupawala, M., Meek, J., et al. (2022). Widespread nociceptive maps in the human neonatal somatosensory cortex. *Elife* 11:e71655. doi: 10.7554/eLife.71655
- Kelly, C. E., Cheong, J. L. Y., Gabra Fam, L., Leemans, A., Seal, M. L., Doyle, L. W., et al. (2016a). Moderate and late preterm infants exhibit widespread brain white matter microstructure

- alterations at term-equivalent age relative to term-born controls. *Brain Imaging Behav.* 10, 41–49. doi: 10.1007/s11682-015-9361-0
- Kelly, C. E., Thompson, D. K., Chen, J., Leemans, A., Adamson, C. L., Inder, T. E., et al. (2016b). Axon density and axon orientation dispersion in children born preterm. *Hum. Brain Mapp.* 37, 3080–3102. doi: 10.1002/hbm.23227
- Kelly, C. E., Thompson, D. K., Genc, S., Chen, J., Yang, J. Y., Adamson, C., et al. (2020). Long-term development of white matter fibre density and morphology up to 13 years after preterm birth: A voxel-based analysis. *NeuroImage* 220, 117068. doi: 10.1016/j.neuroimage.2020.117068
- Keunen, K., Counsell, S. J., and Benders, M. J. N. L. (2017). The emergence of functional architecture during early brain development. *NeuroImage* 160, 2–14. doi: 10.1016/j.neuroimage.2017.01.047
- Keunen, K., Kersbergen, K. J., Groenendaal, F., Isgum, I., de Vries, L. S., and Benders, M. J. N. L. (2012). Brain tissue volumes in preterm infants: prematurity, perinatal risk factors and neurodevelopmental outcome: A systematic review. *J. Matern.-Fetal Neonatal Med.* 25, 89–100. doi: 10.3109/14767058.2012.664343
- Kimpton, J. A., Batalle, D., Barnett, M. L., Hughes, E. J., Chew, A. T. M., Falconer, S., et al. (2021). Diffusion magnetic resonance imaging assessment of regional white matter maturation in preterm neonates. *Neuroradiology* 63, 573–583. doi: 10.1007/s00234-020-02584-9
- Klein, A., and Tourville, J. (2012). 101 labeled brain images and a consistent human cortical labeling protocol. *Front. Neurosci.* 6:171. doi: 10.3389/fnins.2012.00171
- Knight, M. J., Smith-Collins, A., Newell, S., Denbow, M., and Kauppinen, R. A. (2018). Cerebral White Matter Maturation Patterns in Preterm Infants: An MRI T2 Relaxation Anisotropy and Diffusion Tensor Imaging Study. *J. Neuroimaging* 28, 86–94. doi: 10.1111/jon.12486
- Kostović, I., Sedmak, G., and Judaš, M. (2019). Neural histology and neurogenesis of the human fetal and infant brain. *NeuroImage* 188, 743–773. doi: 10.1016/j.neuroimage.2018.12.043
- Kulikova, S., Hertz-Pannier, L., Dehaene-Lambertz, G., Buzmakov, A., Poupon, C., and Dubois, J. (2015). Multi-parametric evaluation of the white matter maturation. *Brain Struct. Funct.* 220, 3657–3672. doi: 10.1007/s00429-014-0881-y
- Kunz, N., Zhang, H., Vasung, L., O'Brien, K. R., Assaf, Y., Lazeyras, F., et al. (2014). Assessing white matter microstructure of the newborn with multi-shell diffusion MRI and biophysical compartment models. *NeuroImage* 96, 288–299. doi: 10.1016/j.neuroimage.2014.03.057
- Leisman, G., Braun-Benjamin, O., and Melillo, R. (2014). Cognitive-motor interactions of the basal ganglia in development. *Front. Syst. Neurosci.* 8:16. doi: 10.3389/fnsys.2014.00016
- Li, X., Li, M., Wang, M., Wu, F., Liu, H., Sun, Q., et al. (2022). Mapping white matter maturational processes and degrees on neonates by diffusion kurtosis imaging with multiparametric analysis. *Hum. Brain Mapp.* 43, 799–815. doi: 10.1002/hbm.25689
- Linsell, L., Malouf, R., Morris, J., Kurinczuk, J. J., and Marlow, N. (2015). Prognostic Factors for Poor Cognitive Development in Children Born Very Preterm or With Very Low Birth Weight: A Systematic Review. *JAMA Pediatr.* 169, 1162–1172. doi: 10.1001/jamapediatrics.2015.2175
- Loh, W. Y., Anderson, P. J., Cheong, J. L. Y., Spittle, A. J., Chen, J., Lee, K. J., et al. (2017). Neonatal basal ganglia and thalamic volumes: Very preterm birth and 7-year neurodevelopmental outcomes. *Pediatr. Res.* 82, 970–978. doi: 10.1038/pr.2017.161
- Loh, W. Y., Anderson, P. J., Cheong, J. L. Y., Spittle, A. J., Chen, J., Lee, K. J., et al. (2020). Longitudinal growth of the basal ganglia and thalamus in very preterm children. *Brain Imaging Behav.* 14, 998–1011. doi: 10.1007/s11682-019-00057-z
- Machado-Rivas, F., Afacan, O., Khan, S., Marami, B., Velasco-Annis, C., Lidov, H., et al. (2021). Spatiotemporal changes in diffusivity and anisotropy in fetal brain tractography. *Hum. Brain Mapp.* 42, 5771–5784. doi: 10.1002/hbm.25653

- Mah, A., Geeraert, B., and Lebel, C. (2017). Detailing neuroanatomical development in late childhood and early adolescence using NODDI. *PLoS One* 12:e0182340. doi: 10.1371/journal.pone.0182340
- Maitre, N. L., Key, A. P., Chorna, O. D., Slaughter, J. C., Matusz, P. J., Wallace, M. T., et al. (2017). The Dual Nature of Early-Life Experience on Somatosensory Processing in the Human Infant Brain. *Curr. Biol.* 27, 1048–1054. doi: 10.1016/j.cub.2017.02.036
- Makropoulos, A., Gousias, I. S., Ledig, C., Aljabar, P., Serag, A., Hajnal, J. V., et al. (2014). Automatic whole brain MRI segmentation of the developing neonatal brain. *IEEE Trans. Med. Imaging* 33, 1818–1831. doi: 10.1109/TMI.2014.2322280
- Makropoulos, A., Robinson, E. C., Schuh, A., Wright, R., Fitzgibbon, S., Bozek, J., et al. (2018). The developing human connectome project: A minimal processing pipeline for neonatal cortical surface reconstruction. *NeuroImage* 173, 88–112. doi: 10.1016/j.neuroimage.2018.01.054
- McClendon, E., Chen, K., Gong, X., Sharifnia, E., Hagen, M., Cai, V., et al. (2014). Prenatal cerebral ischemia triggers dysmaturation of caudate projection neurons. *Ann. Neurol.* 75, 508–524. doi: 10.1002/ana.24100
- Miceli, P. J., Goeke-Morey, M. C., Whitman, T. L., Kolberg, K. S., Miller-Loncar, C., and White, R. D. (2000). Brief report: Birth status, medical complications, and social environment: Individual differences in development of preterm, very low birth weight infants. *J. Pediatr. Psychol.* 25, 353–358. doi: 10.1093/jpepsy/25.5.353
- Mörelus, E., Hellström-Westas, L., Carlén, C., Norman, E., and Nelson, N. (2006). Is a nappy change stressful to neonates? *Early Hum. Dev.* 82, 669–676. doi: 10.1016/j.earlhumdev.2005.12.013
- Nosarti, C., Nam, K. W., Walshe, M., Murray, R. M., Cuddy, M., Rifkin, L., et al. (2014). Preterm birth and structural brain alterations in early adulthood. *NeuroImage Clin.* 6, 180–191. doi: 10.1016/j.nicl.2014.08.005
- Odd, D. E., Lingam, R., Emond, A., and Whitelaw, A. (2013). Movement outcomes of infants born moderate and late preterm. *Acta Paediatr.* 1992, 876–882. doi: 10.1111/apa.12320
- Ouyang, M., Dubois, J., Yu, Q., Mukherjee, P., and Huang, H. (2019). Delineation of early brain development from fetuses to infants with diffusion MRI and beyond. *NeuroImage* 185, 836–850. doi: 10.1016/j.neuroimage.2018.04.017
- Padilla, N., Alexandrou, G., Blennow, M., Lagercrantz, H., and Ådén, U. (2015). Brain Growth Gains and Losses in Extremely Preterm Infants at Term. *Cereb. Cortex* 1991, 1897–1905. doi: 10.1093/cercor/bht431
- Pannek, K., George, J. M., Boyd, R. N., Colditz, P. B., Rose, S. E., and Fripp, J. (2020). Brain microstructure and morphology of very preterm-born infants at term equivalent age: Associations with motor and cognitive outcomes at 1 and 2 years. *NeuroImage* 221:117163. doi: 10.1016/j.neuroimage.2020.117163
- Pannek, K., Scheck, S. M., Colditz, P. B., Boyd, R. N., and Rose, S. E. (2014). Magnetic resonance diffusion tractography of the preterm infant brain: A systematic review. *Dev. Med. Child Neurol.* 56, 113–124. doi: 10.1111/dmcn.12250
- Parikh, M. N., Chen, M., Braimah, A., Kline, J., McNally, K., Logan, J. W., et al. (2021). Diffusion MRI Microstructural Abnormalities at Term-Equivalent Age Are Associated with Neurodevelopmental Outcomes at 3 Years of Age in Very Preterm Infants. *Am. J. Neuroradiol.* 42, 1535–1542. doi: 10.3174/ajnr.A7135
- Pecheva, D., Kelly, C., Kimpton, J., Bonthron, A., Batalle, D., Zhang, H., et al. (2018). Recent advances in diffusion neuroimaging: Applications in the developing preterm brain. *F1000Research* 7, F1000FacultyRev–1326. doi: 10.12688/f1000research.15073.1

- Pines, A. R., Cieslak, M., Larsen, B., Baum, G. L., Cook, P. A., Adebimpe, A., et al. (2020). Leveraging multi-shell diffusion for studies of brain development in youth and young adulthood. *Dev. Cogn. Neurosci.* 43:100788. doi: 10.1016/j.dcn.2020.100788
- Pogribna, U., Yu, X., Burson, K., Zhou, Y., Lasky, R. E., Narayana, P. A., et al. (2013). Perinatal Clinical Antecedents of White Matter Microstructural Abnormalities on Diffusion Tensor Imaging in Extremely Preterm Infants. *PLoS One* 8:e72974. doi: 10.1371/journal.pone.0072974
- Raghavan, S., Reid, R. I., Przybelski, S. A., Lesnick, T. G., Graff-Radford, J., Schwarz, C. G., et al. (2021). Diffusion models reveal white matter microstructural changes with ageing, pathology and cognition. *Brain Commun.* 3:fcab106. doi: 10.1093/braincomms/fcab106
- Rose, J., Mirmiran, M., Butler, E. E., Lin, C. Y., Barnes, P. D., Kermoian, R., et al. (2007). Neonatal microstructural development of the internal capsule on diffusion tensor imaging correlates with severity of gait and motor deficits. *Dev. Med. Child Neurol.* 49, 745–750. doi: 10.1111/j.1469-8749.2007.00745.x
- Schneider, J., Duerden, E. G., Guo, T., Ng, K., Hagmann, P., Bickle Graz, M., et al. (2018). Procedural pain and oral glucose in preterm neonates: Brain development and sex-specific effects. *Pain* 159, 515–525. doi: 10.1097/j.pain.0000000000001123
- Skranes, J., Vangberg, T. R., Kulseng, S., Indredavik, M. S., Evensen, K. A., Martinussen, M., et al. (2007). Clinical findings and white matter abnormalities seen on diffusion tensor imaging in adolescents with very low birth weight. *Brain J. Neurol.* 130, 654–666. doi: 10.1093/brain/awm001
- Spittle, A. J., and Orton, J. (2014). Cerebral palsy and developmental coordination disorder in children born preterm. *Semin. Fetal Neonatal Med.* 19, 84–89. doi: 10.1016/j.siny.2013.11.005
- Suzuki, K. (2007). Neuropathology of developmental abnormalities. *Brain Dev.* 29, 129–141. doi: 10.1016/j.braindev.2006.08.006
- Thompson, D. K., Inder, T. E., Faggian, N., Johnston, L., Warfield, S. K., Anderson, P. J., et al. (2011). Characterization of the corpus callosum in very preterm and full-term infants utilizing MRI. *NeuroImage* 55, 479–490. doi: 10.1016/j.neuroimage.2010.12.025
- Thompson, D. K., Kelly, C. E., Chen, J., Beare, R., Alexander, B., Seal, M. L., et al. (2019). Characterisation of brain volume and microstructure at term-equivalent age in infants born across the gestational age spectrum. *NeuroImage Clin.* 21:101630. doi: 10.1016/j.nicl.2018.101630
- Thompson, D. K., Loh, W. Y., Connelly, A., Cheong, J. L. Y., Spittle, A. J., Chen, J., et al. (2020). Basal ganglia and thalamic tract connectivity in very preterm and full-term children; associations with 7-year neurodevelopment. *Pediatr. Res.* 87, 48–56. doi: 10.1038/s41390-019-0546-x
- Thompson, R. J. Jr., Catlett, A. T., Oehler, J. M., Gustafson, K. E., Goldstein, R. F., and Prochaska, J. J. (1998). Home Environment and Developmental Outcome of African American and White Infants With Very Low Birthweight. *Child. Health Care* 27, 1–14. doi: 10.1207/s15326888chc2701_1
- Tomasino, B., and Gremese, M. (2016). The Cognitive Side of M1. *Front. Hum. Neurosci.* 10:298. doi: 10.3389/fnhum.2016.00298
- van den Heuvel, M. P., Kersbergen, K. J., de Reus, M. A., Keunen, K., Kahn, R. S., Groenendaal, F., et al. (2015). The Neonatal Connectome During Preterm Brain Development. *Cereb. Cortex* 1991, 3000–3013. doi: 10.1093/cercor/bhu095
- Van Hus, J. W., Potharst, E. S., Jeukens-Visser, M., Kok, J. H., and Van Wassenae-Leemhuis, A. G. (2014). Motor impairment in very preterm-born children: Links with other developmental deficits at 5 years of age. *Dev. Med. Child Neurol.* 56, 587–594. doi: 10.1111/dmcn.12295

- van Kooij, B. J. M., de Vries, L. S., Ball, G., van Haastert, I. C., Benders, M. J. N. L., Groenendaal, F., et al. (2012). Neonatal tract-based spatial statistics findings and outcome in preterm infants. *AJNR Am. J. Neuroradiol.* 33, 188–194. doi: 10.3174/ajnr.A2723
- van Pul, C., van Kooij, B. J. M., de Vries, L. S., Benders, M. J. N. L., Vilanova, A., and Groenendaal, F. (2012). Quantitative fiber tracking in the corpus callosum and internal capsule reveals microstructural abnormalities in preterm infants at term-equivalent age. *AJNR Am. J. Neuroradiol.* 33, 678–684. doi: 10.3174/ajnr.A2859
- Volpe, J. J. (2021). Primary neuronal dysmaturation in preterm brain: Important and likely modifiable. *J. Neonatal Perinat. Med.* 14, 1–6. doi: 10.3233/NPM-200606
- Williams, J., Lee, K. J., and Anderson, P. J. (2010). Prevalence of motor-skill impairment in preterm children who do not develop cerebral palsy: A systematic review. *Dev. Med. Child Neurol.* 52, 232–237. doi: 10.1111/j.1469-8749.2009.03544.x
- Wu, D., Chang, L., Akazawa, K., Oishi, K., Skranes, J., Ernst, T., et al. (2017). Mapping the Critical Gestational Age at Birth that Alters Brain Development in Preterm-born Infants using Multi-Modal MRI. *NeuroImage* 149, 33–43. doi: 10.1016/j.neuroimage.2017.01.046
- Yakovlev, P. I., and Lecours, A. R. (1967). “The Myelogenetic Cycles of Regional Maturation of the Brain,” in *Regional Development of the Brain in early Life* ScienceOpen, ed. A. Minkowski (Oxford: Blackwell), 3–69. doi: 10.1007/BF00192215
- Young, J. M., Vandewouw, M. M., Mossad, S. I., Morgan, B. R., Lee, W., Smith, M. L., et al. (2019). White matter microstructural differences identified using multi-shell diffusion imaging in six-year-old children born very preterm. *NeuroImage Clin.* 23:101855. doi: 10.1016/j.nicl.2019.101855
- Zhang, H., Schneider, T., Wheeler-Kingshott, C. A., and Alexander, D. C. (2012). NODDI: Practical in vivo neurite orientation dispersion and density imaging of the human brain. *NeuroImage* 61, 1000–1016. doi: 10.1016/j.neuroimage.2012.03.072
- Zhao, T., Mishra, V., Jeon, T., Ouyang, M., Peng, Q., Chalak, L., et al. (2019). Structural network maturation of the preterm human brain. *NeuroImage* 185, 699–710. doi: 10.1016/j.neuroimage.2018.06.047
- Zwicker, J. G. (2014). Motor impairment in very preterm infants: Implications for clinical practice and research. *Dev. Med. Child Neurol.* 56, 514–515. doi: 10.1111/dmcn.12454
- Zwicker, J. G., Grunau, R. E., Adams, E., Chau, V., Brant, R., Poskitt, K. J., et al. (2013). Score for neonatal acute physiology-II and neonatal pain predict corticospinal tract development in premature newborns. *Pediatr. Neurol.* 48, 123–129.e1. doi: 10.1016/j.pediatrneurol.2012.10.016

Afterword

The presented study aimed to characterize the effects of prematurity on the tracts of the primary SM network in a population of 59 low-risk preterm-born infants at TEA. We used DTI and NODDI-derived diffusion metrics to characterize the microstructure of specific SM tracts and compared them to a reference group of full-term infants using a multiparametric Mahalanobis distance. This approach allowed us to assess the effects of prematurity while considering the natural developmental variability and complementarity of multiple diffusion metrics.

Our findings suggested that prematurity affects the primary SM network at TEA, with more pronounced effects in infants born at earlier gestational ages. We revealed complex patterns of prematurity's impact, showing greater effects in more rostral and peripheral tracts. This trajectory aligns with known global white matter maturation patterns that progress in caudal-to-rostral and central-to-peripheral fashion (Yakovlev & Lecours, 1967).

The use of multiparametric Mahalanobis distance, instead of univariate approaches, provided a more detailed and easier to interpret description of SM network vulnerability to preterm birth. The sensitivity of our approach to the alteration of the SM microstructure with potential neurodevelopmental consequences was further supported by the uncovered associations between the (NODDI-derived) Mahalanobis distances for certain tracts with the infant motor and cognitive outcomes at 18mCA.

In summary, our investigation of the SM network at TEA within the context of prematurity offered valuable insights into atypical brain development. However, while this group-wise assessment enhanced our understanding of potential origins of neurodevelopmental delays, it was not well adapted to guide the individual early identification of at-risk infants which would be beneficial for instructing timely interventions. In the next chapter, we explore machine learning techniques for more personalized predictions of neurodevelopmental outcomes.

Poster:

Early structural connectivity within the sensorimotor networks: evaluating the impact of prematurity with a multiparametric approach

Andrea Gondova^{1,2*}, Sara Neumann^{1,2,3*}, Yann Leprince², Lucie Hertz-Pannier^{1,2}, Tomoki Arichi^{3,4}, Jessica Dubois^{1,2}

¹Université Paris Cité, Inserm, NeuroDiderot, F-75019 Paris, France

²Université Paris-Saclay, CEA, NeuroSpin, UNIACT, F-91191, Gif-sur-Yvette, France

³Centre for the Developing Brain, School of Biomedical Engineering and Imaging Sciences, King's College London, London SE1 7EH, United Kingdom

⁴Paediatric Neurosciences, Evelina London Children's Hospital, Guy's and St Thomas' NHS Foundation Trust, London SE1 7EH, United Kingdom

* These authors have contributed equally to this work and share first authorship

* Corresponding Author: Andrea.Gondova@cea.fr



Introduction

Sensorimotor (SM) system:

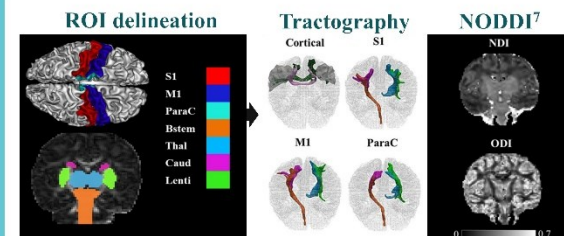
- network of cortical and subcortical grey matter regions
- rapid maturation during the perinatal period^{1,2}
- supports development of sensory and motor functions³
- particularly vulnerable to preterm birth⁴

AIMS:

- Explore prematurity impact on the microstructural maturation of SM tracts (in infants at term-equivalent age)
- Investigate relationship with neurodevelopmental outcome
- (at 18 months of corrected age)

Methods

- 3T anatomical and diffusion MRI data (developing Human Connectome Project)^{5,6}
- **33 extremely/very preterm (PT) infants**
 - (no major brain lesions)
 - 54.5 % male
 - Gestational age at birth: [23.7-31.9]w
 - Post-menstrual age at MRI: [38.4-45.0]w
- **59 term-born (FT) infants**
 - 55.9% male
 - Gestational age at birth: [37.4-42.3]w
 - Post-menstrual age at MRI: [38.4-44.9]w



SI: postcentral gyrus, MI: precentral gyrus, ParaC: paracentral area, Bstem: brainstem, Thal: thalamus, Caud: caudate nucleus, Lenti: lentiform nucleus *intra-hemispheric tracts evaluated in left and right hemispheres, then averaged.

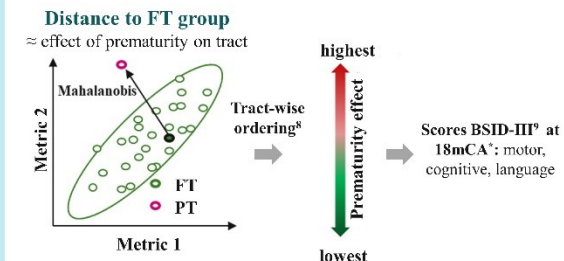


Figure 1. Overview of the processing pipeline

Results

- Microstructural differences in all SM tracts between PT and FT infants at TEA
- Weak or no effect of main perinatal clinical risk factors (including sex, preterm comorbidities, multiple pregnancy, intra-uterine growth restriction and parenteral nutrition), likely due to the limited cohort size

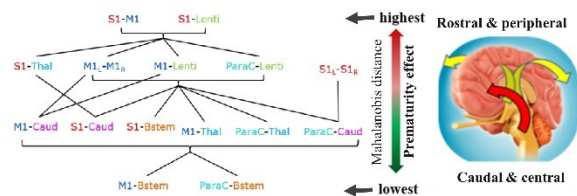


Figure 2. SM tract ordering in the PT group based on Mahalanobis distance for NDI and ODI metrics (higher values on top). The pairwise lines link the tracts that differ significantly in terms of their vulnerability to prematurity (paired t-tests Benjamini-Hochberg false discovery rate correction, $p < 0.1$).

- Vulnerability patterns of the tract microstructure: i. follows the established WM caudo-rostral developmental sequence: rostral tracts present the strongest alterations at TEA and ii., presents differences between somatosensory and motor tracts (Figure 2).
- For some tracts, the maturational distances related to prematurity seemed correlated to cognitive and fine motor neurodevelopmental outcome at 18 m corrected age (Figure 3).

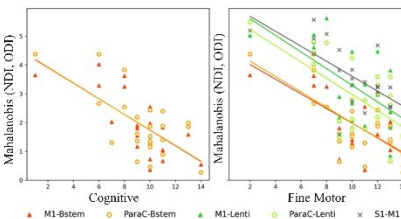


Figure 3. Significant correlations between Mahalanobis distances and BSID-III scores at 18-m CA presented for some tracts as scatter plots of the significant Pearson correlations.

Conclusion

- We described differential alterations of the SM network in relation to prematurity and long-term neurodevelopment,
- The study highlighted interest in using multiparametric approaches to characterize microstructural development
- We demonstrated potential for the identification of neuroimaging markers of neurodevelopmental disorders in infants, with special interest for subtle neuromotor impairments frequently observed in preterm-born children.

References

[1] Dubois et al., (2014), Neuroscience [2] Kostović et al., (2019), NeuroImage [3] Gilmore et al., (2018), Nat. Rev. Neurosci. [4] Parikh et al., (2021), J. Neurosci. [5] Makropoulos et al., (2018), NeuroImage [6] Christiaens et al., (2021), NeuroImage [7] Zhang et al., (2012), NeuroImage [8] Kulikova et al., (2015), Brain Struct. Funct. [9] Bayley (2006), Tech. Man. Psychol. Corp.

Acknowledgements

This project has received funding from the European Union's Horizon 2020 research and innovation programme under grant agreement No 800945 – NUMERICS – 112020-MSCA-COFUND-2017. The developing Human Connectome Project was funded by the European Research Council under the European Union Seventh Framework Programme (FP7/2007–2013)/ERC Grant Agreement no. 319456.

Chapter 4: Individual prediction of specific features and developmental outcomes

Preface

Numerous studies have demonstrated the importance of early MRI in detecting significant brain alterations in premature infants (Banihani et al., 2021) and their association with later outcomes (van't Hooft et al., 2015; Vo Van et al., 2022). While group studies provide valuable insights, they are not adapted for individual outcome prediction. To mitigate this, recent research has turned to predictive modelling using supervised machine learning to establish data-driven relationships between early MRI-derived markers and output labels, for example to detect new patterns of atypical development between preterm and full-term infants or predict adverse neurodevelopmental outcomes. These advancements might facilitate the development of reliable descriptive, predictive, and recommendation tools to enhance our understanding of altered brain development and improve early detection and intervention strategies in the future.

In this chapter, we present three studies in which we employed machine learning to evaluate the implications of early brain developmental markers on later outcomes. Firstly (*section 4.1*), we outline our attempt at predicting adverse neurodevelopmental alterations by analysing microstructural descriptors of the sensorimotor network derived in the preceding chapter. Next (*section 4.2*), we present a conceptual replication of a previous study that described a successful neurodevelopmental outcome prediction strategy based on the cortical microstructure (Ouyang et al., 2020). However, our inability to replicate the findings despite a larger dataset and extended validation steps, emphasized the need for more standardized approaches and external validation to ensure the reliability and positive impact of these applications in infant care in the future. It further brings to the forefront the ongoing discussion about the replicability problems facing machine learning applications. Lastly (*section 4.3*), we present our study on the prematurity status prediction that aimed to discriminate PT infants at TEA and FT neonates based on their cortical microstructure, confirming significant alterations between the two populations in a data-driven manner.

4.1. Potential of the SM network characterization for predicting outcomes

In the preceding chapter, we demonstrated the significant impact of prematurity on the microstructural characteristics of the SM network, even in infants classified as low-risk. Moreover, we suggested a plausible connection between alterations in the SM network and subsequent neurodevelopmental outcomes through “simple” correlation analyses. In this study, we aimed to expand on this observation by attempting to establish a link between the early microstructural features of the SM network at TEA and neurodevelopmental outcomes at 18m CA using predictive modelling. This is a relevant clinical question as 18mCA corresponds to a key period for assessing severe neurodevelopmental impairments, some of which lead to specific diagnoses like cerebral palsy. By identifying potential biomarkers of neurodevelopmental delays from early scans at TEA, this and similar studies might offer new avenues to improve the early identification of at-risk individuals, which is essential to set up timely interventions to improve long-term outcomes and quality of life for these children.

This section first presents briefly the previously post-processed dHCP data of preterm and full-term born infants, then provides a description of the implemented predictive pipeline, followed by a short summary of the results. The chapter ends with the poster presented at the annual scientific meeting of the Organisation for Human Brain Mapping (OHBM) 2023 which summarizes this work (Gondová et al., 2023c).

4.1.1. Methods

4.1.1.1. Description of the data

- **Subjects**

The presented study included anatomical and diffusion MRI data from the dHCP database of 118 infants (59 FT and 59 PT, 56% males, gestational age (GA) at birth: median 36.7 weeks [23.7w–42.3w]; post-menstrual age (PMA) at MRI: median 41.3 weeks [38.3w–44.9w]). None of the subjects had brain abnormalities detected on MR images (Neumane et al, 2022).

- **Subject-specific SM microstructural profile**

The SM microstructural profiles for each subject were characterized by tract-specific diffusion metrics (AD, RD, MD, FA, NDI, and ODI) derived from probabilistic dissections of the SM network performed in Neumane et al., (2022). The six weighted average diffusion metrics were calculated per tract, with intra-hemispheric tracts

evaluated in left and right hemispheres separately and then averaged. Resulting individual infant microstructural profiles consisted of 90 features (15 tracts x 6 diffusion metrics). These profiles were used as inputs to continuous machine learning (ML) models after dimensionality reduction with linear principal component analysis (PCA).

- **Subject characteristics at 18 months of corrected age (CA)**

Neurodevelopmental assessment was available for 88 out of 118 subjects with Bayley Scales of Infant and Toddler Development, Third Edition (BSID-III) at median corrected age 18 months (range: 17–21). As expected in this low-risk cohort, we did not observe any major developmental delays or specific disabilities in the included infants, with the majority of the scaled (and composite) BSID-III scores falling into the norm (Neumane et al., (2022): Figure 2; in this manuscript *Figure 3.2.*). As we expected potential neuromotor impairments to have a bigger impact on the fine than gross motor skills of the infants, we chose to focus mostly on the analysis of the scaled BSID-III scores: cognitive, receptive language, expressive language, fine motor, and gross motor scaled scores.

- **Clinical features**

Although exploring the associations between early brain markers and long-term outcomes is a relevant clinical question, it is essential to recognize that as infants develop, perinatal risk factors may become less influential compared to environmental factors, for example socio-familiar context, which gain importance in the neurodevelopmental interindividual variability (Miceli et al., 2000; Anderson & Doyle, 2008; Linsell et al., 2015). Incorporating information on such factors might enhance outcome prediction at 18m CA. Thus, alongside the SM microstructural characteristics, we assessed the advantages of integrating selected sociodemographic and clinical features previously associated with neurodevelopmental outcomes. These features include sex, GA at birth, birth weight, multiple pregnancy, intrauterine growth restriction (IUGR), preterm comorbidities, Apgar scores at 1 and 5 min, and index of multiple deprivation (IMD) scores (Chandwani et al., 2021; Pierrat et al., 2021b and others).

For more detailed description of the cohort, MRI acquisition and preprocessing, delineation of ROIs, SM network dissections, and estimation of tract-based microstructural characteristics, we refer readers to our publication: Neumane et al., 2022.

4.1.1.2. Predictive pipeline

To address the challenge posed by the high dimensionality of our input data (consisting of 90 SM features) compared to the limited sample size of infants with available BSID-III outcomes (88 preterm and full-term infants), we first performed a dimensionality reduction step using Principal Component Analysis (PCA) (Hotelling, 1933). PCA decomposition was performed on a separate set of 30 subjects, referred to as the ‘PCA set’, which included 21 infants with SM descriptors but lacking outcome measures (including 9 extreme-very preterm, 6 moderate-low preterm, and 6 full-term infants), and 9 randomly selected full-term infants to balance the preterm/full-term ratio. During the PCA, each input feature was first independently standardized across the ‘PCA set’. Any missing values in the clinical inputs were imputed with medians. It's worth noting that the computation of medians for imputations and normalization scaling parameters, as well as fitting of the PCA model were limited to the 'PCA set' and subsequently applied to the remaining 88 infants. This approach minimized the necessity of incorporating PCA into the internal validation loop and ensured there was no information leakage between PCA fits and the training and validation of the predictive algorithms. The number of principal components retained as inputs for the predictive models was determined based on a 95% threshold of cumulative explained variance.

Subsequently, we carried out prediction of each BSID-III scaled score at 18mCA based on individual SM microstructural profiles using both linear regression and Gradient Boosting (GB) regression models. Additionally, to leverage the known high internal consistency among BSID-III scores, implying relationships between prediction tasks, we explored a multi-task setting employing Multi-task Lasso Regression (ML), which combined the 5 different BSID-III scaled scores.

The predictive models were implemented using scikit-learn 1.0.1 (Pedregosa et al., 2011). During model training, 75% of the data (66 infants for the train/test set) was employed for initial assessments and hyperparameter optimization in both single and multi-task settings. Random search hyperparameter optimization for both GB and Multi-task Lasso regression models was assessed using leave-one-out cross-validation (LOOCV).

We evaluated the performance of these trained models in predicting the 5 continuous BSID-III scaled scores using two key metrics: the coefficient of determination (R^2) and the mean absolute error (MAE). R^2 serves as a widely recognized metric for assessing predictive regressors. Positive R^2 scores nearing one indicate effective prediction, while values equal to or below zero signify either a model that disregards the inputs entirely (constant) or one that

performs worse than a constant model. MAE, on the other hand, calculates the arithmetic mean of the absolute differences between paired observations, with lower MAE values indicating closer alignment between the predictive model outputs and the known scores in the testing set.

For the final evaluation, we first established a baseline prediction by running a dummy (constant) regression model that consistently predicted the mean of the outcome scores. This baseline provided a theoretical threshold for our prediction setting. Linear regression models, along with GB and Lasso models with hyperparameter settings associated with the lowest MAE and highest R2 during the optimisation step, were subsequently retrained on the entire training dataset. These models were then assessed on a previously unseen hold-out set (25% of the data involving 22 subjects). Predictive performance was once again quantified using R2 and MAE scores, allowing for a comparison with the theoretical baseline threshold.

An overview of the predictive pipeline is visualized in *Figure 4.1*.

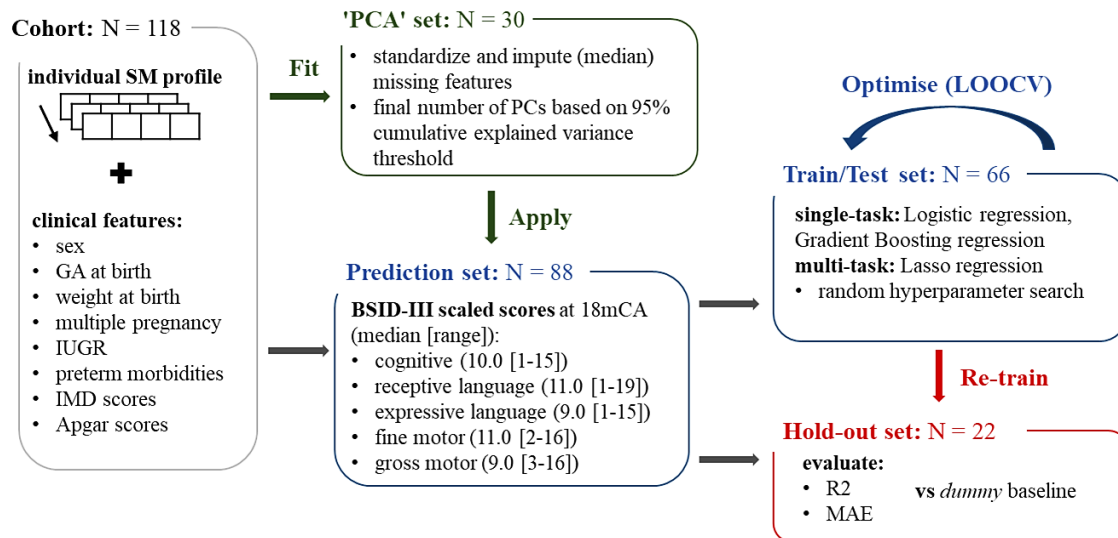


Figure 4.1. Overview of the predictive pipeline. Inputs to the pipeline consisted of individual SM profiles and clinical features (to determine the optimal input vector, different combinations of clinical and tract-specific diffusion features were tested). PCA was first performed on the independent 'PCA set' (N=30 without outcome BSID-III data) to reduce the input dimensionality and applied to the *prediction set* (N=88) before the training, optimisation, and testing of the continuous single-task and multi-task models using train/test subsets (N=66). The overall predictive performance was evaluated on a hold-out set (N=22) with coefficient of determination (R2) and mean absolute error (MAE) and compared to the results of a *dummy* baseline (outputting mean of the training data). **Legend:** IUGR: intrauterine growth restriction; IMD: Index of multiple deprivation; PC: principal component; LOOCV: leave-one-out cross-validation.

4.1.2. Results

Among PT and FT subjects with available outcome assessment (training set N=88), SM network microstructure at TEA was not found to be predictive of BSID-III scaled scores at 18mCA. Including the selected clinical and environmental features did not improve the predictive models. The predictive models (linear regression, GB, and multi-task Lasso) in all of the input settings performed worse or equally to a baseline predictor (dummy predictor outputting mean of the training data) which produced R^2 of -0.083 for Cognitive, -0.068 for Receptive Communication, -0.005 for Expressive Communication, -0.019 for Fine Motor, and -0.006 for Gross Motor scaled scores.

4.1.3. Conclusion

In our investigation of the link between SM network microstructure and neurodevelopmental outcomes using machine learning, the limited sample size posed challenges due to dimensionality issues, affecting model performance and generalization. To address this, we employed PCA to reduce feature dimensions, aiming to balance data reduction with information retention by selecting components based on a 95% cumulative explained variance threshold. Overall, only a small number of PCs were retained suggesting rather high information redundancy within the SM network. However, it is possible that linear PCA might not be completely appropriate to describe potential non-linear relationships between the SM features and the investigation into the use of non-linear dimensionality reduction strategy might be beneficial (although, our experiments with non-linear kernel PCA did not improve the predictive results). Despite these efforts, our predictive models, including linear regression, GB, and multi-task Lasso, performed similarly or worse than a baseline predictor on the independent hold-out set. These results indicate that the dimensionality reduction approach may not be suitable for our specific context. Alternatively, the estimated SM network microstructure in our analysis pipeline may not contain information relevant to explaining the subtle differences observed in the outcomes of our cohort.

Several additional factors likely contributed to these negative outcomes. The most straightforward explanation is that the selected inputs lack predictive power for neurodevelopmental outcomes at 18mCA. This could be attributed to the relatively low functional variability of SM tract microstructure at TEA, which may require the inclusion of additional brain networks related to higher-order functions for reliable predictions.

Another plausible explanation is the homogeneity of our cohort, primarily composed of low-risk preterm infants and healthy full-term newborns. Their limited variability in

neurodevelopmental scores might have hindered predictive modelling. Furthermore, the inclusion of additional environmental and clinical variables did not improve predictions, possibly due to the narrow distribution of available clinical information and BSID-III scores within our training data.

To address these limitations, future research may benefit from a larger and more diverse dataset with greater outcome variability, potentially enabling a more robust relationship between SM network microstructure and neurodevelopmental outcomes.

Poster:

Predicting neurodevelopmental outcomes from the early sensorimotor structural connectivity

Gondova Andrea^{1,2*}, Neumane Sara^{1,2,3}, Leprince Yann², Arichi Tomoki^{3,4}, Mangin Jean-François⁵, Dubois Jessica^{1,2}

¹Université Paris Cité, Inserm, NeuroDiderot, F-75019 Paris, France

²UNIACT, NeuroSpin, CEA, Université Paris-Saclay, F-91191, Gif-sur-Yvette, France

³Centre for the Developing Brain, School of Biomedical Engineering and Imaging Sciences, King's College London, London SE1 7EH, United Kingdom

⁴Paediatric Neurosciences, Evelina London Children's Hospital, Guy's and St Thomas' NHS Foundation Trust, London SE1 7EH, United Kingdom

⁵Université Paris-Saclay, CEA, CNRS, NeuroSpin, BAOBAB, Gif-sur-Yvette, France

* Corresponding Author: Andrea.Gondova@cea.fr



Introduction

Sensorimotor (SM) system:

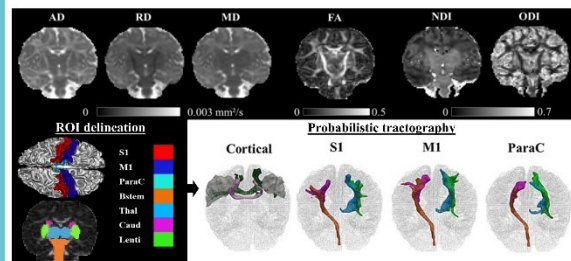
- distributed cortical and subcortical grey matter regions connected through white matter tracts
- rapid and critical maturation during early human life, as emphasized by the adverse effects of preterm birth¹⁻⁴.
- systematic relationship between early SM network structural alterations and later behavioural impairment has been little explored in low-risk preterm infants (moderate to late preterm and/or without perinatal brain injury).

AIMS:

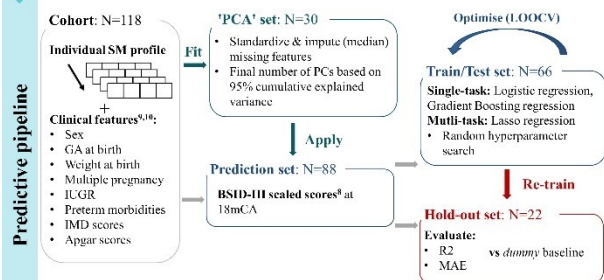
- explore whether the microstructural properties of the SM tracts in full-term (FT) and preterm (PT) infants at term equivalent age (TEA) can predict later neurodevelopmental outcome at 18 months of age.

Methods

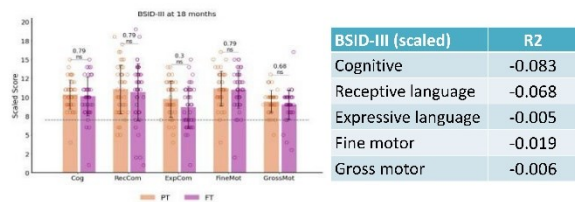
- 3T anatomical and diffusion MRI data (developing Human Connectome Project)^{5,6}
- 118 infants without major brain lesions:
 - 59 full-term and 59 preterm
 - 56% male
 - Gestational age at birth: median 36.7 [23.7–42.3]w
 - Post-menstrual age at MRI: median 41.3 [38.3–44.9]w



SI: postcentral gyrus, M1: precentral gyrus, ParaC: paracentral area, Bstem: brainstem, Thal: thalamus, Caud: caudate nucleus, Lenti: lentiform nucleus *intra-hemispheric tracts evaluated in left and right hemispheres, then averaged.



Results



- predictive models in all of the input settings performed worse or similar to baseline predictor
- results were not improved by clinical features previously described as associated with neurodevelopmental outcome¹⁰

Conclusion

- primary SM network microstructure at TEA was not predictive of BSID-III scaled scores at 18mCA
- multiple factors might explain the current results, e.g.:
 - cohort selection bias towards the low-risk infants leading to low microstructural variability of inputs and/or narrow distribution of the BSID-III scores and clinical features
 - sub-optimal SM microstructure description with tract-specific diffusion metrics followed by dimensionality reduction
 - focus limited to the SM network combination with higher-order functional networks might be necessary for the prediction of complex behavioural scores

FUTURE PERSPECTIVE:

- acute need for reliable early identification of at-risk infants to personalise care, several perspectives to be explored in future:
 - use of a larger, more heterogeneous dataset
 - refinement of SM microstructural profiles and the predictive pipeline
 - incorporating complementary MRI markers

References

[1] Gilmore et al., (2018), Nat. Rev. Neurosci. [2] Suzuki et al., (2007), Brain Dev. [3] Pierrat et al., (2021), BMJ [4] Dewey et al., (2019), Acta Paediatr. Oslo Nor. [5] Makropoulos et al., (2018), NeuroImage [6] Christiaens et al., (2021), NeuroImage [7] Hernandez-Fernandez et al., (2019), NeuroImage [8] Bayley (2006), Tech. Man. Psychol. Corp. [9] Neumane et al., (2022), Front. Neurosci. [10] Parikh et al., (2021), J. Neuroradiol.

Acknowledgements



This project has received funding from the European Union's Horizon 2020 research and innovation programme under grant agreement No 800945 – NUMERICS – H2020-MSCA-COFUND-2017. The developing Human Connectome Project was funded by the European Research Council under the European Union Seventh Framework Programme (FP/2007–2013)/ERC Grant Agreement no. 319456.

4.2. Cortical microstructure as a biomarker for early prediction of outcomes

In the preceding section, we reported that despite the significant relationship between SM alterations and later neurodevelopmental outcomes in PT infants, utilizing tract-based microstructural descriptors of the SM alone proved insufficient for successful individual outcome prediction in our study and highlighted the difficulties of translating group-based observation to specific individual subjects. Given the important need for early and reliable identification of infants at risk of adverse neurodevelopmental outcomes, we were interested to further explore alternative inputs to the predictive modelling strategy.

Prior research has reported successful prediction in PT and FT infants using diverse sets of input features derived from anatomical, diffusion, as well as resting-state functional MRI (*Section 1.3.4*). One of those studies presented promising results at predicting continuous neurodevelopmental outcomes at 2 years based on cortical microstructural fractional anisotropy (Ouyang et al., 2020). However, this study was conducted on a limited dataset of 46 PT and FT subjects and was evaluated using a leave-one-out-validation strategy. Acknowledging the potential for inflated predictive results in such settings, we aimed to conceptually replicate this approach by incorporating a much larger dataset of subjects (dHCP) with similar ages at birth and at scan (295 infants). Additionally, we extended the validation strategy to nested cross-validation, which included additional hyperparameter tuning, and used baseline predictors to validate the implementation of the predictive pipeline for simpler predictive tasks: gestational age (GA) at birth, prediction of infant prematurity status (categorized GA at birth with 37 weeks threshold), as well as categorized outcome scores.

Our inability to conceptually replicate the reported results of the original study aligns with previously reported replicability issues within the machine learning domain and underscores the challenges with establishing a robust set of practices for implementing reliable and generalisable predictive tools in the early neurodevelopmental research, as well as other related fields. The presented investigations were published as a full-length article in the journal *Neuroimage: Reports* (see the article included in the following section: Gondová et al., (2023a)).

Paper: Predicting neurodevelopmental outcomes from neonatal cortical microstructure: A conceptual replication study.

Andrea Gondova^{1,2}, Sara Neumane^{1,2,6}, Yann Leprince², Jean-François Mangin³, Tomoki Arichi^{4,5} Jessica Dubois^{1,2}

1. Université Paris Cité, Inserm, NeuroDiderot, F-75019 Paris, France

2. Université Paris-Saclay, CEA, NeuroSpin UNIACT, F-91191, Gif-sur-Yvette, France

3. Université Paris-Saclay, CEA, CNRS, NeuroSpin, BAOBAB, Gif-sur-Yvette, France

4. Centre for the Developing Brain, School of Biomedical Engineering and Imaging Sciences, King's College London, London SE1 7EH, United Kingdom

5. Paediatric Neurosciences, Evelina London Children's Hospital, Guy's and St Thomas' NHS Foundation Trust, London SE1 7EH, United Kingdom

Reference: Gondova, A., Neumane, S., Leprince, Y., Mangin, J.F., Arichi, T., & Dubois, J. (2023). Predicting neurodevelopmental outcomes from neonatal cortical microstructure: A conceptual replication study. *Neuroimage: Reports*.

#1 Abstract

Machine learning combined with large-scale neuroimaging databases has been proposed as a promising tool for improving our understanding of the behavioural emergence and early prediction of the neurodevelopmental outcome. A recent example of this strategy is a study by Ouyang et al., (2020) which suggested that cortical microstructure quantified by diffusion MRI through fractional anisotropy (FA) metric in preterm and full-term neonates can lead to effective prediction of language and cognitive outcomes at 2 years of corrected age as assessed by *Bayley Scales of Infant and Toddler Development, Third Edition* (BSID-III) composite scores. Given the important need for robust and generalisable tools which can reliably predict the neurodevelopmental outcome of preterm infants, we aimed to replicate the conclusions of this work using a larger independent dataset from the *developing Human Connectome Project* dataset (dHCP, third release) with early MRI and BSID-III evaluation at 18 months of corrected age. We then aimed to extend the validation of the proposed predictive pipeline through the study of different cohorts (the largest one included 295 neonates, with gestational age between 29 and 42 week and post-menstrual age at MRI between 31 and 45 weeks). This allowed us to evaluate whether some limitations of the original study (mainly small sample size and limited variability in the input and output features used in the predictive models) would influence the prediction results. In contrast to the original study that inspired the current work, our prediction results did not outcompete the random levels. Furthermore, these negative results persisted even when the study settings were expanded. Our findings

* first co-authors

suggest that the cortical microstructure close to birth described by DTI-FA measures might not be sufficient for a reliable prediction of BSID-III scores during toddlerhood, at least in the current setting, i.e. generally older cohorts and a different processing pipeline. Our inability to conceptually replicate the results of the original study is in line with the previously reported replicability issues within the machine learning field and demonstrates the challenges in defining the good set of practices for the implementation and validation of reliable predictive tools in the neurodevelopmental (and other) fields.

#2 Introduction

The human brain undergoes dynamic and complex structural and functional development during the pre- and perinatal period (Silbereis, et al., 2016; Parikh, 2016; Ouyang, et al., 2019a; Kostović, et al., 2019), driven by several cellular and molecular mechanisms that show heterogenous progression at both spatial and temporal levels. Deviations from the normal developmental sequence due to events like preterm birth can have profound and long-term effects, including motor, cognitive, and language deficits (Johnston, 2009; Hadaya & Nosarti, 2020). However, these are typically not observed until their acquisition during early childhood (e.g. around 18 months for independent walking) leading to relatively late diagnosis despite the perinatal onset of underlying brain abnormalities (Arpi & Ferrari, 2013; Parikh, 2016; Marín, 2016). As personalised neuroprotective and rehabilitation interventions are likely to be most effective early in infancy when neuroplasticity is enhanced (Blauw-Hospers, et al., 2007; Pickler, et al., 2010; Müller, et al., 2017), the ability to identify at-risk neonates in the first few weeks after birth could have major public health benefits through improving the quality of life of potentially affected children and their families. In this context, markers of abnormal early brain development such as those provided by non-invasive magnetic resonance imaging (MRI) have a clear role in predicting brain development trajectories and infant behavioural outcomes. Moreover, this can be further enhanced by combining extracted features with sophisticated, infant-adapted machine learning (ML) strategies (see Baker & Kandasamy (2022) for a review focused on premature infants).

In this vein, Ouyang et al., (2020) recently proposed one such strategy based on diffusion tensor imaging (DTI) and cortical microstructure at birth using regional fractional anisotropy (FA) measures as inputs. FA is thought to directly reflect the cellular and molecular processes underlying cortical development during the preterm period (e.g. growth of radial glia projections and apical dendrites, development of multi-orientation intra-cortical connections, proliferation of membranes) (Ball, et al., 2013; Ouyang, et al., 2019a). Ouyang's study thus

tested the hypothesis that regional FA measures in preterm and full-term neonates could serve as a useful biomarker for the prediction of distinctive aspects of later neurodevelopmental outcome assessed with *Bayley Scales of Infant and Toddler Development, Third Edition* (BSID-III) at around 2 years of corrected age. Their results suggested that inter-individual variability of cortical microstructure at birth provided sufficient information for successful and robust prediction of later cognitive and language outcomes using linear support vector regression (SVR). Additionally, based on the evaluation of model feature importance, the authors suggested that the distinctive features were encoded in uniquely distributed patterns across the cerebral cortex.

Despite these promising results, the authors of this original study remained cautious given the limitations of their strategy, highlighting the small dataset (46 infants) as one of the major problems affecting the potential generalisability of their proposed method to the wider population. Additionally, motor outcomes in their dataset could not be predicted, although they suggested that it was unclear whether these null results resulted from insufficient heterogeneity within the cohort (in terms of cortical inputs and/or outcome scores) or other factors such as low signal-to-noise ratio (SNR) of cortical FA in primary sensorimotor cortical regions associated with motor function. Given these limitations and the important need for robust and generalisable tools which can reliably predict the neurodevelopmental outcome of preterm infants, this original study seemed to us an ideal target for conceptual replication. As opposed to direct replication, conceptual replication aims to test the generality of the original suggestion, i.e. that cortical FA close to birth is predictive of later neurodevelopmental outcome, with a different but similarly reliable method (Zwaan et al., 2017).

In short, in the present study, we aimed to examine whether cortical microstructure close to birth –assessed with regional FA measures - is predictive of later neurodevelopmental outcomes in an independent dataset with early MRI acquired in neonates and behavioural follow-up as part of the “developing Human Connectome Project” (dHCP). To test this, our goal was to replicate the original study of Ouyang et al., (2020) as closely as possible given the available information. Importantly, we opted for a different but robust processing pipeline: differences are specified in detail within the methods and discussion sections. Additionally, we expanded the predictive pipeline by incorporating model tuning and nested validation for a more robust evaluation of the results. To validate the implementation of the pipeline, we also developed predictive baselines on simpler predictive tasks, i.e. prediction of the gestational age (GA) at birth, infant prematurity status (categorised GA at birth with 37 weeks threshold), as well as categorised behavioural scores.

#3 Materials and Methods

#3.1. Data

We included a sample of preterm and full-term neonates participating in the open-source developing Human Connectome Project (<http://www.developingconnectome.org/>). Detailed subject demographic and clinical information can be found in the section Cohort Description. Data collection for the dHCP took place in London, UK from 2015 to 2020 with UK NHS research ethics committee approval (14/LO/1169, IRAS 138070), and written informed consent obtained from parents.

#3.2. Cohort Description

By taking advantage of the large sample size of available dHCP data, we were able to perform this replication study on different cohort profiles, starting from the cohort with the largest heterogeneity and subsequently limiting the inclusion criteria to approximate the composition of the original study of Ouyang et al. (2020).

- **Cohort A**

Cohort A included all subjects available in the dHCP 3rd data release with complete diffusion and anatomical MRI which passed the quality control (QC) (Edwards et al., 2022), and with available BSID-III composite scores assessed between 17-20 months of age. In cases of subjects with multiple sessions, we prioritised the session at the youngest age to approximate the original study that aimed to scan subjects as close to birth as possible. Additionally, we included only infants that were considered healthy and without major brain focal lesions (i.e. who did not present any visible abnormality of possible clinical significance on structural MRI evaluated by an expert Paediatric Neuroradiologist, recorded in dHCP databases as radiological score range 1–3). To approximate the exclusion criteria described in the original study from the clinical information available in the dHCP database as closely as possible, we additionally excluded 63 additional subjects who had a history of hypoxic-ischemic encephalopathy, lung disease or bronchopulmonary dysplasia, necrotizing enterocolitis requiring intestinal resection or complex feeding/nutritional disorders, maternal drug or alcohol abuse or smoking during pregnancy in their records. Additionally, 12 subjects were excluded as the quality of the registration to the neonate atlas and subsequent projection to the cortex was insufficient (see *section #3.4.1. Extraction of cortical diffusion metrics*).

The final Cohort A then included 295 infants (54% males, gestational age at birth –GA at birth: median 39.9 weeks, range [29.9w –42.3w]; scanned at median post-menstrual age –PMA: 40.9w, range [31.1w –45.1w]).

- **Cohort B**

We additionally restricted the subject space by removing infants whose PMA at scan and GA at birth were outside the range of the original study (i.e. [31.9w-41.7w] PMA at scan and [25.0w-41.4w] GA at birth). We thus aimed to investigate whether prediction models can leverage wider age variability or whether the original results were limited to a narrow range of GA at birth and PMA at scan. Additionally, this allowed us to test whether low variability in motor outcome score in the original study may have been the reason for a lack of prediction by leveraging the larger size of the dHCP dataset through selecting for increased variability in the neurodevelopmental outcomes. With the GA at birth and PMA at scan matched as close as possible to the data in the original study, Cohort B then included 196 subjects (57% male, median GA at birth 39.1w, range [29.9w-41.3w], median PMA at scan 39.9, range [32.3w-41.6w]).

- **Cohort C**

Additionally, Cohort C's subjects were further selected from Cohort B based on matching the ranges of BSID-III composite scores ([65 – 110] for cognitive, [59 – 112] for language, and [73 – 107] for motor scores) to the original study. In this setting, the cohort was therefore highly similar to the original one in terms of PMA at scan, GA at birth, and the BSID-III score ranges but had a larger sample size of 126 subjects which could allow investigation of the effect of the training sample size on predictive performance. The subjects within Cohort C were 58% male with median GA at birth 39.1w, range [29.9w-41.3w] and median PMA at scan 40.0, range [32.7w – 41.6w]) in contrast to the original study which included 72% of males.

- **Cohort D**

Finally, Cohort D served as a close replication of the original study where subjects were limited to the same number (n=46) with similar ranges of PMA at scan, GA at birth and BSID-III score ranges. Randomly sampling 46 subjects from the Cohort C for the training and testing allowed us to test the robustness of the predictive pipeline relatively to the training set size, and thus the generalisability of the predictions.

The detailed description of the Cohorts A, B, and C can be found in *Table 4.1*.

	Cohort A (n = 295)		Cohort B (n = 196)		Cohort C (n = 126)	
	Mean (std)	Median [range]	Mean (std)	Median [range]	Mean (std)	Median [range]
<i>PMA at scan (weeks)</i>	40.43 (2.446)	40.86 [31.14, 45.14]	39.29 (2.014)	39.86 [32.29, 41.57]	39.46 (1.793)	40.00 [32.71, 41.57]
<i>GA at birth (weeks)</i>	39.15 (2.361)	39.86 [29.86, 42.29]	38.50 (2.417)	39.14 [29.86, 41.29]	38.65 (2.172)	39.14 [29.86, 41.29]
<i>* Pearson correlation</i>	r = 0.81, p<0.001*		r = 0.91, p<0.001*		r = 0.86, p<0.001*	
<i>Scan – birth delay (weeks)</i>	1.28 (1.469)	0.57 [0.00, 8.7]	0.79 (1.033)	0.29 [0.00, 6.85]	0.81 (1.120)	0.29 [0.00, 6.85]
<i>Age at BSID-III assessment (months CA)</i>	18.17 (0.860)	18.00 [17.00, 20.00]	18.31 (0.827)	18.00 [17.00, 20.00]	18.24 (0.821)	18.00 [17.00, 20.00]
<i>Weight at birth (kg)</i>	3.18 (0.689)	3.30 [0.76, 4.61]	3.03 (0.700)	3.11 [0.76, 4.59]	3.09 (0.646)	3.18 [1.25, 4.59]
<i>Male: number (%)</i>	158 (53.6%)		111 (56.6%)		73 (58.0%)	
<i>White: number (%)</i>	158 (53.6%)		93 (47.5%)		52 (41.3%)	
<i>Mode of delivery: number</i>	V: 155, I: 67, Cem: 73, Cel: 0		V: 102, I: 40, Cem: 54, Cel: 0		V: 60, I: 32, Cem: 34, Cel: 0	
<i>Subject per template age: number</i>	33w: 7, 36w: 29, 39w: 259		33: 6, 36: 29, 39: 161		33: 3, 36: 15, 39: 108	
<i>BSID-III composite scores</i>	Mean (std)	Median [range]	Mean (std)	Median [range]	Mean (std)	Median [range]
<i>Cognitive</i>	101.1 (11.18)	100 [60, 130]	99.6 (11.40)	100 [60, 130]	95.7 (9.14)	95 [65, 110]
<i>Language</i>	97.0 (16.05)	97 [47, 153]	95.4 (16.22)	97 [47, 153]	90.9 (12.81)	91 [59, 112]
<i>Motor</i>	101.7 (9.48)	103 [70, 127]	100.8 (9.78)	100 [70, 127]	97.2 (7.98)	98 [73, 107]

*Pearson correlation between GA at birth and PMA at scan.

Table 4.1. Description of Cohort A, B, C (Cohort D is a random subset of C). BSID-III - Bayley Scales of Infant and toddler Development, 3rd edition; CA – corrected age; mode of delivery: V – vaginal, C_{em} – emergency Caesarean section, C_{el} – elective Caesarean section; PMA – post-menstrual age; std – standard deviation; subjects per template age: categorization of infants to age-standardized template according to their PMA at scan.

#3.3. Description of available data

#3.3.1. Diffusion MRI

MRI data was acquired using a Philips 3-Tesla Achieva scanner (Philips Medical Systems, Best, The Netherlands). All infants were scanned during natural sleep in a scanner environment optimised for neonatal imaging including a dedicated transport system, positioning device and an optimally sized neonatal 32-channel receive coil with a custom-made acoustic hood as previously described (Hughes, et al., 2017).

The diffusion MRI data was used in its pre-processed state available from the dHCP 3rd data release. In sum, diffusion-weighted (DW) images were acquired following a multi-shell high angular resolution diffusion imaging (HARDI) protocol (with $b=0, 400, 1000, 2600$ s/mm²) (Tournier, et al., 2019) and pre-processed with correction for motion artefacts and slice-to-volume reconstruction using the SHARD approach, leading to a final isotropic voxel size of 1.5mm (Christiaens, et al., 2021; Hutter, et al., 2018). All included data passed SHARD QC provided in the dHCP (Edwards et al., 2022). Quantitative metric maps resulting from the diffusion tensor imaging (DTI) model, including fractional anisotropy (FA) maps, were computed based on $b=0$ and 1000s/mm² images using FSL's DTIFIT. For distribution of motion across the dataset as well as example FA maps for two subjects, see *Annexe 3.2. Supp. Figure 1*.

#3.3.2. Structural MRI

The structural data was acquired and reconstructed following optimized protocols (Cordero-Grande, et al., 2018) leading to super-resolved T2w images with an isotropic spatial resolution of 0.5mm. Subsequent processing followed a dedicated pipeline for segmentation and cortical surface extraction for T2w neonatal brain images (Bozek, et al., 2018; Makropoulos, et al., 2018) with bias-correction, brain extraction, and segmentation using the Draw-EM (Developing brain Region Annotation with Expectation Maximisation) algorithm (Makropoulos, et al., 2014). Available meshes of inner cortical surface (corresponding to white matter surface) were used for the cortical parcellations and extraction of DTI metrics such as FA.

#3.3.3. Neurodevelopmental assessment and infant characteristics at 18 months

Neurodevelopmental outcome was assessed at St Thomas' Hospital, London by two experienced assessors (a paediatrician and a chartered psychologist) using the Bayley Scales of Infant and Toddler Development, Third Edition (BSID-III) (Bayley, 2006). We only

considered evaluations performed at around 18 months of age (between 17 and 20m; corrected for GA at birth in PT infants). Three distinct developmental categories – motor, cognition, and language functions – were assessed yielding age-standardized respective composite scores, with higher values indicating better infant development and scores below 85 (i.e., lower than – 1SD of the mean at 100) indicating a developmental delay.

BSID-III composite scores in the Cohort A were the following: median cognitive score of 100, range [60 –130]; median language score of 97, range [47 –153]; and median motor score of 103, range [70 –127]. The score medians and ranges were identical for the Cohort B. In case of the Cohort C, the median BSID-III composite scores were the following: cognitive score of 95, range [60 –110]; language score of 91, range [59 –112]; and motor score of 98, range [73 –107]. Cohort D was a random subset of the Cohort C.

Additionally, family socio-economic status (SES) was measured using the Index of multiple deprivation (IMD) which is a UK geographically defined composite social risk score comprising data on income, employment, health, education, living environment, and crime calculated at 18mCA assessment from the mother's home address at the time of birth.

#3.4. Data processing

Additionally, we used cortical surfaces extracted as meshes from the structural MRI data, to obtain a cortical parcellation and extract the DTI metrics in the cortical ribbon.

#3.4.1. Extraction of cortical DTI metrics

We registered and projected the FA values to the inner cortical surface using a cylindrical approach guided by the spatial location of the local minimum of axial diffusivity (AD). This has been shown to reliably locate the DTI metrics in the cortical ribbon (details available in (Lebenberg, et al., 2019)): this method robustly excludes values from surrounding cerebrospinal fluid (CSF) and underlying white matter at the individual level, since these tissues show higher AD values than the grey matter in the immature brain of neonates. This approach for cortical FA extraction has been reliably used and validated in different studies (Lebenberg et al, 2019; Rolland et al, 2019; Adibpour et al, 2020) but it differed from the one of the original study (pipeline not available at the time of this conceptual replication study) which used a cortical skeleton and a fast-marching correction. Visual and quantitative validation suggested 12 subjects with small local mistakes in the metric projection, leading to their exclusion from all cohorts (see *section #3.2. Cohorts description*).

#3.4.2. Cortical parcellation

Neonate atlas

As in the original study, FA maps were registered to the neonate segmentation atlas described in Feng et al. (2019) and Oishi et al. (2011). But, as recommended by the atlas' authors (brainmrmap.org, n.d), we found it more reliable to use FSL's FNIRT for the subject-to-atlas projections rather than the large deformation diffeomorphic metric mapping (LDDMM) registration that was used in the original study.

Firstly, subjects were split into 3 groups based on their PMA at scan: the 33w group (31.1, 34.5): 14 subjects; the 36w group [34.5, 37.5): 42 subjects; the 39w group [37.5, 45.1): 239 subjects. The linear transformations were then estimated between subject FA map and the corresponding age-specific atlas spaces, which were then used to initiate the non-linear registration. The resulting warps were inverted and used to project the atlas parcellations to the native DW subject space. Labelling information and the list of the 52 cortical ROIs (26 per hemisphere) used in the study as well as examples of cortical parcellation are presented in *Figure 4.2a*. Segmented labels were then projected to the subject' cortical surface with the same method as the diffusion metric maps.

Visual QC of the registration results and parcellation projections on the cortical mesh were performed with a specific focus on the subjects with the highest distance of their PMA at scan to the atlas template age. We noticed small errors stemming from the registration especially in the cingulate area and regions where the opposite gyri banks were close in volumetric space, which led to multiple parcels per label. To correct the errors, we developed a post-processing step which iteratively reassigned the small unconnected labelled regions to their nearest neighbour main label, based on the path distance along the cortical surface; this was run until only one parcel per label remained.

Random parcellation

Additionally, cortical surfaces were parcellated into random bilateral parcels with similar area (k-means based on Dijkstra-path, optimized to balance the vertex numbers per region). The numbers were more than double the atlas parcels: 128, 256, 512, 1024. The random parcellation was performed in the dHCP surface template space after manual segmentation of the cingulate area, which was excluded from the final parcellations to avoid possible inclusion of non-cortical tissues (*Figure 4.2b*). The random parcellations were then

projected to the subjects' anatomical space using the transformations available from the dHCP database.

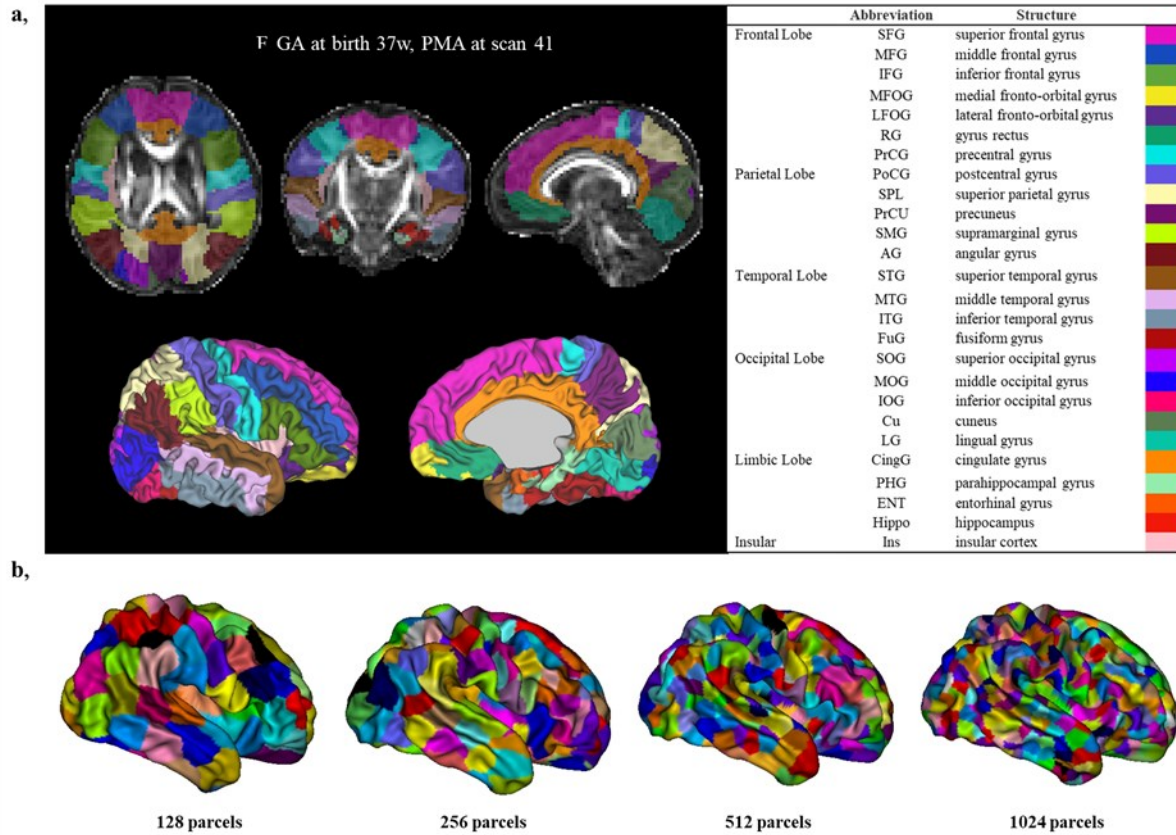


Figure 4.2. Example parcellation of 52 cortical parcels in volumetric view and on the cortical surface. More details on the used atlas can be found in Feng et al. (2019) **(a)**. Example of random parcellation in the dHCP template space for the different number of parcels **(b)**.

#3.4.3. Extraction of DTI metrics in cortical parcels

For both the atlas and the random parcellations, individual DTI metrics were reliably extracted from every cortical region using the DTI maps projected to the subjects' inner cortical surfaces and extracting the median FA per region (as this has similar values to the mean but higher robustness to potential outliers). We then created individual subject feature vectors, considering all cortical parcels and to serve as an input to the subsequent predictive pipeline.

Age correction

To address the likely confounding effect of various PMA at scan across subjects on the predictive performance observed during the piloting stages of our replication (see #4 *Results* section), we decided to adjust the regional FA values for PMA at scan. Following on from

previous studies, we assumed a relationship between global FA (median over the whole cortical surface) and PMA at scan with an inflection point between 35 and 43w (Batalle, et al., 2019; Ouyang, et al., 2020). We fitted a continuous piecewise linear regression to Cohort A assuming two linear segments with external knots being the minimal and maximal PMA at scan within the cohort and the middle inflection point between the above specified range. Results of the fits evaluated by Akaike information criterion (AIC), and Bayesian information criterion (BIC) metrics suggested that the ideal inflection point in our data is 36w PMA which was then used as a separation age to perform the corrections over the younger and older age ranges. The line segments were estimated only from the training data and applied to the testing data within the predictive pipeline to avoid data leakage. Although we acknowledge that this inflection point might not be optimal for all parcels given their heterogeneous maturation with age, a single inflection point was preferred for all parcels to avoid heterogeneous FA corrections.

#3.5. Predictive pipeline

Wherever possible, the replication pipeline followed the original study as closely as possible given the provided description of methods in the original and referenced publications (Ouyang et al., 2020, Ouyang et al., 2019b, Yu et al., 2016).

#3.5.1. Prediction of continuous composite scores

We recreated the individualised prediction using the SVR algorithm (nu-SVR with a linear kernel and C of 9) to predict continuous variables – cognitive, language, and motor composite BSID-III scores. As the authors of the original study did not report any tuning of the hyperparameters during their implementation or between tasks, we re-used their hyperparameter settings. Given the different sample sizes of our cohorts, we adopted k-fold cross-validation with 46 folds to recreate the training-testing split proportions used in the original study. Leave-one-out cross-validation (LOOCV) is a special case of k-fold where n of the testing set is 1, and thus Cohort D was evaluated exactly like in the original study.

The individual feature vectors of FA metrics from cortical parcels (either from atlas or random parcellation) were then used to predict the outcome scores. During training, features were independently scaled between 0 and 1 using the training splits to determine the scaling factors which were then applied to the testing set. Predictive results were evaluated using a Pearson correlation coefficient (r) and mean absolute error (MAE) between the predicted and real composite scores. Additionally, we evaluated the coefficient of determination (R^2), which is bounded between $(-\infty, 1]$ with 0 suggesting the random prediction. In contrast to Pearson's r

which is insensitive to scale with potential high correlations possible even for large differences between predicted and actual target value, R2 quantifies a portion of variation in the target predicted by the model and is thus a more indicative measure of predictive performance. However, as the outcome variance might differ between samples, R2 does not allow comparisons across different datasets: MAE measuring the predictive error in the units of the original target measure is then a useful metric.

Replicating the original study, we also performed a permutation test to assess the predictive performance. In short, we randomly shuffled the BSID-III scores 1000 times to generate null distributions for random predictors for both the Pearson's correlation coefficient and MAE. P-values of observing the reported r (or MAE) by chance is then calculated as the ratio of number of permutation tests with r higher than the observed r value over the number of permutation tests (reverse for the MAE).

Additionally, to test the impact of random small differences in the dataset on the robustness of the predictive results, we randomised the inputs and outputs 100 times and repeated the same evaluation to derive the mean and standard deviation of predictive results across the independent runs to determine how sensitive the results are to small changes in the inputs upon shuffling.

We performed the same training and evaluation as a continuous prediction of GA at birth to further validate the implementation of the pipeline.

#3.5.2. Categorical predictors

Additionally, we also simplified the predictive task by categorising the independent variables. In the case of BSID-III scores, infants were categorised based on a threshold into Typical (>85) and Atypical (≤ 85) outcome groups. We then tested prediction of whether the infant developed typically or not, given the cortical FA features using the support vector classifier (SVC) algorithm with predictive results evaluated using Area Under the (Receiver Operating Characteristic) Curve (AUC), Specificity (SPEC), and Sensitivity (SENS) scores. The same permutation testing (reported p-value being the proportion of permutation tests with AUC above the reported AUC divided by number of permutation tests) and shuffling as described in the previous section were also performed.

Similarly, in the case of GA at birth prediction, we performed a classification using categorised GA at birth into *prematurity status* as outputs: preterm (PT) born before 37 weeks of gestation vs full-term (FT), which served to validate the predictive pipeline's implementation as well as the input features.

#3.5.3. Hyperparameter tuning & nested validation (Cohort D)

The larger size of the dHCP available data compared to the original work allows us to perform a more thorough validation of the predictive pipeline (*Figure 4.3*). To do this, we randomly selected a subset n times ($n=10$) of 46 infants from the Cohort C keeping them as an independent testing set (to recreate the validation from the original study). The remaining data, i.e. 80 subjects, was used within the inner validation LOOCV loop (79 subjects to train and one as validation) which allowed us to tune the hyperparameters of the SVR. The best model was then re-trained on the 80 subjects and evaluated on the independent testing split. The mean R2 and MEA results across the 10 repetitions are reported as the final predictive results. Again, the prediction of GA at birth and the binarized outcome scores were used as the *sanity* check and performed the same evaluation in the form of a categorical predictive task.

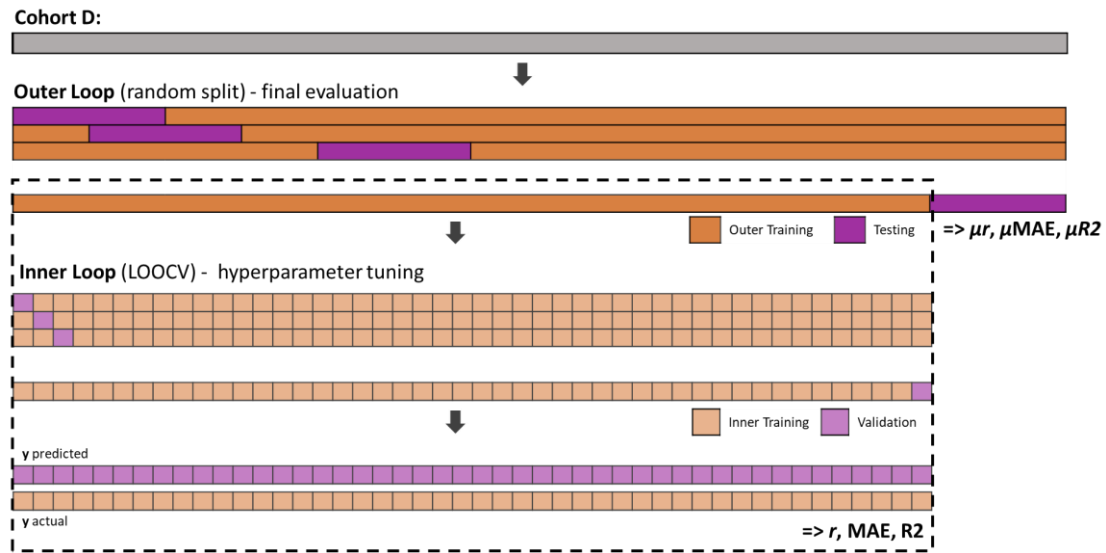


Figure 4.3. Nested validation pipeline. μr : mean Pearson's r ; μMAE : mean absolute error, $\mu R2$: mean R2, n : number of outer loop repetitions, k : number of inner loop repetitions.

#4 Results

#4.1. Evaluation of cortical microstructure

As expected, the change in global cortical FA with PMA at scan did not appear to follow a simple linear relationship but showed a steep decrease for young ages followed by an inflection point identified at 36w PMA for Cohort A (*Annexe 3.2. Supp. Figure 2*). Additionally, the FA metrics differed significantly between the preterm- and term-born subjects even after correcting for PMA at scan in all cohorts (*Annexe 3.2. Supp. Table 1*). We also incorporated

two major risk factors – GA at birth and sex – in an ANCOVA model to investigate their effect on global cortical FA (corrected for PMA at scan). The results suggested a significant effect of sex on cortical FA, but not of GA at birth, which is likely due to the skew within the Cohort A towards the older neonates.

Visual assessment of the distribution of median FA metrics over the 52 parcels of the atlas for Cohort A (*Figure 4.4*) revealed individual and regional variability in cortical microstructure across the sample. However, it is interesting to note that we observed globally lower FA values in comparison to the original study: more than effects related to PMA at scan, image quality or to the method for extracting cortical FA measures, we suspect that this relates to the SHARD pre-processing pipeline (Christiaens et al., 2021) for correction of motion artefacts and geometric distortions.

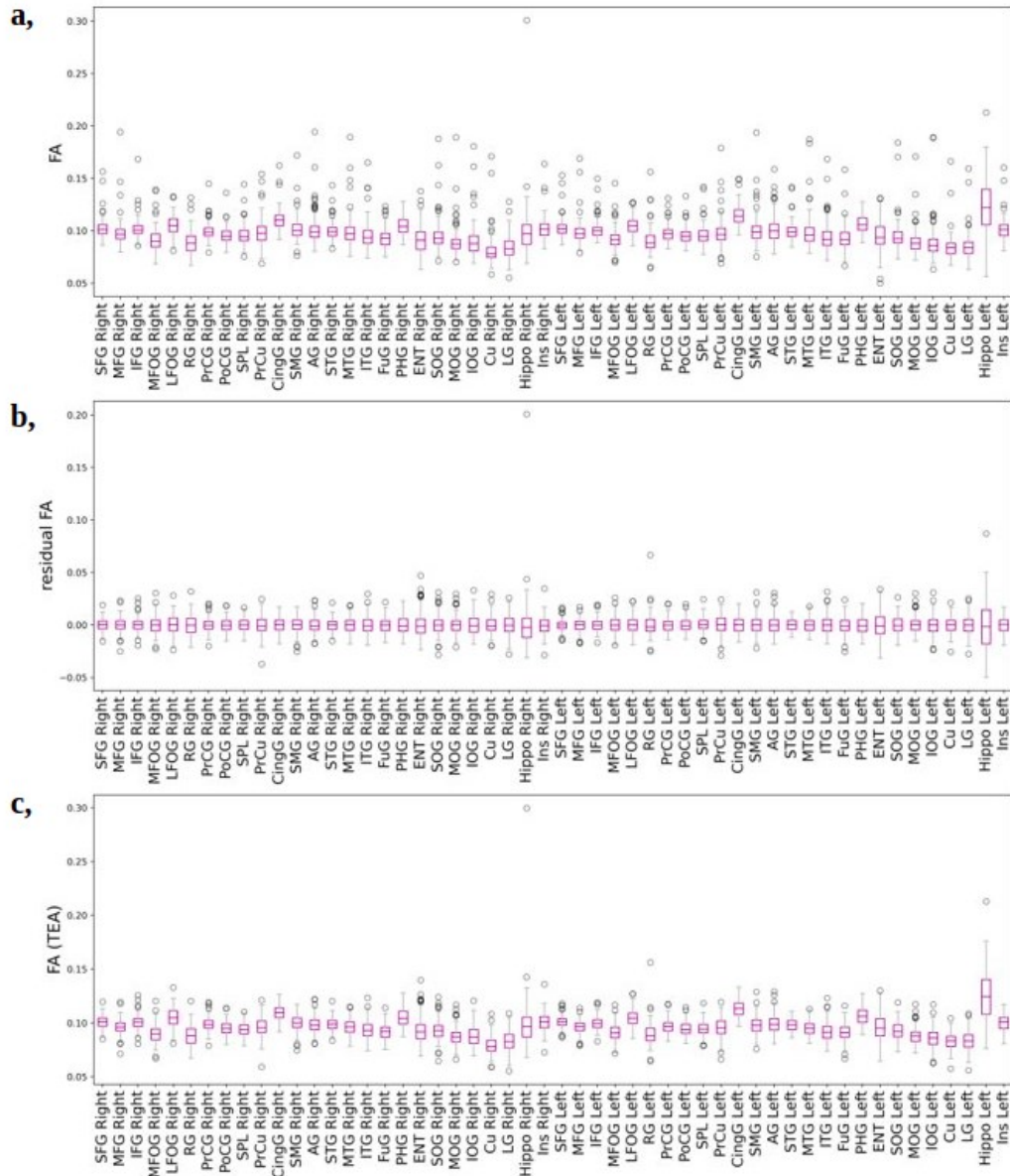


Figure 4.4. Distribution of cortical FA. **a**, Distribution of median FA per cortical region (atlas parcellation) suggesting inter-individual and inter-regional microstructural variability (Cohort A). **b**, Distribution of the residual FA estimated as the residual of a piecewise linear regression considering the regional FA as the function of PMA at scan with inflection at 36w. **c**, Distribution of the corrected FA after the reintroduction of expected regional FA values at term equivalent age (TEA = 40w PMA) (predicted from the correction models represented in b). Labelling abbreviations are detailed in *Figure 1*.

#4.2. Neurodevelopmental outcomes at 18 months

For Cohort A the BSID-III composite scores at 18 months ranged from 60 to 130 (mean \pm std 101.1 ± 11.2) for cognition, 47 to 153 (97.0 ± 16.0) for language, and 70 to 127 (101.7 ± 9.5) for motor outcomes. BSID-III score distribution was very similar in Cohort B. Cohort C showed, by design, more restricted BSID-III scores. The descriptive values are detailed in *Table 4.1*. No significant differences between preterm and full-term infants were found in any of the

BSID-III scores across cohorts (*Figure 4.5*). Additionally, we did not observe any significant correlation between any specific age (i.e. GA at birth, PMA at scan, age at BSID-III assessment) and neurodevelopmental outcome scores across the cohorts or within preterm and full-term subgroups (*Annexe 3.2. Supp. Table 2*) except for Cognitive and Language scores and PMA at scan within the FT group of Cohort A after the FDR corrections for multiple comparisons.

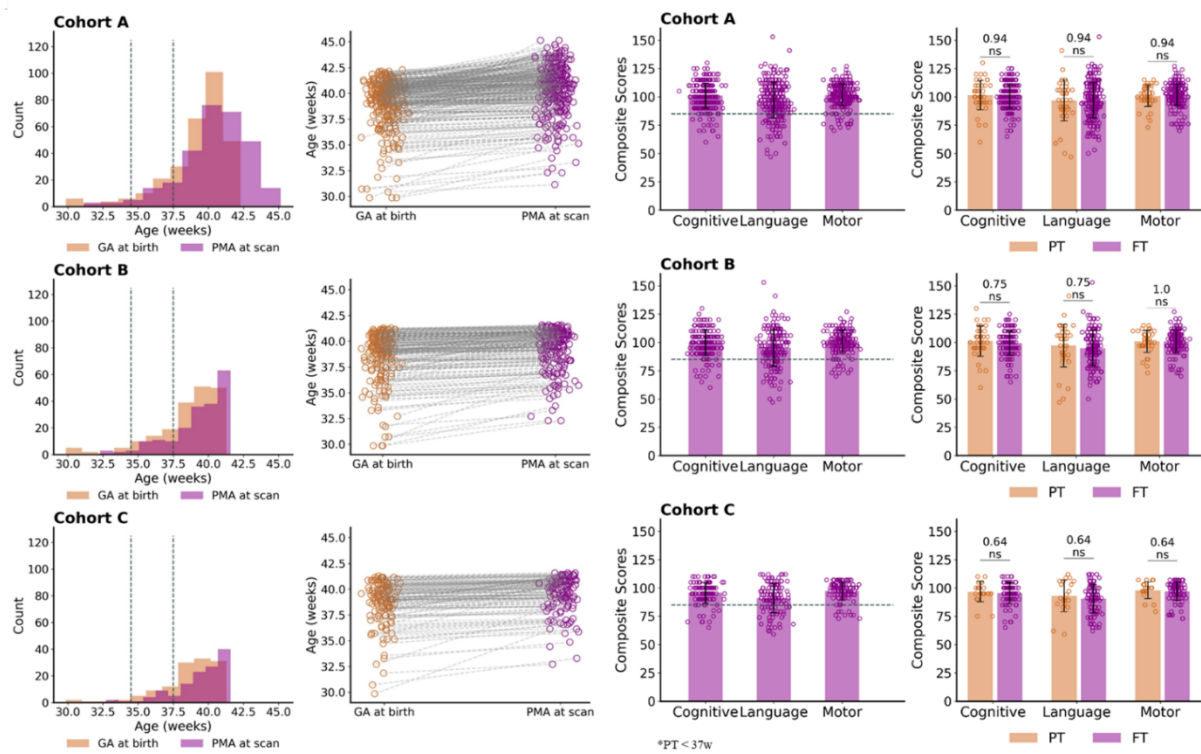


Figure 4.5. Visual description of the Cohorts A,B, and C showing distribution of GA at birth and PMA at scan as well as BSID-III composite scores.

Composition of the evaluated cohorts in terms of their Atypical/Typical subject numbers is shown in *Table 4.2*. Percentage of PT (or FT) group of the whole PT (or FT) population within the cohort is also shown. The distribution of the PT and FT infants across the Atypical and Typical categories for the 3 scores are very similar, although in the case of motor score in all cohorts, the PT subjects seem to be somewhat overrepresented. Interestingly, in the case of language scores, it is the FT population that seems to have a higher proportion of subjects with Atypical scores.

Additionally, we performed an ANCOVA modelling to study the effect of environment approximated by the IMD on BSID-III scores, and including the global cortical FA and risk factors – GA at birth and sex – within the descriptive analysis (*Annexe 3.2. Supp. Table 3*). We

observed the effects of global cortical FA on Cognitive, Language, but not the Motor scores which is in line with the predictive results presented in the original paper. As expected, IMD (and sex for cognitive and language scores) seemed to affect the neurodevelopmental outcomes.

	Atypical (scores ≤ 85)			Typical	
Cohort A (N=295)	Number	PT vs FT	$ \Delta\% $	Number	PT vs FT
Cognitive	24	PT: 4 (9.3%) FT: 20 (7.9%)	1.4	271	PT: 39 (90.7%) FT: 232 (92.1%)
Language	57	PT: 7 (16.3%) FT: 50 (19.8%)	3.5	238	PT: 36 (83.7%) FT: 202 (80.2%)
Motor	21	PT: 5 (11.6%) FT: 16 (6.3%)	5.3	274	PT: 38 (88.4%) FT: 236 (93.7%)
Cohort B (N=196)					
Cognitive	20	PT: 4 (10.3%) FT: 16 (10.2%)	0.1	176	PT: 35 (89.7%) FT: 141 (89.8%)
Language	42	PT: 6 (15.4%) FT: 36 (22.9%)	7.5	154	PT: 33 (84.6%) FT: 121 (77.1%)
Motor	17	PT: 5 (12.8%) FT: 12 (7.6%)	5.2	179	PT: 34 (87.2%) FT: 145 (92.4%)
Cohort C (N=126)					
Cognitive	16	PT: 2 (9.5%) FT: 14 (13.3%)	3.8	110	PT: 19 (90.5%) FT: 91 (86.7%)
Language	36	PT: 4 (19.0%) FT: 32 (30.5%)	11.5	90	PT: 17 (81.0%) FT: 73 (69.5%)
Motor	14	PT: 3 (14.3%) FT: 11 (10.5%)	6.2	112	PT: 18 (85.7%) FT: 94 (89.5%)

Table 4.2. Composition of Cohorts A,B, and C in terms of categorised BSID-III composite scores. In the *PT vs FT* columns, the percentages refer to percent of given PT (or FT) group from the entire PT (or FT) population within the cohort. $|\Delta\%|$ is a relative difference between PT and FT % prevalence within the Atypical group.

#4.3. Prematurity status & GA at birth prediction

#4.3.1. Prematurity status & GA at birth prediction

Prediction of prematurity status (preterm vs full-term categorised depending on GA at birth) using different inputs served two goals: i, validation of the predictive pipeline implementation, and ii, validation of the input features. Overall, cortical FA seemed predictive of prematurity status at birth in all cohorts (*Annexe 3.2. Supp. Materials: Predictive results, Figure 4.6a*). However, the predictive power tended to decrease (sometimes reaching random predictor levels) after the correction of the inputs for PMA at scan which might be explained by the high correlation between PMA at scan and GA at birth in all cohorts (*Table 4.1*). This suggests that some, but not all of the prediction was driven by the distribution of this confounding variable, thus stressing the importance of correcting for PMA at scan in all of the

following predictive settings. Therefore, all the following reported results are based on the inputs corrected for the PMA at scan.

Interestingly, the random parcellations led to consistently higher predictive results than the atlas parcellation with a tendency of the predictive power to increase with number of regions. This is possibly due to larger number of parcels providing more granular information than when collapsed too much within the atlas parcels.

Another observed tendency was the general trend of decreasing predictive power across the cohorts as the dataset gets progressively limited in variability of inputs and sample sizes. Interestingly, in the case of Cohort D, which is the closest replication of the original study, we observed a substantial drop in predictive power of prematurity status. Comparing these results to those in the Cohort C suggests this is largely due to insufficient sample size leading to negative results rather than the limited variability within the data given the similar distribution of input and output features.

We also performed a similar prediction aiming to categorise infants into three classes by additionally subdividing the preterm group of Cohort A into extreme-very preterm (EVP, GA at birth <32w, N=8) and moderate-late preterm (MLP, GA at birth \geq 32w, N= 35) groups. In this setting, only the atlas parcellation led to higher than random prediction (*Annexe 3.2. Supp. Table 4*). Results are in line with previous findings demonstrating the differential effect of the degree of prematurity on brain measures and suggest that the categorisation within the preterm group is possible. Nevertheless, it is important to note that practical issues, such as size of the dataset or class imbalance, are likely to impact the reliability of these observations, at least in our limited sample.

When attempting to predict continuous GA at birth rather than categorised prematurity status, the predictive models did not outperform random levels (*Annexe 3.2. Supp. Materials: Predictive results, Figure 4.6c*). Overall, these results at the same time validate the implementation of our pipeline and suggest there might be at least some information within the estimated cortical microstructure that allows differentiation of subjects in terms of their prematurity status, although it is conceivable that the predictive results might be driven by some other confounding factors, such as motion (*Annexe 3.2. Supp. Materials: Motion Correction* section). This information is however insufficient for the more difficult prediction of the continuous GA at birth.

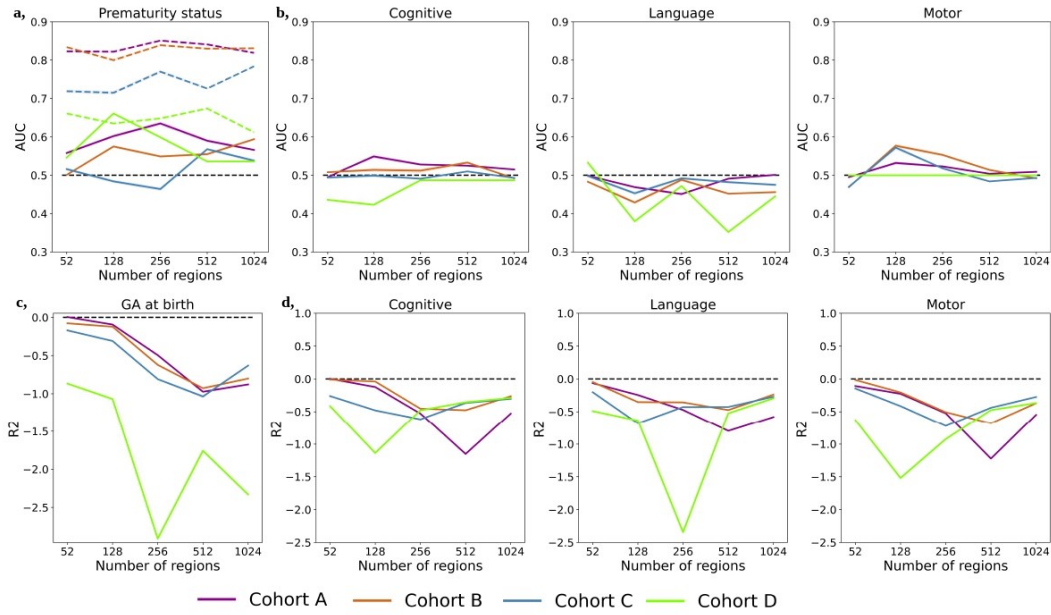


Figure 4.6. Predictive results of categorical tasks (upper row) for **a**, prematurity status and **b**, categorized BSID-III scores with increasing region numbers across the Cohorts A, B, C and D, and the predictive results of the continuous tasks (lower row) for **c**, GA at birth and **d**, BSID-III scores. Coloured dotted lines in the prematurity status subplot show predictive results before the adjustment for PMA at scan. Grey dotted lines represent the random predictive level (0.5 for AUC and 0 for R2 metric).

#4.3.2. BSID-III score prediction

Our results of the predictive models for BSID-III outcome suggested limited ability to distinguish Atypical vs Typical categories for cognitive, language, and motor composite scores (Figure 4.6b). All models generally performed poorly, with the performance depending on the combination of the cohort and parcellation strategy. Once again, the random parcellation seemed to lead to better results supporting the idea there might be more granular information than that contained within 52 atlas parcels. However, the results were too heterogeneous and close to random levels to make conclusions on optimal number of parcels with confidence. The erratic behaviour observed for Cohort D (especially for language and motor scores) might be due to the lower stability of the model to the small variations within the data caused by the randomly sampled small dataset, i.e. due to a less robust model which is unlikely to generalise well.

In contrast to the original study, the prediction results for the BSID-III continuous scores using cortical microstructure did not outcompete random levels (*Annexe 3.2. Supp. Materials: Predictive results, Figure 4.6d*). Given the results on the categorised scores, it is possible that some information pertaining to later developmental outcome is contained within

the input data of early cortical microstructure, but was insufficient to predict the continuous scores like in the case of birth age prediction.

#4.3.3. Nested validation (hyperparameter tuning & independent test set)

To expand on the validation strategy, we also performed a nested validation on all 4 predictive tasks: prematurity status, GA at birth, categorical BSID-III, and continuous BSID-III scores based on cortical features corrected for PMA at scan. This strategy enabled evaluation of mean metrics as well as calculation of confidence intervals for the predictive results (*Table 4.3*). Again, predicting prematurity status from the cortical microstructure was possible, but the more complex task of continuous GA at birth prediction was not successful. In the case of BSID-III scores, no model was better than random in neither categorised nor continuous setting.

a, Categorical (corrected for PMA at scan)

Outcome	Inputs	AUC [CI]	SPEC [CI]	SENS [CI]
Prematurity status	ROIs (52)	0.571 [0.5279;0.6148]	0.929 [0.8865;0.9723]	0.213 [0.0862;0.3404]
	Random (128)	0.564 [0.5135;0.6145]	0.821 [0.7435;0.8993]	0.307 [0.1569;0.4564]
	Random (256)	0.562 [0.5025;0.6223]	0.951 [0.9278;0.9750]	0.173 [0.0599;0.2868]
	Random (512)	0.502 [0.4341;0.5694]	0.864 [0.8037;0.9234]	0.140 [0.0185;0.2615]
	Random (1024)	0.512 [0.4414;0.5829]	0.864 [0.7723;0.9564]	0.160 [0.0324;0.2876]
Cognitive Score	ROIs (52)	0.474 [0.4340;0.5138]	0.881 [0.8203;0.9419]	0.067 [-0.0160;0.1493]
	Random (128)	0.475 [0.4594;0.4899]	0.916 [0.8858;0.9462]	0.033 [-0.0080;0.0747]
	Random (256)	0.478 [0.4657;0.4900]	0.956 [0.9314;0.9801]	0.000 [0.0000;0.0000]
	Random (512)	0.498 [0.4944;0.5006]	0.995 [0.9888;1.0012]	0.000 [0.0000;0.0000]
	Random (1024)	0.493 [0.4836;0.5018]	0.985 [0.9672;1.0035]	0.000 [0.0000;0.0000]
Language Score	ROIs (52)	0.496 [0.4906;0.5010]	0.945 [0.8778;1.0131]	0.046 [-0.0111;0.1034]
	Random (128)	0.460 [0.4261;0.4930]	0.887 [0.7969;0.9771]	0.032 [0.0077;0.0564]
	Random (256)	0.479 [0.4525;0.5051]	0.958 [0.9050;1.0102]	0.000 [0.0000;0.0000]
	Random (512)	0.491 [0.4793;0.5025]	0.934 [0.8844;0.9844]	0.047 [0.0089;0.0860]
	Random (1024)	0.490 [0.4693;0.5107]	0.920 [0.8725;0.9684]	0.060 [0.0076;0.1115]
Motor Score	ROIs (52)	0.512 [0.4789;0.5446]	0.894 [0.8482;0.9390]	0.130 [0.0270;0.2330]
	Random (128)	0.501 [0.4713;0.5302]	0.962 [0.9376;0.9855]	0.040 [-0.0096;0.0896]
	Random (256)	0.493 [0.4865;0.4988]	0.985 [0.9731;0.9976]	0.000 [0.0000;0.0000]
	Random (512)	0.500 [0.5000;0.5000]	1.000 [1.0000;1.0000]	0.000 [0.0000;0.0000]
	Random (1024)	0.498 [0.4948;0.5006]	0.995 [0.9896;1.0011]	0.000 [0.0000;0.0000]

b, Continuous (corrected for PMA at scan)

Outcome	Inputs	RHO [CI]	MAE [CI]	R2 [CI]
GA at birth	ROIs (52)	0.092 [-0.0038;0.1887]	1.464 [1.3303;1.5976]	-0.069 [-0.1599;0.0212]

	Random (128)	0.046 [-0.0915;0.1834]	1.597 [1.4775;1.7163]	-0.185 [-0.3618;-0.0073]
	Random (256)	-0.018 [-0.1568;0.1206]	1.646 [1.4598;1.8321]	-0.295 [-0.4497;-0.1411]
	Random (512)	-0.080 [-0.2404;0.0809]	1.594 [1.4665;1.7211]	-0.392 [-0.5363;-0.2480]
	Random (1024)	0.017 [-0.0970;0.1316]	1.493 [1.3944;1.5907]	-0.320 [-0.5269;-0.1121]
Cognitive Score	ROIs (52)	-0.026 [-0.0981;0.0466]	6.613 [6.2772;6.9489]	-0.081 [-0.1129;-0.0485]
	Random (128)	0.002 [-0.0476;0.0508]	6.517 [6.2554;6.7794]	-0.076 [-0.0959;-0.0567]
	Random (256)	-0.044 [-0.1063;0.0177]	6.739 [6.5065;6.9717]	-0.141 [-0.2019;-0.0804]
	Random (512)	0.043 [-0.0379;0.1238]	6.461 [6.1927;6.7291]	-0.045 [-0.0630;-0.0265]
	Random (1024)	0.065 [-0.0103;0.1407]	6.430 [6.1602;6.7006]	-0.043 [-0.0605;-0.0246]
Language Score	ROIs (52)	-0.072 [-0.1417;-0.0014]	10.500 [10.0920;10.9080]	-0.079 [-0.1176;-0.0406]
	Random (128)	-0.060 [-0.1348;0.0156]	10.535 [9.9543;11.1153]	-0.079 [-0.1409;-0.0172]
	Random (256)	-0.011 [-0.0645;0.0417]	10.822 [10.0066;11.6369]	-0.137 [-0.2700;-0.0046]
	Random (512)	-0.099 [-0.1536;-0.0444]	10.778 [10.0128;11.5437]	-0.154 [-0.2992;-0.0097]
	Random (1024)	-0.080 [-0.1296;-0.0309]	10.717 [10.0147;11.4201]	-0.118 [-0.2220;-0.0149]
Motor Score	ROIs (52)	-0.206 [-0.2345;-0.1780]	6.074 [5.7814;6.3665]	-0.074 [-0.1148;-0.0340]
	Random (128)	-0.045 [-0.0768;-0.0142]	6.013 [5.5622;6.4639]	-0.065 [-0.0874;-0.0426]
	Random (256)	-0.019 [-0.0194;-0.0194]	6.061 [5.5185;6.6033]	-0.083 [-0.1388;-0.0264]
	Random (512)	0 [0;0]	5.865 [5.4868;6.2437]	-0.031 [-0.0449;-0.0162]
	Random (1024)	0 [0;0]	5.865 [5.4868;6.2437]	-0.031 [-0.0449;-0.0162]

Table 4.3. Results of the nested validation for **a**, categorical tasks and **b**, continuous tasks. CI: 95% confidence interval.

To investigate whether an alternative model, incorporating information on the infant cortical microstructure with additional clinical risk factors and environmental information could lead to different results, we performed an additional prediction analysis using the global FA (corrected for PMA at scan), GA at birth, sex, and IMD score as inputs for the prediction of the prematurity status and categorised BSID-III scores. Despite the global effects (observed with ANCOVA) between the scores and the input variables within the Cohort A, such information did not lead to successful predictions within the nested validation setting (*Annexe 3.2. Supp. Table 5*).

Additionally, because of a potential relationship between the whole-brain cortical FA metrics and motion parameters (Christiaens et al., 2021) (*Annexe 3.2. Supp. Table 6*), we analysed whether this confounder might have an impact on predictive results after the correction for PMA at scan. This was not the case (see *Annexe 3.2. Supp. Materials: Predictive Results, Supp. Table 7*), suggesting that correction for motion might not be necessary in the context of this study.

#4.4. *Overlap of input metrics*

We were also interested in evaluating whether the observed predictive results could be explained by analysis of the overlap of the inputs (global median FA as well as the regional FA of the atlas parcellations) during the classification considering only Cohort A as an example (Figure 4.7.). In short, we first estimated the distribution of FA medians over subjects per category (for prematurity status: PT/FT; for scores: Typical/Atypical) and then quantified the measure of similarity between the two categories as the intersection of the areas under the two curves (normalized between 0 and 1). Overall, the overlap in terms of global cortical FA, after correction for PMA at scan, was around 80% for preterm vs term-born infants, which was lower than in the case of BSID-III scores where the FA overlap was above 85% for all scores. This overlap difference between categories might potentially explain the higher prediction of prematurity status compared with the BSID-III scores, i.e. the heterogeneity between BSID-III categories might not be sufficient to allow reliable prediction.

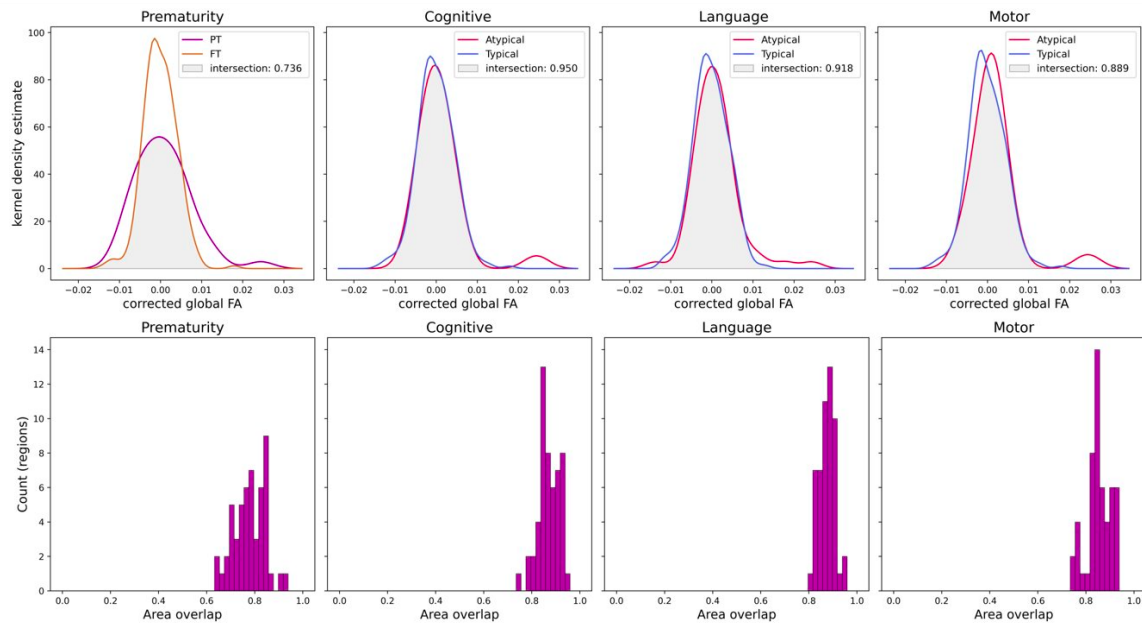


Figure 4.7. Overlap of global FA between PT and FT infants and between Atypical and Typical infants assessed by BSID-III scores (top row). Same assessment across 52 atlas parcells collapsed into a histogram (bottom row).

#5 *Discussion*

In this study, we were unable to conceptually replicate the findings of Ouyang et al. (2020) that cortical microstructure at birth as assessed by DTI-based FA can reliably predict later neurodevelopmental outcome as evaluated with BSID-III in infants born preterm and full-

term. Nevertheless, the performance on the prematurity task allowed us to draw limited conclusions: i) a sufficiently large and heterogeneous dataset appeared to be an indispensable factor for successful training and reliable validation of ML algorithms; ii) age corrections of the cortical FA features appeared to be required, and iii) random parcellations with higher number of parcels seemed beneficial compared with atlas based parcellations. Differences between the original study and our observations are discussed below in the light of deviations between methodologies and possible limitations.

#5.1. Methodological considerations

In this replication study, we had to deviate from the original methodology used for regional FA extraction, mainly due to our inability to exactly re-implement the processing steps and software settings of the original study. Additionally, the potential replication using a different, but equally robust methodology would serve to strengthen the claim that cortical FA at birth might serve as a useful biomarker of later neurodevelopmental outcomes. In short, the diffusion data was pre-processed with correction for motion artefact and slice-to-volume reconstruction using the SHARD approach with all data passing the stringent dHCP quality control assessment (Edwards et al., 2022). To parcellate the cortex into 52 parcels based on an atlas (Feng et al., 2019), we first categorized all subjects into three template groups based on PMA at scan (33w,36w,39w). To register individual subject FA maps to a DTI-based relevant age-group atlas template, we opted to apply FSL's FNIRT following the recommendations of the atlas' authors (brainmrmap.org, n.d) whereas the original study used the LDDMM method (Miller et al., 2002). We then inverted the FNIRT computed transformation warps to bring cortical parcellations to individual subject space.

Instead of cortical FA extraction through cortical skeletons, we next projected the FA map and cortical parcellation for each subject to the individual inner cortical surface using a previously validated cylindrical approach, guided by the local minimum of axial diffusivity (AD) in the cortical ribbon (Lebenberg et al., 2019). This ensured that FA measures and parcel labels were extracted from the same spatial location at each voxel and in a reliable way at the individual level. Moreover, the current extraction method used in this study is robust across the wide range of ages at scan, since it relies on the local AD minimum which is consistently observed in the cortex at all ages rather than relying on FA measures which become low around term equivalent age (Batalle et al., 2019). Despite this, some errors in the subject parcellations were observed particularly in areas where the opposing gyral banks were in close spatial proximity in volumetric space for example at the level of the central sulcus. This was mainly

due to the propagation of registration problems, perhaps related to the difference between PMA at scan and template age (i.e. lower registration quality when there was a larger age gap between a subject and the template). This might have particularly affected the predictive results of Cohort A which included more infants with ages distant to the 39w group template than other cohorts. To minimize the effects of the potential remaining errors of cortical parcellation after iterative corrections, we finally extracted the median rather than mean regional FA, due to its better robustness to outlier values particularly in small cortical regions (e.g. angular gyrus, parahippocampal gyrus). Together, we feel that this would mean it is unlikely that these methodological differences in our optimised pipeline for cortical FA extraction compared with the original study would have impacted the observation of robust prediction results, although this cannot be excluded.

Observed differences between extracted regional FA metrics across subjects and regions could stem from differences in infants' developmental stage (related to GA at birth and PMA at scan) and in intrinsic differences in local regional microstructure observed also in mature adult brains (Fukotomi et al., 2018). As both the original and this study focused on infants scanned close to birth, taking into account the inter-individual variability in cortical microstructure related to PMA at scan was necessary to reduce the impact of this potential confounding factor. In line with the original study and for the sake of simplicity, we then adjusted the regional cortical FA using a biphasic piecewise linear regression with inflection point at 36w PMA, although a region-dependent age cut-off might have been more appropriate to consider the spatially and temporally heterogeneous maturation of cortical microstructure. This FA adjustment led to a substantial reduction in the prediction of prematurity status, suggesting that the initial results were driven mostly by differences in PMA at scan rather than in cortical microstructure per se. These results stressed the importance of appropriate corrections of inputs (such as PMA at scan) to dissociate the impact of cortical microstructure on predictive performance from the incidental effects of potential confounders. Reintroducing inter-regional differences (e.g. through regional value interpolation at TEA, *Figure 4.4c*) could be done in the future to keep the inherent but potentially informative differences between the cortical parcels. For the same reason, it might also be worthwhile scaling all input FA features across regions simultaneously, as here (like in the original study), each input FA feature was scaled to lie in the range (0,1) over the group for each parcel independently.

Another important methodological aspect for prediction studies relies on the implemented pipeline. Results of ML studies are by nature, highly dependent on the dataset and its learning procedure, and on data splitting strategies. Approaches can be highly variable

and thus results often generalize poorly to other datasets, especially in the context of small datasets (Woods, 2018, Varoquaux, 2018, Poldrack et al., 2019). In our case, even the largest Cohort A, which is six times larger than the dataset in the original study, would typically be considered small in a ML context and might also suffer from these generalization limitations. We attempted to remedy this by a thorough assessment of predictive performance which is a crucial step to dissociate whether the reported results are reliable or whether they might stem from performance fluctuations. Although the leave-one-out cross-validation strategy is popular for small datasets since it maximizes the training set size by keeping only a single subject for the testing, its main limitation is reduced estimation of generalization performance due to the depleted test set (Bouthillier et al., 2021). We thus aimed to leverage our larger cohort which allowed us to assess how, holding the algorithm constant, the performance changes under small perturbations to the data by performing randomized repetitions of the k-fold validation. Testing the prediction pipeline performance multiple times using multiple splits and thus test sets in this manner can improve estimation of performance variability (Poldrack et al., 2019, Bouthillier et al., 2021)

Finally, predictive performance is highly sensitive to hyperparameter settings with suboptimal settings leading to unfairly low performance (Poldrack et al., 2019). Noting that the hyperparameters used in the original study might be suboptimal in our input/target setting, we decided to incorporate the hyperparameter tuning within the nested cross-validation loop. However, neither the extended validation nor tuning led to behavioural outcome prediction results similar to those reported in the original study.

An important finding was that for prematurity status prediction, we observed significant differences in prediction performance in relation to the cortical parcellation used. One possible explanation is that summarising cortical microstructure into 52 regional metrics using a neonatal atlas might be insufficient for the behavioural predictions. We found that random parcellations led to better prediction of prematurity status, potentially simply due to the increased granularity of inputs associated with a larger number of parcels. However, there is also evidence that in the absence of a substantial sample size to train meaningful models, adding dimensions can negatively impact model performance and generalisability (Koutroumbas & Theodoridis, 2009). This is not only because of the ‘curse of dimensionality’, but also because more granular parcellations will be more sensitive to noise within the data and likely suffer from large multi-collinearity between the inputs (discussed below). Although outside the scope of our replication study, this suggested that future studies will clearly benefit from first

identifying the study-specific optimal number of parcels that represent a good trade-off between information granularity and dimensionality reduction.

Another limitation to the atlas parcellations potentially stems from methodological difficulties regarding the delineation of cortical regions in the neonate cortex. This is particularly relevant for regions such as the hippocampus or entorhinal gyrus, which are small and difficult to delineate. As a result, FA values in these types of areas had substantially larger variability compared to other parcels. Such (heterogeneously) noisy measurements could thus negatively affect predictive performance. Although the benefits of atlas informed parcellations on predictive results should be investigated further in the future, our findings suggest random parcellations could provide a simpler and neutral strategy to extract cortical microstructure descriptors for use in predictive models. Alternatively, regularized voxel-based strategies combined with deep learning able to automatically extract the relevant features from the large dataset images might be an additional avenue to explore to avoid the difficulties associated with the cortical parcellations.

#5.2. Possible causes for negative prediction results

Our inability to recreate the conclusions of the original study might stem from deviations to the original methodology as discussed in the previous sections, as well as from differences in PMA at scan between cohorts and in image characteristics. For instance, the PMA distribution for Cohort A is skewed towards somewhat older ages, which is of relevance as the reliability of measures of cortical microstructure at these ages is still debated. Some authors have suggested that above 40w PMA, FA measures might be as low as noise values, and thus no longer sensitive to microstructural characteristics (Ball et al., 2013, Ouyang et al., 2019), whereas others have proposed that FA provides relevant information even above 41w PMA (Batalle et al., 2019). Here, we observed inter-subject and inter-regional variability in the extracted FA metrics, even in the Cohort A where the skew towards the older subjects was the largest. This suggested that FA might hold some information about the underlying microstructural differences across subjects which, if useful for the establishment of relationship with the later neurodevelopment, should be able to drive the predictions. Nevertheless, given the ongoing discussion regarding FA's lack of sensitivity to microstructural changes in the cortex in older infants (>38w PMA), its usefulness for neurodevelopmental outcome prediction might be limited to the preterm cohorts.

Additionally, differences in the spatial resolution and signal-to-noise ratio of diffusion MRI images between studies might have led to different partial volume effects (critical at the

level of the thin cortical ribbon of neonates) and variable estimation of DTI model and thus FA. However, the high quality of the dHCP dataset for anatomical and diffusion MRI has been highlighted by several studies from different groups. We are also confident about the reliability of our measures and analyses having observed successful prediction of prematurity status based on cortical FA (corrected for PMA at scan), even in reduced cohorts.

Besides, development of cortical microstructure is defined by multiple ongoing processes such as the growth of dendritic arborisation, synaptogenesis, and myelination of intracortical white matter, combined with the large-scale complex process of cortical folding. As in the original study, we focused on the widely used DTI-derived FA measure. In the preterm period, cortical FA is initially high due to the early radial orientation of apical dendrites and radial glia, and then decreases: which has been suggested to reflect increased neurite growth in all orientations as the cortex matures (McKinstry et al., 2002; Kroenke et al., 2007; Huang et al., 2008; Ball et al., 2013; Dubois et al., 2014; Smyser et al., 2016; Ouyang et al., 2019a; Ouyang et al., 2019b). However, the non-monotonic FA developmental profile in relation to PMA at scan suggests a more complex underlying biological picture where the later stages (around the age of full-term bir0h) may be dominated by increasing cellular and organelle density (Batalle et al., 2019). This complex relationship potentially makes FA a difficult input feature for linear predictive models requiring a robust age correction strategy. It is possible that a different DTI-derived metric with a simpler age-related profile, such as mean or axial diffusivity that continuously decreases with age, might be a more straightforward choice. Nevertheless, none of the DTI-derived metrics is likely to completely capture the diversity of properties of the underlying microstructure on its own. Thus, expansion of the input feature space to include the complementary DTI-derived metrics could be required. Such increase of the input space dimensions however would likely need to be combined with an appropriate feature selection strategy before (or during) the training of the predictive models (Gondová et al., 2022).

Moreover, the specificity of the DTI method might be limited even when combining metrics (Vos et al., 2012) and ‘overlook’ important cortical modifications that relate to functional outcomes. Using more elaborate diffusion MRI models, such as diffusion kurtosis imaging (DKI) (Jensen et al., 2005) or a multi-compartment neurite orientation dispersion and density imaging (NODDI) (Zhang et al., 2012) may improve description of complex cortical cytoarchitecture during gestation (Genc et al., 2017; Mah et al., 2017; Kimpton et al., 2020). However, these complex models require multi-shell diffusion data which likely limits the future potential applications of predictive models with clinical applications. Although possible with

the dHCP data used here, estimating these more complex models was beyond the scope this replication.

Additionally, cortical microstructure alone might provide too limited a view of the complex developmental stage that a brain has reached at birth. In this respect, the unimodal nature of diffusion imaging at birth might be unable to prognosticate about the complex combination of neurodevelopmental processes underlying later behavioural acquisitions. Assuming that information sufficient for the prediction of later outcomes relies mainly on the brain, incorporating other sources of information such as cortical morphology (Seidlitz et al., 2018, Fenchel et al., 2022), white matter connectivity (Ball et al., 2015, Wee et al., 2017, Girault et al., 2019), or even functional connectivity (He et al., 2021) might be beneficial. Nevertheless, timing of the imaging will have an important impact on what ‘developmental information’ can be accessed as the maturation occurs within a spatially heterogeneous and temporally asynchronous progression (both within grey and white matter) (Kulikova et al., 2014, Croteau-Chonka et al., 2016, Gilmore et al., 2018, Lebenberg et al., 2019, Yu et al., 2019). It is also likely that developmental trajectories capturing the dynamism that characterises brain development at multiple timepoints can provide more reliable information for predictive models compared to a single snapshot of the brain at birth. Thus, investing into the acquisition of longitudinal cohorts, even if difficult to implement in practice, might be required for developing successful outcome prognostic tools in the future. As a more practical alternative at large scale, it might be useful to further investigate what is the optimal timing for a single MRI exploration to provide relevant markers for prediction.

A further consideration is that as children develop after birth, environmental information (e.g. sensory stimulation, nutrition, social interaction, socio-economic factors) also significantly impacts on neurodevelopment. This has been shown to explain a large part of observed interindividual variability in sensorimotor and cognitive skill acquisition, with the influence of perinatal risk factors diminishing over time (Pierrat et al., 2021; Boardman & Counsell, 2019; Gui et al., 2019; Beauregard et al., 2018; Mangin et al., 2017). Thus, it is unlikely that brain features at birth alone, in the absence of socio-economic and clinical information, can truly capture the complex relationships between a given child’s development and outcomes. Adding these factors to predict outcome could thus provide useful complementary information. Nevertheless, given the high resource requirements for large population level MRI studies, it will be important to investigate whether the imaging data brings additional benefits to outcome prognostication compared to readily available clinical information.

Another aspect that might partly explain our negative prediction results is the low heterogeneity within our study population who were at relatively low risk of neurodevelopmental impairment. In contrast to the original study which used the BSID-III scores assessed around 2 years of corrected age, the neurodevelopmental outcome assessment available in the dHCP database was performed at around 18 months. The overall neurodevelopmental stage in terms of language, cognitive and motor acquisitions between the two ages is very similar and is unlikely to change the significance or conclusions derived from our results. Additionally, assessment at 18 months corresponds to a strategic age for identifying neurodevelopmental impairment in preterm infants, and thus examining whether cortical microstructure at birth relates to outcomes at this age is of interest even in low-risk preterm populations without obvious brain anomalies who can still develop subtle neuromotor disorders (e.g. developmental coordination disorder) (Groeschel et al., 2019; Spittle & Orton, 2014; Edwards et al., 2011; Zwicker et al., 2012). Although in our study, prematurely born infants were over-represented in the atypical category of the BSID-III motor score compared with full-terms, no major development delays or specific disabilities were neither expected nor observed within the specific low-risk cohort analysed in our replication study. Therefore, an important question raised in the original study of insufficient heterogeneity within the input and outputs remained pertinent in our work.

As an extension, we performed the training and evaluation of the outcome predictions on different cohorts with expanded variability for the targets (Cohort B) as well as both targets and inputs (Cohort A), but without success in terms of prediction results. The limited variance within the input features combined with the relatively narrow distribution of the BSID-III scores across the dataset may have still been insufficient to allow the ML models to establish relationships with outcomes even if such relationships do exist. Moreover, cohort selection bias towards a low-risk population might remain problematic, given that even in the presence of inherent but subtle microstructural variability that could be predictive of the later outcomes, this might remain undetected because of the noisy metric extraction: detecting this relevant and predictive variability would thus require more precise measurements of cortical FA. Developing targeted models for a specific narrow age range may alleviate problems with feature extraction and provide more reliable inputs, which coupled with wider BSID-III outcome distributions (including more infants with atypical outcomes) could lead to more reliable results.

#5.3. ML & interpretation

Finally, we would like to discuss limitations regarding the generalizability and interpretation of ML results, although we did not recreate the evaluation of model feature importance as in the original study, given the poor prediction of BSID-III scores we obtained. In the context of linear SVR, the high correlation between cortical features observed in our cohort (*Annexe 3.2. Supp. Figure 5*) and similar trends expected in the original study might be a critical issue to keep in mind. Firstly, input collinearity might affect the generalizability of the trained models. This is because during training, predictive models aim to minimize the prediction error, not to explain the true relationships between input features and the target. Thus, any of the highly correlated features can be selected as a strong predictor while the impact of other features with similar relationships with the target is minimized, leading to a lower performance on new data that does not follow the same correlation patterns.

In the future, it might be appropriate to attempt to decorrelate the inputs for all cortical parcels using a dimensionality reduction method such as PCA (Hotelling, 1993). Such a strategy might have additional benefits by decreasing the number of input dimensions and capturing only the components with the greatest amount of variance, while retaining most of the original information content and additionally “denoising” the data. Nevertheless, interpreting the feature weights in such a setting in terms of regional association with outcome suffers from the same pitfall. Post-hoc analysis of the feature weights will only allow evaluation of the use of features within the ML model, which is not the same as evaluating the data itself. Thus, our ability to draw links between the interpretation of predictive models and the underlying region-target functional associations will remain limited without additional hypothesis-driven experiments.

#6 Conclusions

Machine learning has become a major focus of research as a promising tool for early behavioural outcome prediction. However, very few clinical questions, including the neurodevelopmental assessments, represent well posed discrimination tasks that can be naturally framed as ML problems (Baker & Kandasamy, 2022). Careful consideration of potential confounders that might drive predictions instead of the inputs of interest is required before ML can become useful in the clinical practice. This is further compounded by a lack of standardized methodologies for model implementation with some validation methods in current ML applications leading to highly variable and potentially inflated ML performance estimation, in particular in small datasets (Varoquaux, 2018). As in many other areas,

reproducibility failures in ML-based science appears prevalent without any systemic solutions (Kapoor et al. 2022). In light of these limitations, our inability to corroborate conclusions of the study by Ouyang et al., (2020) does not come as a surprise. Importantly, it should not be seen as a discouragement either. As a reminder, the normative charts used in clinical practice, even though proposing much simpler features for the prognosis, are often derived from very large cohorts. Successful leveraging of the complexity of brain imaging data now requires reaching (at minimum) similar large scales. Additionally, it might be useful to admit that replication problems, whether they involve direct or conceptual replication efforts, are an unescapable component of the current *early* stage of the field which could drive increased efforts to establish good practices for implementation and careful validation of the promising prediction tools.

#7 References

- Adibpour, P., Lebenberg, J., Kabdebon, C., Dehaene-Lambertz, G., & Dubois, J. (2020, April). Anatomic-functional correlates of auditory development in infancy. *Developmental Cognitive Neuroscience*, 42, 100752.
- Arpi, E., & Ferrari, F. (2013). Preterm birth and behaviour problems in infants and preschool-age children: a review of the recent literature. *Developmental Medicine & Child Neurology*, 55.
- Baker, S. B., & Kandasamy, Y. (2022). Machine learning for understanding and predicting neurodevelopmental outcomes in premature infants: a systematic review. *Pediatric Research*, 1-7.
- Ball, G., Pazderová, L., Chew, A. T., Tusor, N., Merchant, N., Arichi, T., . . . Counsell, S. J. (2015). Thalamocortical Connectivity Predicts Cognition in Children Born Preterm. *Cerebral Cortex* (New York, NY), 25, 4310-4318.
- Ball, G., Srinivasan, L., Aljabar, P., Counsell, S. J., Durighel, G., Hajnal, J. V., . . . Edwards, A. D. (2013). Development of cortical microstructure in the preterm human brain. *Proceedings of the National Academy of Sciences*, 110, 9541-9546.
- Bastiani, M., Cottaar, M., Fitzgibbon, S., Suri, S., Alfaro-Almagro, F., Sotiropoulos, S., . . . Andersson, J. (2019, January). Automated quality control for within and between studies diffusion MRI data using a non-parametric framework for movement and distortion correction. *NeuroImage*, 184, 801-812.
- Batalle, D., O'Muircheartaigh, J., Makropoulos, A., Kelly, C. J., Dimitrova, R., Hughes, E. J., . . . Counsell, S. J. (2019). Different patterns of cortical maturation before and after 38 weeks gestational age demonstrated by diffusion MRI in vivo. *Neuroimage*, 185, 764-775.
- Bayley, N. (2012). *Bayley Scales of Infant and Toddler Development*, Third Edition.
- Beauregard, J. L., Drews-Botsch, C., Sales, J. M., Flanders, W. D., & Kramer, M. R. (2018). Does Socioeconomic Status Modify the Association Between Preterm Birth and Children's Early Cognitive Ability and Kindergarten Academic Achievement in the United States? *American Journal of Epidemiology*, 187, 1704-1713.
- Blauw-Hospers, C. H., de Graaf-Peters, V. B., Dirks, T., Bos, A. F., & Hadders-Algra, M. (2007). Does early intervention in infants at high risk for a developmental motor disorder improve motor and cognitive development? *Neuroscience & Biobehavioral Reviews*, 31, 1201-1212.

- Bozek, J., Makropoulos, A., Schuh, A., Fitzgibbon, S. P., Wright, R., Glasser, M. F., . . . Robinson, E. C. (2018). Construction of a neonatal cortical surface atlas using Multimodal Surface Matching in the Developing Human Connectome Project. *NeuroImage*, 179, 11-29.
- Boardman, J. P., & Counsell, S. J. (2019). Factors associated with atypical brain development in preterm infants: insights from magnetic resonance imaging.
- Bouthillier, X., Delaunay, P., Bronzi, M., Trofimov, A., Nichyporuk, B., Szeto, J., . . . Vincent, P. (2021). Accounting for Variance in Machine Learning Benchmarks. *ArXiv*, abs/2103.03098.
- Brainmap, & Org. (n.d.). Penn CHOP age specific neonate and infant brain atlases. Penn CHOP age specific neonate and infant brain atlases.
- Christiaens, D., Cordero-Grande, L., Pietsch, M., Hutter, J., Price, A. N., Hughes, E. J., . . . Tournier, J. D. (2021). Scattered slice SHARD reconstruction for motion correction in multi-shell diffusion MRI. *Neuroimage*, 225.
- Cordero-Grande, L., Hughes, E. J., Hutter, J., Price, A. N., & Hajnal, J. V. (2018). Three-dimensional motion corrected sensitivity encoding reconstruction for multi-shot multi-slice MRI: Application to neonatal brain imaging. *Magnetic Resonance in Medicine*, 79, 1365-1376.
- Croteau-Chonka, E. C., Dean, D. C., Remer, J., Dirks, H., O'Muircheartaigh, J., & Deoni, S. C. (2016). Examining the relationships between cortical maturation and white matter myelination throughout early childhood. *NeuroImage*, 125, 413-421.
- Dubois, J., Dehaene-Lambertz, G., Kulikova, S., Poupon, C., Hüppi, P. S., & Hertz-Pannier, L. (2014). The early development of brain white matter: A review of imaging studies in fetuses, newborns and infants. *Neuroscience*, 276, 48-71.
- Edwards, A. D., Rueckert, D., Smith, S. M., Seada, S. A., Alansary, A., Almalbis, J. F., . . . Hajnal, J. V. (2022). The Developing Human Connectome Project Neonatal Data Release. *Frontiers in Neuroscience*, 16.
- Edwards, J. K., Berube, M., Erlandson, K., Haug, S., Johnstone, H., Meagher, M., . . . Zwicker, J. G. (2011). Developmental Coordination Disorder in School-Aged Children Born Very Preterm and/or at Very Low Birth Weight: A Systematic Review. *Journal of Developmental & Behavioral Pediatrics*, 32, 678-687.
- Fenchel, D., Dimitrova, R., Robinson, E. C., Batalle, D., Chew, A. T., Falconer, S., . . . O'Muircheartaigh, J. (2022). Neonatal multi-modal cortical profiles predict 18-month developmental outcomes. *Developmental Cognitive Neuroscience*, 54.
- Feng, L., Li, H., Oishi, K., Mishra, V. R., Song, L., Peng, Q., . . . Huang, H. (2019). Age-specific gray and white matter DTI atlas for human brain at 33, 36 and 39 postmenstrual weeks. *NeuroImage*, 185, 685-698.
- Fukutomi, H., Glasser, M. F., Zhang, H., Autio, J. A., Coalson, T. S., Okada, T., . . . Hayashi, T. (2018). Neurite imaging reveals microstructural variations in human cerebral cortical gray matter. *NeuroImage*, 182, 488-499.
- Genc, S., Malpas, C. B., Holland, S. K., Beare, R., & Silk, T. J. (2017). Neurite density index is sensitive to age related differences in the developing brain. *NeuroImage*, 148, 373-380.
- Gilmore, J. H., Knickmeyer, R. C., & Gao, W. (2018). Imaging structural and functional brain development in early childhood. *Nature Reviews Neuroscience*, 19, 123-137.
- Girault, J. B., Munsell, B. C., Puechmaille, D., Goldman, B. D., Prieto, J. C., Styner, M., & Gilmore, J. H. (2019). White matter connectomes at birth accurately predict cognitive abilities at age 2. *NeuroImage*, 192, 145-155.
- Gondová, A., Neumane, S., Leprince, Y., Mangin, J., & Dubois, J. (2022, June 19). Infant cortical microstructure at term-equivalent age accurately predicts prematurity status at birth. In *OHBM 2022 annual meeting*. Glasgow, UK.

- Groeschel, S., Holmström, L., Northam, G. B., Tournier, J. D., Baldeweg, T., Latal, B., . . . Vollmer, B. (2019). Motor Abilities in Adolescents Born Preterm Are Associated With Microstructure of the Corpus Callosum. *Frontiers in Neurology*, 10.
- Gui, L., Loukas, S., Lazeyras, F., Huppi, P. S., Meskaldji, D. E., & Borradori-Tolsa, C. (2019). Longitudinal study of neonatal brain tissue volumes in preterm infants and their ability to predict neurodevelopmental outcome. *NeuroImage*, 185, 728-741.
- Hadaya, L., & Nosarti, C. (2020). The neurobiological correlates of cognitive outcomes in adolescence and adulthood following very preterm birth. *Seminars in fetal & neonatal medicine*, 101117.
- He, L., Li, H., Chen, M., Wang, J., Altaye, M., Dillman, J. R., & Parikh, N. A. (2021). Deep Multimodal Learning From MRI and Clinical Data for Early Prediction of Neurodevelopmental Deficits in Very Preterm Infants. *Frontiers in Neuroscience*, 15.
- Hotelling, H. (1933). Analysis of a complex of statistical variables into principal components. *Journal of Educational Psychology*, 24, 498-520.
- Huang, H., Yamamoto, A., Hossain, M. A., Younes, L., & Mori, S. (2008). Quantitative Cortical Mapping of Fractional Anisotropy in Developing Rat Brains. *The Journal of Neuroscience*, 28, 1427-1433.
- Hughes, E. J., Winchman, T., Padormo, F., Teixeira, R. P., Wurie, J., Sharma, M., . . . Hajnal, J. V. (2017). A dedicated neonatal brain imaging system. *Magnetic Resonance in Medicine*, 78, 794-804.
- Hutter, J., Tournier, J. D., Price, A. N., Cordero-Grande, L., Hughes, E. J., Malik, S. J., . . . Hajnal, J. V. (2018). Time-efficient and flexible design of optimized multishell HARDI diffusion. *Magnetic Resonance in Medicine*, 79, 1276-1292.
- Jensen, J. H., Helpert, J. A., Ramani, A., Lu, H., & Kaczynski, K. (2005). Diffusional kurtosis imaging: The quantification of non-gaussian water diffusion by means of magnetic resonance imaging. *Magnetic Resonance in Medicine*, 53.
- Johnston, M. V. (2009). Plasticity in the developing brain: implications for rehabilitation. *Developmental disabilities research reviews*, 15 2, 94-101.
- Kapoor, S., & Narayanan, A. (2022). Leakage and the Reproducibility Crisis in ML-based Science. *Leakage and the Reproducibility Crisis in ML-based Science*. arXiv.
- Kimpton, J. A., Bataille, D., Barnett, M. L., Hughes, E. J., Chew, A. T., Falconer, S., . . . Counsell, S. J. (2020). Diffusion magnetic resonance imaging assessment of regional white matter maturation in preterm neonates. *Neuroradiology*, 63, 573-583.
- Kostović, I., Sedmak, G., & Judas, M. (2019). Neural histology and neurogenesis of the human fetal and infant brain. *NeuroImage*, 188, 743-773.
- Kroenke, C. D., Essen, D. C., Inder, T. E., Rees, S., Bretthorst, G. L., & Neil, J. J. (2007). Microstructural Changes of the Baboon Cerebral Cortex during Gestational Development Reflected in Magnetic Resonance Imaging Diffusion Anisotropy. *The Journal of Neuroscience*, 27, 12506-12515.
- Kulikova, S., Hertz-Pannier, L., Dehaene-Lambertz, G., Buzmakov, A., Poupon, C., & Dubois, J. (2014). Multi-parametric evaluation of the white matter maturation. *Brain Structure & Function*, 220, 3657-3672.
- Lebenberg, J., Mangin, J. F., Thirion, B., Poupon, C., Hertz-Pannier, L., Leroy, F., . . . Dubois, J. (2019). Mapping the asynchrony of cortical maturation in the infant brain: A MRI multi-parametric clustering approach. *NeuroImage*, 185, 641-653.
- Mah, A., Geeraert, B. L., & Lebel, C. A. (2017). Detailing neuroanatomical development in late childhood and early adolescence using NODDI. *PLoS ONE*, 12.

- Makropoulos, A., Gousias, I. S., Ledig, C., Aljabar, P., Serag, A. M., Hajnal, J. V., . . . Rueckert, D. (2014). Automatic Whole Brain MRI Segmentation of the Developing Neonatal Brain. *IEEE Transactions on Medical Imaging*, 33, 1818-1831.
- Makropoulos, A., Robinson, E. C., Schuh, A., Wright, R., Fitzgibbon, S. P., Bo\varez, J., . . . Rueckert, D. (2018). The developing human connectome project: A minimal processing pipeline for neonatal cortical surface reconstruction. *NeuroImage*, 173, 88-112.
- Mangin, K. S., Horwood, L. J., & Woodward, L. J. (2017). Cognitive Development Trajectories of Very Preterm and Typically Developing Children. *Child development*, 88 1, 282-298.
- Marín, O. (2016). Developmental timing and critical windows for the treatment of psychiatric disorders. *Nature Medicine*, 22, 1229-1238.
- McKinstry, R. C., Mathur, A. M., Miller, J. H., Ozcan, A., Snyder, A. Z., Schefft, G. L., . . . Neil, J. J. (2002). Radial organization of developing preterm human cerebral cortex revealed by non-invasive water diffusion anisotropy MRI. *Cerebral cortex*, 12 12, 1237-43.
- Miller, M. I., Trouvé, A., & Younes, L. (2002). On the metrics and euler-lagrange equations of computational anatomy. *Annual review of biomedical engineering*, 4, 375-405.
- Müller, A. B., Saccani, R., & Valentini, N. C. (2017). Impact of compensatory intervention in 6- to 18-month-old babies at risk of motor development delays. *Early Child Development and Care*, 187, 1707-1717.
- Oishi, K., Mori, S., Donohue, P. K., Ernst, T., Anderson, L., Buchthal, S., . . . Chang, L. (2011). Multi-contrast human neonatal brain atlas: Application to normal neonate development analysis. *NeuroImage*, 56, 8-20.
- Ouyang, M., Dubois, J., Yu, Q., Mukherjee, P., & Huang, H. (2019). Delineation of early brain development from fetuses to infants with diffusion MRI and beyond. *NeuroImage*, 185, 836-850.
- Ouyang, M., Jeon, T., Sotiras, A., Peng, Q., Mishra, V. R., Halovanic, C., . . . Huang, H. (2019). Differential cortical microstructural maturation in the preterm human brain with diffusion kurtosis and tensor imaging. *Proceedings of the National Academy of Sciences of the United States of America*, 116, 4681-4688.
- Ouyang, M., Peng, Q., Jeon, T., Heyne, R., Chalak, L., & Huang, H. (2020). Diffusion-MRI-based regional cortical microstructure at birth for predicting neurodevelopmental outcomes of 2-year-olds. *eLife*, 9.
- Parikh, N. A. (2016). Advanced neuroimaging and its role in predicting neurodevelopmental outcomes in very preterm infants. *Seminars in perinatology*, 40 8, 530-541.
- Pickler, R. H., Mcgrath, J. M., Reyna, B. A., McCain, N. L., Lewis, M., Cone, S., . . . Best, A. M. (2010). A Model of Neurodevelopmental Risk and Protection for Preterm Infants. *The Journal of Perinatal & Neonatal Nursing*, 24, 356–365.
- Pierrat, V., Marchand-martin, L., Marret, S., Arnaud, C., Benhammou, V., Cambonie, G., . . . Ancel, P.-Y. (2021). Neurodevelopmental outcomes at age 5 among children born preterm: EPIPAGE-2 cohort study. *The BMJ*, 373.
- Poldrack, R. A., Huckins, G., & Varoquaux, G. (2019). Establishment of Best Practices for Evidence for Prediction: A Review. *JAMA psychiatry*.
- Rolland, C., Lebenberg, J., Leroy, F., Moulton, E., Adibpour, P., Riviere, D., . . . Dubois, J. (2019, April). Exploring Microstructure Asymmetries in the Infant Brain Cortex: A Methodological Framework Combining Structural and Diffusion Mri. In 2019 IEEE 16th International Symposium on Biomedical Imaging (ISBI 2019) (pp. 426–429).
- Seidlitz, J., Vá\vsá, F., Shinn, M., Romero-García, R., Whitaker, K. J., Vértes, P. E., . . . Bullmore, E. T. (2018). Morphometric Similarity Networks Detect Microscale Cortical Organization and Predict Inter-Individual Cognitive Variation. *Neuron*, 97, 231-247.e7.

- Silbereis, J. C., Pochareddy, S., Zhu, Y., Li, M., & Sestan, N. (2016). The Cellular and Molecular Landscapes of the Developing Human Central Nervous System. *Neuron*, 89, 248-268.
- Smyser, C. D., Dosenbach, N. U., Smyser, T. A., Snyder, A. Z., Rogers, C. E., Inder, T. E., . . . Neil, J. J. (2016). Prediction of brain maturity in infants using machine-learning algorithms. *NeuroImage*, 136, 1-9.
- Smyser, T. A., Smyser, C. D., Rogers, C. E., Gillespie, S. K., Inder, T. E., & Neil, J. J. (2016). Cortical Gray and Adjacent White Matter Demonstrate Synchronous Maturation in Very Preterm Infants. *Cerebral cortex*, 26 8, 3370-3378.
- Spittle, A. J., & Orton, J. (2014). Cerebral palsy and developmental coordination disorder in children born preterm. *Seminars in fetal & neonatal medicine*, 19 2, 84-9.
- Theodoridis, S., & Koutroumbas, K. D. (2008). *Pattern Recognition*, Fourth Edition.
- Tournier, J. D., Christiaens, D., Hutter, J., Price, A. N., Cordero-Grande, L., Hughes, E. J., . . . Hajnal, J. V. (2019). A data-driven approach to optimising the encoding for multi-shell diffusion MRI with application to neonatal imaging. *NMR in biomedicine*, 33, e4348 - e4348.
- Varoquaux, G. (2018). Cross-validation failure: Small sample sizes lead to large error bars. *NeuroImage*, 180, 68-77.
- Vos, S. B., Jones, D. K., Jeurissen, B., Viergever, M. A., & Leemans, A. (2012). The influence of complex white matter architecture on the mean diffusivity in diffusion tensor MRI of the human brain. *NeuroImage*, 59, 2208-2216.
- Wee, C.-Y., Tuan, T. A., Broekman, B. F., Ong, M. Y., Chong, Y.-S., Kwek, K., . . . Qiu, A. (2017). Neonatal neural networks predict children behavioral profiles later in life. *Human Brain Mapping*, 38.
- Woods, B. (2018). Expanding search in the space of empirical ML. *ArXiv*, abs/1812.01495.
- Yu, Q., Ouyang, A., Chalak, L., Jeon, T., Chia, J. M., Mishra, V. R., . . . Huang, H. (2016). Structural Development of Human Fetal and Preterm Brain Cortical Plate Based on Population-Averaged Templates. *Cerebral cortex*, 26 11, 4381-4391.
- Yu, Q., Peng, Y., Kang, H., Peng, Q., Ouyang, M., Slinger, M., . . . Huang, H. (2019). Differential White Matter Maturation from Birth to 8 Years of Age. *Cerebral Cortex (New York, NY)*, 30, 2674-2690.
- Zhang, H., Schneider, T., Wheeler-Kingshott, C. A., & Alexander, D. C. (2012). NODDI: Practical in vivo neurite orientation dispersion and density imaging of the human brain. *NeuroImage*, 61, 1000-1016.
- Zwaan, R., Etz, A., Lucas, R., & Donnellan, B. (2017, October 20). Making Replication Mainstream. *Behavioral and Brain Sciences*, 41.
- Zwicker, J. G., Yoon, S. W., Mackay, M., Petrie-Thomas, J., Rogers, M., & Synnes, A. R. (2012). Perinatal and neonatal predictors of developmental coordination disorder in very low birthweight children. *Archives of Disease in Childhood*, 98, 118-122.

4.3. Cortical microstructure as a biomarker of prematurity at birth

In the preceding section and article, we showed that utilizing cortical fractional anisotropy alone did not enable reliable individual predictions of later neurodevelopmental outcomes. However, consistent differences in cortical microstructure between PT and FT infants at TEA have been previously reported in addition to the typical heterogeneity of maturation progression across the cortex (Parikh, 2016). Thus, studying differences in cortical microstructure between PT and FT infants with a supervised machine learning approach might still be of interest to provide insights into atypical developmental trajectories resulting from the premature birth.

To explore this perspective, we aimed to assess the early microstructural properties of the neonate cortex using diffusion MRI and employ machine learning to distinguish between preterm and full-term infants studied at around TEA. This section first briefly describes the used dHCP data for PT and FT infants, followed by a description of the implemented predictive pipeline and concise summary of the results. The chapter concludes with a related poster presented at the annual scientific meeting of the Organisation for Human Brain Mapping (OHBM) 2022 (Gondová et al., 2022).

4.3.1. Methods

In this study, we examined data from 59 PT infants (55.9% males, GA at birth: [23.7-36.0] weeks; PMA at scan: [38.4-44.9] weeks) and 59 FT infants, matched for PMA and sex, selected from the dHCP database. DTI-derived metric maps (AD, RD, and FA) estimated from the SHARD-processed diffusion MRI data ($b=0-1000$ sec/mm² shells) were reliably projected to the cortical surface (Lebenberg et al., 2019) and averaged for each of the 36 bilateral cortical ROIs defined using the infant-specific M-CRIB-S tool (Adamson et al., 2020). The resulting 216 features (3 metrics x 2 hemispheres x 36 ROIs) for each subject were used to predict the prematurity status at birth.

To reduce input dimensionality and enhance model interpretability, we addressed existing collinearities among features through feature selection. Initially, we calculated a distance matrix between all the evaluated features based on Pearson's correlation coefficient. Using this matrix, we performed Ward's linkage collinearity hierarchical clustering to describe the hierarchy of relationships between features. Subsequently, we selected a single representative feature from each cluster for use in the predictive models to reduce the redundancy of information. Our selection prioritized features that exhibited the greatest

distance from other clusters. The clustering threshold, determining the final number of features for the predictive models, was considered an additional hyperparameter during the fine-tuning of the gradient boosting classifier within the inner loop of the nested stratified 5-fold cross validation. We evaluated feature importance through permutation testing and SHAP (SHapley Additive exPlanations) analysis (Lundberg et al., 2020).

4.3.2. Results

As expected, significant differences in global cortical AD, RD, and FA were observed between the PT and FT groups (paired t-test: $p < 0.001$). The performance of predictive models for classifying prematurity status, i.e. whether an infant was born preterm or not, depended on the chosen clustering threshold. Through hyperparameter optimisation, specifically tuning the clustering threshold (optimal at 0.9), we achieved the best classifier capable of distinguishing between the two groups with high performance using 18 features (mean AUC: 0.80 ± 0.07 , recall: 0.79 ± 0.11 , precision: 0.80 ± 0.09 , f1-score: 0.79 ± 0.08). Notably, we were able to reduce the feature set to as few as 5 features while still achieving a non-random prediction (clustering threshold of 2, mean AUC: 0.7 ± 0.08 , recall: 0.7 ± 0.13 , precision: 0.71 ± 0.10 , f1-score: 0.70 ± 0.09), confirming the relatively widespread differences in cortical microstructure between the two groups (*Figure 4.8a*).

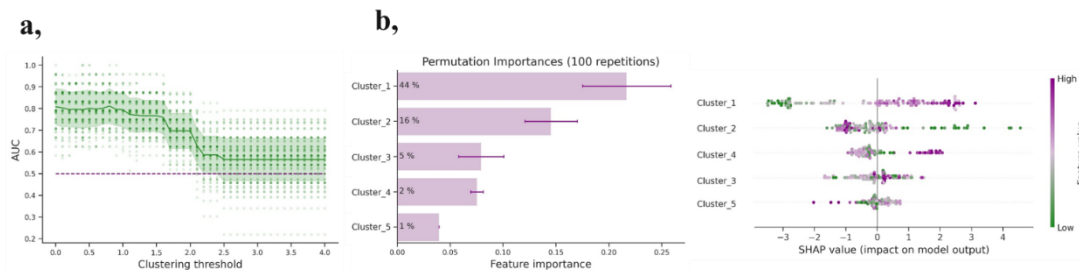


Figure 4.8. Results of the prematurity status prediction. **a.** Evolution of the AUC score with the collinearity clustering threshold. The green line represents the mean results over 20 repetitions of the nested stratified 5-fold cross validation, while the purple line shows the theoretical random classification baseline. This highlights a non-random prediction of prematurity status at birth for clustering thresholds below or equal to 2. **b.** Results of permutation testing and SHAP analysis of feature importance with the clustering threshold set to 2 (corresponding to 5 clusters). These results revealed the significance of clusters 1 and 2 for the prediction of prematurity status.

During validation, permutation testing, corroborated by the SHAP analysis (*Figure 4.8b*), revealed the importance of two distinct bilateral clusters for distinguishing between PT and FT infants at TEA: clusters 1 and 2, primarily localized in inferior frontal regions (*Figure 4.9*). Further analyses indicated that within cluster 1, most regions exhibited a reduction in

both AD and RD with GA at birth, while in cluster 2 regions, there was a minimal relationship between FA and GA.

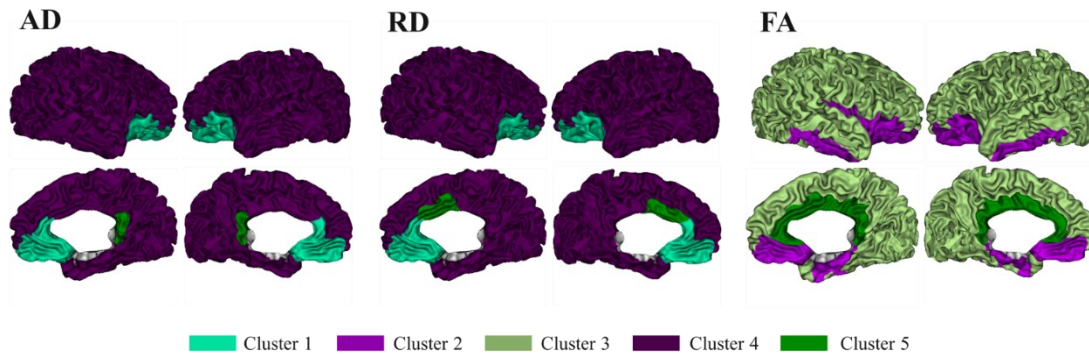


Figure 4.9. Localisation of 5 clusters for prematurity prediction, i.e. the minimum number of representative features allowing a non-random prediction of prematurity status. In particular, cluster 1 corresponds to 4 bilateral regions for both AD and RD, while cluster 2 corresponds to 6 bilateral regions and right insula for FA.

4.3.3. Conclusion

Our findings align with prior research, highlighting early global differences in cortical microstructure associated with preterm birth around TEA (Ball, Srinivasan, et al., 2013). Moreover, our original approach combining clustering analysis for feature selection with prematurity status prediction, identified specific regions that could discriminate between PT and FT infants, predominantly located in lateral and medial inferior frontal lobes. Prior machine learning-based studies also noted significant alterations in frontal regions between PT and FT infants in terms of functional (Ball et al., 2016) and structural connectivity (Taoudi-Benchekroun et al., 2022). These findings might imply broader systemic impacts of prematurity, potentially linked to relative immaturity of the frontal regions at the time of preterm birth. In future studies, extending the analysis to include a microstructural assessment of subcortical regions, including the thalamus - known to be particularly susceptible to the effects of preterm birth (Ball, Boardman, et al., 2013; Smyser et al., 2010) - could offer further insights into how prematurity shapes early microstructural development. Importantly, all three DTI metrics proved informative when distinguishing PT from FT infants, emphasizing their utility as complementary descriptors of diverse maturational processes occurring in the initial postnatal weeks (Ouyang, Dubois, et al., 2019), such as dendritic arborization growth and intra-cortical fibre myelination.

Poster:

Infant cortical microstructure at term-equivalent age accurately predicts prematurity status at birth.

Gondova Andrea^{1,2,*}, Neumane Sara^{1,2,3}, Leprince Yann², Mangin Jean-François⁴, Dubois Jessica^{1,2}

¹Université Paris Cité, INSERM, NeuroDiderot Unit UMR1141, F-75019, Paris, France, ²Université Paris-Saclay, CEA, NeuroSpin U1212, F-91191, Gif-sur-Yvette, France, ³Centre for Developing Brain, School of Biomedical Engineering and Imaging Sciences, King's College London, London, UK, ⁴Université Paris-Saclay, CEA, CNRS, BAOBAB, Gif-sur-Yvette, France
*andrea.gondova@cea.fr



Introduction

- **Preterm** birth has a profound, long-term effect on brain development.
- Related **grey-matter (GM) abnormalities** (e.g. lower volume, altered cortical gyration and maturation) have been described in preterm-born subjects across the lifespan with **MRI**^{1,2}.

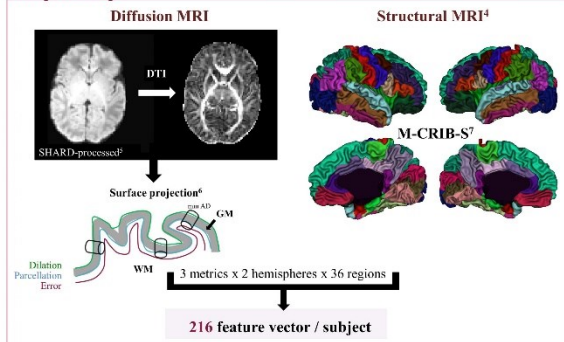
AIMS:

- ✓ Leverage **diffusion MRI** to evaluate early microstructural properties of the cortex
- ✓ **Differentiate between preterm- and full-term-born** infants studied at around term equivalent age (TEA).

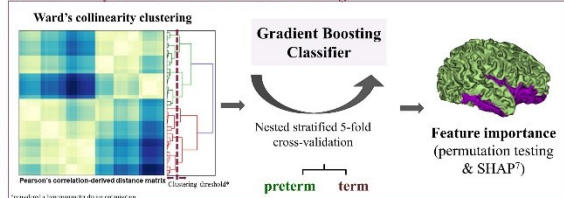
Methods

- 3T-MRI structural and diffusion MRI data (developing Human Connectome Project (dHCP))³.
- **59 preterm-born** infants without major brain lesions:
 - 55.9% males
 - gestational age (GA) at birth: [23.7–36.0] weeks
 - post-menstrual age (PMA) at MRI: [38.4–44.9] weeks
- **59 term-born** infants matched for PMA and sex
- DTI model: Axial Diffusivity (AD), Radial Diffusivity (RD), Fractional Anisotropy (FA)

Data processing



Dimensionality Reduction & Predictive Modelling



Results

- **Significant differences in average cortical AD, RD, and FA** between preterm and full-term infants (Fig 1A).
- Representative features from **5 clusters** relevant for prediction of infant prematurity status (Fig 1B and C)

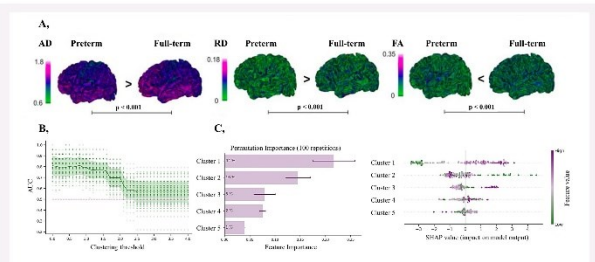


Figure 1. A, Example AD, RD, and FA cortical maps (paired t-test). AD and RD in $\times 10^{-3}$ mm²/sec. B, AUC score vs collinearity clustering threshold. — average result nested stratified 5-fold cross validation, — theoretical baseline. C, Feature importance (permutation testing and SHAP analysis with clustering threshold of 2).

- Predictive regions mainly localized in **lateral and medial inferior frontal lobes**(Fig 2A)
- Average AD over all regions of **cluster 1** significantly associated with GA at birth (Fig 2B)

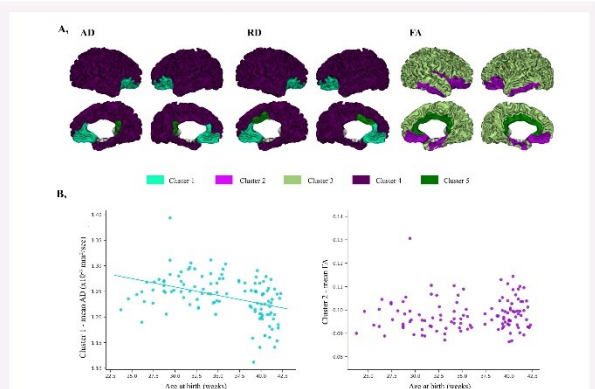


Figure 2. A, 5 clusters predictive of infant prematurity status. B, Average DTI metric (AD or FA) of **cluster 1** and **cluster 2** vs GA at birth. The line shows robust linear correlation.

Conclusions

- **Global differences** in cortical microstructure at TEA associated with preterm birth⁸
- All three DTI metrics informative for the classification - **the importance of using complementary metrics** when exploring early cortical development.
- In the future, similar approach to predict long-term neurodevelopmental outcome from cortical microstructure

References:

[1] Parikh (2015) Seminars in perinatology [2] Madaya & Nosarti (2020) Seminars in fetal & neonatal medicine [3] Hughes et al. (2017) Magnetic Resonance in Medicine [4] Makropoulos et al. (2018) NeuroImage [5] Christiaens et al. (2021) NeuroImage [6] Leibenberg et al. (2019) NeuroImage [7] Adanson et al. (2020) Scientific Reports [8] Lueken et al. (2020) Nature Machine Learning [9] Ball et al. (2013) PNAS

Acknowledgments:

AG was supported by the CEA NUMERICS program, which has received funding from the European Union's Horizon 2020 research and innovation program under the Marie Skłodowska-Curie grant agreement No 800945. The developing Human Connectome Project was funded by the European Research Council under the European Union Seventh Framework Programme (FP7/2007–2013/ERC Grant Agreement no. 319456). JD was supported by the Fondation Médicite (FDF-18-00092867) and the IdEx Université de Paris (ANR-18-IDEX-0001).

Afterword

The three presented studies of this *Chapter 4* aimed to utilize supervised machine learning tools for predicting neurodevelopmental characteristics (prematurity status) and outcomes based on microstructural features of the SM network (*Chapter 4.1*) and cortical microstructure (*Chapter 4.2, Chapter 4.3*). Our efforts met with variable degrees of success due to several methodological limitations discussed throughout the studies, underscoring the need for further refinement of predictive strategies, including the exploration of different machine learning models and feature selection strategies, along with the collection of more heterogeneous datasets.

Moreover, it is worth considering that no single MRI modality alone may effectively bridge the extensive temporal gap between early scans and outcomes evaluated months or even years later. Recent efforts have explored the integration of complementary MRI modalities, resulting in promising predictive outcomes (Janjic et al., 2020; He et al., 2021; Fenchel et al., 2022). However, the interindividual variability in neurodevelopmental outcomes likely arises from a combination of multiple factors, including dynamically developing brain features and “extracranial” factors which might be captured through supplementary clinical, demographic, and environmental information. Improved understanding of the infant brain development as a multimodal system resulting from structural, functional, and environmental interactions could guide the identification of the most appropriate MRI, clinical and environmental markers to guide future predictive studies. In this vein, the following chapter presents our work focusing on investigating potential relationships between developing inter-regional microstructural similarities across cortical and subcortical regions and functional connectivity during the preterm period, and their alterations in the context of prematurity.

Chapter 5: Relationship between grey-matter microstructural similarity and functional connectivity

Preface

The following section presents our recent work investigating the developmental changes and the relationships between grey matter microstructural similarity derived from complementary diffusion MRI metrics (DTI and NODDI-derived), and the functional connectivity (assessed from resting-state functional MRI) across cortical and subcortical brain regions with the aim to provide potential insights into their coordinated maturation during the preterm period. The analyses relied on longitudinal information between groups of PT infants scanned close to birth and at TEA, as well as a group of FT neonates to investigate the potential alterations with prematurity. The presented study is currently in preparation for submission to eLife (and thus follows eLife's ordering of sections, i.e. Results follow the Introduction, Methods are included towards the end).

Paper: Bridging the gap between microstructural grey-matter similarity and functional connectome: A multi-modal MRI study in preterm and full-term infants

#1 Introduction

The third trimester of pregnancy and the perinatal period are characterized by complex macro- and micro-structural changes, essential for establishing the structural and functional brain networks that support behavioural acquisitions and optimal neurodevelopmental outcomes later in life (Gilmore et al., 2018). In recent years, significant advances in neuroimaging, particularly diffusion magnetic resonance imaging (dMRI) and resting-state functional MRI (rs-fMRI), have provided unprecedented access to study this critical period *in vivo* (Dubois et al., 2021).

The microstructural organization of cortical and subcortical grey matter (GM) regions can be effectively characterized by complementary dMRI measures obtained from diffusion models like Diffusion Tensor Imaging (DTI) (Basser et al., 1994) and Neurite Orientation Dispersion and Density Imaging (NODDI) (H. Zhang et al., 2012) which can inform on the developmental modifications in neuronal and glial density, neurite complexity, synaptic overproduction and pruning, and reduction in brain water content (Ouyang, Dubois, et al., 2019). Changes in diffusion properties show a marked heterogeneity between regions in terms of their spatio-temporal profile in neonates and infants (Ball et al., 2013; Batalle et al., 2019; Ouyang, Jeon, et al., 2019; Yuan et al., 2023). Nevertheless, while some synchrony across GM regions belonging to the same developing functional network is expected, investigating the co-variation of microstructure across different GM regions remains relatively unexplored. This could provide insights into coordinated maturational changes across the cortical and subcortical regions (Alexander-Bloch et al., 2013), and potentially reveal commonalities in microstructural profiles among functionally connected regions.

Studies relying on brain morphometric markers, like cortical thickness that reflects microstructure in an indirect way, have previously suggested the biological significance of measuring co-variations across grey matter areas (Alexander-Bloch et al., 2013; King & Wood, 2020). Evidence from non-human primate tracing studies supports this notion, suggesting stronger axonal connectivity between structurally similar brain regions (Barbas, 2015; Goulas et al., 2016; Goulas et al., 2017; Seidlitz et al., 2018). Likewise, studies in human adults and adolescents have demonstrated that morphologically similar grey matter regions are more likely to be anatomically connected (Goulas et al., 2016; Goulas et al., 2017). These regions

also display similarities in genetic and transcriptomic profiles (Alexander-Bloch et al., 2013; Yee et al., 2018) and are associated with changes in disease and cognitive function (Wu et al., 2023; Y. Zhang et al., 2021). In the early stages of development (first 2 years), researchers have explored regional covariation based on factors such as grey matter volume (Fan et al., 2011), cortical thickness (Geng et al., 2016; Nie et al., 2014), cortical folding (Nie et al., 2014), and fibre density (Fan et al., 2011; Nie et al., 2014). Notably, covariance based on grey matter volumes has shown the potential to differentiate neonates with a familial risk of schizophrenia (Shi et al., 2012). However, these studies used single descriptors, which could significantly influence the estimated covariance relationships by specific spatial and temporal patterns exhibited by the given metrics during infancy (Gilmore et al., 2012; Lyall et al., 2015; Nie et al., 2014; Seidlitz et al., 2018). Recently, multiparametric approaches taking advantage of the combination of multiple morphological and microstructural descriptors were reported for estimating individual similarity networks in the neonatal brain and delineating modules consistent with known cytoarchitectonic tissue classes and functional systems (Fenchel et al., 2020). Such approaches applied to full-term (FT) newborns have also allowed the prediction of social-emotional performance at 18 months (Fenchel et al., 2022), and the discrimination of preterm (PT) and FT individuals at term-equivalent age (TEA) (Galdi et al., 2020).

In this context, the first objective of this study was to investigate the developmental evolution of microstructural similarity across cortical and subcortical regions (referred to as grey matter connectivity, GC, in the following), based on complementary microstructural descriptors derived from DTI and NODDI models, expected to reflect cytoarchitectural and maturational processes. We extended previous investigations to an earlier period, constructing group-wise GC for PT infants from the developing Human Connectome Project (dHCP), without overt brain abnormalities and with a longitudinal follow-up involving two scans—one acquired close to birth (PT:ses1) and the second at TEA (PT:ses2). A group of FT neonates was also considered as a reference. Contrary to previous studies (Fenchel et al., 2020; Galdi et al., 2020), a group-wise, potentially more robust approach was preferred, first because the number of metrics for regional similarity estimation was reduced to focus on microstructure, and because the group comparisons required corrections for confounders such as gestational age at birth.

Additionally, functional connectivity (FC) during early brain development has also been explored extensively using rs-fMRI, showing a strengthening of cortico-cortical and cortico-subcortical connections with distinct developmental patterns across different functional networks (Doria et al., 2010; Fransson et al., 2009; Jakab et al., 2014; Smyser et al., 2010; van

den Heuvel et al., 2015), and progressive refinements to form complex regional relationships and inter-hemispheric asymmetries (Taymourtash et al., 2023; Williams et al., 2023). By TEA, the topological architecture of functional connectivity resembles that of adults, although connectivity hubs are still primarily located in sensory-motor regions (Dall’Orso et al., 2022; Eyre et al., 2021; Fransson et al., 2009; Toulmin et al., 2015; Turk et al., 2019; van den Heuvel & Hulshoff Pol, 2010). Postnatally, the maturation and specialization of functional connectivity seem to progress asynchronously, following a primary-to-higher function order from sensorimotor/auditory to visual and default-mode networks (Cao et al., 2017; Eyre et al., 2021; Gao et al., 2015; Hoff et al., 2013).

This maturational progression is, at least superficially, suggestive of the observed spatiotemporal maturation of the grey matter, where maturation of primary sensorimotor regions was described to precede that of association areas and prefrontal cortices (Ball et al., 2013; Monson et al., 2018; Neil & Smyser, 2018; Yu et al., 2016). Thus, in this study, we aimed to explore the potential relationships between the evaluated GC derived from microstructural features and the changes in FC within the three infant groups of interest (PT:ses1, PT:ses2, FT), hypothesizing that regions within the same functional network should exhibit stronger GC. Our analyses included direct comparisons of connectivity profiles between GC and FC, as well as network-level assessments achieved through hierarchical clustering of connectivity matrices. Additionally, we envisioned that early developing microstructural clusters likely serve as the foundation for developing functionality and might provide insights into synchronized functional maturation between brain areas (Alexander-Bloch et al., 2013). To investigate this, we evaluated the evolution of both GC and FC between birth and TEA in PT subjects and related them with the hypothesis that the size and direction of GC-FC longitudinal changes might provide insights into potential co-development of the microstructural and functional networks during the preterm period.

Finally, we aimed to explore the effects of prematurity on the development of GC and FC by comparing the PT groups with the group of FT infants, matched for sex and postmenstrual age (PMA) at TEA scan. In fact, disrupting normal gestation, premature birth leads to notable alterations of grey matter maturation, in a heterogeneous and region-specific way, as observed with dMRI measures at TEA, suggesting the differential effects of prematurity on different brain areas (Ball et al., 2013, 2020; Batalle et al., 2019; Dimitrova et al., 2021; Eaton-Rosen et al., 2015, 2017; McKinstry et al., 2002; Ouyang, Jeon, et al., 2019; T. A. Smyser et al., 2016; Yu et al., 2016). Prematurity also affects functional connectivity, resulting in spatially diffuse alterations in functional connections involving cortico-cortical and

cortico-subcortical regions (Ball et al., 2016; Brenner et al., 2021; Keunen et al., 2017; C. D. Smyser et al., 2010), with plausibly fewer long-range connections and generally reduced connectivity strength in PT at TEA than FT (Ball et al., 2016; Brenner et al., 2021; Chiarelli et al., 2021; Eyre et al., 2021; Keunen et al., 2017; Scheinost et al., 2016; C. D. Smyser et al., 2010). The PT-FT group comparisons we performed aimed to investigate the effects of prematurity on the developing GC and FC, and analyse their changing relationships within the context of prematurity.

#2 Results

#2.1. Evaluating GM microstructural similarity in infant groups

As univariate analyses of diffusion metrics (resulting from DTI: AD, RD, MD, FA; and from NODDI: NDI, and ODI) in cortical and subcortical regions revealed regionally-dependent differences between groups of infants (*Annexe 3.3. Supp. Methods and Results: #1*), we first aimed to investigate the regional relationships through a measure of GM microstructural similarity defining a “grey matter connectivity” (GC) in each group of infants: 45 preterm-born scanned close to birth (PT:ses1, median postmenstrual age (PMA) at scan 34.9 weeks, range [28.3w–36.9w]), the same infants scanned at TEA (PT:ses2, median PMA at scan 41.3 weeks, range [38.4w–44.9w]), and 45 full-term control neonates matched for PMA at scan and sex (FT). GC was defined as a Pearson’s correlation (R coefficient) between pairs of regions, over all subjects within each group, considering all diffusion metrics (corrected for PMA at scan, gestational age (GA) at birth, and a residual of the global median GM diffusion metric corrected for PMA at scan and GA at birth) together (*Annexe 3.3. Supp. Figure 2.1.*). The resulting GC matrices are presented for each infant group in circular form (*Figure 5.1a*), grouping cortical ROIs into 6 cortical lobes and sub-cortical ROIs within 1 group, and showing only the connections corresponding to the 25% highest absolute correlation coefficients across all infant groups or for each infant group independently.

A visual comparison across groups suggested a global reinforcement of microstructural similarity with development between most ROI pairs in both positive and negative direction of correlations when comparing the GC at birth (PT:ses1) and TEA (PT:ses2 and FT). Disappearance of some relationships from the strongest top 25% was also observed, especially with cingular lobe and some of the subcortical regions. Strong negative correlations were observed in PT:ses2 and FT groups, especially between cortical and subcortical ROIs, involving mostly brainstem and bilateral thalamus connectivity. While challenging to attribute to a single factor, these negative relationships likely arise from differences in microstructural

profiles between ROIs, most likely due to FA and ODI profiles, opposite between subcortical regions and specific cortical regions (which largely overlapped when comparing the negative connections related to brainstem and thalamus).

Adapting connectivity threshold to reveal top 25% connections within each group allowed to present the evolving patterns of GM similarity. Overall, the GC correlations were not only weaker, but also more widespread across ROI pairs at birth (PT:ses1), and seemed to selectively strengthen during development (PT:ses2, FT), with preference for stronger connections between lobes. Comparing the ROI pair strengths between groups (*Figure 5.1b*) confirmed significant changes to the GM structural similarity with age, and showed significant differences between PT and FT infants at TEA (paired Wilcoxon test across absolute region pair connections, corrected for multiple comparisons*: PT:ses2 > PT:ses1, $W=915823$ $p<0.001$; PT:ses2 > FT, $W=1521116$ $p<0.001$; *NB: multiple comparison correction refers to Benjamini–Hochberg false-discovery rate correction across the manuscript; histograms, scatter plots, and statistical comparisons include only the upper triangle of symmetric connectivity matrices). Low (although significant) correlation between the PT GC at birth compared to TEA suggested that the profile of microstructural connections is far from developed in preterms at birth. On the contrary, much stronger correlation between GC link strengths were observed between the PT:ses2 and FT groups (*Figure 5.1c*). But despite this high correlation, relative patterns of GM similarity seemed affected in PT at TEA as apparent when visualizing the difference in top 25% connections between the two infant groups (*Figure 5.1a*).

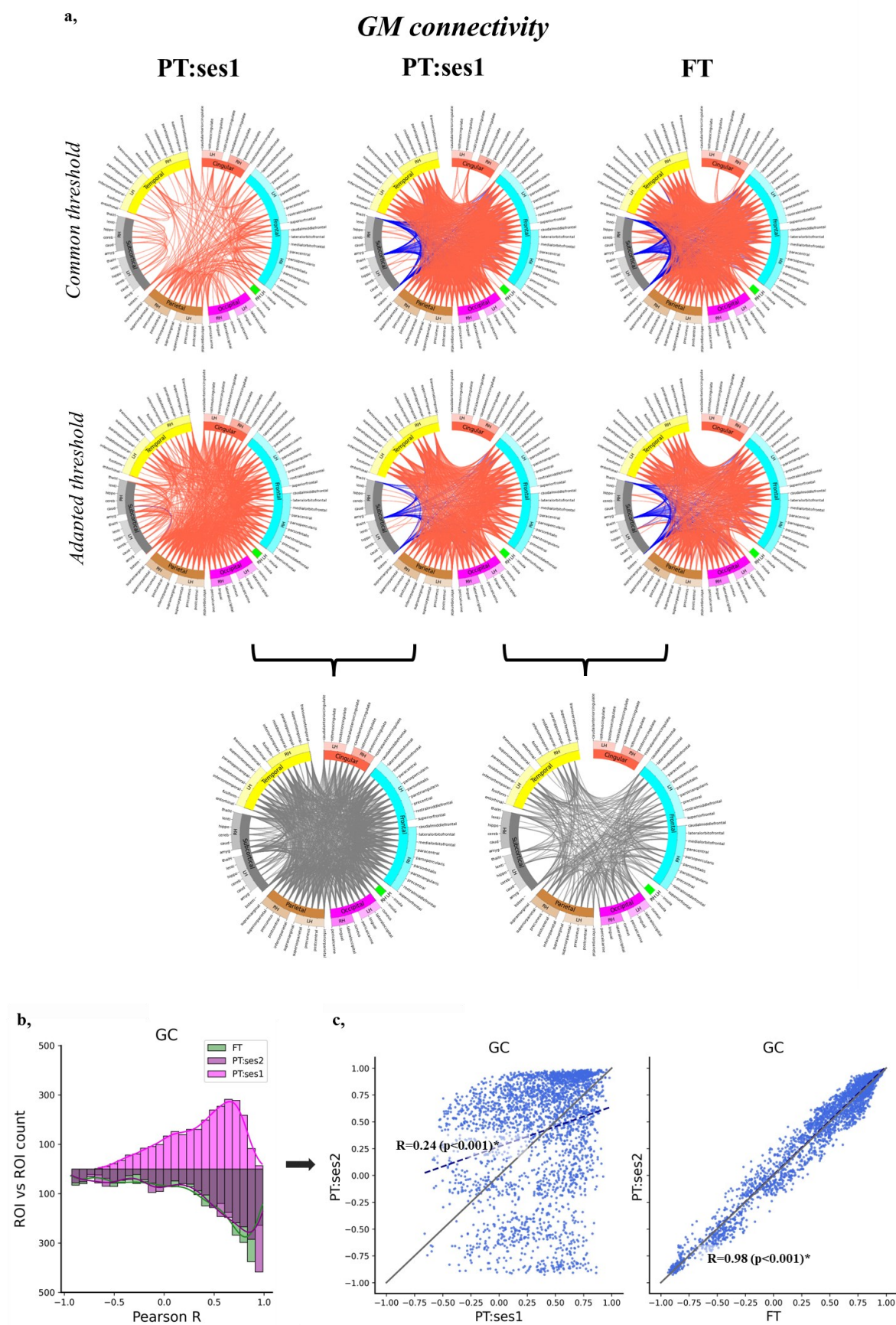


Figure 5.1. Grey matter connectome in infant groups. **a**, Circular plots representing correlation matrices and visualizing top 25 % GC connections for each infant group. Top row: common GC threshold of 0.786. Middle row: adapted threshold of 0.657 for PT:ses1, 0.856 for PT:ses2, and 0.833 for FT. For the ease of visualization, cortical ROIs were grouped into 6 lobes (frontal in light blue, parietal in brown, temporal in yellow, occipital in pink, cingular in red, and insular in green) and subcortical ROIs in 1 group (in grey) (see *Annexe 3.3. Supp. Table 1.* for ROI naming conventions and assignment to lobes). Positive correlations are shown in red, negative in blue. Bottom row: ROI pair connections that differ between the two groups in terms of their belonging to the top 25% strongest connections determined by adapted thresholds: PT:ses1 vs PT:ses2 comparison on the left, PT:Ses2 vs FT on the right. This visualization serves as a (limited) proxy for assessment of overall relationships of the connectivity relationships between the groups. **b**, Distribution of ROI pair correlations (Pearson coefficient R) across infant groups (NB: throughout the manuscript, histograms, scatter plots, and statistical comparisons include only the upper triangle of symmetric matrices). **c**, Scatter plots showing relationships between the GC ROI pair similarity between PT:ses1 vs PT:ses2 (middle) and FT vs PT:ses2 (left). The dotted line shows the group correlation (with R: Pearson's coefficient), while the solid line represents the identity relationship.

To extend the direct comparisons between the infant groups, we used the correlation strengths between ROI pairs to define ‘microstructural networks’. Using ward clustering, we defined hierarchical trees of regional similarity based on GC for each infant group. The resulting dendrograms, as well as examples of clustering for selected cluster numbers are presented in *Supp. Figure 2.3*. The dynamic evolution of differences of the ROI pair correlation strengths prevented selecting a final cluster number that would appropriately reflect the studied relationships across the infant-groups. To compare the networks across groups, we instead evaluated the mutual information (MI) between hierarchical trees, for all possible cluster numbers from 2 to 75 (corresponding to a cluster size=1). Only the MI values that survived the permutation testing (described in the *#4 Materials and Methods*) were further described, as these would approximate the overlap of the infant group-derived networks. In agreement with the previous section observations, the comparison of clustering results between infant groups showed higher, although imperfect, overlap between PT and FT subjects at TEA than between the 2 PT sessions (*Figure 5.2a&5.2c*), while differences between PT and FT subjects at TEA supported potential effects of prematurity on microstructural relationships across regions.

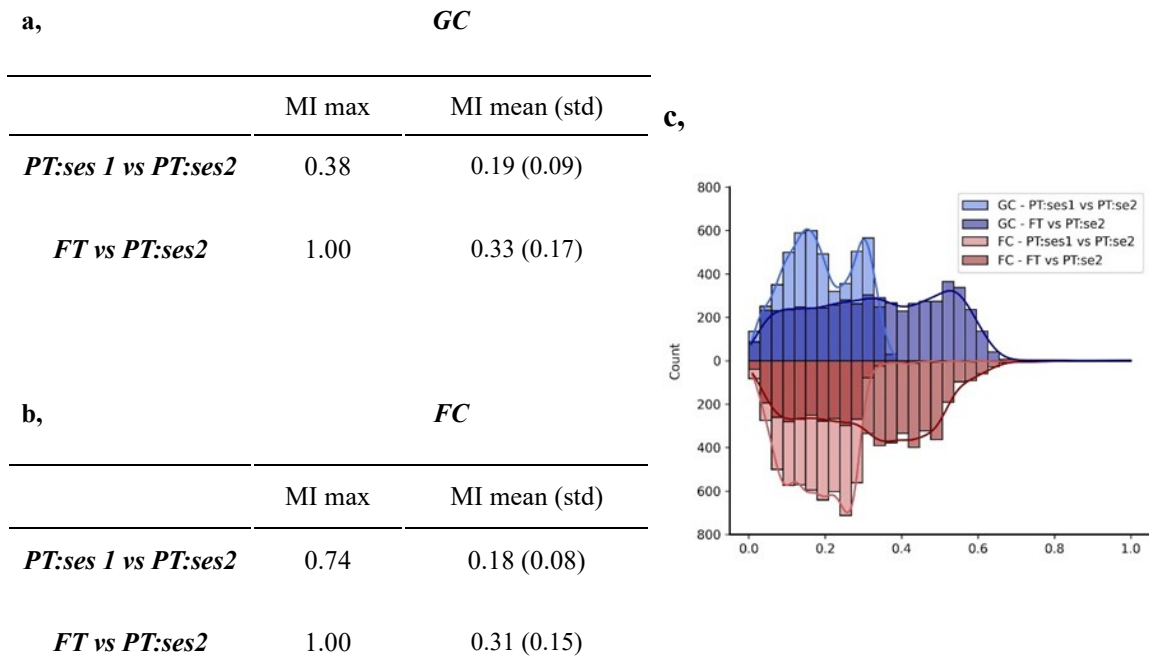


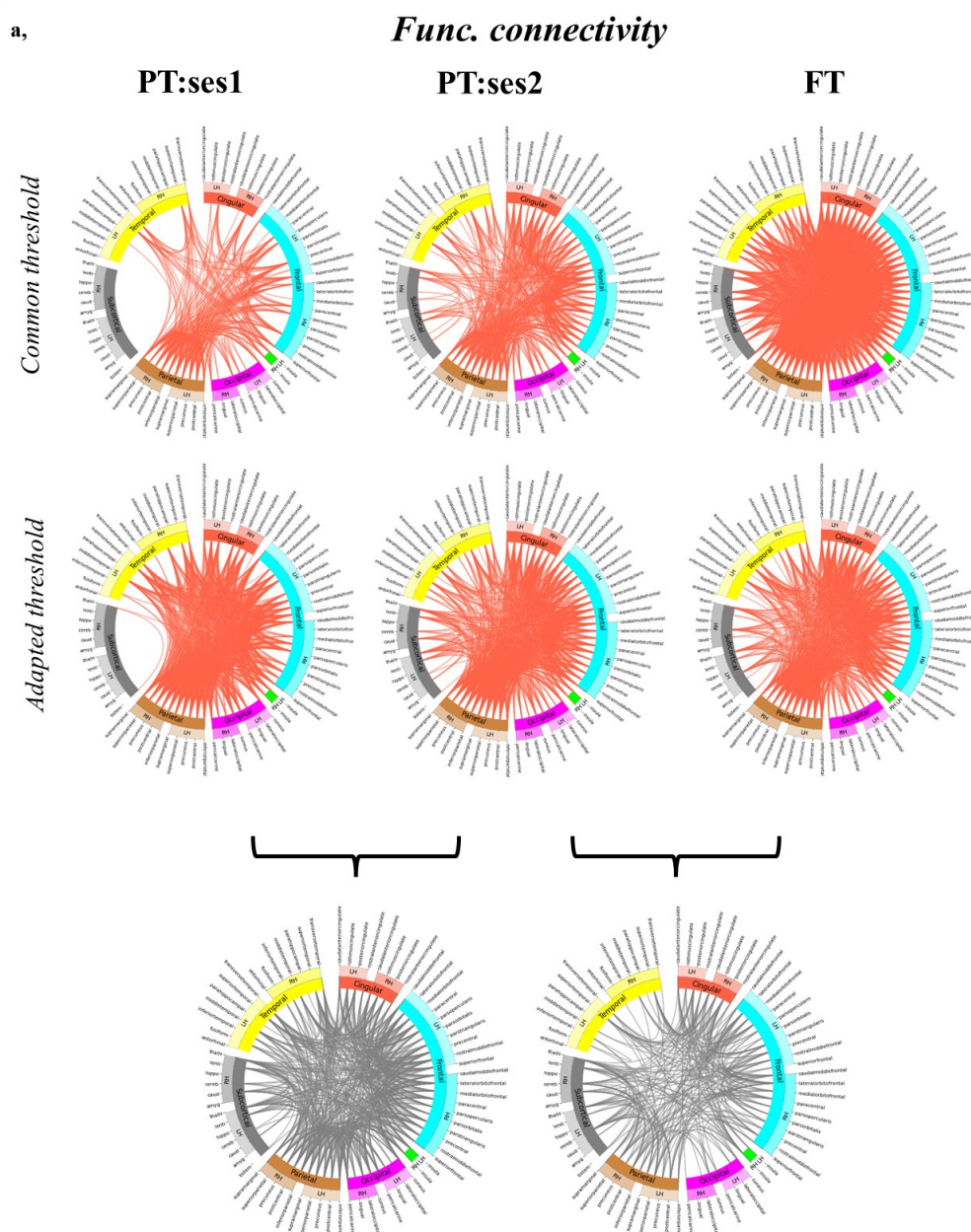
Figure 5.2. Mutual information (MI) results of groups comparisons. **a,b.** Summary of distribution of mutual information MI for group comparisons of clustering results derived from GC (a) or FC (b). **c,** Distribution of MI values visualizing differences in network overlap between infant groups (PT:ses1 vs PT:ses2 in deep colour, FT vs PT:ses2 in light colour) for each modality (GC in blue, FC in red).

#2.2. Evaluating functional connectivity (FC) in infant groups

Similarly to the GC analyses, we performed comparisons in terms of group-wise functional connectivity, defined as the infant group average of the temporal correlations of median functional signal between pairs of ROIs. Visualizing the top 25% connections, we observed globally a similar reinforcement of the correlations between ROI pairs with development (PT:ses1 vs PT:ses2 and FT) (*Figure 5.3a*), in particular for cortico-subcortical connections that did not appear in the top 25% of connections for the PT:ses1 group. This might be due to the higher within-cortical connectivity at birth compared to later ages, when synchronization of subcortical and cortical activity becomes more important. But, it is also possible that the low correlations at birth are driven by the age-dependent effects of the signal-to-noise ratio, which might be lower in the subcortical regions (Maugeri et al., 2018; Risk et al., 2021).

As for GC, significant differences between groups were observed in terms of ROI pair correlation strengths (paired Wilcoxon test corrected for multiple comparisons: PT:ses2 > PT:ses1, $W = 562652$ $p < 0.001$; PT:ses2 < FT, $W = 125$ $p < 0.001$) (*Figure 5.3b*). The results again suggested an ongoing development of the FC connectivity between the two sessions in preterms

as well as potential effect of prematurity at TEA. Besides, as for GC, connection strength was highly correlated between PT:ses2 and FT across ROI pairs (*Figure 5.3c*), suggesting that while impacted by prematurity, the FC profile was not drastically modified at TEA. Additionally, PT:ses1 and PT:ses2 groups seemed much closer in terms of FC than GC, suggesting that FC profiles are already in place close to birth, or on the reverse, that FC changes stem from global increase of FC strengths.



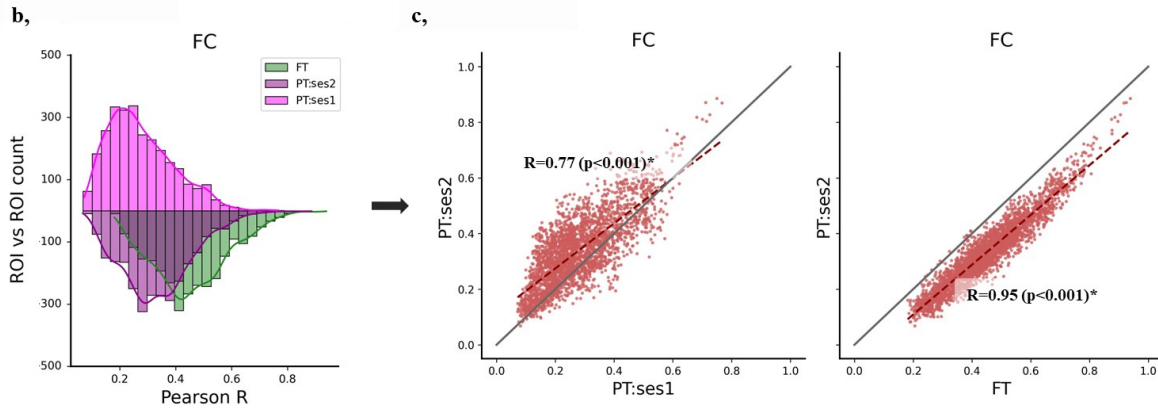


Figure 5.3. Functional connectome in infant groups. **a**, Circular plots representing correlation matrices and visualizing top 25 % FC connections for each infant group. Top row: common FC threshold of 0.448. Middle row: adapted threshold of 0.349 for PT:ses1, 0.409 for PT:ses2, and 0.537 for FT. For the ease of visualization, cortical ROIs were grouped into 6 lobes (frontal in light blue, parietal in brown, temporal in yellow, occipital in pink, cingular in red, and insular in green) and subcortical ROIs in 1 group (in grey) (see *Annexe 3.3. Supp. Table 1.* for ROI naming conventions and assignment to lobes). Positive correlations are shown in red. Bottom row: ROI pair connections that differ between the two groups in terms of their belonging to the top 25% strongest connections determined by adapted thresholds: PT:ses1 vs PT:ses2 comparison on the left, PT:ses2 vs FT on the right. **b**, Distribution of ROI pair correlations across (Pearson coefficient R) infant groups. **c**, Scatter plots show relationships between the FC ROI pair correlations between PT:ses1 vs PT:ses2 (middle) and FT vs PT:ses2 (left). The dotted line shows the group correlation (with R: Pearson's coefficient), while the solid line represents the identity relationship.

As for GC, we extended the FC descriptions and comparisons by evaluating the similarity in inter-regional relationships on the network-level. The FC-derived dendrograms resulting from hierarchical clustering for each infant group, as well as examples of clustering for selected cluster numbers are presented in *Annexe 3.3. Supp. Figure 2.4*. Comparisons of FC clustering based on MI and permutation testing allowed us to describe the overlap of FC networks between infant groups (*Figures 5.2b&5.2c*): clustering overlap was higher (but imperfect) between PT and FT subjects at TEA than between the PT:ses1 and PT:ses2. Interestingly, despite higher relationships between PT:ses1 and PT:ses2 groups in terms of FC than GC in terms of strength of whole-brain connectivity (*Figures 5.3c vs 5.1c*), the group overlap was very similar in FC and GC network spaces (*Figure 5.2*), potentially suggesting that network structures observed at TEA are already in place close to birth to a certain extent for both FC and GC.

#2.3. Relating GM similarity and functional connectivity in infant groups

We further compared the two connectivity modalities in each group to investigate the potential GC-FC relationships during development. Across all ROI-pair connections, GC and

FC were strongly correlated in each infant group (*Figure 5.4*). Interestingly, this GC-FC relationship was strongest in the youngest group (PT:ses1) (Pearson's R of 0.57) and seemed to decrease with development, with statistically-different slopes between the 2 PT sessions ($Z=17.39$, $p<0.001$) but not-statistically-different slopes between PT:ses2 and FT (Z -score=1.054, $p=0.293$).

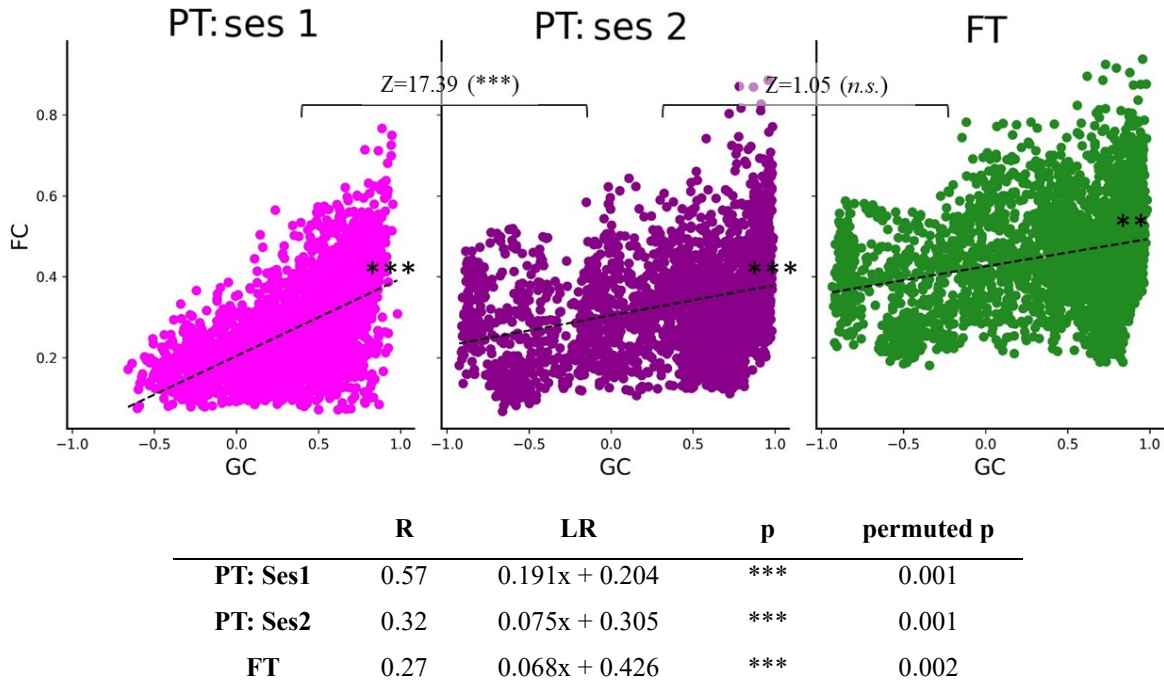


Figure 5.4. Relationship between GC and FC connectivity per ROI pair (upper triangle of symmetric matrices). The table summarizes Pearson's correlation (R) and features of the linear relationship (LR) between the two connectomes ($p < 0.001$ ***, $p > 0.05$ *n.s.*). Z: Z-score comparing the slopes of linear regression.

As for the between-group comparisons for GC and FC separately, we evaluated the similarity between the inter-regional relationships of GC and FC in each group at the network level using the clustering approach. This revealed a trend towards low but increasing mutual information between GC and FC-derived networks with development (i.e., lower mean values in PT:ses1 than in FT, *Figure 5.5, Annexe 3.3. Supp. Figure 2.5.*), suggesting a potential emergence of the shared underlying network structures between GC and FC throughout development.

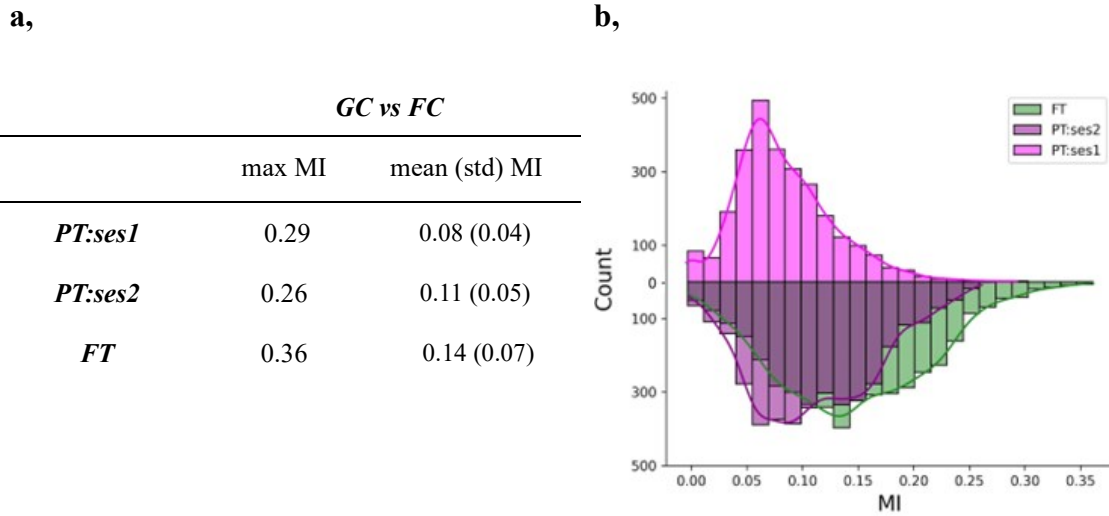


Figure 5.5. Mutual information (MI) between GC and FC. a, Summary of distribution of MI comparing GC and FC clustering for each infant group. b, Distribution of MI values visualizing differences in GC-FC network overlap in each group.

#2.4. Evaluating the longitudinal evolution of GC and FC connectomes

As a last step, we aimed to investigate the GC-FC relationships based on the evolution of microstructural and functional connectomes by taking advantage of the longitudinal evaluations of PT infants. We first computed the matrices of developmental change between PT:ses1 and PT:ses2 separately for GC and FC (referred to these as ΔGC and ΔFC , respectively), and summarized the resulting matrices in circular plots (*Figure 5.6*). Both modalities showed both increases and decreases of the link strengths between birth and TEA. On the ΔGC level, most connections increased in strength, and the most pronounced decreases mostly concerned the connections involving the cingular lobe and some subcortical ROIs (for example cerebellum and amygdala). On the ΔFC level, connections involving subcortical ROIs seemed to increase in strength while the global decrease was more pronounced than for ΔGC and involved especially the long-range connectivity across cortical regions.

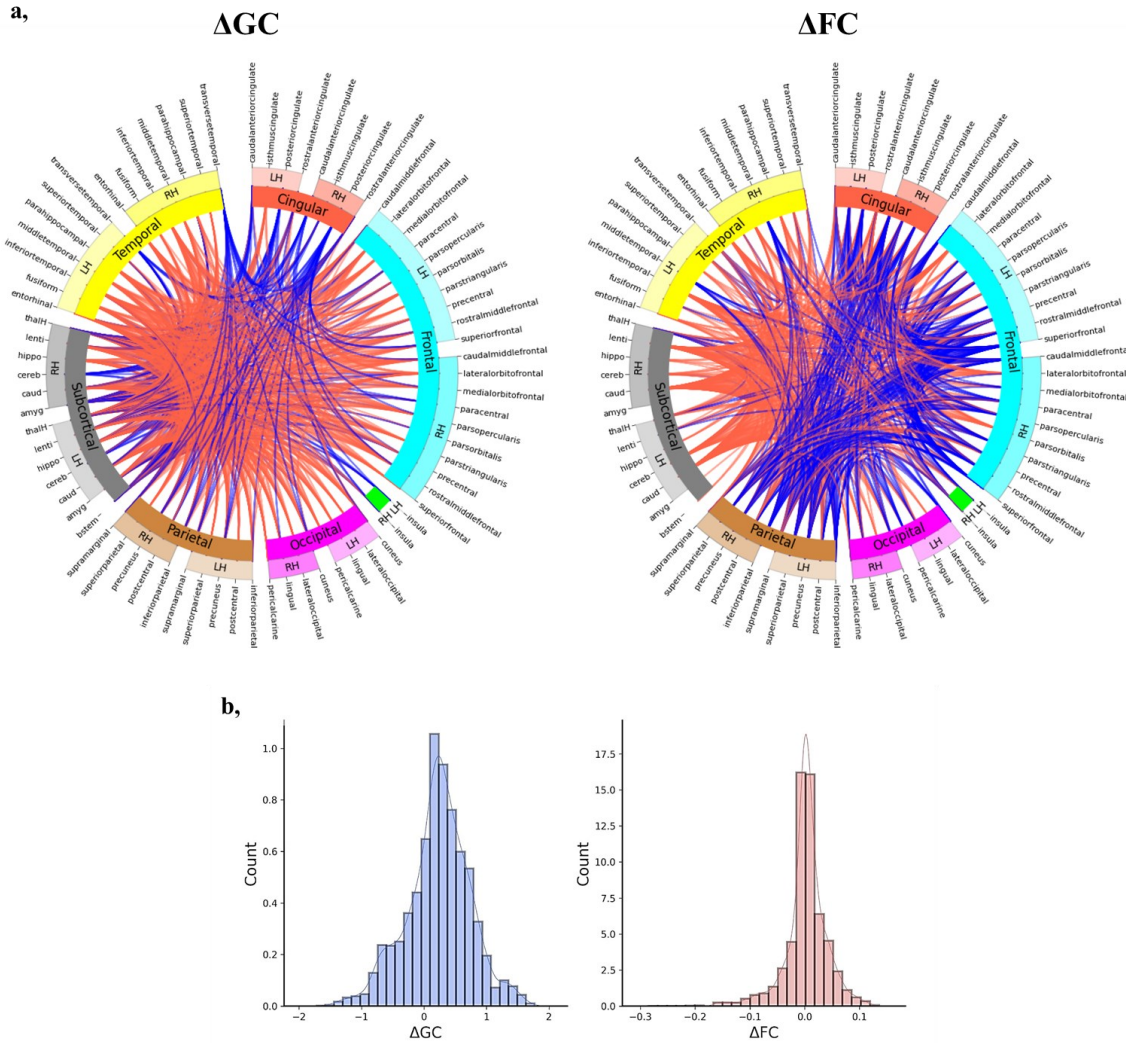


Figure 5.6. Longitudinal evolution of GC and FC. **a**, Circular plots visualizing top 25 % connections for ΔGC and ΔFC modalities in PT infants (respective thresholds: 0.656 and 0.037). Connections with increasing strength of relationships between with age are shown in red, decreasing in blue. The ROI naming conventions and assignment to lobes is detailed in *Annexe 3.3. Supp. Table 1*. **b**, Distribution of changes in connectivity strength between ROI pairs with age.

Furthermore, we aimed to investigate the potential directionality of relationships between the developing GC and FC by comparing ΔGC , ΔFC , and connectivities at specific ages. More specifically, different comparisons allowed us to test three hypotheses regarding the relationships between microstructural and functional development of connectivity (*Figure 5.7a*): 1) if FC and GC co-evolve, ΔGC and ΔFC should be strongly correlated; 2) if GC relies on FC, FC at ses1 should drive ΔGC while ΔFC should drive GC at ses2; 3) on the reverse, if FC relies on GC, GC at ses1 should drive ΔFC , while ΔGC should drive FC at ses2. These hypotheses and the results of these relationships are summarized in *Figure 5.7b*. The direct comparison between ΔGC and ΔFC suggested a low but significant positive relationship across

ROI-pair connections (robust linear regression: slope=0.008, $p<0.001$), suggesting some co-evolution of microstructural and functional connectomes. Besides, the developmental change in each modality was significantly related to the connectivity in the other modality at early session (ΔGC vs FC-PT:ses1: slope -1.29, $p<0.001$; ΔFC vs GC-PT:ses1: slope -0.03, $p<0.001$), but the slope of the relationship was significantly higher for ΔGC than ΔFC ($Z=17.6$, $p<0.001$), hinting at a potential higher dependency of FC development on the early underlying GC than the reverse. Comparing the ΔGC and ΔFC to the other modality at a later session suggested similar trend, with significant microstructural-functional relationships in both directions (ΔGC vs FC-PT:ses2: slope -0.82, $p<0.001$; ΔFC vs GC-PT:ses2: slope -0.004, $p<0.001$) but again with a higher slope for ΔGC than ΔFC ($Z=11.3$). Finally, the relationships seemed stronger when comparing the evolution of GC and FC to the other modality at session 1 than at session 2 (ΔGC - FC-PT:ses1 vs FC-PT:ses2: $Z=15.7$; ΔFC - GC-PT:ses1 vs GC-PT:ses2: $Z=4.6$), suggesting that changes in both GC and FC rely more on the early connectivity organization than they impact the later one.

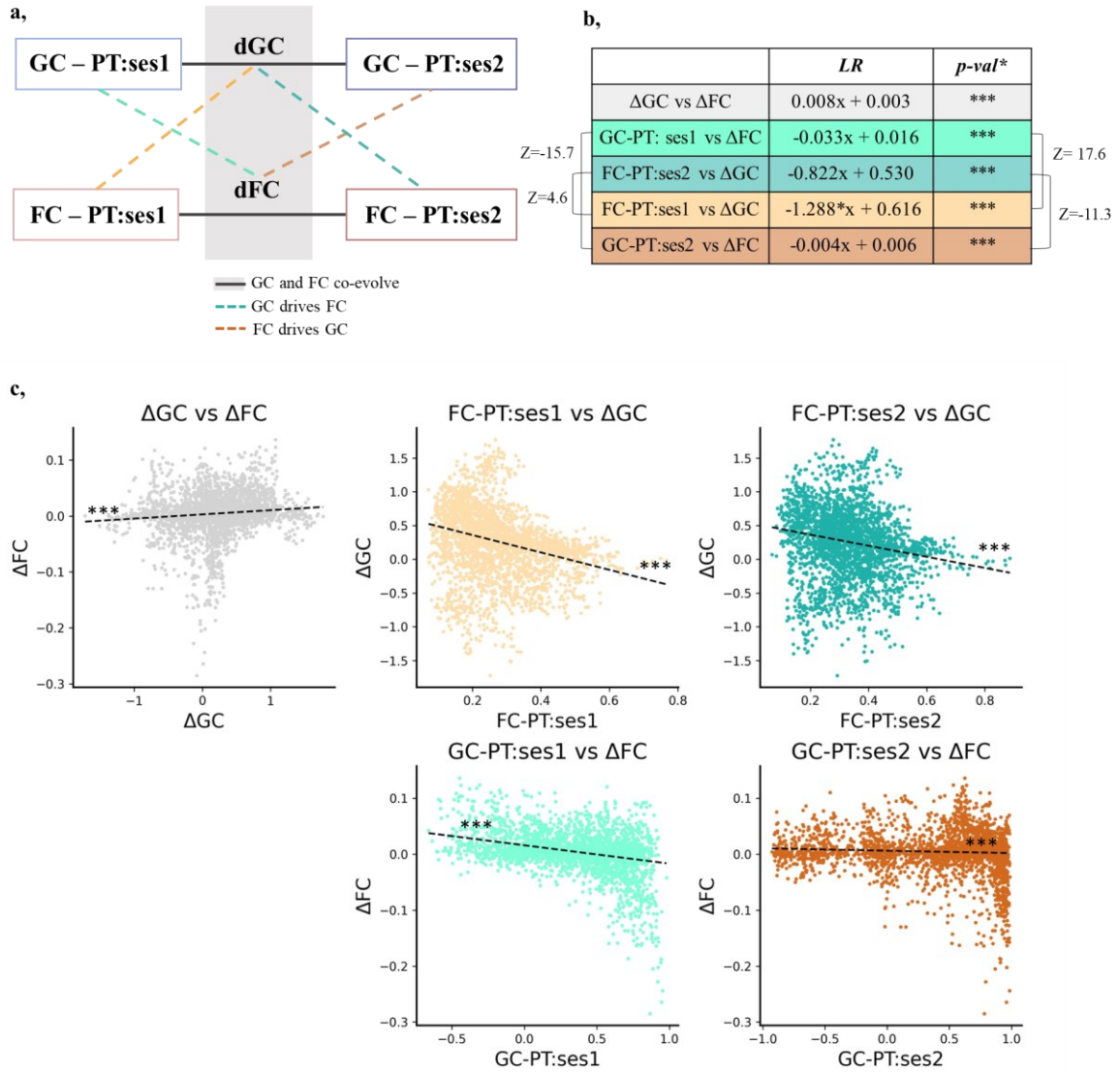


Figure 5.7. Directionality of GC-FC relationships. **a,** 3 possible hypotheses on the developing causal relationships between microstructural and functional connectivity. **b,** The table summarizes relationships between the two connectomes estimated with robust linear regression (LR) (p-val *** < 0.001 corrected for multiple comparisons). Z: Z-score comparing the estimated slopes. **c,** Relationship between dGC and dFC connectivity per ROI pair as well as the comparison to the connectivities of the opposite modality at different sessions. We colour coded the subplots by hypothesis tested by the given comparison: GC and FC co-evolve (grey), GC drives FC (cyan, dark cyan), and FC drives GC (orange, dark orange).

Finally, as in previous sections, we performed analyses of hierarchical clustering separately on ΔGC and ΔFC to evaluate the longitudinal networks. Derived ΔGC and ΔFC dendrograms are presented in *Annexe 3.3. Supp. Figure 6.3*. Examples of clustering results for selected cluster numbers are presented in *Figure 5.8a*, showing some visual similarities but also some dissimilarities between ΔGC and ΔFC , and to a lesser extent between the two hemispheres.

As previously, these longitudinal networks, and the PT networks at each session (described in #2.1 and #2.2) were compared based on hierarchical clustering to test the relationship hypotheses we proposed (*Figure 5.7.a*). Evaluation of the MI between Δ GC and Δ FC derived networks suggested a significant overlap, which tended to be higher than for all the other comparisons between each longitudinal network and the opposite modality at a given session (all reached significant but similar MI overlaps except for Δ FC vs GC-ses2 which reached the lowest MI) (*Figure 5.8b,c*). comparable results suggested commonalities between the network development in both GC and FC modalities but did not allow us to ascertain which of the three hypotheses about GC-FC co-evolution is the most probable on the network level.

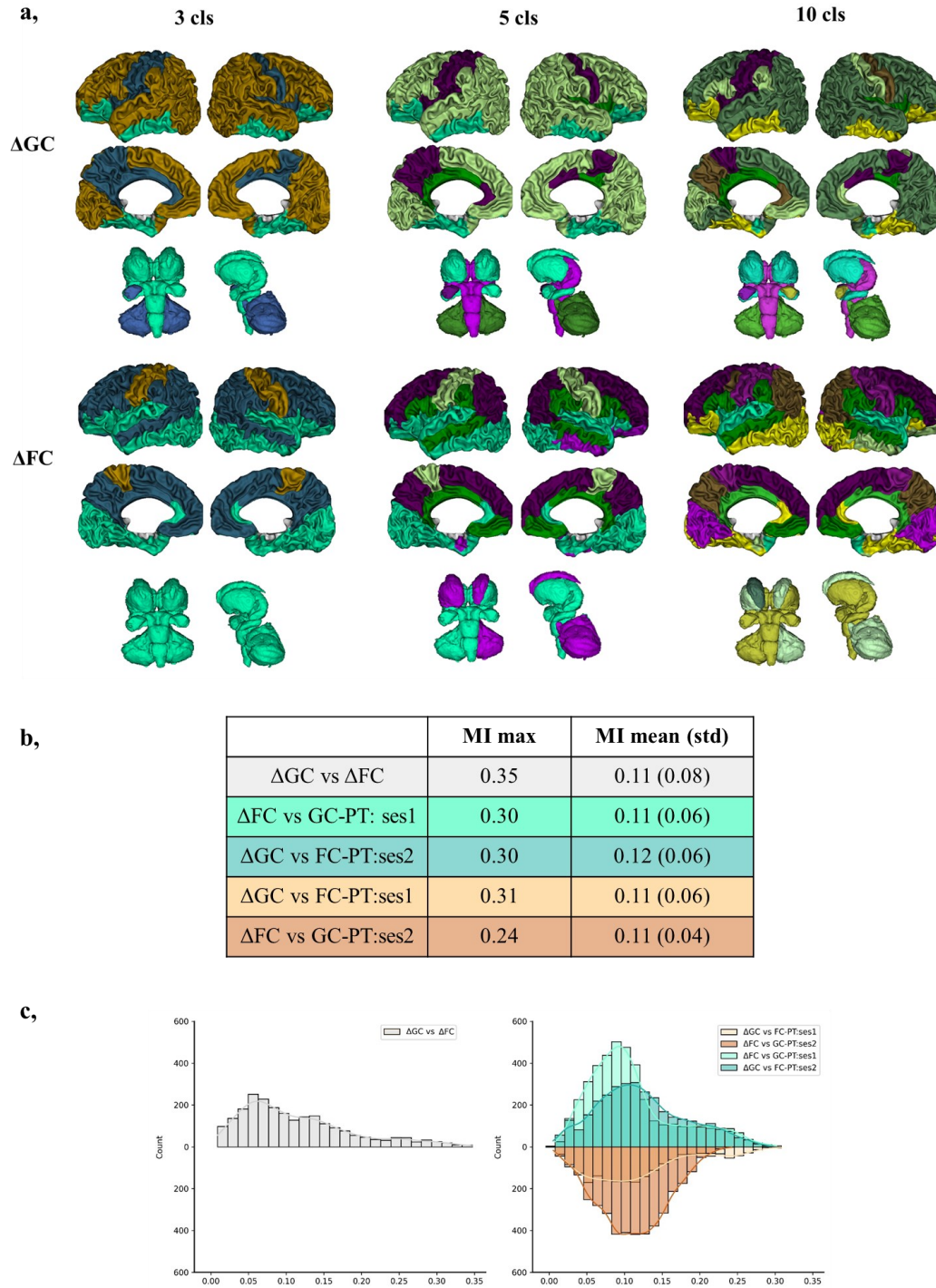


Figure 5.8. Network-based comparisons of longitudinal GC-FC relationships. **a,** Example clustering results based on the developmental change in GC and FC between scans at ses1 and ses2 for selected cluster numbers. **b,** Mutual information between clustering results derived from ΔGC and ΔFC matrices as well as the comparison to the networks derived from the opposite modality at ses1 or ses2. As in *Figure 5.7*, we colour coded the columns by hypothesis tested by the given comparison: GC and FC co-evolve (grey), GC drives FC (cyan), and FC drives GC (orange). **c,** Distribution of MI values visualizing GC-FC network overlaps in each setting.

#3 Discussion

In our study, we explored the developmental changes and the relationships between grey matter microstructural similarity (i.e. grey matter connectome, GC) and the functional connectivity (FC) across cortical and subcortical brain regions to provide potential insights into their coordinated maturation. Using a longitudinal cohort of PT infants scanned close to birth and at TEA, we observed a global reinforcement of inter-regional relationships in both GC and FC modalities with age, with marked connection-specific variability. Direct comparison of GC and FC matrices in terms of connectivity strengths revealed significant relationships that decreased with age. Interestingly, we found an increasing overlap of GC and FC-derived networks with age, suggesting an evolving commonalities and progressive refinement in network development across both microstructural and functional levels. Notably, GC and FC connectivity strengths and GC-FC network-level relationships were significantly altered by prematurity, as observed through comparisons between PT infants at TEA and FT neonates.

#3.1. Evaluations of GC and FC in the developing brain

Previous studies focusing on covariation of regional similarities across grey matter during the first two years of life primarily relied on single morphometric markers like grey matter volume (Fan et al., 2011), cortical thickness (Geng et al., 2016; Nie et al., 2014), cortical folding (Nie et al., 2014), and fibre density (Fan et al., 2011; Nie et al., 2014). However, these markers, while informative, offer rather indirect measures of the microstructural processes underlying grey matter development during the early period. Moreover, univariate estimates of grey matter similarities can be significantly biased by specific spatial and temporal patterns exhibited during infancy by individual descriptors (Gilmore et al., 2012; Lyall et al., 2015; Nie et al., 2014; Seidlitz et al., 2018). To address this limitation, we employed a set of 6 microstructural metrics derived from DTI and NODDI models with the aim of obtaining a more comprehensive view of the developing inter-regional relationships across the grey matter.

Such multiparametric approach was previously proposed in FT infants (Fenchel et al., 2020). Authors derived cortical similarity matrices in individual infants using a combination of morphological and microstructural descriptors and identified modules consistent with known cytoarchitectonic tissue classes and functional systems, suggesting that inter-regional similarities within grey matter could provide meaningful functional insights. Similarly, in a cohort of PT and FT neonates at TEA, multiparametric inter-regional similarity across brain regions (including GM as well as white matter) was successfully used for classification of an individual's prematurity status (Galdi et al., 2020). Extending these investigations to an earlier

period in PT infants, we evaluated both the evolution of the grey matter microstructural similarities across cortical and subcortical regions during the preterm period and analysed the effects of prematurity on the GC at TEA. However, contrarily to previous studies which performed intra-individual correlation analyses (Fenchel et al., 2020; Galdi et al., 2020), we could only perform group-wise correlation analyses, to ensure the robust estimation of the microstructural similarity across GM regions. This choice was related to the limited number of regional microstructural descriptors we used per subject (6), which aimed to provide more focused information on the maturing cytoarchitecture, and to the intra-group corrections required in the analyses by the inter-individual heterogeneity in PMA at scan in PT-ses1 particularly.

An additional novelty of our study involved the comparison of estimated GC to FC to explore the relationship between microstructural and functional development in the preterm period. It involved a direct comparison of GC and FC, considering all cortical and subcortical regions, and employed a network approach based on hierarchical clustering to compare the overlap between networks derived from these two modalities and their changes with age during the preterm period. Previous research investigating structure-function coupling primarily focused on white matter connectivity in older subjects (toddler and older) (Grayson et al., 2014; Hagmann et al., 2010; Zhang et al., 2021). In PT infants, positive coupling in the white matter and functional connectivity was described and seemed to increase with age (van den Heuvel et al., 2015). At similar ages, maturational progression of grey matter was shown associated with white matter tracts (Friedrichs-Maeder et al., 2017; Smyser et al., 2016). In this study, we suggested that microstructural similarity across cortical and subcortical regions can act as a proxy measure of brain connectivity. However, unlike structural white matter connectivity, GC might reflect the microstructural similarity of spatially distinct regions of GM even in the absence of established structural links. The evolution of GC with age might then reflect the coordinated maturation of potentially meaningful functional networks.

#3.2. Limitations

Our study offered several advantages such as longitudinal follow-up of PT infants, optimized data acquisition and analysis protocols for this age group, utilization of multiple diffusion metrics for comprehensive microstructure characterization, and a novel approach linking microstructural and functional development. However, it also had recognized limitations.

One major limitation concerned the choice of ROI parcellation scheme and the inter- and intra-individual variability in parcellation quality. As expected, a good parcellation performance was generally achieved in subjects with similar age to the cohort used to define the atlas template (infants at TEA), but the quality decreased with the distance to the cohort (*Annexe 3.3. Supp. Figure 4.1*) with potential down-stream effects on the analysis and comparisons of results in younger subjects. The effects were also likely to be non-homogeneous across regions, with smaller regions more likely to suffer larger effects and potential parcellation errors. The use of anatomical parcellations could also introduce bias into connectivity estimates, particularly to estimate functional connectivity, since anatomically-driven parcellation schemes are likely to not accurately represent functional regions, not align with dynamic functional development and variability within seemingly homogenous regions. but ROI selection based on prior knowledge could also have introduced significant bias into the connectivity estimates (Smith & Beckmann, 2017). We made the choice of anatomical parcellation to provide a common useful framework facilitating comparisons between GC and FC modalities. However, future studies should validate results with different parcellation atlases dedicated to early infants, to validate our findings. Alternative methods for ROI delineation, such as previously employed random parcellation (Fenchel et al., 2020) could also be explored but might prevent the inclusion of subcortical regions.

Another limitation regards the use of group-wise analyses, which were chosen to address the constraints of a limited descriptor set for evaluating GC similarity matrices. These group analyses also required corrections for confounding factors (PMA at scan, GA at birth, and a residual of the global median diffusion metric corrected for PMA and GA) to reduce inter-individual variability within the evaluated groups. This was crucial to ensure that the observed relationships were specific to inter-regional microstructure variations and not confounded by other sources of variability. While this approach did not allow investigation into individual longitudinal changes in GC and FC, it potentially helped mitigate the impact of occasional parcellation errors, especially in the youngest subjects where such errors might be more pronounced in individual GC matrices.

Furthermore, we acknowledged the difficulties with estimating group-wise functional connectivity. In all infant groups (PT:ses1, PT:ses2, FT), we observed notable effects of PMA at scan on estimated median connectivities in individual functional FC matrices that were difficult to correct for at the level of individual ROI pair connection. We attempted to mitigate this by considering the variability between infants within the groups for each ROI pair when computing the group-wise FC longitudinal change between birth and TEA, weighted by the

overlap of confidence intervals for each ROI pair between groups. However, it's evident that age effects significantly influenced the reliability of the group-wise FC estimates in our study.

The reliability of microstructural connectivity estimates was also likely influenced by recognized limitations in the employed diffusion models. These include challenges with the DTI model in regions with complex microstructure and potential suboptimal estimation of NODDI parameters in infant brains due to model optimization for adults. In the future, accounting for the unique diffusion properties of immature brains and exploring additional microstructural descriptors like diffusion kurtosis metrics (Jensen et al., 2005) might be beneficial.

Finally, we utilized ward hierarchical clustering to delineate GC and FC networks, which might be open to question. Hierarchical clustering was chosen explicitly as we expected the regional relationships across grey matter to be hierarchical in nature, i.e. regions not changing their network belonging depending on the granularity of network analysis. In future research, testing additional clustering methods and criteria in addition to ward methods to assess agreement in the clustering results and estimate their robustness is warranted. Mutual information methods, as utilized in our study to compare overlap across different networks, could be valuable for this purpose. However, we acknowledge that mutual information estimates might offer only a broad measure of overlap across the GC and FC-derived networks, stemming from the challenge of determining an optimal cluster number that could match both modalities and various infant groups. In the future, this approach could be extended by more robust comparative evaluation of the resulting dendrograms such as those proposed for comparisons of phylogenetic trees (Cardona et al., 2013).

#3.3. Evolution of GC and FC with age

Our findings indicated significant changes in grey matter microstructural similarities across cortical and subcortical regions with age, including a global reinforcement of GC strength between ROI pairs. Initially weaker and widespread connections across ROI pairs at birth (PT:ses1) seemed to selectively strengthen during development (PT:ses2, FT) in both positive and negative directions. Most notable connectivity strengthening was observed between lobes, while cingulate regions became more dissimilar. Previous studies have also reported complex patterns of microstructural similarity profiles, including increases across occipital, parietal, and temporal areas, and decreases in limbic and cingulate regions in both FT and PT infants at TEA (Fenchel et al., 2020; Galdi et al., 2020). Our findings also suggested a strengthening of similarities for the frontal regions at TEA compared to PT scans at birth,

consistent with Galdi et al., (2020), but differing from Fenchel et al., (2020). These differences can be likely attributed to the use of PT infants within our cohort resulting in alterations of brain maturation (Ball et al., 2017). In our study, we also observed increasing negative connectivity between thalamus and brainstem to cortical regions with age. This was in line with previously rapid developmental changes in connections to and from deep grey matter structures during the studied period (Batalle et al., 2017a), combined with varying trends observed in thalamus and cortex development (Eaton-Rosen et al., 2015). More globally, previous work indicated that inter-regional similarities within GM and WM increase with age, while similarities between cortical GM and WM decrease and subcortical ROIs become more similar to WM and more dissimilar to cortical GM (Galdi et al., 2020).

At the network level, we noted a significant but not extensive overlap between the two PT sessions, indicating that GM similarity undergoes notable convergences and divergences of microstructural relationships during the preterm period. Nevertheless, some patterns of inter-regional similarities, reflecting potential network properties, seem to be already established by birth in PT subjects and further refined with development.

Similar trends were observed in terms of FC, including global reinforcement of connectivity strengths with age, in particular for cortico-subcortical connections, but also affecting cortico-cortical connectivities. This was consistent with previous observations of both cortico-cortical and thalamo-cortical connectivity increases in the preterm period (Taymourtash et al., 2023; Thomason et al., 2015). We might wonder if some biases in FC estimation might come from potential age-dependent effects on the signal-to-noise ratio (SNR) of rs-fMRI images (Denisova, 2019), which may be even lower in subcortical regions (Maugeri et al., 2018; Risk et al., 2021) and may limit the ability to derive existing cortical-subcortical connectivity at an early age.

Interestingly, the connectivity strengths across FC connectome showed closer alignment between birth and TEA in PT subjects compared to GC. However, it's challenging to ascertain whether this indicates that functional connections are established earlier than microstructural connectivity or if it reflects a temporal asynchrony of refinement of inter-regional relationships which might occur later and is not captured within the period assessed in our study. Similarly to GC network comparisons, FC-derived networks showed rather low but not insignificant overlap between the two PT sessions. This suggested that although significant development of functional networks occurs during the preterm period (Doria et al., 2010; Smyser et al., 2010; van den Heuvel et al., 2015) to reach an architecture that resembles

that of adults at TEA, some of these networks are already discernible at the time of PT birth (median 35 weeks gestational age in our study).

#3.4. Relationships between GC and FC during development

Comparisons of GC and FC modalities in terms of connectivity strength first highlighted strongest relationships in PT infants at birth and a decrease with development. This was likely driven by the divergence between GC and FC in terms of their changing profiles with age. For instance, GC seemingly underwent more pronounced changes in terms of strength between the two sessions compared to FC, whose profile in PT:ses2 was much more similar to PT:ses1. To investigate if these results might be affected by potential limitations of including the subcortical regions in the functional analysis, we also performed the GC-FC comparison while excluding the subcortical ROIs (*Annexe 3.3. Supp. Figure 2.2*). Focusing solely on cortical regions revealed a similar trend, with a strong relationship between GC and FC connectivity in PT: ses1, which disappeared in FT infants.

Interestingly, the trend was reversed when comparing GC and FC-derived networks instead of connectivity strengths. We hypothesize that this reflects that although both modalities exhibit distinct temporal patterns of change between the two sessions, the fundamental and shared network properties for both might already be established at preterm birth and further align as the networks refine on both microstructural and functional levels. This hints at a potential emergence of shared underlying network structures between GC and FC throughout development, suggested at later ages (Geng et al., 2016). The value of the 'network-approach' is underscored by the fact that although direct comparison of the two PT sessions within each modality suggested a higher similarity of FC than GC, the GC-FC network overlap remained the same. This indicates the preservation of at least some consistent patterns of inter-regional relationships across ages and modalities.

#3.5. Alterations of GC and FC with prematurity

Our results when comparing the PT infants at TEA to their FT counterparts confirmed the expected significant impact of prematurity in terms GC (Batalle et al., 2019b; Dimitrova et al., 2021; Eaton-Rosen et al., 2015, 2017; Ouyang, Jeon, et al., 2019; Smyser et al., 2016; Yu et al., 2016). Interestingly, we observed globally stronger microstructural strengths in PT than FT infants. Despite globally high correlation between GC in PT and FT infants, the relative patterns of GM similarity seemed altered between the two groups, affecting diverse ROI pairs including bilateral thalamus and hippocampus, as well as widespread regions across the cortex.

In terms of FC, we also observed a significant effect of prematurity, characterized by a global decrease in connectivity strength, consistent with previous observations (Scheinost et al., 2016). Prematurity was also associated with diffuse alterations of connectivity strengths across a broad range of subcortical and cortical regions, aligning with prior research (Ball et al., 2016; Brenner et al., 2021; Chiarelli et al., 2021; Eyre et al., 2021; Keunen et al., 2017; Smyser et al., 2010).

Interestingly, direct comparison of GC and FC connectivities did not reveal differences between PT infants at TEA and FT neonates. However, comparisons of GC and FC-derived networks indicated a lower overlap in PT than FT subjects, suggesting a higher, network-level dissociation between FC and the underlying GM microstructure due to prematurity.

#3.6. Longitudinal comparisons of GC and FC

To extend the GC-FC comparisons, we took advantage of the longitudinal PT data to describe the evolution of GC and FC connectomes with age by computing matrices of developmental change (ΔGC , ΔFC) that indicated both magnitude and direction of connectivity strength changes between birth and TEA. Consistently with previous findings on group comparisons, both modalities exhibited a spectrum of both increases and decreases of the link strengths during the preterm period.

In terms of ΔGC , the most pronounced decreases mostly concerned the connections involving the cingulate lobe and certain subcortical ROIs (for example cerebellum and amygdala). In ΔFC , global decreases were more prominent across cortical regions, particularly in long-range connectivity, while connections involving subcortical ROIs displayed an increase in strength. The direct comparison between ΔGC and ΔFC suggested a low but significant relationship, suggesting a potential co-evolution of microstructural and functional connectivities. However, this relationship was considerably weaker compared to the GC-FC relationships within each session (PT:ses1 and PT:ses2), likely due to the relatively small changes in the FC modality compared to GC between sessions.

Unfortunately, our results did not provide clear differentiation among the three hypotheses intended to test the directionality of GC and FC co-development: 1) FC and GC co-evolution; 2) if GC relying on FC; 3) FC relying on GC.

Although we could not determine whether GC relies on FC or vice versa, we might derive some suggestions from our observations. Overall, estimated slopes of all comparisons were significantly different. However, the relationships involving ΔGC were notably stronger than others, reinforcing the idea that the changes captured in ΔGC are reflected in FC. Our

findings might also suggest that within the short developmental period assessed in our study, ΔFC might not undergo sufficient change to provide adequate descriptors which could relate to GC.

In contrast, network-based comparisons of ΔGC and ΔFC to the opposite modalities reached similar overlaps, further implying commonalities in the network development in GC and FC modalities. Again, we were not able to ascertain which of the three hypotheses about GC-FC co-evolution is the most probable on the network level. Additionally, the complexity of whole-brain comparisons and the known regional and network level differences in their maturation timing of both the gray matter microstructure (Fukutomi et al., 2018; Lebenberg et al., 2019) and the FC (Cao et al., 2017; Eyre et al., 2021; Larivière et al., 2020) make it challenging to pinpoint the most probable hypothesis about GC-FC co-evolution at the network level. It is possible that the information on the potential relationships between FC and GC during development is buried within the complexity of the whole-brain comparisons. Future investigations might focus on early maturing areas like primary sensory regions to gain more insight into their relationship during development. In addition, the evaluation of GC-FC co-evolution was limited to PT subjects, which showed altered development in both modalities at TEA compared to FT neonates, suggesting this population might not be adequate to make conclusions on typical connectivity development. Future research should extend this comparison to typically developing individuals, for example foetuses, to provide better understanding into the directionality of GC-FC relationships suggested by our results.

In conclusion, our work presents an alternative approach for studying complex structure-function relationships during the early development and their alterations with prematurity by focusing on the grey matter microstructural similarities across cortical and subcortical regions. As an extension, it will be interesting to investigate how the altered GC-FC relationships in the early period relate to later neurodevelopmental outcomes.

#4 Materials and Methods

#4.1. Data presentation

#4.1.1. Subjects

This study included a sample of preterm and full-term neonates taken from the developing Human Connectome Project (dHCP) cohort (Edwards et al., 2022), collected at St Thomas' Hospital London, UK from 2015 to 2020. This project received UK NHS research

ethics committee approval (14/LO/1169, IRAS 138070), and written informed consent was obtained from the parents of all participant infants.

From the overall cohort, we identified 45 preterm (PT) infants (26 males, gestational age at birth – GA at birth – median 32.3 weeks, range [25.6w–36.0w]) who were scanned at two time points and whose dMRI and rs-fMRI data passed the quality control as described in 3rd dHCP release notes. For the session 1, the infants were scanned close to birth at median postmenstrual age – PMA at scan – 34.9 weeks, range [28.3w–36.9w]; median delay between birth-scan 1.7 weeks, range [0.1w–9.3w], and at the near term-equivalent age (TEA, i.e. session 2) (median PMA at scan 41.3 weeks, range [38.4w–44.9w], median birth-scan delay 9.1 weeks, range [3.6w–15.6w], median Ses1-Ses2 scan delay 7.3 weeks, range [2.7w–11.9w]). Additionally, we used a group of 45 full-term born (FT) infants (GA at birth: median 40.1w, range [37.4w–42.3w], median birth-scan delay 0.4 weeks, range [0.1w–3.9w]) matched to the preterm population on age at MRI at TEA and sex. All included infants were deemed healthy at scan, i.e., were without major brain focal lesions or any overt abnormality of clinical significance on anatomical MRI as evaluated by an expert paediatric neuroradiologist, (i.e. dHCP radiological scores were in the range [1-3]). More subject details for all three groups are available in *Annexe 3.3. Supplementary Table 3.1*.

#4.1.2. Acquisition and preprocessing of MRI data

MRI data was acquired using a Philips 3-Tesla Achieva scanner (Philips Medical Systems, Best, Netherlands). All infants were scanned during natural sleep using a neonatal head coil and imaging system optimized for the dHCP study as previously described (E. J. Hughes et al., 2017). In our work, we used anatomical, diffusion, and resting-state functional MRI data available in its pre-processed state from the dHCP database (3rd release) (Edwards et al., 2022).

The *anatomical data* resulted from acquisition and reconstruction using optimized protocols (Cordero-Grande et al., 2019), leading to super-resolved T2w images with an isotropic spatial voxel size of 0.5 mm. Processing followed a dedicated pipeline for segmentation and cortical surface extraction for T2w images of neonatal brains (Makropoulos et al., 2018a), with bias-correction, brain extraction, volumetric segmentation using Draw-EM (Developing brain Region Annotation with Expectation Maximization) algorithm (Makropoulos et al., 2014), and reconstruction of white matter surface (inner cortical surface) meshes. These anatomical data were used for the extraction of GM regions of interest (ROIs) (see section #4.2.1. *Delineation of ROIs*).

Acquisition and reconstruction of the *diffusion data* (dMRI) followed a multi-shell high angular resolution diffusion imaging (HARDI) protocol with 4 b-shells ($b = 0$ s/mm²: 20 repeats; and $b = 400, 1,000, 2,600$ s/mm²: 64, 88, and 128 directions, respectively) (Hutter et al., 2018) and was pre-processed with correction for motion artifacts and slice-to-volume reconstruction using the SHARD approach, leading to an isotropic voxel size of 1.5 mm (D. Christiaens et al., 2021). Pre-processed data were used for the fitting of diffusion models and the measure of GM microstructure (see section #4.2.2. *GM microstructural connectivity*).

Resting state functional data (rs-fMRI) was acquired for 15 minutes using a high temporal resolution multiband EPI protocol (TE=38 ms; TR=392 ms; MB factor=9x; 2.15 mm isotropic) (Price, 2015) and was processed following an automated processing framework specifically developed for neonates (Fitzgibbon et al., 2020a). Available data was used for the estimation of the whole-brain functional connectivity (see section #4.2.3. *Functional connectivity*).

#4.2. Estimation of connectivity matrices

#4.2.1. Delineation of ROIs

Firstly, regions of interest (ROIs) were defined as sub-regions of the cortical and subcortical grey matter to provide a framework for a focused and potentially interpretable assessment of the brain connectivity. Anatomically-driven parcellation strategy was used to provide a more reliable region correspondence between subjects and to allow the direct comparison of results between dMRI and rs-fMRI modalities. To define the ROIs, pre-processed anatomical data was used to parcellate the GM into 31 bilateral cortical and 13 subcortical regions. Cortical parcels were defined on the cortical surface of each hemisphere using the M-CRIB-S surface-based parcellation tool optimized for the term-born neonates (Adamson et al., 2020) whose labelling scheme replicates the Desikan-Killiany-Tourville (DKT) atlas (Klein & Tourville, 2012). The subcortical ROIs were defined using a volumetric GM parcellation based on Draw-EM algorithm segmentation (Makropoulos et al., 2014), and included medial brainstem (Bstem), and for each hemisphere: thalamus (Thal, fusing high and low intensity regions), caudate nucleus (Caud), lenticular nucleus (Lenti), amygdala (Amg), hippocampus (Hpc), and cerebellum (Crb). The 75 cortical and subcortical ROIs were combined and aligned to the subject diffusion and functional space with FSL 6.0's FLIRT using precomputed warps provided within the dHCP database. The list of ROIs used in this work is detailed in *Annexe 3.3. Supp. Table 1.* and visualized in *Annexe 3.3. Supp. Figure 4.1.*

Because the M-CRIB-S approach was developed for full-term neonates, visual inspection of the ROI segmentation quality was performed on the 25 youngest PT infants at scan. While we observed an expected trend of an increase in the segmentation quality with PMA at scan (errors for the youngest subjects could be explained by the landmarks missing or being less pronounced, i.e. shallower, for the successful surface-based registration to atlas, for example secondary and tertiary sulci), the parcellations remained satisfactory enough so as not to exclude any additional infants. Examples of the ROI longitudinal segmentations are shown in *Annexe 3.3. Supp. Figure 4.1*.

#4.2.2. GM microstructural connectivity (GC)

The DTI model was fitted to the diffusion data using a single shell ($b = 1,000 \text{ s/mm}^2$) and calculated with FSL's DTIFIT to estimate metric maps for four metrics: fractional anisotropy (FA), axial diffusivity (AD), radial diffusivity (RD), and mean diffusivity (MD) maps were estimated. Additionally, multi-shell diffusion data was used to derive the neurite density index (NDI) and orientation dispersion index (ODI) maps from the NODDI model (H. Zhang et al., 2012) using the CUDA 9.1 Diffusion Modelling Toolbox (cuDIMOT) NODDI Watson model implementation for GPUs (Hernandez-Fernandez et al., 2019). Derived maps were then corrected as described in Neumane et al., (2022).

To create subject-specific regional microstructural fingerprints, we extracted median diffusion metrics for each cortical and subcortical ROI. Beforehand, volumetric parcellations for subcortical regions underwent 1-voxel erosion to address potential border parcellation errors with surrounding white matter and cerebro-spinal fluid. For cortical regions, diffusion metrics were projected to the white-grey matter surface using a cylindrical approach guided by the minimum of AD, as described in (Lebenberg et al., 2019) and (Gondová et al., 2023a). Four hemispheres with locally imperfect projections in the superior frontal gyrus were identified, but the error impact on median computations within such a large region was minimal.

To focus on the microstructural variability between regions, we aimed to correct for potential confounding factors influencing dMRI metrics and the resulting correlations between pairs of regions before computing the group connectivity matrices. Regional metric values were corrected independently over the 3 groups for PMA at scan, GA at birth, and a residual of the global median diffusion metric corrected for PMA and GA (see Gondová et al., 2023a). Metric values were then scaled between $[0,1]$ for each region and for each subject group (PT: Ses1, PT: Ses2, FT). Group-specific GM connectivity matrices (GC) were then computed using

Pearson's correlation across the individual microstructural fingerprints including all 6 diffusion metrics together (4 DTI, 2 NODDI) and considering all pairs of grey matter ROIs.

#4.2.3. Functional connectivity (FC)

Based on pre-processed rs-fMRI individual data, we computed median BOLD activity over labelled ROIs, applied low-pass filtering (0.1 Hz), and standardized the time-series into z-scores. Data was smoothed (full-width at half maximum of 3.225 mm) and trimmed (first and last 50 time-points). For each subject, Pearson's correlation was used to compute a region-based connectivity matrix from the time series of each region pair. Group-level connectivity matrices were then obtained by averaging individual matrices within each group (PT-Ses1, PT-Ses2, FT). Even though the anatomically-driven parcellation might not be completely adequate for delineating the functional regions in the developing brain (*Annexe 3.3. Supp. Figure 4.3.*) we decided to keep this common framework to reduce the dimensionality of the connectomes and to allow for direct comparisons with the GC.

#4.3. Evaluation of group-wise connectivity matrices

#4.3.1. Comparing GM microstructural similarity between infant groups

On the GC level, we investigated the differences of the ROI-pair connections in terms of their microstructural profile between groups (comparing PT:ses2 and FT, and PT:ses1 and PT:ses2). Taking only the upper triangle of the GC matrix into account (because of matrix symmetry), we compared the distribution of the correlations between groups. As the correlation coefficients were not distributed normally in each group, as assessed by the Shapiro-Wilk test, and were considered as paired measures between groups PT:ses1 vs PT:ses 2 and PT:ses2 vs FT, we used a non-parametric Wilcoxon signed-rank test to assess the differences of distributions across the group pairs. Distribution of connectivity strength between infant groups was also assessed using Pearson's correlation to describe potential relationships in the patterns of GC connectivity.

For visual aid, we represented the GC connectomes as circle plots connecting ROIs. To ease the visualization, the GC matrices were thresholded to show only the top 25% connection with: *i*, a common threshold across all three infant groups to uncover potential global changes of GC with age and prematurity (GC threshold r of 0.786), and *ii*, with threshold adapted to each infant group to visualize potential changes in the relative connectivity strengths between groups (adapted threshold of 0.657 for PT:ses1, 0.856 for PT:ses2, and 0.833 for FT).

#4.3.2. Comparing group-wise functional connectomes (FC)

We performed similar analyses as in the case of GC to evaluate the differences in FC between the infant groups. For the creation of the circle plots from the FC connectomes, we used common FC thresholds of 0.448, and adapted thresholds of 0.349 for PT:ses1, 0.409 for PT:ses2, and 0.537 for FT.

#4.3.3. Associating GC and FC connectivity

The relationship between groupwise GC and FC was evaluated by a linear regression applied to the components of the upper triangle of the connectomes for each infant group separately. The reported p-value for the described relationship was obtained by permutation testing during which the null distribution was generated by randomly shuffling the GC and FC inputs to the linear regressor. The final value was then computed as the proportion of observations more extreme than the one observed for the unshuffled inputs after 1000 random runs. The slopes of the comparisons were compared using Z-scores.

#4.4. *Delineation and assessment of GC and FC networks*

#4.4.1. Group-wise networks

To extend our analyses beyond the direct comparisons of matrices in terms of ROI pair correlation, we aimed to evaluate the spatial similarity between the inter-regional relationships to compare either the groups or the two connectomic modalities. With this goal, we sought to extract ‘networks’, i.e. clusters, that would regroup ROIs with similar connectivity profiles for each group and each modality separately and then to assess potential overlaps between such defined GC/FC networks. For each modality and infant group, we firstly computed Euclidean distances from the correlation coefficients to create group-wise GC and FC distance matrices using cosine theorem:

$$d = \sqrt{2(1 - r)}$$

We then performed hierarchical clustering with the ward linkage to group regions with similar connectivity patterns. As deciding the ideal number of clusters that would appropriately reflect the studied relationships across modalities and infant groups is difficult, especially given the dynamic evolution of developing infant brain on both structural and functional level, we decided to split the derived hierarchical trees (dendrograms) into all possible cluster sizes from 2 to 75 (max number where cluster size is 1 because of the number of parcels) instead.

The commonalities between clustering results were then compared (either between groups for a single modality, or between modalities for a single group) using mutual

information (MI) between all possible cluster pairs as this measure is expected to approximate to a certain extent the overlap of the networks. Similarly to previous GC-FC comparisons, we performed permutation testing to define a threshold for the individual values of the mutual information (MI derived for a given cluster pair) by randomly shuffling the inputs (i.e. randomly re-labelling the cluster assignments) to obtain the null distribution (100 times) for each comparison. Only the mutual information scores that were higher than 95% of the null distribution scores were retained when reporting means and standard deviations of the obtained MI results.

#4.4.2. Longitudinal networks

Based on the idea that regions that participate in the same networks might show similar developmental evolution, we further aimed to regroup ROIs based on their changing connectivity profiles into structural and functional ‘longitudinal networks’ and compare these GC and FC longitudinal networks in terms of their overlap with MI. To evaluate potential similarities between GC and FC connectomes in the evolution with age, we leveraged the longitudinal aspect of our dataset. We first computed the matrices of developmental change between PT:ses1 and PT:ses2 for GC and FC separately (referred to as ΔGC and ΔFC , respectively). For ΔGC , as the diffusion metrics were corrected for within-group age effects before the computation of the connectome, the change between connectomic strengths with age was computed as a simple absolute difference between the sessions. The direction of the change was then added to the matrix to indicate the increases or decreases of the connectivity strength between given ROI pairs between Ses1 and Ses2, i.e. positive values mean increases in the structural similarity with age, while negative values capture the weakening of the similarities with development.

For ΔFC , the computation of matrices of developmental change between Ses1 and Ses2 was similar but included an additional step to account for the variance across the individual FC matrices within PT:ses1 and PT:ses2 groups whose median correlations were significantly associated with the infants’ ages (PMA at Ses1 vs Ses2 were not correlated, Pearson’s $R=0.18$, $p=0.17$). As an attempt to remedy this, we first computed group-wise confidence intervals for each ROI pair using the standard deviations of pair’s connectivity strength across subjects within the considered infant group. The absolute FC differences between the 2 sessions were then weighted by overlap of the confidence interval (meaning that a high overlap leads to a decreased difference). The sign was once again added to the resulting matrices of

developmental change like for ΔGC , to indicate the direction (i.e. increase or decrease) of the ROI pairs' evolution with age.

The relationship between ΔGC and ΔFC was evaluated by a linear regression applied to the components of the upper triangle of the matrices. Additionally, we compared ΔGC and ΔFC to the connectivity matrices of the opposite modality derived at two sessions (i.e. ΔGC vs $FC - PT:ses1$ and $FC - PT:ses2$, and ΔFC vs $GC - PT:ses1$ and $GC - PT:ses2$). We believed such analysis might allow us to assess hypotheses regarding the potential co-evolution of the GC and FC connectivity, in case such co-evolution exists in the age-ranges of the subjects available in this study. Specifically, if the GC and FC networks co-evolve, their ΔGC and ΔFC -derived networks should be highly similar. In case of stronger effect of GC on FC in the early period, we would expect ΔFC to depend on GC in the $PT:ses1$ group while FC at $PT:Ses2$ would depend on ΔGC . The opposite would be true if GC is based on FC. As an attempt to mitigate the outliers, we evaluated the relationships using robust linear regression. To decipher if one of these hypotheses is more relevant than the others in our PT group, we compared the regression slopes of the evaluated relationships using a Z-scores like before.

To get a proxy of longitudinal GC and FC networks, the derived ΔGC and ΔFC matrices were used to cluster ROIs with similar developmental connectivity change. As previously done for within-group connectivity matrices, we used the ward hierarchical clustering and created all possible cluster sizes from 2 to 75 and evaluated the MI between the clustering pairs considering different combinations. Additionally, we compared the networks derived from the ΔGC and ΔFC to the networks from the respective opposite modality derived at both sessions (i.e. ΔGC vs $FC - PT:ses1$ and $FC - PT:ses2$, and ΔFC vs $GC - PT:ses1$ and $GC - PT:ses2$) to assess the potential co-evolution of the GC and FC networks.

#5 References

- Alexander-Bloch, A., Giedd, J. N., & Bullmore, E. (2013). Imaging structural co-variance between human brain regions. *Nature Reviews Neuroscience*, 14(5), 322–336. <https://doi.org/10.1038/nrn3465>
- Ball, G., Aljabar, P., Arichi, T., Tusor, N., Cox, D., Merchant, N., Nongena, P., Hajnal, J. V., Edwards, A. D., & Counsell, S. J. (2016). Machine-learning to characterise neonatal functional connectivity in the preterm brain. *NeuroImage*, 124, 267–275. <https://doi.org/10.1016/j.neuroimage.2015.08.055>
- Ball, G., Aljabar, P., Nongena, P., Kennea, N., Gonzalez-Cinca, N., Falconer, S., Chew, A. T. M., Harper, N., Wurie, J., Rutherford, M. A., Counsell, S. J., & Edwards, A. D. (2017). Multimodal image analysis of clinical influences on preterm brain development. *Annals of Neurology*, 82(2), 233–246. <https://doi.org/10.1002/ana.24995>

- Ball, G., Seidlitz, J., O’Muircheartaigh, J., Dimitrova, R., Fenchel, D., Makropoulos, A., Christiaens, D., Schuh, A., Passerat-Palmbach, J., Hutter, J., Cordero-Grande, L., Hughes, E., Price, A., Hajnal, J. V., Rueckert, D., Robinson, E. C., & Edwards, A. D. (2020). Cortical morphology at birth reflects spatiotemporal patterns of gene expression in the fetal human brain. *PLOS Biology*, 18(11), e3000976. <https://doi.org/10.1371/journal.pbio.3000976>
- Ball, G., Srinivasan, L., Aljabar, P., Counsell, S. J., Durighel, G., Hajnal, J. V., Rutherford, M. A., & Edwards, A. D. (2013). Development of cortical microstructure in the preterm human brain. *Proceedings of the National Academy of Sciences*, 110(23), 9541–9546. <https://doi.org/10.1073/pnas.1301652110>
- Barbas, H. (2015). General Cortical and Special Prefrontal Connections: Principles from Structure to Function. *Annual Review of Neuroscience*, 38(1), 269–289. <https://doi.org/10.1146/annurev-neuro-071714-033936>
- Basser, P. J., Mattiello, J., & Lebihan, D. (1994). Estimation of the Effective Self-Diffusion Tensor from the NMR Spin Echo. *Journal of Magnetic Resonance, Series B*, 103(3), 247–254. <https://doi.org/10.1006/jmrb.1994.1037>
- Batalle, D., Hughes, E. J., Zhang, H., Tournier, J.-D., Tusor, N., Aljabar, P., Wali, L., Alexander, D. C., Hajnal, J. V., Nosarti, C., Edwards, A. D., & Counsell, S. J. (2017). Early development of structural networks and the impact of prematurity on brain connectivity. *NeuroImage*, 149, 379–392. <https://doi.org/10.1016/j.neuroimage.2017.01.065>
- Batalle, D., O’Muircheartaigh, J., Makropoulos, A., Kelly, C. J., Dimitrova, R., Hughes, E. J., Hajnal, J. V., Zhang, H., Alexander, D. C., Edwards, A. D., & Counsell, S. J. (2019). Different patterns of cortical maturation before and after 38 weeks gestational age demonstrated by diffusion MRI in vivo. *NeuroImage*, 185, 764–775. <https://doi.org/10.1016/j.neuroimage.2018.05.046>
- Brenner, R. G., Wheelock, M. D., Neil, J. J., & Smyser, C. D. (2021). Structural and functional connectivity in premature neonates. *Seminars in Perinatology*, 45(7), 151473. <https://doi.org/10.1016/j.semperi.2021.151473>
- Cao, M., Huang, H., & He, Y. (2017). Developmental Connectomics from Infancy through Early Childhood. *Trends in Neurosciences*, 40(8), 494–506. <https://doi.org/10.1016/j.tins.2017.06.003>
- Cardona, G., Mir, A., Rosselló, F., Rotger, L., & Sánchez, D. (2013). Cophenetic metrics for phylogenetic trees, after Sokal and Rohlf. *BMC Bioinformatics*, 14(1), 3. <https://doi.org/10.1186/1471-2105-14-3>
- Chiarelli, A. M., Sestieri, C., Navarra, R., Wise, R. G., & Caulo, M. (2021). Distinct effects of prematurity on MRI metrics of brain functional connectivity, activity, and structure: Univariate and multivariate analyses. *Human Brain Mapping*, 42(11), 3593–3607. <https://doi.org/10.1002/hbm.25456>
- Christiaens, D., Cordero-Grande, L., Pietsch, M., Hutter, J., Price, A. N., Hughes, E. J., Vecchiato, K., Deprez, M., Edwards, A. D., Hajnal, J. V., & Tournier, J.-D. (2021). Scattered slice SHARD reconstruction for motion correction in multi-shell diffusion MRI. *NeuroImage*, 225, 117437. <https://doi.org/10.1016/j.neuroimage.2020.117437>
- Cordero-Grande, L., Christiaens, D., Hutter, J., Price, A. N., & Hajnal, J. V. (2019). Complex diffusion-weighted image estimation via matrix recovery under general noise models. *NeuroImage*, 200, 391–404. <https://doi.org/10.1016/j.neuroimage.2019.06.039>
- Dall’Orso, S., Arichi, T., Fitzgibbon, S. P., Edwards, A. D., Burdet, E., & Muceli, S. (2022). Development of functional organization within the sensorimotor network across the perinatal period. *Human Brain Mapping*, 43(7), 2249–2261. <https://doi.org/10.1002/hbm.25785>
- Denisova, K. (2019). Age attenuates noise and increases symmetry of head movements during sleep resting-state fMRI in healthy neonates, infants, and toddlers. *Infant Behavior and Development*, 57, 101317. <https://doi.org/10.1016/j.infbeh.2019.03.008>

- Dimitrova, R., Pietsch, M., Ciarrusta, J., Fitzgibbon, S. P., Williams, L. Z. J., Christiaens, D., Cordero-Grande, L., Batalle, D., Makropoulos, A., Schuh, A., Price, A. N., Hutter, J., Teixeira, R. P., Hughes, E., Chew, A., Falconer, S., Carney, O., Egloff, A., Tournier, J.-D., ... O'Muircheartaigh, J. (2021). Preterm birth alters the development of cortical microstructure and morphology at term-equivalent age. *NeuroImage*, 243, 118488. <https://doi.org/10.1016/j.neuroimage.2021.118488>
- Doria, V., Beckmann, C. F., Arichi, T., Merchant, N., Groppo, M., Turkheimer, F. E., Counsell, S. J., Murgasova, M., Aljabar, P., Nunes, R. G., Larkman, D. J., Rees, G., & Edwards, A. D. (2010). Emergence of resting state networks in the preterm human brain. *Proceedings of the National Academy of Sciences*, 107(46), 20015–20020. <https://doi.org/10.1073/pnas.1007921107>
- Dubois, J., Alison, M., Counsell, S. J., Hertz-Pannier, L., Hüppi, P. S., & Benders, M. J. N. L. (2021). MRI of the Neonatal Brain: A Review of Methodological Challenges and Neuroscientific Advances. *Journal of Magnetic Resonance Imaging*, 53(5), 1318–1343. <https://doi.org/10.1002/jmri.27192>
- Eaton-Rosen, Z., Melbourne, A., Orasanu, E., Cardoso, M. J., Modat, M., Bainbridge, A., Kendall, G. S., Robertson, N. J., Marlow, N., & Ourselin, S. (2015). Longitudinal measurement of the developing grey matter in preterm subjects using multi-modal MRI. *NeuroImage*, 111, 580–589. <https://doi.org/10.1016/j.neuroimage.2015.02.010>
- Eaton-Rosen, Z., Scherrer, B., Melbourne, A., Ourselin, S., Neil, J. J., & Warfield, S. K. (2017). Investigating the maturation of microstructure and radial orientation in the preterm human cortex with diffusion MRI. *NeuroImage*, 162, 65–72. <https://doi.org/10.1016/j.neuroimage.2017.08.013>
- Edwards, A. D., Rueckert, D., Smith, S. M., Abo Seada, S., Alansary, A., Almalbis, J., Allsop, J., Andersson, J., Arichi, T., Arulkumaran, S., Bastiani, M., Batalle, D., Baxter, L., Bozek, J., Braithwaite, E., Brandon, J., Carney, O., Chew, A., Christiaens, D., ... Hajnal, J. V. (2022). The Developing Human Connectome Project Neonatal Data Release. *Frontiers in Neuroscience*, 16. <https://doi.org/10.3389/fnins.2022.886772>
- Eyre, M., Fitzgibbon, S. P., Ciarrusta, J., Cordero-Grande, L., Price, A. N., Poppe, T., Schuh, A., Hughes, E., O'Keeffe, C., Brandon, J., Cromb, D., Vecchiato, K., Andersson, J., Duff, E. P., Counsell, S. J., Smith, S. M., Rueckert, D., Hajnal, J. V., Arichi, T., ... Edwards, A. D. (2021). The Developing Human Connectome Project: typical and disrupted perinatal functional connectivity. *Brain*, 144(7), 2199–2213. <https://doi.org/10.1093/brain/awab118>
- Fan, Y., Shi, F., Smith, J. K., Lin, W., Gilmore, J. H., & Shen, D. (2011). Brain anatomical networks in early human brain development. *NeuroImage*, 54(3), 1862–1871. <https://doi.org/10.1016/j.neuroimage.2010.07.025>
- Fenchel, D., Dimitrova, R., Robinson, E. C., Batalle, D., Chew, A., Falconer, S., Kyriakopoulou, V., Nosarti, C., Hutter, J., Christiaens, D., Pietsch, M., Brandon, J., Hughes, E. J., Allsop, J., O'Keeffe, C., Price, A. N., Cordero-Grande, L., Schuh, A., Makropoulos, A., ... O'Muircheartaigh, J. (2022). Neonatal multi-modal cortical profiles predict 18-month developmental outcomes. *Developmental Cognitive Neuroscience*, 54, 101103. <https://doi.org/10.1016/j.dcn.2022.101103>
- Fenchel, D., Dimitrova, R., Seidlitz, J., Robinson, E. C., Batalle, D., Hutter, J., Christiaens, D., Pietsch, M., Brandon, J., Hughes, E. J., Allsop, J., O'Keeffe, C., Price, A. N., Cordero-Grande, L., Schuh, A., Makropoulos, A., Passerat-Palmbach, J., Bozek, J., Rueckert, D., ... O'Muircheartaigh, J. (2020). Fench et Development of Microstructural and Morphological Cortical Profiles in the Neonatal Brain. *Cerebral Cortex*, 30(11), 5767–5779. <https://doi.org/10.1093/cercor/bhaa150>
- Fitzgibbon, S. P., Harrison, S. J., Jenkinson, M., Baxter, L., Robinson, E. C., Bastiani, M., Bozek, J., Karolis, V., Cordero Grande, L., Price, A. N., Hughes, E., Makropoulos, A., Passerat-Palmbach,

- J., Schuh, A., Gao, J., Farahibozorg, S. R., O’Muircheartaigh, J., Ciarrusta, J., O’Keeffe, C., ... Andersson, J. (2020). The developing Human Connectome Project (dHCP) automated resting-state functional processing framework for newborn infants. *NeuroImage*, 223(August), 117303. <https://doi.org/10.1016/j.neuroimage.2020.117303>
- Fransson, P., Skiöld, B., Engström, M., Hallberg, B., Mosskin, M., Åden, U., Lagercrantz, H., & Blennow, M. (2009). Spontaneous Brain Activity in the Newborn Brain During Natural Sleep—An fMRI Study in Infants Born at Full Term. *Pediatric Research*, 66(3), 301–305. <https://doi.org/10.1203/PDR.0b013e3181b1bd84>
- Friedrichs-Maeder, C. L., Griffo, A., Schneider, J., Hüppi, P. S., Truttmann, A., & Hagmann, P. (2017). Exploring the role of white matter connectivity in cortex maturation. *PLOS ONE*, 12(5), e0177466. <https://doi.org/10.1371/journal.pone.0177466>
- Fukutomi, H., Glasser, M. F., Zhang, H., Autio, J. A., Coalson, T. S., Okada, T., Togashi, K., Van Essen, D. C., & Hayashi, T. (2018). Neurite imaging reveals microstructural variations in human cerebral cortical gray matter. *NeuroImage*, 182, 488–499. <https://doi.org/10.1016/j.neuroimage.2018.02.017>
- Galdi, P., Blesa, M., Stoye, D. Q., Sullivan, G., Lamb, G. J., Quigley, A. J., Thrippleton, M. J., Bastin, M. E., & Boardman, J. P. (2020). Neonatal morphometric similarity mapping for predicting brain age and characterizing neuroanatomic variation associated with preterm birth. *NeuroImage: Clinical*, 25, 102195. <https://doi.org/10.1016/j.nicl.2020.102195>
- Gao, W., Alcauter, S., Elton, A., Hernandez-Castillo, C. R., Smith, J. K., Ramirez, J., & Lin, W. (2015). Functional Network Development During the First Year: Relative Sequence and Socioeconomic Correlations. *Cerebral Cortex*, 25(9), 2919–2928. <https://doi.org/10.1093/cercor/bhu088>
- Geng, X., Li, G., Lu, Z., Gao, W., Wang, L., Shen, D., Zhu, H., & Gilmore, J. H. (2016). Structural and Maturation Covariance in Early Childhood Brain Development. *Cerebral Cortex*, bhw022. <https://doi.org/10.1093/cercor/bhw022>
- Gilmore, J. H., Knickmeyer, R. C., & Gao, W. (2018). Imaging structural and functional brain development in early childhood. *Nature Reviews Neuroscience*, 19(3), 123–137. <https://doi.org/10.1038/nrn.2018.1>
- Gilmore, J. H., Shi, F., Woolson, S. L., Knickmeyer, R. C., Short, S. J., Lin, W., Zhu, H., Hamer, R. M., Styner, M., & Shen, D. (2012). Longitudinal Development of Cortical and Subcortical Gray Matter from Birth to 2 Years. *Cerebral Cortex*, 22(11), 2478–2485. <https://doi.org/10.1093/cercor/bhr327>
- Gondová, A., Neumane, S., Leprince, Y., Mangin, J.-F., Arichi, T., & Dubois, J. (2023). Predicting neurodevelopmental outcomes from neonatal cortical microstructure: A conceptual replication study. *Neuroimage: Reports*, 3(2), 100170. <https://doi.org/10.1016/j.ynirp.2023.100170>
- Goulas, A., Werner, R., Beul, S. F., Saering, D., Heuvel, M. P., T. L. C., & Hilgetag, C. C. (2016). Cytoarchitectonic similarity is a wiring principle of the human connectome. *BioRxiv*.
- Goulas, A., Uylings, H. B. M., & Hilgetag, C. C. (2017). Principles of ipsilateral and contralateral cortico-cortical connectivity in the mouse. *Brain Structure and Function*, 222(3), 1281–1295. <https://doi.org/10.1007/s00429-016-1277-y>
- Grayson, D. S., Ray, S., Carpenter, S., Iyer, S., Dias, T. G. C., Stevens, C., Nigg, J. T., & Fair, D. A. (2014). Structural and Functional Rich Club Organization of the Brain in Children and Adults. *PLoS ONE*, 9(2), e88297. <https://doi.org/10.1371/journal.pone.0088297>
- Hagmann, P., Sporns, O., Madan, N., Cammoun, L., Pienaar, R., Wedeen, V. J., Meuli, R., Thiran, J.-P., & Grant, P. E. (2010). White matter maturation reshapes structural connectivity in the late developing human brain. *Proceedings of the National Academy of Sciences*, 107(44), 19067–19072. <https://doi.org/10.1073/pnas.1009073107>

- Hernandez-Fernandez, M., Reguly, I., Jbabdi, S., Giles, M., Smith, S., & Sotiropoulos, S. N. (2019). Using GPUs to accelerate computational diffusion MRI: From microstructure estimation to tractography and connectomes. *NeuroImage*, 188, 598–615. <https://doi.org/10.1016/j.neuroimage.2018.12.015>
- Hoff, G. E. A.-J., Van den Heuvel, M. P., Benders, M. J. N. L., Kersbergen, K. J., & De Vries, L. S. (2013). On development of functional brain connectivity in the young brain. *Frontiers in Human Neuroscience*, 7. <https://doi.org/10.3389/fnhum.2013.00650>
- Hughes, E. J., Winchman, T., Padormo, F., Teixeira, R., Wurie, J., Sharma, M., Fox, M., Hutter, J., Cordero-Grande, L., Price, A. N., Allsop, J., Bueno-Conde, J., Tusor, N., Arichi, T., Edwards, A. D., Rutherford, M. A., Counsell, S. J., & Hajnal, J. V. (2017). A dedicated neonatal brain imaging system. *Magnetic Resonance in Medicine*, 78(2), 794–804. <https://doi.org/10.1002/mrm.26462>
- Hutter, J., Tournier, J. D., Price, A. N., Cordero-Grande, L., Hughes, E. J., Malik, S., Steinweg, J., Bastiani, M., Sotiropoulos, S. N., Jbabdi, S., Andersson, J., Edwards, A. D., & Hajnal, J. V. (2018). Time-efficient and flexible design of optimized multishell HARDI diffusion. *Magnetic Resonance in Medicine*, 79(3), 1276–1292. <https://doi.org/10.1002/mrm.26765>
- Jakab, A., Schwartz, E., Kasprian, G., Gruber, G. M., Prayer, D., Schopf, V., & Langs, G. (2014). Fetal functional imaging portrays heterogeneous development of emerging human brain networks. *Frontiers in Human Neuroscience*, 8. <https://doi.org/10.3389/fnhum.2014.00852>
- Jensen, J. H., Helpert, J. A., Ramani, A., Lu, H., & Kaczynski, K. (2005). Diffusional kurtosis imaging: The quantification of non-gaussian water diffusion by means of magnetic resonance imaging. *Magnetic Resonance in Medicine*, 53(6), 1432–1440. <https://doi.org/10.1002/mrm.20508>
- Keunen, K., Counsell, S. J., & Benders, M. J. N. L. (2017). The emergence of functional architecture during early brain development. *NeuroImage*, 160, 2–14. <https://doi.org/10.1016/j.neuroimage.2017.01.047>
- King, D. J., & Wood, A. G. (2020). Clinically feasible brain morphometric similarity network construction approaches with restricted magnetic resonance imaging acquisitions. *Network Neuroscience*, 4(1), 274–291. https://doi.org/10.1162/netn_a_00123
- Klein, A., & Tourville, J. (2012). 101 Labeled Brain Images and a Consistent Human Cortical Labeling Protocol. *Frontiers in Neuroscience*, 6. <https://doi.org/10.3389/fnins.2012.00171>
- Larivière, S., Vos de Wael, R., Hong, S.-J., Paquola, C., Tavakol, S., Lowe, A. J., Schrader, D. V., & Bernhardt, B. C. (2020). Multiscale Structure–Function Gradients in the Neonatal Connectome. *Cerebral Cortex*, 30(1), 47–58. <https://doi.org/10.1093/cercor/bhz069>
- Lebenberg, J., Mangin, J.-F., Thirion, B., Poupon, C., Hertz-Pannier, L., Leroy, F., Adibpour, P., Dehaene-Lambertz, G., & Dubois, J. (2019). Mapping the asynchrony of cortical maturation in the infant brain: A MRI multi-parametric clustering approach. *NeuroImage*, 185, 641–653. <https://doi.org/10.1016/j.neuroimage.2018.07.022>
- Lyall, A. E., Shi, F., Geng, X., Woolson, S., Li, G., Wang, L., Hamer, R. M., Shen, D., & Gilmore, J. H. (2015). Dynamic Development of Regional Cortical Thickness and Surface Area in Early Childhood. *Cerebral Cortex*, 25(8), 2204–2212. <https://doi.org/10.1093/cercor/bhu027>
- Makropoulos, A., Gousias, I. S., Ledig, C., Aljabar, P., Serag, A., Hajnal, J. V., Edwards, A. D., Counsell, S. J., & Rueckert, D. (2014). Automatic Whole Brain MRI Segmentation of the Developing Neonatal Brain. *IEEE Transactions on Medical Imaging*, 33(9), 1818–1831. <https://doi.org/10.1109/TMI.2014.2322280>
- Makropoulos, A., Robinson, E. C., Schuh, A., Wright, R., Fitzgibbon, S., Bozek, J., Counsell, S. J., Steinweg, J., Vecchiato, K., Passerat-Palmbach, J., Lenz, G., Mortari, F., Tenev, T., Duff, E. P., Bastiani, M., Cordero-Grande, L., Hughes, E., Tusor, N., Tournier, J. D., ... Rueckert, D. (2018). The developing human connectome project: A minimal processing pipeline for neonatal cortical

- surface reconstruction. *NeuroImage*, 173(April 2017), 88–112. <https://doi.org/10.1016/j.neuroimage.2018.01.054>
- Maugeri, L., Moraschi, M., Summers, P., Favilla, S., Mascali, D., Cedola, A., Porro, C. A., Giove, F., & Fratini, M. (2018). Assessing denoising strategies to increase signal to noise ratio in spinal cord and in brain cortical and subcortical regions. *Journal of Instrumentation*, 13(02), C02028–C02028. <https://doi.org/10.1088/1748-0221/13/02/C02028>
- McKinstry, R. C., Mathur, A. M., Miller, J. H., Ozcan, A., Snyder, A. Z., Schefft, G., Almlil, C. R., Shiran, S. I., Conturo, T. E., & Neil, J. J. (2002). Radial Organization of Developing Preterm Human Cerebral Cortex Revealed by Non-invasive Water Diffusion Anisotropy MRI. *Cerebral Cortex*, 12(12), 1237–1243. <https://doi.org/10.1093/cercor/12.12.1237>
- Monson, B. B., Eaton-Rosen, Z., Kapur, K., Liebenthal, E., Brownell, A., Smyser, C. D., Rogers, C. E., Inder, T. E., Warfield, S. K., & Neil, J. J. (2018). Differential Rates of Perinatal Maturation of Human Primary and Nonprimary Auditory Cortex. *Eneuro*, 5(1), ENEURO.0380-17.2017. <https://doi.org/10.1523/ENEURO.0380-17.2017>
- Neil, J. J., & Smyser, C. D. (2018). Recent advances in the use of MRI to assess early human cortical development. *Journal of Magnetic Resonance*, 293, 56–69. <https://doi.org/10.1016/j.jmr.2018.05.013>
- Neumane, S., Gondova, A., Leprince, Y., Hertz-Pannier, L., Arichi, T., & Dubois, J. (2022). Early structural connectivity within the sensorimotor network: Deviations related to prematurity and association to neurodevelopmental outcome. *Frontiers in Neuroscience*, 16. <https://doi.org/10.3389/fnins.2022.932386>
- Nie, J., Li, G., Wang, L., Shi, F., Lin, W., Gilmore, J. H., & Shen, D. (2014). Longitudinal development of cortical thickness, folding, and fiber density networks in the first 2 years of life. *Human Brain Mapping*, 35(8), 3726–3737. <https://doi.org/10.1002/hbm.22432>
- Ouyang, M., Dubois, J., Yu, Q., Mukherjee, P., & Huang, H. (2019). Delineation of early brain development from fetuses to infants with diffusion MRI and beyond. *NeuroImage*, 185, 836–850. <https://doi.org/10.1016/j.neuroimage.2018.04.017>
- Ouyang, M., Jeon, T., Sotiras, A., Peng, Q., Mishra, V., Halovanic, C., Chen, M., Chalak, L., Rollins, N., Roberts, T. P. L., Davatzikos, C., & Huang, H. (2019). Differential cortical microstructural maturation in the preterm human brain with diffusion kurtosis and tensor imaging. *Proceedings of the National Academy of Sciences*, 116(10), 4681–4688. <https://doi.org/10.1073/pnas.1812156116>
- Price, A. N. (2015). Accelerated Neonatal fMRI Using Multiband EPI.
- Risk, B. B., Murden, R. J., Wu, J., Nebel, M. B., Venkataraman, A., Zhang, Z., & Qiu, D. (2021). Which multiband factor should you choose for your resting-state fMRI study? *NeuroImage*, 234, 117965. <https://doi.org/10.1016/j.neuroimage.2021.117965>
- Scheinost, D., Kwon, S. H., Shen, X., Lacadie, C., Schneider, K. C., Dai, F., Ment, L. R., & Constable, R. T. (2016). Preterm birth alters neonatal, functional rich club organization. *Brain Structure and Function*, 221(6), 3211–3222. <https://doi.org/10.1007/s00429-015-1096-6>
- Seidlitz, J., Váša, F., Shinn, M., Romero-Garcia, R., Whitaker, K. J., Vértes, P. E., Wagstyl, K., Kirkpatrick Reardon, P., Clasen, L., Liu, S., Messinger, A., Leopold, D. A., Fonagy, P., Dolan, R. J., Jones, P. B., Goodyer, I. M., Raznahan, A., & Bullmore, E. T. (2018). Morphometric Similarity Networks Detect Microscale Cortical Organization and Predict Inter-Individual Cognitive Variation. *Neuron*, 97(1), 231-247.e7. <https://doi.org/10.1016/j.neuron.2017.11.039>
- Shi, F., Yap, P.-T., Gao, W., Lin, W., Gilmore, J. H., & Shen, D. (2012). Altered structural connectivity in neonates at genetic risk for schizophrenia: A combined study using morphological and white matter networks. *NeuroImage*, 62(3), 1622–1633. <https://doi.org/10.1016/j.neuroimage.2012.05.026>

- Smyser, C. D., Inder, T. E., Shimony, J. S., Hill, J. E., Degnan, A. J., Snyder, A. Z., & Neil, J. J. (2010). Longitudinal Analysis of Neural Network Development in Preterm Infants. *Cerebral Cortex*, 20(12), 2852–2862. <https://doi.org/10.1093/cercor/bhq035>
- Smyser, T. A., Smyser, C. D., Rogers, C. E., Gillespie, S. K., Inder, T. E., & Neil, J. J. (2016). Cortical Gray and Adjacent White Matter Demonstrate Synchronous Maturation in Very Preterm Infants. *Cerebral Cortex*, 26(8), 3370–3378. <https://doi.org/10.1093/cercor/bhv164>
- Taymourtash, A., Schwartz, E., Nenning, K.-H., Sobotka, D., Licandro, R., Glatter, S., Diogo, M. C., Golland, P., Grant, E., Prayer, D., Kasprian, G., & Langs, G. (2023). Fetal development of functional thalamocortical and cortico–cortical connectivity. *Cerebral Cortex*, 33(9), 5613–5624. <https://doi.org/10.1093/cercor/bhac446>
- Thomason, M. E., Grove, L. E., Lozon, T. A., Vila, A. M., Ye, Y., Nye, M. J., Manning, J. H., Pappas, A., Hernandez-Andrade, E., Yeo, L., Mody, S., Berman, S., Hassan, S. S., & Romero, R. (2015). Age-related increases in long-range connectivity in fetal functional neural connectivity networks in utero. *Developmental Cognitive Neuroscience*, 11, 96–104. <https://doi.org/10.1016/j.dcn.2014.09.001>
- Toulmin, H., Beckmann, C. F., O’Muircheartaigh, J., Ball, G., Nongena, P., Makropoulos, A., Ederies, A., Counsell, S. J., Kennea, N., Arichi, T., Tusor, N., Rutherford, M. A., Azzopardi, D., Gonzalez-Cinca, N., Hajnal, J. V., & Edwards, A. D. (2015). Specialization and integration of functional thalamocortical connectivity in the human infant. *Proceedings of the National Academy of Sciences*, 112(20), 6485–6490. <https://doi.org/10.1073/pnas.1422638112>
- Turk, E., van den Heuvel, M. I., Benders, M. J., de Heus, R., Franx, A., Manning, J. H., Hect, J. L., Hernandez-Andrade, E., Hassan, S. S., Romero, R., Kahn, R. S., Thomason, M. E., & van den Heuvel, M. P. (2019). Functional Connectome of the Fetal Brain. *The Journal of Neuroscience*, 39(49), 9716–9724. <https://doi.org/10.1523/JNEUROSCI.2891-18.2019>
- van den Heuvel, M. P., & Hulshoff Pol, H. E. (2010). Exploring the brain network: A review on resting-state fMRI functional connectivity. *European Neuropsychopharmacology*, 20(8), 519–534. <https://doi.org/10.1016/j.euroneuro.2010.03.008>
- van den Heuvel, M. P., Kersbergen, K. J., de Reus, M. A., Keunen, K., Kahn, R. S., Groenendaal, F., de Vries, L. S., & Benders, M. J. N. L. (2015). The Neonatal Connectome During Preterm Brain Development. *Cerebral Cortex*, 25(9), 3000–3013. <https://doi.org/10.1093/cercor/bhu095>
- Williams, L. Z. J., Fitzgibbon, S. P., Bozek, J., Winkler, A. M., Dimitrova, R., Poppe, T., Schuh, A., Makropoulos, A., Cupitt, J., O’Muircheartaigh, J., Duff, E. P., Cordero-Grande, L., Price, A. N., Hajnal, J. V., Rueckert, D., Smith, S. M., Edwards, A. D., & Robinson, E. C. (2023). Structural and functional asymmetry of the neonatal cerebral cortex. *Nature Human Behaviour*, 7(6), 942–955. <https://doi.org/10.1038/s41562-023-01542-8>
- Wu, X., Palaniyappan, L., Yu, G., Zhang, K., Seidlitz, J., Liu, Z., Kong, X., Schumann, G., Feng, J., Sahakian, B. J., Robbins, T. W., Bullmore, E., & Zhang, J. (2023). Morphometric dis-similarity between cortical and subcortical areas underlies cognitive function and psychiatric symptomatology: a preadolescence study from ABCD. *Molecular Psychiatry*, 28(3), 1146–1158. <https://doi.org/10.1038/s41380-022-01896-x>
- Yee, Y., Fernandes, D. J., French, L., Ellegood, J., Cahill, L. S., Vousden, D. A., Spencer Noakes, L., Scholz, J., van Eede, M. C., Nieman, B. J., Sled, J. G., & Lerch, J. P. (2018). Structural covariance of brain region volumes is associated with both structural connectivity and transcriptomic similarity. *NeuroImage*, 179, 357–372. <https://doi.org/10.1016/j.neuroimage.2018.05.028>
- Yu, Q., Ouyang, A., Chalak, L., Jeon, T., Chia, J., Mishra, V., Sivarajan, M., Jackson, G., Rollins, N., Liu, S., & Huang, H. (2016). Structural Development of Human Fetal and Preterm Brain Cortical

Plate Based on Population-Averaged Templates. *Cerebral Cortex*, 26(11), 4381–4391. <https://doi.org/10.1093/cercor/bhv201>

Yuan, S., Liu, M., Kim, S., Yang, J., Barkovich, A. J., Xu, D., & Kim, H. (2023). Cyto/myeloarchitecture of cortical gray matter and superficial white matter in early neurodevelopment: multimodal MRI study in preterm neonates. *Cerebral Cortex*, 33(2), 357–373. <https://doi.org/10.1093/cercor/bhac071>

Zhang, H., Schneider, T., Wheeler-Kingshott, C. A., & Alexander, D. C. (2012). NODDI: Practical in vivo neurite orientation dispersion and density imaging of the human brain. *NeuroImage*, 61(4), 1000–1016. <https://doi.org/10.1016/j.neuroimage.2012.03.072>

Zhang, Y., Ma, M., Xie, Z., Wu, H., Zhang, N., & Shen, J. (2021). Bridging the Gap Between Morphometric Similarity Mapping and Gene Transcription in Alzheimer’s Disease. *Frontiers in Neuroscience*, 15. <https://doi.org/10.3389/fnins.2021.731292>

PART III: Discussion and general conclusion

Chapter 6: Discussion

Early brain development is accompanied by a complex set of diverse processes and can be significantly perturbed in the context of prematurity. In our PhD work, we aimed to investigate the prematurity-linked alterations to the typical developmental trajectories using multimodal *in vivo* **MRI**. To achieve this, we employed a large database of imaging data available from the *dHCP* and evaluated preterm and full-term infants at multiple scales, including grey matter microstructure and white matter structural connectivity estimated from diffusion MRI, and functional connectivity derived from resting-state functional MRI data. Throughout the thesis, we provided examples of adapted multivariate approaches that consider complementary information from different MRI markers, suggesting the benefits of these approaches for the study of atypical brain development and identification of markers of adverse neurodevelopmental outcomes.

Firstly, we aimed to characterize prematurity effects on the microstructural properties of tracts within the primary sensorimotor network, employing complementary DTI and NODDI measures to capture microstructural changes (Neumane, Gondova et al., 2022; Gondová, et al., 2023b). Notably, we employed the Mahalanobis distance approach to quantify tract-specific vulnerability to prematurity in a multivariate manner while accounting for typical variability within the reference group of full-term infants. The results confirmed the vulnerability of sensorimotor tracts, with stronger effects in infants born at earlier gestational ages with distinct patterns across tracts. Suggested associations of some of the tract-specific alterations with neurodevelopmental outcomes highlighted the potential of the Mahalanobis distance approach for evaluating other atypical or pathological states in the future.

Besides, a large part of our PhD work aimed to relate early brain alterations described by MRI markers to later individual neurodevelopmental outcomes. Initially, we attempted predictive modelling using microstructural descriptors of the sensorimotor network but could not achieve successful individual outcome predictions (Gondová et al., 2023c). Including relevant clinical and environmental features did not enhance predictive models. Given the critical need for early identification of at-risk infants, we also explored using markers of cortical microstructure, previously shown to be highly predictive of adverse neurodevelopmental outcomes. However, we faced challenges in externally validating the conclusions of the reported predictive study (Ouyang et al., 2020), highlighting the necessity for standardized methodologies and thorough validation in machine learning studies, especially with small datasets (Gondová et al., 2023a). We further employed a machine learning approach

to investigate differences in global cortical microstructure between preterm and full-term infants at term-equivalent age. This analysis unveiled significant changes predominantly located in the lateral and medial inferior frontal lobes (Gondová et al., 2022).

Lastly, we explored the interplay between development of cortical microstructure and functional maturation. Traditionally, studies examining structure-function relationships during development focused on the white matter structural connectivity derived from tractography (van den Heuvel et al., 2015; Zhang et al., 2019) but we expected that exploring the relationships between functional connectivity and microstructural similarities across cortical and subcortical regions would add original insights into the complex interplay between different aspects of early brain development. Our work demonstrated how these complex microstructural-functional relationships evolve during development and are altered with prematurity.

Despite the original findings they provided, our studies share several limitations, including sensitivity to acquisition and post-processing settings which restricts comparisons with other studies, and reported age-related effects on the post-processing quality which might confound the results if not effectively corrected (for example, the quality of anatomically driven parcellation diminished with the distance from the population used for atlas derivation). Moreover, our studies primarily relied on group analysis, and revealed difficulties in translating group-wise associations into individualized predictions.

As specific limitations of each study are detailed within relevant chapters of the experimental section of this manuscript, we reserved the following section to address some of the overarching challenges we encountered when evaluating early brain development. This includes the discussion on interpreting employed MRI descriptors, as well as benefits and challenges of early prediction of neurodevelopmental outcomes.

6.1. Non-invasive examination of early brain development

6.1.1. Magnetic resonance imaging of typical and atypical populations

In vivo neuroimaging, particularly MRI, has proven a powerful tool for studying early brain development in preterm and early postnatal periods, providing non-invasive insights into brain structure, function, and connectivity with implications for later neurodevelopmental outcomes. However, newborn imaging poses distinct challenges across MRI modalities, rooted in inherent differences between the immature brains compared to adults, including brain size, different water and lipid content, tissue characteristics, immature neurovascular coupling, and

differences in hemodynamic response function (Norman & O’kusky, 1986; Arichi et al., 2012; Dubois et al., 2021; Korom et al., 2022). These factors impact both diffusion properties of the brain assessed in dMRI and hemodynamic response temporal profiles in rs-fMRI. Many infant-specific adaptations in MRI acquisition protocols and processing pipelines were developed to address these challenges and employed within the dHCP database, including dedicated coils optimized for head size to enhance signal-to-noise ratio (SNR) in images, improved spatial resolutions to mitigate partial volume effects, implementation of specialized motion-tolerant acquisition and reconstruction approaches, and development of post-processing tools adapted to signal and contrast properties of immature brains (Cordero-Grande et al., 2018c; Bastiani et al., 2019; Dubois et al., 2021; Korom et al., 2022).

Our PhD investigations contributed to the extensive body of evidence highlighting the significant impact of prematurity on typical brain development, resulting in distinct alterations in brain microstructural properties, as well as structural and functional connectivity in preterm infants (Volpe, 2019; Wallois et al., 2020). Thus, while studying atypical brain trajectories in preterm infants provides a vital contrast to postnatal development in typical populations and offers insights into critical features related to neurodevelopmental consequences, these alterations caution against directly using preterm infants as a model of typical development during the preterm period. Recent advances in foetal imaging offer new avenues for studying ‘healthy’ populations, confirming the feasibility of effective characterisation of foetal structural and functional connectivity using *in utero* dMRI (Jakab et al., 2015, 2017; Song et al., 2017; Jaimes et al., 2020; Wilson et al., 2023) and rs-fMRI (Schöpf et al., 2012; Turk et al., 2019; Karolis et al., 2023).

However, foetal imaging, in addition to the newborn imaging challenges, poses additional difficulties. These include pronounced motion artifacts caused by maternal and foetal movements, and confounding effects from surrounding maternal organs and amniotic fluid (Rousseau et al., 2016; Jakab, 2019). While post-processing techniques are advancing to improve data quality, correct motion, and reconstruct foetal rs-fMRI and dMRI data at increasingly higher resolutions (Marami et al., 2017; Kuklisova-Murgasova et al., 2018), prenatal MRI applications remain challenging and predominantly conducted in specialized imaging centres. Open data initiatives like the upcoming release of foetal dataset within the dHCP hold promise for enabling broader research contributions to the study of *in utero* development (for example: Karolis et al., 2023; Uus et al., 2023; Wilson et al., 2023).

6.1.2. Prematurity: modulator of brain development or clinical phenotype?

Given the lasting neurodevelopmental consequences linked to prematurity-related brain alterations, studying preterm populations is important and holds potential medical and societal implications (Saigal & Doyle, 2008; Fernández de Gamarra-Oca et al., 2021). Prematurity, defined as birth before 37wGA, is typically categorized into four groups based on the age at birth, typically: extremely preterm (<28w GA), very preterm (28-32w GA), moderate (32–34 wGA), and late preterm (34–36 wGA). This categorisation aligns with the increasing impact of prematurity with lower gestational age, aids neonatal prognosis and medical decision-making (Moutquin, 2003; Harrison & Goldenberg, 2016), and allow robust group-based evaluations of the brain alterations linked to prematurity. For example, in our study on prematurity's impact on sensorimotor network, we categorized preterm infants into two groups: extremely to very preterm (GA at birth < 32w) and moderate to late preterm (GA at birth ≥ 32w). This categorization helped us to confirm microstructural differences in sensorimotor tracts between PT and FT infants, especially pronounced in the extremely to very preterm group.

However, conventional categorisations using somewhat arbitrary gestational age cutoffs may oversimplify the diverse spectrum of brain as well as developmental alterations within preterm populations. Analysing prematurity effects as a continuous trend may reveal more subtle associations and/or non-linear relationships relative to gestational age at birth. For example, extending our Mahalanobis approach to continuous assessment might allow creation of tract-specific 'trajectories' of prematurity effect providing a more elaborate view of the atypical brain development. Additionally, our group-based assessments demonstrated significant correlations between the Mahalanobis distances of specific sensorimotor tracts with neurodevelopmental outcomes, but focusing on the continuous gestational age spectrum may provide more nuanced prognostic markers better aligned with the individual's positioning on the continuous spectrum. However, practical limitations, such as a small number of infants for reliable continuous trajectory estimation and a high inter-individual variability, need addressing for meaningful assessments. Advanced statistical methods involving data normalization and identification of relevant covariates will be vital to isolate the effects of interest and control for confounding variables.

Additionally, such 'normative' models of atypical development would necessarily assume homogeneity within the preterm population, which is also a problematic question. Although the conventional prematurity definitions, whether continuous or categorical, still rely

solely on gestational age, overlooking the multifactorial aetiology of preterm labour and birth highly dependent on many risk factors (Moutquin, 2003; Offiah et al., 2012) seems incomplete. Neglecting the variability in its origins and treating prematurity as an entity defined by time rather than a distinct clinical phenotype might contribute to challenges with investigations into prematurity impact on brain development and subsequent neurodevelopmental consequences (Muglia & Katz, 2010). Thus, shifting our attitude to prematurity might be beneficial. Possible inspiration could come from the psychiatric field's evolving approach which explores disorder heterogeneity using unsupervised machine learning to identify new subgroups within the population based on cognitive, genetic, and/or brain profiles (Arnedo et al., 2015; Wu et al., 2017). In the neurodevelopmental field, similar efforts might lead to novel classifications for premature infants that could improve our understanding of subject heterogeneity required for accurate predictions of neurodevelopmental outcomes.

6.1.3. What can we gain from 'almost healthy' cohorts?

In our PhD research, we employed the dHCP database which consists predominantly of healthy full-term and preterm infants without overt brain injuries.

On one hand, the dHCP can be considered fairly representative of the general population given that such low-risk PT infants make up a majority of preterm births (Blencowe et al., 2012). The homogeneity in the dHCP PT and FT populations also likely enhanced our statistical comparisons and allowed more accurate accounts of PT and FT differences from a smaller sample by reducing the sources of error and variability in the analysis (Jager et al., 2017).

However, this inter-individual 'homogeneity' might limit generalizability beyond similar cohorts and, together with the bias towards a healthy cohort (as we proposed in our predictive studies: *Chapter 4.1.* and *4.2.*), might limit our ability to build effective predictive models of neurodevelopmental outcomes. In *Chapter 4*, we explored several reasons for our unsuccessful efforts to relate individual MRI markers to later neurodevelopmental outcomes, suspecting that the input and output homogeneity, particularly a notable class imbalance and bias towards high scores indicating normal outcomes, played an important role in poor predictability. Consequently, although large databases like dHCP are immensely valuable for enhancing our understanding of the early period, their usefulness for the development of essential predictive tools might be constrained by the limited variability within their subject population.

Importantly, we do not intend this observation to discourage the creation of large databases of healthy or nearly healthy infants. Large-scale databases that encompass multimodal MRI data with a comprehensive demographic profiling and behavioural tests like dHCP, Baby Connectome Project (Howell et al., 2019), or the 'Utrecht Baby MRI Youth Project' are essential for a thorough and systematic assessment of early brain development. Instead, we aim to emphasize the limitation of a 'one-size-fits-all strategy', a criticism often echoed in the context of patient care, which is equally applicable in selecting tailored datasets for specific research aims and questions. We believe that diversifying data sources to construct sizable datasets with a broader range of neurodevelopmental outcomes will be useful to enhance outcome predictions in the future.

For example, initiatives like the project ENSEMBLE, which aims to coordinate diverse centres and partner institutions across Europe for early cerebral palsy detection (Benders et al., 2022), represent a significant step towards enhanced data reuse and commitment to open science practices more generally and could inspire similar projects targeting improved prediction of diverse neurodevelopmental outcomes. For successful applications, mitigating complexities associated with statistical site effects resulting from technical variations and diverse sample characteristics and their impact on distribution of MRI markers in neuroimaging data will be necessary (for review: Bayer et al., 2022). Looking forward, federated learning approaches, as exemplified in ENIGMA (Thompson et al., 2020), hold promise as future directions by enabling distributed neural network training without exposing raw data, addressing some challenges in combining data from multiple sites for collective analysis, including security and privacy concerns (Stripelis et al., 2022).

6.1.4. Would a single snapshot be ever enough?

Our PhD studies effectively demonstrated differences between preterm and term-born subjects at TEA through cross-sectional evaluation. However, early brain development is a dynamic process characterized by spatially heterogeneous and temporally asynchronous structural changes in grey and white matter, as well as functionally (Kulikova et al., 2015; Gilmore et al., 2018; Lebenberg et al., 2019). Cross-sectional studies offer a snapshot of this complex system at a specific data collection timepoint – this timing constraints the 'developmental information' that can be accessed and overlooks dynamic changes to typical trajectories caused by prematurity. Additionally, practical constraints introduce variance in data collection, underscoring the need for effective control and corrections for confounding effects like age at scan (among others). Studying developmental trajectories in preterm infants

longitudinally could be beneficial to overcome these limitations (Monson et al., 2018). For instance, we can imagine extending our Mahalanobis approach to encompass longitudinal evaluations of the prematurity effects on different sensorimotor tracts that could enable assessment of individual developmental trajectories in the context of prematurity. These trajectories, derived from multiple scans, may capture deviations from other preterm infants or alternatively individual's developmental 'catch-ups' with the FT subjects, potentially providing an enhanced descriptors for individual neurodevelopmental prognosis.

However, implementing longitudinal approaches is challenging in practice due to the difficulty of collecting large datasets of infant MRI, which is already demanding for single scans. Challenges include the impracticality of sampling multiple time points for many subjects and ensuring precise timings across scans. Maintaining identical experimental settings across scans in the same individual might also be difficult due to rapid changes in brain characteristics with development, potentially introducing methodological and processing artifacts. Despite these difficulties, exploring developmental trajectories in individual infants from multiple scans could offer valuable insights into the evolving brain, provided a careful consideration of associated challenges.

6.2. What can we 'see' with MRI?: link to underlying neurobiology

The developing brain can be effectively observed and measured using a range of structural and functional neuroimaging techniques. In the preceding sections, we described some methodological constraints in newborn neuroimaging stemming from differences in immature and adult brain structures, as well as the practical challenges associated with scanning infants (e.g., limited acquisition windows during sleep and the requirement for specialized equipment). In this section, we explore the connections between MRI markers and their underlying neurobiological mechanisms, highlighting the constraints that influence which aspects of early development can be investigated with the MRI methods employed in our PhD work.

6.2.1. Assessing brain's microstructure: dMRI as a tool for 'virtual histology and dissection'

Diffusion MRI allows precise, non-invasive exploration of brain microstructure by detecting changes in cellular architecture, providing quantitative descriptors of underlying developmental processes. However, it's important to recognise that dMRI generates tissue

descriptions at the voxel size (in order of cubic millimetres), averaging information about mesostructural axonal fibres and microstructural geometrical neuronal sizes, shapes and densities, resulting in a significant loss of specificity. While this limited detail is acceptable for broader analysis, for example estimating overall development of white matter pathways, or discriminating different cortical regions based on microstructural composition, it complicates interpretation of the observations in terms of underlying neurobiology.

As described in *Chapter 2*, microstructural assessments also heavily rely on signal or biophysical models that link tissue features to MR signal with all of them presenting their specific methodological challenges, such as DTI's known difficulties with areas with complex geometries (Jones & Cercignani, 2010), or reliance of more complex models like NODDI on assumptions about water diffusion within different voxel compartments often derived from observations in adults which might be suboptimal for fitting the models in immature infants brains (Guerrero et al., 2019). These limitations affect the reliability of metric estimates, likely decreasing with the distance to the population to which the models were originally optimised. Given that developmental studies investigate changes in diffusion metrics in a similar direction to these potential processing artifacts, interpreting changing metrics derived from these complex models requires caution. In the future, tailoring the diffusion models more specifically to newborns will be useful to enhance the reliability and accuracy of our observations.

Moreover, while dMRI data analysis primarily focuses on neuronal interpretations, non-neuronal cell types are also reflected within the voxel measurements (Alexander et al., 2019), which cannot be easily distinguished with commonly employed diffusion models. However, as numerous developmental processes involve modulations of specific cell types and their microstructures (Dyrby et al., 2018). Analysing their profiles with alternative imaging approaches, such as diffusion-weighted magnetic resonance spectroscopy (DW-MRS) that allows the identification of cell type-specific metabolites (Palombo et al., 2018) or multidimensional diffusion encoding (MDE) that allows the sub-voxel discrimination of cell types through descriptions of microscopic anisotropy (μ FA) (Dyrby et al., 2018), could be used to complement our current, quickly evolving understanding of the early development and its alterations with prematurity.

The white matter pathways can be inferred from virtual dissections that link the local fibre orientations derived from dMRI through tractography, with many successful examples in infants brain despite their immaturity (Dubois et al., 2006; Kulikova et al., 2015; Y. Wu et al., 2023; Yepes-Calderon et al., 2017). However, tractography methods, whether based on simple DTI or more sophisticated tools relying on estimation of fibre orientation distribution function

(fODF), still suffer from significant biases. Insights gained from synthetic diffusion data and animal models which compare the quality of resulting tractograms to ground-truth connectivity consistently highlight the presence of significant false positives, most frequent in bundles connecting adjacent regions and particularly prevalent in probabilistic methods, and false negatives, including premature termination of tracts which tends to increase with spatial distance between connected regions and frequent in non-dominant bundles with low connection strengths, across all methods (Maier-Hein et al., 2017; Sinke et al., 2018; Jeurissen et al., 2019; Sarwar et al., 2019; Schilling et al., 2019; Girard et al., 2023). Although limitations observed in diffusion phantoms and animal models do not replicate the complexity of a real brain, they suggest similar limitations in real adult data.

These challenges are further exacerbated in newborn diffusion data due to lower effective resolutions and lower diffusion anisotropies in unmyelinated white matter. Moreover, the spatiotemporal heterogeneity of white matter maturation likely impacts diffusion signal properties in different manner depending on age and evaluated spatial locations within the brain. The implications of these effects on connectivity estimate reliability, especially in whole-brain connectivity assessments, remain a critical area for further investigation.

In addition to the methodological difficulties, interpreting resulting tractograms poses a significant challenge from a biological perspective. The estimated streamlines are only indirectly linked to the underlying axonal pathways, relying on models of water diffusion, with different fibre configurations, including bending, fanning, crossing, and kissing fibres often yielding identical fibre estimates (Jeurissen et al., 2019). Moreover, as mentioned previously, single voxel contains a substantial number of divers microstructural components in addition to the axonal fibres, including glial cells and blood vessels which exhibit particularly distinct orientations during the early development that might influence the accuracy of axonal orientation estimates (Xu et al., 2014). Consequently, even the most advanced tracking algorithms and diffusion models can only crudely approximate the actual underlying structural connectome within the developing brain.

Multiparametric evaluations of microstructure

Traditionally, evaluations of diffusion properties of different grey and white matter regions with development have employed univariate approaches, where each variable of interest is examined independently. In our PhD work, we aimed to integrate complementary multiparametric information in a joint examination of different diffusion metrics in one model.

We employed different multivariate analyses throughout our work. For example, using the Mahalanobis approach, we integrated different diffusion measures of the preterm sensorimotor network in respect to a reference population of full-term infants, confirming the differential effects of prematurity on different tracts (*Chapter 3*). In another study, we employed a multivariate approach to estimate cross-correlations across microstructural characteristics of cortical and subcortical regions to evaluate regional similarities, followed by hierarchical clustering to identify regions with similar profiles and describe the evolving regional relationships with development (*Chapter 5*).

Additionally, supervised machine learning was employed to utilize multiple parameters together to differentiate preterm and full-term subjects at term-equivalent age (TEA), offering an alternative 'prior-free' approach to evaluating alterations of cortical microstructure linked to prematurity (*Chapter 4*). However, within machine learning, the potential multicollinearity between metrics and non-independence across regions can negatively affect the performance of predictive models (Schuit et al., 2013). In this context, the critical goal was to identify the subset of features that are most useful for prediction, i.e., finding the combination of regions and descriptors that maximizes complementarity while minimizing potential information overlap.

Like any approach, the multivariate analyses are not without limitations. In the previous sections, we highlighted that NODDI model might not be fully optimized for use in infant populations. DTI limitations in voxels with more complex architectures are also well-documented. How these different influences interact when combined within multivariate analysis remains unclear and would require further investigation.

Overall, our PhD studies emphasized the potential of utilizing multiple microstructural markers to better capture the intricate and interconnected maturation mechanisms within both grey and white matter tissues. Additionally, the utility of additional MRI parameters, such as T1w and T2w relaxation times which are sensitive to rapid changes in water content and myelination, and less dependent on the prior assumptions compared to diffusion-based models, might be useful to include in the future multivariate assessments. Additional diffusion metrics, for example kurtosis imaging (Jensen et al., 2005) for the microstructural evaluation of cortical regions or fixel-based methods for complex white matter regions and tracts (Dhollander et al., 2021), should also be explored in the future.

Whole-brain vs network specific evaluations

In our PhD work, we explored structural connectivity in the newborns using both whole-brain and network-specific approaches, each offering unique insights. By focusing on the sensorimotor network, informed by prior knowledge of its crucial role in early brain development and infant behavioural acquisitions, we could precisely characterize the impact of prematurity on specific tracts within the networks and establish links between some of the tract-specific prematurity-related alterations and the later neurodevelopmental outcomes (*Chapter 3*).

However, such targeted network-specific approaches may inadvertently overlook broader systemic interactions. In contrast, whole-brain approaches, aiming to minimize biases from prior knowledge by adopting a more data-driven attitude, offer a comprehensive view of structural connectivity patterns across the brain during development and allow to assess more global impact of prematurity on emerging networks. Yet, these approaches often resort to summarizing the whole-brain estimates using global graph network measures to reduce interpretative noise from numerous connections, risking oversimplifications of the intricate connectivity details.

Additionally, ensuring the quality and reliability of estimated whole-brain connectomes remains challenging due to processing artifacts, resulting in numerous false positive and false negative connections. While these challenges are also present in network-specific evaluations, correcting them in whole-brain approaches can be particularly difficult due to the sheer number of connections and the lack of gold standards (*Annexe 2*).

Nevertheless, network-specific and whole-brain approaches offer complementary avenues for investigating structural connectivity (Smyser et al., 2019; Vértes & Bullmore, 2015). For example, whole-brain approaches were previously used to describe evolution of brain-wide network properties during brain development in PT and FT infants (Tymofiyeva et al., 2012; Ball et al., 2014; Brown et al., 2014; Lee et al., 2019; Sa de Almeida et al., 2021; Ciarrusta et al., 2022; Zheng, Wang, et al., 2023). The insights derived from these observations can then inspire more focused evaluations. For example, the proposed network-specific investigations performed to study spatiotemporal maturational changes in thalamus of PT/FT neonates as well as foetuses (Wilson et al., 2023; Zheng, Zhao, et al., 2023) or linguistic, visual, and auditory pathways in infants (Adibpour et al., 2015; Dubois, Poupon, et al., 2016). As always, the selection of the best approach closely depends on the specific research questions,

and both methodologies will significantly contribute to our understanding of early brain development in healthy infants as well as preterm populations.

It is also good to note that although we focused in this section on contrasting whole-brain and network-specific structural connectivity because we employed both approaches during the PhD project, similar concerns also apply to the microstructural and functional evaluations. In *Chapter 5*, we focused on a whole-brain investigation of relationships between grey matter microstructural similarities with functional connectivity. In the future, focusing more narrowly on specific networks, for example the sensorimotor regions, might be interesting to complement our analysis of prematurity-linked alterations of sensorimotor tracts presented in the *Chapter 3*.

6.2.2. Resting state functional connectivity in infants

Resting-state functional MRI is a widely used modality to study functional connectivity. In contrast to task-based methods, rs-fMRI is especially useful in newborn (and increasingly in *in utero* foetal) populations as it avoids the need for performing in-scanner tasks (Fransson et al., 2007; Arichi et al., 2010; Doria et al., 2010; Smyser et al., 2010; Ferrazzi et al., 2014; Thomason et al., 2015; Kanel et al., 2021). However, analysing rs-fMRI in newborns involves considerations of distinct characteristics of their data acquisitions. For example, during the preterm period, rs-fMRI studies are typically conducted during natural sleep to minimize motion (Copeland et al., 2021). Considering the differences in neonatal sleep patterns and the impact of sleep states on brain activity is essential when interpreting rs-fMRI connectivity estimates (Dehaene-Lambertz et al., 2002; Melbourne et al., 2004; Tagliazucchi et al., 2012; Mitra et al., 2017).

During the analysis, the captured coordinated patterns of BOLD signal are regrouped to networks believed to be credible from anatomical and functional perspectives due to their similarity to adult-derived resting state networks associated with specific cognitive tasks or structural connectivity (Fransson et al., 2007; Greicius et al., 2009). However, it's important to acknowledge that rs-fMRI provides only an indirect measure of functional connectivity tied to assumption of tight coupling between neuronal activity and the activity-induced BOLD signal. This relationship can differ in immature developing brains compared to adults (Baxter et al., 2019) due to changes in the cerebral blood flow and local neurovascular coupling underlying the BOLD response (Baxter et al., 2019), requiring a careful control of the 'resting' condition during rs-fMRI measurements in newborns (Arichi, 2012). Additionally, due to its dependence on time delay and duration of the hemodynamic response, rs-fMRI can achieve only relatively

low temporal resolutions. Integrating insights provided by electrophysiological techniques like magnetoencephalography (MEG) or electroencephalography (EEG) that offer superior temporal resolution, although at the cost of spatial resolution, by directly detecting variations in electrical and magnetic fields (Glover, 2011) might provide both an enhanced understanding of the neurovascular coupling in developing brain (Scarapicchia et al., 2017) as well as complementary descriptors of the functional connectivity (Zhang et al., 2019).

Additionally, the interpretation of estimated functional connectivity heavily depends on the model of regional signal synchronicity used to define the relationships. For instance, in our PhD work (*Chapter 5*), we utilized Pearson's correlation across predefined set of anatomical parcellations to compare the evolution of derived functional connectivity between birth and term-equivalent age in the preterm infants with maturation. Recently, a more dynamic approach that directly considers the age-related changes in functional connectivity within network estimation has also been proposed to characterize the rapid emergence of organized patterns of spontaneous brain activity in fetuses (Karolis et al., 2023). Extending such evaluations to the preterm populations might lead to additional insights of functional maturation between preterm and typically developing subjects.

Nevertheless, linking functional connectivity to underlying neurobiology and disentangling its role in immature brains are challenging. In early development, functional systems rapidly evolve with age to accommodate emerging behavioural and cognitive functions (Gao et al., 2015) and undergo functional specialization (Wylie et al., 2014). These changes are likely influenced by the progressive maturation of the underlying structural connectivity, although the precise nature and role of structure-function interactions remains subjects of debate (Luhmann et al., 2016). In *Chapter 1* we suggested that spontaneous neural activity during early development is also tightly intertwined with structural changes, impacting neurogenesis, cell apoptosis, neuronal migration, axonal development, and myelination (Luhmann et al., 2016). The question of whether distinct activity patterns govern different developmental stages and processes remains open, but it is conceivable that resting-state activity during the early period serves a different role compared to that in adults.

6.2.3. Relating functional and structural development

Structural and functional analyses provide unique and complementary descriptions of early brain development. In neonates and infants, both structural and functional connectivity, as well as grey matter microstructure has been linked to behavioural function and their alterations in preterm-born individuals to abnormal neurodevelopmental outcomes (Vo Van et

al., 2022). However, establishing a clear link between these modalities during early development is not straightforward.

In healthy adults, structurally connected regions tend to exhibit similar patterns of functional connectivity (Greicius et al., 2009; Rykhlevskaia et al., 2008; van den Heuvel et al., 2009). Studies in newborns that have compared the developing functional and structural connectivity patterns using rs-fMRI and diffusion MRI also suggest at least a partial alignment between structural and physiological functional connectome (Smyser et al., 2019; van den Heuvel et al., 2015). This alignment seems to depend on the systems, with greater overlap in sensory regions and pathways than in higher-order association ones (Larivière et al., 2020; van den Heuvel et al., 2015), potentially reflecting the differences in maturation between different networks.

Nevertheless, it is important to note that comparing structural and functional connectivity is challenging due to significant biases related to spatiotemporally heterogeneous maturation across brain regions, which affects both reliability of tractography reconstructions of structural connections and dynamically developing properties affecting functional connectivity. The direct comparison is further complicated by the observation that functional connectivity between regions can be detected even in absence of direct structural links (Smyser et al., 2010). This is not unexpected given the conceptual differences in estimating connectivity for the two modalities: tracking direct regional connections in structural connectomes, as opposed to evaluating more diffuse BOLD signal synchronicity in functional connectivity.

Inspired by this conceptual difference between direct and indirect connectivities, we were interested in exploring an additional type of structural ‘connectivity’ based on the microstructural features of the developing grey matter. This idea was grounded in the assumption that similar regions on a cytoarchitectonic and maturation level may reflect meaningful functional areas. Our results have suggested a certain level of overlap between functional connectivity profiles and the microstructural similarity of cortical and subcortical regions. Nevertheless, our approach showed methodological limitations, was constrained to group-wise assessments, and included only direct temporal correlations within functional comparisons. It is improbable that such a simplistic view could fully encapsulate the intricate nature of structure-function relationships that take place at multiple scales during early development. Moreover, both structural and functional connectivity are only partially accessible through the diffusion and rs-fMRI modalities. In the future, integrating additional microstructural descriptors of grey matter, structural connectivity, and possibly more direct neuronal recordings, such as EEG, within advance modelling approaches will likely be

essential for more effective linking of structure and function in the developing brain (Babaeeghazvini et al., 2021).

6.3. Linking the early brain features to later neurodevelopment

6.3.1. Machine learning for personalized predictions

In recent years, progress in medical care has significantly improved outcomes for premature newborns (Arnaud et al., 2021). However, the persistent high incidence of preterm births, alongside improved survival rates, has led to a rise in survivors facing adverse neurodevelopmental outcomes, posing substantial economic and societal challenges (Banihani et al., 2021; Parikh, 2016). Studies emphasize that even mild prematurity can adversely affect neurodevelopment (Lundequist et al., 2015; Pierrat et al., 2021b).

Early identification of infants at risk for adverse neurodevelopmental outcomes before symptoms manifest is crucial for targeted follow-up programs and neuroprotective interventions, potentially leading to improved prognosis (Allotey et al., 2018). With the increasingly large amounts of available neuroimaging data in the preterm populations, a substantial rise in data-driven applications, particularly in machine learning, were reported that aim to use the early MRI markers for individual prediction of outcome. Machine learning is a versatile toolbox that can be optimized to various neuroimaging problems, including prediction of neurodevelopmental outcomes, but also used to detect potentially novel imaging signatures of brain structure and function (as in the case of preterm vs full-term prediction for example, *Chapter 4.3.*). Hence, the integration of MRI-derived markers with machine learning holds great potential for improving our understanding of brain development and consequently significantly enhancing care for this vulnerable population.

However, it is important to acknowledge the fragility and potential unreliability of machine learning models outside their training/testing conditions (exemplified in frequent differences between reported predictive performance and external validation or real-world setting) (Davatzikos, 2019). These generalization challenges can often be attributed to methodological pitfalls, for example data leakage (van Boven et al., 2022). To address this, rigorous validation schemes including predictions on unseen data and nested cross-validation approaches, combined with appropriate evaluation metrics, need to be implemented to avoid inflated performance reports which might be contributing to well-documented reproducibility issues (Kapoor & Narayanan, 2022). Representativeness of training data and class imbalance,

i.e. small number of high-risk compared to low-risk infants, can also significantly affect the learning ability of predictive models warranting careful consideration (Haixiang et al., 2017).

In the context of imaging premature infants, and early MRI more broadly, acquisition challenges and costs often limit size of available datasets. Our efforts to predict neurodevelopmental outcomes from cortical microstructure included 295 PT and FT infants (*Chapter 4.2.*), which was the largest sample size among the previously reported studies whose majority involved fewer than 100 subject (*Chapter 1.*). Data augmentation, synthetic data generation, transfer learning approaches, or leveraging multiple datasets through data sharing initiatives (Shirwaikar et al., 2018; Spitzer et al., 2015) might be useful to mitigate the limitations due to smaller sample sizes (van Boven et al., 2022). Tailoring algorithms to the specific research context, informed by domain expertise, can also outcompete generic complex models trained on large datasets (Savadjiev et al., 2020).

Additionally, reliability of machine learning models heavily depends on the quality of input data and outcomes. Considering the limitations and potential errors associated with processing newborn data described in the previous sections, a thorough assessment of the data quality requiring expertise in processing of early MRI will be crucial to dissociate predictors of the neurodevelopmental outcomes from processing artifacts or noise.

Another topic often raised within machine learning is its interpretability (Gerlings et al., 2021), especially when aiming to uncover novel brain-outcome relationships. Data-driven approaches use inductive reasoning to reveal correlations in a bottom-up manner and their interpretation involves examining contributions of different features during learning. However, currently reported neurodevelopmental outcome prediction studies mostly utilize discriminative machine learning models. Inherently, these models are only concerned with determining the patterns in data that allow the best categorization (or regression) as evaluated by similarity of their predictions to known labels. However, it's been previously reported that even highly positive predictive results can be driven by noise or spurious correlations (Savadjiev et al., 2020), or that models can fit randomly assigned labels (Zhang et al., 2023). Even in the case of 'real' predictions, biases originating from data selection, assumptions on model inputs, and methodological limitations influence the model's data representation, revealing certain patterns while excluding others, emphasizing the need to differentiate between predictive usefulness and comprehensive scientific understanding (Mazzocchi, 2015). As suggested in other fields, combining discriminative models with generative methods, which investigate the likely data signal sources, might allow to take advantage of prior expert

knowledge, enhancing model performance and generating more reliable hypotheses from the data (Savadjiev et al., 2020; Yuille & Liu, 2018).

6.3.2. Difficulties with predicting later outcomes from early MRI

The application of early MRI as a standalone imaging tool holds promise for identifying brain alterations that could enable individualized prediction of neurodevelopmental outcomes when coupled with advanced machine learning approaches. Recent efforts have also explored the integration of multimodal neuroimaging inputs and complementary MRI modalities, yielding encouraging predictive results. However, prognosticating neurodevelopmental outcomes solely from early brain MRI is challenging due to the temporal gap between imaging data acquisition and behavioural assessments. This underscores the fact that interindividual variability in neurodevelopmental outcomes likely stems from the interplay of diverse factors, encompassing neurobiology as well as environmental influences (Miceli et al., 2000; Anderson & Doyle, 2008; Linsell et al., 2015). Additionally, although in this research we mostly emphasized the impact of preterm birth on neurodevelopment, prematurity is a risk factor for various other adverse events, including respiratory, cardiac, renal, and endocrine disorders (Pravia & Benni, 2021). Understanding the intricate interplay of these concurrent conditions and incorporating the associated clinical information in predictive models might provide additional benefits for outcome predictions.

Looking forward, the potential of early MRI in combination with machine learning holds a great promise for advancing efficient care by facilitating accurate early diagnoses. However, the significance of MRI markers will depend on the routine clinical use of MRI in preterm infants (van Boven et al., 2022). The challenge lies in determining whether added value of early MRI can effectively outweigh the significant barriers to use, including costs, technical challenges, and required expertise (Banihani et al., 2021). Fostering increased collaboration between clinicians and ML researchers to deepen our understanding of early brain markers and their relationship to predicted outcomes in preterm infants, and development of novel strategies of care for preterm infants labelled 'at risk', will be essential in the future to ensure that the potential improved prognostic capabilities of MRI will unequivocally translate into enhanced outcomes of this vulnerable population. To enhance the individual prognosis, considering descriptors of an individual's developmental trajectories derived from longitudinal assessments instead of a single time point as well as integrating known predictors of neurodevelopmental outcomes, including clinical and environmental factors such as socio-familial context (Miceli

et al., 2000; Anderson & Doyle, 2008; Linsell et al., 2015), might be beneficial to better account for inter-individual variability in brain development and neurodevelopmental acquisitions.

Chapter 7: General conclusion

The preterm period and early postnatal months are critical for human brain development. The dynamic nature and complexity of the ongoing cellular and molecular events make the developing brain highly vulnerable to adverse events such as prematurity. These events can lead to significant alterations in brain microstructural properties, as well as in structural and functional connectivity in preterm-born infants. Investigating these alterations not only adds to our comprehension of typical and atypical developmental trajectories but also provides valuable insights into their potential neurodevelopmental consequences.

Within our PhD work, we investigated these prematurity-linked alterations using a rich multimodal *in vivo* MRI dataset from the developing Human Connectome Project (dHCP). Our multivariate analyses contributed to a finer quantitative description of the tract-specific vulnerabilities to prematurity within the sensorimotor network with potential correlates to altered neurodevelopmental outcomes. Moreover, we explored the potential of MRI markers, including descriptors of cortical and white matter microstructure, for individual outcome prediction and differentiation between preterm and full-term infants using machine learning approaches. Lastly, we explored relationships between cortical microstructure development and functional maturation to describe the complex evolution of microstructural-functional relationships during early development and their alterations with prematurity.

Building on these insights, several directions might be investigated in the future to further refine our understanding of early brain development in the context of prematurity, such as shifting from group-wise analyses towards longitudinal approaches by leveraging individuals with multiple scans within the dHCP cohort. Comparing prematurity-related brain alterations with effects of other perinatal insults, such as neonatal stroke or hypoxic-ischemic encephalopathy, might also be beneficial to shed light on potential common pathways of brain injury and vulnerability, or conversely, describe distinctive effects of various perinatal insults. Additionally, estimating specific vulnerabilities to prematurity effects with multiparametric approaches such as Mahalanobis distance might offer additional direction for identifying infants with distinct vulnerability patterns, acting as potential markers for adverse neurodevelopmental outcomes or brain-related pathologies.

Moreover, expanding the predictive modelling strategy by integrating multimodal MRI markers with clinical and environmental features and diversifying the training cohort to encompass subjects with varying neurodevelopmental outcomes might enhance our ability to predict individual motor, cognitive, and language neurodevelopmental outcomes. Similar

strategies could be employed for early prediction of other prematurity-related adverse events such as social-emotional difficulties.

Overall, our research work and proposed future directions aim to advance our understanding of brain development and prediction of neurodevelopmental outcomes through early neuroimaging. The overarching goal is to enhance care and quality of life for the vulnerable preterm population through early and reliable prognosis that might facilitate effective individualized interventions by taking advantage of the intense brain plasticity observed in the first months after birth.

Global references

- Adamson, C. L., Alexander, B., Ball, G., Beare, R., Cheong, J. L. Y., Spittle, A. J., Doyle, L. W., Anderson, P. J., Seal, M. L., & Thompson, D. K. (2020). Parcellation of the neonatal cortex using Surface-based Melbourne Children's Regional Infant Brain atlases (M-CRIB-S). *Scientific Reports*, 10(1), 1–11. <https://doi.org/10.1038/s41598-020-61326-2>
- Adibpour, P., Dehaene-Lambertz, G., & Dubois J. (2015). Relating the structural and functional maturation of visual and auditory white matter pathways with diffusion imaging and event-related potentials in infants. *Proceedings of ISMRM*, 645.
- Ajayi-Obe, M., Saeed, N., Cowan, F., Rutherford, M., & Edwards, A. (2000). Reduced development of cerebral cortex in extremely preterm infants. *The Lancet*, 356(9236), 1162–1163. [https://doi.org/10.1016/S0140-6736\(00\)02761-6](https://doi.org/10.1016/S0140-6736(00)02761-6)
- Alexander, D. C., Dyrby, T. B., Nilsson, M., & Zhang, H. (2019). Imaging brain microstructure with diffusion MRI: practicality and applications. *NMR in Biomedicine*, 32(4). <https://doi.org/10.1002/nbm.3841>
- Aljabar, P., Heckemann, R. A., Hammers, A., Hajnal, J. V., & Rueckert, D. (2009). Multi-atlas based segmentation of brain images: Atlas selection and its effect on accuracy. *NeuroImage*, 46(3), 726–738. <https://doi.org/10.1016/j.neuroimage.2009.02.018>
- Allen, N. J. (2013). Role of glia in developmental synapse formation. *Current Opinion in Neurobiology*, 23(6), 1027–1033. <https://doi.org/10.1016/j.conb.2013.06.004>
- Allison, C., Baron-Cohen, S., Wheelwright, S., Charman, T., Richler, J., Pasco, G., & Brayne, C. (2008). The Q-CHAT (Quantitative CHECKlist for Autism in Toddlers): A Normally Distributed Quantitative Measure of Autistic Traits at 18–24 Months of Age: Preliminary Report. *Journal of Autism and Developmental Disorders*, 38(8), 1414–1425. <https://doi.org/10.1007/s10803-007-0509-7>
- Allotey, J., Zamora, J., Cheong-See, F., Kalidindi, M., Arroyo-Manzano, D., Asztalos, E., van der Post, J., Mol, B., Moore, D., Birtles, D., Khan, K., & Thangaratinam, S. (2018). Cognitive, motor, behavioural and academic performances of children born preterm: a meta-analysis and systematic review involving 64 061 children. *BJOG: An International Journal of Obstetrics & Gynaecology*, 125(1), 16–25. <https://doi.org/10.1111/1471-0528.14832>
- Anand, K. J. S., & Hickey, P. R. (1987). Pain and Its Effects in the Human Neonate and Fetus. *New England Journal of Medicine*, 317(21), 1321–1329. <https://doi.org/10.1056/NEJM198711193172105>
- Anderson, P. J., & Doyle, L. W. (2008). Cognitive and Educational Deficits in Children Born Extremely Preterm. *Seminars in Perinatology*, 32(1), 51–58. <https://doi.org/10.1053/j.semperi.2007.12.009>
- Andersson, J. L. R., Skare, S., & Ashburner, J. (2003). How to correct susceptibility distortions in spin-echo echo-planar images: application to diffusion tensor imaging. *NeuroImage*, 20(2), 870–888. [https://doi.org/10.1016/S1053-8119\(03\)00336-7](https://doi.org/10.1016/S1053-8119(03)00336-7)
- Andersson, J. L. R., & Sotiropoulos, S. N. (2016). An integrated approach to correction for off-resonance effects and subject movement in diffusion MR imaging. *NeuroImage*, 125, 1063–1078. <https://doi.org/10.1016/j.neuroimage.2015.10.019>
- Ardekani, B. A., Guckemus, S., Bachman, A., Hoptman, M. J., Wojtaszek, M., & Nierenberg, J. (2005). Quantitative comparison of algorithms for inter-subject registration of 3D volumetric brain MRI scans. *Journal of Neuroscience Methods*, 142(1), 67–76. <https://doi.org/10.1016/j.jneumeth.2004.07.014>
- Arichi, T. (2012). Functional MRI of the developing neonatal brain: potential and challenges for the future. *Developmental Medicine & Child Neurology*, 54(8), 680–680. <https://doi.org/10.1111/j.1469-8749.2012.04355.x>

- Arichi, T., Counsell, S. J., Allievi, A. G., Chew, A. T., Martinez-Biarge, M., Mondì, V., Tusor, N., Merchant, N., Burdet, E., Cowan, F. M., & Edwards, A. D. (2014). The effects of hemorrhagic parenchymal infarction on the establishment of sensori-motor structural and functional connectivity in early infancy. *Neuroradiology*, 56(11), 985–994. <https://doi.org/10.1007/s00234-014-1412-5>
- Arichi, T., Fagiolo, G., Varela, M., Melendez-Calderon, A., Allievi, A., Merchant, N., Tusor, N., Counsell, S. J., Burdet, E., Beckmann, C. F., & Edwards, A. D. (2012). Development of BOLD signal hemodynamic responses in the human brain. *NeuroImage*, 63(2), 663–673. <https://doi.org/10.1016/j.neuroimage.2012.06.054>
- Arichi, T., Moraux, A., Melendez, A., Doria, V., Groppo, M., Merchant, N., Combs, S., Burdet, E., Larkman, D. J., Counsell, S. J., Beckmann, C. F., & Edwards, A. D. (2010). Somatosensory cortical activation identified by functional MRI in preterm and term infants. *NeuroImage*, 49(3), 2063–2071. <https://doi.org/10.1016/j.neuroimage.2009.10.038>
- Arichi, T., Whitehead, K., Barone, G., Pressler, R., Padormo, F., Edwards, A. D., & Fabrizi, L. (2017). Localization of spontaneous bursting neuronal activity in the preterm human brain with simultaneous EEG-fMRI. *ELife*, 6. <https://doi.org/10.7554/eLife.27814>
- Arnaud, C., Ehlinger, V., Delobel-Ayoub, M., Klapouszczak, D., Perra, O., Hensey, O., Neubauer, D., Hollódy, K., Virella, D., Rackauskaite, G., Greitane, A., Himmelmann, K., Ortibus, E., Dakovic, I., Andersen, G. L., Papavasiliou, A., Sellier, E., Platt, M. J., & Krägeloh-Mann, I. (2021). Trends in Prevalence and Severity of Pre/Perinatal Cerebral Palsy Among Children Born Preterm From 2004 to 2010: A SCPE Collaboration Study. *Frontiers in Neurology*, 12. <https://doi.org/10.3389/fneur.2021.624884>
- Arnedo, J., Svrakic, D. M., del Val, C., Romero-Zaliz, R., Hernández-Cuervo, H., Fanous, A. H., Pato, M. T., Pato, C. N., de Erausquin, G. A., Cloninger, C. R., & Zwir, I. (2015). Uncovering the Hidden Risk Architecture of the Schizophrenias: Confirmation in Three Independent Genome-Wide Association Studies. *American Journal of Psychiatry*, 172(2), 139–153. <https://doi.org/10.1176/appi.ajp.2014.14040435>
- Assaf, Y., & Basser, P. J. (2005). Composite hindered and restricted model of diffusion (CHARMED) MR imaging of the human brain. *NeuroImage*, 27(1), 48–58. <https://doi.org/10.1016/j.neuroimage.2005.03.042>
- Auzias, G., Coulon, O., & Brovelli, A. (2016). MarsAtlas: A cortical parcellation atlas for functional mapping. *Human Brain Mapping*, 37(4), 1573–1592. <https://doi.org/10.1002/hbm.23121>
- Auzias, G., Lefevre, J., Le Troter, A., Fischer, C., Perrot, M., Regis, J., & Coulon, O. (2013). Model-Driven Harmonic Parameterization of the Cortical Surface: HIP-HOP. *IEEE Transactions on Medical Imaging*, 32(5), 873–887. <https://doi.org/10.1109/TMI.2013.2241651>
- Babaeeghazvini, P., Rueda-Delgado, L. M., Gooijers, J., Swinnen, S. P., & Daffertshofer, A. (2021). Brain Structural and Functional Connectivity: A Review of Combined Works of Diffusion Magnetic Resonance Imaging and Electro-Encephalography. *Frontiers in Human Neuroscience*, 15. <https://doi.org/10.3389/fnhum.2021.721206>
- Baker, S., & Kandasamy, Y. (2023). Machine learning for understanding and predicting neurodevelopmental outcomes in premature infants: a systematic review. *Pediatric Research*, 93(2), 293–299. <https://doi.org/10.1038/s41390-022-02120-w>
- Bakken, T. E., Miller, J. A., Ding, S.-L., Sunkin, S. M., Smith, K. A., Ng, L., Szafer, A., Dalley, R. A., Royall, J. J., Lemon, T., Shapouri, S., Aiona, K., Arnold, J., Bennett, J. L., Bertagnolli, D., Bickley, K., Boe, A., Brouner, K., Butler, S., ... Lein, E. S. (2016). A comprehensive transcriptional map of primate brain development. *Nature*, 535(7612), 367–375. <https://doi.org/10.1038/nature18637>
- Baldassano, C., Beck, D. M., & Fei-Fei, L. (2015). Parcellating connectivity in spatial maps. *PeerJ*, 3, e784. <https://doi.org/10.7717/peerj.784>

- Ball, G., Aljabar, P., Arichi, T., Tusor, N., Cox, D., Merchant, N., Nongena, P., Hajnal, J. V., Edwards, A. D., & Counsell, S. J. (2016). Machine-learning to characterise neonatal functional connectivity in the preterm brain. *NeuroImage*, 124, 267–275. <https://doi.org/10.1016/j.neuroimage.2015.08.055>
- Ball, G., Aljabar, P., Nongena, P., Kennea, N., Gonzalez-Cinca, N., Falconer, S., Chew, A. T. M., Harper, N., Wurie, J., Rutherford, M. A., Counsell, S. J., & Edwards, A. D. (2017). Multimodal image analysis of clinical influences on preterm brain development. *Annals of Neurology*, 82(2), 233–246. <https://doi.org/10.1002/ana.24995>
- Ball, G., Aljabar, P., Zebari, S., Tusor, N., Arichi, T., Merchant, N., Robinson, E. C., Ogundipe, E., Rueckert, D., Edwards, A. D., & Counsell, S. J. (2014). Rich-club organization of the newborn human brain. *Proceedings of the National Academy of Sciences*, 111(20), 7456–7461. <https://doi.org/10.1073/pnas.1324118111>
- Ball, G., Boardman, J. P., Aljabar, P., Pandit, A., Arichi, T., Merchant, N., Rueckert, D., Edwards, A. D., & Counsell, S. J. (2013). The influence of preterm birth on the developing thalamocortical connectome. *Cortex*, 49(6), 1711–1721. <https://doi.org/10.1016/j.cortex.2012.07.006>
- Ball, G., Boardman, J. P., Rueckert, D., Aljabar, P., Arichi, T., Merchant, N., Gousias, I. S., Edwards, A. D., & Counsell, S. J. (2012). The Effect of Preterm Birth on Thalamic and Cortical Development. *Cerebral Cortex*, 22(5), 1016–1024. <https://doi.org/10.1093/cercor/bhr176>
- Ball, G., Srinivasan, L., Aljabar, P., Counsell, S. J., Durighel, G., Hajnal, J. V., Rutherford, M. A., & Edwards, A. D. (2013). Development of cortical microstructure in the preterm human brain. *Proceedings of the National Academy of Sciences*, 110(23), 9541–9546. <https://doi.org/10.1073/pnas.1301652110>
- Banihani, R., Seesahai, J., Asztalos, E., & Terrien Church, P. (2021). Neuroimaging at Term Equivalent Age: Is There Value for the Preterm Infant? A Narrative Summary. *Children*, 8(3), 227. <https://doi.org/10.3390/children8030227>
- Barnes, K. A., Cohen, A. L., Power, J. D., Nelson, S. M., Dosenbach, Y. B., Miezin, F. M., Petersen, S. E., & Schlaggar, B. L. (2010). Identifying basal ganglia divisions in individuals using resting-state functional connectivity MRI. *Frontiers in System Neuroscience*. <https://doi.org/10.3389/fnsys.2010.00018>
- Barrera, K., Chu, P., Abramowitz, J., Steger, R., Ramos, R. L., & Brumberg, J. C. (2013). Organization of myelin in the mouse somatosensory barrel cortex and the effects of sensory deprivation. *Developmental Neurobiology*, 73(4), 297–314. <https://doi.org/10.1002/dneu.22060>
- Basser, P. J., Mattiello, J., & Lebihan, D. (1994). Estimation of the Effective Self-Diffusion Tensor from the NMR Spin Echo. *Journal of Magnetic Resonance, Series B*, 103(3), 247–254. <https://doi.org/10.1006/jmrb.1994.1037>
- Bassi, L., Chew, A., Merchant, N., Ball, G., Ramenghi, L., Boardman, J., Allsop, J. M., Doria, V., Arichi, T., Mosca, F., Edwards, A. D., Cowan, F. M., Rutherford, M. A., & Counsell, S. J. (2011). Diffusion Tensor Imaging in Preterm Infants With Punctate White Matter Lesions. *Pediatric Research*, 69(6), 561–566. <https://doi.org/10.1203/PDR.0b013e3182182836>
- Bassi, L., Ricci, D., Volzone, A., Allsop, J. M., Srinivasan, L., Pai, A., Ribes, C., Ramenghi, L. A., Mercuri, E., Mosca, F., Edwards, A. D., Cowan, F. M., Rutherford, M. A., & Counsell, S. J. (2008). Probabilistic diffusion tractography of the optic radiations and visual function in preterm infants at term equivalent age. *Brain*, 131(2), 573–582. <https://doi.org/10.1093/brain/awm327>
- Bastiani, M., Andersson, J. L. R., Cordero-Grande, L., Murgasova, M., Hutter, J., Price, A. N., Makropoulos, A., Fitzgibbon, S. P., Hughes, E., Rueckert, D., Victor, S., Rutherford, M., Edwards, A. D., Smith, S. M., Tournier, J.-D., Hajnal, J. V., Jbabdi, S., & Sotiropoulos, S. N. (2019). Automated processing pipeline for neonatal diffusion MRI in the developing Human Connectome Project. *NeuroImage*, 185, 750–763. <https://doi.org/10.1016/j.neuroimage.2018.05.064>

- Batalle, D., Edwards, A. D., & O'Muirheartaigh, J. (2018). Annual Research Review: Not just a small adult brain: understanding later neurodevelopment through imaging the neonatal brain. *Journal of Child Psychology and Psychiatry*, 59(4), 350–371. <https://doi.org/10.1111/jcpp.12838>
- Batalle, D., Hughes, E. J., Zhang, H., Tournier, J.-D., Tusor, N., Aljabar, P., Wali, L., Alexander, D. C., Hajnal, J. V., Nosarti, C., Edwards, A. D., & Counsell, S. J. (2017a). Early development of structural networks and the impact of prematurity on brain connectivity. *NeuroImage*, 149, 379–392. <https://doi.org/10.1016/j.neuroimage.2017.01.065>
- Batalle, D., Hughes, E. J., Zhang, H., Tournier, J.-D., Tusor, N., Aljabar, P., Wali, L., Alexander, D. C., Hajnal, J. V., Nosarti, C., Edwards, A. D., & Counsell, S. J. (2017b). Early development of structural networks and the impact of prematurity on brain connectivity. *NeuroImage*, 149, 379–392. <https://doi.org/10.1016/j.neuroimage.2017.01.065>
- Batalle, D., O'Muirheartaigh, J., Makropoulos, A., Kelly, C. J., Dimitrova, R., Hughes, E. J., Hajnal, J. V., Zhang, H., Alexander, D. C., Edwards, A. D., & Counsell, S. J. (2019a). Different patterns of cortical maturation before and after 38 weeks gestational age demonstrated by diffusion MRI in vivo. *NeuroImage*, 185, 764–775. <https://doi.org/10.1016/j.neuroimage.2018.05.046>
- Batalle, D., O'Muirheartaigh, J., Makropoulos, A., Kelly, C. J., Dimitrova, R., Hughes, E. J., Hajnal, J. V., Zhang, H., Alexander, D. C., Edwards, A. D., & Counsell, S. J. (2019b). Different patterns of cortical maturation before and after 38 weeks gestational age demonstrated by diffusion MRI in vivo. *NeuroImage*, 185, 764–775. <https://doi.org/10.1016/j.neuroimage.2018.05.046>
- Baum, G. L., Cui, Z., Roalf, D. R., Ciric, R., Betzel, R. F., Larsen, B., Cieslak, M., Cook, P. A., Xia, C. H., Moore, T. M., Ruparel, K., Oathes, D. J., Alexander-Bloch, A. F., Shinohara, R. T., Raznahan, A., Gur, R. E., Gur, R. C., Bassett, D. S., & Satterthwaite, T. D. (2020). Development of structure–function coupling in human brain networks during youth. *Proceedings of the National Academy of Sciences*, 117(1), 771–778. <https://doi.org/10.1073/pnas.1912034117>
- Baumann, N., Bartmann, P., & Wolke, D. (2016). Health-Related Quality of Life Into Adulthood After Very Preterm Birth. *Pediatrics*, 137(4). <https://doi.org/10.1542/peds.2015-3148>
- Baumann, N., & Pham-Dinh, D. (2001). Biology of Oligodendrocyte and Myelin in the Mammalian Central Nervous System. *Physiological Reviews*, 81(2), 871–927. <https://doi.org/10.1152/physrev.2001.81.2.871>
- Baumgartner, R., Ryner, L., Richter, W., Summers, R., Jarmasz, M., & Somorjai, R. (2000). Comparison of two exploratory data analysis methods for fMRI: fuzzy clustering vs. principal component analysis. *Magnetic Resonance Imaging*, 18(1), 89–94. [https://doi.org/10.1016/S0730-725X\(99\)00102-2](https://doi.org/10.1016/S0730-725X(99)00102-2)
- Baxter, L., Fitzgibbon, S., Moultrie, F., Goksan, S., Jenkinson, M., Smith, S., Andersson, J., Duff, E., & Slater, R. (2019). Optimising neonatal fMRI data analysis: Design and validation of an extended dHCP preprocessing pipeline to characterise noxious-evoked brain activity in infants. *NeuroImage*, 186, 286–300. <https://doi.org/10.1016/j.neuroimage.2018.11.006>
- Bayer, J. M. M., Thompson, P. M., Ching, C. R. K., Liu, M., Chen, A., Panzenhagen, A. C., Jahanshad, N., Marquand, A., Schmaal, L., & Sämann, P. G. (2022). Site effects how-to and when: An overview of retrospective techniques to accommodate site effects in multi-site neuroimaging analyses. *Frontiers in Neurology*, 13. <https://doi.org/10.3389/fneur.2022.923988>
- Bayley, N. (2006). *Bayley Scales of Infant and Toddler Development, 3rd Edn.: Vol. Harcourt Assessment*.
- Bazacliu, C., & Neu, J. (2019). Necrotizing Enterocolitis: Long Term Complications. *Current Pediatric Reviews*, 15(2), 115–124. <https://doi.org/10.2174/1573396315666190312093119>
- Behrens, T. E. J., Berg, H. J., Jbabdi, S., Rushworth, M. F. S., & Woolrich, M. W. (2007). Probabilistic diffusion tractography with multiple fibre orientations: What can we gain? *NeuroImage*, 34(1), 144–155. <https://doi.org/10.1016/j.neuroimage.2006.09.018>

- Behrens, T. E. J., Woolrich, M. W., Jenkinson, M., Johansen-Berg, H., Nunes, R. G., Clare, S., Matthews, P. M., Brady, J. M., & Smith, S. M. (2003). Characterization and propagation of uncertainty in diffusion-weighted MR imaging. *Magnetic Resonance in Medicine*, 50(5), 1077–1088. <https://doi.org/10.1002/mrm.10609>
- Bekiesinska-Figatowska, M., Romaniuk-Doroszewska, A., Duczkowska, A., Duczkowski, M., Iwanowska, B., & Szkudlińska-Pawlak, S. (2016). Fetal MRI versus postnatal imaging in the MR-compatible incubator. *La Radiologia Medica*, 121(9), 719–728. <https://doi.org/10.1007/s11547-016-0649-y>
- Benders, M. J., Palmu, K., Menache, C., Borradori-Tolsa, C., Lazeyras, F., Sizonenko, S., Dubois, J., Vanhatalo, S., & Hüppi, P. S. (2015). Early Brain Activity Relates to Subsequent Brain Growth in Premature Infants. *Cerebral Cortex*, 25(9), 3014–3024. <https://doi.org/10.1093/cercor/bhu097>
- Benders, M., Mangin, J., Guzzetta, A., Ketelaar, M., & and other members of the project ENSEMBL. (2022). Projet ENSEMBLE : Détecter plus tôt pour intervenir plus tôt. *Cahier de La Recherche N.31*.
- Benzies, K. M., Magill-Evans, J. E., Hayden, K., & Ballantyne, M. (2013). Key components of early intervention programs for preterm infants and their parents: a systematic review and meta-analysis. *BMC Pregnancy and Childbirth*, 13(Suppl 1), S10. <https://doi.org/10.1186/1471-2393-13-S1-S10>
- Berman, J. I., Mukherjee, P., Partridge, S. C., Miller, S. P., Ferriero, D. M., Barkovich, A. J., Vigneron, D. B., & Henry, R. G. (2005). Quantitative diffusion tensor MRI fiber tractography of sensorimotor white matter development in premature infants. *NeuroImage*, 27(4), 862–871. <https://doi.org/10.1016/j.neuroimage.2005.05.018>
- Bhutta, A. T., Cleves, M. A., Casey, P. H., Cradock, M. M., & Anand, K. J. S. (2002). Cognitive and Behavioral Outcomes of School-Aged Children Who Were Born Preterm. *JAMA*, 288(6), 728. <https://doi.org/10.1001/jama.288.6.728>
- Bielczyk, N. Z., Uithol, S., van Mourik, T., Anderson, P., Glennon, J. C., & Buitelaar, J. K. (2019). Disentangling causal webs in the brain using functional magnetic resonance imaging: A review of current approaches. *Network Neuroscience*, 3(2), 237–273. https://doi.org/10.1162/netn_a_00062
- Bijsterbosch, J., Smith, S., & Beckman, C. (2017). *Introduction to Resting State fMRI Functional Connectivity*. Oxford Neuroimaging Primers.
- Blencowe, H., Cousens, S., Oestergaard, M. Z., Chou, D., Moller, A.-B., Narwal, R., Adler, A., Vera Garcia, C., Rohde, S., Say, L., & Lawn, J. E. (2012). National, regional, and worldwide estimates of preterm birth rates in the year 2010 with time trends since 1990 for selected countries: a systematic analysis and implications. *The Lancet*, 379(9832), 2162–2172. [https://doi.org/10.1016/S0140-6736\(12\)60820-4](https://doi.org/10.1016/S0140-6736(12)60820-4)
- Borne, L., Rivière, D., Mancip, M., & Mangin, J. F. (2020). Automatic labeling of cortical sulci using patch- or CNN-based segmentation techniques combined with bottom-up geometric constraints. *Medical Image Analysis*, 62. <https://doi.org/10.1016/j.media.2020.101651>
- Bosch-Bayard, J., Biscay, R. J., Fernandez, T., Otero, G. A., Ricardo-Garcell, J., Aubert-Vazquez, E., Evans, A. C., & Harmony, T. (2022). EEG effective connectivity during the first year of life mirrors brain synaptogenesis, myelination, and early right hemisphere predominance. *NeuroImage*, 252, 119035. <https://doi.org/10.1016/j.neuroimage.2022.119035>
- Bozek, J., Makropoulos, A., Schuh, A., Fitzgibbon, S., Wright, R., Glasser, M. F., Coalson, T. S., O’Muircheartaigh, J., Hutter, J., Price, A. N., Cordero-Grande, L., Teixeira, R. P. A. G., Hughes, E., Tusor, N., Baruteau, K. P., Rutherford, M. A., Edwards, A. D., Hajnal, J. V., Smith, S. M., ... Robinson, E. C. (2018). Construction of a neonatal cortical surface atlas using Multimodal Surface Matching in the Developing Human Connectome Project. *NeuroImage*, 179, 11–29. <https://doi.org/10.1016/j.neuroimage.2018.06.018>

- Breeman, L. D., Jaekel, J., Baumann, N., Bartmann, P., & Wolke, D. (2016). Attention problems in very preterm children from childhood to adulthood: the Bavarian Longitudinal Study. *Journal of Child Psychology and Psychiatry*, 57(2), 132–140. <https://doi.org/10.1111/jcpp.12456>
- Brenner, R. G., Wheelock, M. D., Neil, J. J., & Smyser, C. D. (2021). Structural and functional connectivity in premature neonates. *Seminars in Perinatology*, 45(7), 151473. <https://doi.org/10.1016/j.semperi.2021.151473>
- Brodman, K. (1908). Beiträge zur histologischen Lokalisation der Grosshirnrinde. VI. Mitteilung: Die Cortexgliederung des Menschen. *Journal Für Psychologie Und Neurologie*, 10, 231–246.
- Brouwer, M. J., de Vries, L. S., Kersbergen, K. J., van der Aa, N. E., Brouwer, A. J., Viergever, M. A., Išgum, I., Han, K. S., Groenendaal, F., & Benders, M. J. N. L. (2016). Effects of Posthemorrhagic Ventricular Dilatation in the Preterm Infant on Brain Volumes and White Matter Diffusion Variables at Term-Equivalent Age. *The Journal of Pediatrics*, 168, 41–49.e1. <https://doi.org/10.1016/j.jpeds.2015.09.083>
- Brown, C. J., Miller, S. P., Booth, B. G., Andrews, S., Chau, V., Poskitt, K. J., & Hamarneh, G. (2014). Structural network analysis of brain development in young preterm neonates. *NeuroImage*, 101, 667–680. <https://doi.org/10.1016/j.neuroimage.2014.07.030>
- Brown, C. J., Miller, S. P., Booth, B. G., Zwicker, J. G., Grunau, R. E., Synnes, A. R., Chau, V., & Hamarneh, G. (2019). Predictive connectome subnetwork extraction with anatomical and connectivity priors. *Computerized Medical Imaging and Graphics*, 71, 67–78. <https://doi.org/10.1016/j.compmedimag.2018.08.009>
- Burger, B., Nenning, K.-H., Schwartz, E., Margulies, D. S., Goulas, A., Liu, H., Neubauer, S., Dauwels, J., Prayer, D., & Langs, G. (2022). Disentangling cortical functional connectivity strength and topography reveals divergent roles of genes and environment. *NeuroImage*, 247, 118770. <https://doi.org/10.1016/j.neuroimage.2021.118770>
- BURNS, Y. R., ENSBEY, R. M., & NORRIE, M. A. (1989). The Neuro-sensory Motor Developmental Assessment Part 1: Development and Administration of the Test. *Australian Journal of Physiotherapy*, 35(3), 141–149. [https://doi.org/10.1016/S0004-9514\(14\)60503-1](https://doi.org/10.1016/S0004-9514(14)60503-1)
- Bystron, I., Blakemore, C., & Rakic, P. (2008). Development of the human cerebral cortex: Boulder Committee revisited. *Nature Reviews Neuroscience*, 9(2), 110–122. <https://doi.org/10.1038/nrn2252>
- Cadwell, C. R., Bhaduri, A., Mostajo-Radji, M. A., Keefe, M. G., & Nowakowski, T. J. (2019). Development and Arealization of the Cerebral Cortex. *Neuron*, 103(6), 980–1004. <https://doi.org/10.1016/j.neuron.2019.07.009>
- Cahill-Rowley, K., & Rose, J. (2016). Toddler temporal-spatial deviation index: Assessment of pediatric gait. *Gait & Posture*, 49, 226–231. <https://doi.org/10.1016/j.gaitpost.2016.06.040>
- Cao, J., & Worsley, K. (1999). The geometry of correlation fields with an application to functional connectivity of the brain. *The Annals of Applied Probability*, 9(4). <https://doi.org/10.1214/aoap/1029962864>
- Cao, M., Huang, H., & He, Y. (2017). Developmental Connectomics from Infancy through Early Childhood. *Trends in Neurosciences*, 40(8), 494–506. <https://doi.org/10.1016/j.tins.2017.06.003>
- Cardona, G., Mir, A., Rosselló, F., Rotger, L., & Sánchez, D. (2013). Cophenetic metrics for phylogenetic trees, after Sokal and Rohlf. *BMC Bioinformatics*, 14(1), 3. <https://doi.org/10.1186/1471-2105-14-3>
- Carmody, D. P., Dunn, S. M., Boddie-Willis, A. S., DeMarco, J. K., & Lewis, M. (2004). A quantitative measure of myelination development in infants, using MR images. *Neuroradiology*, 46(9), 781–786. <https://doi.org/10.1007/s00234-004-1241-z>

- Chandwani, R., Kline, J. E., Harpster, K., Tkach, J., & Parikh, N. A. (2021). Early micro- and macrostructure of sensorimotor tracts and development of cerebral palsy in high risk infants. *Human Brain Mapping*, 42(14), 4708–4721. <https://doi.org/10.1002/hbm.25579>
- Chen, M., Li, H., Wang, J., Yuan, W., Altaye, M., Parikh, N. A., & He, L. (2020). Early Prediction of Cognitive Deficit in Very Preterm Infants Using Brain Structural Connectome With Transfer Learning Enhanced Deep Convolutional Neural Networks. *Frontiers in Neuroscience*, 14. <https://doi.org/10.3389/fnins.2020.00858>
- Chiarelli, A. M., Sestieri, C., Navarra, R., Wise, R. G., & Caulo, M. (2021). Distinct effects of prematurity on MRI metrics of brain functional connectivity, activity, and structure: Univariate and multivariate analyses. *Human Brain Mapping*, 42(11), 3593–3607. <https://doi.org/10.1002/hbm.25456>
- Christiaens, D., Cordero-Grande, L., Hutter, J., Price, A. N., O’Murcheartaigh, J., Vecchiato, K., Hajnal, J. V., & Tournier, J.-D. (2020). Fat-shift suppression in diffusion MRI using rotating phase encoding and localised outlier weighting. *ISMRM*, 0981.
- Christiaens, D., Cordero-Grande, L., Pietsch, M., Hutter, J., Price, A. N., Hughes, E. J., Vecchiato, K., Deprez, M., Edwards, A. D., Hajnal, J. V., & Tournier, J.-D. (2021). Scattered slice SHARD reconstruction for motion correction in multi-shell diffusion MRI. *NeuroImage*, 225, 117437. <https://doi.org/10.1016/j.neuroimage.2020.117437>
- Ciarrusta, J., Christiaens, D., Fitzgibbon, S. P., Dimitrova, R., Hutter, J., Hughes, E., Duff, E., Price, A. N., Cordero-Grande, L., Tournier, J.-D., Rueckert, D., Hajnal, J. V., Arichi, T., McAlonan, G., Edwards, A. D., & Batalle, D. (2022). The developing brain structural and functional connectome fingerprint. *Developmental Cognitive Neuroscience*, 55, 101117. <https://doi.org/10.1016/j.dcn.2022.101117>
- Cismaru, A. L., Gui, L., Vasung, L., Lejeune, F., Barisnikov, K., Truttmann, A., Borradori Tolsa, C., & Hüppi, P. S. (2016). Altered Amygdala Development and Fear Processing in Prematurely Born Infants. *Frontiers in Neuroanatomy*, 10. <https://doi.org/10.3389/fnana.2016.00055>
- Coalson, T. S., Van Essen, D. C., & Glasser, M. F. (2018). The impact of traditional neuroimaging methods on the spatial localization of cortical areas. *Proceedings of the National Academy of Sciences*, 115(27). <https://doi.org/10.1073/pnas.1801582115>
- Cohen, A. L., Fair, D. A., Dosenbach, N. U. F., Miezin, F. M., Dierker, D., Van Essen, D. C., Schlaggar, B. L., & Petersen, S. E. (2008). Defining functional areas in individual human brains using resting functional connectivity MRI. *NeuroImage*, 41(1), 45–57. <https://doi.org/10.1016/j.neuroimage.2008.01.066>
- Cole, D. M., Smith, M. S., & Beckmann, C. (2010). Advances and pitfalls in the analysis and interpretation of resting-state FMRI data. *Frontiers in Systems Neuroscience*. <https://doi.org/10.3389/fnsys.2010.00008>
- Copeland, A., Silver, E., Korja, R., Lehtola, S. J., Merisaari, H., Saukko, E., Sinisalo, S., Saunavaara, J., Lähdesmäki, T., Parkkola, R., Nolvi, S., Karlsson, L., Karlsson, H., & Tuulari, J. J. (2021). Infant and Child MRI: A Review of Scanning Procedures. *Frontiers in Neuroscience*, 15, 666020. <https://doi.org/10.3389/fnins.2021.666020>
- Cordero-Grande, L., Christiaens, D., Hutter, J., Price, A. N., & Hajnal, J. V. (2019). Complex diffusion-weighted image estimation via matrix recovery under general noise models. *NeuroImage*, 200, 391–404. <https://doi.org/10.1016/j.neuroimage.2019.06.039>
- Cordero-Grande, L., Hughes, E. J., Hutter, J., Price, A. N., & Hajnal, J. V. (2018a). Three-dimensional motion corrected sensitivity encoding reconstruction for multi-shot multi-slice MRI: Application to neonatal brain imaging. *Magnetic Resonance in Medicine*, 79(3), 1365–1376. <https://doi.org/10.1002/mrm.26796>

- Cordero-Grande, L., Hughes, E. J., Hutter, J., Price, A. N., & Hajnal, J. V. (2018b). Three-dimensional motion corrected sensitivity encoding reconstruction for multi-shot multi-slice MRI: Application to neonatal brain imaging. *Magnetic Resonance in Medicine*, 79(3), 1365–1376. <https://doi.org/10.1002/mrm.26796>
- Cordero-Grande, L., Hughes, E. J., Hutter, J., Price, A. N., & Hajnal, J. V. (2018c). Three-dimensional motion corrected sensitivity encoding reconstruction for multi-shot multi-slice MRI: Application to neonatal brain imaging. *Magnetic Resonance in Medicine*, 79(3), 1365–1376. <https://doi.org/10.1002/mrm.26796>
- Counsell, S. J., Allsop, J. M., Harrison, M. C., Larkman, D. J., Kennea, N. L., Kapellou, O., Cowan, F. M., Hajnal, J. V., Edwards, A. D., & Rutherford, M. A. (2003). Diffusion-Weighted Imaging of the Brain in Preterm Infants With Focal and Diffuse White Matter Abnormality. *Pediatrics*, 112(1), 1–7. <https://doi.org/10.1542/peds.112.1.1>
- Counsell, S. J., Edwards, A. D., Chew, A. T. M., Anjari, M., Dyet, L. E., Srinivasan, L., Boardman, J. P., Allsop, J. M., Hajnal, J. V., Rutherford, M. A., & Cowan, F. M. (2008). Specific relations between neurodevelopmental abilities and white matter microstructure in children born preterm. *Brain*, 131(12), 3201–3208. <https://doi.org/10.1093/brain/awn268>
- Dale, A. M., Liu, A. K., Fischl, B. R., Buckner, R. L., Belliveau, J. W., Lewine, J. D., & Halgren, E. (2000). Dynamic Statistical Parametric Mapping. *Neuron*, 26(1), 55–67. [https://doi.org/10.1016/S0896-6273\(00\)81138-1](https://doi.org/10.1016/S0896-6273(00)81138-1)
- Dall’Orso, S., Arichi, T., Fitzgibbon, S. P., Edwards, A. D., Burdet, E., & Muceli, S. (2022). Development of functional organization within the sensorimotor network across the perinatal period. *Human Brain Mapping*, 43(7), 2249–2261. <https://doi.org/10.1002/hbm.25785>
- Damaraju. (2010). Resting-state functional connectivity differences in premature children. *Frontiers in Systems Neuroscience*. <https://doi.org/10.3389/fnsys.2010.00023>
- Davatzikos, C. (2019). Machine learning in neuroimaging: Progress and challenges. *NeuroImage*, 197, 652–656. <https://doi.org/10.1016/j.neuroimage.2018.10.003>
- de Vareilles, H., Rivière, D., Mangin, J., & Dubois, J. (2023). Development of cortical folds in the human brain: An attempt to review biological hypotheses, early neuroimaging investigations and functional correlates. *Developmental Cognitive Neuroscience*, 61, 101249. <https://doi.org/10.1016/j.dcn.2023.101249>
- Dehaene-Lambertz, G., Dehaene, S., & Hertz-Pannier, L. (2002). Functional Neuroimaging of Speech Perception in Infants. *Science*, 298(5600), 2013–2015. <https://doi.org/10.1126/science.1077066>
- Del Rosario, C., Slevin, M., Molloy, E. J., Quigley, J., & Nixon, E. (2021). How to use the Bayley Scales of Infant and Toddler Development. *Archives of Disease in Childhood - Education & Practice Edition*, 106(2), 108–112. <https://doi.org/10.1136/archdischild-2020-319063>
- Demerens, C., Stankoff, B., Logak, M., Anglade, P., Allinquant, B., Couraud, F., Zalc, B., & Lubetzki, C. (1996). Induction of myelination in the central nervous system by electrical activity. *Proceedings of the National Academy of Sciences*, 93(18), 9887–9892. <https://doi.org/10.1073/pnas.93.18.9887>
- Denisova, K. (2019). Age attenuates noise and increases symmetry of head movements during sleep resting-state fMRI in healthy neonates, infants, and toddlers. *Infant Behavior and Development*, 57, 101317. <https://doi.org/10.1016/j.infbeh.2019.03.008>
- Deoni, S. C. L., Dean, D. C., O’Muircheartaigh, J., Dirks, H., & Jerskey, B. A. (2012). Investigating white matter development in infancy and early childhood using myelin water fraction and relaxation time mapping. *NeuroImage*, 63(3), 1038–1053. <https://doi.org/10.1016/j.neuroimage.2012.07.037>

- Destrieux, C., Fischl, B., Dale, A., & Halgren, E. (2010). Automatic parcellation of human cortical gyri and sulci using standard anatomical nomenclature. *NeuroImage*, 53(1), 1–15. <https://doi.org/10.1016/j.neuroimage.2010.06.010>
- Devisscher, L., Labra, N., Aubrain, K., Leroy, F., Hertz-pannier, L., & Dubois, J. (n.d.). *Disentangling the differential maturation of sensorimotor cortices in newborns compared to adults Institutions : First Author :*
- Dhollander, T., Clemente, A., Singh, M., Boonstra, F., Civier, O., Duque, J. D., Egorova, N., Enticott, P., Fuelscher, I., Gajamange, S., Genc, S., Gottlieb, E., Hyde, C., Imms, P., Kelly, C., Kirkovski, M., Kolbe, S., Liang, X., Malhotra, A., ... Caeyenberghs, K. (2021). Fixel-based Analysis of Diffusion MRI: Methods, Applications, Challenges and Opportunities. *NeuroImage*, 241, 118417. <https://doi.org/10.1016/j.neuroimage.2021.118417>
- Dhollander, T., & Connelly, A. (2016). A novel iterative approach to reap the benefits of multi-tissue CSD from just single-shell ($+b=0$) diffusion MRI data. *24th International Society of Magnetic Resonance in Medicine*.
- Dhollander, T., Mito, R., Raffelt, D., & Connelly, A. (2019). Improved white matter response function estimation for 3-tissue constrained spherical deconvolution. *27th International Society of Magnetic Resonance in Medicine*.
- Dimitrova, R., Pietsch, M., Ciarrusta, J., Fitzgibbon, S. P., Williams, L. Z. J., Christiaens, D., Cordero-Grande, L., Bataille, D., Makropoulos, A., Schuh, A., Price, A. N., Hutter, J., Teixeira, R. P., Hughes, E., Chew, A., Falconer, S., Carney, O., Egloff, A., Tournier, J.-D., ... O'Muircheartaigh, J. (2021). Preterm birth alters the development of cortical microstructure and morphology at term-equivalent age. *NeuroImage*, 243, 118488. <https://doi.org/10.1016/j.neuroimage.2021.118488>
- Doria, V., Beckmann, C. F., Arichi, T., Merchant, N., Groppo, M., Turkheimer, F. E., Counsell, S. J., Murgasova, M., Aljabar, P., Nunes, R. G., Larkman, D. J., Rees, G., & Edwards, A. D. (2010). Emergence of resting state networks in the preterm human brain. *Proceedings of the National Academy of Sciences*, 107(46), 20015–20020. <https://doi.org/10.1073/pnas.1007921107>
- Drobyshevsky, A., Song, S.-K., Gamkrelidze, G., Wyrwicz, A. M., Derrick, M., Meng, F., Li, L., Ji, X., Trommer, B., Beardsley, D. J., Luo, N. L., Back, S. A., & Tan, S. (2005). Developmental Changes in Diffusion Anisotropy Coincide with Immature Oligodendrocyte Progression and Maturation of Compound Action Potential. *The Journal of Neuroscience*, 25(25), 5988–5997. <https://doi.org/10.1523/JNEUROSCI.4983-04.2005>
- Dubois, J., Adibpour, P., Poupon, C., Hertz-Pannier, L., & Dehaene-Lambertz, G. (2016). MRI and M/EEG studies of the White Matter Development in Human Fetuses and Infants: Review and Opinion. *Brain Plasticity*, 2(1), 49–69. <https://doi.org/10.3233/BPL-160031>
- Dubois, J., Alison, M., Counsell, S. J., Hertz-Pannier, L., Hüppi, P. S., & Benders, M. J. N. L. (2021). MRI of the Neonatal Brain: A Review of Methodological Challenges and Neuroscientific Advances. *Journal of Magnetic Resonance Imaging*, 53(5), 1318–1343. <https://doi.org/10.1002/jmri.27192>
- Dubois, J., Dehaene-Lambertz, G., Kulikova, S., Poupon, C., Hüppi, P. S., & Hertz-Pannier, L. (2014). The early development of brain white matter: A review of imaging studies in fetuses, newborns and infants. *Neuroscience*, 276, 48–71. <https://doi.org/10.1016/j.neuroscience.2013.12.044>
- Dubois, J., Dehaene-Lambertz, G., Perrin, M., Mangin, J.-F., Cointepas, Y., Duchesnay, E., Le Bihan, D., & Hertz-Pannier, L. (2008). Asynchrony of the early maturation of white matter bundles in healthy infants: Quantitative landmarks revealed noninvasively by diffusion tensor imaging. *Human Brain Mapping*, 29(1), 14–27. <https://doi.org/10.1002/hbm.20363>
- Dubois, J., Hertz-Pannier, L., Cachia, A., Mangin, J. F., Le Bihan, D., & Dehaene-Lambertz, G. (2009). Structural Asymmetries in the Infant Language and Sensori-Motor Networks. *Cerebral Cortex*, 19(2), 414–423. <https://doi.org/10.1093/cercor/bhn097>

- Dubois, J., Hertz-Pannier, L., Dehaene-Lambertz, G., Cointepas, Y., & Le Bihan, D. (2006). Assessment of the early organization and maturation of infants' cerebral white matter fiber bundles: A feasibility study using quantitative diffusion tensor imaging and tractography. *NeuroImage*, 30(4), 1121–1132. <https://doi.org/10.1016/j.neuroimage.2005.11.022>
- Dubois, J., Kostovic, I., & Judas, M. (2015). Development of structural and functional connectivity. In *Brain Mapping: An Encyclopedic Reference* (Vol. 2, pp. 423–437).
- Dubois, J., Lefèvre, J., Angleys, H., Leroy, F., Fischer, C., Lebenberg, J., Dehaene-Lambertz, G., Borradori-Tolsa, C., Lazeyras, F., Hertz-Pannier, L., Mangin, J.-F., Hüppi, P. S., & Germanaud, D. (2019a). The dynamics of cortical folding waves and prematurity-related deviations revealed by spatial and spectral analysis of gyrification. *NeuroImage*, 185, 934–946. <https://doi.org/10.1016/j.neuroimage.2018.03.005>
- Dubois, J., Lefèvre, J., Angleys, H., Leroy, F., Fischer, C., Lebenberg, J., Dehaene-Lambertz, G., Borradori-Tolsa, C., Lazeyras, F., Hertz-Pannier, L., Mangin, J.-F., Hüppi, P. S., & Germanaud, D. (2019b). The dynamics of cortical folding waves and prematurity-related deviations revealed by spatial and spectral analysis of gyrification. *NeuroImage*, 185, 934–946. <https://doi.org/10.1016/j.neuroimage.2018.03.005>
- Dubois, J., Poupon, C., Thirion, B., Simonnet, H., Kulikova, S., Leroy, F., Hertz-Pannier, L., & Dehaene-Lambertz, G. (2016). Exploring the Early Organization and Maturation of Linguistic Pathways in the Human Infant Brain. *Cerebral Cortex*, 26(5), 2283–2298. <https://doi.org/10.1093/cercor/bhv082>
- Dudink, J., Lequin, M., van Pul, C., Buijs, J., Conneman, N., van Goudoever, J., & Govaert, P. (2007). Fractional anisotropy in white matter tracts of very-low-birth-weight infants. *Pediatric Radiology*, 37(12), 1216–1223. <https://doi.org/10.1007/s00247-007-0626-7>
- Dyrby, T. B., Innocenti, G. M., Bech, M., & Lundell, H. (2018). Validation strategies for the interpretation of microstructure imaging using diffusion MRI. *NeuroImage*, 182, 62–79. <https://doi.org/10.1016/j.neuroimage.2018.06.049>
- Eaton-Rosen, Z., Melbourne, A., Orasanu, E., Cardoso, M. J., Modat, M., Bainbridge, A., Kendall, G. S., Robertson, N. J., Marlow, N., & Ourselin, S. (2015). Longitudinal measurement of the developing grey matter in preterm subjects using multi-modal MRI. *NeuroImage*, 111, 580–589. <https://doi.org/10.1016/j.neuroimage.2015.02.010>
- Eaton-Rosen, Z., Scherrer, B., Melbourne, A., Ourselin, S., Neil, J. J., & Warfield, S. K. (2017). Investigating the maturation of microstructure and radial orientation in the preterm human cortex with diffusion MRI. *NeuroImage*, 162, 65–72. <https://doi.org/10.1016/j.neuroimage.2017.08.013>
- Edwards, A. D., Rueckert, D., Smith, S. M., Abo Seada, S., Alansary, A., Almalbis, J., Allsop, J., Andersson, J., Arichi, T., Arulkumaran, S., Bastiani, M., Batalle, D., Baxter, L., Bozek, J., Braithwaite, E., Brandon, J., Carney, O., Chew, A., Christiaens, D., ... Hajnal, J. V. (2022). The Developing Human Connectome Project Neonatal Data Release. *Frontiers in Neuroscience*, 16. <https://doi.org/10.3389/fnins.2022.886772>
- Erickson, G., Dobson, N. R., & Hunt, C. E. (2021). Immature control of breathing and apnea of prematurity: the known and unknown. *Journal of Perinatology*, 41(9), 2111–2123. <https://doi.org/10.1038/s41372-021-01010-z>
- Eyre, M., Fitzgibbon, S. P., Ciarrusta, J., Cordero-Grande, L., Price, A. N., Poppe, T., Schuh, A., Hughes, E., O'Keeffe, C., Brandon, J., Cromb, D., Vecchiato, K., Andersson, J., Duff, E. P., Counsell, S. J., Smith, S. M., Rueckert, D., Hajnal, J. V., Arichi, T., ... Edwards, A. D. (2021). The Developing Human Connectome Project: typical and disrupted perinatal functional connectivity. *Brain*, 144(7), 2199–2213. <https://doi.org/10.1093/brain/awab118>
- Fagard, J., Esseily, R., Jacquey, L., O'Regan, K., & Somogyi, E. (2018). Fetal Origin of Sensorimotor Behavior. *Frontiers in Neurobotics*, 12. <https://doi.org/10.3389/fnbot.2018.00023>

- Fan, Y., Shi, F., Smith, J. K., Lin, W., Gilmore, J. H., & Shen, D. (2011). Brain anatomical networks in early human brain development. *NeuroImage*, 54(3), 1862–1871. <https://doi.org/10.1016/j.neuroimage.2010.07.025>
- Farahani, F. V., & Karwowski, W. (2019). *Computational Methods for Analyzing Functional and Effective Brain Network Connectivity Using fMRI* (pp. 101–112). https://doi.org/10.1007/978-3-319-94866-9_10
- Farquharson, S., Tournier, J.-D., Calamante, F., Fabinyi, G., Schneider-Kolsky, M., Jackson, G. D., & Connelly, A. (2013). White matter fiber tractography: why we need to move beyond DTI. *Journal of Neurosurgery*, 118(6), 1367–1377. <https://doi.org/10.3171/2013.2.JNS121294>
- Fenchel, D., Dimitrova, R., Robinson, E. C., Batalle, D., Chew, A., Falconer, S., Kyriakopoulou, V., Nosarti, C., Hutter, J., Christiaens, D., Pietsch, M., Brandon, J., Hughes, E. J., Allsop, J., O’Keeffe, C., Price, A. N., Cordero-Grande, L., Schuh, A., Makropoulos, A., ... O’Muirheartaigh, J. (2022). Neonatal multi-modal cortical profiles predict 18-month developmental outcomes. *Developmental Cognitive Neuroscience*, 54, 101103. <https://doi.org/10.1016/j.dcn.2022.101103>
- Fenchel, D., Dimitrova, R., Seidlitz, J., Robinson, E. C., Batalle, D., Hutter, J., Christiaens, D., Pietsch, M., Brandon, J., Hughes, E. J., Allsop, J., O’Keeffe, C., Price, A. N., Cordero-Grande, L., Schuh, A., Makropoulos, A., Passerat-Palmbach, J., Bozek, J., Rueckert, D., ... O’Muirheartaigh, J. (2020). Fench et Development of Microstructural and Morphological Cortical Profiles in the Neonatal Brain. *Cerebral Cortex*, 30(11), 5767–5779. <https://doi.org/10.1093/cercor/bhaa150>
- Fenn-Moltu, S., Fitzgibbon, S. P., Ciarrusta, J., Eyre, M., Cordero-Grande, L., Chew, A., Falconer, S., Gale-Grant, O., Harper, N., Dimitrova, R., Vecchiato, K., Fenchel, D., Javed, A., Earl, M., Price, A. N., Hughes, E., Duff, E. P., O’Muirheartaigh, J., Nosarti, C., ... Batalle, D. (2023). Development of neonatal brain functional centrality and alterations associated with preterm birth. *Cerebral Cortex*, 33(9), 5585–5596. <https://doi.org/10.1093/cercor/bhac444>
- Fernández de Gamarra-Oca, L., Ojeda, N., Gómez-Gastiasoro, A., Peña, J., Ibarretxe-Bilbao, N., García-Guerrero, M. A., Loureiro, B., & Zubiaurre-Elorza, L. (2021). Long-Term Neurodevelopmental Outcomes after Moderate and Late Preterm Birth: A Systematic Review. *The Journal of Pediatrics*, 237, 168–176.e11. <https://doi.org/10.1016/j.jpeds.2021.06.004>
- Ferrazzi, G., Kuklisova Murgasova, M., Arichi, T., Malamateniou, C., Fox, M. J., Makropoulos, A., Allsop, J., Rutherford, M., Malik, S., Aljabar, P., & Hajnal, J. V. (2014). Resting State fMRI in the moving fetus: A robust framework for motion, bias field and spin history correction. *NeuroImage*, 101, 555–568. <https://doi.org/10.1016/j.neuroimage.2014.06.074>
- Fischi-Gomez, E., Muñoz-Moreno, E., Vasung, L., Griffa, A., Borradori-Tolsa, C., Monnier, M., Lazeyras, F., Thiran, J.-P., & Hüppi, P. S. (2016). Brain network characterization of high-risk preterm-born school-age children. *NeuroImage: Clinical*, 11, 195–209. <https://doi.org/10.1016/j.nicl.2016.02.001>
- Fischi-Gómez, E., Vasung, L., Meskaldji, D.-E., Lazeyras, F., Borradori-Tolsa, C., Hagmann, P., Barisnikov, K., Thiran, J.-P., & Hüppi, P. S. (2015). Structural Brain Connectivity in School-Age Preterm Infants Provides Evidence for Impaired Networks Relevant for Higher Order Cognitive Skills and Social Cognition. *Cerebral Cortex*, 25(9), 2793–2805. <https://doi.org/10.1093/cercor/bhu073>
- Fischl, B. (2004). Automatically Parcellating the Human Cerebral Cortex. *Cerebral Cortex*, 14(1), 11–22. <https://doi.org/10.1093/cercor/bhg087>
- Fischl, B. (2012). FreeSurfer. *NeuroImage*, 62(2), 774–781. <https://doi.org/10.1016/j.neuroimage.2012.01.021>
- Fitzgibbon, S. P., Harrison, S. J., Jenkinson, M., Baxter, L., Robinson, E. C., Bastiani, M., Bozek, J., Karolis, V., Cordero Grande, L., Price, A. N., Hughes, E., Makropoulos, A., Passerat-Palmbach, J., Schuh, A., Gao, J., Farahibozorg, S. R., O’Muirheartaigh, J., Ciarrusta, J., O’Keeffe, C., ...

- Andersson, J. (2020a). The developing Human Connectome Project (dHCP) automated resting-state functional processing framework for newborn infants. *NeuroImage*, 223(August), 117303. <https://doi.org/10.1016/j.neuroimage.2020.117303>
- Fitzgibbon, S. P., Harrison, S. J., Jenkinson, M., Baxter, L., Robinson, E. C., Bastiani, M., Bozek, J., Karolis, V., Cordero Grande, L., Price, A. N., Hughes, E., Makropoulos, A., Passerat-Palmbach, J., Schuh, A., Gao, J., Farahibozorg, S.-R., O'Muirheartaigh, J., Ciarrusta, J., O'Keeffe, C., ... Andersson, J. (2020b). The developing Human Connectome Project (dHCP) automated resting-state functional processing framework for newborn infants. *NeuroImage*, 223, 117303. <https://doi.org/10.1016/j.neuroimage.2020.117303>
- Flechsig, P. (1901). Developmental (myelogenetic) localisation of the cerebral cortex in the human subject. *Lancet*, 1027(9).
- Flechsig, P. (1920). *Anatomie des menschlichen Gehirns und Rückenmarks auf myelogenetischer Grundlage (Vol. 1): G. Thieme*.
- Fletcher, J. L., Makowiecki, K., Cullen, C. L., & Young, K. M. (2021). Oligodendrogenesis and myelination regulate cortical development, plasticity and circuit function. *Seminars in Cell & Developmental Biology*, 118, 14–23. <https://doi.org/10.1016/j.semcdb.2021.03.017>
- Foster-Cohen, S. H., Friesen, M. D., Champion, P. R., & Woodward, L. J. (2010). High Prevalence/Low Severity Language Delay in Preschool Children Born Very Preterm. *Journal of Developmental & Behavioral Pediatrics*, 31(8), 658–667. <https://doi.org/10.1097/DBP.0b013e3181e5ab7e>
- Fransson, P., Skiöld, B., Engström, M., Hallberg, B., Mosskin, M., Åden, U., Lagercrantz, H., & Blennow, M. (2009). Spontaneous Brain Activity in the Newborn Brain During Natural Sleep—An fMRI Study in Infants Born at Full Term. *Pediatric Research*, 66(3), 301–305. <https://doi.org/10.1203/PDR.0b013e3181b1bd84>
- Fransson, P., Skiöld, B., Horsch, S., Nordell, A., Blennow, M., Lagercrantz, H., & Åden, U. (2007). Resting-state networks in the infant brain. *Proceedings of the National Academy of Sciences*, 104(39), 15531–15536. <https://doi.org/10.1073/pnas.0704380104>
- Friedrichs-Maeder, C. L., Griffo, A., Schneider, J., Hüppi, P. S., Truttmann, A., & Hagmann, P. (2017). Exploring the role of white matter connectivity in cortex maturation. *PLOS ONE*, 12(5), e0177466. <https://doi.org/10.1371/journal.pone.0177466>
- Friston, K. J. (2011). Functional and Effective Connectivity: A Review. *Brain Connectivity*, 1(1), 13–36. <https://doi.org/10.1089/brain.2011.0008>
- Friston, K. J. (1994). Functional and effective connectivity in neuroimaging: a synthesis. *Hum Brain Mapp*, 2, 56–78.
- Fukutomi, H., Glasser, M. F., Zhang, H., Autio, J. A., Coalson, T. S., Okada, T., Togashi, K., Van Essen, D. C., & Hayashi, T. (2018). Neurite imaging reveals microstructural variations in human cerebral cortical gray matter. *NeuroImage*, 182, 488–499. <https://doi.org/10.1016/j.neuroimage.2018.02.017>
- Galdi, P., Blesa, M., Stoye, D. Q., Sullivan, G., Lamb, G. J., Quigley, A. J., Thrippleton, M. J., Bastin, M. E., & Boardman, J. P. (2020). Neonatal morphometric similarity mapping for predicting brain age and characterizing neuroanatomic variation associated with preterm birth. *NeuroImage: Clinical*, 25, 102195. <https://doi.org/10.1016/j.nicl.2020.102195>
- Gao, W., Alcauter, S., Elton, A., Hernandez-Castillo, C. R., Smith, J. K., Ramirez, J., & Lin, W. (2015). Functional Network Development During the First Year: Relative Sequence and Socioeconomic Correlations. *Cerebral Cortex*, 25(9), 2919–2928. <https://doi.org/10.1093/cercor/bhu088>
- Garel, C., Chantrel, E., Brisse, H., Elmaleh, M., Luton, D., Oury, J. F., Sebag, G., & Hassan, M. (2001). Fetal cerebral cortex: normal gestational landmarks identified using prenatal MR imaging. *AJNR. American Journal of Neuroradiology*, 22(1), 184–189.

- Geng, X., Gouttard, S., Sharma, A., Gu, H., Styner, M., Lin, W., Gerig, G., & Gilmore, J. H. (2012). Quantitative tract-based white matter development from birth to age 2 years. *NeuroImage*, 61(3), 542–557. <https://doi.org/10.1016/j.neuroimage.2012.03.057>
- Geng, X., Li, G., Lu, Z., Gao, W., Wang, L., Shen, D., Zhu, H., & Gilmore, J. H. (2016). Structural and Maturational Covariance in Early Childhood Brain Development. *Cerebral Cortex*, bhw022. <https://doi.org/10.1093/cercor/bhw022>
- Gerlings, J., Shollo, A., & Constantiou, I. (2021). *Reviewing the Need for Explainable Artificial Intelligence (xAI)*. <https://doi.org/10.24251/HICSS.2021.156>
- Geyer, S., Weiss, M., Reimann, K., Lohmann, G., & Turner, R. (2011). Microstructural Parcellation of the Human Cerebral Cortex – From Brodmann’s Post-Mortem Map to in vivo Mapping with High-Field Magnetic Resonance Imaging. *Frontiers in Human Neuroscience*, 5. <https://doi.org/10.3389/fnhum.2011.00019>
- Gilmore, J. H., Knickmeyer, R. C., & Gao, W. (2018). Imaging structural and functional brain development in early childhood. *Nature Reviews Neuroscience*, 19(3), 123–137. <https://doi.org/10.1038/nrn.2018.1>
- Gilmore, J. H., Shi, F., Woolson, S. L., Knickmeyer, R. C., Short, S. J., Lin, W., Zhu, H., Hamer, R. M., Styner, M., & Shen, D. (2012). Longitudinal Development of Cortical and Subcortical Gray Matter from Birth to 2 Years. *Cerebral Cortex*, 22(11), 2478–2485. <https://doi.org/10.1093/cercor/bhr327>
- Ginzburg, F., Aubrain, K., Leroy, F., Devisscher, L., Hertz-pannier, L., & Dubois, J. (2021). Exploring the cortex microstructure in newborns : A clustering approach of diffusion MRI parameters Institutions : First Author : *OHBM 2021*.
- Girard, G., Rafael-Patiño, J., Truffet, R., Aydogan, D. B., Adluru, N., Nair, V. A., Prabhakaran, V., Bendlin, B. B., Alexander, A. L., Bosticardo, S., Gabusi, I., Ocampo-Pineda, M., Battocchio, M., Piskorova, Z., Bontempi, P., Schiavi, S., Daducci, A., Stafiej, A., Ciupek, D., ... Thiran, J.-P. (2023). Tractography passes the test: Results from the diffusion-simulated connectivity (disco) challenge. *NeuroImage*, 277, 120231. <https://doi.org/10.1016/j.neuroimage.2023.120231>
- Girault, J. B., Munsell, B. C., Puechmaille, D., Goldman, B. D., Prieto, J. C., Styner, M., & Gilmore, J. H. (2019). White matter connectomes at birth accurately predict cognitive abilities at age 2. *NeuroImage*, 192, 145–155. <https://doi.org/10.1016/j.neuroimage.2019.02.060>
- Glasser, M. F., Coalson, T. S., Robinson, E. C., Hacker, C. D., Harwell, J., Yacoub, E., Ugurbil, K., Andersson, J., Beckmann, C. F., Jenkinson, M., Smith, S. M., & Van Essen, D. C. (2016). A multi-modal parcellation of human cerebral cortex. *Nature*, 536(7615), 171–178. <https://doi.org/10.1038/nature18933>
- Glover, G. H. (2011). Overview of Functional Magnetic Resonance Imaging. *Neurosurgery Clinics of North America*, 22(2), 133–139. <https://doi.org/10.1016/j.nec.2010.11.001>
- Goldenberg, R. L., Culhane, J. F., Iams, J. D., & Romero, R. (2008). Epidemiology and causes of preterm birth. *The Lancet*, 371(9606), 75–84. [https://doi.org/10.1016/S0140-6736\(08\)60074-4](https://doi.org/10.1016/S0140-6736(08)60074-4)
- Gondová, A., Neumane, S., Leprince, Y., Arichi, T., Mangin, J., & Dubois, J. (2023c). Predicting neurodevelopmental outcomes from the early sensorimotor structural connectivity. *OHBM 2023 Annual Meeting*.
- Gondová, A., Neumane, S., Leprince, Y., Hertz-Pannier, L., Arichi, T., & Dubois, J. (2023b). Structural connectivity of sensorimotor network: evaluating the impact of prematurity. *OHBM 2023 Annual Meeting*.
- Gondová, A., Neumane, S., Leprince, Y., Mangin, J., & Dubois, J. (2022). Infant cortical microstructure at term-equivalent age accurately predicts prematurity status at birth. *OHBM 2022 Annual Meeting*.

- Gondová, A., Neumane, S., Leprince, Y., Mangin, J.-F., Arichi, T., & Dubois, J. (2023a). Predicting neurodevelopmental outcomes from neonatal cortical microstructure: A conceptual replication study. *Neuroimage: Reports*, 3(2), 100170. <https://doi.org/10.1016/j.ynirp.2023.100170>
- Gordon, E. M., Laumann, T. O., Adeyemo, B., Huckins, J. F., Kelley, W. M., & Petersen, S. E. (2016). Generation and Evaluation of a Cortical Area Parcellation from Resting-State Correlations. *Cerebral Cortex*, 26(1), 288–303. <https://doi.org/10.1093/cercor/bhu239>
- Goulas, A., Uylings, H. B. M., & Stiers, P. (2012). Unravelling the Intrinsic Functional Organization of the Human Lateral Frontal Cortex: A Parcellation Scheme Based on Resting State fMRI. *Journal of Neuroscience*, 32(30), 10238–10252. <https://doi.org/10.1523/JNEUROSCI.5852-11.2012>
- Gousias, I. S., Edwards, A. D., Rutherford, M. A., Counsell, S. J., Hajnal, J. V., Rueckert, D., & Hammers, A. (2012). Magnetic resonance imaging of the newborn brain: Manual segmentation of labelled atlases in term-born and preterm infants. *NeuroImage*, 62(3), 1499–1509. <https://doi.org/10.1016/j.neuroimage.2012.05.083>
- Grayson, D. S., Ray, S., Carpenter, S., Iyer, S., Dias, T. G. C., Stevens, C., Nigg, J. T., & Fair, D. A. (2014). Structural and Functional Rich Club Organization of the Brain in Children and Adults. *PLoS ONE*, 9(2), e88297. <https://doi.org/10.1371/journal.pone.0088297>
- Greicius, M. D., Krasnow, B., Reiss, A. L., & Menon, V. (2003). Functional connectivity in the resting brain: A network analysis of the default mode hypothesis. *Proceedings of the National Academy of Sciences*, 100(1), 253–258. <https://doi.org/10.1073/pnas.0135058100>
- Greicius, M. D., Supekar, K., Menon, V., & Dougherty, R. F. (2009). Resting-State Functional Connectivity Reflects Structural Connectivity in the Default Mode Network. *Cerebral Cortex*, 19(1), 72–78. <https://doi.org/10.1093/cercor/bhn059>
- Grinberg, F., Farrher, E., Kaffanke, J., Oros-Peusquens, A.-M., & Shah, N. J. (2011). Non-Gaussian diffusion in human brain tissue at high b-factors as examined by a combined diffusion kurtosis and biexponential diffusion tensor analysis. *NeuroImage*, 57(3), 1087–1102. <https://doi.org/10.1016/j.neuroimage.2011.04.050>
- Guerrero, J. M., Adluru, N., Bendlin, B. B., Goldsmith, H. H., Schaefer, S. M., Davidson, R. J., Kecsckemeti, S. R., Zhang, H., & Alexander, A. L. (2019). Optimizing the intrinsic parallel diffusivity in NODDI: An extensive empirical evaluation. *PLOS ONE*, 14(9), e0217118. <https://doi.org/10.1371/journal.pone.0217118>
- Guilbert, J., Légaré, A., De Koninck, P., Desrosiers, P., & Desjardins, M. (2022). Toward an integrative neurovascular framework for studying brain networks. *Neurophotonics*, 9(03). <https://doi.org/10.1117/1.NPh.9.3.032211>
- Hagmann, C. F., De Vita, E., Bainbridge, A., Gunny, R., Kapetanakis, A. B., Chong, W. K., Cady, E. B., Gadian, D. G., & Robertson, N. J. (2009). T2 at MR Imaging Is an Objective Quantitative Measure of Cerebral White Matter Signal Intensity Abnormality in Preterm Infants at Term-equivalent Age. *Radiology*, 252(1), 209–217. <https://doi.org/10.1148/radiol.2522080589>
- Hagmann, P., Sporns, O., Madan, N., Cammoun, L., Pienaar, R., Wedeen, V. J., Meuli, R., Thiran, J.-P., & Grant, P. E. (2010). White matter maturation reshapes structural connectivity in the late developing human brain. *Proceedings of the National Academy of Sciences*, 107(44), 19067–19072. <https://doi.org/10.1073/pnas.1009073107>
- Haixiang, G., Yijing, L., Shang, J., Mingyun, G., Yuanyue, H., & Bing, G. (2017). Learning from class-imbalanced data: Review of methods and applications. *Expert Systems with Applications*, 73, 220–239. <https://doi.org/10.1016/j.eswa.2016.12.035>
- Hanganu-Opatz, I. L. (2010). Between molecules and experience: Role of early patterns of coordinated activity for the development of cortical maps and sensory abilities. *Brain Research Reviews*, 64(1), 160–176. <https://doi.org/10.1016/j.brainresrev.2010.03.005>

- Harrison, M. S., & Goldenberg, R. L. (2016). Global burden of prematurity. *Seminars in Fetal and Neonatal Medicine*, 21(2), 74–79. <https://doi.org/10.1016/j.siny.2015.12.007>
- Haslbeck, F. B., Jakab, A., Held, U., Bassler, D., Bucher, H.-U., & Hagmann, C. (2020). Creative music therapy to promote brain function and brain structure in preterm infants: A randomized controlled pilot study. *NeuroImage: Clinical*, 25, 102171. <https://doi.org/10.1016/j.nicl.2020.102171>
- He, L., Li, H., Chen, M., Wang, J., Altaye, M., Dillman, J. R., & Parikh, N. A. (2021). Deep Multimodal Learning From MRI and Clinical Data for Early Prediction of Neurodevelopmental Deficits in Very Preterm Infants. *Frontiers in Neuroscience*, 15. <https://doi.org/10.3389/fnins.2021.753033>
- He, L., Li, H., Holland, S. K., Yuan, W., Altaye, M., & Parikh, N. A. (2018). Early prediction of cognitive deficits in very preterm infants using functional connectome data in an artificial neural network framework. *NeuroImage: Clinical*, 18, 290–297. <https://doi.org/10.1016/j.nicl.2018.01.032>
- He, L., Li, H., Wang, J., Chen, M., Gozdas, E., Dillman, J. R., & Parikh, N. A. (2020). A multi-task, multi-stage deep transfer learning model for early prediction of neurodevelopment in very preterm infants. *Scientific Reports*, 10(1), 15072. <https://doi.org/10.1038/s41598-020-71914-x>
- He, L., & Parikh, N. A. (2015). Aberrant Executive and Frontoparietal Functional Connectivity in Very Preterm Infants With Diffuse White Matter Abnormalities. *Pediatric Neurology*, 53(4), 330–337. <https://doi.org/10.1016/j.pediatrneurol.2015.05.001>
- Heckemann, R. A., Hajnal, J. V., Aljabar, P., Rueckert, D., & Hammers, A. (2006). Automatic anatomical brain MRI segmentation combining label propagation and decision fusion. *NeuroImage*, 33(1), 115–126. <https://doi.org/10.1016/j.neuroimage.2006.05.061>
- Heineman, K. R., Schendelaar, P., Van den Heuvel, E. R., & Hadders-Algra, M. (2018). Motor development in infancy is related to cognitive function at 4 years of age. *Developmental Medicine & Child Neurology*, 60(11), 1149–1155. <https://doi.org/10.1111/dmcn.13761>
- Hermoye, L., Saint-Martin, C., Cosnard, G., Lee, S.-K., Kim, J., Nassogne, M.-C., Menten, R., Clapuyt, P., Donohue, P. K., Hua, K., Wakana, S., Jiang, H., van Zijl, P. C. M., & Mori, S. (2006). Pediatric diffusion tensor imaging: Normal database and observation of the white matter maturation in early childhood. *NeuroImage*, 29(2), 493–504. <https://doi.org/10.1016/j.neuroimage.2005.08.017>
- Hernandez-Fernandez, M., Reguly, I., Jbabdi, S., Giles, M., Smith, S., & Sotiropoulos, S. N. (2019). Using GPUs to accelerate computational diffusion MRI: From microstructure estimation to tractography and connectomes. *NeuroImage*, 188, 598–615. <https://doi.org/10.1016/j.neuroimage.2018.12.015>
- Hoff, G. E. A.-J., Van den Heuvel, M. P., Benders, M. J. N. L., Kersbergen, K. J., & De Vries, L. S. (2013). On development of functional brain connectivity in the young brain. *Frontiers in Human Neuroscience*, 7. <https://doi.org/10.3389/fnhum.2013.00650>
- Hotelling, H. (1933). Analysis of a complex of statistical variables into principal components. *Journal of Educational Psychology*, 24(6), 417–441. <https://doi.org/10.1037/h0071325>
- Howell, B. R., Styner, M. A., Gao, W., Yap, P.-T., Wang, L., Baluyot, K., Yacoub, E., Chen, G., Potts, T., Salzwedel, A., Li, G., Gilmore, J. H., Piven, J., Smith, J. K., Shen, D., Ugurbil, K., Zhu, H., Lin, W., & Elison, J. T. (2019). The UNC/UMN Baby Connectome Project (BCP): An overview of the study design and protocol development. *NeuroImage*, 185, 891–905. <https://doi.org/10.1016/j.neuroimage.2018.03.049>
- Huang, H., Jeon, T., Sedmak, G., Pletikos, M., Vasung, L., Xu, X., Yarowsky, P., Richards, L. J., Kostovic, I., Sestan, N., & Mori, S. (2013). Coupling Diffusion Imaging with Histological and Gene Expression Analysis to Examine the Dynamics of Cortical Areas across the Fetal Period of Human Brain Development. *Cerebral Cortex*, 23(11), 2620–2631. <https://doi.org/10.1093/cercor/bhs241>

- Huang, H., Xue, R., Zhang, J., Ren, T., Richards, L. J., Yarowsky, P., Miller, M. I., & Mori, S. (2009). Anatomical Characterization of Human Fetal Brain Development with Diffusion Tensor Magnetic Resonance Imaging. *The Journal of Neuroscience*, 29(13), 4263–4273. <https://doi.org/10.1523/JNEUROSCI.2769-08.2009>
- Huang, Y., Wu, Z., Wang, F., Hu, D., Li, T., Guo, L., Wang, L., Lin, W., & Li, G. (2022). Mapping developmental regionalization and patterns of cortical surface area from 29 post-menstrual weeks to 2 years of age. *Proceedings of the National Academy of Sciences*, 119(33). <https://doi.org/10.1073/pnas.2121748119>
- Hughes, A. J., Redsell, S. A., & Glazebrook, C. (2016). Motor Development Interventions for Preterm Infants: A Systematic Review and Meta-analysis. *Pediatrics*, 138(4). <https://doi.org/10.1542/peds.2016-0147>
- Hughes, E. J., Winchman, T., Padormo, F., Teixeira, R., Wurie, J., Sharma, M., Fox, M., Hutter, J., Cordero-Grande, L., Price, A. N., Allsop, J., Bueno-Conde, J., Tusor, N., Arichi, T., Edwards, A. D., Rutherford, M. A., Counsell, S. J., & Hajnal, J. V. (2017). A dedicated neonatal brain imaging system. *Magnetic Resonance in Medicine*, 78(2), 794–804. <https://doi.org/10.1002/mrm.26462>
- Hüppi, P. S., Schuknecht, B., Boesch, C., Bossi, E., Felblinger, J., Fusch, C., & Herschkowitz, N. (1996). Structural and Neurobehavioral Delay in Postnatal Brain Development of Preterm Infants. *Pediatric Research*, 39(5), 895–901. <https://doi.org/10.1203/00006450-199605000-00026>
- Hutter, J., Tournier, J. D., Price, A. N., Cordero-Grande, L., Hughes, E. J., Malik, S., Steinweg, J., Bastiani, M., Sotiropoulos, S. N., Jbabdi, S., Andersson, J., Edwards, A. D., & Hajnal, J. V. (2018). Time-efficient and flexible design of optimized multishell HARDI diffusion. *Magnetic Resonance in Medicine*, 79(3), 1276–1292. <https://doi.org/10.1002/mrm.26765>
- Ide, J. S., Shenoy, P., Yu, A. J., & Li, C. R. (2013). Bayesian Prediction and Evaluation in the Anterior Cingulate Cortex. *The Journal of Neuroscience*, 33(5), 2039–2047. <https://doi.org/10.1523/JNEUROSCI.2201-12.2013>
- Inder, T. E., de Vries, L. S., Ferriero, D. M., Grant, P. E., Ment, L. R., Miller, S. P., & Volpe, J. J. (2021). Neuroimaging of the Preterm Brain: Review and Recommendations. *The Journal of Pediatrics*, 237, 276–287.e4. <https://doi.org/10.1016/j.jpeds.2021.06.014>
- Irzan, H., Molteni, E., Hütel, M., Ourselin, S., Marlow, N., & Melbourne, A. (2021). White matter analysis of the extremely preterm born adult brain. *NeuroImage*, 237, 118112. <https://doi.org/10.1016/j.neuroimage.2021.118112>
- Jaekel, J., Baumann, N., Bartmann, P., & Wolke, D. (2019). General cognitive but not mathematic abilities predict very preterm and healthy term born adults' wealth. *PLOS ONE*, 14(3), e0212789. <https://doi.org/10.1371/journal.pone.0212789>
- Jager, J., Putnick, D. L., & Bornstein, M. H. (2017). II. MORE THAN JUST CONVENIENT: THE SCIENTIFIC MERITS OF HOMOGENEOUS CONVENIENCE SAMPLES. *Monographs of the Society for Research in Child Development*, 82(2), 13–30. <https://doi.org/10.1111/mono.12296>
- Jaimes, C., Cheng, H. H., Soul, J., Ferradal, S., Rath, Y., Gagoski, B., Newburger, J. W., Grant, P. E., & Zöllei, L. (2018). Probabilistic tractography-based thalamic parcellation in healthy newborns and newborns with congenital heart disease. *Journal of Magnetic Resonance Imaging*, 47(6), 1626–1637. <https://doi.org/10.1002/jmri.25875>
- Jaimes, C., Machado-Rivas, F., Afacan, O., Khan, S., Marami, B., Ortinau, C. M., Rollins, C. K., Velasco-Annis, C., Warfield, S. K., & Gholipour, A. (2020). In vivo characterization of emerging white matter microstructure in the fetal brain in the third trimester. *Human Brain Mapping*, 41(12), 3177–3185. <https://doi.org/10.1002/hbm.25006>
- Jain, A. K. (2008). Data clustering: 50 years beyond K-means. *Pattern Recognit. Lett.*, 31, 651–666.
- Jakab, A. (2019). Developmental Pathoconnectomics and Advanced Fetal MRI. *Topics in Magnetic Resonance Imaging*, 28(5), 275–284. <https://doi.org/10.1097/RMR.0000000000000220>

- Jakab, A., Pogledic, I., Schwartz, E., Gruber, G., Mitter, C., Brugger, P. C., Langs, G., Schöpf, V., Kasprian, G., & Prayer, D. (2015). Fetal Cerebral Magnetic Resonance Imaging Beyond Morphology. *Seminars in Ultrasound, CT and MRI*, 36(6), 465–475. <https://doi.org/10.1053/j.sult.2015.06.003>
- Jakab, A., Schwartz, E., Kasprian, G., Gruber, G. M., Prayer, D., Schöpf, V., & Langs, G. (2014). Fetal functional imaging portrays heterogeneous development of emerging human brain networks. *Frontiers in Human Neuroscience*, 8. <https://doi.org/10.3389/fnhum.2014.00852>
- Jakab, A., Tuura, R., Kellenberger, C., & Scheer, I. (2017). In utero diffusion tensor imaging of the fetal brain: A reproducibility study. *NeuroImage: Clinical*, 15, 601–612. <https://doi.org/10.1016/j.nicl.2017.06.013>
- Janjic, T., Pereverzyev, S., Hammerl, M., Neubauer, V., Lerchner, H., Wallner, V., Steiger, R., Kiechl-Kohlendorfer, U., Zimmermann, M., Buchheim, A., Grams, A. E., & Gizewski, E. R. (2020). Feed-forward neural networks using cerebral MR spectroscopy and DTI might predict neurodevelopmental outcome in preterm neonates. *European Radiology*, 30(12), 6441–6451. <https://doi.org/10.1007/s00330-020-07053-8>
- Jbabdi, S., Sotiropoulos, S. N., Savio, A. M., Graña, M., & Behrens, T. E. J. (2012). Model-based analysis of multishell diffusion MR data for tractography: How to get over fitting problems. *Magnetic Resonance in Medicine*, 68(6), 1846–1855. <https://doi.org/10.1002/mrm.24204>
- Jelescu, I. O., Veraart, J., Adisetiyo, V., Milla, S. S., Novikov, D. S., & Fieremans, E. (2015). One diffusion acquisition and different white matter models: How does microstructure change in human early development based on WMTI and NODDI? *NeuroImage*, 107, 242–256. <https://doi.org/10.1016/j.neuroimage.2014.12.009>
- Jenkinson, M., Bannister, P., Brady, M., & Smith, S. (2002). Improved Optimization for the Robust and Accurate Linear Registration and Motion Correction of Brain Images. *NeuroImage*, 17(2), 825–841. <https://doi.org/10.1006/nimg.2002.1132>
- Jenkinson, M., & Smith, S. (2001). A global optimisation method for robust affine registration of brain images. *Medical Image Analysis*, 5(2), 143–156. [https://doi.org/10.1016/S1361-8415\(01\)00036-6](https://doi.org/10.1016/S1361-8415(01)00036-6)
- Jensen, J. H., & Helpert, J. A. (2010). MRI quantification of non-Gaussian water diffusion by kurtosis analysis. *NMR in Biomedicine*, 23(7), 698–710. <https://doi.org/10.1002/nbm.1518>
- Jensen, J. H., Helpert, J. A., Ramani, A., Lu, H., & Kaczynski, K. (2005). Diffusional kurtosis imaging: The quantification of non-gaussian water diffusion by means of magnetic resonance imaging. *Magnetic Resonance in Medicine*, 53(6), 1432–1440. <https://doi.org/10.1002/mrm.20508>
- Jeurissen, B., Descoteaux, M., Mori, S., & Leemans, A. (2019). Diffusion MRI fiber tractography of the brain. *NMR in Biomedicine*, 32(4). <https://doi.org/10.1002/nbm.3785>
- Jeurissen, B., Leemans, A., Tournier, J.-D., Jones, D. K., & Sijbers, J. (2013). Investigating the prevalence of complex fiber configurations in white matter tissue with diffusion magnetic resonance imaging. *Human Brain Mapping*, 34(11), 2747–2766. <https://doi.org/10.1002/hbm.22099>
- Jeurissen, B., Tournier, J.-D., Dhollander, T., Connelly, A., & Sijbers, J. (2014). Multi-tissue constrained spherical deconvolution for improved analysis of multi-shell diffusion MRI data. *NeuroImage*, 103, 411–426. <https://doi.org/10.1016/j.neuroimage.2014.07.061>
- Jha, S. C., Xia, K., Ahn, M., Girault, J. B., Li, G., Wang, L., Shen, D., Zou, F., Zhu, H., Styner, M., Gilmore, J. H., & Knickmeyer, R. C. (2019). Environmental Influences on Infant Cortical Thickness and Surface Area. *Cerebral Cortex*, 29(3), 1139–1149. <https://doi.org/10.1093/cercor/bhy020>
- Jones, D. K. (2008). Tractography Gone Wild: Probabilistic Fibre Tracking Using the Wild Bootstrap With Diffusion Tensor MRI. *IEEE Transactions on Medical Imaging*, 27(9), 1268–1274. <https://doi.org/10.1109/TMI.2008.922191>

- Jones, D. K., & Cercignani, M. (2010). Twenty-five pitfalls in the analysis of diffusion MRI data. *NMR in Biomedicine*, 23(7), 803–820. <https://doi.org/10.1002/nbm.1543>
- Jones, D. K., Simmons, A., Williams, S. C. R., & Horsfield, M. A. (1999). Non-invasive assessment of axonal fiber connectivity in the human brain via diffusion tensor MRI. *Magnetic Resonance in Medicine*, 42(1), 37–41. [https://doi.org/10.1002/\(SICI\)1522-2594\(199907\)42:1<37::AID-MRM7>3.0.CO;2-O](https://doi.org/10.1002/(SICI)1522-2594(199907)42:1<37::AID-MRM7>3.0.CO;2-O)
- Judas, M., Rados, M., Jovanov-Milosevic, N., Hrabac, P., Stern-Padovan, R., & Kostovic, I. (2005). Structural, immunocytochemical, and mr imaging properties of periventricular crossroads of growing cortical pathways in preterm infants. *AJNR. American Journal of Neuroradiology*, 26(10), 2671–2684.
- Jung, W. H., Jang, J. H., Park, J. W., Kim, E., Goo, E.-H., Im, O.-S., & Kwon, J. S. (2014). Unravelling the Intrinsic Functional Organization of the Human Striatum: A Parcellation and Connectivity Study Based on Resting-State fMRI. *PLoS ONE*, 9(9), e106768. <https://doi.org/10.1371/journal.pone.0106768>
- Kanel, D., Counsell, S. J., & Nosarti, C. (2021). Advances in functional and diffusion neuroimaging research into the long-term consequences of very preterm birth. *Journal of Perinatology*, 41(4), 689–706. <https://doi.org/10.1038/s41372-020-00865-y>
- Kang, H. J., Kawasawa, Y. I., Cheng, F., Zhu, Y., Xu, X., Li, M., Sousa, A. M. M., Pletikos, M., Meyer, K. A., Sedmak, G., Guennel, T., Shin, Y., Johnson, M. B., Krsnik, Ž., Mayer, S., Fertuzinhos, S., Umlauf, S., Lisgo, S. N., Vortmeyer, A., ... Šestan, N. (2011). Spatio-temporal transcriptome of the human brain. *Nature*, 478(7370), 483–489. <https://doi.org/10.1038/nature10523>
- Kapoor, S., & Narayanan, A. (2022). Leakage and the Reproducibility Crisis in ML-based Science. *ArXiv*.
- Karimi, D., Vasung, L., Jaimes, C., Machado-Rivas, F., Khan, S., Warfield, S. K., & Gholipour, A. (2021). A machine learning-based method for estimating the number and orientations of major fascicles in diffusion-weighted magnetic resonance imaging. *Medical Image Analysis*, 72, 102129. <https://doi.org/10.1016/j.media.2021.102129>
- Karolis, V. R., Fitzgibbon, S. P., Cordero-Grande, L., Farahibozorg, S.-R., Price, A. N., Hughes, E. J., Fetit, A. E., Kyriakopoulou, V., Pietsch, M., Rutherford, M. A., Rueckert, D., Hajnal, J. V., Edwards, A. D., O’Muirheartaigh, J., Duff, E. P., & Arichi, T. (2023). Maturation networks of human fetal brain activity reveal emerging connectivity patterns prior to ex-utero exposure. *Communications Biology*, 6(1), 661. <https://doi.org/10.1038/s42003-023-04969-x>
- Kawahara, J., Brown, C. J., Miller, S. P., Booth, B. G., Chau, V., Grunau, R. E., Zwicker, J. G., & Hamarneh, G. (2017). BrainNetCNN: Convolutional neural networks for brain networks; towards predicting neurodevelopment. *NeuroImage*, 146, 1038–1049. <https://doi.org/10.1016/j.neuroimage.2016.09.046>
- Kellner, E., Dhital, B., Kiselev, V. G., & Reiser, M. (2016). Gibbs-ringing artifact removal based on local subvoxel-shifts. *Magnetic Resonance in Medicine*, 76(5), 1574–1581. <https://doi.org/10.1002/mrm.26054>
- Kesler, S. R., Reiss, A. L., Vohr, B., Watson, C., Schneider, K. C., Katz, K. H., Maller-Kesselman, J., Silbereis, J., Constable, R. T., Makuch, R. W., & Ment, L. R. (2008). Brain Volume Reductions within Multiple Cognitive Systems in Male Preterm Children at Age Twelve. *The Journal of Pediatrics*, 152(4), 513–520.e1. <https://doi.org/10.1016/j.jpeds.2007.08.009>
- Keunen, K., Counsell, S. J., & Benders, M. J. N. L. (2017). The emergence of functional architecture during early brain development. *NeuroImage*, 160, 2–14. <https://doi.org/10.1016/j.neuroimage.2017.01.047>
- Khan, S., Vasung, L., Marami, B., Rollins, C. K., Afacan, O., Ortinau, C. M., Yang, E., Warfield, S. K., & Gholipour, A. (2019). Fetal brain growth portrayed by a spatiotemporal diffusion tensor MRI

- atlas computed from in utero images. *NeuroImage*, 185, 593–608. <https://doi.org/10.1016/j.neuroimage.2018.08.030>
- Khosla, M., Jamison, K., Ngo, G. H., Kuceyeski, A., & Sabuncu, M. R. (2019). Machine learning in resting-state fMRI analysis. *Magnetic Resonance Imaging*, 64, 101–121. <https://doi.org/10.1016/j.mri.2019.05.031>
- Khurana, S., Kane, A. E., Brown, S. E., Tarver, T., & Dusing, S. C. (2020). Effect of neonatal therapy on the motor, cognitive, and behavioral development of infants born preterm: a systematic review. *Developmental Medicine & Child Neurology*, 62(6), 684–692. <https://doi.org/10.1111/dmcn.14485>
- Kidokoro, H., Anderson, P. J., Doyle, L. W., Woodward, L. J., Neil, J. J., & Inder, T. E. (2014). Brain Injury and Altered Brain Growth in Preterm Infants: Predictors and Prognosis. *Pediatrics*, 134(2), e444–e453. <https://doi.org/10.1542/peds.2013-2336>
- Kimpton, J. A., Batalle, D., Barnett, M. L., Hughes, E. J., Chew, A. T. M., Falconer, S., Tournier, J. D., Alexander, D., Zhang, H., Edwards, A. D., & Counsell, S. J. (2021). Diffusion magnetic resonance imaging assessment of regional white matter maturation in preterm neonates. *Neuroradiology*, 63(4), 573–583. <https://doi.org/10.1007/s00234-020-02584-9>
- Kinney, H. C., Ann brody, B., Kloman, A. S., & Gilles, F. H. (1988). Sequence of Central Nervous System Myelination in Human Infancy. II. Patterns of Myelination in Autopsied Infants. *Journal of Neuropathology and Experimental Neurology*, 47(3), 217–234. <https://doi.org/10.1097/00005072-198805000-00003>
- Klein, A., & Tourville, J. (2012). 101 Labeled Brain Images and a Consistent Human Cortical Labeling Protocol. *Frontiers in Neuroscience*, 6. <https://doi.org/10.3389/fnins.2012.00171>
- Kline, J. E., Illapani, V. S. P., Li, H., He, L., Yuan, W., & Parikh, N. A. (2021). Diffuse white matter abnormality in very preterm infants at term reflects reduced brain network efficiency. *NeuroImage: Clinical*, 31, 102739. <https://doi.org/10.1016/j.nicl.2021.102739>
- Kline, J. E., Yuan, W., Harpster, K., Altaye, M., & Parikh, N. A. (2021). Association between brain structural network efficiency at term-equivalent age and early development of cerebral palsy in very preterm infants. *NeuroImage*, 245(November), 118688. <https://doi.org/10.1016/j.neuroimage.2021.118688>
- Kolasinski, J., Takahashi, E., Stevens, A. A., Benner, T., Fischl, B., Zöllei, L., & Grant, P. E. (2013). Radial and tangential neuronal migration pathways in the human fetal brain: Anatomically distinct patterns of diffusion MRI coherence. *NeuroImage*, 79, 412–422. <https://doi.org/10.1016/j.neuroimage.2013.04.125>
- Korom, M., Camacho, M. C., Filippi, C. A., Licandro, R., Moore, L. A., Dufford, A., Zöllei, L., Graham, A. M., Spann, M., Howell, B., Shultz, S., & Scheinost, D. (2022). Dear reviewers: Responses to common reviewer critiques about infant neuroimaging studies. *Developmental Cognitive Neuroscience*, 53, 101055. <https://doi.org/10.1016/j.dcn.2021.101055>
- Kostovic, I., Kostovic-Srzentic, M., Benjak, V., Jovanov-Milosevic, N., & Rados, M. (2014). Developmental Dynamics of Radial Vulnerability in the Cerebral Compartments in Preterm Infants and Neonates. *Frontiers in Neurology*, 5. <https://doi.org/10.3389/fneur.2014.00139>
- Kostović, I. (2020). The enigmatic fetal subplate compartment forms an early tangential cortical nexus and provides the framework for construction of cortical connectivity. *Progress in Neurobiology*, 194, 101883. <https://doi.org/10.1016/j.pneurobio.2020.101883>
- Kostović, I., & Jovanov-Milošević, N. (2006). The development of cerebral connections during the first 20–45 weeks' gestation. *Seminars in Fetal and Neonatal Medicine*, 11(6), 415–422. <https://doi.org/10.1016/j.siny.2006.07.001>

- Kostović, I., & Judaš, M. (2010). The development of the subplate and thalamocortical connections in the human foetal brain. *Acta Paediatrica*, 99(8), 1119–1127. <https://doi.org/10.1111/j.1651-2227.2010.01811.x>
- Kostović, I., & Judaš, M. (2015). Embryonic and Fetal Development of the Human Cerebral Cortex. In *Brain Mapping* (pp. 167–175). Elsevier. <https://doi.org/10.1016/B978-0-12-397025-1.00193-7>
- Kostovic, I., Judas, M., Rados, M., & Hrabac, P. (2002). Laminar Organization of the Human Fetal Cerebrum Revealed by Histochemical Markers and Magnetic Resonance Imaging. *Cerebral Cortex*, 12(5), 536–544. <https://doi.org/10.1093/cercor/12.5.536>
- Kostović, I., Petanjek, Z., & Judaš, M. (1993). Early areal differentiation of the human cerebral cortex: Entorhinal area. *Hippocampus*, 3(4), 447–458. <https://doi.org/10.1002/hipo.450030406>
- Kostovic, I., & Rakic, P. (1980). Cytology and time of origin of interstitial neurons in the white matter in infant and adult human and monkey telencephalon. *Journal of Neurocytology*, 9(2), 219–242. <https://doi.org/10.1007/BF01205159>
- Kostovic, I., & Rakic, P. (1990). Developmental history of the transient subplate zone in the visual and somatosensory cortex of the macaque monkey and human brain. *The Journal of Comparative Neurology*, 297(3), 441–470. <https://doi.org/10.1002/cne.902970309>
- Kostović, I., Sedmak, G., & Judaš, M. (2019). Neural histology and neurogenesis of the human fetal and infant brain. *NeuroImage*, 188, 743–773. <https://doi.org/10.1016/j.neuroimage.2018.12.043>
- Kostovic, I., & Vasung, L. (2009). Insights From In Vitro Fetal Magnetic Resonance Imaging of Cerebral Development. *Seminars in Perinatology*, 33(4), 220–233. <https://doi.org/10.1053/j.semperi.2009.04.003>
- Kriegstein, A., & Alvarez-Buylla, A. (2009). The Glial Nature of Embryonic and Adult Neural Stem Cells. *Annual Review of Neuroscience*, 32(1), 149–184. <https://doi.org/10.1146/annurev.neuro.051508.135600>
- Kroll, J., Karolis, V., Brittain, P. J., Tseng, C.-E. J., Froudust-Walsh, S., Murray, R. M., & Nosarti, C. (2017). Real-Life Impact of Executive Function Impairments in Adults Who Were Born Very Preterm. *Journal of the International Neuropsychological Society*, 23(5), 381–389. <https://doi.org/10.1017/S1355617717000169>
- Krsnik, Ž., Majić, V., Vasung, L., Huang, H., & Kostović, I. (2017). Growth of Thalamocortical Fibers to the Somatosensory Cortex in the Human Fetal Brain. *Frontiers in Neuroscience*, 11. <https://doi.org/10.3389/fnins.2017.00233>
- Kuban, K., Sanocka, U., Leviton, A., Allred, E. N., Pagano, M., Dammann, O., Share, J., Rosenfeld, D., Abiri, M., DiSalvo, D., Doubilet, P., Kairam, R., Kazam, E., Kirpekar, M., & Schonfeld, S. (1999). White matter disorders of prematurity: Association with intraventricular hemorrhage and ventriculomegaly. *The Journal of Pediatrics*, 134(5), 539–546. [https://doi.org/10.1016/S0022-3476\(99\)70237-4](https://doi.org/10.1016/S0022-3476(99)70237-4)
- Kuklisova-Murgasova, M., Lockwood Estrin, G., Nunes, R. G., Malik, S. J., Rutherford, M. A., Rueckert, D., & Hajnal, J. V. (2018). Distortion Correction in Fetal EPI Using Non-Rigid Registration With a Laplacian Constraint. *IEEE Transactions on Medical Imaging*, 37(1), 12–19. <https://doi.org/10.1109/TMI.2017.2667227>
- Kulikova, S., Hertz-Pannier, L., Dehaene-Lambertz, G., Buzmakov, A., Poupon, C., & Dubois, J. (2015). Multi-parametric evaluation of the white matter maturation. *Brain Structure and Function*, 220(6), 3657–3672. <https://doi.org/10.1007/s00429-014-0881-y>
- Kunz, N., Zhang, H., Vasung, L., O'Brien, K. R., Assaf, Y., Lazeyras, F., Alexander, D. C., & Hüppi, P. S. (2014). Assessing white matter microstructure of the newborn with multi-shell diffusion MRI and biophysical compartment models. *NeuroImage*, 96, 288–299. <https://doi.org/10.1016/j.neuroimage.2014.03.057>

- Lacoste, B., Comin, C. H., Ben-Zvi, A., Kaeser, P. S., Xu, X., Costa, L. da F., & Gu, C. (2014). Sensory-Related Neural Activity Regulates the Structure of Vascular Networks in the Cerebral Cortex. *Neuron*, 83(5), 1117–1130. <https://doi.org/10.1016/j.neuron.2014.07.034>
- Lagercrantz, H. (2016). *Infant Brain Development: Formation of the Mind and the Emergence of Consciousness*. Springer.
- Lagercrantz, H., & Changeux, J.-P. (2009). The Emergence of Human Consciousness: From Fetal to Neonatal Life. *Pediatric Research*, 65(3), 255–260. <https://doi.org/10.1203/PDR.0b013e3181973b0d>
- Larivière, S., Vos de Wael, R., Hong, S.-J., Paquola, C., Tavakol, S., Lowe, A. J., Schrader, D. V., & Bernhardt, B. C. (2020). Multiscale Structure–Function Gradients in the Neonatal Connectome. *Cerebral Cortex*, 30(1), 47–58. <https://doi.org/10.1093/cercor/bhz069>
- Lean, R. E., Han, R. H., Smyser, T. A., Kenley, J. K., Shimony, J. S., Rogers, C. E., Limbrick, D. D., & Smyser, C. D. (2019). Altered neonatal white and gray matter microstructure is associated with neurodevelopmental impairments in very preterm infants with high-grade brain injury. *Pediatric Research*, 86(3), 365–374. <https://doi.org/10.1038/s41390-019-0461-1>
- Lebel, C., Gee, M., Camicioli, R., Wieler, M., Martin, W., & Beaulieu, C. (2012). Diffusion tensor imaging of white matter tract evolution over the lifespan. *NeuroImage*, 60(1), 340–352. <https://doi.org/10.1016/j.neuroimage.2011.11.094>
- Lebenberg, J., Mangin, J.-F., Thirion, B., Poupon, C., Hertz-Pannier, L., Leroy, F., Adibpour, P., Dehaene-Lambertz, G., & Dubois, J. (2019). Mapping the asynchrony of cortical maturation in the infant brain: A MRI multi-parametric clustering approach. *NeuroImage*, 185, 641–653. <https://doi.org/10.1016/j.neuroimage.2018.07.022>
- Lee, J. Y., Park, H.-K., & Lee, H. J. (2019). Accelerated Small-World Property of Structural Brain Networks in Preterm Infants at Term-Equivalent Age. *Neonatology*, 115(2), 99–107. <https://doi.org/10.1159/000493087>
- Lee, S. J., Ralston, H. J. P., Drey, E. A., Partridge, J. C., & Rosen, M. A. (2005). Fetal Pain. *JAMA*, 294(8), 947. <https://doi.org/10.1001/jama.294.8.947>
- Lewis, T. L., Courchet, J., & Polleux, F. (2013). Cellular and molecular mechanisms underlying axon formation, growth, and branching. *Journal of Cell Biology*, 202(6), 837–848. <https://doi.org/10.1083/jcb.201305098>
- Li, K., Guo, L., Nie, J., Li, G., & Liu, T. (2009). Review of methods for functional brain connectivity detection using fMRI. *Computerized Medical Imaging and Graphics*, 33(2), 131–139. <https://doi.org/10.1016/j.compmedimag.2008.10.011>
- Li, K., Sun, Z., Han, Y., Gao, L., Yuan, L., & Zeng, D. (2015). Fractional anisotropy alterations in individuals born preterm: a diffusion tensor imaging meta-analysis. *Developmental Medicine & Child Neurology*, 57(4), 328–338. <https://doi.org/10.1111/dmcn.12618>
- Li, M., Xu, X., Cao, Z., Chen, R., Zhao, R., Zhao, Z., Dang, X., Oishi, K., & Wu, D. (2023). Multi-modal multi-resolution atlas of the human neonatal cerebral cortex based on microstructural similarity. *NeuroImage*, 272, 120071. <https://doi.org/10.1016/j.neuroimage.2023.120071>
- Li, X., Li, M., Wang, M., Wu, F., Liu, H., Sun, Q., Zhang, Y., Liu, C., Jin, C., & Yang, J. (2022). Mapping white matter maturational processes and degrees on neonates by diffusion kurtosis imaging with multiparametric analysis. *Human Brain Mapping*, 43(2), 799–815. <https://doi.org/10.1002/hbm.25689>
- Liang, W., Yu, Q., Wang, W., Dhollander, T., Suluba, E., Li, Z., Xu, F., Hu, Y., Tang, Y., & Liu, S. (2022). A comparative study of the superior longitudinal fasciculus subdivisions between neonates and young adults. *Brain Structure and Function*, 227(8), 2713–2730. <https://doi.org/10.1007/s00429-022-02565-z>

- Liégeois, R., Santos, A., Matta, V., Van De Ville, D., & Sayed, A. H. (2020). Revisiting correlation-based functional connectivity and its relationship with structural connectivity. *Network Neuroscience*, 4(4), 1235–1251. https://doi.org/10.1162/netn_a_00166
- Lin, Z., Gong, T., Wang, K., Li, Z., He, H., Tong, Q., Yu, F., & Zhong, J. (2019). Fast learning of fiber orientation distribution function for <scp>MR</scp> tractography using convolutional neural network. *Medical Physics*, 46(7), 3101–3116. <https://doi.org/10.1002/mp.13555>
- Lindström, K., Lindblad, F., & Hjern, A. (2011). Preterm Birth and Attention-Deficit/Hyperactivity Disorder in Schoolchildren. *Pediatrics*, 127(5), 858–865. <https://doi.org/10.1542/peds.2010-1279>
- Linsell, L., Malouf, R., Morris, J., Kurinczuk, J. J., & Marlow, N. (2015). Prognostic Factors for Poor Cognitive Development in Children Born Very Preterm or With Very Low Birth Weight. *JAMA Pediatrics*, 169(12), 1162. <https://doi.org/10.1001/jamapediatrics.2015.2175>
- Lobo, M. A., Harbourne, R. T., Dusing, S. C., & McCoy, S. W. (2013). Grounding Early Intervention: Physical Therapy Cannot Just Be About Motor Skills Anymore. *Physical Therapy*, 93(1), 94–103. <https://doi.org/10.2522/ptj.20120158>
- Longo, S., Caporali, C., Pisoni, C., Borghesi, A., Perotti, G., Tritto, G., Olivieri, I., La Piana, R., Tonduti, D., Decio, A., Ariaudo, G., Spairani, S., Naboni, C., Gardella, B., Spinillo, A., Manzoni, F., Tinelli, C., Stronati, M., & Orcesi, S. (2021). Neurodevelopmental outcome of preterm very low birth weight infants admitted to an Italian tertiary center over an 11-year period. *Scientific Reports*, 11(1), 16316. <https://doi.org/10.1038/s41598-021-95864-0>
- Lowe, M. J. (2012). The emergence of doing “nothing” as a viable paradigm design. *NeuroImage*, 62(2), 1146–1151. <https://doi.org/10.1016/j.neuroimage.2012.01.014>
- Lu, D., He, L., Xiang, W., Ai, W.-M., Cao, Y., Wang, X.-S., Pan, A., Luo, X.-G., Li, Z., & Yan, X.-X. (2013). Somal and Dendritic Development of Human CA3 Pyramidal Neurons From Midgestation to Middle Childhood: A Quantitative Golgi Study. *The Anatomical Record: Advances in Integrative Anatomy and Evolutionary Biology*, 296(1), 123–132. <https://doi.org/10.1002/ar.22616>
- Luhmann, H. J., Sinning, A., Yang, J.-W., Reyes-Puerta, V., Stüttgen, M. C., Kirischuk, S., & Kilb, W. (2016). Spontaneous Neuronal Activity in Developing Neocortical Networks: From Single Cells to Large-Scale Interactions. *Frontiers in Neural Circuits*, 10. <https://doi.org/10.3389/fncir.2016.00040>
- Lund, L. K., Vik, T., Skranes, J., Brubakk, A.-M., & Indredavik, M. S. (2011). Psychiatric morbidity in two low birth weight groups assessed by diagnostic interview in young adulthood. *Acta Paediatrica*, 100(4), 598–604. <https://doi.org/10.1111/j.1651-2227.2010.02111.x>
- Lundberg, S. M., Erion, G., Chen, H., DeGrave, A., Prutkin, J. M., Nair, B., Katz, R., Himmelfarb, J., Bansal, N., & Lee, S.-I. (2020). From local explanations to global understanding with explainable AI for trees. *Nature Machine Intelligence*, 2(1), 56–67. <https://doi.org/10.1038/s42256-019-0138-9>
- Lundequist, A., Böhm, B., Lagercrantz, H., Forssberg, H., & Smedler, A. (2015). Cognitive outcome varies in adolescents born preterm, depending on gestational age, intrauterine growth and neonatal complications. *Acta Paediatrica*, 104(3), 292–299. <https://doi.org/10.1111/apa.12864>
- Luu, T. M., Rehman Mian, M. O., & Nuyt, A. M. (2017). Long-Term Impact of Preterm Birth. *Clinics in Perinatology*, 44(2), 305–314. <https://doi.org/10.1016/j.clp.2017.01.003>
- Lyall, A. E., Shi, F., Geng, X., Woolson, S., Li, G., Wang, L., Hamer, R. M., Shen, D., & Gilmore, J. H. (2015). Dynamic Development of Regional Cortical Thickness and Surface Area in Early Childhood. *Cerebral Cortex*, 25(8), 2204–2212. <https://doi.org/10.1093/cercor/bhu027>
- Maalouf, E. F., Duggan, P. J., Rutherford, M. A., Counsell, S. J., Fletcher, A. M., Battin, M., Cowan, F., & Edwards, A. D. (1999). Magnetic resonance imaging of the brain in a cohort of extremely

- preterm infants. *The Journal of Pediatrics*, 135(3), 351–357. [https://doi.org/10.1016/S0022-3476\(99\)70133-2](https://doi.org/10.1016/S0022-3476(99)70133-2)
- Maier-Hein, K. H., Neher, P. F., Houde, J.-C., Côté, M.-A., Garyfallidis, E., Zhong, J., Chamberland, M., Yeh, F.-C., Lin, Y.-C., Ji, Q., Reddick, W. E., Glass, J. O., Chen, D. Q., Feng, Y., Gao, C., Wu, Y., Ma, J., He, R., Li, Q., ... Descoteaux, M. (2017). The challenge of mapping the human connectome based on diffusion tractography. *Nature Communications*, 8(1), 1349. <https://doi.org/10.1038/s41467-017-01285-x>
- Makropoulos, A., Gousias, I. S., Ledig, C., Aljabar, P., Serag, A., Hajnal, J. V., Edwards, A. D., Counsell, S. J., & Rueckert, D. (2014). Automatic Whole Brain MRI Segmentation of the Developing Neonatal Brain. *IEEE Transactions on Medical Imaging*, 33(9), 1818–1831. <https://doi.org/10.1109/TMI.2014.2322280>
- Makropoulos, A., Robinson, E. C., Schuh, A., Wright, R., Fitzgibbon, S., Bozek, J., Counsell, S. J., Steinweg, J., Vecchiato, K., Passerat-Palmbach, J., Lenz, G., Mortari, F., Tenev, T., Duff, E. P., Bastiani, M., Cordero-Grande, L., Hughes, E., Tusor, N., Tournier, J. D., ... Rueckert, D. (2018a). The developing human connectome project: A minimal processing pipeline for neonatal cortical surface reconstruction. *NeuroImage*, 173(April 2017), 88–112. <https://doi.org/10.1016/j.neuroimage.2018.01.054>
- Makropoulos, A., Robinson, E. C., Schuh, A., Wright, R., Fitzgibbon, S., Bozek, J., Counsell, S. J., Steinweg, J., Vecchiato, K., Passerat-Palmbach, J., Lenz, G., Mortari, F., Tenev, T., Duff, E. P., Bastiani, M., Cordero-Grande, L., Hughes, E., Tusor, N., Tournier, J.-D., ... Rueckert, D. (2018b). The developing human connectome project: A minimal processing pipeline for neonatal cortical surface reconstruction. *NeuroImage*, 173, 88–112. <https://doi.org/10.1016/j.neuroimage.2018.01.054>
- Malavolti, A. M., Chau, V., Brown-Lum, M., Poskitt, K. J., Brant, R., Synnes, A., Grunau, R. E., & Miller, S. P. (2017). Association between corpus callosum development on magnetic resonance imaging and diffusion tensor imaging, and neurodevelopmental outcome in neonates born very preterm. *Developmental Medicine & Child Neurology*, 59(4), 433–440. <https://doi.org/10.1111/dmcn.13364>
- Mangin, J.-F., Fillard, P., Cointepas, Y., Le Bihan, D., Frouin, V., & Poupon, C. (2013). Toward global tractography. *NeuroImage*, 80, 290–296. <https://doi.org/10.1016/j.neuroimage.2013.04.009>
- Mangold, C., Zoretic, S., Thallapureddy, K., Moreira, A., Chorath, K., & Moreira, A. (2021). Machine Learning Models for Predicting Neonatal Mortality: A Systematic Review. *Neonatology*, 118(4), 394–405. <https://doi.org/10.1159/000516891>
- Marami, B., Mohseni Salehi, S. S., Afacan, O., Scherrer, B., Rollins, C. K., Yang, E., Estroff, J. A., Warfield, S. K., & Gholipour, A. (2017). Temporal slice registration and robust diffusion-tensor reconstruction for improved fetal brain structural connectivity analysis. *NeuroImage*, 156, 475–488. <https://doi.org/10.1016/j.neuroimage.2017.04.033>
- Margulies, D. S., Böttger, J., Long, X., Lv, Y., Kelly, C., Schäfer, A., Goldhahn, D., Abbushi, A., Milham, M. P., Lohmann, G., & Villringer, A. (2010). Resting developments: a review of fMRI post-processing methodologies for spontaneous brain activity. *Magnetic Resonance Materials in Physics, Biology and Medicine*, 23(5–6), 289–307. <https://doi.org/10.1007/s10334-010-0228-5>
- Marret, S., Marchand-Martin, L., Picaud, J.-C., Hascoët, J.-M., Arnaud, C., Rozé, J.-C., Truffert, P., Larroque, B., Kaminski, M., Ancel, P.-Y., & for the EPIPAGE Study Group. (2013). Brain Injury in Very Preterm Children and Neurosensory and Cognitive Disabilities during Childhood: The EPIPAGE Cohort Study. *PLoS ONE*, 8(5), e62683. <https://doi.org/10.1371/journal.pone.0062683>
- Mars, R. B., Jbabdi, S., Sallet, J., O'Reilly, J. X., Croxson, P. L., Olivier, E., Noonan, M. P., Bergmann, C., Mitchell, A. S., Baxter, M. G., Behrens, T. E. J., Johansen-Berg, H., Tomassini, V., Miller, K. L., & Rushworth, M. F. S. (2011). Diffusion-Weighted Imaging Tractography-Based Parcellation

- of the Human Parietal Cortex and Comparison with Human and Macaque Resting-State Functional Connectivity. *The Journal of Neuroscience*, 31(11), 4087–4100. <https://doi.org/10.1523/JNEUROSCI.5102-10.2011>
- Maugeri, L., Moraschi, M., Summers, P., Favilla, S., Mascali, D., Cedola, A., Porro, C. A., Giove, F., & Fratini, M. (2018). Assessing denoising strategies to increase signal to noise ratio in spinal cord and in brain cortical and subcortical regions. *Journal of Instrumentation*, 13(02), C02028–C02028. <https://doi.org/10.1088/1748-0221/13/02/C02028>
- Mazzocchi, F. (2015). Could Big Data be the end of theory in science? *EMBO Reports*, 16(10), 1250–1255. <https://doi.org/10.15252/embr.201541001>
- McGowan, E. C., & Vohr, B. R. (2019). Neurodevelopmental Follow-up of Preterm Infants. *Pediatric Clinics of North America*, 66(2), 509–523. <https://doi.org/10.1016/j.pcl.2018.12.015>
- McKinstry, R. C., Mathur, A. M., Miller, J. H., Ozcan, A., Snyder, A. Z., Schefft, G., Almlie, C. R., Shiran, S. I., Conturo, T. E., & Neil, J. J. (2002). Radial Organization of Developing Preterm Human Cerebral Cortex Revealed by Non-invasive Water Diffusion Anisotropy MRI. *Cerebral Cortex*, 12(12), 1237–1243. <https://doi.org/10.1093/cercor/12.12.1237>
- Melbourne, A., Eaton-Rosen, Z., Orasanu, E., Price, D., Bainbridge, A., Cardoso, M. J., Kendall, G. S., Robertson, N. J., Marlow, N., & Ourselin, S. (2016). Longitudinal development in the preterm thalamus and posterior white matter: MRI correlations between diffusion weighted imaging and T2 relaxometry. *Human Brain Mapping*, 37(7), 2479–2492. <https://doi.org/10.1002/hbm.23188>
- Melbourne, A., Eaton-Rosen, Z., Orasanu, E., Price, D., Bainbridge, A., Cardoso, M. J., & Middlemiss, W. (2004). Infant sleep: a review of normative and problematic sleep and interventions. *Early Child Development and Care*, 174, 99–122.
- Miceli, P. J., Miceli P. J., Goeke-Morey M. C., Whitman T. L., Kolberg K. S., Miller-Loncar C., & White R. D. (2000). Brief Report : Birth Status, Medical Complications, and Social Environment : Individual Differences in Development of Preterm, Very Low Birth Weight Infants. *Journal of Pediatric Psychology*, 25(5), 353–358. <https://doi.org/10.1093/jpepsy/25.5.353>
- Milh, M., Kaminska, A., Huon, C., Lapillonne, A., Ben-Ari, Y., & Khazipov, R. (2007). Rapid Cortical Oscillations and Early Motor Activity in Premature Human Neonate. *Cerebral Cortex*, 17(7), 1582–1594. <https://doi.org/10.1093/cercor/bhl069>
- Mire, E., Mezzera, C., Leyva-Díaz, E., Paternain, A. V., Squarzone, P., Bluy, L., Castillo-Paterna, M., López, M. J., Peregrín, S., Tessier-Lavigne, M., Garel, S., Galcerán, J., Lerma, J., & López-Bendito, G. (2012). Spontaneous activity regulates Robo1 transcription to mediate a switch in thalamocortical axon growth. *Nature Neuroscience*, 15(8), 1134–1143. <https://doi.org/10.1038/nn.3160>
- Mishra, V., Cheng, H., Gong, G., He, Y., Dong, Q., & Huang, H. (2013). Differences of inter-tract correlations between neonates and children around puberty: a study based on microstructural measurements with DTI. *Frontiers in Human Neuroscience*, 7. <https://doi.org/10.3389/fnhum.2013.00721>
- Mitra, A., Snyder, A. Z., Tagliazucchi, E., Laufs, H., Elison, J., Emerson, R. W., Shen, M. D., Wolff, J. J., Botteron, K. N., Dager, S., Estes, A. M., Evans, A., Gerig, G., Hazlett, H. C., Paterson, S. J., Schultz, R. T., Styner, M. A., Zwaigenbaum, L., Schlaggar, B. L., ... Raichle, M. (2017). Resting-state fMRI in sleeping infants more closely resembles adult sleep than adult wakefulness. *PLOS ONE*, 12(11), e0188122. <https://doi.org/10.1371/journal.pone.0188122>
- Mitter, C., Jakab, A., Brugger, P. C., Ricken, G., Gruber, G. M., Bettelheim, D., Scharrer, A., Langs, G., Hainfellner, J. A., Prayer, D., & Kasprian, G. (2015). Validation of In utero Tractography of Human Fetal Commissural and Internal Capsule Fibers with Histological Structure Tensor Analysis. *Frontiers in Neuroanatomy*, 9. <https://doi.org/10.3389/fnana.2015.00164>

- Mizuno, H., Hirano, T., & Tagawa, Y. (2010). Pre-synaptic and post-synaptic neuronal activity supports the axon development of callosal projection neurons during different post-natal periods in the mouse cerebral cortex. *European Journal of Neuroscience*, 31(3), 410–424. <https://doi.org/10.1111/j.1460-9568.2009.07070.x>
- Moeskops, P., Išgum, I., Keunen, K., Claessens, N. H. P., van Haastert, I. C., Groenendaal, F., de Vries, L. S., Viergever, M. A., & Benders, M. J. N. L. (2017). Prediction of cognitive and motor outcome of preterm infants based on automatic quantitative descriptors from neonatal MR brain images. *Scientific Reports*, 7(1), 2163. <https://doi.org/10.1038/s41598-017-02307-w>
- Moghim, P., Dang, A. T., Netoff, T. I., Lim, K. O., & Atluri, G. (2021). A Review on MR Based Human Brain Parcellation Methods. *ArXiv*.
- Molloy, M. F., & Saygin, Z. M. (2022). Individual variability in functional organization of the neonatal brain. *NeuroImage*, 253, 119101. <https://doi.org/10.1016/j.neuroimage.2022.119101>
- Molnár, Z., Luhmann, H. J., & Kanold, P. O. (2020). Transient cortical circuits match spontaneous and sensory-driven activity during development. *Science*, 370(6514), eabb2153. <https://doi.org/10.1126/science.abb2153>
- Monson, B. B., Eaton-Rosen, Z., Kapur, K., Liebenthal, E., Brownell, A., Smyser, C. D., Rogers, C. E., Inder, T. E., Warfield, S. K., & Neil, J. J. (2018). Differential Rates of Perinatal Maturation of Human Primary and Nonprimary Auditory Cortex. *Eneuro*, 5(1), ENEURO.0380-17.2017. <https://doi.org/10.1523/ENEURO.0380-17.2017>
- Montagna, A., & Nosarti, C. (2016). Socio-Emotional Development Following Very Preterm Birth: Pathways to Psychopathology. *Frontiers in Psychology*, 7. <https://doi.org/10.3389/fpsyg.2016.00080>
- Moore, G. P., Lemyre, B., Barrowman, N., & Daboval, T. (2013). Neurodevelopmental Outcomes at 4 to 8 Years of Children Born at 22 to 25 Weeks' Gestational Age. *JAMA Pediatrics*, 167(10), 967. <https://doi.org/10.1001/jamapediatrics.2013.2395>
- Mori, S., Crain, B., Chacko, V., & van Zijl, P. (1999). Three-dimensional tracking of axonal projections in the brain by magnetic resonance imaging. *Ann Neurol.*, 45, 265–269.
- Moutquin, J. (2003). Classification and heterogeneity of preterm birth. *BJOG: An International Journal of Obstetrics and Gynaecology*, 110, 30–33. [https://doi.org/10.1016/S1470-0328\(03\)00021-1](https://doi.org/10.1016/S1470-0328(03)00021-1)
- Mrzljak, L., Uylings, H. B. M., Kostovic, I., & van Eden, C. G. (1988). Prenatal development of neurons in the human prefrontal cortex: I. A qualitative Golgi study. *The Journal of Comparative Neurology*, 271(3), 355–386. <https://doi.org/10.1002/cne.902710306>
- Mrzljak, L., Uylings, H. B. M., Kostovic, I., & van Eden, C. G. (1992). Prenatal development of neurons in the human prefrontal cortex. II. A quantitative Golgi study. *The Journal of Comparative Neurology*, 316(4), 485–496. <https://doi.org/10.1002/cne.903160408>
- Muglia, L. J., & Katz, M. (2010). The Enigma of Spontaneous Preterm Birth. *New England Journal of Medicine*, 362(6), 529–535. <https://doi.org/10.1056/NEJMra0904308>
- Mukherjee, D., & Kanold, P. O. (2023). Changing subplate circuits: Early activity dependent circuit plasticity. *Frontiers in Cellular Neuroscience*, 16. <https://doi.org/10.3389/fncel.2022.1067365>
- Mulder, H., Pitchford, N. J., & Marlow, N. (2010). Processing speed and working memory underlie academic attainment in very preterm children. *Archives of Disease in Childhood - Fetal and Neonatal Edition*, 95(4), F267–F272. <https://doi.org/10.1136/adc.2009.167965>
- Mullen, E. M. (1995). *Mullen Scales of Early Learning*. AGS.
- Nath, V., Lyu, I., Schilling, K. G., Parvathaneni, P., Hansen, C. B., Huo, Y., Janve, V. A., Gao, Y., Stepniewska, I., Anderson, A. W., & Landman, B. A. (2019). Enabling Multi-shell b-Value Generalizability of Data-Driven Diffusion Models with Deep SHORE (pp. 573–581). https://doi.org/10.1007/978-3-030-32248-9_64

- Neil, J. J., & Smyser, C. D. (2018). Recent advances in the use of MRI to assess early human cortical development. *Journal of Magnetic Resonance*, 293, 56–69. <https://doi.org/10.1016/j.jmr.2018.05.013>
- Neumane, S., Gondova, A., Leprince, Y., Hertz-Pannier, L., Arichi, T., & Dubois, J. (2022). Early structural connectivity within the sensorimotor network: Deviations related to prematurity and association to neurodevelopmental outcome. *Frontiers in Neuroscience*, 16. <https://doi.org/10.3389/fnins.2022.932386>
- Ní Bhroin, M., Abo Seada, S., Bonthron, A. F., Kelly, C. J., Christiaens, D., Schuh, A., Pietsch, M., Hutter, J., Tournier, J.-D., Cordero-Grande, L., Rueckert, D., Hajnal, J. V., Pushparajah, K., Simpson, J., Edwards, A. D., Rutherford, M. A., Counsell, S. J., & Batalle, D. (2020). Reduced structural connectivity in cortico-striatal-thalamic network in neonates with congenital heart disease. *NeuroImage: Clinical*, 28, 102423. <https://doi.org/10.1016/j.nicl.2020.102423>
- Nie, J., Li, G., Wang, L., Shi, F., Lin, W., Gilmore, J. H., & Shen, D. (2014). Longitudinal development of cortical thickness, folding, and fiber density networks in the first 2 years of life. *Human Brain Mapping*, 35(8), 3726–3737. <https://doi.org/10.1002/hbm.22432>
- Norman, M. G., & O’kusky, J. R. (1986). The Growth and Development of Microvasculature in Human Cerebral Cortex. *Journal of Neuropathology and Experimental Neurology*, 45(3), 222. <https://doi.org/10.1097/00005072-198605000-00003>
- NOSARTI, C., GIOUROUKOU, E., MICALI, N., RIFKIN, L., MORRIS, R. G., & MURRAY, R. M. (2007). Impaired executive functioning in young adults born very preterm. *Journal of the International Neuropsychological Society*, 13(04). <https://doi.org/10.1017/S1355617707070725>
- Nosarti, C., Reichenberg, A., Murray, R. M., Cnattingius, S., Lambe, M. P., Yin, L., MacCabe, J., Rifkin, L., & Hultman, C. M. (2012). Preterm Birth and Psychiatric Disorders in Young Adult Life. *Archives of General Psychiatry*, 69(6). <https://doi.org/10.1001/archgenpsychiatry.2011.1374>
- Nossin-Manor, R., Card, D., Morris, D., Noormohamed, S., Shroff, M. M., Whyte, H. E., Taylor, M. J., & Sled, J. G. (2013a). Quantitative MRI in the very preterm brain: Assessing tissue organization and myelination using magnetization transfer, diffusion tensor and T1 imaging. *NeuroImage*, 64, 505–516. <https://doi.org/10.1016/j.neuroimage.2012.08.086>
- Nossin-Manor, R., Card, D., Morris, D., Noormohamed, S., Shroff, M. M., Whyte, H. E., Taylor, M. J., & Sled, J. G. (2013b). Quantitative MRI in the very preterm brain: Assessing tissue organization and myelination using magnetization transfer, diffusion tensor and T1 imaging. *NeuroImage*, 64, 505–516. <https://doi.org/10.1016/j.neuroimage.2012.08.086>
- Nossin-Manor, R., Card, D., Raybaud, C., Taylor, M. J., & Sled, J. G. (2015). Cerebral maturation in the early preterm period—A magnetization transfer and diffusion tensor imaging study using voxel-based analysis. *NeuroImage*, 112, 30–42. <https://doi.org/10.1016/j.neuroimage.2015.02.051>
- Offiah, I. , O’Donoghue, K. , & Kenny, L. (2012). Clinical risk factors for preterm birth. In *Preterm birth-mother and child* (pp. 73–95). InTech.
- Ogawa, S. , Lee, T. M. , Kay, A. R. , & Tank, D. W. (1990). Brain magnetic resonance imaging with contrast dependent on blood oxygenation. *Proceedings of the National Academy of Sciences of the United States of America*, 87(24), 9868–9872.
- O’Leary, D. D. M., Chou, S.-J., & Sahara, S. (2007). Area Patterning of the Mammalian Cortex. *Neuron*, 56(2), 252–269. <https://doi.org/10.1016/j.neuron.2007.10.010>
- Oliveira, F. P. M., & Tavares, J. M. R. S. (2014). Medical image registration: a review. *Computer Methods in Biomechanics and Biomedical Engineering*, 17(2), 73–93. <https://doi.org/10.1080/10255842.2012.670855>
- Ouyang, M., Dubois, J., Yu, Q., Mukherjee, P., & Huang, H. (2019). Delineation of early brain development from fetuses to infants with diffusion MRI and beyond. *NeuroImage*, 185, 836–850. <https://doi.org/10.1016/j.neuroimage.2018.04.017>

- Ouyang, M., Jeon, T., Mishra, V., Du, H., Wang, Y., Peng, Y., & Huang, H. (2016). *Global and regional cortical connectivity maturation index (CCMI) of developmental human brain with quantification of short-range association tracts* (B. Gimi & A. Krol, Eds.; p. 97881B). <https://doi.org/10.1117/12.2218029>
- Ouyang, M., Jeon, T., Sotiras, A., Peng, Q., Mishra, V., Halovanic, C., Chen, M., Chalak, L., Rollins, N., Roberts, T. P. L., Davatzikos, C., & Huang, H. (2019). Differential cortical microstructural maturation in the preterm human brain with diffusion kurtosis and tensor imaging. *Proceedings of the National Academy of Sciences*, 116(10), 4681–4688. <https://doi.org/10.1073/pnas.1812156116>
- Ouyang, M., Peng, Q., Jeon, T., Heyne, R., Chalak, L., & Huang, H. (2020). Diffusion-MRI-based regional cortical microstructure at birth for predicting neurodevelopmental outcomes of 2-year-olds. *ELife*, 9. <https://doi.org/10.7554/eLife.58116>
- Palisano, R. J., Hanna, S. E., Rosenbaum, P. L., Russell, D. J., Walter, S. D., Wood, E. P., Raina, P. S., & Galuppi, B. E. (2000). Validation of a model of gross motor function for children with cerebral palsy. *Physical Therapy*, 80(10), 974–985.
- Palombo, M., Shemesh, N., Ronen, I., & Valette, J. (2018). Insights into brain microstructure from in vivo DW-MRS. *NeuroImage*, 182, 97–116. <https://doi.org/10.1016/j.neuroimage.2017.11.028>
- Pandit, A. S., Robinson, E., Aljabar, P., Ball, G., Gousias, I. S., Wang, Z., Hajnal, J. V., Rueckert, D., Counsell, S. J., Montana, G., & Edwards, A. D. (2014). Whole-Brain Mapping of Structural Connectivity in Infants Reveals Altered Connection Strength Associated with Growth and Preterm Birth. *Cerebral Cortex*, 24(9), 2324–2333. <https://doi.org/10.1093/cercor/bht086>
- Parikh, N. A. (2016). Advanced neuroimaging and its role in predicting neurodevelopmental outcomes in very preterm infants. *Seminars in Perinatology*, 40(8), 530–541. <https://doi.org/10.1053/j.semperi.2016.09.005>
- Passingham, R. E., Stephan, K. E., & Kötter, R. (2002). The anatomical basis of functional localization in the cortex. *Nature Reviews Neuroscience*, 3(8), 606–616. <https://doi.org/10.1038/nrn893>
- Pedregosa, F., Varoquaux, G., Gramfort, A., Michel, V., Thirion, B., Grisel, O., Blondel, M., Prettenhofer, P., Weiss, R., Dubourg, V., Vanderplas, A., Passos, A., Cournapeau, D., Brucher, M., Perrot, M., & Duchesnay, E. (2011). Scikit-learn: Machine Learning in Python. *The Journal of Machine Learning Research*, 12, 2825–2830.
- Penn, A. A., & Shatz, C. J. (1999). Brain Waves and Brain Wiring: The Role of Endogenous and Sensory-Driven Neural Activity in Development. *Pediatric Research*, 45(4, Part 1 of 2), 447–458. <https://doi.org/10.1203/00006450-199904010-00001>
- Penny, W. D., Friston, K. J., Ashburner, J., Kiebel, S. J., & Nichols, T. E. (2007). *Statistical Parametric Mapping: The Analysis of Functional Brain Images*.
- Pereira, C. B., Heimann, K., Czaplik, M., Blazek, V., Venema, B., & Leonhardt, S. (2016). Thermoregulation in premature infants: A mathematical model. *Journal of Thermal Biology*, 62, 159–169. <https://doi.org/10.1016/j.jtherbio.2016.06.021>
- Persad, E., Jost, K., Honoré, A., Forsberg, D., Coste, K., Olsson, H., Rautiainen, S., & Herlenius, E. (2021). Neonatal sepsis prediction through clinical decision support algorithms: A systematic review. *Acta Paediatrica*, 110(12), 3201–3226. <https://doi.org/10.1111/apa.16083>
- Peterson, B. S., Vohr, B., Staib, L., Cannistraci, C. J., Dolberg, A., Schneider, K. C., Katz, K. H., Westerveld, M., Sparrow, S., Anderson, A. W., Duncan, C. C., Makuch, R. W., Gore, J. C., & Ment, L. R. (2000). Regional Brain Volume Abnormalities and Long-term Cognitive Outcome in Preterm Infants. *JAMA*, 284(15), 1939. <https://doi.org/10.1001/jama.284.15.1939>
- Piao, X., Hill, R. S., Bodell, A., Chang, B. S., Basel-Vanagaite, L., Straussberg, R., Dobyns, W. B., Qasrawi, B., Winter, R. M., Innes, A. M., Voit, T., Ross, M. E., Michaud, J. L., Descarrie, J.-C., Barkovich, A. J., & Walsh, C. A. (2004). G Protein-Coupled Receptor-Dependent Development

- of Human Frontal Cortex. *Science*, 303(5666), 2033–2036. <https://doi.org/10.1126/science.1092780>
- Pierrat, V., Marchand-Martin, L., Arnaud, C., Kaminski, M., Resche-Rigon, M., Lebeaux, C., Bodeau-Livinec, F., Morgan, A. S., Goffinet, F., Marret, S., & Ancel, P.-Y. (2017). Neurodevelopmental outcome at 2 years for preterm children born at 22 to 34 weeks' gestation in France in 2011: EPIPAGE-2 cohort study. *BMJ*, j3448. <https://doi.org/10.1136/bmj.j3448>
- Pierrat, V., Marchand-Martin, L., Marret, S., Arnaud, C., Benhammou, V., Cambonie, G., Debillon, T., Dufourg, M.-N., Gire, C., Goffinet, F., Kaminski, M., Lapillonne, A., Morgan, A. S., Rozé, J.-C., Twilhaar, S., Charles, M.-A., & Ancel, P.-Y. (2021a). Neurodevelopmental outcomes at age 5 among children born preterm: EPIPAGE-2 cohort study. *BMJ*, n741. <https://doi.org/10.1136/bmj.n741>
- Pierrat, V., Marchand-Martin, L., Marret, S., Arnaud, C., Benhammou, V., Cambonie, G., Debillon, T., Dufourg, M.-N., Gire, C., Goffinet, F., Kaminski, M., Lapillonne, A., Morgan, A. S., Rozé, J.-C., Twilhaar, S., Charles, M.-A., & Ancel, P.-Y. (2021b). Neurodevelopmental outcomes at age 5 among children born preterm: EPIPAGE-2 cohort study. *BMJ*, n741. <https://doi.org/10.1136/bmj.n741>
- Pietsch, M., Christiaens, D., Hajnal, J. V., & Tournier, J.-D. (2021). dStripe: Slice artefact correction in diffusion MRI via constrained neural network. *Medical Image Analysis*, 74, 102255. <https://doi.org/10.1016/j.media.2021.102255>
- Pietsch, M., Christiaens, D., Hutter, J., Cordero-Grande, L., Price, A. N., Hughes, E., Edwards, A. D., Hajnal, J. V., Counsell, S. J., & Tournier, J.-D. (2019). A framework for multi-component analysis of diffusion MRI data over the neonatal period. *NeuroImage*, 186, 321–337. <https://doi.org/10.1016/j.neuroimage.2018.10.060>
- Pines, A. R., Cieslak, M., Larsen, B., Baum, G. L., Cook, P. A., Adebimpe, A., Dávila, D. G., Elliott, M. A., Jirsaraie, R., Murtha, K., Oathes, D. J., Piiwaa, K., Rosen, A. F. G., Rush, S., Shinohara, R. T., Bassett, D. S., Roalf, D. R., & Satterthwaite, T. D. (2020). Leveraging multi-shell diffusion for studies of brain development in youth and young adulthood. *Developmental Cognitive Neuroscience*, 43, 100788. <https://doi.org/10.1016/j.dcn.2020.100788>
- Pittet, M. P., Vasung, L., Huppi, P. S., & Merlini, L. (2019). Newborns and preterm infants at term equivalent age: A semi-quantitative assessment of cerebral maturity. *NeuroImage: Clinical*, 24, 102014. <https://doi.org/10.1016/j.nicl.2019.102014>
- Plaisier, A., Govaert, P., Lequin, M. H., & Dudink, J. (2014). Optimal Timing of Cerebral MRI in Preterm Infants to Predict Long-Term Neurodevelopmental Outcome: A Systematic Review. *American Journal of Neuroradiology*, 35(5), 841–847. <https://doi.org/10.3174/ajnr.A3513>
- Pletikos, M., Sousa, A. M. M., Sedmak, G., Meyer, K. A., Zhu, Y., Cheng, F., Li, M., Kawasawa, Y. I., & Šestan, N. (2014). Temporal Specification and Bilaterality of Human Neocortical Topographic Gene Expression. *Neuron*, 81(2), 321–332. <https://doi.org/10.1016/j.neuron.2013.11.018>
- Pollatou, A., Filippi, C. A., Aydin, E., Vaughn, K., Thompson, D., Korom, M., Dufford, A. J., Howell, B., Zöllei, L., Martino, A. Di, Graham, A., Scheinost, D., & Spann, M. N. (2022). An ode to fetal, infant, and toddler neuroimaging: Chronicling early clinical to research applications with MRI, and an introduction to an academic society connecting the field. *Developmental Cognitive Neuroscience*, 54, 101083. <https://doi.org/10.1016/j.dcn.2022.101083>
- Power, J. D., Fair, D. A., Schlaggar, B. L., & Petersen, S. E. (2010). The Development of Human Functional Brain Networks. *Neuron*, 67(5), 735–748. <https://doi.org/10.1016/j.neuron.2010.08.017>
- Prastawa, M., Sadeghi, N., Gilmore, J. H., Lin, W., & Gerig, G. (2010). A new framework for analyzing white matter maturation in early brain development. *2010 IEEE International Symposium on Biomedical Imaging: From Nano to Macro*, 97–100. <https://doi.org/10.1109/ISBI.2010.5490404>

- Prayer, D., Barkovich, A. J., Kirschner, D. A., Prayer, L. M., Roberts, T. P., Kucharczyk, J., & Moseley, M. E. (2001). Visualization of nonstructural changes in early white matter development on diffusion-weighted MR images: evidence supporting premyelination anisotropy. *AJNR. American Journal of Neuroradiology*, 22(8), 1572–1576.
- Price, A. N. (2015). *Accelerated Neonatal fMRI Using Multiband EPI*.
- Qiu, A., Fortier, M. V., Bai, J., Zhang, X., Chong, Y.-S., Kwek, K., Saw, S.-M., Godfrey, K. M., Gluckman, P. D., & Meaney, M. J. (2013). Morphology and microstructure of subcortical structures at birth: A large-scale Asian neonatal neuroimaging study. *NeuroImage*, 65, 315–323. <https://doi.org/10.1016/j.neuroimage.2012.09.032>
- Qiu, A., Mori, S., & Miller, M. I. (2015). Diffusion Tensor Imaging for Understanding Brain Development in Early Life. *Annual Review of Psychology*, 66(1), 853–876. <https://doi.org/10.1146/annurev-psych-010814-015340>
- Rakic, P., Ayoub, A. E., Breunig, J. J., & Dominguez, M. H. (2009). Decision by division: making cortical maps. *Trends in Neurosciences*, 32(5), 291–301. <https://doi.org/10.1016/j.tins.2009.01.007>
- Rheault, F., Schilling, K. G., Obaid, S., Begnoche, J. P., Cutting, L. E., Descoteaux, M., Landman, B. A., & Petit, L. (2022). The influence of regions of interest on tractography virtual dissection protocols: general principles to learn and to follow. *Brain Structure and Function*, 227(6), 2191–2207. <https://doi.org/10.1007/s00429-022-02518-6>
- Risk, B. B., Murden, R. J., Wu, J., Nebel, M. B., Venkataraman, A., Zhang, Z., & Qiu, D. (2021). Which multiband factor should you choose for your resting-state fMRI study? *NeuroImage*, 234, 117965. <https://doi.org/10.1016/j.neuroimage.2021.117965>
- Roberts, T. P. L., Khan, S. Y., Blaskey, L., Dell, J., Levy, S. E., Zarnow, D. M., & Christopher Edgar, J. (2009). Developmental correlation of diffusion anisotropy with auditory-evoked response. *NeuroReport*, 20(18), 1586–1591. <https://doi.org/10.1097/WNR.0b013e3283306854>
- Robinson, E. C., Garcia, K., Glasser, M. F., Chen, Z., Coalson, T. S., Makropoulos, A., Bozek, J., Wright, R., Schuh, A., Webster, M., Hutter, J., Price, A., Cordero Grande, L., Hughes, E., Tusor, N., Bayly, P. V., Van Essen, D. C., Smith, S. M., Edwards, A. D., ... Rueckert, D. (2018). Multimodal surface matching with higher-order smoothness constraints. *NeuroImage*, 167, 453–465. <https://doi.org/10.1016/j.neuroimage.2017.10.037>
- Roca, P., Rivière, D., Guevara, P., Poupon, C., & Mangin, J.-F. (2009). *Tractography-Based Parcellation of the Cortex Using a Spatially-Informed Dimension Reduction of the Connectivity Matrix* (pp. 935–942). https://doi.org/10.1007/978-3-642-04268-3_115
- Roca, P., Tucholka, A., Rivière, D., Guevara, P., Poupon, C., & Mangin, J.-F. (2010). *Inter-subject Connectivity-Based Parcellation of a Patch of Cerebral Cortex* (pp. 347–354). https://doi.org/10.1007/978-3-642-15745-5_43
- Rousseau, F., Studholme, C., Jardri, R., & Thomason, M. E. (2016). In Vivo Human Fetal Brain Analysis Using MR Imaging. In *Fetal Development* (pp. 407–427). Springer International Publishing. https://doi.org/10.1007/978-3-319-22023-9_20
- Roze, E., Harris, P. A., Ball, G., Elorza, L. Z., Braga, R. M., Allsop, J. M., Merchant, N., Porter, E., Arichi, T., Edwards, A. D., Rutherford, M. A., Cowan, F. M., & Counsell, S. J. (2012). Tractography of the corticospinal tracts in infants with focal perinatal injury: comparison with normal controls and to motor development. *Neuroradiology*, 54(5), 507–516. <https://doi.org/10.1007/s00234-011-0969-5>
- Rubarth, L. B., & Quinn, J. (2015). Respiratory Development and Respiratory Distress Syndrome. *Neonatal Network*, 34(4), 231–238. <https://doi.org/10.1891/0730-0832.34.4.231>

- Rubinov, M., & Sporns, O. (2010). Complex network measures of brain connectivity: Uses and interpretations. *NeuroImage*, 52(3), 1059–1069. <https://doi.org/10.1016/j.neuroimage.2009.10.003>
- Rykhlevskaia, E., Gratton, G., & Fabiani, M. (2008). Combining structural and functional neuroimaging data for studying brain connectivity: A review. *Psychophysiology*, 45(2), 173–187. <https://doi.org/10.1111/j.1469-8986.2007.00621.x>
- Sa de Almeida, J., Meskaldji, D.-E., Loukas, S., Lordier, L., Gui, L., Lazeyras, F., & Hüppi, P. S. (2021). Preterm birth leads to impaired rich-club organization and fronto-paralimbic/limbic structural connectivity in newborns. *NeuroImage*, 225, 117440. <https://doi.org/10.1016/j.neuroimage.2020.117440>
- Sadeghi, N., Prastawa, M., Fletcher, P. T., Wolff, J., Gilmore, J. H., & Gerig, G. (2013). Regional characterization of longitudinal DT-MRI to study white matter maturation of the early developing brain. *NeuroImage*, 68, 236–247. <https://doi.org/10.1016/j.neuroimage.2012.11.040>
- Saha, S., Pagnozzi, A., Bourgeat, P., George, J. M., Bradford, D., Colditz, P. B., Boyd, R. N., Rose, S. E., Fripp, J., & Pannek, K. (2020). Predicting motor outcome in preterm infants from very early brain diffusion MRI using a deep learning convolutional neural network (CNN) model. *NeuroImage*, 215, 116807. <https://doi.org/10.1016/j.neuroimage.2020.116807>
- Saigal, S., & Doyle, L. W. (2008). An overview of mortality and sequelae of preterm birth from infancy to adulthood. *The Lancet*, 371(9608), 261–269. [https://doi.org/10.1016/S0140-6736\(08\)60136-1](https://doi.org/10.1016/S0140-6736(08)60136-1)
- Salimi-Khorshidi, G., Douaud, G., Beckmann, C. F., Glasser, M. F., Griffanti, L., & Smith, S. M. (2014). Automatic denoising of functional MRI data: Combining independent component analysis and hierarchical fusion of classifiers. *NeuroImage*, 90, 449–468. <https://doi.org/10.1016/j.neuroimage.2013.11.046>
- Sarker, I. H. (2021). Machine Learning: Algorithms, Real-World Applications and Research Directions. *SN Computer Science*, 2(3), 160. <https://doi.org/10.1007/s42979-021-00592-x>
- Sarwar, T., Ramamohanarao, K., & Zalesky, A. (2019). Mapping connectomes with diffusion MRI: deterministic or probabilistic tractography? *Magnetic Resonance in Medicine*, 81(2), 1368–1384. <https://doi.org/10.1002/mrm.27471>
- Savadjiev, P., Reinhold, C., Martin, D., & Forghani, R. (2020). Knowledge Based Versus Data Based. *Neuroimaging Clinics of North America*, 30(4), 401–415. <https://doi.org/10.1016/j.nic.2020.06.002>
- Scarapicchia, V., Brown, C., Mayo, C., & Gawryluk, J. R. (2017). Functional Magnetic Resonance Imaging and Functional Near-Infrared Spectroscopy: Insights from Combined Recording Studies. *Frontiers in Human Neuroscience*, 11. <https://doi.org/10.3389/fnhum.2017.00419>
- Schadl, K., Vassar, R., Cahill-Rowley, K., Yeom, K. W., Stevenson, D. K., & Rose, J. (2018). Prediction of cognitive and motor development in preterm children using exhaustive feature selection and cross-validation of near-term white matter microstructure. *NeuroImage: Clinical*, 17, 667–679. <https://doi.org/10.1016/j.nicl.2017.11.023>
- Scheinost, D., Kwon, S. H., Shen, X., Lacadie, C., Schneider, K. C., Dai, F., Ment, L. R., & Constable, R. T. (2016). Preterm birth alters neonatal, functional rich club organization. *Brain Structure and Function*, 221(6), 3211–3222. <https://doi.org/10.1007/s00429-015-1096-6>
- Scherrer, B., Schwartzman, A., Taquet, M., Sahin, M., Prabhu, S. P., & Warfield, S. K. (2016). Characterizing brain tissue by assessment of the distribution of anisotropic microstructural environments in diffusion-compartment imaging (DIAMOND). *Magnetic Resonance in Medicine*, 76(3), 963–977. <https://doi.org/10.1002/mrm.25912>
- Schilling, K. G., Daducci, A., Maier-Hein, K., Poupon, C., Houde, J.-C., Nath, V., Anderson, A. W., Landman, B. A., & Descoteaux, M. (2019). Challenges in diffusion MRI tractography – Lessons

- learned from international benchmark competitions. *Magnetic Resonance Imaging*, 57, 194–209. <https://doi.org/10.1016/j.mri.2018.11.014>
- Schilling, K. G., Rheault, F., Petit, L., Hansen, C. B., Nath, V., Yeh, F.-C., Girard, G., Barakovic, M., Rafael-Patino, J., Yu, T., Fischl-Gomez, E., Pizzolato, M., Ocampo-Pineda, M., Schiavi, S., Canales-Rodríguez, E. J., Daducci, A., Granziera, C., Innocenti, G., Thiran, J.-P., ... Descoteaux, M. (2021). Tractography dissection variability: What happens when 42 groups dissect 14 white matter bundles on the same dataset? *NeuroImage*, 243, 118502. <https://doi.org/10.1016/j.neuroimage.2021.118502>
- Schöpf, V., Kasprian, G., Brugger, P. C., & Prayer, D. (2012). Watching the fetal brain at ‘rest’. *International Journal of Developmental Neuroscience*, 30(1), 11–17. <https://doi.org/10.1016/j.ijdevneu.2011.10.006>
- Schuit, E., Groenwold, R. H. H., Harrell, F. E., de Kort, W. L. A. M., Kwee, A., Mol, B. W. J., Riley, R. D., & Moons, K. G. M. (2013). Unexpected predictor–outcome associations in clinical prediction research: causes and solutions. *Canadian Medical Association Journal*, 185(10), E499–E505. <https://doi.org/10.1503/cmaj.120812>
- Schultz, T. (2012). *Learning a Reliable Estimate of the Number of Fiber Directions in Diffusion MRI* (pp. 493–500). https://doi.org/10.1007/978-3-642-33454-2_61
- SCIL. (2023). *The Sherbrooke Connectivity Imaging Lab (SCIL) Python dMRI processing toolbox*.
- Seidlitz, J., Váša, F., Shinn, M., Romero-Garcia, R., Whitaker, K. J., Vértes, P. E., Wagstyl, K., Kirkpatrick Reardon, P., Clasen, L., Liu, S., Messinger, A., Leopold, D. A., Fonagy, P., Dolan, R. J., Jones, P. B., Goodyer, I. M., Raznahan, A., & Bullmore, E. T. (2018). Morphometric Similarity Networks Detect Microscale Cortical Organization and Predict Inter-Individual Cognitive Variation. *Neuron*, 97(1), 231–247.e7. <https://doi.org/10.1016/j.neuron.2017.11.039>
- Serenius, F., Ewald, U., Farooqi, A., Fellman, V., Hafström, M., Hellgren, K., Maršál, K., Ohlin, A., Olhager, E., Stjernqvist, K., Strömberg, B., Ådén, U., & Källén, K. (2016). Neurodevelopmental Outcomes Among Extremely Preterm Infants 6.5 Years After Active Perinatal Care in Sweden. *JAMA Pediatrics*, 170(10), 954. <https://doi.org/10.1001/jamapediatrics.2016.1210>
- Seunarine KK, & Alexander DC. (2014). *Multiple fibers: beyond the diffusion tensor: Vol. Diffusion MRI*. Elsevier.
- Shankle, W. R., Rafii, M. S., Landing, B. H., & Fallon, J. H. (1999). Approximate Doubling of Numbers of Neurons in Postnatal Human Cerebral Cortex and in 35 Specific Cytoarchitectural Areas from Birth to 72 Months. *Pediatric and Developmental Pathology*, 2(3), 244–259. <https://doi.org/10.1007/s100249900120>
- Shin, Y., Nam, Y., Shin, T., Choi, J. W., Lee, J. H., Jung, D. E., Lim, J., & Kim, H. G. (2021). Brain MRI radiomics analysis may predict poor psychomotor outcome in preterm neonates. *European Radiology*, 31(8), 6147–6155. <https://doi.org/10.1007/s00330-021-07836-7>
- Shirwaikar, R. D., Acharya U, D., Makkithaya, K., Mallayaswamy, S., & Lewis, L. E. S. (2018). Design Framework for a Data Mart in the Neonatal Intensive Care Unit. *Critical Reviews in Biomedical Engineering*, 46(3), 221–243. <https://doi.org/10.1615/CritRevBiomedEng.2018027067>
- Simons, M., & Nave, K.-A. (2016). Oligodendrocytes: Myelination and Axonal Support. *Cold Spring Harbor Perspectives in Biology*, 8(1), a020479. <https://doi.org/10.1101/cshperspect.a020479>
- Sinke, M. R. T., Otte, W. M., Christiaens, D., Schmitt, O., Leemans, A., van der Toorn, A., Sarabdjitsingh, R. A., Joëls, M., & Dijkhuizen, R. M. (2018). Diffusion MRI-based cortical connectome reconstruction: dependency on tractography procedures and neuroanatomical characteristics. *Brain Structure and Function*, 223(5), 2269–2285. <https://doi.org/10.1007/s00429-018-1628-y>

- Smith, R. E., Tournier, J.-D., Calamante, F., & Connelly, A. (2013). SIFT: Spherical-deconvolution informed filtering of tractograms. *NeuroImage*, 67, 298–312. <https://doi.org/10.1016/j.neuroimage.2012.11.049>
- Smith, R. E., Tournier, J.-D., Calamante, F., & Connelly, A. (2015). SIFT2: Enabling dense quantitative assessment of brain white matter connectivity using streamlines tractography. *NeuroImage*, 119, 338–351. <https://doi.org/10.1016/j.neuroimage.2015.06.092>
- Smith, S. M., & Beckmann, C. F. (2017). *Introduction to Resting State fMRI Functional Connectivity*.
- Smith, S. M., Fox, P. T., Miller, K. L., Glahn, D. C., Fox, P. M., Mackay, C. E., Filippini, N., Watkins, K. E., Toro, R., Laird, A. R., & Beckmann, C. F. (2009). Correspondence of the brain's functional architecture during activation and rest. *Proceedings of the National Academy of Sciences*, 106(31), 13040–13045. <https://doi.org/10.1073/pnas.0905267106>
- Smith, S. M., Miller, K. L., Salimi-Khorshidi, G., Webster, M., Beckmann, C. F., Nichols, T. E., Ramsey, J. D., & Woolrich, M. W. (2011). Network modelling methods for FMRI. *NeuroImage*, 54(2), 875–891. <https://doi.org/10.1016/j.neuroimage.2010.08.063>
- Smyser, C. D., Inder, T. E., Shimony, J. S., Hill, J. E., Degnan, A. J., Snyder, A. Z., & Neil, J. J. (2010). Longitudinal Analysis of Neural Network Development in Preterm Infants. *Cerebral Cortex*, 20(12), 2852–2862. <https://doi.org/10.1093/cercor/bhq035>
- Smyser, C. D., Snyder, A. Z., Shimony, J. S., Blazey, T. M., Inder, T. E., & Neil, J. J. (2013). Effects of White Matter Injury on Resting State fMRI Measures in Prematurely Born Infants. *PLoS ONE*, 8(7), e68098. <https://doi.org/10.1371/journal.pone.0068098>
- Smyser, C. D., Wheelock, M. D., Limbrick, D. D., & Neil, J. J. (2019). Neonatal brain injury and aberrant connectivity. *NeuroImage*, 185, 609–623. <https://doi.org/10.1016/j.neuroimage.2018.07.057>
- Smyser, T. A., Smyser, C. D., Rogers, C. E., Gillespie, S. K., Inder, T. E., & Neil, J. J. (2016). Cortical Gray and Adjacent White Matter Demonstrate Synchronous Maturation in Very Preterm Infants. *Cerebral Cortex*, 26(8), 3370–3378. <https://doi.org/10.1093/cercor/bhv164>
- Snaidero, N., Möbius, W., Czopka, T., Hekking, L. H. P., Mathisen, C., Verkleij, D., Goebbels, S., Edgar, J., Merkler, D., Lyons, D. A., Nave, K.-A., & Simons, M. (2014). Myelin Membrane Wrapping of CNS Axons by PI(3,4,5)P3-Dependent Polarized Growth at the Inner Tongue. *Cell*, 156(1–2), 277–290. <https://doi.org/10.1016/j.cell.2013.11.044>
- Solano-Castiella, E., Anwender, A., Lohmann, G., Weiss, M., Docherty, C., Geyer, S., Reimer, E., Friederici, A. D., & Turner, R. (2010). Diffusion tensor imaging segments the human amygdala in vivo. *NeuroImage*, 49(4), 2958–2965. <https://doi.org/10.1016/j.neuroimage.2009.11.027>
- Song, L., Mishra, V., Ouyang, M., Peng, Q., Slinger, M., Liu, S., & Huang, H. (2017). Human Fetal Brain Connectome: Structural Network Development from Middle Fetal Stage to Birth. *Frontiers in Neuroscience*, 11. <https://doi.org/10.3389/fnins.2017.00561>
- Sotiropoulos, S. N., Hernández-Fernández, M., Vu, A. T., Andersson, J. L., Moeller, S., Yacoub, E., Lenglet, C., Ugurbil, K., Behrens, T. E. J., & Jbabdi, S. (2016). Fusion in diffusion MRI for improved fibre orientation estimation: An application to the 3T and 7T data of the Human Connectome Project. *NeuroImage*, 134, 396–409. <https://doi.org/10.1016/j.neuroimage.2016.04.014>
- Spittle, A. J., & Orton, J. (2014). Cerebral palsy and developmental coordination disorder in children born preterm. *Seminars in Fetal and Neonatal Medicine*, 19(2), 84–89. <https://doi.org/10.1016/j.siny.2013.11.005>
- Spittle, A., & Treyvaud, K. (2016). The role of early developmental intervention to influence neurobehavioral outcomes of children born preterm. *Seminars in Perinatology*, 40(8), 542–548. <https://doi.org/10.1053/j.semperi.2016.09.006>

- Spitzer, A. R., Ellsbury, D., & Clark, R. H. (2015). The Pediatrix BabySteps® Data Warehouse — A Unique National Resource for Improving Outcomes for Neonates. *The Indian Journal of Pediatrics*, 82(1), 71–79. <https://doi.org/10.1007/s12098-014-1585-2>
- Srinivasan, L., Dutta, R., Counsell, S. J., Allsop, J. M., Boardman, J. P., Rutherford, M. A., & Edwards, A. D. (2007). Quantification of Deep Gray Matter in Preterm Infants at Term-Equivalent Age Using Manual Volumetry of 3-Tesla Magnetic Resonance Images. *Pediatrics*, 119(4), 759–765. <https://doi.org/10.1542/peds.2006-2508>
- Stahl, R., Walcher, T., De Juan Romero, C., Pilz, G. A., Cappello, S., Irmeler, M., Sanz-Aquela, J. M., Beckers, J., Blum, R., Borrell, V., & Götz, M. (2013). Trnp1 Regulates Expansion and Folding of the Mammalian Cerebral Cortex by Control of Radial Glial Fate. *Cell*, 153(3), 535–549. <https://doi.org/10.1016/j.cell.2013.03.027>
- Stahlmann, N., Eisemann, N., Thyen, U., Herting, E., & Rapp, M. (2016). Long-Term Health Outcomes and Health-Related Quality of Life in Adolescents from a Cohort of Extremely Premature Infants Born at Less Than 27 Weeks of Gestation in Northern Germany. *Neuropediatrics*, 47(06), 388–398. <https://doi.org/10.1055/s-0036-1593373>
- Stahlmann, N., Rapp, M., Herting, E., & Thyen, U. (2009). Outcome of Extremely Premature Infants at Early School Age: Health-Related Quality of Life and Neurosensory, Cognitive, and Behavioral Outcomes in a Population-Based Sample in Northern Germany. *Neuropediatrics*, 40(03), 112–119. <https://doi.org/10.1055/s-0029-1243166>
- Stiles, J., & Jernigan, T. L. (2010). The basics of brain development. *Neuropsychology Review*, 20(4), 327–348. <https://doi.org/10.1007/s11065-010-9148-4>
- Stokes, P. A., & Purdon, P. L. (2017). A study of problems encountered in Granger causality analysis from a neuroscience perspective. *Proceedings of the National Academy of Sciences*, 114(34). <https://doi.org/10.1073/pnas.1704663114>
- Stripelis, D., Gupta, U., Saleem, H., Dhinagar, N., Ghai, T., Anastasiou, R. C., Asghar, A., Steeg, G. Ver, Ravi, S., Naveed, M., Thompson, P. M., & Ambite, J. L. (2022). *Secure & Private Federated Neuroimaging*.
- Sun, F. T., Miller, L. M., & D’Esposito, M. (2004). Measuring interregional functional connectivity using coherence and partial coherence analyses of fMRI data. *NeuroImage*, 21(2), 647–658. <https://doi.org/10.1016/j.neuroimage.2003.09.056>
- Sun, F. T., Miller, L. M., & D’Esposito, M. (2005). Measuring temporal dynamics of functional networks using phase spectrum of fMRI data. *NeuroImage*, 28(1), 227–237. <https://doi.org/10.1016/j.neuroimage.2005.05.043>
- Sur, M., & Rubenstein, J. L. R. (2005). Patterning and Plasticity of the Cerebral Cortex. *Science*, 310(5749), 805–810. <https://doi.org/10.1126/science.1112070>
- Tagliazucchi, E., von Wegner, F., Morzelewski, A., Borisov, S., Jahnke, K., & Laufs, H. (2012). Automatic sleep staging using fMRI functional connectivity data. *NeuroImage*, 63(1), 63–72. <https://doi.org/10.1016/j.neuroimage.2012.06.036>
- Takahashi, E., Folkerth, R. D., Galaburda, A. M., & Grant, P. E. (2012). Emerging Cerebral Connectivity in the Human Fetal Brain: An MR Tractography Study. *Cerebral Cortex*, 22(2), 455–464. <https://doi.org/10.1093/cercor/bhr126>
- Takemura, H., Caiafa, C. F., Wandell, B. A., & Pestilli, F. (2016). Ensemble Tractography. *PLOS Computational Biology*, 12(2), e1004692. <https://doi.org/10.1371/journal.pcbi.1004692>
- Tam, E. W. Y., Ferriero, D. M., Xu, D., Berman, J. I., Vigneron, D. B., Barkovich, A. J., & Miller, S. P. (2009). Cerebellar Development in the Preterm Neonate: Effect of Supratentorial Brain Injury. *Pediatric Research*, 66(1), 102–106. <https://doi.org/10.1203/PDR.0b013e3181a1fb3d>
- Taoudi-Benchekroun, Y., Christiaens, D., Grigorescu, I., Gale-Grant, O., Schuh, A., Pietsch, M., Chew, A., Harper, N., Falconer, S., Poppe, T., Hughes, E., Hutter, J., Price, A. N., Tournier, J.-D.,

- Cordero-Grande, L., Counsell, S. J., Rueckert, D., Arichi, T., Hajnal, J. V., ... Batalle, D. (2022). Predicting age and clinical risk from the neonatal connectome. *NeuroImage*, 257, 119319. <https://doi.org/10.1016/j.neuroimage.2022.119319>
- Tau, G. Z., & Peterson, B. S. (2010). Normal Development of Brain Circuits. *Neuropsychopharmacology*, 35(1), 147–168. <https://doi.org/10.1038/npp.2009.115>
- Taymourtash, A., Schwartz, E., Nenning, K.-H., Sobotka, D., Licandro, R., Glatte, S., Diogo, M. C., Golland, P., Grant, E., Prayer, D., Kasprian, G., & Langs, G. (2023). Fetal development of functional thalamocortical and cortico–cortical connectivity. *Cerebral Cortex*, 33(9), 5613–5624. <https://doi.org/10.1093/cercor/bhac446>
- Thibault, S., Py, R., Gervasi, A. M., Salemme, R., Koun, E., Lövdén, M., Boulenger, V., Roy, A. C., & Brozzoli, C. (2021). Tool use and language share syntactic processes and neural patterns in the basal ganglia. *Science*, 374(6569). <https://doi.org/10.1126/science.abe0874>
- Thomason, M. E., Grove, L. E., Lozon, T. A., Vila, A. M., Ye, Y., Nye, M. J., Manning, J. H., Pappas, A., Hernandez-Andrade, E., Yeo, L., Mody, S., Berman, S., Hassan, S. S., & Romero, R. (2015). Age-related increases in long-range connectivity in fetal functional neural connectivity networks in utero. *Developmental Cognitive Neuroscience*, 11, 96–104. <https://doi.org/10.1016/j.dcn.2014.09.001>
- Thompson, D. K., Inder, T. E., Faggian, N., Warfield, S. K., Anderson, P. J., Doyle, L. W., & Egan, G. F. (2012). Corpus callosum alterations in very preterm infants: Perinatal correlates and 2 year neurodevelopmental outcomes. *NeuroImage*, 59(4), 3571–3581. <https://doi.org/10.1016/j.neuroimage.2011.11.057>
- Thompson, D. K., Lee, K. J., Egan, G. F., Warfield, S. K., Doyle, L. W., Anderson, P. J., & Inder, T. E. (2014). Regional white matter microstructure in very preterm infants: Predictors and 7 year outcomes. *Cortex*, 52, 60–74. <https://doi.org/10.1016/j.cortex.2013.11.010>
- Thompson, E., Mohammadi-Nejad, A. R., Robinson, E. C., Andersson, J. L. R., Jbabdi, S., Glasser, M. F., Bastiani, M., & Sotiropoulos, S. N. (2020). Non-negative data-driven mapping of structural connections with application to the neonatal brain. *NeuroImage*, 222, 117273. <https://doi.org/10.1016/j.neuroimage.2020.117273>
- Thompson, P. M., Jahanshad, N., Ching, C. R. K., Salminen, L. E., Thomopoulos, S. I., Bright, J., Baune, B. T., Bertolín, S., Bralten, J., Bruin, W. B., Bülow, R., Chen, J., Chye, Y., Dannlowski, U., de Kovel, C. G. F., Donohoe, G., Eyler, L. T., Faraone, S. V., Favre, P., ... Zelman, V. (2020). ENIGMA and global neuroscience: A decade of large-scale studies of the brain in health and disease across more than 40 countries. *Translational Psychiatry*, 10(1), 100. <https://doi.org/10.1038/s41398-020-0705-1>
- Toulmin, H., Beckmann, C. F., O’Muircheartaigh, J., Ball, G., Nongena, P., Makropoulos, A., Ederies, A., Counsell, S. J., Kennea, N., Arichi, T., Tusor, N., Rutherford, M. A., Azzopardi, D., Gonzalez-Cinca, N., Hajnal, J. V., & Edwards, A. D. (2015). Specialization and integration of functional thalamocortical connectivity in the human infant. *Proceedings of the National Academy of Sciences*, 112(20), 6485–6490. <https://doi.org/10.1073/pnas.1422638112>
- Tournier, D., Calamante, F., & Connelly, A. (2010). Improved probabilistic streamlines tractography by 2nd order integration over fibre orientation distributions. *Proceedings of ISMRM*.
- Tournier, J.-D., Calamante, F., & Connelly, A. (2013). Determination of the appropriate *b* value and number of gradient directions for high-angular-resolution diffusion-weighted imaging. *NMR in Biomedicine*, 26(12), 1775–1786. <https://doi.org/10.1002/nbm.3017>
- Tournier, J.-D., Calamante, F., Gadian, D. G., & Connelly, A. (2004). Direct estimation of the fiber orientation density function from diffusion-weighted MRI data using spherical deconvolution. *NeuroImage*, 23(3), 1176–1185. <https://doi.org/10.1016/j.neuroimage.2004.07.037>

- Tournier, J.-D., Smith, R., Raffelt, D., Tabbara, R., Dhollander, T., Pietsch, M., Christiaens, D., Jeurissen, B., Yeh, C.-H., & Connelly, A. (2019). MRtrix3: A fast, flexible and open software framework for medical image processing and visualisation. *NeuroImage*, 202, 116137. <https://doi.org/10.1016/j.neuroimage.2019.116137>
- Tuch, D. S. (2004). Q-ball imaging. *Magnetic Resonance in Medicine*, 52(6), 1358–1372. <https://doi.org/10.1002/mrm.20279>
- Turk, E., van den Heuvel, M. I., Benders, M. J., de Heus, R., Franx, A., Manning, J. H., Hect, J. L., Hernandez-Andrade, E., Hassan, S. S., Romero, R., Kahn, R. S., Thomason, M. E., & van den Heuvel, M. P. (2019). Functional Connectome of the Fetal Brain. *The Journal of Neuroscience*, 39(49), 9716–9724. <https://doi.org/10.1523/JNEUROSCI.2891-18.2019>
- Tusor, N., Benders, M. J., Counsell, S. J., Nongena, P., Ederies, M. A., Falconer, S., Chew, A., Gonzalez-Cinca, N., Hajnal, J. V., Gangadharan, S., Chatzi, V., Kersbergen, K. J., Kennea, N., Azzopardi, D. V., & Edwards, A. D. (2017). Punctate White Matter Lesions Associated With Altered Brain Development And Adverse Motor Outcome In Preterm Infants. *Scientific Reports*, 7(1), 13250. <https://doi.org/10.1038/s41598-017-13753-x>
- Tymofiyeva, O., Hess, C. P., Ziv, E., Tian, N., Bonifacio, S. L., McQuillen, P. S., Ferriero, D. M., Barkovich, A. J., & Xu, D. (2012). Towards the “Baby Connectome”: Mapping the Structural Connectivity of the Newborn Brain. *PLoS ONE*, 7(2), e31029. <https://doi.org/10.1371/journal.pone.0031029>
- Uus, A., Kyriakopoulou, V., Makropoulos, A., Fukami-Gartner, A., Cromb, D., Davidson, A., Cordero-Grande, L., Price, A., Grigorescu, I., Williams, L., Robinson, E., Lloyd, D., Pushparajah, K., Story, L., Hutter, J., Counsell, S., Edwards, D., Rutherford, M., Hajnal, J., & Deprez, M. (2023). BOUNTI: Brain vOlumetry and aUtomated parcellatioN for 3D feTal MRI. *ArXiv*.
- Valavani, E., Blesa, M., Galdi, P., Sullivan, G., Dean, B., Cruickshank, H., Sitko-Rudnicka, M., Bastin, M. E., Chin, R. F. M., MacIntyre, D. J., Fletcher-Watson, S., Boardman, J. P., & Tsanas, A. (2022). Language function following preterm birth: prediction using machine learning. *Pediatric Research*, 92(2), 480–489. <https://doi.org/10.1038/s41390-021-01779-x>
- van Boven, M. R., Henke, C. E., Leemhuis, A. G., Hoogendoorn, M., van Kaam, A. H., Königs, M., & Oosterlaan, J. (2022). Machine Learning Prediction Models for Neurodevelopmental Outcome After Preterm Birth: A Scoping Review and New Machine Learning Evaluation Framework. *Pediatrics*, 150(1). <https://doi.org/10.1542/peds.2021-056052>
- van den Heuvel, M. P., & Hulshoff Pol, H. E. (2010). Exploring the brain network: A review on resting-state fMRI functional connectivity. *European Neuropsychopharmacology*, 20(8), 519–534. <https://doi.org/10.1016/j.euroneuro.2010.03.008>
- van den Heuvel, M. P., Kersbergen, K. J., de Reus, M. A., Keunen, K., Kahn, R. S., Groenendaal, F., de Vries, L. S., & Benders, M. J. N. L. (2015). The Neonatal Connectome During Preterm Brain Development. *Cerebral Cortex*, 25(9), 3000–3013. <https://doi.org/10.1093/cercor/bhu095>
- van den Heuvel, M. P., Mandl, R. C. W., Kahn, R. S., & Hulshoff Pol, H. E. (2009). Functionally linked resting-state networks reflect the underlying structural connectivity architecture of the human brain. *Human Brain Mapping*, 30(10), 3127–3141. <https://doi.org/10.1002/hbm.20737>
- van der Fels, I. M. J., Smith, J., de Bruijn, A. G. M., Bosker, R. J., Königs, M., Oosterlaan, J., Visscher, C., & Hartman, E. (2019). Relations between gross motor skills and executive functions, controlling for the role of information processing and lapses of attention in 8-10 year old children. *PLOS ONE*, 14(10), e0224219. <https://doi.org/10.1371/journal.pone.0224219>
- Van der Knaap, M. S., & Valk, J. (1993). *Myelin and white matter: Magnetic resonance of myelin, myelination and myelin disorders*.

- Van Essen, D. C., Smith, S. M., Barch, D. M., Behrens, T. E. J., Yacoub, E., & Ugurbil, K. (2013). The WU-Minn Human Connectome Project: An overview. *NeuroImage*, 80, 62–79. <https://doi.org/10.1016/j.neuroimage.2013.05.041>
- Vanhatalo, S., & Kaila, K. (2006). Development of neonatal EEG activity: From phenomenology to physiology. *Seminars in Fetal and Neonatal Medicine*, 11(6), 471–478. <https://doi.org/10.1016/j.siny.2006.07.008>
- van't Hooft, J., van der Lee, J. H., Opmeer, B. C., Aarnoudse-Moens, C. S. H., Leenders, A. G. E., Mol, B. W. J., & de Haan, T. R. (2015). Predicting developmental outcomes in premature infants by term equivalent MRI: systematic review and meta-analysis. *Systematic Reviews*, 4(1), 71. <https://doi.org/10.1186/s13643-015-0058-7>
- Vardhan, A., Prastawa, M., Gouttard, S., Piven, J., & Gerig, G. (2012). Quantifying regional growth patterns through longitudinal analysis of distances between multimodal MR intensity distributions. *2012 9th IEEE International Symposium on Biomedical Imaging (ISBI)*, 1156–1159. <https://doi.org/10.1109/ISBI.2012.6235765>
- Varoquaux, G. (2018). Cross-validation failure: Small sample sizes lead to large error bars. *NeuroImage*, 180, 68–77. <https://doi.org/10.1016/j.neuroimage.2017.06.061>
- Vassar, R., Schadl, K., Cahill-Rowley, K., Yeom, K., Stevenson, D., & Rose, J. (2020). Neonatal Brain Microstructure and Machine-Learning-Based Prediction of Early Language Development in Children Born Very Preterm. *Pediatric Neurology*, 108, 86–92. <https://doi.org/10.1016/j.pediatrneurol.2020.02.007>
- Vasung, L., Abaci Turk, E., Ferradal, S. L., Sutin, J., Stout, J. N., Ahtam, B., Lin, P.-Y., & Grant, P. E. (2019). Exploring early human brain development with structural and physiological neuroimaging. *NeuroImage*, 187, 226–254. <https://doi.org/10.1016/j.neuroimage.2018.07.041>
- Vasung, L., Huang, H., Jovanov-Milošević, N., Pletikos, M., Mori, S., & Kostović, I. (2010). Development of axonal pathways in the human fetal fronto-limbic brain: histochemical characterization and diffusion tensor imaging. *Journal of Anatomy*, 217(4), 400–417. <https://doi.org/10.1111/j.1469-7580.2010.01260.x>
- Vasung, L., Lepage, C., Radoš, M., Pletikos, M., Goldman, J. S., Richiardi, J., Raguz, M., Fisch-Gómez, E., Karama, S., Huppi, P. S., Evans, A. C., & Kostovic, I. (2016). Quantitative and Qualitative Analysis of Transient Fetal Compartments during Prenatal Human Brain Development. *Frontiers in Neuroanatomy*, 10. <https://doi.org/10.3389/fnana.2016.00011>
- Vasung, L., Raguz, M., Kostovic, I., & Takahashi, E. (2017). Spatiotemporal Relationship of Brain Pathways during Human Fetal Development Using High-Angular Resolution Diffusion MR Imaging and Histology. *Frontiers in Neuroscience*, 11. <https://doi.org/10.3389/fnins.2017.00348>
- Vecchierini, M.-F., André, M., & d'Allest, A. M. (2007). Normal EEG of premature infants born between 24 and 30 weeks gestational age: Terminology, definitions and maturation aspects. *Neurophysiologie Clinique/Clinical Neurophysiology*, 37(5), 311–323. <https://doi.org/10.1016/j.neucli.2007.10.008>
- Vértes, P. E., & Bullmore, E. T. (2015). Annual Research Review: Growth connectomics – the organization and reorganization of brain networks during normal and abnormal development. *Journal of Child Psychology and Psychiatry*, 56(3), 299–320. <https://doi.org/10.1111/jcpp.12365>
- Vo Van, P., Alison, M., Morel, B., Beck, J., Bednarek, N., Hertz-Pannier, L., & Loron, G. (2022). Advanced Brain Imaging in Preterm Infants: A Narrative Review of Microstructural and Connectomic Disruption. *Children*, 9(3), 356. <https://doi.org/10.3390/children9030356>
- Volpe, J. J. (2019). Dysmaturation of Premature Brain: Importance, Cellular Mechanisms, and Potential Interventions. *Pediatric Neurology*, 95, 42–66. <https://doi.org/10.1016/j.pediatrneurol.2019.02.016>

- Vos, T., Lim, S. S., Abbafati, C., Abbas, K. M., Abbasi, M., Abbasifard, M., Abbasi-Kangevari, M., Abbastabar, H., Abd-Allah, F., Abdelalim, A., Abdollahi, M., Abdollahpour, I., Abolhassani, H., Aboyans, V., Abrams, E. M., Abreu, L. G., Abrigo, M. R. M., Abu-Raddad, L. J., Abushouk, A. I., ... Murray, C. J. L. (2020). Global burden of 369 diseases and injuries in 204 countries and territories, 1990–2019: a systematic analysis for the Global Burden of Disease Study 2019. *The Lancet*, 396(10258), 1204–1222. [https://doi.org/10.1016/S0140-6736\(20\)30925-9](https://doi.org/10.1016/S0140-6736(20)30925-9)
- Wagner, M. W., So, D., Guo, T., Erdman, L., Sheng, M., Ufkes, S., Grunau, R. E., Synnes, A., Branson, H. M., Chau, V., Shroff, M. M., Ertl-Wagner, B. B., & Miller, S. P. (2022). MRI based radiomics enhances prediction of neurodevelopmental outcome in very preterm neonates. *Scientific Reports*, 12(1), 11872. <https://doi.org/10.1038/s41598-022-16066-w>
- Wake, H., Ortiz, F. C., Woo, D. H., Lee, P. R., Angulo, M. C., & Fields, R. D. (2015). Nonsynaptic junctions on myelinating glia promote preferential myelination of electrically active axons. *Nature Communications*, 6(1), 7844. <https://doi.org/10.1038/ncomms8844>
- Wallois, F. (2010). Synopsis of maturation of specific features in EEG of premature neonates. *Neurophysiologie Clinique/Clinical Neurophysiology*, 40(2), 125–126. <https://doi.org/10.1016/j.neucli.2010.02.001>
- Wallois, F., Routier, L., & Bourel-Ponchel, E. (2020). *Impact of prematurity on neurodevelopment* (pp. 341–375). <https://doi.org/10.1016/B978-0-444-64150-2.00026-5>
- Walsh, J. M., Doyle, L. W., Anderson, P. J., Lee, K. J., & Cheong, J. L. Y. (2014). Moderate and Late Preterm Birth: Effect on Brain Size and Maturation at Term-Equivalent Age. *Radiology*, 273(1), 232–240. <https://doi.org/10.1148/radiol.14132410>
- Wang, J., Xinian Zuo, & Yong He. (2010). Graph-based network analysis of resting-state functional MRI. *Frontiers in Systems Neuroscience*. <https://doi.org/10.3389/fnsys.2010.00016>
- Wedeer, V. J., Hagmann, P., Tseng, W. I., Reese, T. G., & Weisskoff, R. M. (2005). Mapping complex tissue architecture with diffusion spectrum magnetic resonance imaging. *Magnetic Resonance in Medicine*, 54(6), 1377–1386. <https://doi.org/10.1002/mrm.20642>
- Wehrle, F. M., Michels, L., Guggenberger, R., Huber, R., Latal, B., O’Gorman, R. L., & Hagmann, C. F. (2018). Altered resting-state functional connectivity in children and adolescents born very preterm short title. *NeuroImage: Clinical*, 20, 1148–1156. <https://doi.org/10.1016/j.nicl.2018.10.002>
- White, R., & Krämer-Albers, E.-M. (2014). Axon-glia interaction and membrane traffic in myelin formation. *Frontiers in Cellular Neuroscience*, 7. <https://doi.org/10.3389/fncel.2013.00284>
- Whitehead, K., Pressler, R., & Fabrizi, L. (2017). Characteristics and clinical significance of delta brushes in the EEG of premature infants. *Clinical Neurophysiology Practice*, 2, 12–18. <https://doi.org/10.1016/j.cnp.2016.11.002>
- Whiteus, C., Freitas, C., & Grutzendler, J. (2014). Perturbed neural activity disrupts cerebral angiogenesis during a postnatal critical period. *Nature*, 505(7483), 407–411. <https://doi.org/10.1038/nature12821>
- Wiegell, M. R., Tuch, D. S., Larsson, H. B. W., & Wedeen, V. J. (2003). Automatic segmentation of thalamic nuclei from diffusion tensor magnetic resonance imaging. *NeuroImage*, 19(2), 391–401. [https://doi.org/10.1016/S1053-8119\(03\)00044-2](https://doi.org/10.1016/S1053-8119(03)00044-2)
- Wilkinson, M., Kane, T., Wang, R., & Takahashi, E. (2017). Migration Pathways of Thalamic Neurons and Development of Thalamocortical Connections in Humans Revealed by Diffusion MR Tractography. *Cerebral Cortex*, 27(12), 5683–5695. <https://doi.org/10.1093/cercor/bhw339>
- Williams, J. E., & Pugh, Y. (2018). The Late Preterm. *Critical Care Nursing Clinics of North America*, 30(4), 431–443. <https://doi.org/10.1016/j.cnc.2018.07.001>
- Williams, L. Z. J., Fitzgibbon, S. P., Bozek, J., Winkler, A. M., Dimitrova, R., Poppe, T., Schuh, A., Makropoulos, A., Cupitt, J., O’Muircheartaigh, J., Duff, E. P., Cordero-Grande, L., Price, A. N.,

- Hajnal, J. V., Rueckert, D., Smith, S. M., Edwards, A. D., & Robinson, E. C. (2023). Structural and functional asymmetry of the neonatal cerebral cortex. *Nature Human Behaviour*, 7(6), 942–955. <https://doi.org/10.1038/s41562-023-01542-8>
- Wilson, S., Pietsch, M., Cordero-Grande, L., Christiaens, D., Uus, A., Karolis, V. R., Kyriakopoulou, V., Colford, K., Price, A. N., Hutter, J., Rutherford, M. A., Hughes, E. J., Counsell, S. J., Tournier, J.-D., Hajnal, J. V., Edwards, A. D., O’Muircheartaigh, J., & Arichi, T. (2023). Spatiotemporal tissue maturation of thalamocortical pathways in the human fetal brain. *ELife*, 12. <https://doi.org/10.7554/eLife.83727>
- Wilson, S., Pietsch, M., Cordero-Grande, L., Price, A. N., Hutter, J., Xiao, J., McCabe, L., Rutherford, M. A., Hughes, E. J., Counsell, S. J., Tournier, J.-D., Arichi, T., Hajnal, J. V., Edwards, A. D., Christiaens, D., & O’Muircheartaigh, J. (2021). Development of human white matter pathways in utero over the second and third trimester. *Proceedings of the National Academy of Sciences*, 118(20). <https://doi.org/10.1073/pnas.2023598118>
- Wimberger, D., Roberts, T., Barkovich, A., Prayer, L., Moseley, M., & Kucharczyk, J. (1995). Identification of “Premyelination” by Diffusion-Weighted MRI. *Journal of Computer Assisted Tomography*.
- Woodward, L. J., Anderson, P. J., Austin, N. C., Howard, K., & Inder, T. E. (2006). Neonatal MRI to Predict Neurodevelopmental Outcomes in Preterm Infants. *New England Journal of Medicine*, 355(7), 685–694. <https://doi.org/10.1056/NEJMoa053792>
- World Health Organization, Partnership for Maternal, N. and C. H. U. N. C. F. (UNICEF), & United Nations Population Fund. (2023). *Born too soon: decade of action on preterm birth*. World Health Organization. .
- Wu, M.-J., Mwangi, B., Bauer, I. E., Passos, I. C., Sanches, M., Zunta-Soares, G. B., Meyer, T. D., Hasan, K. M., & Soares, J. C. (2017). Identification and individualized prediction of clinical phenotypes in bipolar disorders using neurocognitive data, neuroimaging scans and machine learning. *NeuroImage*, 145, 254–264. <https://doi.org/10.1016/j.neuroimage.2016.02.016>
- Wu, Y., Vasung, L., Calixto, C., Gholipour, A., & Karimi, D. (2023). Characterizing normal perinatal development of the human brain structural connectivity. *ArXiv*.
- Wylie, K., Rojas, D., Ross, R., Hunter, S., Maharajh, K., Cornier, M.-A., & Tregellas, J. (2014). Reduced brain resting-state network specificity in infants compared with adults. *Neuropsychiatric Disease and Treatment*, 1349. <https://doi.org/10.2147/NDT.S63773>
- Xu, G., Takahashi, E., Folkerth, R. D., Haynes, R. L., Volpe, J. J., Grant, P. E., & Kinney, H. C. (2014). Radial Coherence of Diffusion Tractography in the Cerebral White Matter of the Human Fetus: Neuroanatomic Insights. *Cerebral Cortex*, 24(3), 579–592. <https://doi.org/10.1093/cercor/bhs330>
- Yakovlev, P. I., & Lecours, A. (1967). *The myelogenetic cycles of regional maturation of the brain. Regional Development of the Brain in Early Life* (A. Minkowski, Ed.). Blackwell.
- Yeo, B. T., Krienen, F. M., Sepulcre, J., Sabuncu, M. R., Lashkari, D., Hollinshead, M., Roffman, J. L., Smoller, J. W., Zöllei, L., Polimeni, J. R., Fischl, B., Liu, H., & Buckner, R. L. (2011). The organization of the human cerebral cortex estimated by intrinsic functional connectivity. *Journal of Neurophysiology*, 106(3), 1125–1165. <https://doi.org/10.1152/jn.00338.2011>
- Yepes-Calderon, F., Lao, Y., Fillard, P., Nelson, M. D., Panigrahy, A., & Lepore, N. (2017). Tractography in the clinics: Implementing a pipeline to characterize early brain development. *NeuroImage: Clinical*, 14, 629–640. <https://doi.org/10.1016/j.nicl.2016.12.029>
- Yu, Q., Du, Y., Chen, J., Sui, J., Adali, T., Pearlson, G. D., & Calhoun, V. D. (2018). Application of Graph Theory to Assess Static and Dynamic Brain Connectivity: Approaches for Building Brain Graphs. *Proceedings of the IEEE*, 106(5), 886–906. <https://doi.org/10.1109/JPROC.2018.2825200>

- Yu, Q., Ouyang, A., Chalak, L., Jeon, T., Chia, J., Mishra, V., Sivarajan, M., Jackson, G., Rollins, N., Liu, S., & Huang, H. (2016). Structural Development of Human Fetal and Preterm Brain Cortical Plate Based on Population-Averaged Templates. *Cerebral Cortex*, 26(11), 4381–4391. <https://doi.org/10.1093/cercor/bhv201>
- Yu, Q., Peng, Y., Mishra, V., Ouyang, A., Li, H., Zhang, H., Chen, M., Liu, S., & Huang, H. (2014). Microstructure, Length, and Connection of Limbic Tracts in Normal Human Brain Development. *Frontiers in Aging Neuroscience*, 6. <https://doi.org/10.3389/fnagi.2014.00228>
- Yu, X., Ferradal, S. L., Sliva, D. D., Dunstan, J., Carruthers, C., Sanfilippo, J., Zuk, J., Zöllei, L., Boyd, E., Gagoski, B., Ou, Y., Grant, P. E., & Gaab, N. (2021). Functional Connectivity in Infancy and Toddlerhood Predicts Long-Term Language and Preliteracy Outcomes. *Cerebral Cortex*. <https://doi.org/10.1093/cercor/bhab230>
- Yuille, A. L., & Liu, C. (2018). Deep Nets: What have they ever done for Vision? *ArXiv*.
- Yun, H. J., Vasung, L., Tarui, T., Rollins, C. K., Ortinau, C. M., Grant, P. E., & Im, K. (2020). Temporal Patterns of Emergence and Spatial Distribution of Sulcal Pits During Fetal Life. *Cerebral Cortex*, 30(7), 4257–4268. <https://doi.org/10.1093/cercor/bhaa053>
- Zanin, E., Ranjeva, J., Confort-Gouny, S., Guye, M., Denis, D., Cozzone, P. J., & Girard, N. (2011). White matter maturation of normal human fetal brain. An in vivo diffusion tensor tractography study. *Brain and Behavior*, 1(2), 95–108. <https://doi.org/10.1002/brb3.17>
- Zhang, C., Bengio, S., Hardt, M., Recht, B., & Vinyals, O. (2023). Understanding deep learning requires rethinking generalization. *International Conference on Learning Representations*.
- Zhang, H., Schneider, T., Wheeler-Kingshott, C. A., & Alexander, D. C. (2012). NODDI: Practical in vivo neurite orientation dispersion and density imaging of the human brain. *NeuroImage*, 61(4), 1000–1016. <https://doi.org/10.1016/j.neuroimage.2012.03.072>
- Zhang, H., Shen, D., & Lin, W. (2019). Resting-state functional MRI studies on infant brains: A decade of gap-filling efforts. *NeuroImage*, 185, 664–684. <https://doi.org/10.1016/j.neuroimage.2018.07.004>
- Zhang, J., Liu, Y., Mitsuhashi, T., & Matsuo, T. (2021). Accuracy of Deep Learning Algorithms for the Diagnosis of Retinopathy of Prematurity by Fundus Images: A Systematic Review and Meta-Analysis. *Journal of Ophthalmology*, 2021, 1–11. <https://doi.org/10.1155/2021/8883946>
- Zhang, Y., Ma, M., Xie, Z., Wu, H., Zhang, N., & Shen, J. (2021). Bridging the Gap Between Morphometric Similarity Mapping and Gene Transcription in Alzheimer's Disease. *Frontiers in Neuroscience*, 15. <https://doi.org/10.3389/fnins.2021.731292>
- Zhao, T., Mishra, V., Jeon, T., Ouyang, M., Peng, Q., Chalak, L., Wisnowski, J. L., Heyne, R., Rollins, N., Shu, N., & Huang, H. (2019). Structural network maturation of the preterm human brain. *NeuroImage*, 185, 699–710. <https://doi.org/10.1016/j.neuroimage.2018.06.047>
- Zhao, X., Shi, J., Dai, F., Wei, L., Zhang, B., Yu, X., Wang, C., Zhu, W., & Wang, H. (2021). Brain Development From Newborn to Adolescence: Evaluation by Neurite Orientation Dispersion and Density Imaging. *Frontiers in Human Neuroscience*, 15. <https://doi.org/10.3389/fnhum.2021.616132>
- Zheng, W., Wang, X., Liu, T., Hu, B., & Wu, D. (2023). Preterm-birth alters the development of nodal clustering and neural connection pattern in brain structural network at term-equivalent age. *Human Brain Mapping*, 44(16), 5372–5386. <https://doi.org/10.1002/hbm.26442>
- Zheng, W., Zhao, L., Zhao, Z., Liu, T., Hu, B., & Wu, D. (2023). Spatiotemporal Developmental Gradient of Thalamic Morphology, Microstructure, and Connectivity from the Third Trimester to Early Infancy. *The Journal of Neuroscience*, 43(4), 559–570. <https://doi.org/10.1523/JNEUROSCI.0874-22.2022>

- Zhuang, F., Qi, Z., Duan, K., Xi, D., Zhu, Y., Zhu, H., Xiong, H., & He, Q. (2021). A Comprehensive Survey on Transfer Learning. *Proceedings of the IEEE*, 109(1), 43–76. <https://doi.org/10.1109/JPROC.2020.3004555>
- Zilles, K. (2018). Brodmann: a pioneer of human brain mapping—his impact on concepts of cortical organization. *Brain*, 141(11), 3262–3278. <https://doi.org/10.1093/brain/awy273>
- Zilles, K., & Amunts, K. (2015). *Anatomical Basis for Functional Specialization* (pp. 27–66). https://doi.org/10.1007/978-1-4899-7591-1_4
- Zöllei, L., Jaimes, C., Saliba, E., Grant, P. E., & Yendiki, A. (2019). TRActs constrained by UnderLying INfant anatomy (TRACULInA): An automated probabilistic tractography tool with anatomical priors for use in the newborn brain. *NeuroImage*, 199, 1–17. <https://doi.org/10.1016/j.neuroimage.2019.05.051>

Annexe 1: Résumé des travaux de thèse

Liste des abréviations

AET – âge équivalent au terme

CF – connectivité fonctionnelle

CG – connectivité de la substance grise

dHCP – *developing Human Connectome Project*

DTI – *Diffusion Tensor Imaging*

IRM – imagerie par résonance magnétique

IRMa – imagerie par résonance magnétique anatomique

IRMd – imagerie par résonance magnétique de diffusion

IRMfr – imagerie par résonance magnétique fonctionnelle au repos

NODDI – *Neurite Orientation Dispersion and Density Imaging*

1. Introduction

Le développement du cerveau repose sur des processus complexes qui commencent précocement durant la gestation et s'étendent jusqu'à la fin de l'adolescence. Il est marqué par d'importants changements structurels et fonctionnels, en particulier pendant la période prénatale et les premiers mois après la naissance (Lagercrantz, 2016). Les processus développementaux précoces ont été étudiés à l'aide de diverses approches méthodologiques, notamment par des méthodes histologiques *post-mortem* et par neuro-imagerie *in vivo* non invasive, en particulier l'imagerie par résonance magnétique (IRM). Ces études ont décrit une séquence de maturation stéréotypée, c'est-à-dire spatio-temporellement hétérogène entre les régions de substance grise et entre les faisceaux de substance blanche, ainsi qu'une progression de l'activité et de la connectivité fonctionnelle (Dubois et al., 2015; Ouyang, Dubois, et al., 2019).

L'importance de cette période a été soulignée par la vulnérabilité précoce des trajectoires neurodéveloppementales aux événements périnataux défavorables, tels que la prématurité (Volpe, 2019). Les études de comparaison des enfants nés prématurément, évalués à l'âge équivalent au terme (AET) de la grossesse, avec leurs pairs nés à terme ont révélé systématiquement des différences dans les caractéristiques cérébrales, y compris des altérations morphologiques (Dubois et al., 2019b; Pittet et al., 2019; Chiarelli et al., 2021), des lésions fréquentes et des anomalies diffuses de la substance blanche (Malavolti et al., 2017; Lean et al., 2019; Smyser et al., 2019; Kline, Illapani, et al., 2021), des différences de microstructure

des régions corticales et sous-corticales (Ouyang, Jeon, et al., 2019; Dimitrova et al., 2021), ainsi qu'une altération de la connectivité fonctionnelle (Brenner et al., 2021; Chiarelli et al., 2021; Eyre et al., 2021).

De plus, un rapport mondial a récemment révélé une statistique inquiétante : 1 enfant sur 10 est né prématurément (avant 37 semaines d'âge gestationnel) (WHO, 2023), et les survivants prématurés seraient confrontés à des conséquences sanitaires tout au long de leur vie, notamment une probabilité accrue de handicap, y compris des déficiences graves telles que la paralysie cérébrale (première cause de handicap moteur chez l'enfant), des déficiences sensorielles et des déficits cognitifs notables (Longo et al., 2021; Marret et al., 2013; McGowan & Vohr, 2019; Serenius et al., 2016), ces troubles du neurodéveloppement ayant un impact sur l'éducation, la santé, les résultats sociaux et la qualité de vie globale des enfants (Pierrat et al., 2014) mais aussi avec des conséquences tout au long de leur vie.

Face à ces enjeux, mieux évaluer les nouveau-nés, de façon fiable et précoce, semble essentiel. De nombreuses études ont alors souligné le rôle important de l'IRM précoce dans l'identification des altérations cérébrales substantielles chez les prématurés (Banihani et al., 2021). Cette détection est utile pour développer des biomarqueurs de diagnostic et de pronostic basés sur l'IRM afin de prédire le devenir neurodéveloppemental, facilitant ainsi les interventions individualisées permettant d'améliorer les perceptions, les acquisitions et les apprentissages des nourrissons nés prématurément. Des modèles prédictifs s'appuyant sur l'apprentissage automatique (approche d'intelligence artificielle) ont été mis au point pour prédire des aspects variés, tels que la mortalité (Mangold et al., 2021), la septicémie (Persad et al., 2021) et la rétinopathie du prématuré (Zhang et al., 2021). Cependant, les études ayant exploré les liens avec le neurodéveloppement ultérieur sont plus rares. Les recherches antérieures se sont concentrées principalement sur le devenir moteur, cognitif et langagier et ont fait état d'une prédiction réussie à l'aide de divers ensembles de caractéristiques d'entrée, dérivées de l'IRM anatomique (IRMa), de diffusion (IRMd) et fonctionnelle au repos (IRMfr) (Baker & Kandasamy, 2023; van Boven et al., 2022). Ces exemples suggèrent le potentiel des marqueurs IRM précoces pour prédire le devenir neurodéveloppemental à l'échelle individuelle et devraient servir d'inspiration pour les recherches futures.

2. Méthodes générales

Dans cette thèse, notre objectif principal était d'étudier les altérations du développement précoce du cerveau dans le contexte de la prématurité, par comparaison aux nourrissons se développant de façon typique suite à une naissance à terme. Notre second objectif était

d'explorer le développement précoce du cerveau en termes d'évolution de la connectivité structurelle et fonctionnelle au cours de cette phase critique que constituent les dernières semaines pré-terme.

Pour atteindre ces objectifs, nous avons concentré nos analyses sur une grande base de données : celle du *developing Human Connectome Project* (dHCP) (E. J. Hughes et al., 2017). Cette base comprend des sets individuels d'IRM multimodales (IRMa, IRMd, et IRMfr) acquises et prétraitées avec des outils optimisés pour les cerveaux des nouveau-nés et des nourrissons, ainsi que des informations cliniques complémentaires et des scores neurodéveloppementaux à 18 mois d'âge corrigé (Bayley, 2006). Dans sa troisième publication, la base de données dHCP comprend les données de 783 sujets, incluant à la fois des enfants nés prématurément et des enfants nés à terme.

Nous avons axé notre évaluation du développement cérébral des nourrissons sur différentes mesures de connectivités, notamment la connectivité structurelle de la substance blanche, estimée à partir de l'IRMd à l'aide de méthodes de tractographie basées sur les graines (*seed-based*) et du cerveau entier (*whole-brain*), ainsi que la connectivité fonctionnelle dérivée des données de l'IRMfr. En outre, nous avons étudié une autre mesure originale de connectivité, basée sur la similarité microstructurelle des régions de substance grise, et ses relations avec la connectivité fonctionnelle au cours du développement. L'estimation de ces connectivités était basée sur l'identification des régions corticales et sous-corticales dérivées de parcellisations basées sur l'IRMa (Adamson et al., 2020).

Au cours de ces travaux de thèse, nous avons privilégié des approches multivariées adaptées qui intègrent des informations complémentaires provenant de différents marqueurs IRM, notamment la distance de Mahalanobis pour quantifier les effets de la prématurité sur les réseaux sensorimoteurs (*Chapitre 3*), l'apprentissage automatique pour identifier les modèles distinguant les sujets prématurés des sujets nés à terme ou prédire à l'échelle individuelle le devenir neurodéveloppemental (*Chapitre 4*), ou encore les comparaisons de connectivité de la substance grise et de la connectivité fonctionnelle basées sur des réseaux dérivés d'une classification hiérarchique (*Chapitre 5*). Ces études sont décrites plus en détails dans les sections suivantes.

3. Effet de la prématurité sur le réseau sensorimoteur

Le système sensorimoteur (SM) joue un rôle fondamental dans le développement de l'enfant. Établi précocement (Dubois et al., 2014), le réseau cérébral associé est impliqué dans la formation du connectome structurel et fonctionnel (van den Heuvel et al., 2015; T. Zhao et

al., 2019) et sert de base aux acquisitions comportementales (Heineman et al., 2018; van der Fels et al., 2019). Dans notre étude, nous avons cherché à étudier l'impact de la prématurité sur les caractéristiques microstructurelles de ce réseau chez les nourrissons à l'AET et son association potentielle avec le devenir neurodéveloppemental. Notre étude s'est concentrée sur les connexions au sein d'un sous-ensemble de régions corticales primaires et sous-corticales du système sensorimoteur, disséquées à l'aide d'une approche de tractographie probabiliste (Behrens et al., 2007).

Pour évaluer quantitativement les altérations du réseau SM dans le groupe de 59 nourrissons prématurés considérés (l'âge médian de gestation 31.7 semaines entre [23.7s–36.0s], sans anomalie cérébrale détectée), nous avons comparé ses caractéristiques microstructurelles estimées par les modèles de Diffusion Tensor Imaging (DTI) (Basser et al., 1994) et de Neurite Orientation Dispersion and Density Imaging (NODDI) (Zhang et al., 2012) aux valeurs typiques d'un groupe de référence de 59 nouveau-nés à terme et en bonne santé, en utilisant une distance de Mahalanobis multivariée. Nos résultats ont démontré que la prématurité affecte le réseau SM primaire à l'AET, avec des effets plus prononcés chez les nourrissons nés à des âges gestationnels plus précoces. En outre, notre approche a révélé des schémas complexes de l'impact de la prématurité, montrant des effets plus importants au niveau des voies rostrales et périphériques en comparaison des voies caudales et centrales, en accord avec la trajectoire connue de la progression de la maturation globale de la substance blanche (Yakovlev & Lecours, 1967). En outre, notre approche a suggéré que certaines de ces altérations dans des voies spécifiques étaient associées au devenir moteur et cognitif des nourrissons à l'âge corrigé de 18 mois.

4. Prédiction individuelle des caractéristiques spécifiques et du devenir neurodéveloppemental

Si les études de groupe fournissent des informations précieuses sur les altérations du développement cérébral dans le contexte de la prématurité, elles ne sont pas adaptées à la prédiction des résultats individuels. Pour pallier ce problème, des recherches récentes se sont tournées vers la modélisation prédictive à l'aide de l'apprentissage automatique supervisé qui peut aider à établir des relations fondées sur des données entre les marqueurs précoces dérivés de l'IRM et les exemples annotées, par exemple pour détecter de nouveaux modèles de développement atypique entre enfants nés prématurés et enfants nés à terme ou pour prédire un devenir neurodéveloppemental défavorable. Étant donné l'importance et l'enjeu d'identifier de

façon précoce et fiable des nourrissons présentant un risque de trouble du neurodéveloppement, nous avons voulu explorer cette stratégie dans le cadre de trois études.

Premièrement, nous avons cherché à utiliser les descripteurs microstructuels du réseau SM pour prédire le devenir neurodéveloppemental à 18 mois d'âge corrigé sur les mêmes nourrissons que l'étude précédente (N=59x2), mais nous n'avons pas réussi à prédire les résultats individuels, même en incluant d'autres caractéristiques cliniques et environnementales pertinentes.

Deuxièmement, nous avons exploré le potentiel de marqueurs de la microstructure corticale, car une étude précédente avait suggéré leur pouvoir prédictif élevé du devenir neurodéveloppemental (Ouyang et al., 2020). Malgré nos tentatives d'élargir la taille et les caractéristiques des données d'entraînement et d'étendre la validation de l'étude originale, nous n'avons pas été en mesure de reproduire ces résultats, ce qui met en évidence les difficultés de reproductibilité et la nécessité de méthodologies normalisées et d'une validation approfondie dans les études d'apprentissage automatique, en particulier avec de petits ensembles de données.

Troisièmement, nous avons utilisé les mesures de microstructure corticale pour distinguer les nourrissons prématurés à l'AET et les nouveau-nés avant terme (N=59x2) avec une approche guidée par les données, confirmant des différences globales précoces associées à la prématurité.

5. Relations entre la similarité microstructurale de la substance grise et le connectome fonctionnel au cours du développement précoce

Dans cette dernière étude, nous avons étudié l'évolution de la connectivité de la substance grise (CG) et de la connectivité fonctionnelle (CF) au sein des régions corticales et sous-corticales chez 45 sujets prématurés, évalués de la naissance à l'âge équivalent au terme, par rapport à 45 nouveau-nés à terme. Nos analyses ont montré un renforcement global de la connectivité avec le développement dans les modalités CG et CF. L'utilisation d'une approche de classification hiérarchique des connectivités CG et CF a permis une comparaison au niveau des réseaux, révélant un chevauchement croissant entre les modalités de CG et CF et suggérant des modèles partagés dans les structures de réseau à la fois au niveau microstructurel et fonctionnel. De plus, les nourrissons prématurés à l'AET montraient, par rapport aux

nourrissons nés à terme, des altérations significatives des forces de connectivité CG et CF et des relations CG-CF au niveau du réseau. Dans l'ensemble, nos résultats ont mis en évidence que les mesures de similarité microstructurale sont pertinentes sur la période pré-terme, et fournissent des informations précieuses sur le développement des réseaux en lien avec leur fonction.

6. Discussion et conclusion générale

Dans le cadre de cette thèse, nous avons confirmé l'impact significatif de la prématurité sur le développement du cerveau. En utilisant une vaste base de données multimodale d'IRM précoce *in vivo*, nous avons tout d'abord confirmé la vulnérabilité des voies sensorimotrices et suggéré des associations entre certaines altérations et le devenir neurodéveloppemental (Neumane et al., 2022; Gondová, Neumane, Leprince, Hertz-Pannier, et al., 2023). Nous avons par ailleurs tenté d'établir un lien entre les marqueurs IRM du cerveau et le neurodéveloppement ultérieur à l'aide d'une modélisation prédictive, en nous appuyant soit sur les descripteurs microstructuraux du réseau SM (Gondová, Neumane, Leprince, Arichi, et al., 2023), soit sur la microstructure corticale (Gondová, Neumane, Leprince, Mangin, et al., 2023). Nos travaux ont également suggéré que les relations microstructurelles-fonctionnelles évoluent de façon complexe au cours du développement et sont impactées par la prématurité (*Chapitre 5*).

Bien que nos études originales aient fourni des résultats intéressants, elles présentent un certain nombre de limitations liées à la sensibilité des données aux paramètres d'acquisition et aux effets liés à l'âge sur la qualité des post-traitements utilisés. Ces difficultés limitent les comparaisons directes avec d'autres études et peuvent introduire des facteurs de confusion dans les résultats. Les recherches futures pourraient explorer des approches longitudinales en s'appuyant sur les sujets de la cohorte dHCP avec plusieurs imageries afin d'envisager des analyses centrées sur l'individu. Comparer les altérations cérébrales liées à la prématurité avec celles d'autres agressions périnatales, telles que l'accident vasculaire cérébral néonatal ou l'encéphalopathie hypoxique-ischémique, pourrait mettre en évidence des voies potentiellement communes de perturbations neurodéveloppementales et de vulnérabilité.

En outre, il est essentiel d'identifier de manière fiable et précoce les nourrissons qui risquent de souffrir de futurs troubles du neurodéveloppement pour pouvoir mettre en place des interventions efficaces qui tirent parti de la grande plasticité du cerveau au cours des premiers mois post-nataux. Pour parvenir à un pronostic précoce fiable, les efforts futurs devraient se concentrer sur l'affinement des stratégies prédictives à l'aide de divers modèles

d'apprentissage automatique, d'approches de sélection des caractéristiques et d'ensembles de données plus variés. Des études récentes ont exploré l'intégration de modalités IRM complémentaires, ce qui a donné des résultats prédictifs prometteurs (Fenchel et al., 2022; He et al., 2021; Janjic et al., 2020). Cependant, la variabilité inter-individuelle du devenir neurodéveloppemental s'explique par une interaction complexe de facteurs, englobant le développement dynamique des caractéristiques cérébrales et des éléments externes, notamment environnementaux. L'intégration de marqueurs IRM multimodaux et de ces facteurs complémentaires, ainsi que l'élargissement des cohortes d'apprentissage devraient permettre d'obtenir des informations plus complètes sur le développement précoce du cerveau chez les prématurés. Ceci, à son tour, devrait améliorer la précision des modèles de prédiction du devenir neurodéveloppemental à l'échelle individuelle, dans le but ultime d'améliorer les soins, la prise en charge et par conséquent la qualité de vie de cette population vulnérable et de leur famille.

Annexe 2: Whole-brain tractography in PT/FT infants

In *Chapter 5*, we highlighted the ability of microstructural similarity between grey matter regions to offer an alternative point of entry for studying potentially meaningful functional networks. As an extension of this work, we also aimed to integrate the structural white-matter connectivity into the evaluations using the whole-brain tractography approach.

In the past, various methodologies have been employed to estimate connectomes in both preterm infants (PT) at term-equivalent age (TEA) and full-term (FT) neonates using whole-brain tractography. These approaches were based either on DTI (Brown et al., 2014; Lee et al., 2019), probabilistic tractography with BedPostX fibre orientation estimations and ProbTrackX (Ball et al., 2014), fibre orientation distribution estimates derived from single-shell single-tissue (SS1T) constrained spherical deconvolution (CSD) (Sa de Almeida et al., 2021), or multi-shell multi-tissue CSD (MSMT-CSD) (Zheng, Wang, et al., 2023). Recently, the whole-brain tractography analysis was also presented for PT subjects near birth utilizing MSMT-CSD (Ciarrusta et al., 2022).

Given the diversity of the available approaches, it appeared challenging to find a consensus on the method that best suits the complicated nature of reliably tracing the connectomes in the immature brain. Therefore, we tested a number of strategies that led to promising, but imperfect estimations of whole-brain connectomes, affected by different properties of the very young brains. In this section, we present some of the tested methods and intertwine them with our observations, with hope to lay the foundation for further refinement and expansion of this strategy in the future.

Dataset

This section employed the same dMRI data for three groups of infants as in the *Chapter 5*, including 45 PT infants (26 males, GA at birth – median 32.3 weeks, range [25.6w–36.0w]) (PT:ses1) scanned near birth (PMA at scan median 34.9 weeks, range [28.3w–36.9w]) and at TEA (PMA at scan median 41.3 weeks, range [38.4w–44.9w]) (PT:ses2), and a group of FT neonates matched to PT:Ses2 on age at MRI at TEA and sex.

Estimation of fibre orientation distribution

To estimate the fibre orientation distributions within the dMRI dataset, we first aimed to compare different tissue response estimation strategies: single-shell single-tissue (SS1T) (Tournier et al., 2013), single-shell three-tissues (SS3T) (Dhollander & Connelly, 2016), multi-shell three-tissues (MS3T) and multi-shell two-tissues (MS2T) constrained spherical

deconvolution (CSD) (Dhollander et al., 2019; Jeurissen et al., 2014). All methods except for SS3T were implemented in MRtrix3 (Tournier et al., 2019). SS3T was estimated with MRtrix3Tissue (<https://3Tissue.github.io>), a fork of MRtrix3. For the multi-tissue estimates, based on (imperfect) visual evaluation of estimated tissues, we decreased the FA threshold to 0.08 to reflect the lower overall anisotropy within the immature infant brains, as well as generally lower FA that resulted from the SHARD-processing of the diffusion data.

Estimation of the WM tissue components for each of the models was significantly impacted by the subject's PMA at scan (*Figure A2.1a* - only the MS2T estimation shown). To derive the group-average response functions for each model and estimated compartment, we calculated the average over 23 FT individuals whose white matter response at $b=1000\text{s/mm}^2$ fell into the interquartile range of the group to avoid potential error stemming from group's outliers in response estimates (*Figure A2.1a*). Different models were evaluated on a single example subject (PMA at scan 41w, GA at birth 37, female) using the average responses to perform visual evaluation of the tissue estimates and preliminary tractography results (*Figure A2.1b*). Interestingly, in this subject, using only the $b=1000\text{s/mm}^2$ shell for the 3 tissue estimation (SS3T) models seemed to improve the multi-shell estimates (MS3T) which tended to overestimate the GM compartment. Nevertheless, although we acknowledge the limitation of basing this choice only on the one FT subject, we suggested that MS2T-CSD algorithm might be appropriate (at least in FT infants) to deconvolve the dMRI into WM fibre orientation distribution function (fODF) and CSF components. We subsequently corrected each subject's tissue components for global intensity differences using *mtnormalise* (Tournier et al., 2019).

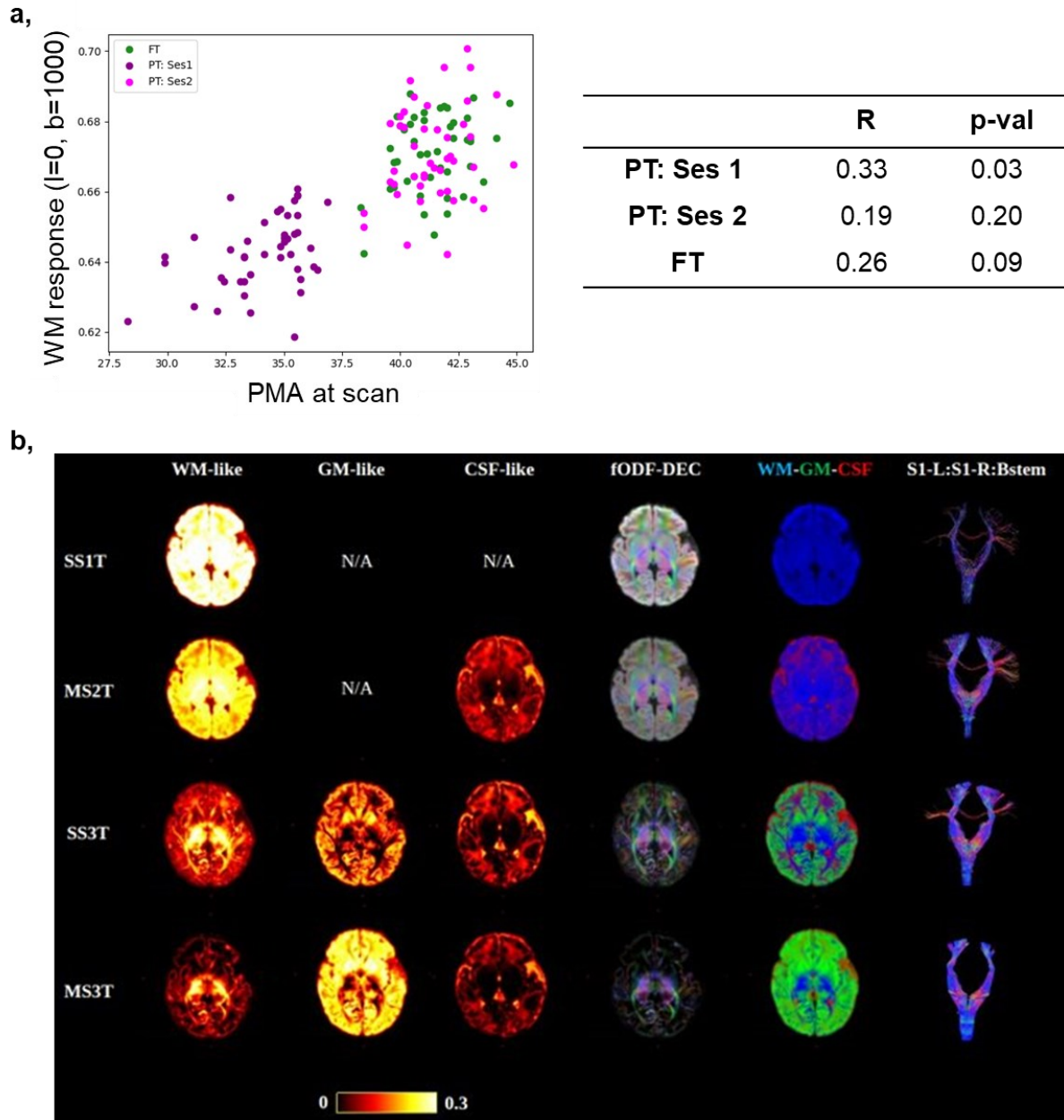


Figure A2.1a, WM tissue estimate (harmonic degree $l=0$) was significantly associated with PMA at scan over all subjects, and within PT:ses1. **b**, Example of tissue response CSD estimates for an example subject (F, PMA at scan 41w) estimated with: **SS1T** algorithm ($b=0,1000s/mm^2$); **MS2T** ($b=0,400,1000,2600s/mm^2$, $FA=0.08$); **SS3T** ($b=0,1000s/mm^2$, $FA=0.08$); and **MS3T** ($b=0,400,1000,2600s/mm^2$, $FA=0.08$) computed based on the corresponding average response function over the 23 FT individuals. The example tractograms (right column) show inter-hemispheric S1-S1, and bilateral S1-brainstem fibre reconstructions estimated with probabilistic tractography (5000k streamlines, WM seed mask, step size of 0.25mm, max. angle of 30° , filtering with SIFT algorithm to 1/10 size). Scaling across images: fODF directionally encoded colour (DEC) scaling between $[0,1]$, WM-GM-CSF $[0,0.3]$.

Tractogram generation

ODF estimates were used as inputs to the probabilistic tracking with second-order Integration over Fiber Orientation Distributions (iFOD2) algorithm (Tournier et al., 2010). Seed masks for the tractography were obtained from the WM segmentation provided within the dHCP database. Additionally, we refined the seed mask by removing voxels with high likelihood of belonging to CSF, i.e. voxels with $MD < 2.10-3\text{mm}^2/\text{s}$ (except voxels with $FA > 0.25$ which might correspond to WM voxels in the corpus callosum but close to the ventricles with some CSF partial volume effects).

Given that tractography outputs are highly dependent on the specific parameter settings (Schilling et al., 2021), we proposed to use an ‘ensemble’ tractography approach which might reduce the parameter dependencies and lead to more robust tractogram estimates (Takemura et al., 2016). We performed 4 tractography runs that performed individually well upon previous visual assessments of inter-hemispheric S1-S1, and bilateral S1-brainstem dissections, using different parameter settings (run 1: 1200k streamlines, step 0.25mm, angle 30°; run 2: 1200k streamlines, step 0.25mm, angle 40°, run 3: 1200k streamlines, step 0.5mm, angle 30°; run 4: 1200k streamlines, step 0.5mm, angle 45°) by randomly seeding from the WM mask. Subsequently, we combined the four partial tractograms together resulting in an ensemble of 5 million streamlines before filtering to 1/10 size with SIFT algorithm (Smith et al., 2013).

Connections between previously parcellated ROIs (as described in *Chapter 5*) were then decomposed using *scil* python package (SCIL, 2023), keeping the longest streamline segment connecting the ROI pairs. Similarly, we used the *scil* package to extract whole ROI-to-ROI connectivity matrices with links between regions quantified by streamline counts and lengths derived from the tractograms as well as average diffusion metrics (FA, AD, RD, MD, NDI, and ODI).

Quality Assessments: Evaluation of link presence with age, region size, length, etc.

We observed a significant effect of PMA at scan on the quality of both the estimated tissue components as well as resulting tractographies. Focusing on the youngest subject in the study (PMA at scan 28w), we observed that the approach was highly different to FT estimations. Higher water content and lower WM anisotropies led to overestimation of GM and CSF compartments in the three tissue models (SS3T, MS3T), and failed to lead to successful tracing of inter-hemispheric S1-S1 (primary somatosensory cortex), and bilateral S1-brainstem

tracts. MS3T led to slightly better estimations but nevertheless failed to result in successful inter-hemispheric S1-S1 connectivity (*Figure A2.2a*). The simplest SS1T model led to overestimation of WM tissue content in cortical areas (likely driven by high anisotropy in the cortex earlier in development which lowers with age) that resulted in some spurious streamlines.

Inter-hemispheric S1-S1, and bilateral S1-brainstem tracts were again used to visually assess the quality of the final ensemble tractography results. We observed a significant inter-individual variation in the quality of reconstructed tracts, especially the inter-hemispheric S1-S1 connections. Qualitative evaluation gave the impression that results were also related to age at scan (*Figure A2.2b*). This again suggested that MS2T model might be the most appropriate (or rather the least inappropriate) choice, but clearly highlighted major differences in young preterms and FT infants which likely affect the reliability of the resulting connectomes.

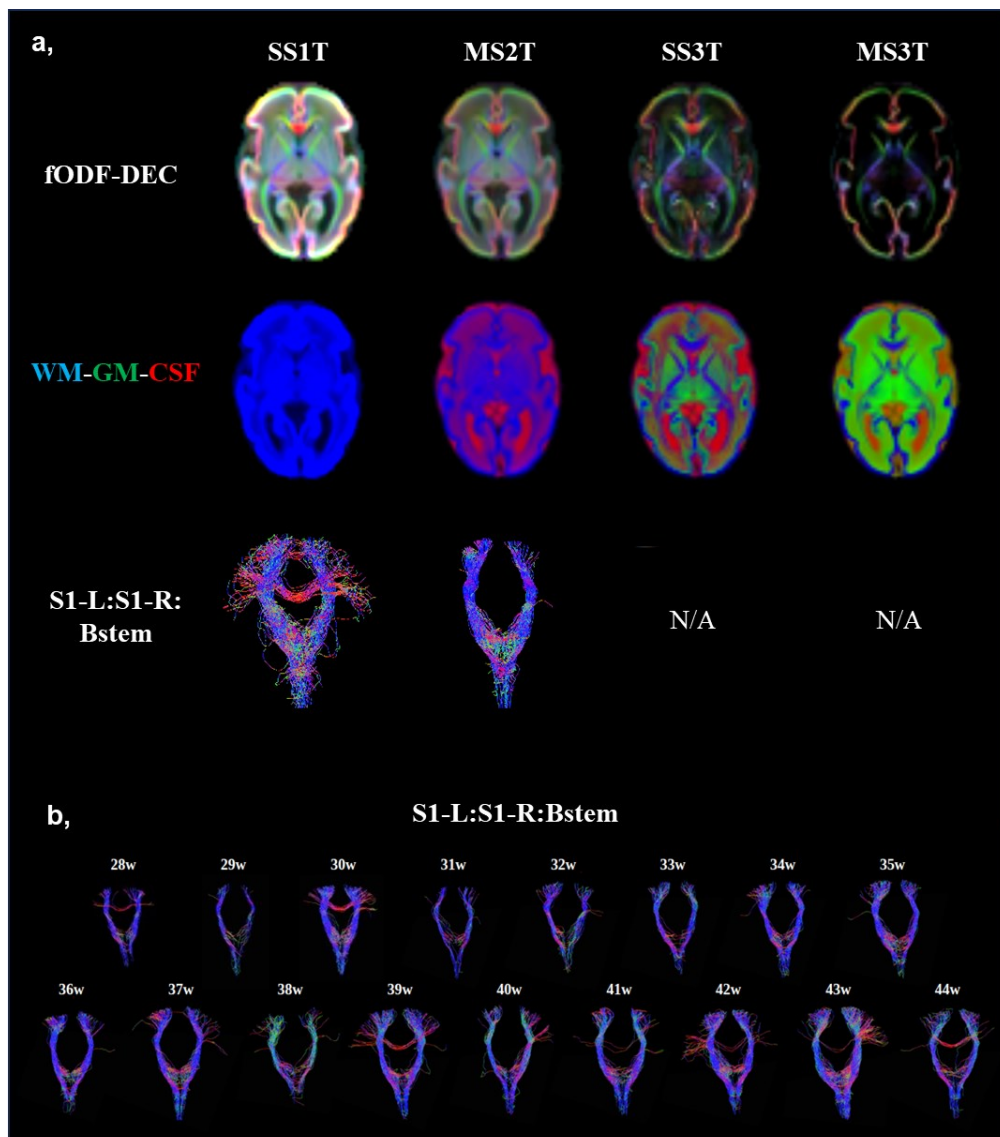


Figure A2.2a, Example of tissue response estimates CSD estimates for the youngest subject at scan (male, PMA at scan 28w) estimated with different algorithms as described in the *Figure A2.1*. Of note, WM and GM tissue estimates seemed ‘reversed’, or rather, the properties of the cortex resembled the white matter (as expected by the models) likely due to higher cortical FA in the early period. **b**, Effect of age on quality of inter-hemispheric S1-S1, and bilateral S1-brainstem tract delineations derived from the ensemble tractography.

Analyses of the derived structural connectivity matrices over all PT and FT infants showed (expected) significant effects of age at scan on the number of delineated connections across the brain (linear regression: all subjects $p\text{-val} < 0.001$, PT:ses1 $p\text{-val} = 0.02$, PT:ses2 $p\text{-val} = 0.02$, FT $p\text{-val} = 0.02$, corrected for multiple comparisons with false-discovery rate approach) (*Figure A2.3*). Overall, we observed that streamline lengths were significantly associated with streamline numbers (linear regression, slope = -0.41, $p\text{-val} < 0.001$) (although this was not corrected for brain size). Importantly, we also observed a significant difference between PT:ses2 and FT in terms of the number of delineated connections (two-tail t-test, $T = -4.27$, $p\text{-val} < 0.01$). In contrast to previous assumption that PT-FT data would be comparable as possible errors from tractography would be similar within the same age range (sa de Almeida et al., 2021), our results suggested that this might not be the case and the estimations might differ for the same tractography setting between the PT and FT infants at TEA. Not considering such differences might have a downstream effect on the conclusion of group-comparison.

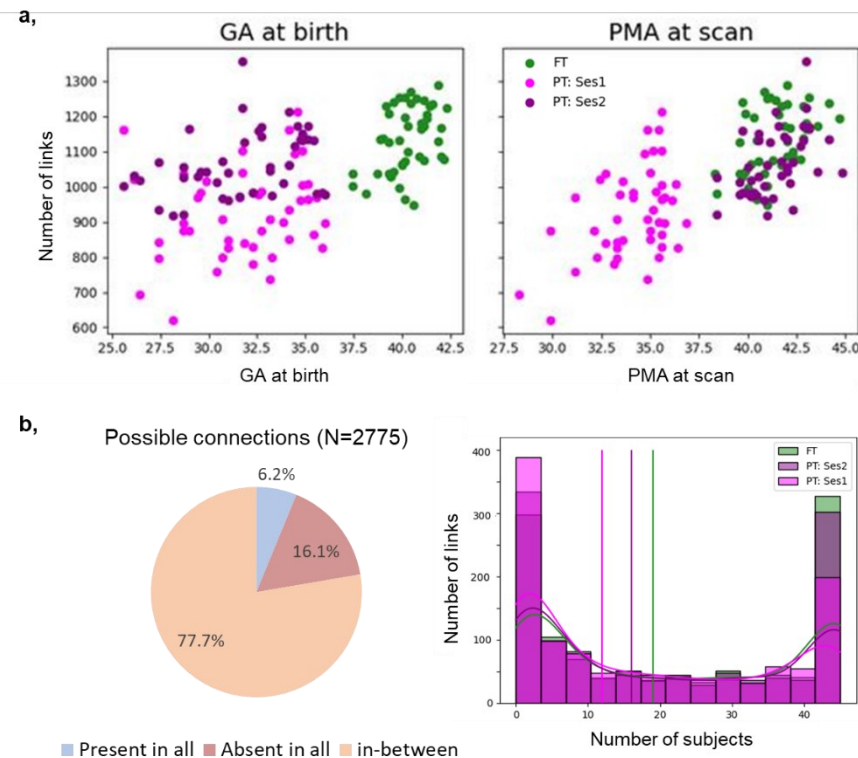


Figure A2.3. Quality assessment of the resulting white-matter connectivity matrices. **a**, Number of identified connections as a function of subject's GA at birth and PMA at scan. **b**, Proportion of connections present in all 135 infants, absent in all infants, and the links that were identified in some subjects (likely representing a combination of false positives, false negatives, and possible progressive formation of some connections with age).

As expected, the effects were even more pronounced in PT:ses1 group. Given the substantial evolution of the different components as a function of age (Pietsch et al., 2019), it is possible that adapting the tissue response estimates to a specific group (rather than using the average estimates from the FT group) might be more appropriate to get more reliable estimates within specific groups in the future. However, this might also limit subsequent between-group comparisons, as differences in scaling of fibre orientation distributions estimated between groups might have complex effects on tractography estimations. Alternatively, focusing analysis only on the subset of tracts that were estimated in all subjects (ignoring the false negatives) might be a viable strategy, but this would, in our study, significantly affect the comparisons with the microstructural grey matter and functional connectomes.

Instead of restricting our focus on subset of connections, we attempted to post-process the derived structural connectivity matrices, for example by using the streamline numbers for non-homotopic inter-hemispheric connections (other than cerebellum) as a threshold for the connection filtering. Even then however, the effect of PMA at scan remained significant in all three groups of infants. Filtering the connectome matrices this way, we observed some (statistically significant) trend between the streamline number for the ROI pairs (corrected for their length) and their microstructural similarity, especially for the cortical regions. However, the current approach had too many limitations to derive any conclusions. That is why we did not include the present analyses in our last study (*Chapter 5*).

Future investigations should focus on improving the tractography results, including larger streamline numbers, or using alternative filtering strategies such as SIFT2 which offers streamline weights rather than removing them completely to be considered during connectivity matrix estimation steps (Smith et al., 2015). Alternatively, global tractography methods (as opposed to the above described local 'step-by-step' reconstruction approaches) might provide benefits as they are not in the same way affected by local mistakes in local fibre orientations (Mangin et al., 2013). Anatomically, informed global approaches adapted to older infant brains were previously reported to lead to promising results (Zöllei et al., 2019). Benefits to the PT population near birth should be tested in the future.

Annexe 3: Supplementary materials

3.1. Supplementary materials for Chapter 3

‘Early structural connectivity within the sensorimotor network: Deviations related to prematurity and association to neurodevelopmental outcome’ (Neumane, Gondova et al., 2023)

Table SupT1. Clinical factors for the 4 infants’ sub-groups used for the adjustments in descriptive models. Preterm infants (PT) were subdivided into those born extremely to very preterm (PT_{EV}) or moderate to late preterm (PT_{ML}) and their corresponding full-term (FT) controls.

	PT _{EV} (N=33)	FT _{EV} ct (N=33)	PT _{ML} (N=26)	FT _{ML} ct (N=26)
GA at birth (<i>weeks</i>) <i>Median (IQR) [range]</i>	29.0 (27.4; 30.7) [23.7; 31.9]	40.4 (39.9; 41.1) [37.4; 42.3]	34.3 (33.2; 35.1) [32.3; 36.0]	40.1 (39.4;40.8) [37.4;42.1]
Sex, <i>male</i>	18 (55%)	18 (55%)	15 (58%)	15 (58%)
Multiple Pregnancy, <i>twins</i>	9 (27%)	0	9 (35%)	1 (4%)
IUGR	10 (33%) <i>NA: 3</i>	0 <i>NA: 1</i>	7 (28%) <i>NA: 1</i>	1 (4%) <i>NA: 1</i>
Preterm Morbidities	21 (64%)	0	4 (36%) <i>NA: 15</i>	0
Parenteral Nutrition >21days	4 (12%)	0	0 <i>NA: 5</i>	0
PMA at MRI (<i>weeks</i>) <i>Median (IQR) [range]</i>	41.3 (40.1; 42.3) [38.4; 44.9]	41.3 (40.3;42.3) [38.3;44.7]	41.1 (40.1;42.0) [38.9;44.1]	41.1 (40.1;42.0) [38.9;44.1]

Refer to Table 1 legend for abbreviations.

Table SupT2. Cohort characteristics and outcome assessment at around 18 months of corrected age.

		Preterm infants (n=59)		Full-term controls (n=59)		<i>p</i>
		<i>NA</i>		<i>NA</i>		
Sex, male	N (%)	15	23 (52.3) □	6	30 (56.6) □	#
Age at assessment (<i>months</i>)	Median (IQR) [Range]	15		6		
Chronological age			20.4 (19.8;21.1) [18.9;23.4]		18.2 (17.8;18.7) [17.3;19.8]	***
Corrected age			18.4 (18.1;18.7) [17.7;20.8]		18.2 (17.9;18.6) [17.3;19.8]	ns
Family socioeconomic status: Index of multiple deprivation (IMD)	Median (IQR) [Range]	17	17.8 (11.1;29.7) [2.7;48.3]	5	26.6 (18.2;33.8) [4.2;46.4]	*
BSID-III: <i>Scaled scores</i>	Mean (SD) [range]	15		6		

Cognitive			10.1 (2.6) [1.0;15.0]		10.2 (2.0) [4.0;15.0]	ns
Receptive communication			10.7 (3.8) [1.0;19.0]		10.8 (3.1) [5.0;18.0]	ns
Expressive communication			8.7 (2.8) [1.0;15.0]		9.6 (2.5) [4.0;14.0]	ns
Fine motor			11.0 (2.5) [2.0;15.0]		11.1 (2.2) [4.0;16.0]	ns
Gross motor			9.0 (2.0) [3.0;16.0]		9.3 (1.6) [5.0;13.0]	ns

□ percentage over the available data (see NA for missing data). Comparisons for ages at assessment and IMD scores were performed with Wilcoxon rank sum test. #: no comparisons done for sex (used for pairing the full-term controls). *p*-values for BSID-III scores were obtained from t-tests corrected for multiple comparisons. Refer to *Table 1* legend for abbreviations. See *Figure 2* for BSID-III scores distributions and graphical comparison between groups.

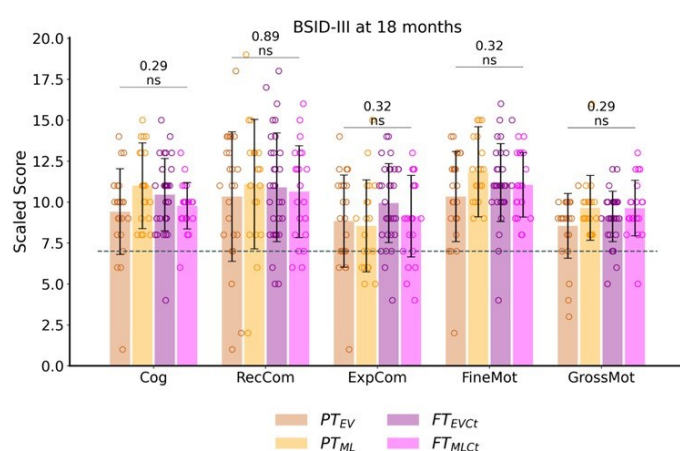


Figure SupF1. Outcome assessment at around 18 months of corrected age: BSID-III scaled scores across subgroups (PT_{EV}, PT_{ML}, FT_{EVct}, and FT_{MLct}), with the results of one-way ANOVA and *p*-values indicating no significant group effect. The dotted line indicates the scores threshold indicating a developmental delay (scores < -1 SD): scaled scores < 7. Cog: cognitive; RecCom: receptive communication, ExpCom: expressive communication; FineMot: fine motor, GrossMot: gross motor scores. ns: not significant.

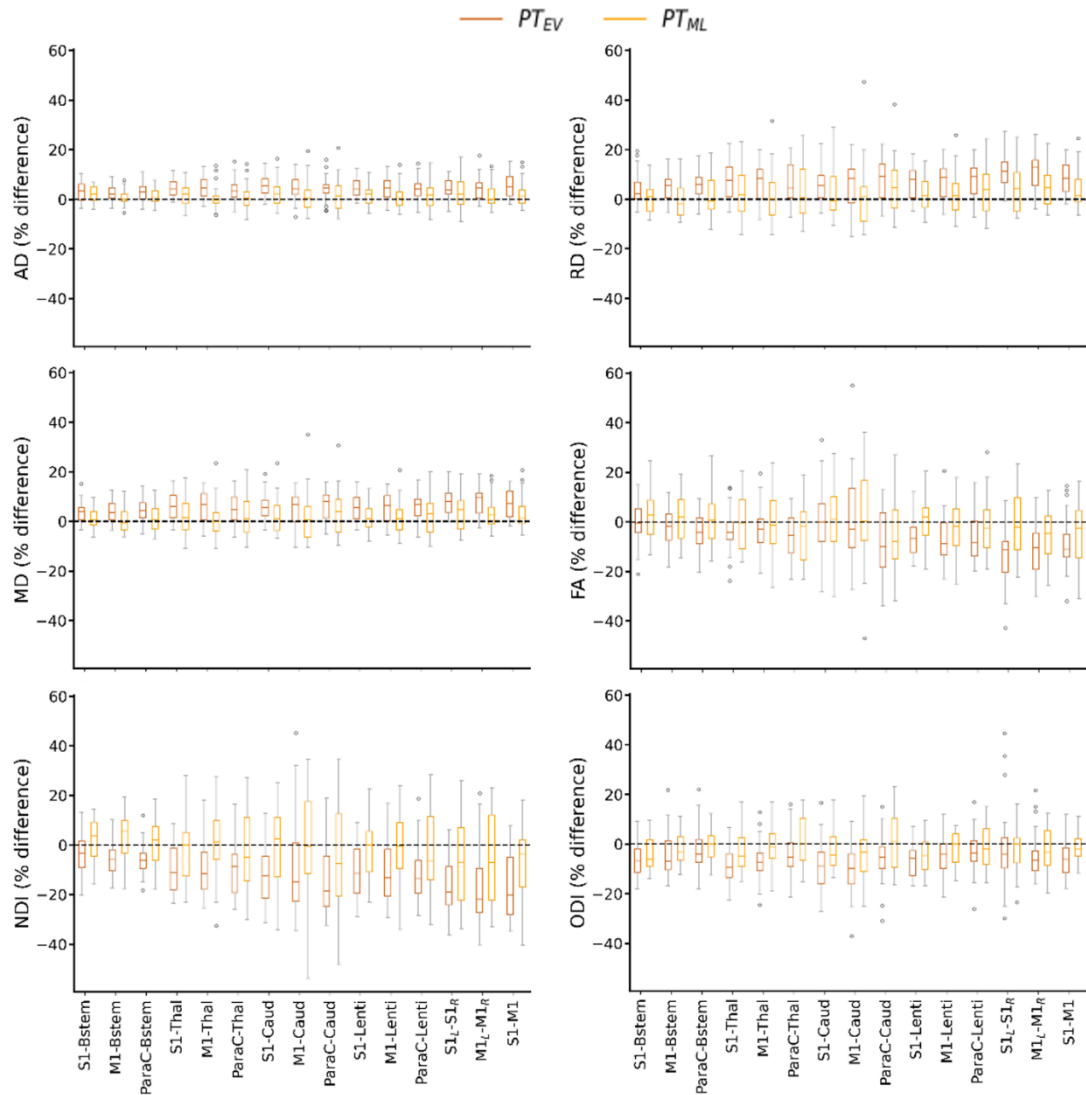


Figure SupF2. Relative percent difference in diffusion metrics between PT_{EV} vs FT_{EVCt} and PT_{ML} vs FT_{MLCt} groups (each PT infant being compared to his/her paired FT newborn) for each SM tract. Refer to *Figure 1* legend for abbreviations.

Table SupT3. ANOVA model studying effects of tract and PT subgroup on Mahalanobis distances, for each set. Refer to *Table 1* for p -value legend.

	Set 1 (AD, RD)	Set 2 (MD, FA)	Set 3 (NDI, ODI)
Tract	****	****	****
Group	****	****	****
Tract : Group	****	****	****

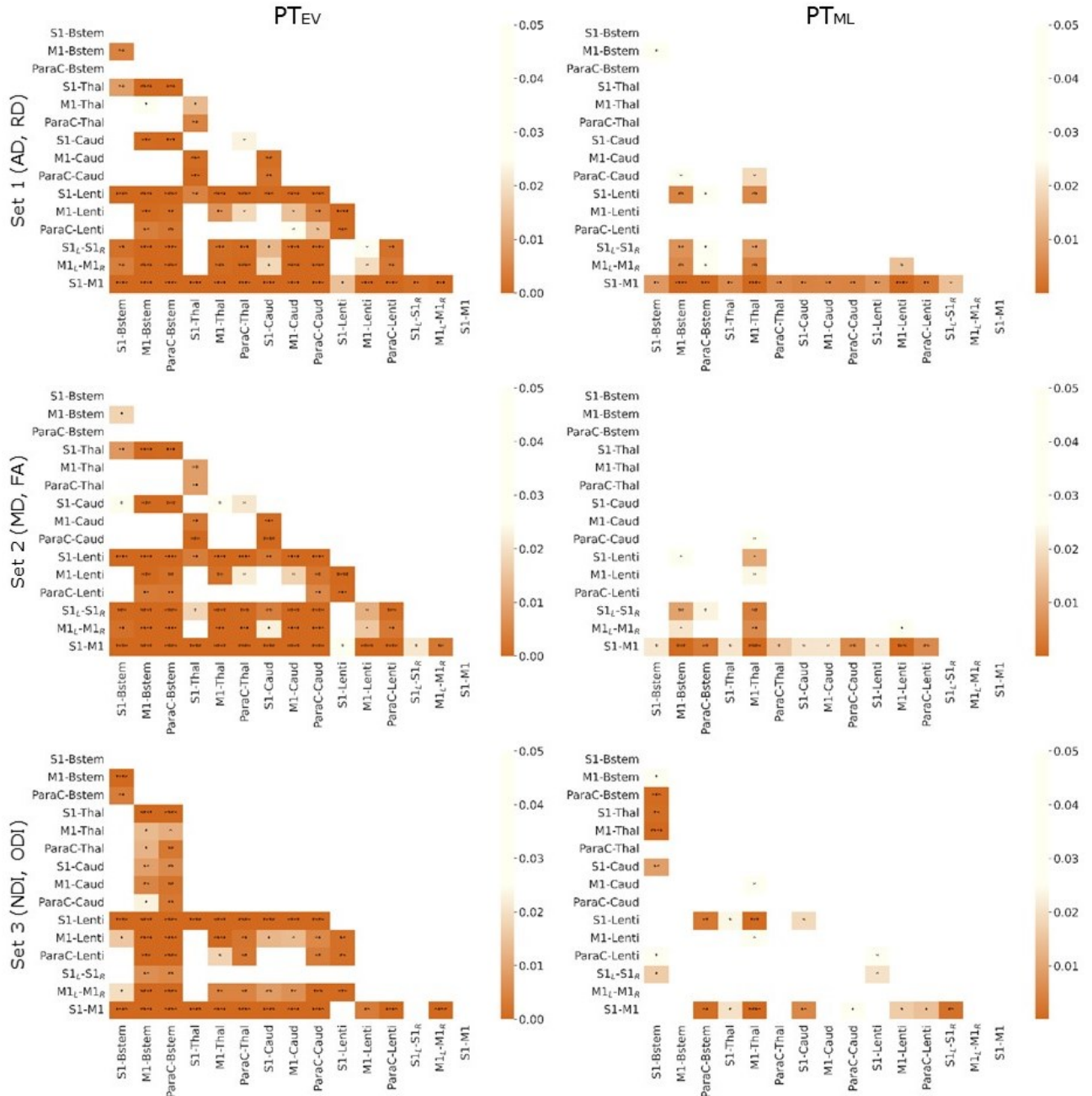


Figure SupF3. Differential effect of prematurity on specific SM tracts. Heatmap of p -values from paired t -tests (corrected for multiple comparisons) of Mahalanobis distances for each pair of SM tracts, for each set of metrics, in each PT subgroup independently (PT_{EV} on the left, PT_{ML} on the right). Legend depicts p -values with respect to heat intensity, with darker colours representing greater statistical significance and white no significant differences. Refer to *Figure 1* legend for abbreviations and to *Table 1* for p -value legend.

Table SupT4. Pearson correlation analyses between Mahalanobis distance and BSID-III scaled scores. Only PT_{EV} results for *set 3* (NODDI) are shown (p-values corrected for multiple comparisons), as no significant correlations were found in *sets 1* and *2*.

Tract	PT _{EV} - Set 3 (NDI, ODI)									
	Cognitive		Receptive Com.		Expressive Com.		Fine Motor		Gross Motor	
	r	p	r	p	r	p	r	p	r	p
S1-Bstem	-0.51	ns	-0.46	ns	-0.31	ns	-0.56	.	0.12	ns
M1-Bstem	-0.7	*	-0.55	.	-0.5	ns	-0.68	*	0.08	ns
ParaC-Bstem	-0.66	*	-0.45	ns	-0.47	ns	-0.69	*	0.03	ns
S1-Thal	-0.35	ns	-0.22	ns	-0.13	ns	-0.48	ns	0.33	ns
M1-Thal	-0.5	ns	-0.43	ns	-0.31	ns	-0.58	.	0.08	ns
ParaC-Thal	-0.34	ns	-0.32	ns	-0.25	ns	-0.54	ns	0.1	ns
S1-Caud	-0.41	ns	-0.12	ns	0.02	ns	-0.31	ns	0.13	ns
M1-Caud	-0.27	ns	-0.15	ns	-0.12	ns	-0.33	ns	0.12	ns
ParaC-Caud	-0.35	ns	-0.39	ns	-0.33	ns	-0.42	ns	-0.02	ns
S1-Lenti	-0.52	ns	-0.48	ns	-0.36	ns	-0.57	.	0.15	ns
M1-Lenti	-0.46	ns	-0.51	ns	-0.4	ns	-0.62	*	0.02	ns
ParaC-Lenti	-0.45	ns	-0.47	ns	-0.41	ns	-0.62	*	-0.02	ns
S1 _L -S1 _R	-0.01	ns	-0.02	ns	0.11	ns	-0.06	ns	0.17	ns
M1 _L -M1 _R	-0.47	ns	-0.49	ns	-0.43	ns	-0.56	.	-0.03	ns
S1-M1	-0.56	.	-0.54	ns	-0.35	ns	-0.68	*	0.1	ns

Refer to *Table 1* for p-value legend and to *Figure 1* for tracts abbreviations.

Descriptive univariate analysis

For the sake of clarity, the tables and figures from this section are referred to as Uni in the text.

To prepare the settings of multivariate analyses, we performed three preparatory univariate analyses on diffusion metrics.

1) We first aimed to evaluate whether differences between left and right tracts were important to consider, and to check that differences were present between groups. As we aimed to perform a single analysis for all tracts together, we add to further introduce this factor.

Considering all tracts except interhemispheric connections, we assessed whether different factors (namely the tract, the hemisphere, and the infant group) have an effect on each diffusion metric by implementing a global ANOVA model. The results (**Table UniT1. A**) confirmed the expected significant effects of tract microstructure and group, as well as the interaction between both, except for FA where the group did not reach the significance level. A significant effect of hemisphere was further observed for FA, RD, and ODI metrics as well as interaction between tract and hemisphere, uncovering asymmetries between left and right tracts. However, given that no significant interaction was observed between hemisphere and group for any of the six

evaluated metrics, we decided not to further explore these differences between left and right tracts, and to consider *averaged diffusion metrics for left and right tracts* in all subsequent analyses.

Additionally, the differences between groups of interest (PT_{EV} vs FT_{EVct}; PT_{ML} vs FT_{MLct}) was studied post-hoc with paired t-tests (over all tracts) corrected for multiple comparisons across the metrics and per each tract independently. The groups analyses which considered all tracts corroborated the existence of significant differences between PT infants and their matched FT controls, with higher AD, RD and MD metrics, opposed to lower FA, NDI, and ODI metrics in PT groups compared to FT, especially in the PT_{EV} vs FT_{EVct} (**Table UniT1. B**). This suggested that the more preterm the infant is, the more “immature” microstructural characteristics are. Group comparisons for PT_{EV} vs FT_{EVct} per tract are presented in **Table UniT2** (group comparisons between PT_{ML} vs FT_{MLct} were not significant).

Tables UniT1. A. ANOVA model studying effects of tract, hemisphere, infant group (considering *extreme to very preterms* (PT_{EV}) / *moderate to late preterms* (PT_{ML}) and their paired controls (FT_{EVct} and FT_{MLct}, respectively), and their interactions on each diffusion metric. **B.** Paired t-test comparisons between PT_{EV}, PT_{ML}, and paired FT controls for each diffusion metric, over all tracts (p-values corrected for multiple comparisons).

Refer to *Table 1* for abbreviations and p-values significance.

A.

	AD	RD	MD	FA	NDI	ODI
Tract	****	****	****	****	****	****
Hemisphere	ns	*	ns	***	ns	****
Group	****	***	****	ns	***	****
Tract : Hemisphere	****	*	****	****	****	****
Tract : Group	****	****	****	****	****	****
Hemisphere : Group	ns	ns	ns	ns	ns	ns

B.

	PT _{EV} vs FT _{EVct} (N= 33)			PT _{ML} vs FT _{MLct} (N = 26)		
	T	CI95%	p-value	T	CI95%	p-value
AD	22.49	[0.; 0.]	****	6.02	[0.;0.]	****
RD	20.98	[0.; 0.]	****	5.49	[0.;0.]	****
MD	22.73	[0.; 0.]	****	5.87	[0.;0.]	****
FA	-11.47	[-0.02;-0.01]	****	-2.11	[-0.01;0.]	**
NDI	-21.76	[-0.03;-0.02]	****	-3.78	[-0.01;0.]	***
ODI	-13.84	[-0.02;-0.01]	****	-4.87	[-0.01;0.]	****

Table UniT2. Group comparisons per tract: paired t-tests for each diffusion metric between PT_{EV} vs FT_{EVct} (N=33 in each group). Left/Right tracts values are averaged, as for all the further supplementary tables. P-values are corrected for multiple comparisons.

Tracts	AD		RD		MD		FA		NDI		ODI	
	T	p	T	p	T	p	T	p	T	p	T	p
S1-Bstem	5.39	****	3.9	***	5.01	****	-0.6	ns	-3.28	**	-4.87	****
M1-Bstem	5.0	****	4.78	****	5.42	****	-1.92	.	-4.22	***	-3.09	**
ParaC-Bstem	4.55	***	6.11	****	6.22	****	-3.53	**	-5.89	****	-1.83	.
S1-Thal	7.48	****	5.6	****	6.34	****	-2.6	*	-6.22	****	-6.31	****
M1-Thal	6.32	****	4.7	****	5.36	****	-1.88	.	-5.34	****	-5.01	****
ParaC-Thal	4.58	****	4.94	****	4.97	****	-3.55	**	-5.3	****	-2.91	**
S1-Caud	8.12	****	4.5	***	5.76	****	-0.24	ns	-5.42	****	-5.36	****
M1-Caud	5.47	****	2.93	**	3.7	**	0.08	ns	-3.78	***	-6.16	****
ParaC-Caud	5.23	****	5.94	****	6.05	****	-3.67	**	-6.35	****	-3.31	**
S1-Lenti	6.84	****	6.18	****	6.52	****	-4.6	****	-6.15	****	-6.12	****
M1-Lenti	5.62	****	5.76	****	5.91	****	-4.1	***	-5.98	****	-3.36	**
ParaC-Lenti	6.11	****	6.04	****	6.33	****	-4.03	***	-6.47	****	-2.57	*
S1 _L -S1 _R	5.75	****	9.23	****	9.08	****	-6.73	****	-7.86	****	-0.91	ns
M1 _L -M1 _R	5.26	****	8.23	****	7.99	****	-6.39	****	-7.22	****	-3.64	**
S1-M1	6.94	****	7.42	****	7.4	****	-5.49	****	-7.24	****	-3.64	**

Positive T values refer to higher values in FT than PT. Refer to *Table 1* for *p*-value legend and to *Figure 1* for metrics and tracts abbreviations.

2) In a second step, we aimed to evaluate whether clinical factors important for preterm development should be considered as confounders in the analyses of tract microstructure. We studied the effect of selected clinical factors (focusing on the ones previously reported as having significant effect on infant WM microstructure, cf. section *Neonatal characteristics at birth*) on the diffusion metrics considering only the preterm infants, by performing additional ANOVA modelling considering all tracts (including interhemispheric tracts (**Table UniT3**)). Confirming previous results, the tract effect was highly significant for all metrics. The group effect (PT_{EV} vs PT_{ML}) as well as the interaction between the tract and group, were less significant than in the previous analyses, probably because only PT infants were considered while larger differences are observed between PT and FT than between PT_{EV} and PT_{ML}. Globally, multiple pregnancy, IUGR and parenteral nutrition were weakly associated with some of the evaluated diffusion metrics. Interestingly, sex and preterm morbidities were not significantly associated with the diffusion metrics, which led us not to retain this latter variable in the next analyses. As a consequence, only the significant clinical factors were considered in further analyses.

Table UniT3. ANOVA analysis including only the preterm infants (PT_{EV} and PT_{ML} groups) to study the effect of selected clinical factors on each diffusion metric.

	AD	RD	MD	FA	NDI	ODI
Tract	****	****	****	****	****	****
Group	*	ns	.	ns	.	*
Sex	ns	ns	ns	ns	ns	ns

Multiple Pregnancy	ns	ns	ns	ns	ns	*
IUGR	*	.	*	ns	*	*
Preterm Morbidities	ns	ns	ns	ns	ns	ns
Parenteral Nutrition >21d	*	.	.	ns	*	*
Tract : Group	ns	**	*	****	ns	ns
Group : Sex	ns	ns	ns	ns	ns	ns
Group : Multiple Pregnancy	ns	ns	ns	ns	ns	*
Group : IUGR	ns	ns	ns	ns	ns	*
Group : Preterm Morbidities	ns	ns	ns	ns	ns	ns
Group : Parenteral Nutrition	NA	NA	NA	NA	NA	NA
Sex : Multiple Pregnancy	ns	ns	ns	ns	ns	ns
Sex : IUGR	ns	ns	ns	ns	ns	ns
Sex : Preterm Morbidities	ns	ns	ns	ns	ns	ns
Sex : Parenteral Nutrition	ns	ns	ns	ns	ns	ns

Refer to *Table 1* legend for abbreviations and *p*-values significance.

3) Our third aim was to evaluate the effects of additional continuous variables that are known to impact the tract microstructure: PMA at scan and whole-brain WM microstructure. GA at birth was then preferred to group categorization in order to better describe the inter-individual variability. Thus, we used a global ANCOVA model with PMA at scan, GA at birth and a proxy of whole-brain WM microstructure. For this latter variable (hereafter named WM residuals), we considered the residuals of the linear model considering the metric averaged over the whole WM mask as a function of GA at birth and PMA at scan, which were shown to be highly associated with the averaged WM metric (**Table UniT4. A**). In the model, we also considered factors that were previously relevant, among which the tracts and a few clinical factors.

For each metric, the modelling uncovered significant associations with the three continuous variables (PMA at scan, GA at birth and a proxy of whole-brain WM microstructure), but the effects of clinical factors, other than IUGR, dropped considerably in significance compared to the previous models probably because these factors are related to GA at birth and WM residuals, leading us not to retain them for the next multivariate analyses. Moreover, as the effect of IUGR was negligible compared to the effects of GA at birth, PMA at scan and WM residuals, this factor was likewise not retained in the subsequent analyses.

To further explore changes in diffusion metrics with GA at birth, we performed a linear regression over the whole cohort after correction for significant variables identified in the previous analyses (PMA at scan and WM residuals) (**Table UniT4. B**). Significant associations with GA at birth were observed in almost all SM tracts and metrics (**Table UniT4.B, Table UniT5** and **Figure UniF1**). Confirming the observations from the group analyses (**Figure 3, Table UniT2**), MD, AD, and RD metrics decreased, and FA, NDI, and ODI increased with the GA at birth. The lower associations for FA (only 10/15 tracts) and ODI (13/15 tracts) (**Table UniT5**) suggested that these

metrics might be less sensitive to detect the variation of microstructure characteristics with GA at birth within some SM tracts, at least at TEA.

Tables UniT4. A. ANCOVA analysis including GA at birth (rather than the group belonging), PMA at scan, WM residuals (corrected for GA at birth and PMA at scan), relevant clinical factors (multiple pregnancy, IUGR, parenteral nutrition >21days), as well as relevant interactions between factors. **B.** Multiple linear regression over the whole cohort of mean WM metrics with PMA at scan and GA at birth, and interactions.

Refer to *Table 1* legend for abbreviations and *p*-values significance.

A.

	AD	RD	MD	FA	NDI	ODI
Tract	****	****	****	****	****	****
GA at birth	****	****	****	****	****	****
PMA at scan	****	****	****	****	****	.
Residual WM	****	****	ns	*	****	ns
Multiple Pregnancy	*	ns	**	.	**	**
IUGR	ns	ns	.	ns	*	ns
Parenteral Nutrition	ns	ns	*	.	***	.
Tract : GA at birth	****	****	****	****	****	****
Tract : PMA at scan	**	****	****	****	****	ns
Tract : Residual WM	****	****	.	****	**	***
Tract : Multiple Pregnancy	ns	.	**	**	***	ns
Tract : IUGR	ns	ns	ns	ns	ns	ns
Tract : Parenteral Nutrition	.	**	***	ns	***	ns

B.

	AD	RD	MD	FA	NDI	ODI
PMA at scan	****	****	****	****	****	****
GA at birth	****	****	****	****	****	*
PMA : GA at birth	ns	ns	ns	ns	ns	ns

Table UniT5. Univariate linear regression analysis: relationship between SM tracts' diffusion metrics (corrected for PMA at scan and WM residuals) and GA at birth over the whole cohort.

	AD		RD		MD		FA		NDI		ODI	
Tracts	T	<i>p</i>	T	<i>p</i>	T	<i>p</i>	T	<i>p</i>	T	<i>p</i>	T	<i>p</i>
S1-Bstem	-7.86	****	-4.83	****	-7.32	****	-0.33	ns	2.98	**	6.28	****
M1-Bstem	-6.43	****	-5.22	****	-6.84	****	0.69	ns	3.41	**	3.74	***
ParaC-Bstem	-6.74	****	-7.58	****	-8.88	****	2.89	**	5.57	****	1.79	ns
S1-Thal	-9.88	****	-8.72	****	-9.81	****	3.14	**	8.29	****	7.74	****
M1-Thal	-7.7	****	-7.22	****	-8.19	****	1.89	ns	7.14	****	5.24	****
ParaC-Thal	-5.76	****	-8.05	****	-7.87	****	4.89	***	7.53	****	2.26	*
S1-Caud	-11.1	****	-6.1	****	-8.19	****	0.36	ns	6.82	****	6.45	****
M1-Caud	-7.82	****	-3.04	**	-4.41	****	-1.19	ns	4.4	****	7.3	****

ParaC-Caud	-6.42	****	-9.52	****	-9.21	****	5.49	***	9.34	****	3.28	**
S1-Lenti	-10.2	****	-10.8	****	-11.7	****	5.1	***	10.2	****	9.3	****
M1-Lenti	-7.87	****	-9.96	****	-10.1	****	5.09	***	9.49	****	4.35	****
ParaC-Lenti	-8.2	****	-10.21	****	-10.9	****	4.49	***	9.26	****	3.09	**
S1L-S1R	-7.22	****	-12.1	****	-12.6	****	7.07	***	9.16	****	1.35	ns
M1L-M1R	-6.62	****	-12.58	****	-11.8	****	9.07	***	10.58	****	4.08	***
S1-M1	-11.5	****	-15.68	****	-14.7	****	9.41	***	13.04	****	4.93	****

Refer to Figure 1 and Table 1 legends for abbreviations. P-values are corrected for multiple comparisons.

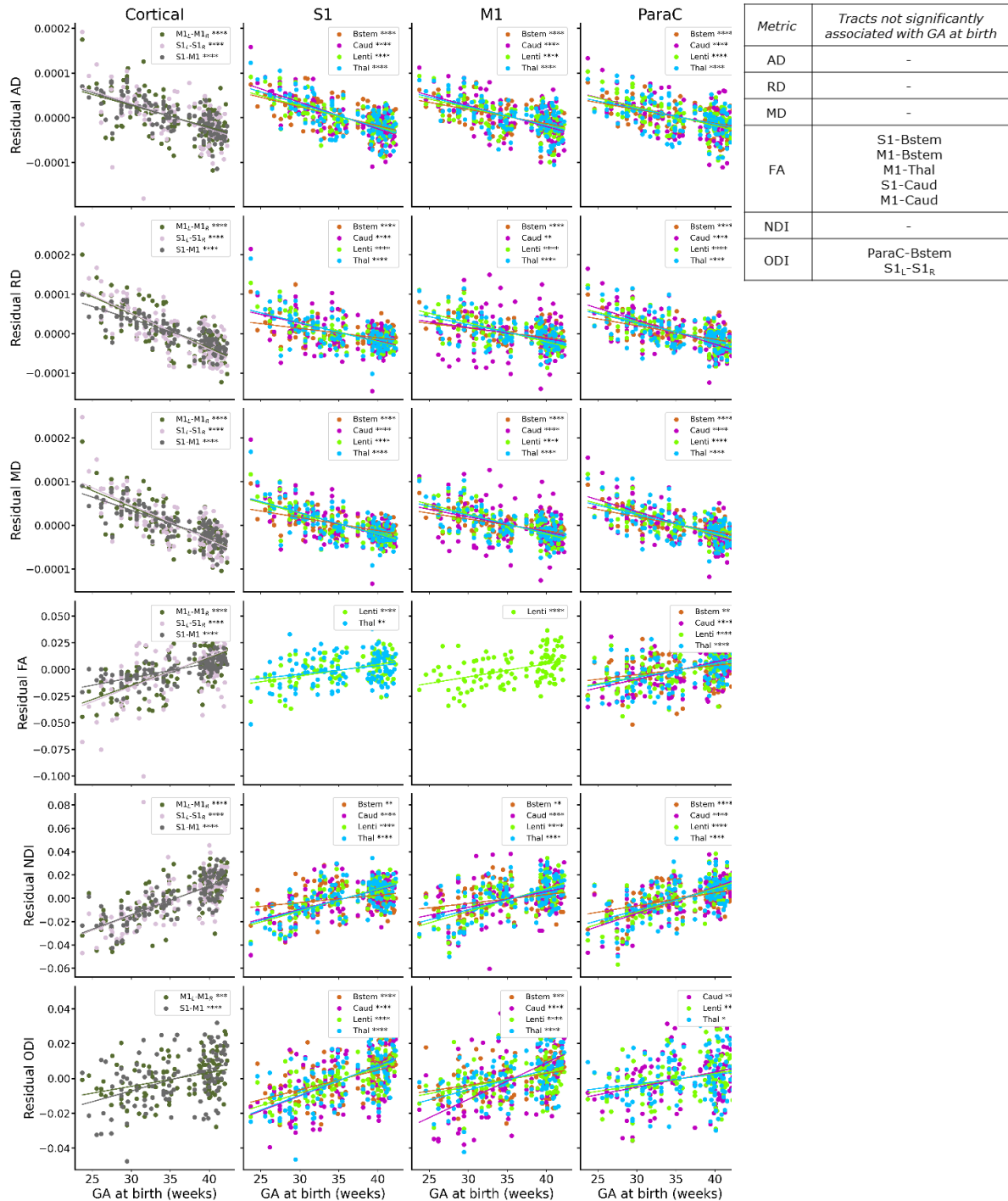


Figure UniF1. Scatterplot of metrics residuals (after correction of PMA at scan and WM residuals) with GA at birth. The regression lines show significant relationship with GA at birth (after correction for multiple comparisons). The table lists the tracts that are not significantly associated with GA at birth for each metric. Refer to *Figure 1* legend for abbreviations.

Results for BSID-III composite scores (CS)

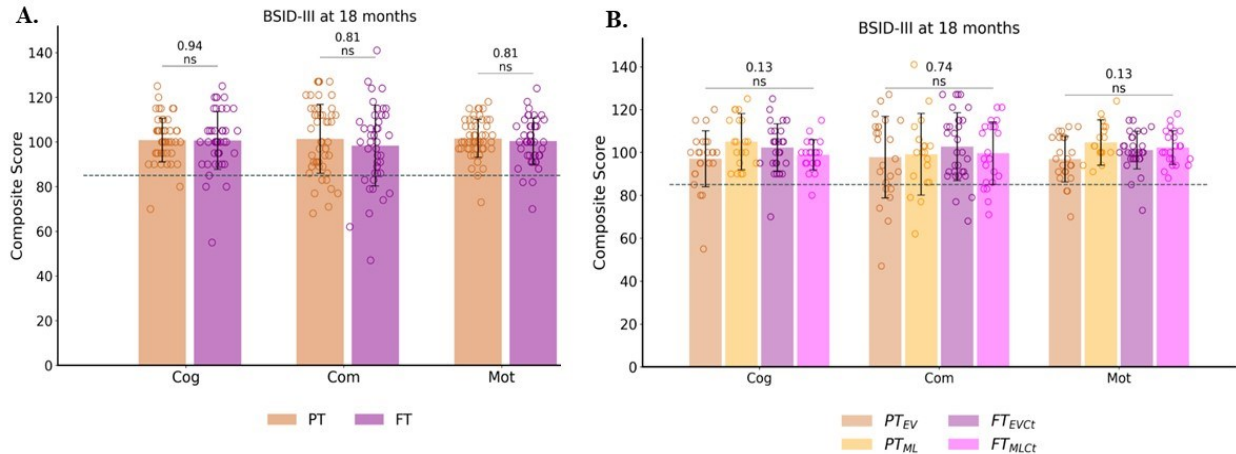


Figure Sup-CS_F1. Outcome assessment at around 18 months of corrected age: BSID-III composite scores between PT and FT groups (A), and subgroups (B: PT_{EV}, PT_{ML}, FT_{EVct} and FT_{MLct}). The dotted line indicates the scores threshold indicating a developmental delay (scores < -1 SD): composite scores < 85. Reported statistics are results of either t-test corrected for multiple comparisons for PT vs FT or one-way ANOVA for the subgroup analysis. Cog: cognitive; Com: communication; Mot: motor. ns: not significant.

Table Sup-CS_T2. Correlation analyses between Mahalanobis distance and BSID-III composite scores. Only PT_{EV} results for set 3 (NDI and ODI) are shown (p-values corrected for multiple comparisons), as no significant correlations were found in sets 1 and 2.

Tract	PT _{EV} - Set 3 (NDI, ODI)					
	Cognitive		Communication		Motor	
	r	p	r	p	r	p
S1-Brainstem	-0.51	ns	-0.41	ns	-0.37	ns
M1-Brainstem	-0.7	*	-0.55	ns	-0.49	ns
ParaC-Brainstem	-0.66	*	-0.48	ns	-0.52	ns
S1-Thal	-0.35	ns	-0.19	ns	-0.18	ns
M1-Thal	-0.5	ns	-0.4	ns	-0.4	ns
ParaC-Thal	-0.34	ns	-0.3	ns	-0.35	ns
S1-Caud	-0.41	ns	-0.06	ns	-0.16	ns
M1-Caud	-0.27	ns	-0.14	ns	-0.18	ns

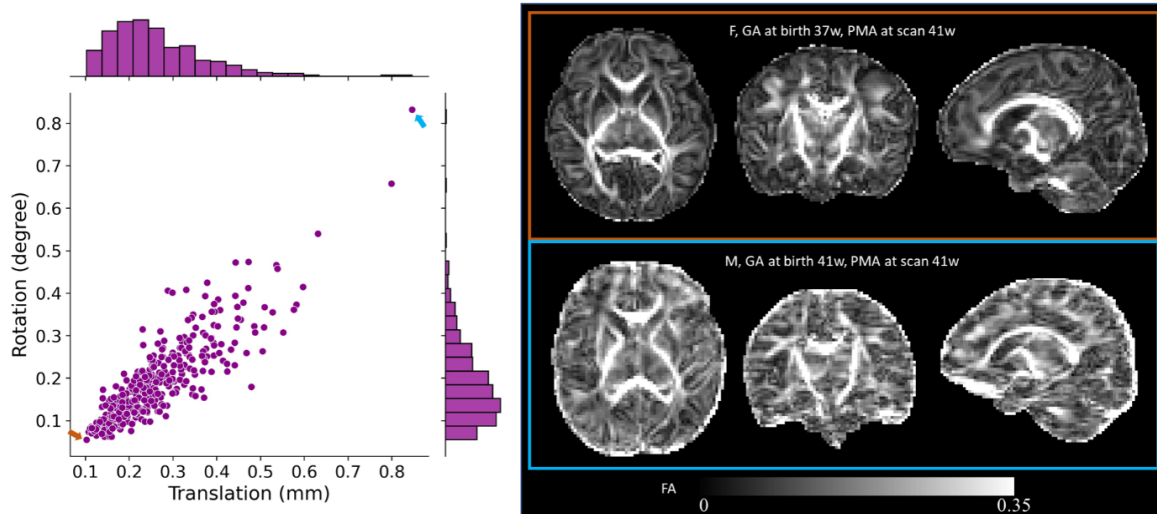
ParacC-Caud	-0.35	ns	-0.38	ns	-0.33	ns
S1-Lenti	-0.52	ns	-0.45	ns	-0.36	ns
M1-Lenti	-0.46	ns	-0.49	ns	-0.47	ns
ParaC-Lenti	-0.45	ns	-0.47	ns	-0.49	ns
S1L-S1R	-0.01	ns	0.03	ns	0.04	ns
M1L-M1R	-0.47	ns	-0.49	ns	-0.45	ns
S1-M1	-0.56	ns	-0.47	ns	-0.48	ns

Refer to *Table 3.1* for p-value legend and to *Figure 1* for tracts abbreviations.

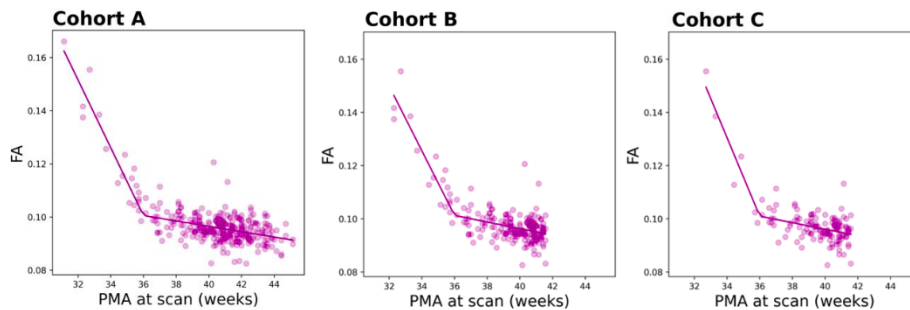
3.2. Supplementary materials for Chapter 4

‘Predicting neurodevelopmental outcomes from neonatal cortical microstructure: A conceptual replication study’ (Gondova et al., 2023).

Supp. Figure 1. SHARD quality control across the Cohort A (left) and example FA maps for the **best** and for the **worst** subjects.



Supp. Figure 2. Continuous piecewise linear regression of global FA with PMA at scan showing inflection points at around 36 weeks in cohorts A, B, and C.



Supp. Table 1. Unpaired comparison of median global cortical FA between preterm and term-born subjects (FDR correction) after correcting for PMA at scan.

	T	p-value
Cohort A	-5.74	7.09e-07
Cohort B	-7.10	2.28e-08
Cohort C	-6.53	7.09e-07

Supp. Table 2. Relationship between BSID-III scores and ages (robust linear correlation) in the entire cohorts (columns All), and for the preterm and term-born infants separately (Pearson's r).

	BSID-III scores	GA at birth			PMA at scan			Age at BSID-III assessment		
		All	PT	FT	All	PT	FT	All	PT	FT
Cohort A	Cognitive	0.04	0.06	0.40	0.06	-0.02	0.14	-0.09	-0.33	-0.07
	Language	0.04	-0.12	0.13	0.06	-0.21	0.18	-0.07	-0.06	-0.08

	Motor	0.07	0.00	0.10	0.07	-0.03	0.09	-0.04	-0.31	0.02
Cohort B	Cognitive	-0.03	0.04	0.04	-0.07	-0.17	0.05	-0.09	-0.33	-0.08
	Language	-0.04	-0.14	0.10	-0.05	-0.29	0.12	-0.07	-0.05	-0.13
	Motor	0.01	-0.05	0.04	-0.04	-0.19	-0.01	-0.02	-0.30	0.05
Cohort C	Cognitive	0.06	0.43	0.09	0.04	0.20	0.08	-0.12	-0.35	-0.12
	Language	-0.01	0.28	0.00	-0.02	0.12	0.03	-0.10	0.00	-0.19
	Motor	-0.01	0.28	-0.03	-0.02	0.24	-0.06	0.02	-0.27	0.06

Supp. Table 3. ANCOVA analysis including global cortical FA, GA at birth, sex and IMD, as well as interactions between them, to explain BSID-III scores.

Cohort A	Cognitive (p-value)	Language (p-value)	Motor (p-value)
Global cortical FA*	0.04 (*)	0.06	0.99
GA at birth	0.44	0.45	0.21
Sex	0.01 (*)	0.002 (**)	0.45
IMD	<0.001 (***)	0.006 (**)	0.02 (*)
FA : GA at birth	0.69	0.75	0.26
FA : Sex	0.66	0.34	0.15
FA : IMD	0.61	0.49	0.34
GA at birth : Sex	0.80	0.38	0.66
GA at birth : IMD	0.03 (*)	0.45	0.29
Sex : IMD	0.28	0.14	0.37

* corrected for PMA at scan (inflection=36w); signific. codes: <0.001: ***, <0.01: **, <0.05: *

Supp. Table 4. Predictive results of 3-class categorical task of prematurity status in Cohort A with increasing region numbers. The dashed line represents the random predictive level (0.5 for AUC).

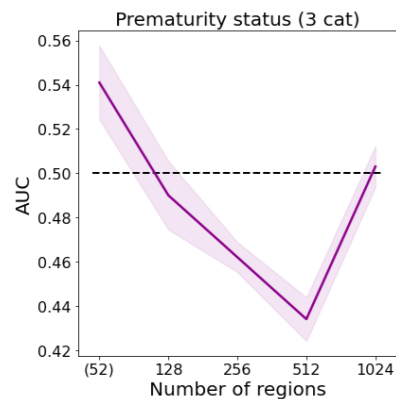
Inputs	AUC [CI][§]	AUC (p-val)[%]
GA birth	1 [1;1]	0.999(0.000000)
Atlas 52*	0.541 [0.5243;0.5577]	0.555(0.040000)
Random 128*	0.49 [0.4745;0.5055]	0.532(0.070000)
Random 256*	0.462 [0.4552;0.4688]	0.465(0.280000)
Random 512*	0.434 [0.4241;0.4439]	0.436(0.410000)
Random 1024*	0.503 [0.4937;0.5123]	0.495(0.160000)

GA at birth input used to validate the implementation.

* corrected for PMA at scan (inflection=36w)

§ mean AUC and confidence interval (CI) across 100 randomly shuffled runs

% permutation testing similar to original study



Supp. Table 5. Results of the nested cross-validation performed in the Cohort D. Inputs: Global FA (corrected for PMA at scan), GA at birth, Sex, IMD score. Prematurity status prediction task was used to validate the implementation.

Outcome	AUC [CI]	SPEC [CI]	SENS [CI]
Prematurity status	0.932 [0.8728;0.9905]	1.000 [1.0000;1.0000]	0.863 [0.7456;0.9811]
Cognitive	0.500 [0.5000;0.5000]	1.000 [1.0000;1.0000]	0.000 [0.0000;0.0000]
Language	0.500 [0.5000;0.5000]	1.000 [1.0000;1.0000]	0.000 [0.0000;0.0000]
Motor	0.500 [0.5000;0.5000]	1.000 [1.0000;1.0000]	0.000 [0.0000;0.0000]

Motion Correction

Additionally, during the QC of the dMRI data, we evaluated potential relationships between the global FA values and motion (quantified by total subject translation and rotation (Christiaens et al., 2021) (*Supp. Table 4*). To address the possible confounding effect of motion on the predictive results, we corrected the input features for the translation and rotation using linear regression before the training and testing of the nested validation (reported results of 5 repetitions instead of 10 used in the main body of the manuscript).

Supp. Table 6. dMRI QC with PMA at scan & global FA. FDR correction within cohort and independent variable.

Cohort	QC metric	PMA scan		Global FA	
		rho	p-val	rho	p-val
A	Translation	0.135842	0.026122	0.043287	0.611863
	Rotation	0.159185	0.012289	0.086068	0.385249
	SNR	-0.197346	0.002611	0.188706	0.004509
	Outlier ratio	0.056062	0.337279	0.014047	0.810137
B	Translation	0.162672	0.045449	0.021483	0.856948
	Rotation	0.176835	0.045449	0.052071	0.856948
	SNR	-0.075229	0.392876	0.140424	0.198537
	Outlier ration	0.046567	0.516904	-0.012958	0.856948
C	Translation	0.081942	0.487254	0.091616	0.307595
	Rotation	0.082551	0.487254	0.146521	0.203196
	SNR	-0.081305	0.487254	0.160733	0.203196
	Outlier ratio	0.009634	0.914735	0.099740	0.307595

Additionally, because cortical FA could be affected by the motion, we tested whether observed predictive results were driven by this confounder rather than cortical information itself by regressing out the effects of total subject translation and rotation from the input features. The prematurity status remained predictable from the cortical microstructure in some cases of random parcellations suggesting a need for higher number of parcels for successful prediction. As in the previous experiments, no model was better than random in case of continuous GA at birth and BSID-III scores settings (*Supp. Table 5*). Predictive results did not seem to be significantly affected by the motion. The prematurity status remained predictable from the cortical microstructure (random parcellations) with similar scores.

Supp. Table 7. a, Results of the nested validation – categorical task after correction for PMA at scan and subject motion. **b,** continuous task after correction for PMA at scan and subject motion.

a, Categorical (corrected for PMA at scan and motion)

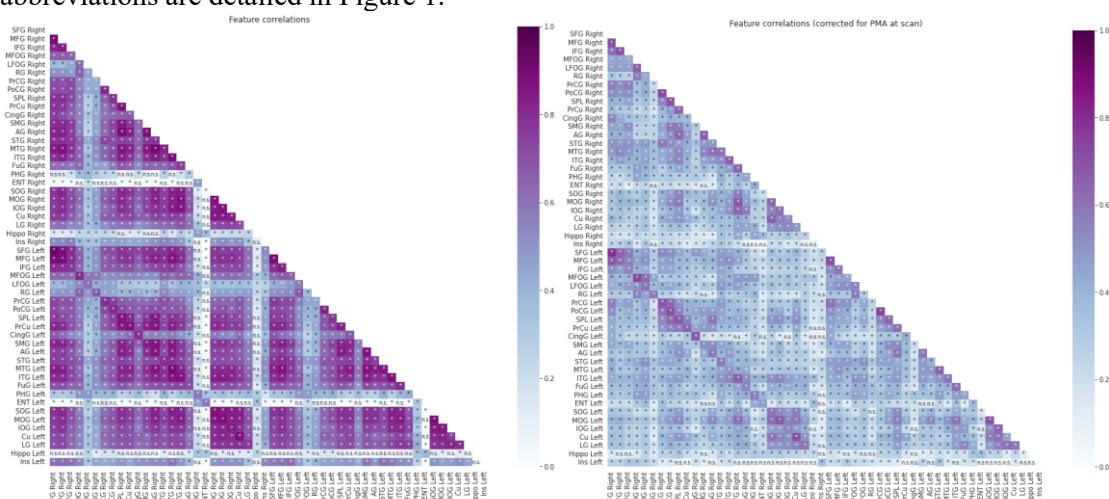
Outcome	Inputs	AUC [CI]	SPEC [CI]	SENS [CI]
Prematurity status	ROIs (52)	0.500 [0.5000;0.5000]	1.000 [1.0000;1.0000]	0.000 [0.0000;0.0000]
	Random (128)	0.498 [0.4967;0.4986]	0.995 [0.9934;0.9971]	0.000 [0.0000;0.0000]
	Random (256)	0.531 [0.5105;0.5508]	0.908 [0.8966;0.9192]	0.153 [0.1172;0.1895]

	Random (512)	0.547 [0.5218;0.5721]	0.907 [0.8997;0.9148]	0.187 [0.1380;0.2353]
	Random (1024)	0.502 [0.4987;0.5062]	0.985 [0.9811;0.9887]	0.020 [0.0122;0.0278]
Cognitive Score	ROIs (52)	0.500 [0.5000;0.5000]	1.000 [1.0000;1.0000]	0.000 [0.0000;0.0000]
	Random (128)	0.490 [0.4836;0.4971]	0.941 [0.9335;0.9480]	0.040 [0.0243;0.0557]
	Random (256)	0.468 [0.4656;0.4705]	0.936 [0.9312;0.9410]	0.000 [0.0000;0.0000]
	Random (512)	0.490 [0.4875;0.4930]	0.980 [0.9749;0.9861]	0.000 [0.0000;0.0000]
	Random (1024)	0.495 [0.4932;0.4970]	0.990 [0.9864;0.9941]	0.000 [0.0000;0.0000]
	ROIs (52)	0.500 [0.5000;0.5000]	1.000 [1.0000;1.0000]	0.000 [0.0000;0.0000]
Language Score	Random (128)	0.492 [0.4896;0.4937]	0.935 [0.9180;0.9511]	0.049 [0.0358;0.0617]
	Random (256)	0.500 [0.5000;0.5000]	1.000 [1.0000;1.0000]	0.000 [0.0000;0.0000]
	Random (512)	0.487 [0.4825;0.4914]	0.944 [0.9297;0.9590]	0.030 [0.0225;0.0368]
	Random (1024)	0.493 [0.4882;0.4977]	0.931 [0.9115;0.9498]	0.055 [0.0420;0.0685]
	ROIs (52)	0.493 [0.4911;0.4947]	0.986 [0.9821;0.9895]	0.000 [0.0000;0.0000]
	Random (128)	0.495 [0.4935;0.4972]	0.991 [0.9871;0.9943]	0.000 [0.0000;0.0000]
Motor Score	Random (256)	0.493 [0.4910;0.4947]	0.986 [0.9820;0.9894]	0.000 [0.0000;0.0000]
	Random (512)	0.493 [0.4916;0.4939]	0.986 [0.9833;0.9879]	0.000 [0.0000;0.0000]
	Random (1024)	0.495 [0.4940;0.4963]	0.990 [0.9880;0.9927]	0.000 [0.0000;0.0000]
	ROIs (52)	0.493 [0.4911;0.4947]	0.986 [0.9821;0.9895]	0.000 [0.0000;0.0000]
	Random (128)	0.495 [0.4935;0.4972]	0.991 [0.9871;0.9943]	0.000 [0.0000;0.0000]

b, Continuous (corrected for PMA at scan and motion)

Outcome	Inputs	RHO [CI]	MAE [CI]	R2 [CI]
GA at birth	ROIs (52)	0.009 [-0.0137;0.0323]	1.444 [1.4090;1.4792]	-0.014 [-0.0185;-0.0098]
	Random (128)	-0.029 [-0.0654;0.0071]	1.473 [1.4401;1.5053]	-0.050 [-0.0659;-0.0331]
	Random (256)	-0.074 [-0.1259;-0.0214]	1.477 [1.4425;1.5116]	-0.091 [-0.1136;-0.0675]
	Random (512)	0.007 [-0.0219;0.0352]	1.457 [1.4222;1.4908]	-0.125 [-0.1493;-0.1003]
	Random (1024)	0.026 [-0.0177;0.0692]	1.484 [1.4354;1.5335]	-0.155 [-0.1848;-0.1246]
Cognitive Score	ROIs (52)	-0.039 [-0.0671;-0.0114]	6.557 [6.4703;6.6427]	-0.076 [-0.0843;-0.0668]
	Random (128)	0.034 [0.0050;0.0633]	6.530 [6.4378;6.6230]	-0.067 [-0.0772;-0.0571]
	Random (256)	0.039 [0.0140;0.0640]	6.565 [6.4694;6.6611]	-0.072 [-0.0826;-0.0612]
	Random (512)	0.045 [0.0247;0.0652]	6.513 [6.4385;6.5876]	-0.060 [-0.0661;-0.0546]
	Random (1024)	0.043 [0.0289;0.0572]	6.517 [6.4361;6.5987]	-0.056 [-0.0607;-0.0506]
Language Score	ROIs (52)	0.077 [0.0666;0.0872]	10.209 [10.0759;10.3414]	-0.039 [-0.0489;-0.0301]
	Random (128)	0.077 [0.0644;0.0897]	10.430 [10.3108;10.5501]	-0.082 [-0.1043;-0.0590]
	Random (256)	0.093 [0.0840;0.1014]	10.496 [10.3878;10.6035]	-0.085 [-0.1070;-0.0638]
	Random (512)	0.056 [0.0404;0.0726]	10.278 [10.1259;10.4306]	-0.032 [-0.0370;-0.0275]
	Random (1024)	0.046 [0.0245;0.0667]	10.348 [10.1981;10.4975]	-0.049 [-0.0563;-0.0414]
Motor Score	ROIs (52)	-0.024 [-0.0440;-0.0032]	5.909 [5.7845;6.0329]	-0.032 [-0.0361;-0.0275]
	Random (128)	-0.088 [-0.0938;-0.0827]	5.926 [5.8041;6.0481]	-0.038 [-0.0416;-0.0343]
	Random (256)	-0.093 [-0.1151;-0.0701]	5.935 [5.8194;6.0502]	-0.042 [-0.0461;-0.0384]
	Random (512)	-0.163 [-0.1627;-0.1627]	5.913 [5.8022;6.0239]	-0.041 [-0.0465;-0.0346]
	Random (1024)	-0.059 [-0.0789;-0.0384]	6.035 [5.9379;6.1317]	-0.070 [-0.0856;-0.0536]

Supp. Figure 5. Feature collinearity before (left) and after (right) correction for PMA at scan. Label abbreviations are detailed in Figure 1.



3.3. Supplementary materials for Chapter 5

‘Bridging the gap between microstructural grey-matter similarity and functional connectome: A multi-modal MRI study in preterm and full-term infants’ (in prep.)

Cortical (left/right)	Frontal	Superior frontal Rostral middle frontal Caudal middle frontal Pars opercularis Pars triangularis	Pars orbitalis Lateral orbitofrontal Medial orbitofrontal Precentral Paracentral
	Parietal	Superior parietal Inferior parietal Supramarginal	Postcentral Precuneus
	Temporal	Superior temporal Middle temporal Inferior temporal Fusiform	Transverse temporal Entorhinal Parahippocampal
	Occipital	Lateral occipital Lingual	Cuneus Pericalcarine
	Cingular	Rostral anterior cingulate Posterior cingulate	Isthmus cingulate
	Insular	Insula	
Subcortical (left/right):		Hippocampus Amygdala Cerebellum Caudate nucleus Thalamus Lenticular nucleus	
Subcortical (medial):		Brainstem	

Supp. Table 1. List of regions of interest used in the study with assignment to the lobes. Color-coding is re-used in the circular plots.

1. Univariate analyses of GM microstructure

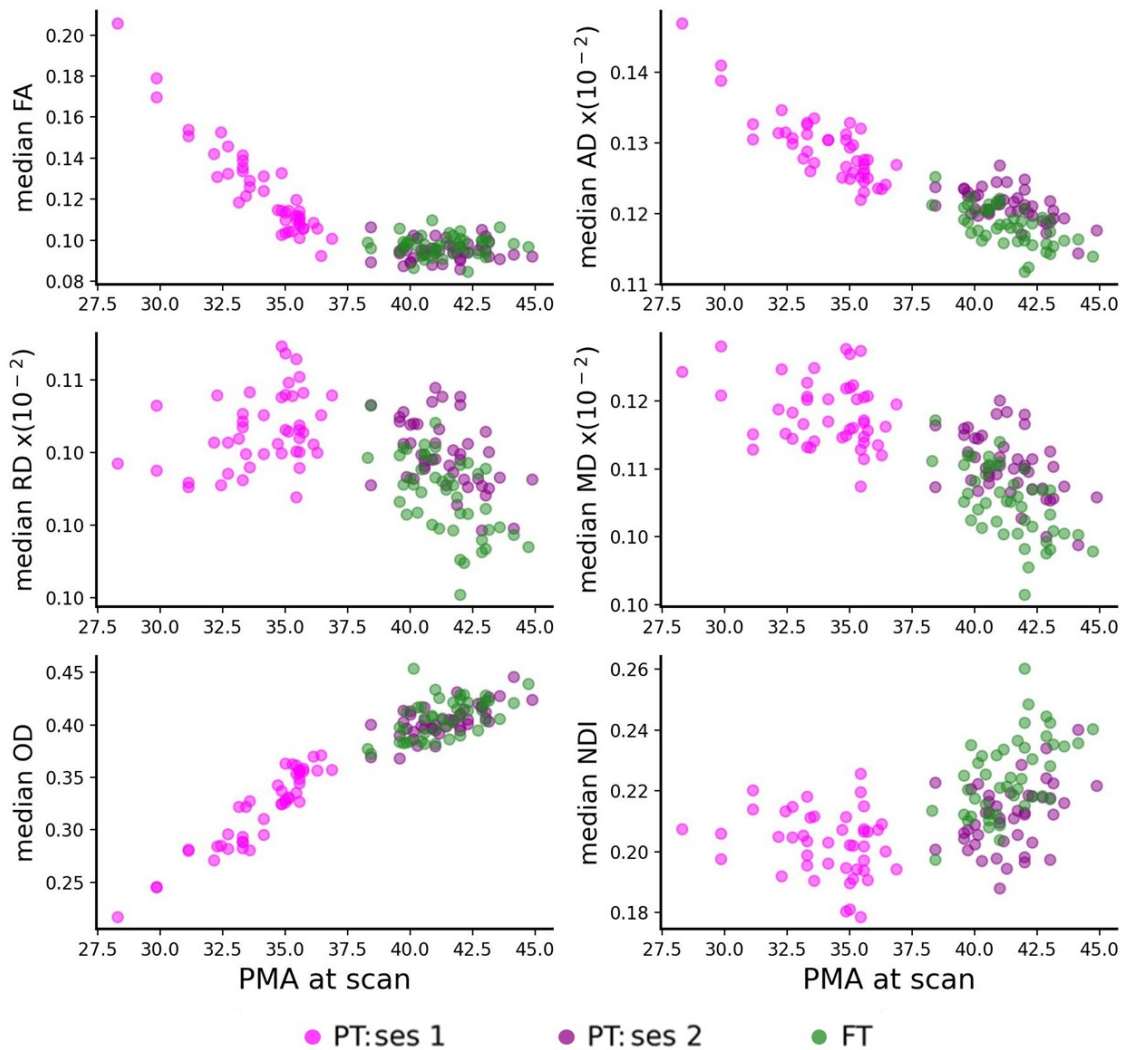
The univariate differences between infant groups in terms of the global microstructural features, i.e. median diffusion metrics across the all cortical and subcortical ROIs detailed in *Supp. Table 1.1.*) were assessed with paired t-tests corrected for multiple comparisons across groups and metrics using the Benjamini–Hochberg false discovery rate (FDR) correction. As expected, the three infant groups (PT:ses1, PT:ses2, and FT) differed significantly in terms of their global median diffusion characteristics, except for ODI in PT: Ses2 vs FT comparisons. Additionally, the global median metrics showed expected evolution with PMA at scan with visible different trends between groups (*Supp. Figure 1.1.*). All DTI-derived metrics (AD, RD, MD, and FA) decreased with PMA at scan, with FA (and of lesser extent RD) showing the biphasic relationship with age previously described in Batalle et al. (2019). Both NODDI-

derived metrics (OD and NDI) increased with age suggesting the increasing complexity of the underlying microstructure.

	PT:ses1 vs PT:ses2		PT:ses1 vs FT		PT:ses2 vs FT	
	T	p-val	T	p-val	T	p-val
FA	9.16	***	7.43	***	-2.21	*
AD	11.68	***	13.34	***	5.96	***
RD	4.23	***	7.38	***	5.49	***
MD	10.25	***	11.96	***	5.55	***
ODI	-17.17	***	-13.03	***	-0.96	n.s.
NDI	-5.06	***	-8.82	***	-5.67	***

*FDR-corrected, paired t-test.

Supp. Table 1.1. Paired t-tests for global median diffusion metric between infant groups: : preterms at session 1 (PT:ses1), preterms at session 2 (PT:ses2), and paired controls (FT). Refer to Table X for abbreviations and p-values significance. p-value ≤ 0.0001 [****], ≤ 0.001 [***], ≤ 0.01 [**], < 0.05 [*], < 0.1 [.] , ≥ 0.1 [ns].



Supp. Figure 1.1. Relationship of median GM diffusion metrics with PMA at scan for the three infant groups: preterms at session 1 (PT:ses1, magenta), preterms at session 2 (PT:ses2, dark magenta), and paired controls (FT, green).

Additionally, we performed ANOVA modeling to investigate the effect of infant group, ROI, and global median diffusion metrics, together with their interactions, on the regional microstructural features. The analysis revealed significant effects of these variables on the evaluated diffusion metrics (*Supp. Table 1.2.*), suggesting the existence of inter-regional differences in terms of their microstructural properties across subjects. ROI-specific diffusion metrics across infant groups are presented in the *Supp. Figure 1.2.*

a,

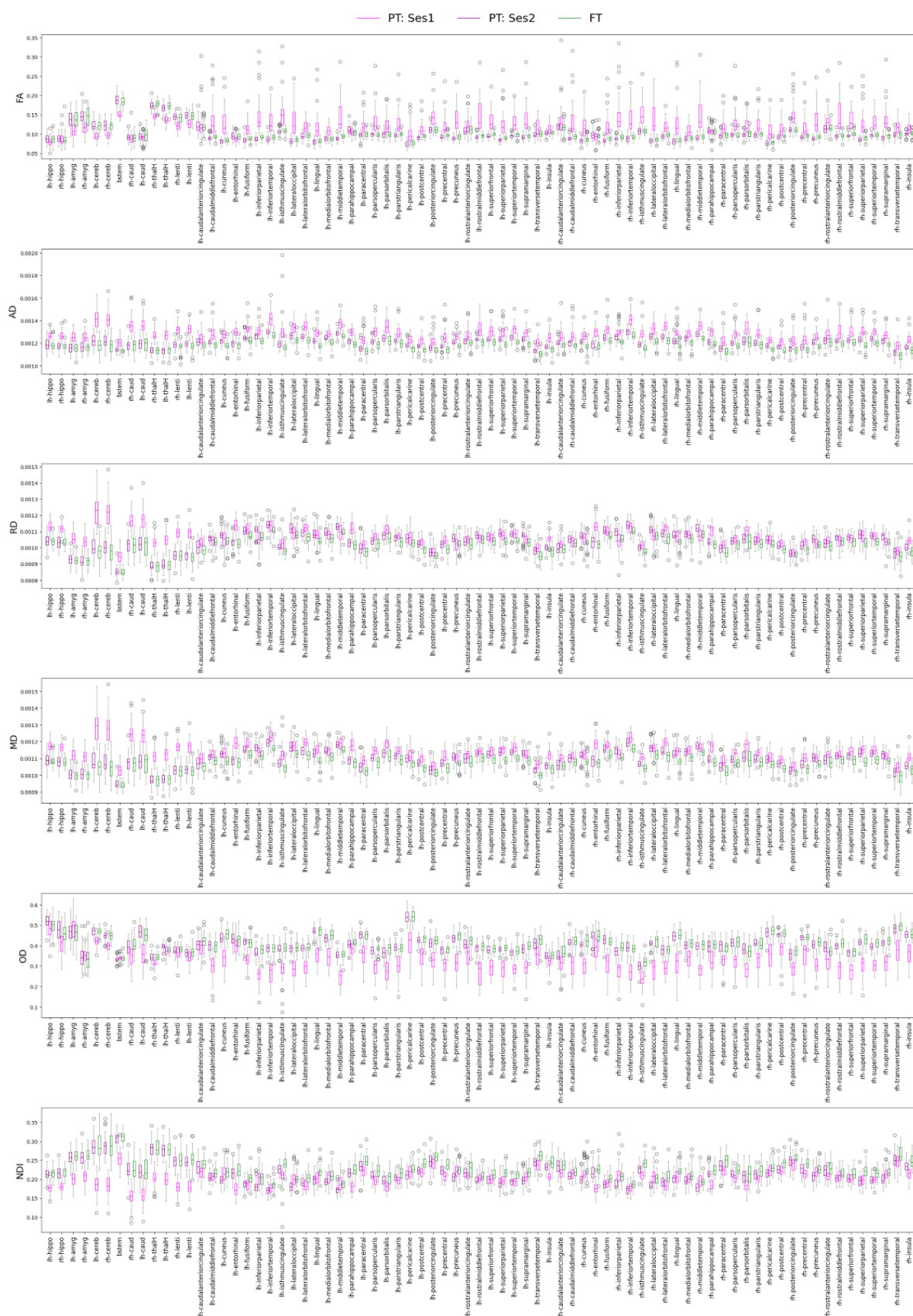
	Global FA	Global AD	Global RD	Global MD	Global OD	Global NDI
<i>PMA scan</i>	***	***	***	***	***	***
<i>GA birth</i>	***	***	***	***	***	***
<i>PMA at scan: GA at birth</i>	***	***	***	***	***	***

b,

	FA	AD	RD	MD	OD	NDI
<i>ROI</i>	***	***	***	***	***	***
<i>Group</i>	***	***	***	***	***	***
<i>Global GM*</i>	***	***	***	***	***	***
<i>ROI: Group</i>	***	***	***	***	***	***
<i>ROI: Global GM*</i>	n.s.	n.s.	***	***	***	***
<i>Group: Global GM*</i>	n.s.	n.s.	*	n.s.	n.s.	n.s.
<i>ROI: Group: Global GM*</i>	n.s.	n.s.	n.s.	n.s.	n.s.	n.s.

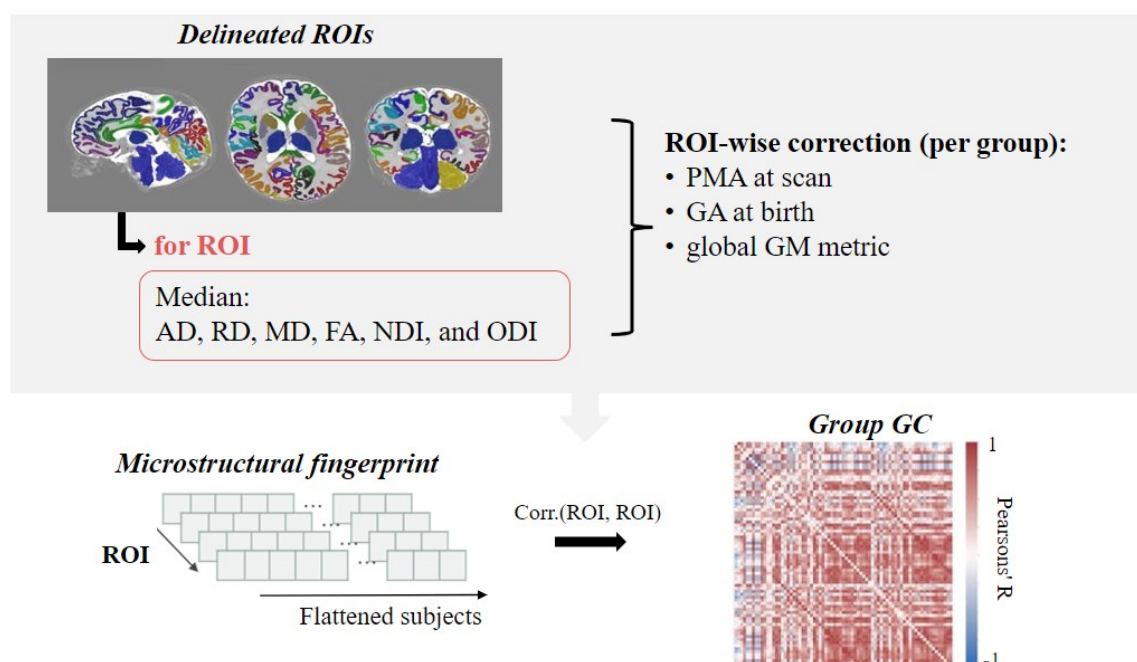
*residual global median diffusion metric after correction for PMA at scan and GA at birth.

Supp. Table 1.2.a: ANOVA model studying effects of PMA at scan and GA at birth on the six global median diffusion metrics. **b:** ANOVA model studying effect of ROI, infant group and residual global median diffusion, and their interactions on each diffusion metric. p-value ≤ 0.0001 [****], ≤ 0.001 [***], ≤ 0.01 [**], < 0.05 [*], < 0.1 [.], ≥ 0.1 [ns].

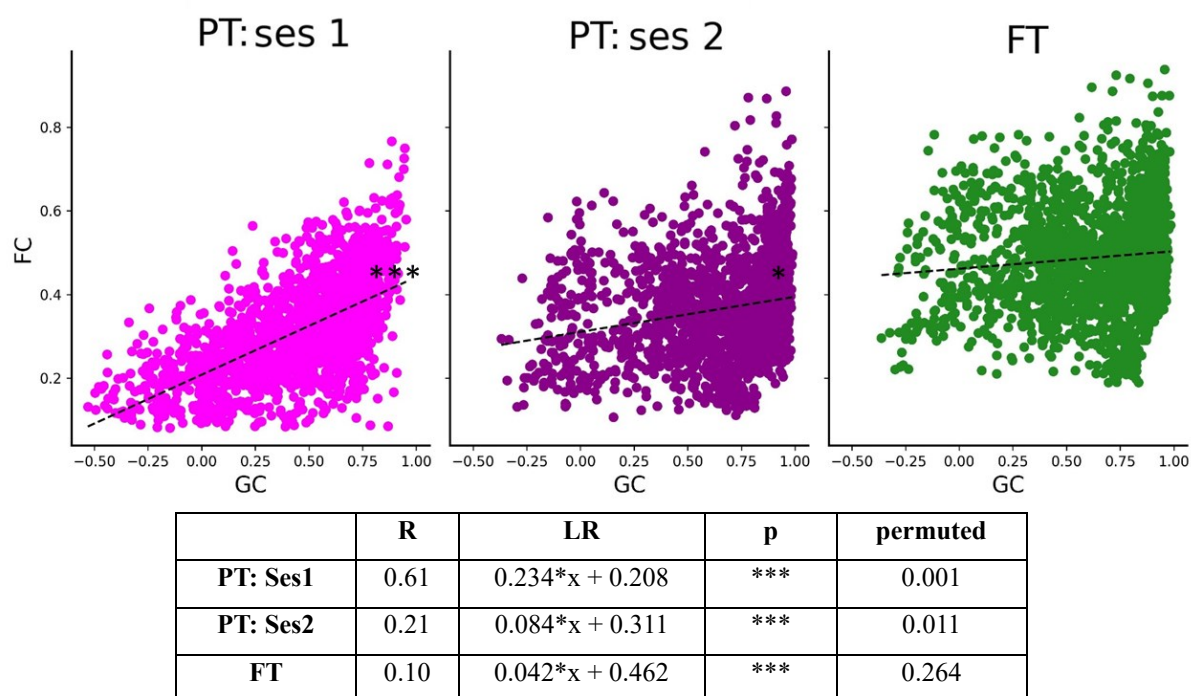


Supp. Figure 1.2. Diffusion metrics across ROIs and infant groups: preterm at session 1 (PT:ses1, magenta), preterm at session 2 (PT:ses2, dark magenta), and paired controls (FT, green). The ROI naming conventions and assignment to lobes is detailed in *Supp. Table 1*.

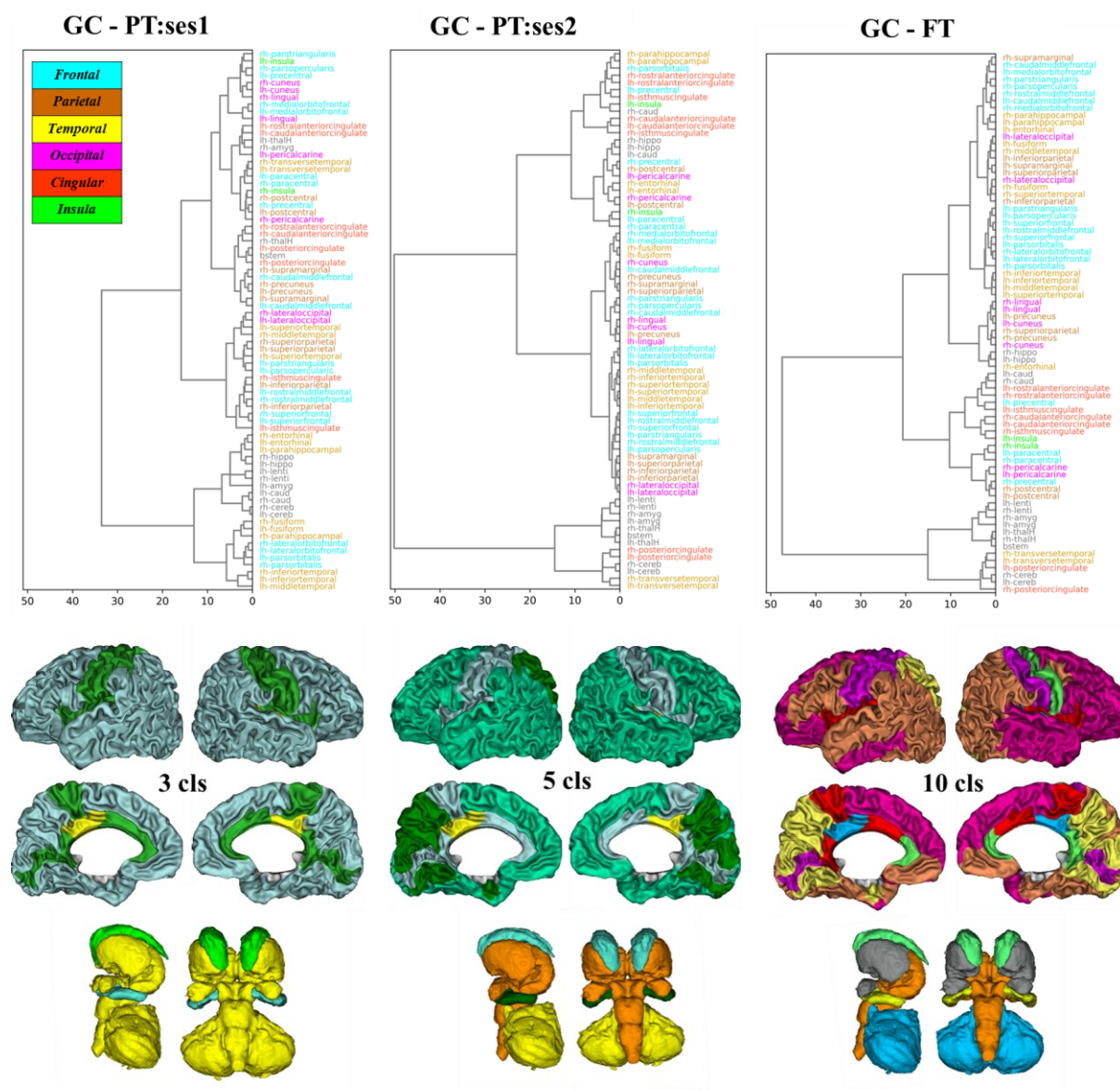
2. Group-wise GC and FC analyses



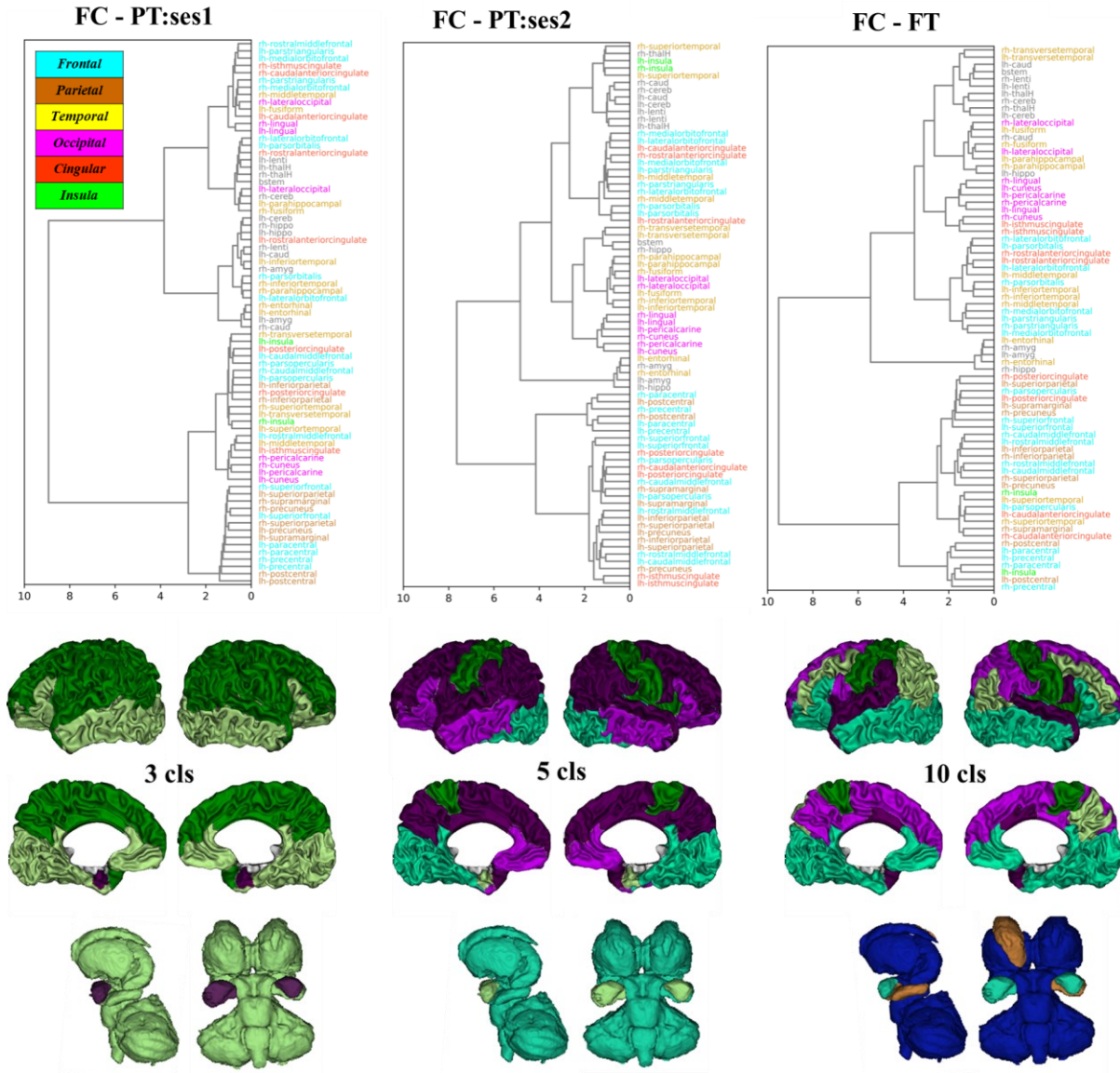
Supp. Figure 2.1. Overview of the steps for the characterisation of the GM structural similarity networks.



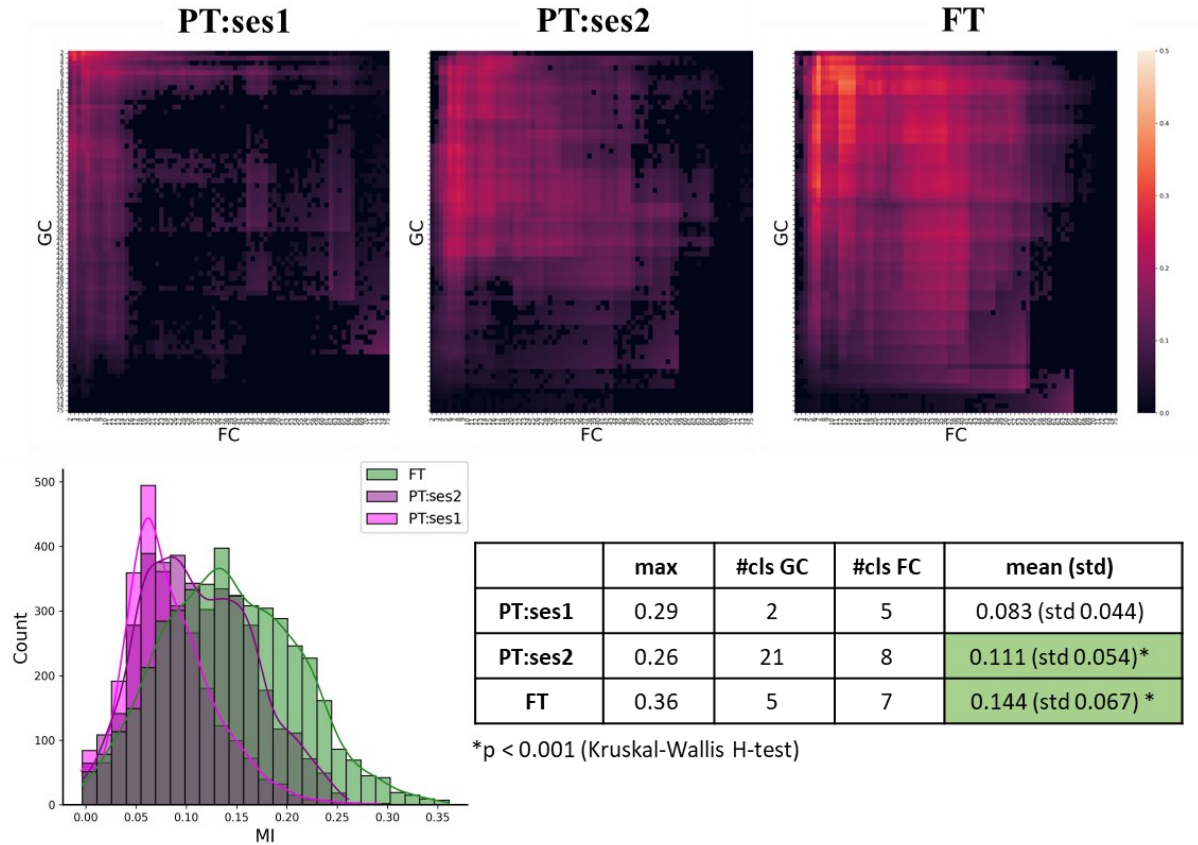
Supp. Figure 2.2. Relationship between GC and FC connectivity per ROI-ROI pair (upper triangle of symmetric matrices) after removal of subcortical regions. The table summarizes the features of the relationship. (PT:ses1 vs PT:ses2 Z-score = 13.12, $p < 0.001$; PT:ses1 vs FT Z-score = 15.85, $p < 0.001$; PT:ses2 vs FT Z-score = 3.16, $p = 0.002$)



Supp. Figure 2.3. GC dendrograms for the three infant groups (a) and example clustering results in FT groups for selected cluster numbers (b). The ROI naming conventions and assignment to lobes is detailed in *Supp. Table 1*.



Supp. Figure 2.4. FC dendrograms for the three infant groups (a) and example clustering results in FT groups for selected cluster numbers (b). The ROI naming conventions and assignment to lobes is detailed in *Supp. Table 1*.

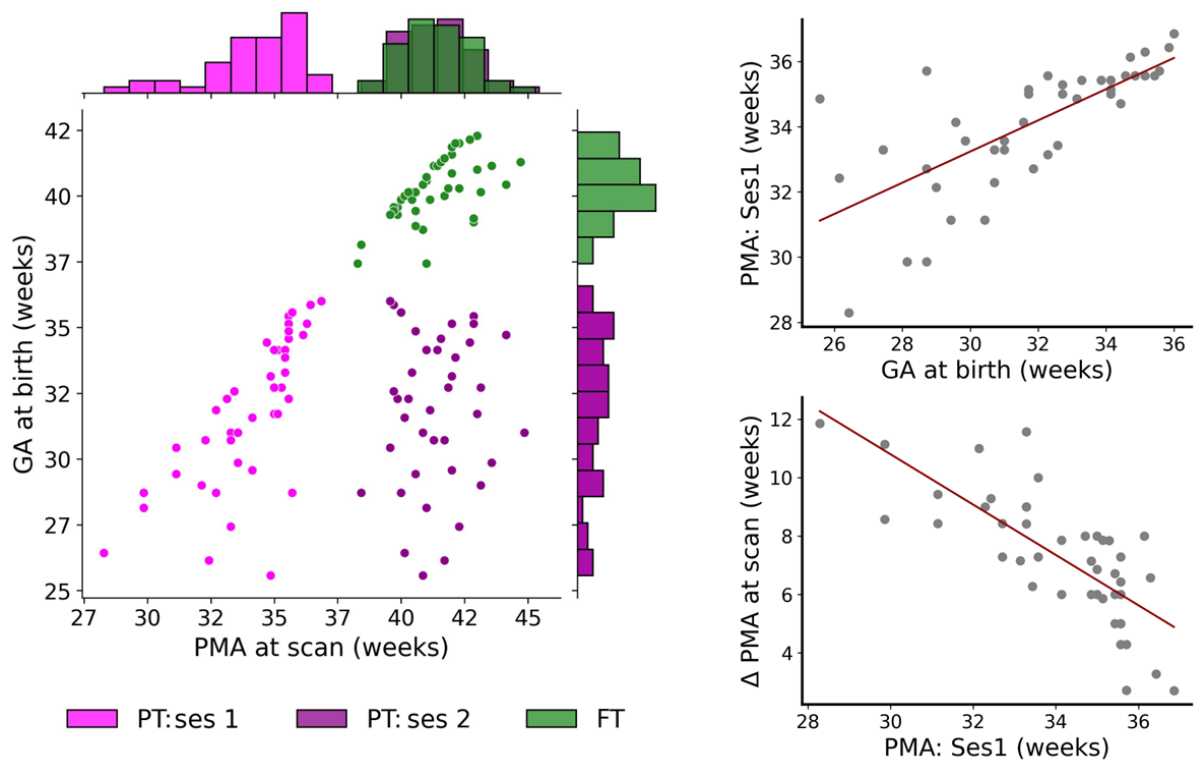


Supp. Figure 2.5. Mutual information between GC and FC clustering results after permutation testing. Histogram summarizes the significant MI values across groups. The table presents the features of the MI evaluations.

3. Cohort description

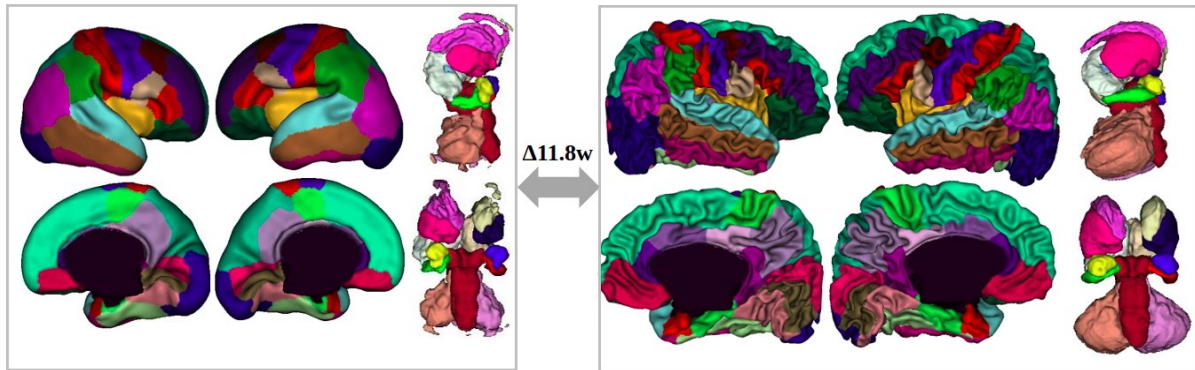
		FT (N = 45)		PT: Ses 1 (N = 45)	
		Mean (std)	Median [range]	Mean (std)	Median [range]
GA at birth		40.3 (1.17)	40.1, [37.4,42.3]	31.8 (2.84)	32.3, [25.6,36.0]
PMA scan: Ses1		-	-	34.1 (1.88)	34.9, [28.3,36.9]
PMA at scan: Ses2 (TEA)		41.4 (1.41)	41.3, [38.3,44.7]	41.4 (1.42)	41.3, [38.4,44.9]
N (%) male		26 (58%)		26 (58%)	
Radiology score:					
	FT (N = 45)	PT: Ses 1	PT: Ses2		
1	29 (64%)	27 (60%)	19 (42%)	p=0.17	
2	11 (24%)	10 (22%)	13 (29%)		
3	5 (11%)	8 (18%)	13 (29%)		

Supp. Table 3.1. Cohort characteristics. *Legend:* FT: Full-term group, PT: Ses1: preterm group scanned at 1st session, PT: Ses2: preterm group scanned at term-equivalent age, GA: gestational age, PMA: post-menstrual age, N: number, std: standard deviation.



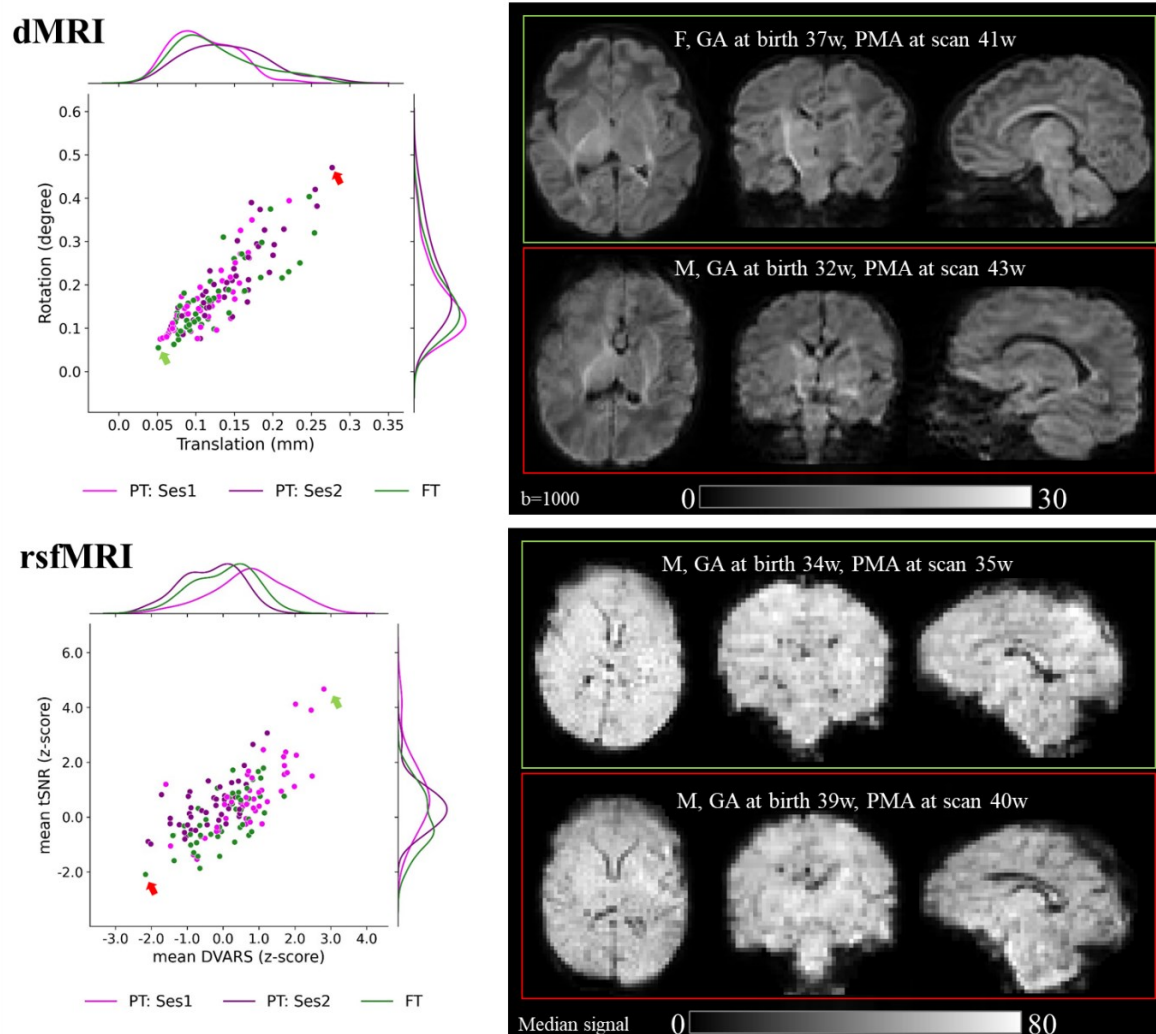
Supp. Figure 3.2. Joint distribution of PMA at scan and GA at birth for the 3 infant groups. Left: significant relationship between the GA at birth with PMA at Ses1, and PMA: Ses1 with delay between PMA at session 1 and 2 (linear regression, $p < 0.001$). *Legend:* FT: Full-term group, PT: Ses1: preterm group scanned at 1st session, PT: Ses2: preterm group scanned at term-equivalent age, GA: gestational age, PMA: post-menstrual age, Δ : difference.

4. ROI delineation

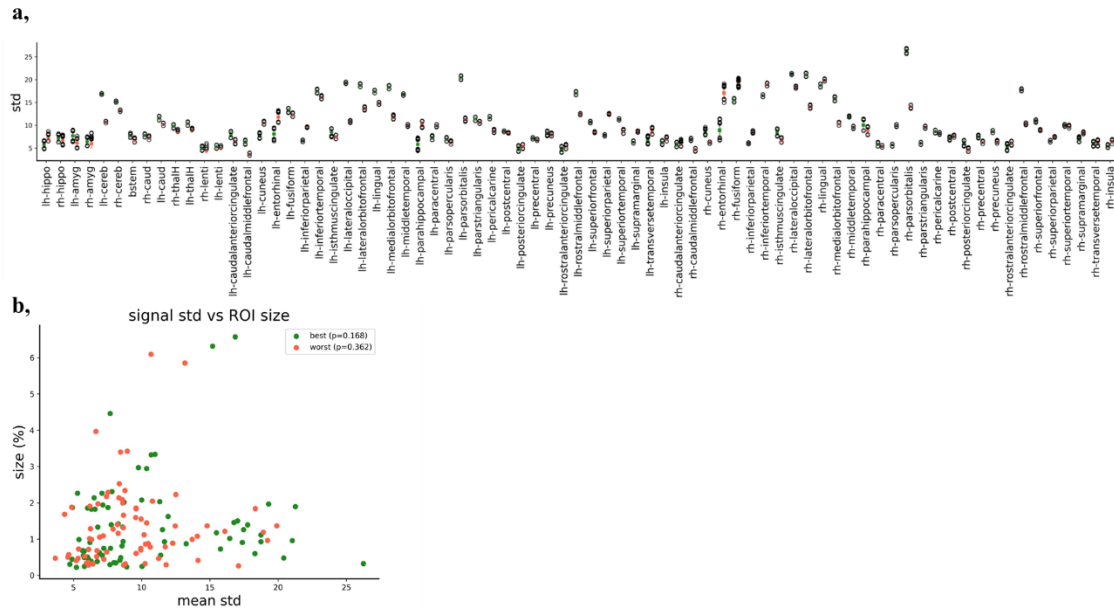


Supp. Figure 4.1. Example of segmentation for the longitudinal subject with the longest scan delay. *Legend:* Δ : difference.

5. Data QC



Supp. Figure 4.2. Example diffusion and resting state functional data for subjects with the highest (in **green**) and the lowest (in **red**) data quality. *Legend:* FT: Full-term group, PT: Ses1: preterm group scanned at 1st session, PT: Ses2: preterm group scanned at term-equivalent age, GA: gestational age, PMA: post-menstrual age, M: male, F: female, tSNR: temporal signal-to-noise ratio, DVARS: the spatial standard deviation of successive difference images.



Supp. Figure 4.3a, Regional coherence of the functional data for delineated ROIs assessed as the standard deviation of the functional signal within the given region. The ROI naming conventions and assignment to lobes is detailed in *Supp. Table 1*. **b,** Scatter plot of ROI's signal standard deviation with its size (as percentage of the whole GM) suggesting no apparent relationship between ROI signal homogeneity with size suggesting that in the analyses aiming to 'equalize' the regions within functional analyses, it might be preferable to sample the regions based on their signal variability rather than size.

6. Longitudinal evaluations

To investigate longitudinal changes between PT:ses1 and PT:ses2 in the PT group in the univariate setting, we first calculated the difference between ses2 and ses1 for each diffusion metric. The effect of the ROI, PMA at scan and GA at birth on the change in the diffusion metric was evaluated in ANOVA analysis, revealing significant effects (*Supp. Table 6.1*). The ROI-wise change in diffusion metrics is visualized in *Supp. Figure 6.1*. Changing profiles for most (but not all) metrics were different from 0 (Wilcoxon test, Benjamini–Hochberg false discovery rate (FDR) correction across ROIs and metrics) (*Supp. Table 6.2*). The relationship of the changing profiles between the pairs of ROIs was also assessed with a Pearson's correlation for six diffusion metrics separately. Results suggested pair-specific similarities in the change of the diffusion metrics between ses1 and ses2 and hinted at the heterogeneous developmental trajectories of the regional microstructure in the preterm group across regions inspiring the delineation of the 'developmental' networks in the main body of this work. The combined results of the comparisons are presented in the *Supp. Figure 6.2*.

a,

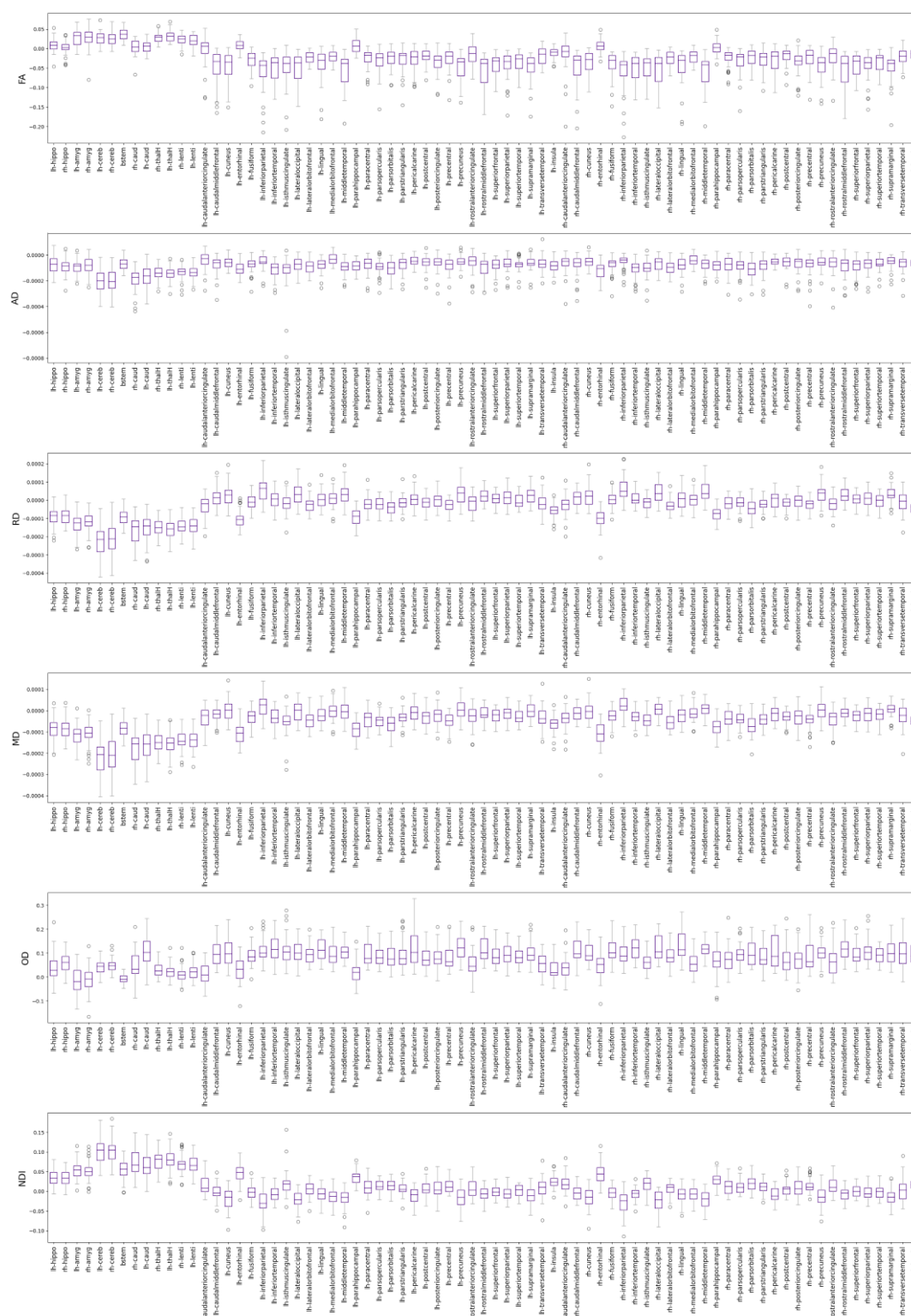
	Global Δ FA	Global Δ AD	Global Δ RD	Global Δ MD	Global Δ OD	Global Δ NDI
Scan delay	***	***	**	***	***	***
PMA Ses1	***	***	***	***	***	***
GA at birth	***	n.s.	**	n.s.	***	***
Scan delay: PMA Ses1	***	***	***	***	n.s.	***
Scan delay: GA at birth	*	n.s.	n.s.	n.s.	*	n.s.
PMA Ses1: GA at birth	***	***	***	***	*	***

<i>Scan delay: PMA Ses1: GA at birth</i>	*	*	***	***	*	*
--	---	---	-----	-----	---	---

b,

	Δ F _A	Δ A _D	Δ R _D	Δ M _D	Δ O _D	Δ N _D I
<i>ROI</i>	***	***	***	***	***	***
<i>Scan delay</i>	***	***	***	***	***	***
<i>PMA Ses1</i>	***	***	***	***	***	***
<i>GA at birth</i>	***	n.s.	***	n.s.	***	***
<i>Global ΔGM*</i>	***	***	***	***	***	***
<i>ROI: Scan delay</i>	***	***	***	***	***	***
<i>ROI: GA at birth</i>	***	**	*	n.s.	***	n.s.

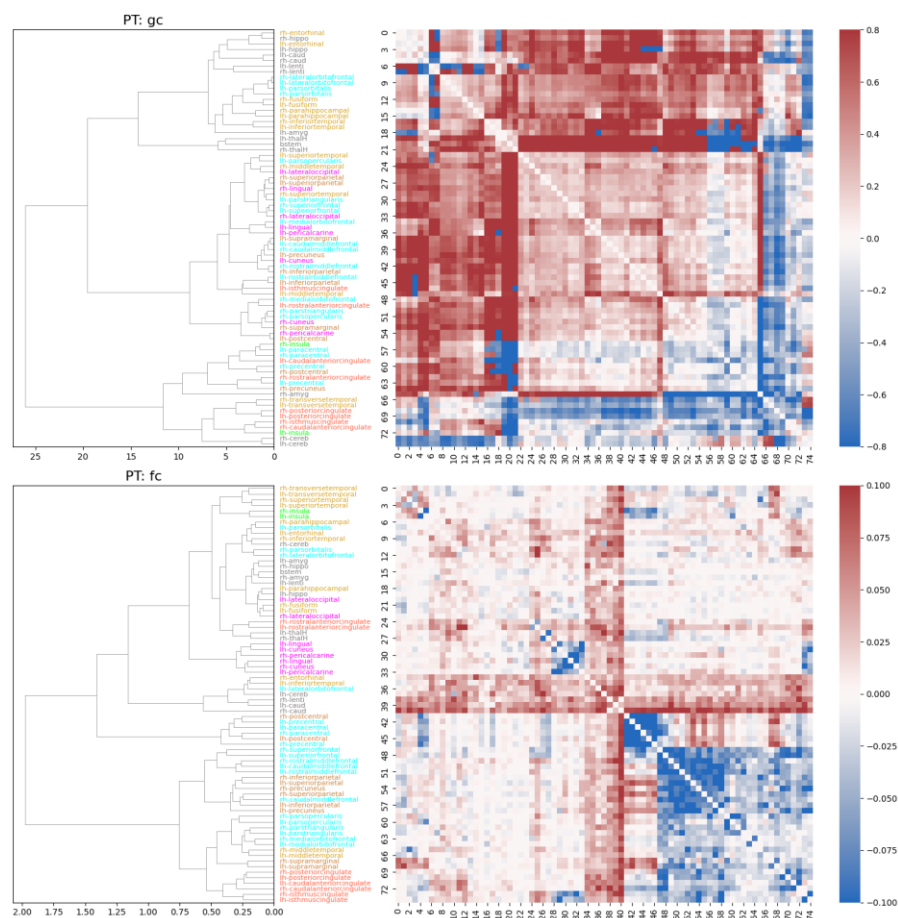
Supp. Table 6.1.a: ANOVA model studying effects of PMA at scan and GA at birth on the six global median diffusion metrics. **b:** ANOVA model studying effects of PMA at scan and GA at birth on the six global median diffusion metrics. p-value ≤ 0.0001 [****], ≤ 0.001 [***], ≤ 0.01 [**], < 0.05 [*], < 0.1 [·], ≥ 0.1 [ns].



Supp. Figure 6.1. Difference in diffusion metrics between PT:ses1 vs PT:ses2 for each ROI corrected for scan delay, PMA at ses1, and GA at birth. (Mean of the difference added back to residuals for visualization purposes). The ROI naming conventions and assignment to lobes is detailed in *Supp. Table 1*.

	Left							Right					
	FA	L1	RD	MD	OD	ND		FA	L1	RD	MD	OD	ND
<i>hippo</i>	***	***	***	***	***	***		n.s.	***	***	***	***	***
<i>amyg</i>	***	***	***	***	n.s.	***		***	***	***	***	n.s.	***
<i>cereb</i>	***	***	***	***	***	***		***	***	***	***	***	***
<i>bstem</i>	***	***	***	***	**	***							
<i>caud</i>	n.s.	***	***	***	***	***		*	***	***	***	***	***
<i>thalH</i>	***	***	***	***	***	***		***	***	***	***	***	***
<i>lenti</i>	***	***	***	***	***	***		***	***	***	***	**	***
<i>caudalanteriorcingulate</i>	n.s.	***	***	***	n.s.	***		**	***	***	***	***	***
<i>caudalmiddlefrontal</i>	***	***	**	**	***	n.s.		***	***	***	*	***	n.s.
<i>cuneus</i>	***	***	***	n.s.	***	***		***	***	**	n.s.	***	***
<i>entorhinal</i>	***	***	***	***	***	***		**	***	***	***	***	***
<i>fusiform</i>	***	***	n.s.	***	***	n.s.		***	***	n.s.	***	***	n.s.
<i>inferiorparietal</i>	***	***	***	***	***	***		***	***	***	***	***	***
<i>inferiortemporal</i>	***	***	n.s.	***	***	*		***	***	**	***	***	***
<i>isthmuscingulate</i>	***	***	*	***	***	***		***	***	*	***	***	***
<i>lateraloccipital</i>	***	***	***	n.s.	***	***		***	***	***	n.s.	***	***
<i>lateralorbitofrontal</i>	***	***	***	***	***	*		***	***	***	***	***	**
<i>lingual</i>	***	***	n.s.	***	***	*		***	***	*	***	***	**
<i>medialorbitofrontal</i>	***	***	*	n.s.	***	***		***	***	n.s.	n.s.	***	**
<i>middletemporal</i>	***	***	***	n.s.	***	***		***	***	***	**	***	***
<i>parahippocampal</i>	*	***	***	***	**	***		n.s.	***	***	***	***	***
<i>paracentral</i>	***	***	***	***	***	***		***	***	***	***	***	***
<i>parsopercularis</i>	***	***	***	***	***	***		***	***	**	***	***	***
<i>parsorbitalis</i>	***	***	***	***	***	***		***	***	***	***	***	***
<i>parstriangularis</i>	***	***	**	***	***	***		***	***	***	***	***	***
<i>pericalcarine</i>	***	***	n.s.	n.s.	***	***		***	***	n.s.	**	***	***
<i>postcentral</i>	***	***	***	***	***	**		***	***	**	***	***	*
<i>posteriorcingulate</i>	***	***	n.s.	***	***	n.s.		***	***	n.s.	***	***	**
<i>precentral</i>	***	***	***	***	***	***		***	***	***	***	***	***
<i>precuneus</i>	***	***	***	n.s.	***	***		***	***	***	n.s.	***	**
<i>rostralanteriorcingulate</i>	***	***	n.s.	***	***	*		***	***	**	***	***	***
<i>rostralmiddlefrontal</i>	***	***	***	*	***	**		***	***	***	n.s.	***	**
<i>superiorfrontal</i>	***	***	n.s.	***	***	n.s.		***	***	n.s.	***	***	n.s.
<i>superiorparietal</i>	***	***	**	*	***	**		***	***	n.s.	**	***	n.s.
<i>superiortemporal</i>	***	***	n.s.	***	***	n.s.		***	***	n.s.	***	***	n.s.
<i>supramarginal</i>	***	***	***	n.s.	***	n.s.		***	***	***	*	***	***
<i>transversetemporal</i>	***	***	*	***	***	**		***	***	n.s.	**	***	n.s.
<i>insula</i>	***	***	***	***	***	***		***	***	***	***	***	***

Supp. Table 6.2. Wilcoxon rank test comparing the distribution of PT:ses1 vs PT:ses2 differences in diffusion metrics to 0 after correction for scan delay, PMA at ses1, and GA at birth. p-values are corrected for multiple comparisons using FDR correction. p-value ≤ 0.0001 [***], ≤ 0.001 [***], ≤ 0.01 [***], < 0.05 [*], < 0.1 [.] , ≥ 0.1 [ns].



Supp. Figure 6.3. Dendrogram derived from the developmental change in GC and FC between scans at ses1 and TEA as well as the Δ GC and Δ FC matrices. The ROI naming conventions and assignment to lobes is detailed in *Supp. Table 2*

Annexe 4: CV and Publications

Andrea Gondová

Doctoral student in Neurosciences

Professional and academic experience

Doctoral student, Neurospin, CEA & Université Paris Cité, FR 2021-

[Horizon 2020: International PhD Program in NUMERICAL Simulation](#)

- *Analysis of large multimodal and multiscale imaging databases for mapping of neonatal brain development.*
 - ✓ Development of the pipeline for processing and analysis of MRI imaging data and the identification of infants at risk of neurodevelopmental disorders
 - ✓ Communication through scientific publications and international congresses
 - ✓ Development of the personal scientific network thanks to collaborators in France and abroad

Graduate scientist in Data Science and AI, Astra Zeneca, SWE 2018-2020

[Early Talent: Data Science & Artificial Intelligence Graduate Programme](#)

Projects:

- *Knowledge graph for identification of patients susceptible to drug-induced interstitial lung disease by the knowledge graph*
- *Improved screening of asthmatic patients with an AI recommendation system*
- *Automated segmentation of CMR images in rats with myocardial infarction*
 - ✓ Implemented and validated AI tools with potential to accelerate drug development and reduce risks within the pharmaceutical industry
 - ✓ Communicated of results to the management team and the R&D community (internal communications, 1 scientific publication, international congress)

MSc project, Chemical & Translational Biology Lab., University of Edinburgh, UK 2018-2018

- *Small molecule target prediction with machine learning*
 - ✓ Developed machine learning models and benchmarked them to cheminformatic standards.

Team member, Edinburgh University Students' Association (EUSA), UK 2015-2018

- ✓ Helped students, staff, and the general public with inquiries about student association's activities
- ✓ Facilitated of the smooth running of events, monitoring and maintaining the safety and cleanliness of EUSA premises

Education

PhD en Neurosciences, Université Paris Cité, FR 2021-

MSc Bioinformatics (with distinction), University of Edinburgh, UK 2017-2018

BSc in Philosophy, Université Paris Nanterre, FR 2022-

BSc (Hons) in Biomedical Sciences, University of Edinburgh, UK 2013-2017

Teaching experiences and science communication

Tutorials' supervisor, Master 2 in Biomedical Imaging, Université Paris-Saclay, FR (from 2022)

- Course: Introduction to artificial intelligence, *INSTN*

Supervision of student internship

- 2023: Master 2 Cognitive and Clinical Neuroscience, Maastricht University
- 2022: Master 2 Computational Neuroscience and Neuro-engineering, Centrale Supélec

Facilitator: 'SciFun Science Road Show' (2013-2017)

- Public science engagement with a primary/secondary school focus
- Participated in festivals and science events across Scotland

Learning Facilitator: 'BioPals' (2014-2015)

- Organized group meetings structured around themes relevant to the university experience of students in learning biology

Volunteering

Secretary: [OHBM* Open Science Special Interest Group](#) (ongoing)

- Coordination of activities and communications between members; co-organization of the 'Open Science Room' during the OHBM* 2023 congress; update of group documentation
- Maintenance of external communication channels (website, social networks)

Project lead 'Train-track': [OHBM* BrainHack 2023](#) (ongoing)

- Identification of educational materials for acquiring the skills required to participate in the hackathon and making them available on the website
- Coordination of tutorials and group work during the event

* Organisation for Human Brain Mapping

Member of the organisational committee: AstraZeneca Data Science Symposium 2020

- Event planning – selection, invitations and coordination of experts for presentations, discussions, and round tables
- 'Back-end' support for the online sessions, co-animation of the round table

Public commitments:

- Speaker at the events:
'Women in Data Science - R&D Early Careers' (2020, online)
'Scottish STEM women Graduate Careers' Fair' (2020, online, represented AstraZeneca)
'Early career in pharmaceutical industry' (2019, Karolinska Institute, SWE)
- Testimonial 'Early career in STEM' published on the University of Edinburgh website

Recognitions

Edinburgh Award: BioPals (2015)

For engagement in peer-support learning scheme

Edinburgh Award: EUSA (2015)

For my activities with the University of Edinburgh Student Union

Data Science Champion, Astra Zeneca (2020)

For my contribution to the symposium organization and representation at numerous events

Scholarships

'Highly Skilled Workforce' (2017)

Covering MSc fees awarded on the basis of academic merit

ERASMUS: international mobility (2015-2016)

Financial aid awarded to motivated students based on academic merit

- 1 year at the Sorbonne University

Publications and communications

Presented PhD work:

<i>Publications</i>	Neumane S*, Gondová A* , Leprince Y, Hertz-Pannier L, Arichi T, Dubois J. Early structural connectivity within the sensorimotor network: Deviations related to prematurity and association to neurodevelopmental outcome. <i>Front Neurosci.</i> 2022 Nov 25;16:932386.
	Gondová A , Neumane S, Leprince Y, Mangin J.F, Arichi T, Dubois J. Predicting neurodevelopmental outcomes from neonatal cortical microstructure: A conceptual replication study. <i>Neuroimage: Reports.</i> 2023.
	Gondová A , et al. Bridging the gap between microstructural gray-matter similarity and functional connectome: A multi-modal MRI study in preterm and full-term infants (in preparation)
<i>Posters</i>	Gondová A , Neumane S, Leprince Y, Hertz-Pannier L, Arichi T, Dubois J. Structural connectivity of sensorimotor network: evaluating the impact of prematurity. OHBM 2023 annual meeting, Montreal, Canada. 2023 July.
	Gondová A , Neumane S, Leprince Y, Arichi T, Mangin J, Dubois J. Predicting neurodevelopmental outcomes from the early sensorimotor structural connectivity. OHBM 2023 annual meeting, Montreal, Canada. 2023 July.
	Gondová A , Neumane S, Leprince Y, Mangin J, Dubois J. Infant cortical microstructure at term-equivalent age accurately predicts prematurity status at birth. OHBM 2022 annual meeting, Glasgow, UK. 2022 June.

*co-first authors